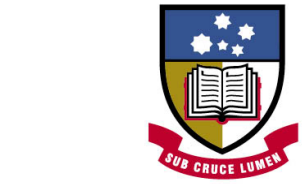

THE UNIVERSITY
of ADELAIDE

The tectonic evolution of the southern Congo Craton

Brandon L. Alessio

Earth Sciences
School of Physical Sciences
University of Adelaide

This thesis is submitted in fulfilment of the requirements
for the degree of Doctor of Philosophy

17th April 2019

Constraining the evolution of continents, and the tectonic plates they reside upon, enables geoscientists to understand phenomena such as mantle dynamics, mineral and energy resource distribution, faunal evolution, and climate development. Thus, there is an underlying necessity to have rigorous palaeogeographic models that constrain plate reconfiguration and interaction throughout earth history. The Congo Craton encompasses present-day central Africa, and is comprised of Archean crustal blocks and Proterozoic orogens. The southern margin of this craton acted as a plate boundary from the Palaeoproterozoic to present. However, the evolution of this margin remains largely enigmatic. This thesis interrogates the tectonic evolution Southern Irumide Belt (SIB), a predominantly Mesoproterozoic orogen located along the southern Congo margin, which serves as a vital proxy for understanding the evolution of the Congo Craton.

U–Pb dating of detrital zircons from metasedimentary rocks within the Zambian terranes of the SIB identifies Palaeoproterozoic to Mesoproterozoic age populations that are equivalent to those preserved in the Muva Supergroup, found in the Irumide Belt (*sensu stricto*) of the Congo Craton. This depositional connection between the SIB and Congo Craton prior to the late-Mesoproterozoic is supportive of a tectonic model where the SIB formed on the southern Congo margin. Neoproterozoic sedimentary rocks identified in the Nyimba–Sinda Terrane highlight subsequent extension in the region that is likely a response to rifting. Full-plate topological models suggest that this rifting was a southern extension of the spreading that separated Australia from Laurentia during Rodinia break-up. An isotopic and geochronological investigation of intrusions throughout this region suggest that the SIB formed on an isotopically evolved Palaeoproterozoic basement. This is equivalent to basement in the neighbouring Irumide Belt, and further supports the SIB forming on the southern Congo margin. During the late stages of Gondwana amalgamation, the Congo Craton collided with the Kalahari Craton to form central Gondwana, generating tectono-metamorphic overprints that are displayed in the rocks of the Southern Irumide and Zambezi belts. These overprints record amphibolite to granulite facies mineral assemblages, and include more exotic, high-pressure 'whiteschist' assemblages. An activity-composition model was created for yoderite, a key mineral in whiteschists, for use with the pressure–temperature (*P–T*) modelling software *THERMOCALC*. Using this model, *P–T* diagrams were calculated for both a retrogressed whiteschist and metapelite from the region, to constrain the features of the Gondwana forming collision. A thermal gradient of 30–90 °C/kbar was calculated for the whiteschist, consistent with those calculated for peak metamorphism, whereas a gradient of 70–165 °C/kbar was calculated for the metapelite. The different thermal gradients relate to different aspects of the collision. Where the amphibolite facies rocks formed in a compressional setting proximal to the southern Congo margin, the whiteschists instead formed directly at the site of continental collision, marking the suture zone between the Congo and Kalahari Cratons. U–Pb apatite and ^{40}Ar–^{39}Ar muscovite data reveal high-temperature cooling ages spanning the late-Neoproterozoic to Cambrian, relating to cooling after Congo–Kalahari collision. Apatite fission track dating identifies periods of low-temperature cooling during the Carboniferous, Triassic, and Cretaceous, with thermal modelling identifying rapid Cenozoic cooling. These periods are interpreted to relate to periods of exhumation in central Africa, which occurred in response to the wider-scale tectonic processes of Karoo rift basin formation, Gondwana break-up, and the development of the East African Rift System (EARS).

These studies provide a framework for understanding the evolution of the Southern Irumide Belt. As a proxy for the evolution of the southern Congo margin, this work serves to constrain palaeogeographic models for the Congo Craton, further elucidating its role within the wider Earth system.

I certify that this work contains no material which has been accepted for the award of any other degree or diploma in my name, in any university or other tertiary institution and, to the best of my knowledge and belief, contains no material previously published or written by another person, except where due reference has been made in the text. In addition, I certify that no part of this work will, in the future, be used in a submission in my name, for any other degree or diploma in any university or other tertiary institution without the prior approval of the University of Adelaide and where applicable, any partner institution responsible for the joint-award of this degree.

I acknowledge that copyright of published works contained within this thesis resides with the copyright holder(s) of those works.

I also give permission for the digital version of my thesis to be made available on the web, via the University's digital research repository, the Library Search and also through web search engines, unless permission has been granted by the University to restrict access for a period of time.

I acknowledge the support I have received for my research through the provision of an Australian Government Research Training Program Scholarship.

Brandon Luke Alessio
21st February, 2019

To my wife Kiara, you are the best thing to have come from my time studying geology. To have done our PhDs together has been a great journey, one that I would have struggled to complete without your love and support. I look forward to our many future adventures.

To Morgan Blades, you were my emotional support throughout honours, though I think that role has swapped between us on many occasions throughout our time together. You were the best man at my wedding, despite being poorly equipped for that role. I've loved every second of our banter and I look forward to much more in the years to come.

To my supervisors Alan Collins and Stijn Glorie, I am extremely grateful for the support and guidance you have provided me throughout this project. Alan, your experience has guided me throughout my PhD, and I appreciate how supportive you've been for me to take this project in my own direction. Stijn, many thanks for always making time to discuss my project and generally being a great person to talk to.

To David Kelsey, your support and expertise has been invaluable throughout this project. The opportunity to conduct and publish our work on yoderite has been one of the highlights of my PhD, and I am immensely grateful for your guidance throughout that study. All the best for your future outside the university.

To Pete Siegfried, our discussions about central African geology have been invaluable for helping to form my own understanding of the region. It has been great to have someone as knowledgeable and enthusiastic about geology as you involved with my project.

JOURNAL ARTICLES

Alessio, B. L.; Blades, M. L.; Murray, G.; Thorpe, B.; Collins, A. S.; Kelsey, D.E.; Foden, J.; Payne, J.; Al-Khirbash, S.; Jourdan, F. (2017). Origin and tectonic evolution of the NE basement of Oman: a window into the Neoproterozoic accretionary growth of India? Geological Magazine, 1-25.

Merdith, A. S.; Collins, A. S.; Williams, S. E.; Pisarevsky, S.; Foden, J.; Archibald, D.; Blades, M. L.; **Alessio, B. L.**; Armistead, S.; Plavsa, D.; Clark, C.; Müller, D. (2017). A full-plate global reconstruction of the Neoproterozoic. Gondwana Research, 50, 84-134.

Alessio, B. L. & Kelsey, D. E. (2018). On yoderite: Using calculated phase equilibria to investigate its rarity in the geological record of whiteschists. Journal of Metamorphic Geology, 36(3), 297-314.

Alessio, B. L.; Collins, A. S.; Siegfried, P.; Glorie, S.; De Waele, B.; Payne, J. L.; Archibald, D. (2018). Neoproterozoic tectonic geography of the south-east Congo Craton in Zambia as deduced from the age and composition of detrital zircons. Geoscience Frontiers.

Dew, R. E. C.; Collins, A. S.; Glorie, S.; Morley, C. K.; King, R.; Foden, J.; De Grave, J.; Kanjanapayont, P.; Evans, N.; **Alessio, B. L.**; Charusiri, P. (2018). Probing into Thailand's basement: New insights from U-Pb geochronology, Sr, Sm-Nd, Pb and Lu-Hf isotopic systems. Lithos.

Alessio, B. L.; Collins, A. S.; Clark, C.; Glorie, S.; Siegfried, P.; Taylor, R. (2019). Age, origin and palaeogeography of the Southern Irumide Belt, Zambia. Journal of the Geological Society.

Blades, M. L.; **Alessio, B. L.**; Collins, A. S.; Foden, J.; Payne, J. L.; Glorie, S.; Holden, P.; Thorpe, B.; Al-Khirbash, S. (Submitted). Unravelling the Neoproterozoic accretionary history of Oman, Using an array of isotopic systems in zircon. Journal of the Geological Society.

Alessio, B. L.; Glorie, S.; Collins, A. S.; Jourdan, F.; Jepson, G.; Nixon, A.; Siegfried, P.; Clark, C. (Submitted). The thermo-tectonic evolution of the southern Congo margin as determined by apatite and muscovite thermochronology. Tectonophysics.

CONFERENCE PRESENTATIONS

Alessio, B. L.; Blades, M. L.; Murray, G.; Thorpe, B.; Collins, A. S.; Kelsey, D.E.; Foden, J.; Payne, J.; Al-Khirbash, S.; Jourdan, F. 2016. Origin and tectonic evolution of the NE basement of Oman: a window into the Neoproterozoic accretionary growth of India? Australian Earth Sciences Convention and 35th International Geological Congress.

Alessio, B. L.; Collins, A. S.; Brick, R.; De Waele, B.; Plavsa, D.; Patranabis-Deb, D.; Foden, J.; Payne J. L.; Clark, C.; Glorie, S.; Blades, M. L. 2016. Testing Azania: using detrital zircon U-Pb ages and Hf isotopic record to constrain tectonic affinities within the East African Orogen. Australian Earth Sciences Convention and 35th International Geological Congress.

Merdith, A. S.; Collins, A. S.; Williams, S. E.; Pisarevsky, S.; Foden, J.; Archibald, D.; Blades, M. L.; **Alessio, B. L.**; Armistead, S.; Plavsa, D.; Clark, C.; Müller, D. 2016. Full-plate topological reconstruction of Gondwana formation. Australian Earth Sciences Convention and 35th International Geological Congress.

Dew, R. E. C.; Collins, A. S.; Glorie, S.; Morley, C. K.; King, R.; Foden, J.; De Grave, J.; Kanjanapayont, P.; Evans, N.; **Alessio, B. L.**; Charusiri, P. 2017. Zircon probes and provenance: new insights in the palaeogeography of Southeast Asia. Gondwana 16.

Alessio, B. L.; Collins, A. S.; Siegfried, P.; Glorie, S.; De Waele, B.; Payne, J. L.; Archibald, D. (2018). 2017. The tectonic evolution of the Southern Irumide Belt: Constraining the plate margin evolution of the southeast Congo–Tanzania–Bangweulu Block. Gondwana 16.

Merdith, A. S.; Collins, A. S.; Williams, S. E.; Pisarevsky, S.; Foden, J.; Archibald, D.; Blades, M. L.; **Alessio, B. L.**; Armistead, S.; Plavsa, D.; Clark, C.; Müller, D. 2018. A full plate topological animation for the Neoproterozoic: a requirement for understanding the feedback between the solid Earth and the greater Earth System. European Geosciences Union general assembly.

Alessio, B.L.; Collins, A.S.; Kelsey, D.E.; Clark, C.; Glorie, S.; Taylor, R. 2018. Identifying the tectono-metamorphic overprints of a Gondwana forming collision: a structural and thermobarometric transect of the Southern Irumide and Zambezi belts, Zambia. European Geosciences Union general assembly.

Alessio, B. L. & Kelsey, D. E. 2018. On yoderite: Using calculated phase equilibria to investigate its rarity in the geological record of whiteschists. European Geosciences Union general assembly.

Collins, A. S.; Blades, M. L.; Cox, G.; **Alessio B. L.**; Foden, J.; Merdith, A.; Williams, S.; Müller, D. 2018. Neoproterozoic Arabia — The Angudan/Malagasy orogenic collision of Neoproterozoic India with Africa in a plate kinematic framework. European Geosciences Union general assembly.

CHAPTER 1

Introduction and thesis outline

INTRODUCTION

The onset of plate tectonics has seen constant evolution and interaction between the Earth's continents. The importance of these interactions cannot be understated as they are intrinsically linked to, and thus hold vital implications for, the development of the greater Earth system (Collins and Pisarevsky, 2005; Merdith et al., 2017; 2019). By understanding the evolution of tectonic plates, and the continents residing on them, geoscientists can further understand changes in mantle dynamics (e.g. Tackley, 2000), mineral and energy resource distribution (e.g. Barley and Groves, 1992), faunal diversity and evolution (e.g. Halverson et al., 2009), and development of the climate (e.g. Hoffman et al., 1998). In recent years, the ability to reconstruct (and thereby understand) the interactions of tectonic plates has evolved beyond simply interpreting relative motions of discrete continental blocks to full plate topological models, which force palaeogeographic interpretations to account for global plate boundary interactions. These advances underline the importance of understanding the evolution of plate boundaries through time, as they control the development and preservation of passive margins, island arcs, and orogens that provide a record of continental evolution (Merdith et al., 2017). Thus, the systematic interrogation of the evolution of Earth's plate margins is a necessary step in producing rigorous palaeogeographic models, which in turn can greatly improve our understanding of wider Earth system processes (Merdith et al. 2019).

The Congo Craton comprises a series of Archaean crustal blocks and Proterozoic orogens that form present-day central Africa, with the southern margin of this craton providing a vital, yet currently underutilised, record of plate margin evolution that spans from the Palaeoproterozoic to present. Understanding the evolution of this margin is crucial for resolving palaeogeographic problems occurring across the last one and a half billion years of Earth evolution, foremost of which are: the position of the Congo Craton in Rodinia (including whether it even formed part of the supercontinent; De Waele et al., 2008; Kröner and Cordani, 2003), the contrasting Neoproterozoic development of the southern Congo margin, the dynamics of collision between the Congo and Kalahari (forming present-day southern Africa) cratons in the late stages of Gondwana amalgamation, and the subsequent thermal evolution and possible reactivation of this relict margin throughout the Phanerozoic. This research revolves around three main foci that seek, at least in part, to resolve the main questions regarding the evolution of the Congo Craton from the Mesoproterozoic to present. First, to determine the extent and evolution of the southern Congo margin throughout the Mesoproterozoic: opposing hypotheses exist for the origin of large swathes of Mesoproterozoic crust located along the (present-day) south-east margin of the Congo Craton and whether or not this crust accreted to, or formed along the craton's margin (Bingen et al., 2009; Johnson et al., 2006; Johnson et al., 2007b). Second, to constrain the Neoproterozoic evolution of the southern Congo Margin: Does the geological record of this region support current palaeogeographic interpretations for the Congo Craton during the Neoproterozoic (Merdith et al., 2017), and what does the metamorphic overprint of this margin imply for the Gondwana forming collision between the Congo and Kalahari cratons. Third, to constrain the Phanerozoic thermal evolution of central Africa, following suturing between the Congo and Kalahari cratons along the southern Congo margin: What implications do the high-temperature thermal evolution of the southern Congo margin hold for Gondwana amalgamation, and what (if any) wider scale tectonic processes are recorded by the regions low-temperature thermal evolution. These foci contribute to understanding the evolution of the Congo Craton's southern plate margin, which is a vital step in constructing the rigor-

ous full-plate, global palaeogeographic models needed to understand the interplay between the evolving continents and greater Earth system.

GEOLOGICAL BACKGROUND

The Congo Craton is a term used by De Waele et al. (2008) to describe the amalgamated central African landmass at the time of Gondwana assembly, and by this time was comprised of several Archaean to Palaeoproterozoic cratons and Palaeoproterozoic to Mesoproterozoic orogens (Fig. 1). Along the southern margin of the Congo Craton, these units include the Palaeoproterozoic Ubendian–Usagaran orogen that records the amalgamation of the Archean to Palaeoproterozoic Bangweulu Block and Archean Tanzanian Craton. Also along this margin is the Mesoproterozoic Irumide Belt, which was interpreted by De Waele et al. (2006b) to act as the boundary of the Bangweulu Block and wider Congo Craton during the Mesoproterozoic. The Irumide Belt is considered to be separate and distinct from the adjacent Southern Irumide Belt on the basis of differing lithologies and overprints in either

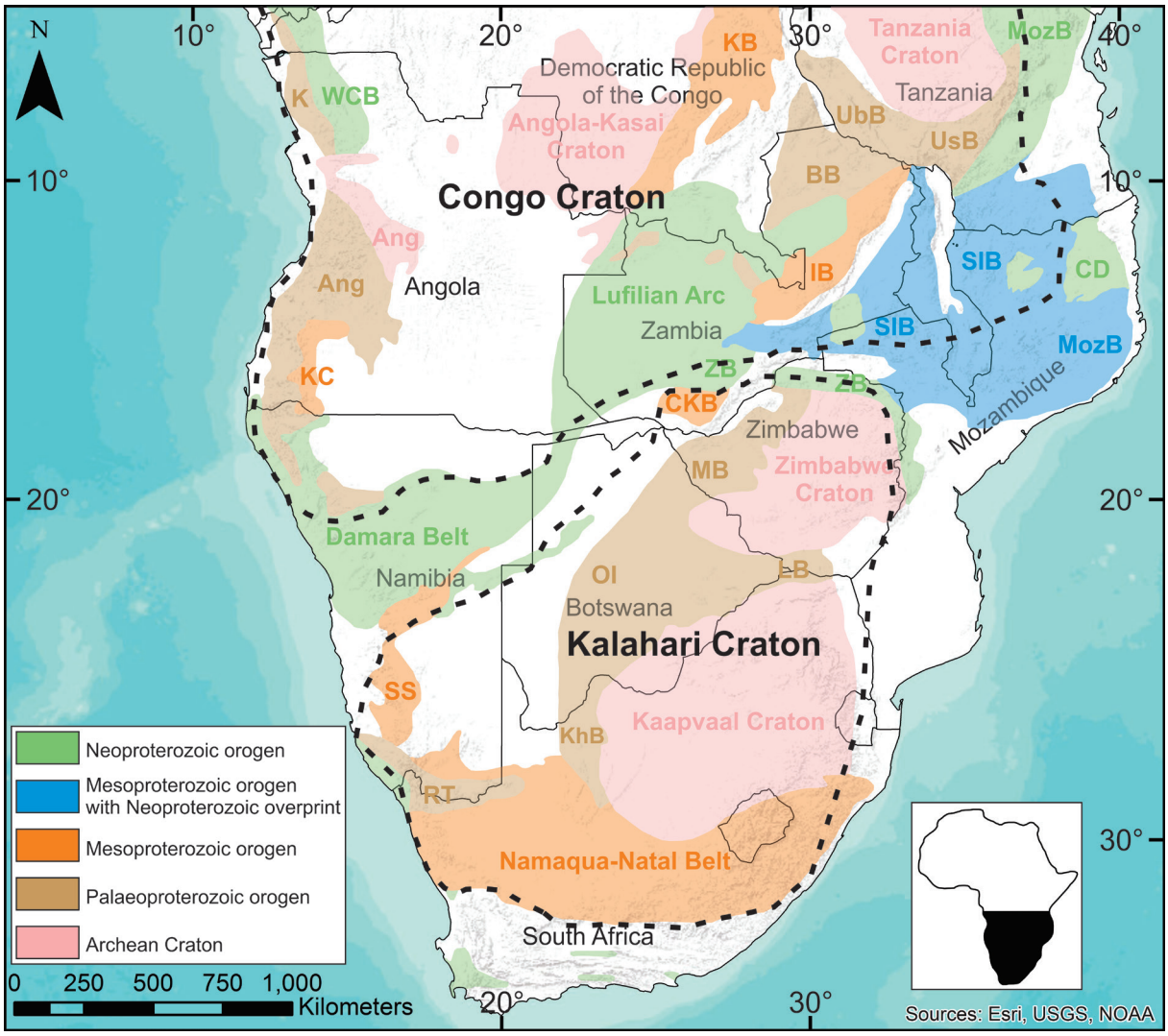

Figure 1. Simplified tectonic map of central Africa adapted from Alessio et al. (2018) following Hanson (2003) and Karmakar and Schenk (2016). The extent of the Congo and Kalahari cratons are denoted by the black dashed lines. Abbreviations: ANG, Angola Block; BB, Bangweulu Block; CKB, Choma-Kalomo Block; CD, Cabo Delgado Nappe Complex; IB, Irumide Belt; K, Kimezian; KB, Kibaran Belt; KC, Kunene Complex; KhB, Kheis Belt; LB, Limpopo Belt; MB, Magondi Belt; MozB, Mozambique Belt; OI, Okwa Inlier; RT, Richtersveld Terrane; SIB, Southern Irumide Belt; UbB, Ubendian Belt; UsB, Usagaran Belt; WCB, West Congo Belt; ZB, Zambezi Belt.

belt, in addition to the contrasting timing of magmatic and metamorphic events recorded therein (Johnson et al., 2006; Johnson et al., 2007b) and structural discontinuity between the orogens (Sarafian et al., 2018). Forming along the southern margin as a result of the late-Neoproterozoic collision between the Congo and Kalahari cratons were the Neoproterozoic Damara, Lufillian, and Zambezi orogens. These orogens are collectively referred to as the Damara–Lufilian–Zambezi orogen that marks the suture zone between the cratons (Hanson et al., 1994; Hutchins and Reeves, 1980; Johnson et al., 2007a; Kampunzu and Cailteux, 1999; Mazac, 1974).

The various orogens located along, or near, the southern Congo margin provide a record of the evolution of this plate margin from the Proterozoic to present. The Ubendian–Usagaran orogen is interpreted to have been a long lived active margin (*c.* 2050–1800 Ma) along the southern margin of the Tanzanian Craton, before its collision with the Bangweulu Block (Boniface et al., 2012; Collins et al., 2004; Tulibonywa et al., 2015). The geological record preserved in the southern Congo Craton suggests relative tectonic quiescence in this region following the amalgamation of these blocks, lasting until the late-Mesoproterozoic when magmatism and metamorphism are recorded in the Irumide and Southern Irumide belts (De Waele et al., 2006a; Johnson et al., 2006). The Irumide Belt (*sensu stricto*) is suggested to have resided along the southern margin of the Congo Craton, acting as an accretionary orogen that was open to an ocean to the present-day south-east (De Waele et al., 2006b; Johnson et al., 2005). Major orogenesis is suggested to have occurred at *c.* 1020 Ma, during which peak metamorphism and widespread granitic magmatism took place. These interpretations suggest that the Southern Irumide Belt (SIB) formed separately to the Irumide Belt (*sensu strictio*), with Johnson et al. (2007b) interpreting that the continental-margin-arc terranes found within this belt formed on a micro-continent during the late-Mesoproterozoic (*c.* 1095–1040 Ma). The magmatism recorded in the SIB is suggested to have ceased upon collision with the southern Congo margin, which initiated the magmatism and metamorphism recorded in the Irumide Belt (Johnson et al., 2007b; Karmakar and Schenk, 2016). Alternatively, Bingen et al. (2009) offer the competing hypothesis that the SIB could have instead acted as the long-lived active margin of the southern Congo Craton prior to these orogenic events, with any discrepancy in the timing of magmatism and metamorphism relating to foreland propagation between *c.* 1020–1005 Ma. Elucidating the true relationship between the SIB and southern Congo margin during the Mesoproterozoic is hampered by the pervasive Neoproterozoic overprint recorded in the SIB, which formed as a result of collision between the Congo and Kalahari cratons during the late stages of Gondwana amalgamation (Johnson et al., 2006). This collision resulted in the suturing of the cratons, which is marked by the Damara–Lufilian–Zambezi origin that runs throughout central Africa (Fig. 1). Following collision, the Congo and Kalahari cratons have remained sutured throughout the Phanerozoic, though large sections of this relict margin have been reactivated during this period and nearby regions record a number of low-temperature thermal events. Permian–Triassic 'Karoo' basins can be found along the Congo–Kalahari cratons and throughout central Africa (Catuneanu et al., 2005), and multiple low-temperature thermal events are recorded throughout this region during the Phanerozoic (e.g. Hurai et al., 2017; Kasanzu et al., 2016; Mackintosh et al., 2017).

This thesis largely investigates the tectonic evolution of the Southern Irumide Belt, which serves as a vital proxy for understanding the plate margin evolution of the southern Congo Craton. The SIB spans a wide portion of the Congo Craton's southern margin, and is defined as a series of terranes extending from southern Zambia to Malawi, Mozambique and

Tanzania (Bingen et al., 2009; Hauzenberger et al., 2014; Johnson et al., 2006; Thomas et al., 2014; Westerhof et al., 2008) that provide a geological record spanning from *c.* 2000 Ma to present. The rocks within this belt can be used to determine the extent of the Congo margin prior to the late-Mesoproterozoic, and whether the SIB represents part of an accreted microcontinent or long lived active margin. The belt preserves sediments and volcanics that formed throughout the Neoproterozoic and can be used to test hypotheses regarding the tectonic geography of the Congo Craton during this time (Merdith et al., 2017). The pervasive tectono-metamorphic overprint recorded throughout the SIB provides a complementary record to that of the Damara–Lufilian–Zambezi orogen, and can be used to understand and constrain the Gondwana forming collision between the Congo and Kalahari cratons. Furthermore, the SIB has a near unconstrained Phanerozoic thermal history, while being located adjacent to regions that record thermal overprints relating to key tectonic events occurring throughout central Africa, including Karoo rift basin formation, Gondwana breakup, and the development of the East African Rift System (Fernandes et al., 2015; Hurai et al., 2017; Kasanzu, 2017; Kasanzu et al., 2016; Mackintosh et al., 2017). As such, understanding the evolution of this belt has the potential to radically improve our understanding of the evolution of the Congo Craton through a vast portion of Earth history.

In Zambia, the SIB is comprised of four structurally imbricated terranes (Johnson et al., 2006) that from west to east are referred to as: Chewore–Rufunsa, Kacholola, Nyimba–Sinda and Chipata terranes (Fig. 2). These terranes are predominantly comprised of late-Mesoproterozoic intrusions that formed on a Palaeoproterozoic basement (Johnson et al., 2006; Johnson et al., 2007b). The Nyimba–Sinda terrane is the only exception, instead being largely comprised of Neoproterozoic gneiss and post-tectonic Cambrian granite. Importantly, each terrane in the belt records a pervasive Neoproterozoic overprint relating to Congo–Kalahari collision (Johns et al., 1989; Keppie, 1977), distinguishing these terranes from the Irumide Belt (sensu stricto; Johnson et al., 2005). Subsequent work in northern Mozambique identified similar terranes that were likely to be extensions of the SIB. Adjacent to the Zambian terranes, in north-west Mozambique, Westerhof et al. (2008) identified Mesoproterozoic terranes with Neoproterozoic structural overprints and Neoproterozoic–Cambrian post-tectonic granite intrusions that they considered to be a southern extension of the belt. In north-east Mozambique, Bingen et al. (2009) identified the Unango and Marrupa complexes, which are similarly comprised of Mesoproterozoic orthogneiss and record a Neoproterozoic overprint. Subsequent work in southern Tanzania identified that the Marrupa Complex likely extended into this region (Hauzenberger et al., 2014; Thomas et al., 2016). Based on the similar characteristics recorded in this region and southern Zambia, these complexes were interpreted as an extension of the SIB (Bingen et al., 2009; Hauzenberger et al., 2014; Thomas et al., 2016), implying that the belt continues through a large section of Malawi (Huang, 2017).

While a number of studies have produced preliminary results and tentative correlations between units within the SIB, significant work remains in understanding and constraining the multiple proxies of the belt's formation and evolution. Initial εNd(t) isotopic data from the Chewore–Rufunsa terrane of the SIB yielded largely evolved values, leading Johnson et al. (2007b) to suggest that the belt formed as a late-Mesoproterozoic continental-margin-arc. On the opposite extent of the belt, Thomas et al. (2016) obtained evolved εHf(t) values for an orthogneiss, supporting the interpretation that the whole belt could have formed in a continental-margin-arc environment. The detrital record of the Zambian terranes remains largely enigmatic, though zircon age

populations of *c.* 2700, 2500, 2100, 1900, 1300 and 1200 Ma have been obtained from north-west Mozambique (Westerhof et al., 2008). Similar detrital ages have been obtained from north-east Mozambique and southern Tanzania, with the Unango and Marrupa complexes yielding detrital age populations of 2700, 2000 and 1100–1000 Ma (Bingen et al., 2009; Thomas et al., 2016). Recent work by Karmakar and Schenk (2016) provides pressure–temperature (*P–T*) information for late-Mesoproterozoic granulite facies metamorphism from the SIB, suggesting that rocks in the Chipata Terrane reached peak conditions of ~5–6 kbar and 900–1000 °C. *P–T* estimates relating to Congo–Kalahari collision are available from the southern margin of the Chewore–Rufunsa terrane, where whiteschists, high pressure metamorphic rocks largely composed of talc and kyanite (Schreyer, 1974), were estimated to record conditions of 12–14 kbar and 725–775 °C (John et al., 2004). These estimates are consistent with nearby whiteschists from the Zambezi Belt, which record coeval peak *P–T* conditions of ~13–21 kbar and 590–650 °C (Johnson and Oliver, 1998). Proximal to these rocks are metapelites that similarly formed from Congo–Kalahari collision and record peak conditions of ~7–9 kbar and 590–720 °C (Goscombe et al., 2000).

The preliminary work done on the SIB suggests it to be an important region for constraining the tectonic geography of the Congo Craton throughout a significant portion of Earth history, though significant work remains for understanding the belt's evolution. As such, the SIB provides an unutilised opportunity to better understand this region's palaeogeography, which can ultimately improve our understanding of the greater Earth system.

THESIS OUTLINE

The aim of this thesis is to develop a framework of understanding for the plate margin evolution of the southern Congo Craton from the Proterozoic to present. This is primarily done through constraining the evolution of the Southern Irumide Belt, which is found along this margin and provides an extensive geological record that can be used to interrogate the questions that surround the evolution of this region. This thesis has been written as a series of individual manuscripts that use an array of methodologies to explore both different aspects and periods of evolution within the Southern Irumide Belt, and by extension the southern Congo margin.

Chapter 2

Chapter 2 is published (online accepted manuscript) in Geoscience Frontiers as: Alessio, B.L.; Collins, A.S.; Siegfried, P.; Glorie, S.; De Waele, B.; Payne J.L.; Archibald, D. 2018 (In press). Neoproterozoic tectonic geography of the south-east Congo Craton in Zambia as deduced from the age and composition of detrital zircons. doi.org/10.1016/j.gsf.2018.07.005.

This chapter constrains the age of metasedimentary sequences throughout the Zambian Southern Irumide Belt. Using these ages, this study aims to establish depositional correlations between the sediments here and elsewhere in central Africa (and further afield) that are used to interrogate the Mesoproterozoic–Neoproterozoic palaeogeographic development of the southern Congo Craton margin. Additionally, these correlations are used to test the pre-existing hypothesis that the Southern Irumide Belt formed on a microcontinent, prior to colliding with and accreting to the southern Congo margin (e.g. Johnson et al., 2007a; Johnson et al., 2006).

Chapter 3

Chapter 3 is published (online accepted manuscript) in the Journal of the Geological Society as: Alessio, B.L.; Collins A.S.; Clark, C.; Glorie, S.; Siegfried, P.; Taylor, R. 2019 (In press). Age, origin and tectonic geography of the Southern Irumide Belt, Zambia. doi.org/10.1144/jgs2018-174.

This chapter provides zircon U–Pb and Lu–Hf isotopic, as well as REE data for igneous and meta-igneous lithologies from terranes throughout the Zambian terranes of the Southern Irumide Belt. The aim of this study is to test whether the belt represents a continental-margin-arc that collided with the southern Congo margin in the late-Mesoproterozoic (Johnson et al., 2007a), or alternatively, if it formed along this margin prior to the late-Mesoproterozoic (Bingen et al. 2009). Supplementing this is a structural investigation of the belt, which aims to constrain the different phases of deformation within the region. The multiple components of this study serve to produce a comprehensive overview of the Zambian portion of the belt, which details its origin and development from the Palaeoproterozoic to Neoproterozoic.

Chapter 4

Chapter 4 is published in the Journal of Metamorphic Geology as: Alessio, B.L.; Kelsey, D.K. 2018. On yoderite: Using calculated phase equilibria to investigate its rarity in the geological record of whiteschists. Journal of Metamorphic Geology 36(3) 297–314. doi.org/10.1111/jmg.12293.

The southern margin of the Congo Craton is intensely deformed as a result of its collision with the Kalahari craton in the final stages of Gondwana amalgamation. Found along this margin as a result of this collision are whiteschists, chemically simple rocks that are suggested to relate to exotic, highly oxidising, deep crustal metasomatism and continental subduction. The southern Congo margin contains the largest exposure of these rocks, therefore, being able to use them in tectono-metamorphic research would provide unique insights to the development of a key Gondwana forming suture-zone. This study provides an activity-composition (*a*–*x*) model for the mineral yoderite, for use with the pressure–temperature modelling software *THERMOCALC*. Yoderite is a key mineral that can form within the MgO, Al_2O_3, SiO_2, H_2O, Fe_2O_3 (MASHO) chemical system that whiteschists are restricted to. The provision of this *a*–*x* file allows for far more rigorous constraints of all whiteschists, including the majority of whiteschists that do not contain the mineral, as it restricts the *P*–*T* stability of the other mineral assemblages found in these rocks. This model is validated by calculating the *P*–*T* stability of various mineral reactions in the MASHO system and comparing them to experimentally derived results. Finally, the utility of the model in tectono-metamorphic research is shown by calculating a *P*–*T* model for a whiteschist of the Zambezi Belt, which also contributes to our understanding of the style and nature of metamorphism experienced during Congo–Kalahari collision.

Chapter 5

Chapter 5 is prepared in manuscript format for submission to Gondwana Research as: Alessio, B.L.; Collins, A.S.; Kelsey, D.E.; Clark, C.; Glorie, S.; Taylor, R. Identifying the tectono-metamorphic overprints of a Gondwana forming collision: a structural and thermobarometric investigation of the Southern Irumide and Zambezi belts, Zambia.

This study aims to constrain the style and nature of the tectono-metamorphic overprints recorded throughout the Southern Irumide and Zambezi belt, which relate to collision between the Congo and Kalahari cratons during Gondwana amalgamation. *P*–*T* modelling (utilising the *a*–*x* model constructed in the previous chapter) is used to investigate the conditions recorded by the more typical amphibolite facies rocks found throughout the region, as well as those recorded by retrogressed whiteschists that are restricted to the southernmost portion of the Southern Irumide Belt and further south, in the Zambezi belt of Zimbabwe. Peak metamorphism is related to deformation observed in the region with an

accompanying structural investigation of the region. This study highlights and discusses the development of distinctly different tectono–metamorphic overprints as a result of a single collisional event, and serve to elucidate the development of a major collisional zone at the heart of Gondwana amalgamation.

Chapter 6

Chapter 6 has been submitted for publication in Tectonophysics as: Alessio, B.L.; Collins, A.S.; Glorie, S.; Jepson, G.; Nixon, A.; Clark, C.; Jourdan, F. The tectono-thermal evolution of central Africa as determined from apatite and muscovite thermochronology. The manuscript forming this chapter is partially revised following favourable reviews.

This study applies high- and low-temperature thermochronology to samples throughout southern Zambia, with the aim of constraining the post-collisional thermal evolution of the region throughout the Phanerozoic. U–Pb apatite and ^{40}Ar–^{39}Ar muscovite thermochronological data are used to constrain the timing of cooling after Congo–Kalahari collision, while apatite fission track data are used to constrain subsequent thermal activity including burial and exhumation. The findings of this study are used to discuss the thermal evolution of central Africa in relation to Neoproterozoic orogenesis, Karoo rifting, Gondwana break-up and the development of the East African Rift System.

Chapter 7

The final chapter summarises for the various findings of this study, providing a holistic explanation of how the southern margin of the Congo Craton developed, largely in reference to the development of the Southern Irumide Belt along this margin. This chapter first summarises the Mesoproterozoic to Neoproterozoic evolution of the Congo Craton's southern margin, which culminated with Congo–Kalahari collision during Gondwana amalgamation. It then outlines the subsequent thermal evolution of central Africa, discussing cooling of the region after Gondwana amalgamation and tectonic events occurring thereafter.

REFERENCES

Barley, M., Groves, D., 1992. Supercontinent cycles and the distribution of metal deposits through time. Geology 20, 291-294.

Bingen, B., Jacobs, J., Viola, G., Henderson, I., Skår, Ø., Boyd, R., Thomas, R., Solli, A., Key, R., Daudi, E., 2009. Geochronology of the Precambrian crust in the Mozambique belt in NE Mozambique, and implications for Gondwana assembly. Precambrian Research 170, 231-255.

Boniface, N., Schenk, V., Appel, P., 2012. Paleoproterozoic eclogites of MORB-type chemistry and three Proterozoic orogenic cycles in the Ubendian Belt (Tanzania): Evidence from monazite and zircon geochronology, and geochemistry. Precambrian Research 192, 16-33.

Catuneanu, O., Wopfner, H., Eriksson, P.G., Cairncross, B., Rubidge, B.S., Smith, R.M.H., Hancox, P.J., 2005. The Karoo basins of south-central Africa. Journal of African Earth Sciences 43, 211-253.

Collins, A.S., Pisarevsky, S.A., 2005. Amalgamating eastern Gondwana: the evolution of the Circum-Indian Orogens. Earth-Science Reviews 71, 229-270.

Collins, A.S., Reddy, S.M., Buchan, C., Mruma, A., 2004. Temporal constraints on Palaeoproterozoic eclogite formation and exhumation (Usagaran Orogen, Tanzania). Earth and Planetary Science Letters 224, 175-192.

De Waele, B., Johnson, S.P., Pisarevsky, S.A., 2008. Palaeoproterozoic to Neoproterozoic growth and evolution of the eastern Congo Craton: Its role in the Rodinia puzzle. Precambrian Research 160, 127-141.

De Waele, B., Kampunzu, A.B., Mapani, B.S.E., Tembo, F., 2006a. The Mesoproterozoic Irumide belt of Zambia. Journal of African

Earth Sciences 46, 36-70.

De Waele, B., Liégeois, J.-P., Nemchin, A.A., Tembo, F., 2006b. Isotopic and geochemical evidence of proterozoic episodic crustal reworking within the irumide belt of south-central Africa, the southern metacratonic boundary of an Archaean Bangweulu Craton. Precambrian Research 148, 225-256.

Fernandes, P., Cogné, N., Chew, D.M., Rodrigues, B., Jorge, R.C., Marques, J., Jamal, D., Vasconcelos, L., 2015. The thermal history of the Karoo Moatize-Minjova Basin, Tete Province, Mozambique: An integrated vitrinite reflectance and apatite fission track thermochronology study. Journal of African Earth Sciences 112, 55-72.

Goscombe, B., Armstrong, R., Barton, J., 2000. Geology of the Chewore Inliers, Zimbabwe: constraining the Mesoproterozoic to Palaeozoic evolution of the Zambezi Belt. Journal of African Earth Sciences 30, 589-627.

Halverson, G.P., Hurtgen, M.T., Porter, S.M., Collins, A.S., 2009. Neoproterozoic-Cambrian biogeochemical evolution. Developments in Precambrian geology 16, 351-365.

Hanson, R.E., Wilson, T.J., Munyanyiwa, H., 1994. Geologic evolution of the Neoproterozoic Zambezi orogenic belt in Zambia. Journal of African Earth Sciences 18, 135-150.

Hauzenberger, C., Tenczer, V., Bauernhofer, A., Fritz, H., Klötzli, U., Košler, J., Wallbrecher, E., Muhongo, S., 2014. Termination of the Southern Irumide Belt in Tanzania: Zircon U/Pb geochronology. Precambrian Research 255, 144-162.

Hoffman, P.F., Kaufman, A.J., Halverson, G.P., Schrag, D.P., 1998. A Neoproterozoic snowball earth. Science 281, 1342-1346.

Huang, L., 2017. Pre-rift evolution of Malawian high-grade basement rocks. University of Cape Town.

Hurai, V., Paquette, J.-L., Huraiová, M., Slobodník, M., Hvožďara, P., Siegfried, P., Gajdošová, M., Milovská, S., 2017. New insights into the origin of the Evate apatite-iron oxide-carbonate deposit, Northeastern Mozambique, constrained by mineralogy, textures, thermochronometry, and fluid inclusions. Ore Geology Reviews 80, 1072-1091.

Hutchins, D., Reeves, C., 1980. Regional geophysical exploration of the Kalahari in Botswana. Tectonophysics 69, 201-220.

John, T., Schenk, V., Mezger, K., Tembo, F., 2004. Timing and PT evolution of whiteschist metamorphism in the Lufilian Arc–Zambezi Belt orogen (Zambia): implications for the assembly of Gondwana. The Journal of geology 112, 71-90.

Johns, C.C., Liyungu, K., Mabuku, S., Mwale, G., Sakungo, F., Tembo, D., Vallance, G., Barr, M.W.C., 1989. The stratigraphic and structural framework of Eastern Zambia: results of a geotraverse. Journal of African Earth Sciences (and the Middle East) 9, 123-136.

Johnson, S., De Waele, B., Evans, D., Banda, W., Tembo, F., Milton, J., Tani, K., 2007a. Geochronology of the Zambezi Supracrustal sequence, southern Zambia: a record of Neoproterozoic divergent processes along the southern margin of the Congo Craton. The Journal of geology 115, 355-374.

Johnson, S., De Waele, B., Liyungu, A., 2006. U-Pb SHRIMP geochronology of granitoid rocks in eastern Zambia: terrane subdivision of the Mesoproterozoic Southern Irumide Belt. Tectonics 25.

Johnson, S., Oliver, G., 1998. A second natural occurrence of yoderite. Journal of Metamorphic Geology 16, 809-818.

Johnson, S.P., De Waele, B., Tembo, F., Katongo, C., Tani, K., Chang, Q., Iizuka, T., Dunkley, D., 2007b. Geochemistry, geochronology and isotopic evolution of the Chewore–Rufunsa Terrane, Southern Irumide Belt: a Mesoproterozoic continental margin arc. Journal of Petrology 48, 1411-1441.

Johnson, S.P., Rivers, T., De Waele, B., 2005. A review of the Mesoproterozoic to early Palaeozoic magmatic and tectonothermal his-

tory of south–central Africa: implications for Rodinia and Gondwana. Journal of the Geological Society 162, 433-450.

Kampunzu, A., Cailteux, J., 1999. Tectonic evolution of the lufilian arc (Central Africa Copper Belt) during Neoproterozoic pan African orogenesis. Gondwana Research 2, 401-421.

Karmakar, S., Schenk, V., 2016. Mesoproterozoic UHT metamorphism in the Southern Irumide Belt, Chipata, Zambia: Petrology and in situ monazite dating. Precambrian Research 275, 332-356.

Kasanzu, C.H., 2017. Apatite fission track and (U-Th)/He thermochronology from the Archean Tanzania Craton: Contributions to cooling histories of Tanzanian basement rocks. Geoscience Frontiers 8, 999-1007.

Kasanzu, C.H., Linol, B., Wit, M.J., Brown, R., Persano, C., Stuart, F.M., 2016. From source to sink in central Gondwana: Exhumation of the Precambrian basement rocks of Tanzania and sediment accumulation in the adjacent Congo basin. Tectonics 35, 2034-2051.

Keppie, J.D., 1977. The geology of the Bulonga Hills area: explanation of degree sheet 1430, SE quarter., In: Zambia, G.S. (Ed.).

Kröner, A., Cordani, U., 2003. African, southern Indian and South American cratons were not part of the Rodinia supercontinent: evidence from field relationships and geochronology. Tectonophysics 375, 325-352.

Mackintosh, V., Kohn, B., Gleadow, A., Tian, Y., 2017. Phanerozoic Morphotectonic Evolution of the Zimbabwe Craton: Unexpected Outcomes From a Multiple Low-Temperature Thermochronology Study. Tectonics 36, 2044-2067.

Mazac, O., 1974. Reconnaissance gravity survey of Zambia. Republic of Zambia, Ministry of Mines and Industry.

Merdith, A.S., Collins, A.S., Williams, S.E., Pisarevsky, S., Foden, J.F., Archibald, D., Blades, M.L., Alessio, B.L., Armistead, S., Plavsa, D., Clark, C., Müller, R.D., 2017. A full-plate global reconstruction of the Neoproterozoic. Gondwana Research 50, 84-134.

Merdith, A. S., Williams, S. E., Brune, S., Collins A. S., Müller, R.D., 2019. Rift and plate boundary evolution across two supercontinent cycles. Global and Planetary Change 173, 1-14.

Sarafian, E., Evans, R.L., Abdelsalam, M.G., Atekwana, E., Elsenbeck, J., Jones, A.G., Chikambwe, E., 2018. Imaging Precambrian lithospheric structure in Zambia using electromagnetic methods. Gondwana Research 54, 38-49.

Schreyer, W., 1974. Whiteschist, a new type of metamorphic rock formed at high pressures. Geologische Rundschau 63, 597-609.

Tackley, P.J., 2000. Mantle convection and plate tectonics: Toward an integrated physical and chemical theory. Science 288, 2002-2007.

Thomas, R.J., Bushi, A.M., Roberts, N.M., Jacobs, J., 2014. Geochronology of granitic rocks from the Ruangwa region, southern Tanzania–Links with NE Mozambique and beyond. Journal of African Earth Sciences 100, 70-80.

Thomas, R.J., Spencer, C., Bushi, A.M., Baglow, N., Boniface, N., de Kock, G., Horstwood, M.S., Hollick, L., Jacobs, J., Kajara, S., 2016. Geochronology of the central Tanzania Craton and its southern and eastern orogenic margins. Precambrian Research 277, 47-67.

Tulibonywa, T., Manya, S., Maboko, M.A., 2015. Palaeoproterozoic volcanism and granitic magmatism in the Ngualla area of the Ubendian Belt, SW Tanzania: Constraints from SHRIMP U–Pb zircon ages, and Sm–Nd isotope systematics. Precambrian Research 256, 120-130.

Westerhof, A.P., Lehtonen, M.I., Mäkitie, H., Manninen, T., Pekkala, Y., Gustafsson, B., Tahon, A., 2008. The Tete-Chipata Belt: A new multiple terrane element from western

Mozambique and southern Zambia. Geological Survey of Finland Special Paper 48, 145-166.

CHAPTER 2

This chapter has been publised in *Geoscience Frontiers* as:
Alessio, B.L.; Collins, A.S.; Siegfried, P.; Glorie, S.; De Waele, B.; Payne J.L.; Archibald, D. 2018. Neoproterozoic tectonic geography of the south-east Congo Craton in Zambia as deduced from the age and composition of detrital zircons.

Statement of Authorship

Title of Paper	Neoproterozoic tectonic geography of the south-east Congo Craton in Zambia as deduced from the age and composition of detrital zircons
Publication Status	☑ Published ☐ Accepted for Publication ☐ Submitted for Publication ☐ Unpublished and Unsubmitted w ork w ritten in manuscript style
Publication Details	Alessio, Brandon L, Collins, Alan S, Siegfried, Peter , Glorie, Stijn , De Waele, Bert, Payne, Justin L , & Archibald, Donnelly (2018). Neoproterozoic tectonic geography of the south-east Congo Craton in Zambia as deduced from the age and composition of detrital zircons. Geoscience Frontiers. doi: https://doi.org/10.1016/j.gsf.2018.07.005

Principal Author

Name of Principal Author (Candidate)	Brandon Luke Alessio		
Contribution to the Paper	Sample preparation, data collection, processing and interpretation, manuscript design and composition, drafting of figures.		
Overall percentage (%)	80		
Certification:	This paper reports on original research I conducted during the period of my Higher Degree by Research candidature and is not subject to any obligations or contractual agreements with a third party that would constrain its inclusion in this thesis. I am the primary author of this paper.		
Signature		Date	07/01/19

Co-Author Contributions

By signing the Statement of Authorship, each author certifies that:

i. the candidate's stated contribution to the publication is accurate (as detailed above);
ii. permission is granted for the candidate in include the publication in the thesis; and
iii. the sum of all co-author contributions is equal to 100% less the candidate's stated contribution.

Name of Co-Author	Alan Collins		
Contribution to the Paper	Fieldwork, guidance in data interpretation and manuscript review.		
Signature		Date	14/01/19

Name of Co-Author	Pete Siegfried		
Contribution to the Paper	Fieldwork, guidance in data interpretation and manuscript review. Fieldwork was based on localities this author had been involved with previously and formed the collected material source.		
Signature		Date	16/01/19

Name of Co-Author	Stijn Glorie		
Contribution to the Paper	Fieldwork, guidance in data interpretation and manuscript review.		
Signature		Date	08/01/19

Name of Co-Author	Bert De Waele		
Contribution to the Paper	Fieldwork, manuscript review.		
Signature	On behalf of Bert De Waele – Agreed via email	Date	07/01/19

Name of Co-Author	Justin Payne		
Contribution to the Paper	Guidance in data collection, interpretation and manuscript review.		
Signature		Date	08/01/19

Name of Co-Author	Donnelly Archibald		
Contribution to the Paper	Collection of data and manuscript review.		
Signature		Date	10/01/19

ABSTRACT

The Southern Irumide Belt (SIB) is an orogenic belt consisting of a number of lithologically varied Mesoproterozoic and Neoproterozoic terranes that were thrust upon each other. The belt lies along the southwest margin of the Archaean to Proterozoic Congo Craton, and bears a Neoproterozoic tectono-thermal overprint relating to the Neoproterozoic–Cambrian collision between the Congo and Kalahari cratons. It preserves a record of about 500 million years of plate interaction along this part of the Congo margin. Detrital zircon samples from the SIB were analysed for U–Pb and Lu–Hf isotopes, as well as trace element compositions. These data are used to constrain sediment-source relationships between SIB terranes and other Gondwanan terranes such as the local Congo Craton and Irumide belt and wider afield to Madagascar (Azania) and India. These correlations are then used to interpret the Mesoproterozoic to Neoproterozoic affinity of the rocks and evolution of the region. Detrital zircon samples from the Chewore–Rufunsa and Kacholola (previously referred to as Luangwa–Nyimba) terranes of the SIB yield zircon U–Pb age populations and evolved εHf(t) values that are similar to the Muva Supergroup found throughout eastern Zambia, primarily correlating with Ubendian–Usagaran (*c.* 2.05–1.80 Ga) phase magmatism and a cryptic basement terrane that has been suggested to underlie the Bangweulu Block and Irumide Belt. These data suggest that the SIB was depositionally connected to the Congo Craton throughout the Mesoproterozoic. The more eastern Nyimba–Sinda terrane of the SIB (previously referred to as Petauke–Sinda terrane) records detrital zircon ages and εHf(t) values that correlate with *c.* 1.1–1.0 Ga magmatism exposed elsewhere in the SIB and Irumide Belt. We ascribe this difference in age populations to the polyphase development of the province, where the sedimentary and volcanic rocks of the Nyimba–Sinda terrane accumulated in extensional basins that developed in the Neoproterozoic. Such deposition would have occurred following late-Mesoproterozoic magmatism that is widespread throughout both the Irumide and Southern Irumide Belts, presently considered to have occurred in response to collision between a possible microcontinental mass and the Irumide Belt. This interpretation implies a multi-staged evolution of the ocean south of the Congo Craton during the mid-Mesoproterozoic to late-Neoproterozoic, which ultimately closed during collision between the Congo and Kalahari cratons.

INTRODUCTION

The southern margin of the Palaeoproterozoic/Archaean Congo Craton is traced from the Namibian Central Damara Belt, to the Lufillian Arc and Zambezi Belt of Zambia, Zimbabwe, Malawi and Mozambique (e.g. Collins and Pisarevsky, 2005; De Waele et al., 2008; Merdith et al., 2017). Collectively, these features are referred to the Damara–Lufilian–Zambezi orogen (Fig. 1). The orogen is of considerable significance as it contains the evidence of the tectonic geography of the Congo Craton through half a billion years of Earth history: from its role in Rodinia, including whether it was a part of Rodinia or not (De Waele et al., 2008; Kröner and Cordani, 2003), to its relationship with the Kalahari continent that is located to its present-day south. One curious feature of this orogen is that the geology of the central Damara region suggests relative tectonic quiescence during much of the Tonian Period, with rifting occurring on the southern Congo Craton at *c.* 760 Ma (McGee et al., 2012). In contrast, the Tonian was a time of volcanic arc magmatism and terrane accretion for the Zambezi Belt region and parts of Mozambique (Bingen et al., 2009a; Johnson et al., 2005). Understanding this contrasting tectonic geography, apparently along orogenic strike, is required to understand the plate margin evolution of this region, a major step towards understanding the plate evolution record of Neoproterozoic central Gondwana (see Merdith et al., 2017).

The Southern Irumide Belt (SIB; Johnson et al., 2006) is a broadly ENE–WSW trending orogenic belt consisting of late Mesoproterozoic and Neoproterozoic metasedimentary and metaigneous rocks. The SIB is located between the Congo and Zimbabwe cratons (the northern part of the Neoproterozoic Kalahari Craton; Fig. 1) and has a Neoproterozoic structural overprint related to Gondwana amalgamation (De Waele et al., 2008; Johnson et al., 2005). In Zambia, the SIB has been the subject of relatively few studies leaving many questions unanswered regarding its origin and tectonic evolution. Late-Mesoproterozoic suprasubduction zone arc magmatism identified in the western-most Chewore–Rufunsa terrane, in conjunction with similar magmatism observed in Malawi and Mozambique (Bingen et al., 2009b), implies the existence of an ocean to the south of the Congo Craton at this time (Begg et al., 2009; Johnson et al., 2007b). However, the evolution of such an ocean is poorly constrained at present. Furthermore, the southern and eastern margins of the Congo Craton were suggested as the source region for the abundant Palaeoproterozoic detrital zircons found in parts of central Madagascar and the Southern Granulite Terrane of India linking these regions to the Congo Craton in the Mesoproterozoic (Archibald et al., 2015; Cox et al., 1998; Cox et al., 2004; Fitzsimons et al., 2004; Plavsa et al., 2014). These relationships were the basis for proposing this region as a separate Neoproterozoic continent named Azania (Collins and Pisarevsky, 2005; Collins and Windley, 2002). However, the correlation was made based on the sparse data available at the time and has not been sufficiently tested, especially using other detrital fingerprints, such as zircon trace element and/or Lu–Hf isotopic compositions.

This study presents detrital zircon laser ablation inductively coupled plasma mass spectrometry (LA–ICP–MS) U–Pb isotope and trace element data in conjunction with multicollector LA–ICP–MS (LA–MC–ICP–MS) Lu–Hf isotope data from the SIB in Zambia. These data are used to constrain both the depositional ages of protoliths and isotopic nature of zircon sources for metasedimentary lithologies found within the three western-most terranes (Chewore–Rufunsa, Kacholola, and Nyimba–Sinda) of the SIB. These data are compared to neighbouring terranes to suggest correlations between major metasedimentary sequences in the SIB, elsewhere in Africa and even further afield in Madagascar and India. These correlations can represent depositional connections, where both basins received input for the same sources, providing palaeogeographic constraints for the southern Congo margin.

REGIONAL GEOLOGY

The eastern Congo Craton

The Congo Craton refers to the amalgamated central African landmass at the time of Gondwana assembly (De Waele et al., 2008), and is comprised of several cratonic blocks. The Bangweulu Block and Tanzanian Craton are located to the eastern side of the Congo Craton (Fig. 1) and are interpreted to have a formed a single continental block from the early Proterozoic onwards, suggested to be marked by the Ubendian–Usagaran orogen. This *c.* 2.05–1.80 Ga orogen is interpreted to have been a long lived active margin that is now located between the two cratons, along the southern margin of the Tanzanian Craton. The Bangweulu Block lies south of the Tanzanian Craton, in northern Zambia. This block is characterised by basement lithologies consisting of schists and coarse to porphyritic granitoids, which are unconformably overlain by fluvial, aeolian and lacustrine sediments of the Paleoproterozoic Muva Supergroup (Daly and Unrug, 1982; De Waele et al., 2006a). De Waele et al. (2006b) suggested that the nucleus of the Bangweulu Block is an Archean craton but contact relationships are obscured by these Palaeoproterozoic sediments. Granitoids in the Bangweulu Block that formed at *c.* 1.85 Ga, are undeformed and have high-K, calc-alkaline ge-

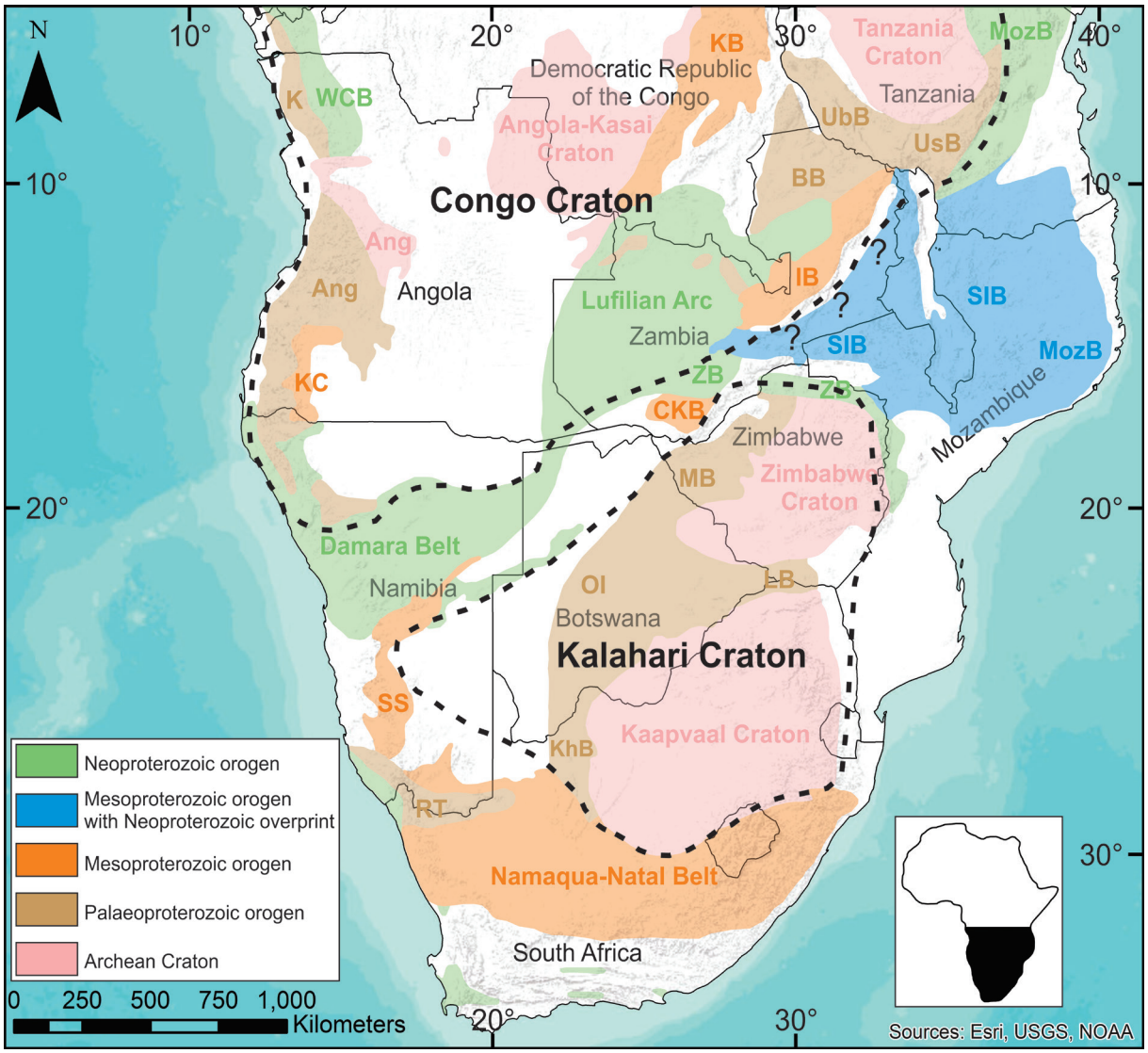

Figure 1. Simplified tectonic map of central Africa adapted from Hanson (2003) and Karmakar and Schenk (2016). The extent of the Congo and Kalahari cratons are denoted by the black dashed lines. Abbreviations: ANG, Angola Block; BB, Bangweulu Block; CKB, Choma-Kalomo Block; IB, Irumide Belt; K, Kimezian; KB, Kibaran Belt; KC, Kunene Complex; KhB, Kheis Belt; LB, Limpopo Belt; MB, Magondi Belt; MozB, Mozambique Belt; OI, Okwa Inlier; RT, Richtersveld Terrane; SIB, Southern Irumide Belt; UbB, Ubendian Belt; UsB, Usagaran Belt; WCB, West Congo Belt; ZB, Zambezi Belt.

ochemical characteristics (Brewer et al., 1979; De Waele et al., 2006b; Schandelmeier, 1980; Schandelmeier, 1983). These were interpreted by Brewer et al. (1979) as shallow intrusions as they are associated with volcanism, which were suggested to represent an active volcanic arc (Daly and Unrug, 1982). De Waele et al. (2006b) noted a lack of evidence for crustal thickening and exhumation in the Bangweulu Block that would be associated with such an arc. De Waele et al. (2006b) additionally noted that the east–west trending schist belts of the Bangweulu Block appear to merge with similar lithologies of the NNW–SSE trending Ubendian Belt at some localities, but are terminated by shear zones in others.

The Irumide Belt

The Irumide Belt sensu stricto (herein referred to as the Irumide Belt) is located to the south of the Bangweulu Block (Fig. 1) and is a NE–SW trending Mesoproterozoic orogenic belt comprised of deformed Palaeoproterozoic granitic basement, folded metasedimentary units and

voluminous granitoid intrusions of *c.* 1.05 to 1.00 Ga age (Daly, 1986; De Waele et al., 2009; De Waele et al., 2006a). The metasedimentary units consist of a succession of quartzites and metapelites and are grouped into the Muva Supergroup, which is interpreted to have been deposited during the Palaeoproterozoic. SHRIMP U–Pb detrital zircon ages from the Muva Supergroup are in the range *c.* 3.2–1.8 Ga with major peaks at *c.* 2.1 and 1.9 Ma. The maximum depositional age is *c.* 1.85 Ga with a minimum depositional age of *c.* 1.6 Ga constrained by granite emplacement in the Irumide Belt (De Waele and Fitzsimons, 2007; De Waele et al., 2003). Peak metamorphism in the Irumide Belt is interpreted to have occurred at *c.* 1020 Ma and is represented by upper-amphibolite facies (7–8 kbar and ~650 °C) mineral assemblages (De Waele, 2004). Peak metamorphism is coincident with large scale structural overprinting along the southern margin of the belt and by the intrusion of primarily calc-alkaline granitoids. The lack of juvenile material present in the Irumide Belt has been used to suggest that the belt acted as a passive margin on the southeast margin of the Congo Craton, and that the active continental margin was further south and is represented by the SIB (De Waele et al., 2006b).

The Southern Irumide Belt

Regional context, extent and correlations

Early work noted deformed Mesoproterozoic rock south of the Irumide Belt, which had been considered as part of the Mozambique Belt and/or Irumide Belt (Johns et al., 1989). The term Southern Irumide Belt was later introduced by Johnson et al. (2005), who consider the belt to be distinct (detailed below) and separate to the Irumide and Mozambique belts. The Southern Irumide Belt remains the focus of ongoing research due to the suggestion that it represents a discrete continental block that was accreted to the Congo crustal assemblage (Begg et al., 2009; De Waele et al., 2008; De Waele et al., 2006b; Johnson et al., 2007b). Lithologies of the SIB crop out in Zambia, Malawi, Mozambique, and Tanzania (Fig. 1). In Zambia, the SIB is located immediately south of the Irumide Belt though any continuity/discontinuity between the SIB and Irumide Belt is obscured by a Permo-Triassic Karoo Graben that forms the Luangwa Valley (Johnson et al., 2006). Aeromagnetic data have been used to interpret that a major shear zone (Mwembeshi Shear Zone) runs between the belts, though this feature is concealed by the graben sediments (Johnson et al., 2006; Sarafian et al., 2018). The Zambian portion of the SIB has been subdivided into four imbricated terranes, from west to east these terranes have been referred to as the Chewore–Rufunsa, Luangwa–Nyimba, Petauke–Sinda, and Chipata terranes (Fig. 2; Johnson et al., 2006; Mapani et al., 2004). Here we partially adopt the nomenclature of these studies, though we instead refer to the Luangwa–Nyimba Terrane as the Kacholola Terrane. This name instead refers to a location within the terrane, as the towns of Luangwa and Nyimba are either on the shear zone boundary or outside the defined area of the terrane. We also refer to the Petauke–Sinda Terrane instead as the Nyinba–Sinda Terrane, which better encompasses the extent of fault-bounded Neoproterozoic lithologies comprising this terrane. In the Tete Province of northwest Mozambique, the SIB has been subdivided into a series of terranes with supracrustal sequences that display little cohesion and granitoids with ages ranging from *c.* 1.2 to 1.05 Ga (Westerhof et al., 2008). The sediments in these terranes display detrital zircon age populations of *c.* 2.7, 2.5, 2.1, 1.9, 1.3 and 1.2 Ga (Westerhof et al., 2008, and references therein). In northeast Mozambique a number of Palaeoproterozoic to Mesoproterozoic complexes that record variable degrees of late-Neoproterozoic metamorphism have been identified (Bingen et al., 2009a; Boyd et al., 2010). The Mesoproterozoic Unango and Marrupa complexes identified in this region primarily consist of *c.* 1.1 to 1 Ga orthog-

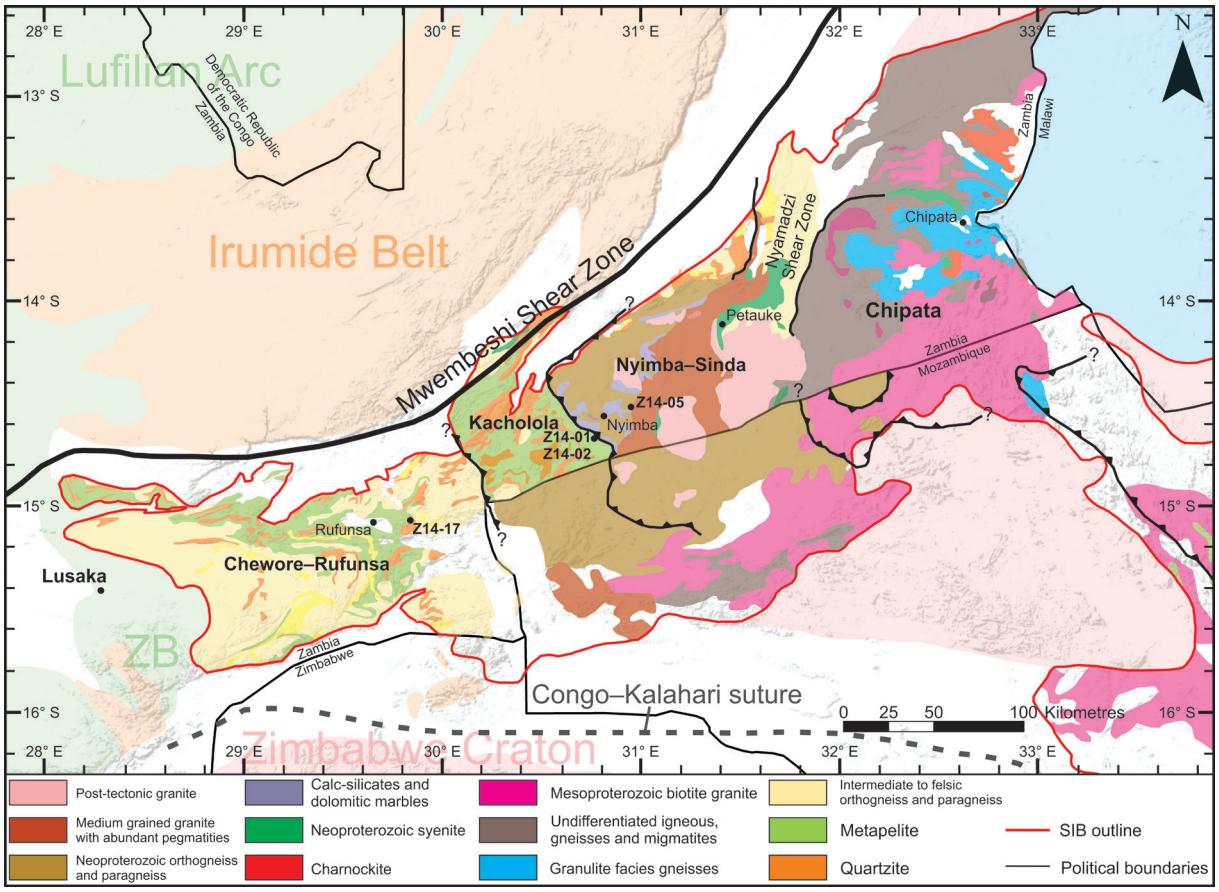

Figure 2. Simplified tectonic map of eastern Zambia adapted from Johnson et al. (2006), with geological units distinguished for the SIB in Zambia and Mozambique. Lithological data for Zambia is adapted from the Geological Survey of Zambia (Agar, 1984; Ray, 1984; Vayrda, 1984) and Johnson et al. (2006). Lithological data for Mozambique is adapted from Westerhof et al. (2008) Shading for Malawi and tectonic units outside of the SIB and Malawi follow the legend in Figure 1.

neiss, and are interpreted to have formed on the Congo margin with the SIB, possibly representing an eastern continuation of the belt. Neoproterozoic granitoids in southern Tanzania have been linked with these rocks in Mozambique, and possibly represent a continuation of the Marrupa Complex (Hauzenberger et al., 2014; Thomas et al., 2014). Later work identified rocks bearing *c.* 1.0 Ga overprints in southern Tanzania, additionally observing an orthogneiss that yields a crystallisation age of *c.* 1.1 Ga. This work also analysed a sample of quartzite in a metasedimentary sequence with marble, which was shown to contain predominantly *c.* 1.1–1.0 Ga detritus with *c.* 2.7 and 2.0 populations. This is suggested to represent a post-Irumide basinal sequence, with no rigorous constraint on a minimum depositional age (Hauzenberger et al., 2014; Thomas et al., 2016). Similar rocks are also preserved in the Nampula Complex of northeast Mozambique, which is also comprised of *c.* 1.1–1.0 Ga orthogneiss that is generally older than that preserved in the Unango and Marrupa complexes. However, this complex is instead interpreted to have accreted to the Kalahari Craton prior to Congo–Kalahari collision (Macey et al., 2010). This collision resulted in its current position, separated from the other Mesoproterozoic complexes by the WSW–ENE trending Lurio Belt that is suggested to represent a suture zone between the Congo and Kalahari cratons (Bingen et al., 2009a).

Timing of magmatism and metamorphism in the SIB

SIB magmatism is constrained to between *c.* 1095 and 1040 Ma in Zambia and northwest

Mozambique (Fig. 3; Johnson et al., 2006; Johnson et al., 2007b; Westerhof et al., 2008) and involved the contamination of juvenile material by silicic continental crust, typical of a continental-margin-arc setting (Johnson et al., 2007b). Here, metamorphism is identified as high-temperature, low-pressure and is contemporaneous with magmatism. The tectonic settings of the eastern terranes in this area are poorly constrained, though preliminary work suggests these to be components of an accreted island arc complex or a continuation of the continental-margin-arc (Johnson et al., 2006; Johnson et al., 2007b; Mapani et al., 2001). In northeast Mozambique, SIB magmatism is constrained to between c. 1060 and 950 Ma (Fig. 3; Bingen et al., 2009a). The magmatism in these Mesoproterozoic complexes is both voluminous and felsic in composition, and as such is also interpreted to have formed in a continental-margin-arc setting. Notably, metamorphism in the Unango and Marrupa complexes is younger than that recorded in Zambia and northwest Mozambique, instead

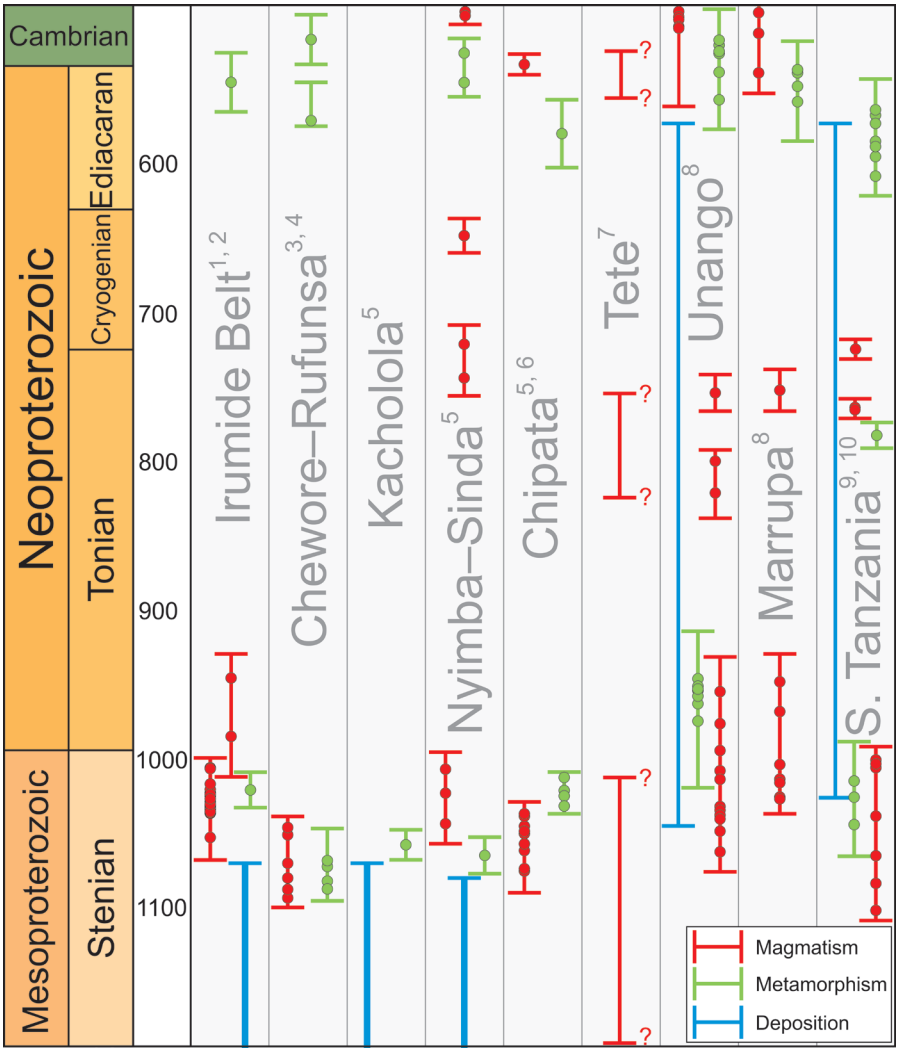

Figure 3. Time-space plot of existing data for the SIB, indicating periods of magmatism (red), metamorphism (green), and deposition (blue) for the belt throughout the Stenian to middle-Cambrian. Bars throughout the plot indicate the duration of events defined by the maximum and minimum error ranges of a series of analyses. Circles along plotted bars indicate mean age values obtained via U–Pb geochronology. References are indicated by the numbers accompanying a given unit's name and are as follows: 1, De Waele et al. (2006a); 2, De Waele et al. (2009); 3, Johnson et al. (2007b); 4, Goscombe et al. (2000); 5, Johnson et al. (2006); 6, Karmakar and Schenk (2016); 7, Westerhof et al. (2008; approximate age ranges); 8, Bingen et al. (2009a); 9, Hauzenberger et al. (2014); 10, Thomas et al. (2016).

dated at *c.* 950 Ma. U–Pb, Hf and Nd isotopic data obtained by Johnson et al. (2007b) suggest that the Zambian terranes of the SIB were formed on variably reworked Palaeoproterozoic basement. Similarly, Archaean to Palaeoproterozoic components are also identified in northeast Mozambique (Bingen et al., 2009a). A marginal basin ophiolite (Chewore Ophiolite) dated at 1393 ± 22 Ma (Oliver et al., 1998) was observed in northern Zimbabwe, though lithological and geochemical characteristics suggest that it is not directly related to the *c.* 1070 Ma continental-margin-arc magmatism (De Waele et al., 2008; Westerhof et al., 2008). Younger magmatic rocks in the belt are broadly restricted to the Nyimba–Sinda Terrane in Zambia as well as the Unango and Marrupa complexes of Mozambique (Fig. 3). A syenite pluton in the Unango Complex yields a crystallisation age of 799 ± 8 Ma, while a charnockite pluton in the Marrupa Complex yielded a crystallisation age of 753 ± 13 Ma and metamorphic age of 549 ± 22 Ma (Bingen et al., 2009a). The ages yielded by this pluton are both within error of similar ages recorded by widespread orthogneiss located within the Nyimba–Sinda Terrane, which yields protolith U–Pb ages of 742 ± 13 Ma and has an interpreted metamorphic age of 536 ± 10 Ma (Johnson et al., 2006). This gneiss is interpreted to be closely associated with predominantly andesitic volcanics that are also located in this terrane (Barr and Drysdall, 1972; Johnson et al., 2006). Direct age constraints are not available for the volcanics, though underlying granite has yielded a crystallisation age of *c.* 1040 Ma. Post-kinematic granite is also widespread throughout the Nyimba–Sinda Terrane and yields a crystallisation age of *c.* 500 Ma. This is broadly consistent with the syenite intrusions found within the prominent Nyamadzi Shear Zone north-east of the Nyimba–Sinda Terrane (Johnson et al., 2006). Broadly coeval post-kinematic magmatism is observed in the complexes of northeast Mozambique, with crystallisation ages ranging from *c.* 550 to 490 Ma (Fig. 3; Bingen et al., 2009a).

Relationship to the Irumide Belt and Congo Craton

Several distinct differences can be observed between the SIB and the Irumide Belt, which has led a number of authors to conclude that there is no genetic relationship between the two belts (De Waele et al., 2008; Hauzenberger et al., 2014; Johnson et al., 2006; Johnson et al., 2007b; Westerhof et al., 2008). While the SIB contains an array of deformed sedimentary, igneous and volcanic units with related intrusions (De Waele et al., 2006b; Hauzenberger et al., 2014; Johnson et al., 2006; Johnson et al., 2007b; Westerhof et al., 2008), the Irumide Belt is largely composed of granitoids and the metasedimentary Muva Supergroup (Daly, 1986; Daly et al., 1984; Daly and Unrug, 1982; De Waele and Mapani, 2002). Metamorphism in the Irumide Belt occurred at *c.* 1020 Ma and involved pressures around 7–8 kbar as a result of crustal thickening processes. This is distinct from metamorphism in the SIB, which was considered to have occurred between *c.* 1090 and 1040 Ma and involved peak pressures below 4 kbar (Goscombe et al., 2000; Johnson et al., 2006; Johnson et al., 2007b). Johnson et al. (2007b) argue that this difference in the timing and nature of metamorphism without a gradual transition is unlikely to be due to the diachronous development of a single Irumide belt. However, recent pressure–temperature estimates obtained for the Chipata Terrane by Karmakar and Schenk (2016) yield values of ~900–1000 °C and 5–6 kbar. These authors also obtained U–Pb monazite ages that indicate that metamorphism was contemporaneous with that in the Irumide Belt. On the basis of contrasting styles and timing of metamorphism, as well as the Mwembeshi dislocation between the SIB and Irumide Belt, Johnson et al. (2006) suggested that there is no genetic relationship between the belts and that the presence of the Luangwa Valley between them masks a key suture along the margin of

the Congo Craton. With no genetic relationship between the belts, Johnson et al. (2007b) argued that the SIB did not develop on the Congo margin and instead developed via subduction of continental crust under the margin of a micro-continental mass later named the Rushinga Microcontinent (Begg et al., 2009), which ultimately lead to ocean closure at *c.* 1040 Ma. This model suggests that collision between the SIB and Congo craton margin led to the cessation of magmatism in the SIB, and initiated compression and crustal melting in the Irumide Belt. Alternatively, Bingen et al. (2009a) suggest that the terranes and complexes identified in the SIB could have always been a part of the southern Congo margin, which acted a long-lived active margin and experienced at least one event of foreland propagation between *c.* 1020 and 1005 Ma.

METHODS

Three samples of quartzite (Z14-01, Z14-02, Z14-17) and one sample of psammite (Z14-05) were collected for detrital zircon U–Pb geochronology, trace element analysis and Lu–Hf isotopic analysis from the SIB in Zambia. Three additional detrital zircon samples from the Irumide Belt were analysed for Lu–Hf isotopic data. These samples were previously age dated using U–Pb geochronology, the details of which are reported in De Waele et al. (2006a). Individual U−Pb, Lu−Hf and trace element analyses can be referred to in the supplementary material.

U–Pb detrital zircon geochronology

U–Pb and trace element data were obtained from separated detrital zircon grains that were extracted from crushed rocks using standard magnetic and heavy liquid techniques. Zircon separates were hand-picked, mounted in epoxy resin and then polished to expose the grains. The grains were imaged using an FEI Quanta 600 Scanning Electron Microscope (SEM) with a Gatan cathodoluminescence detector attached to identify compositional domains that were suitable for analysis. Zircon grains were analysed for U–Pb isotopes and trace elements using an Agilent 7900 ICP-MS and NewWave UP213 Laser Ablation System. Trace elements analysed include the rare earth elements (REE; with the exception of Pm) and P. Ablation of zircon was performed in a He-atmosphere with a frequency of 5 Hz. A spot size of 30 μm was used for all analyses. A total acquisition time of 60 seconds was used consisting of 30 seconds of background acquisition followed by 30 seconds of sample ablation. The Standard GJ ($^{206}Pb/^{238}U$ = 608.5 ± 0.4 Ma; Jackson et al. (2004)) was used as the primary standard for all zircon analyses and Plešovice ($^{206}Pb/^{238}U$ = 337.13 ± 0.37 Ma; Sláma et al. (2008)) was used as a secondary standard. Standard glass NIST SRM 610 was used during trace element analysis as a reference material for corrections to mass bias drift. Plešovice yielded a 95% concordant average $^{206}Pb/^{238}U$ age of 332.1 ± 2.4 Ma (2σ, n = 61) and $^{207}Pb/^{206}Pb$ age of 333.7 ± 9.9 Ma (2σ, n = 61). U–Pb data were reduced using GLITTER (Jackson et al., 2004), while trace element data were reduced using IOLITE (Paton et al., 2011). Upper and lower concordia intercepts of samples were calculated using ISOPLOT (Ludwig, 2004), in addition to the modelling method of Reimink et al. (2016).

Lu–Hf Isotope Analysis

Lu–Hf isotope analysis in zircon was conducted at the University of Adelaide using a New Wave UP-193 Excimer laser attached to a Thermo-Scientific Neptune Multi-Collector ICP–MS. Analytical methods follow Payne et al. (2013). A spot size of ~50 μm was used for all appropriately sized zircon grains, decreasing to 35 μm for smaller grains. Zircons were ablated in a He atmosphere, which was mixed with Ar upstream of the ablation cell, for between 40 to 100 seconds with a 5 Hz repetition rate, a 4 ns pulse rate, and an intensity of ~6–8 J/cm^2. Data were normalised to $^{179}Hf/^{177}Hf$ = 0.7325, using an exponential correction for

mass bias. Yb and Lu isobaric interferences on ^{176}Hf were corrected for following the methodology of Woodhead et al. (2004). Reduction of zircon data was undertaken using the Hf isotope data reduction spreadsheet, HfTRAX (Payne et al., 2013). Known reference materials (Mud Tank and Plešovice) were run throughout the analytical session to verify the stability and performance of the instrument. The primary standard used was Plešovice, which yielded a mean $^{176}Hf/^{177}Hf$ ratio of 0.282470 ± 0.000015 (2σ, n = 7). This is within uncertainty of the known value of 0.282482 ± 0.000013 (Sláma et al., 2008).

SAMPLE INFORMATION AND ANALYTICAL RESULTS

Southern Irumide Belt samples

Z14-17 (15° 03' 09.6" S, 29° 50' 59.8" E)

Z14-17 is a pure quartzite collected from the Chewore–Rufunsa Terrane (Fig. 2), in a road cutting along Great East Road, approximately 20 km north-east of Rufunsa. Zircon grains from this sample range from ~50 to 200 μm in length, and vary from stubby (1:1) or elongated (4:1). They range in appearance from clear to dark and cloudy. Some grains display oscillatory zonation that reflect the igneous growth of the grains and all grains display rounding typical of detrital zircons (Fig. 4). In many cases, the CL zoning indicates that the rims of zircon grains were destroyed, possibly as a result of sedimentary abrasion, metamorphism or chemical alteration (Corfu et al., 2003). Some zircon grains appear to be fragments of a larger grain. One hundred and seventeen (117) zircon cores and six rims were randomly selected for U–Pb LA–ICP–MS analysis, of

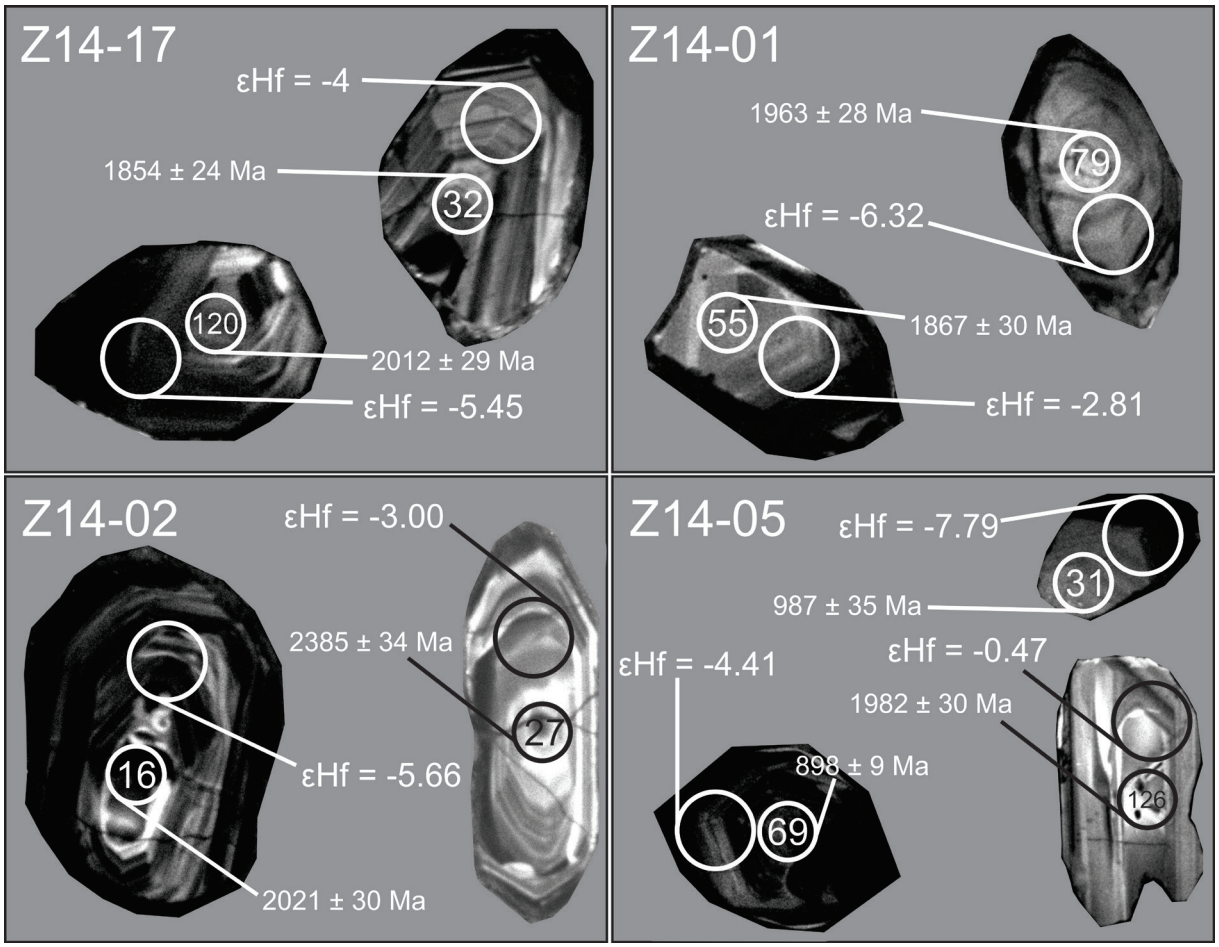

Figure 4. Cathodoluminescence (CL) images of zircons from samples selected for geochronological analysis. Numbered circles represent LA–ICP–MS spot locations of 30 μm diameter and the larger circles on each grain represent MC–LA–ICP–MS spot locations.

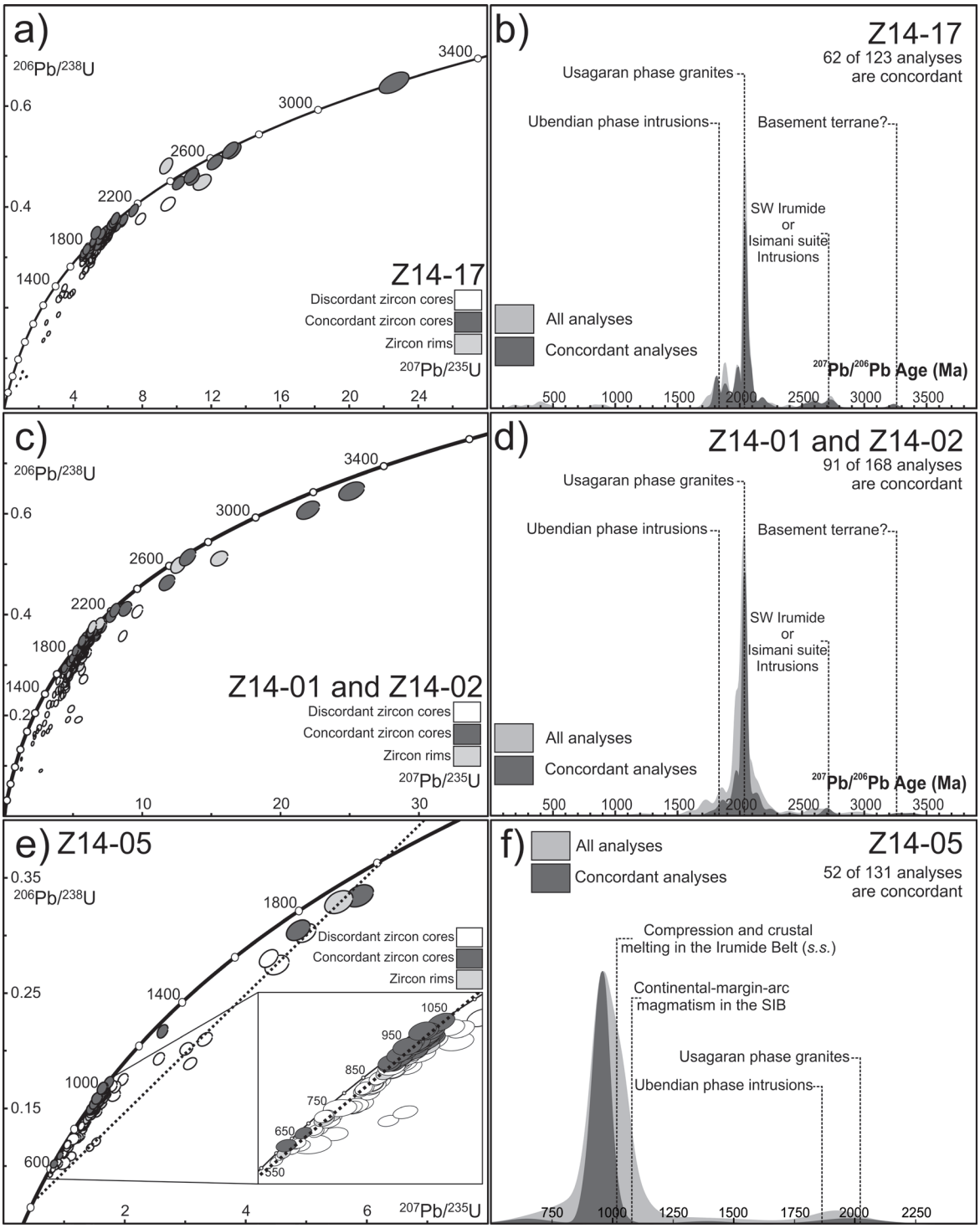

Figure 5. U–Pb concordia diagrams and associated Kernel Density Plots (KDPs) for samples from the Southern Irumide Belt. a) Concordia diagram for sample Z14-17 of the Chewore–Rufunsa Terrane, ≥ 90% concordant zircons are shaded in dark grey and rims in light grey. b) Associated KDP for Z14-17 with $^{207}Pb/^{206}Pb$ ages plotted, likely sources are indicated by the dashed lines. c) Concordia diagram for samples Z14-01 and Z14-02 of the Kacholola Terrane, ≥ 90% concordant zircons are shaded in dark grey and rims in light grey. d) Associated KDP for Z14-01 and Z14-02 with $^{207}Pb/^{206}Pb$ ages plotted, likely sources are indicated by the dashed lines. e) Concordia diagram for sample Z14-05 of the Nyimba–Sinda Terrane, a blowout is also depicted for the c. 1.1–0.55 Ga age range. ≥ 90% concordant zircons are shaded in dark grey and rims in light grey. Interpreted Pb loss lines are indicated by the dashed lines in the concordia plot and blow out. f) Associated KDP for Z14-05 with $^{206}Pb/^{238}U$ ages plotted for ages < 1.2 Ga and $^{207}Pb/^{206}Pb$ ages plotted for ages > 1.2 Ga. Likely sources are indicated by the dashed lines.

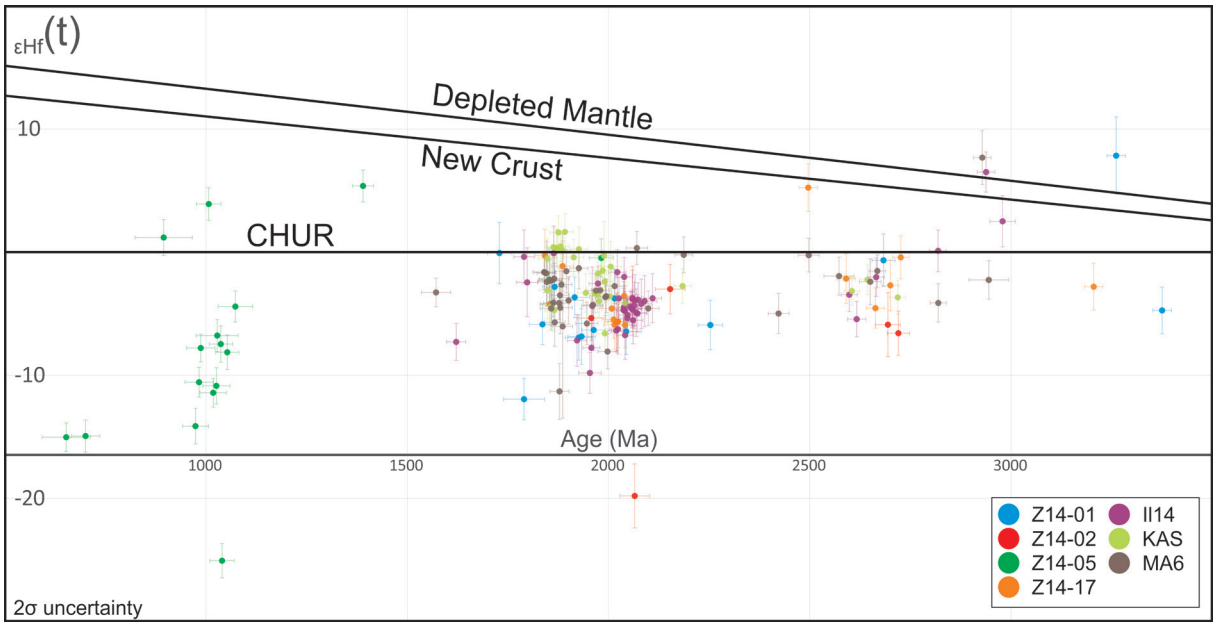

Figure 6. εHf(t) versus U–Pb age plot for detrital zircons from the Irumide Belt and SIB. Uncertainty for age and εHf(t) values are shown at the 2σ level. The depleted mantle curve of Griffin et al. (2002) is plotted, as is the new crust line of Dhuime et al. (2011).

which 62 cores were ≤ 10% discordant (Fig. 5a). The $^{207}Pb/^{206}Pb$ ages of these near-concordant analyses range from *c.* 2726 to 1768 Ma, with the majority of analyses yielding ages around 2.0 Ga. The Kernel Density Plot (KDP) for this sample (Fig. 5b) displays a prominent peak at *c.* 2.0 Ga, with smaller peaks at *c.* 1.8, 2.2, 2.6, 2.7, and 3.2 Ga. Hafnium data was obtained for 15 zircon grains from the *c.* 1.8, 2.0, 2.6 and 3.2 Ga populations (Fig. 6). Each population has negative εHf(t) values, ranging from −5.9 to −0.3. A single grain with a c. 2.5 Ga age has an εHf(t) value of +5.2. Trace element data were obtained for the same 15 zircons (Fig. 7a), which display REE concentrations typical of zircon (Hoskin and Ireland, 2000) that shows a general increase in elemental abundance with increasing atomic mass. Such a trend is also observed in each subsequent sample. Phosphorous contents range from ~100–900 ppm (Fig. 7d), with zircons between *c.* 2.0 and 1.8 Ga having generally higher P contents than older grains. U, Yb and Hf values obtained from all analyses (in every sample) are consistent with zircon derived from a continental source (Fig. 7e, 7f; Grimes et al., 2007).

Z14-01 (14° 38' 02.3" S, 30° 47' 36.7" E) and Z14-02 (14° 38' 04.5" S, 30° 47' 52.3" E)

Z14-01 was collected from the base of Lupiri Hill in the Kacholola Terrane, approximately 9 km SW of Nyimba. Z14-02 was collected from the top of Lupiri Hill (Fig. 2). Both samples are quartzite and contain minor muscovite. Zircons from these samples are ~40 to 200 μm in length, ranging from stubby (1:1) or elongated (4:1). Zircon grains from Z14-01 are generally clear to dark in appearance, with some brownish grains present. Zircon grains from Z14-02 are clear in appearance. Grains in both samples commonly display oscillatory zonation that reflect the igneous growth of the grains, while all grains display rounding (Fig. 4). In sample Z14-01, 136 zircon cores and four rims were randomly selected for U–Pb analysis, from this population 84 grain cores were ≤ 10% discordant. Twenty three (23) zircon core analyses and five rim analyses were obtained from sample Z14-02 and seven cores were ≤ 10% discordant. Due to the proximity, common zircon morphology and similarity in ages obtained, in conjunction with the paucity of near concordant analyses from Z14-02, the analyses from these samples have been com-

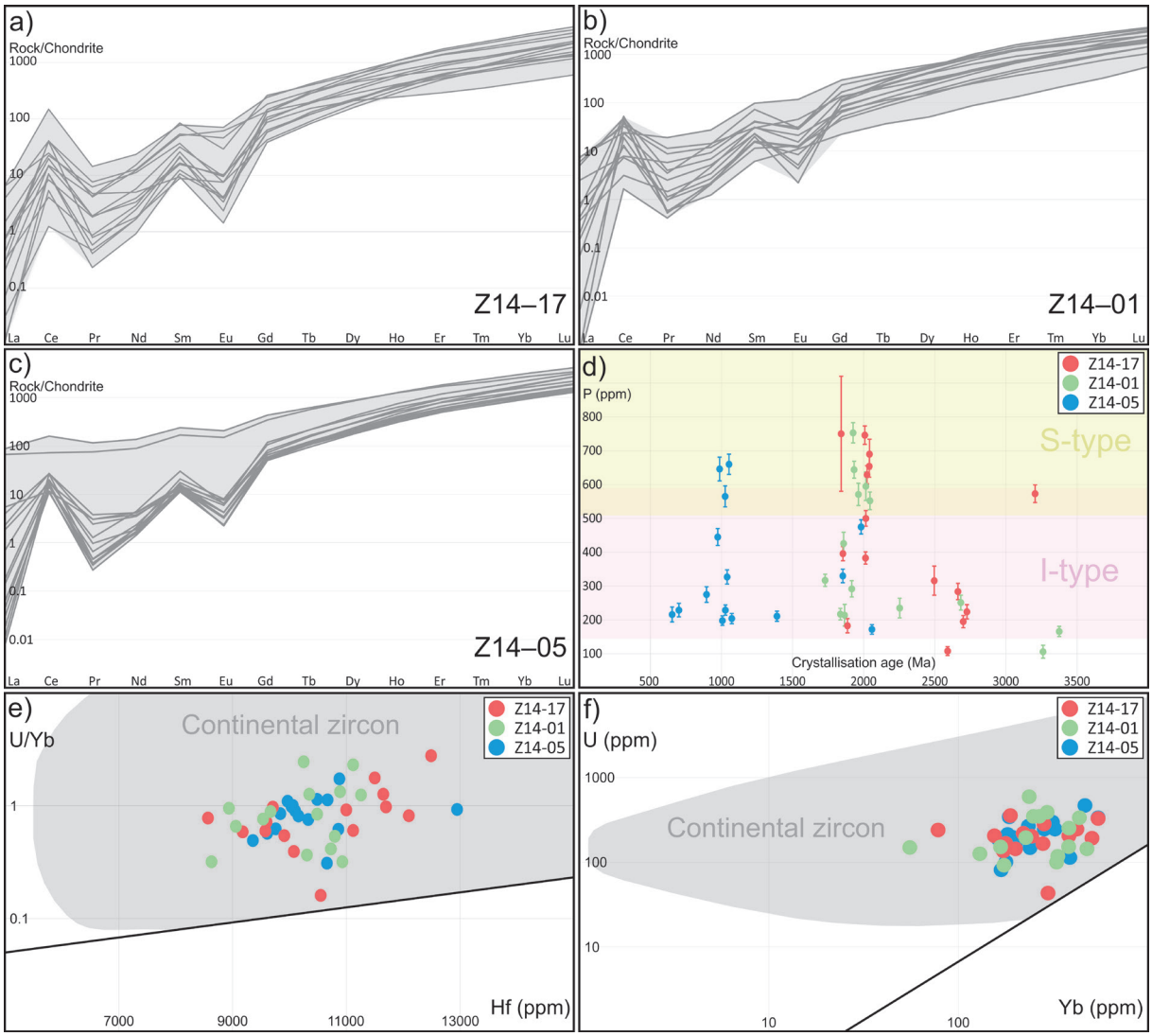

Figure 7. Trace element diagrams for samples from the SIB terranes. a) to c) Rare-earth element diagrams normalised to the average chondrite (McDonough and Sun, 1995) for samples Z14-17, Z14-01 and Z14-05, respectively; d) Phosphorous contents (ppm) versus U–Pb age diagram (Ma) for Z14 samples; e) U/Yb versus Hf (ppm) diagram for Z14 samples, with the grey field outlining the values for continental zircons (Grimes et al., 2007); f) U (ppm) versus Yb (ppm) diagram for Z14 samples, with the grey field outlining the values for continental zircons (Grimes et al., 2007; Burnham and Berry, 2017).

bined and are displayed on a Wetherill concordia diagram (Fig. 5c). The $^{207}Pb/^{206}Pb$ ages of these near-concordant analyses range from *c.* 3376 to 1764 Ma and most ages are *c.* 2.0 Ga. The KDP for this sample (Fig. 5d) displays a large age peak at *c.* 2.0 Ga, with smaller peaks at *c.* 1.85, 2.3, 2.7 and 3.4 Ga. Hafnium isotopic data were obtained for 22 zircons from each of the populations. Each age population has negative εHf(t) values (Fig. 6) that range from −19.8 to −0.1. A single grain with a *c.* 3.3 Ga age displays an εHf(t) value of +7.8. P concentrations in these samples vary between ~100–800 ppm, with a higher variation in P content in zircons of *c.* 2.0–1.8 Ga age in comparison to older grains.

Z14-05 (14° 31' 58.9" S, 30° 57' 50.0" E)

Z14-05 was collected in the Nyimba–Sinda Terrane, from an outcrop approximately 15 km east of Nyimba, along the Great East Road (Fig. 2). The sample is a psammite, being less pure than the previous quartzite samples and containing approximately 10% microcline and minor plagioclase. It also contains minor chlorite, muscovite and rutile. Zircons are between

~20 to 120 μm in length and are stubby (1:1) to elongated (4:1) and are clear in appearance. The zircons typically display oscillatory zonation and all grains are rounded (Fig. 4). Some grains display deformed or discontinuous zonation at the rims, which may reflect partially metamorphosed grains or a later stage of growth. The fractured appearance and zonation of some grains indicates that the grains are fragments of a larger grain. One hundred and twenty two (122) zircon cores and nine rims were randomly selected for U–Pb analysis (Fig. 5e) and 52 core analyses are ≤ 10 % discordant. The $^{206}Pb/^{238}U$ and $^{207}Pb/^{206}Pb$ ages are between *c.* 2.1 to 0.7 Ga, with the majority of analyses clustering at *c.* 1.0 Ga. For grains > 1.2 Ga, the $^{207}Pb/^{206}Pb$ age has been considered, while the $^{206}Pb/^{238}U$ age has been used for younger grains. The KDP for this sample (Fig. 5f) displays a prominent age peak at *c.* 1.0 Ga, with minor populations at *c.* 2.0 and 0.7 Ga. The enlarged section of the concordia diagram for this sample (Fig. 5e), shows several discordant analyses on a near-linear trajectory between the concordant c. 1.0 Ga analyses and *c.* 0.7–0.6 Ga analyses. This may suggest that these younger concordant analyses are part of the *c.* 1.0 Ga population but experienced subsequent Pb loss.

Concordance plotted against the $^{206}Pb/^{238}U$ age (Fig. 8a) for each zircon display a strong linear trend between *c.* 1.1 and 0.8 Ga. This implies that the discordant analyses within this age range that were pulled along a Discordia from *c.* 1.1 Ga and may have formed a coherent single population at that age prior to Pb-loss. The deviation of the < 0.8 Ga ages from the $^{206}Pb/^{238}U$-concordance trendline means that it is not possible to unambiguously assign them to the same population using this method. It does not exclude them from this initial population though as the potential exists for ancient lead loss of a different age to have resulted in a different relationship between $^{206}Pb/^{238}U$ ages and concordance. Assessing the $^{232}Th/^{238}U$ ratios against $^{206}Pb/^{238}U$ ages for the same analyses (Fig. 8b) shows a relatively consistent trend of decreasing $^{232}Th/^{238}U$ with decreasing age, which has been linked to Pb loss (Ashwal et al., 1999; Collins, 2003; Collins et al., 2004; Hoskin and Black, 2000; Kirkland et al., 2015; Pidgeon, 1992; Pidgeon et al., 1998; Vavra et al., 1999). Hf isotope analyses of < *c.* 1 Ga grains show similar Hf_i values to grains from the *c.* 1.0 Ga population (Fig. 8c). The upper and lower concordia intercepts of this population are identifiable using the modelling method of Reimink et al. (2016). This method produces a series of discordia lines and calculates an associated summed probability density, which serves as a measure of the likelihood that a given line contains discordant analyses. Likelihood in this context serves as a relative metric for deciphering upper and lower intercept ages. Figure 8d is a visualisation of these chords and their relative likelihoods, with the most likely upper and lower intercepts for this sample at *c.* 1.1 ± 0.05 Ga and 0.4 ± 0.2 Ga, respectively. There are also minor increases in likelihood for upper intercepts at *c.* 2.0, 2.6, and 3.2 Ga that broadly correspond to age peaks observed in the previous samples. The most likely upper intercept obtained using this method is corroborated with a linear regression in ISOPLOT, which produces an upper intercept of 1071 +98/-44 Ma (MSWD = 0.37; Fig. 8e). The *c.* 1.9 Ga analyses are also suspected to have experienced Pb-loss. A Pb-loss line can be traced through these analyses to the discordant *c.* 1.5–1.3 Ga analyses and even to the most discordant *c.* 0.7 Ga analyses. However an upper concordia intercept of analyses along this line is poorly resolved via the method of Reimink et al. (2016). Instead, an upper intercept calculated using ISOPLOT yields an age of 2006 ± 77 Ma (MSWD = 11.8; Fig. 8f).

Hafnium isotope data were obtained for 17 zircons belonging to the *c.* 1.0 and 2.0 Ga populations, as well as those of *c.* 0.7 and 1.4 Ga age (Fig. 6). The two analyses of zircons of *c.* 650 Ma age returned εHf(t) values of −15.0 and

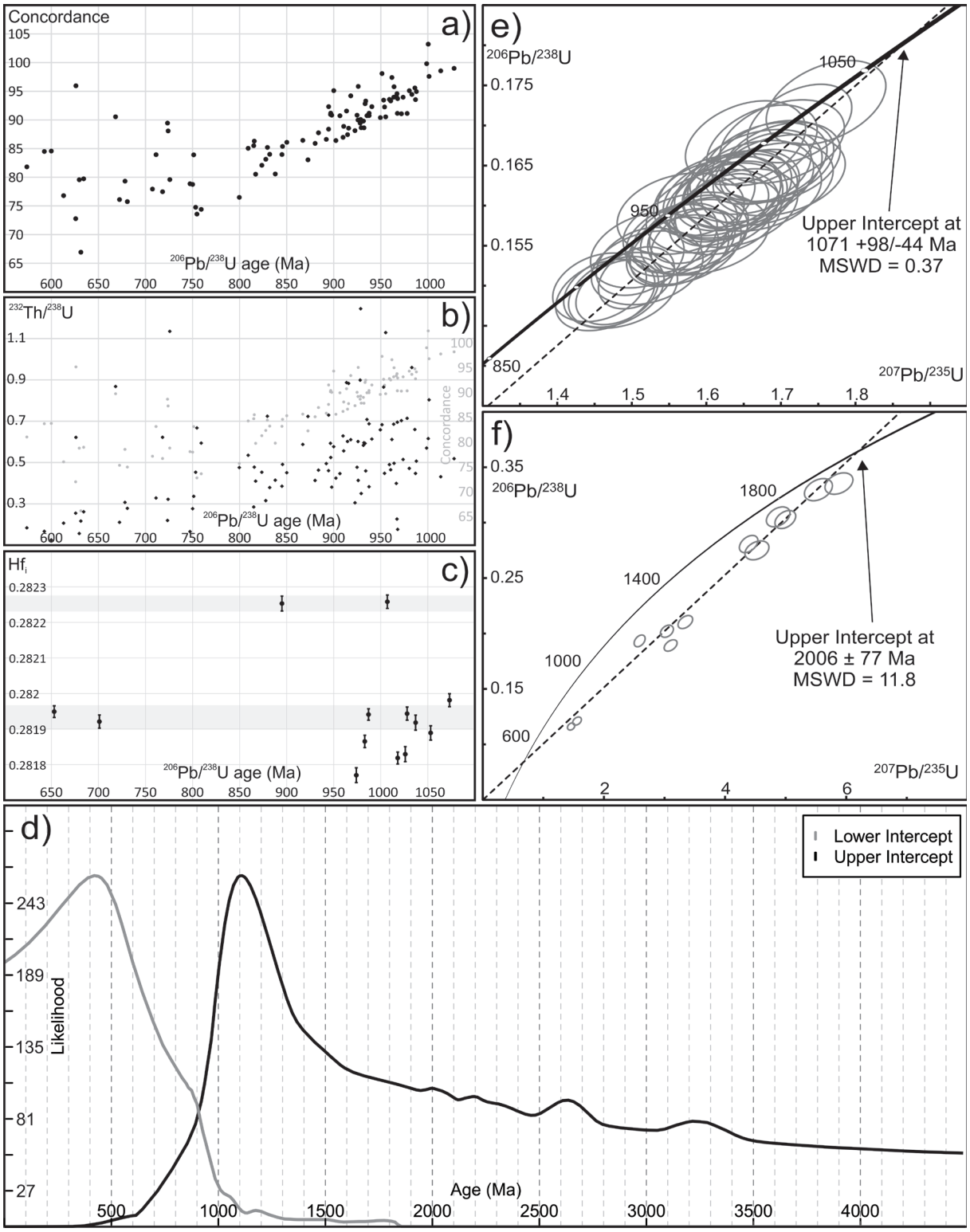

Figure 8. Plots indicating Pb-loss is recorded in zircon grains from sample Z14-05 and calculated concordia intercepts. a) Concordance versus $^{206}Pb/^{238}U$ age plot; b) $^{232}Th/^{238}U$ ratio versus $^{206}Pb/^{238}U$ age plot. Concordance versus $^{206}Pb/^{238}U$ age is additionally shown on the secondary vertical axis (light grey) ; c) Hf_i versus $^{206}Pb/^{238}U$ age plot; d) Upper concordia intercept calculated for the *c.* 1.0 Ga population using ISOPLOT; e) Upper concordia intercept calculated for grains of a suspected *c.* 2 Ga population using ISOPLOT; f) most likely upper and lower concordia intercepts (*c.* 1.1 and 0.4 Ga, respectively) for sample Z14-05, obtained using the modelling method of Reimink et al. (2016).

−14.9, similar to or slightly more evolved than many of the zircon grains from the *c.* 1.0 Ga population, providing a small indication that these grains may have initially belonged to the *c.* 1.0 Ga population. Zircon grains from the *c.* 1.0 Ga population have εHf(t) values ranging from −25.0 to −4.4, with the exception of two grains that have εHf(t) values of +1.2 and +3.9. A single *c.* 1.3 Ga grain yielded an εHf(t) value of +5.4. Analyses from the 1.8 Ga population yielded two εHf(t) values of −2.2 and −0.5, comparable to values obtained for similar populations from the other samples analysed in this study. Trace element data (Fig. 7c) for this sample show a distinct REE enrichment for two analyses in comparison to the other obtained analyses, which is particularly noticeable in the light REE concentrations for these zircons. Such variance may reflect a difference in source material or subsequent metamorphism (Hoskin and Schaltegger, 2003; Wang et al., 2016). These zircons yielded crystallisation ages of *c.* 1.02 and 1.05 Ga, which is temporally indistinct from the majority of analyses from this sample. Morphologically, these zircons are largely indistinct from other grains of similar age in this sample, though are slightly darker in CL. P contents obtained for this sample range from ~150–700 ppm (Fig. 7d).

Irumide Belt samples

Three samples from the Irumide Belt were analysed for Lu–Hf isotopic data. These samples were previously collected and analysed for U–Pb geochronology by De Waele et al. (2006a), with detailed sample descriptions provided therein.

Sample IL14

Sample IL14 is a quartzite sampled from the Ilondola Mission area. The U–Pb zircon data were previously reported in De Waele et al. (2006a) and display prominent age populations at *c.* 1.9, 2.0–2.1, 2.2, 2.4, 2.7, 2.9 and 3.0 Ga Forty-one analyses were undertaken on grains from this sample. εHf(t) values obtained from these analyses range from −9.8 to +6.5 (Fig. 5), with all but three analyses returning a negative εHf(t) value. Notably, the three positive analyses were obtained from the grains with oldest three U–Pb ages (*c.* 3.0–2.7 Ga) obtained from this sample.

Sample KAS

Sample KAS is a quartzite sampled near Kasama. This sample contains zircon age populations of *c.* 1.4, 1.8–1.9, 2.0, 2.1, 2.2 and 2.6 Ga (De Waele et al., 2006a). Twenty-nine analyses were obtained from this sample, with obtained εHf(t) values ranging from −6.6 to +1.7 (Fig. 5). The positive εHf(t) values obtained can be observed to from a cluster at *c.* 1.87 Ga.

Sample MA6

Detrital zircon sample MA6 is a quartzite from near Mansa. Previously collected zircon U–Pb data indicates age populations at *c.* 1.9, 2.0, 2.2, 2.4 and 2.7 Ga (De Waele et al., 2006a). Thirty-nine analyses were obtained from this sample, with εHf(t) values that range from −11.3 to +7.7 (Fig. 5). Only two analyses provide positive values. The analysis returning an εHf(t) value of +7.7 was obtained from the second oldest (*c.* 2.9 Ga) grain analysed for this sample.

DISCUSSION

Depositional age constraints on Southern Irumide Belt protoliths

Sample Z14-17 was sourced from the westernmost Chewore–Rufunsa Terrane of the SIB. From this sample the youngest age population was found to be *c.* 1.8 Ga, the youngest ≤ 10% discordant analysis yielded a $^{207}Pb/^{206}Pb$ age of 1768.1 ± 58.4 Ma (2σ uncertainty) that is interpreted to represent the maximum depositional age of this sample. Johnson et al. (2006) describe quartzite in the Chewore–Rufunsa Terrane as distributed between Mesoproterozoic volcanic and pelitic rocks. This terrane has been shown to have experienced widespread magmatism and metamorphism in the period

between *c.* 1095 and 1040 Ma (Goscombe et al., 2000; Johnson et al., 2006; Johnson et al., 2007b). The sample is interpreted to have been metamorphosed during this event and hence *c.* 1095 Ma is taken to represent the minimum depositional age of this sample.

Samples Z14-01 and Z14-02 were sourced from the Kacholola Terrane. From these samples, the youngest population identified is *c.* 1.85 Ga in age. The youngest ≤ 10% discordant analysis was from Z14-01 yielded a $^{207}Pb/^{206}Pb$ age of 1764.4 ± 74.2 Ma (2σ uncertainty) and is taken to represent the maximum depositional age of both samples. Igneous intrusions are rare within this terrane (Johnson et al., 2006) and there are a general lack of geochronological data that constrain the timing of metamorphism in this terrane. However, low Th/U metamorphic rims from the *c.* 2.6 Ga basement granodiorite were dated at c. 1.04 Ga (Cox et al., 2002). We suggest this metamorphism is contemporaneous with that observed in the overlying sedimentary rocks in this terrane, and thus, reflects the minimum depositional age for these samples.

Sample Z14-05 was collected from the Nyimba–Sinda Terrane, the youngest $^{206}Pb/^{238}U$ age (≤ 5% discordant) is 626.1 ± 17.2 Ma (2σ uncertainty). Depletion in ^{232}Th and a decreasing $^{232}Th/^{238}U$ ratio is typical of post-crystallisation isotope remobilization in zircon (Ashwal et al., 1999; Collins, 2003; Collins et al., 2004; Hoskin and Black, 2000; Kirkland et al., 2015; Pidgeon, 1992; Pidgeon et al., 1998; Vavra et al., 1999) and is a visible feature in the *c.* 850–600 Ma zircon from sample Z14-05 (Fig. 8b). Hf stochiometrically replaces Zr in the zircon crystal structure, and is usually retained in the event of Pb loss. As such, grains that were subjected to post-crystallisation Pb loss are likely to retain their initial Hf values (Finch and Hanchar, 2003; Hawkesworth and Kemp, 2006). Zircon grains with ages that are younger than *c.* 1.0 Ga have Hf_i values that are the same as those displayed in the *c.* 1.0 Ga population (Fig. 8c), indicating that the zircon may have been derived from the same crystallisation event. Given the equivalent Hfi values, decreasing $^{232}Th/^{238}U$ ratios and increasing concordance with increasing age (Fig. 8a, b), it is interpreted that these grains do not record their true age. These grains have likely undergone post-crystallisation isotope remobilization as a result of metamorphism during *c.* 540 Ma collision between the Congo and Kalahari cratons. This suggests that the zircon grains may have been a part of an older (*c.* 1.1–1.0 Ga) population prior to Pb loss. The obtained upper concordia intercept age of 1071 +98/-44 Ma (MSWD = 0.37) and maximum likelihood intercept of ~1.1 Ga (Fig. 7) correspond with magmatism occurring in the SIB between *c.* 1095 and 1040 Ma. The magmatism occurring at this time is suggested to represent the last source of sedimentary input to this sample and therefore, represent the maximum depositional age. We acknowledge that some of these zircon analyses may instead represent slightly younger magmatic events occurring in the Irumide Belt at *c.* 1020 Ma (De Waele et al., 2006b), though resolving this conundrum is difficult with the obtained analyses. This sample of quartzite falls within the broader mapping unit of Neoproterozoic gneiss, which is widespread throughout the Nyimba–Sinda terrane. A sample of this gneiss, located ~40 km south-west of this sampling locality has a protolith age of 742 ± 13 Ma (Johnson et al., 2006). Though early work tentatively suggested that Neoproterozoic gneiss formed the basement to the overlying quartzite (Johns et al., 1989), a rigorous relationship between the gneiss and the quartzite is unclear. If the protolith to the gneiss intruded the metasediments, this would provide a direct constraint on the minimum depositional age of the sample.

Correlation and provenance of Southern Irumide Belt metasedimentary rocks

Chewore–Rufunsa and Kacholola terranes

Samples from the Chewore–Rufunsa (Z14-17) and Kacholola (Z14-01 and Z14-02) ter-

ranes have prominent detrital zircon U−Pb age peaks at *c.* 2.0, 2.7 and 3.3 Ga, with trace element concentrations that reflect continental sources (Fig. 7e, 6f). Recently, the concentration of P in zircon has been used as a tool in distinguishing zircons derived from I- and S-type granites (Burnham and Berry, 2017). If the zircon grains from these samples were sourced from phases of predominantly granitic magmatism, grains older than *c.* 2.0 Ga were likely sourced from I-type granites (Fig. 7d). Zircon grains belonging to the *c.* 2.0 and 1.8 Ga populations display variable P contents that could reflect I- and possibly S-type granite sources. The age populations observed in these samples correlate well with age populations reported by De Waele et al. (2006a) for the Muva Supergroup. Furthermore, the εHf(t) values obtained for Chewore–Rufunsa and Kacholola samples (Z16-17, Z16-01 and Z16-02) are identical to values obtained in this study for these same populations. Both the aforementioned terranes and Muva Supergroup display detrital zircon age peaks that correspond with the main magmatic phases observed within the Bangweulu Block (De Waele et al., 2006a; De Waele et al., 2006b; De Waele et al., 2003). εNd(t) data obtained by De Waele et al. (2006b) clearly demonstrate that the igneous phases in the Bangweulu Block are the result of Proterozoic crustal reworking, which is consistent with the evolved zircons from this study. On the basis of highly correlative age populations and isotopic values, it is interpreted that the sedimentary rocks of the Chewore–Rufunsa and Kacholola terranes were derived from the same or similar source to that of the Muva Supergroup. The prominent *c.* 2.0 Ga zircon grains population are likely sourced from Usagaran or Ubendian phase granites. De Waele et al. (2006b) used this term to not only encompass the magmatism occurring in the Ubendian–Usagaran Belt at this time (Boniface et al., 2012; Ring et al., 1997; Tulibonywa et al., 2015), but also in the SW Irumide Belt. As such, zircons forming the *c.* 2.0 Ga age peak may have been sourced from either region. The *c.* 1.8 Ga age population observed in sample Z14-17 may be derived from Usagaran or Ubendian phase intrusions, granitoids of *c.* 1.85–1.80 Ga age that are speculated to have been part of a widespread plutono-volcanic province ranging from the Ubendian Belt to the Domes region of the Copperbelt in northern Zambia (De Waele et al., 2006b). The south-west Irumide Belt records *c.* 2.7 Ga magmatism (De Waele, 2004; De Waele et al., 2006b) and may explain the presence of the small *c.* 2.7–2.6 Ga detrital zircon age population found in samples from both terranes. Another potential source of this population can be found in the Isimani Suite of the Usagaran Belt. Here, Collins et al. (2004) reported xenocrysts of *c.* 2.7 Ga age in post-tectonic granites. From these data and previous work (Maboko, 1995; Möller et al., 1995; Muhongo et al., 2001; Stern, 2002), a large volume of *c.* 2.7 Ga material (subsequently reworked in the Usagaran orogen) was located to the east of the Tanzanian Craton. Three zircon grains from the three samples record ages over 3 Ga and it is possible that these are derived from a cryptic basement terrane described by De Waele et al. (2008). The proposed terrane possibly underlies both the Bangweulu Block and Irumide Belt. These authors further suggest this may be the same block that collided with the Tanzania Craton between 2 and 1.8 Ga.

The sediments of the Muva Supergroup are suggested to have correlatives in parts of both central Madagascar and Southern India (Cox et al., 2004; Plavsa et al., 2015; Plavsa et al., 2014), an interpretation made with the few data available at the time. In central Madagascar, multiple metasedimentary units preserve detrital age populations that are consistent with those observed in this study. Although the relative population sizes differ between the central Madagascan units and samples obtained in this study, the data indicate that sediments in both regions sourced similarly aged material. The Hf isotopic data obtained in this

study provides a new detrital fingerprint for correlation, and indicates that the age populations common to sedimentary rocks of both the southern Congo margin and central Madagascar display broadly similar εHf(t) values. Zircons with ages between *c.* 2.1 and 1.9 Ga in both regions record εHf(t) values between approximately −10 and +1. Zircons with ages between *c.* 3.0 and 2.5 Ga in central Madagascar record predominantly juvenile εHf(t) values, although a significant portion of samples record evolved values (Archibald et al., 2015) that are consistent with the values recorded by similarly aged grains in the Irumide and Southern Irumide belts. Few data are available for the 3.2 Ga population, although slightly evolved εHf(t) values were recorded for both regions (Archibald et al., 2015). As such, the results of this study are consistent with interpretations of the southern and eastern margins of the Congo Craton were a source region for Archaean–Palaeoproterozoic detrital zircon found in central Madagascar. Plavsa et al. (2014) compared U–Pb and Hf isotope data from southern India to that available for the Congo Craton and central Madagascar, interpreting a correlation between units in each region that was later supported with the data obtained by Archibald et al. (2015). With the exception of the *c.* 3.2 Ga population, U–Pb age populations identified in this study are similarly present in those identified in sediments from southern India. Hf data is not available for *c.* 1.9 Ga zircon grains. For those belonging to older populations εHf(t) values range from approximately −5 to +10 and are predominantly juvenile (Plavsa et al., 2014). This is contrary to Hf data collected in this study, where sediments older than 2.0 Ga have evolved isotopic signatures. More data are required to thoroughly constrain the sediment sources in this region but the southern Congo margin could, at the very least, be a partial sediment source.

Nyimba–Sinda Terrane

Sample Z14-05 was collected from the Nyimba–Sinda Terrane, and displays age peaks at *c.* 1.0 and 1.9 Ga. We interpret the 1.9 Ga population to have been subjected to Pb loss, as such an upper concordia intercept of 2006 ± 77 Ma is used to characterise this peak. This age suggests that this population may have been derived from Usagaran phase granites, similar to the samples from the Chewore–Rufunsa and Kachololа terranes. Similarly, the 1.0 Ga population is interpreted to have been subjected to Pb loss. We instead argue that the upper intercepts show that the analyses formed a single coherent population at *c.* 1.1–1.0 Ga (Fig. 8d, e). This age indicates that the sample and associated sedimentary sequence represent a younger cover sequence post-dating orogenesis in the region at *c.* 1090–1020 Ma. Arc magmatism in the SIB has been shown to have occurred between *c.* 1095 and 1040 Ma (Johnson et al., 2006; Johnson et al., 2007b; Westerhof et al., 2008) and involved the contamination of juvenile material by silicic continental crust, typical of a continental-margin-arc setting (Johnson et al., 2007b). On the basis of the age and isotopic nature of this magmatism, we suggest these intrusions provide an ideal sediment source for Z14-05. Other possible sediment sources can be found along the southern Congo margin, and further afield in Africa. Similarly aged (*c.* 1.1–1 Ga) sediments can be found in southern Zambia, as part of a supracrustal sequence in the Zambezi Belt (Johnson et al., 2007a). These sediments are thought to have been deposited on the southern Congo margin, and sourced directly from underlying basement that could also represent a source for the Nyimba–Sinda sediments. Contemporaneous rocks in western Madagascar (Dabolava Suite; *c.* 1080–980 Ma) were recently interpreted to represent oceanic arc relicts that were part of the same arc as the Irumide Belt at this time (Archibald et al., 2017). Juvenile εHf(t) values with only minor deflection to evolved values in conjunction with δ18O data

were interpreted to indicate the incorporation of young sedimentary or volcanic rocks into evolving juvenile *c.* 1080–980 Ma magmas (Archibald et al., 2017). The εHf(t) values obtained in this study for similarly aged zircons are predominantly evolved, though two grains display juvenile values equivalent with those obtained by Archibald et al. (2017). As such, plutonic and volcanic rocks in western Madagascar are unlikely to be the source for these *c.* 1.1–1.0 Ga detrital zircons.

Palaeogeographic implications

The geochronological data gathered in this study for sedimentary rocks of the Chewore–Rufunsa and Kacholola terranes strongly suggests that they were derived from the same sources as the Muva Supergroup. Such a correlation may indicate that—contrary to previous interpretations—the Chewore–Rufunsa and Kacholola terranes of the SIB were depositionally connected and hence, adjacent to or in close proximity to the Irumide Belt. Such implications may extend to the terranes and complexes in Mozambique and Tanzania that are suggested to be a continuation of the SIB (Bingen et al., 2009a; Thomas et al., 2016; Westerhof et al., 2008). Previous interpreta-

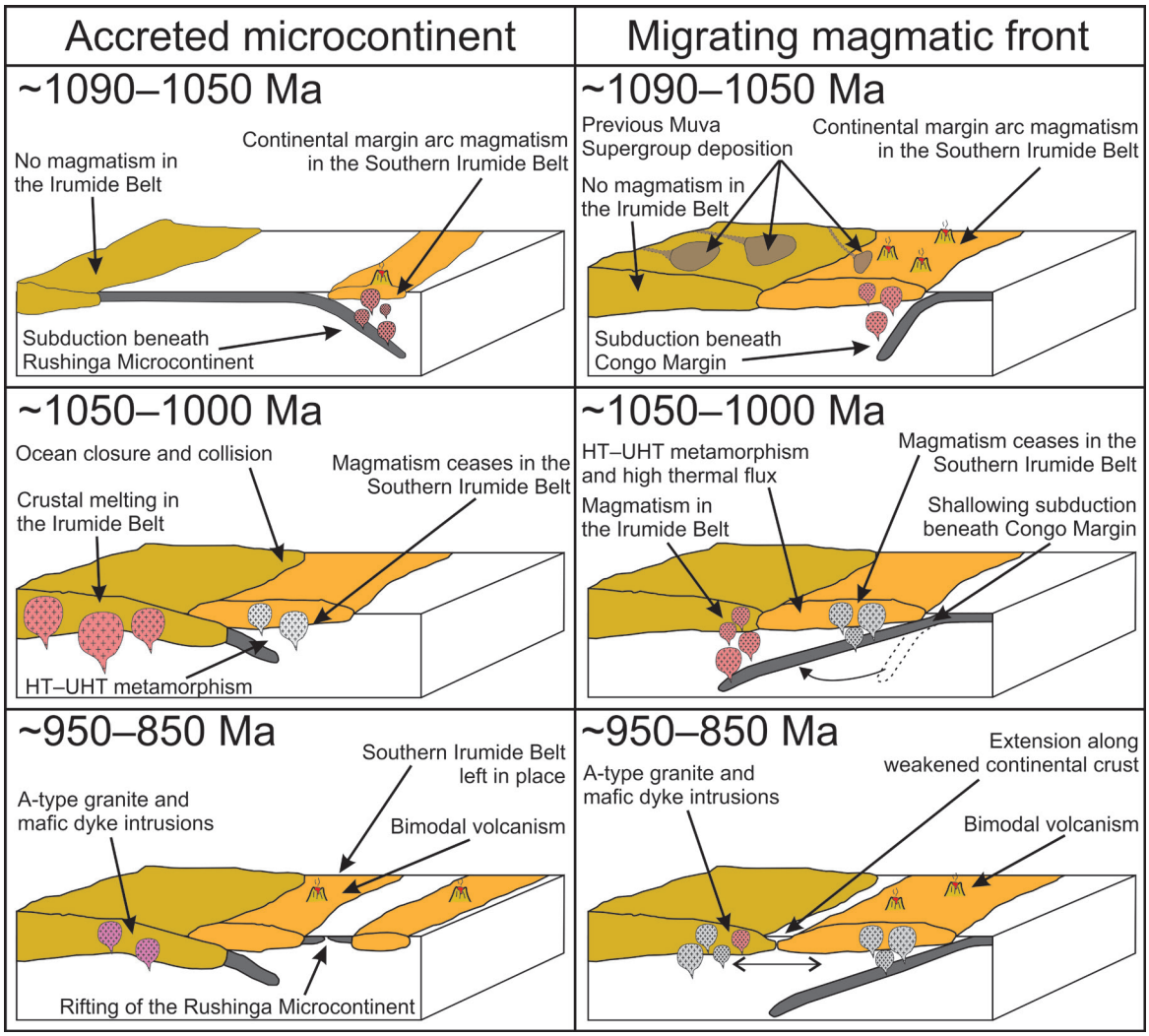

Figure 9. Simplified diagram of the tectonic development of the Irumide and Southern Irumide belts along the southern margin of the Congo Craton from *c.* 1100 to 850 Ma. The left column displays the sequences of events along the southern Congo margin hypothesised by a model where the SIB formed on a microcontinent that subsequently collided with the Irumide Belt (De Waele et al., 2006b; Karmakar and Schenk, 2016). The right column displays the sequence of events hypothesised by a model where the SIB initially formed along the southern Congo margin, and evolved in a similar fashion to the Andes (Ramos and Folguera, 2005).

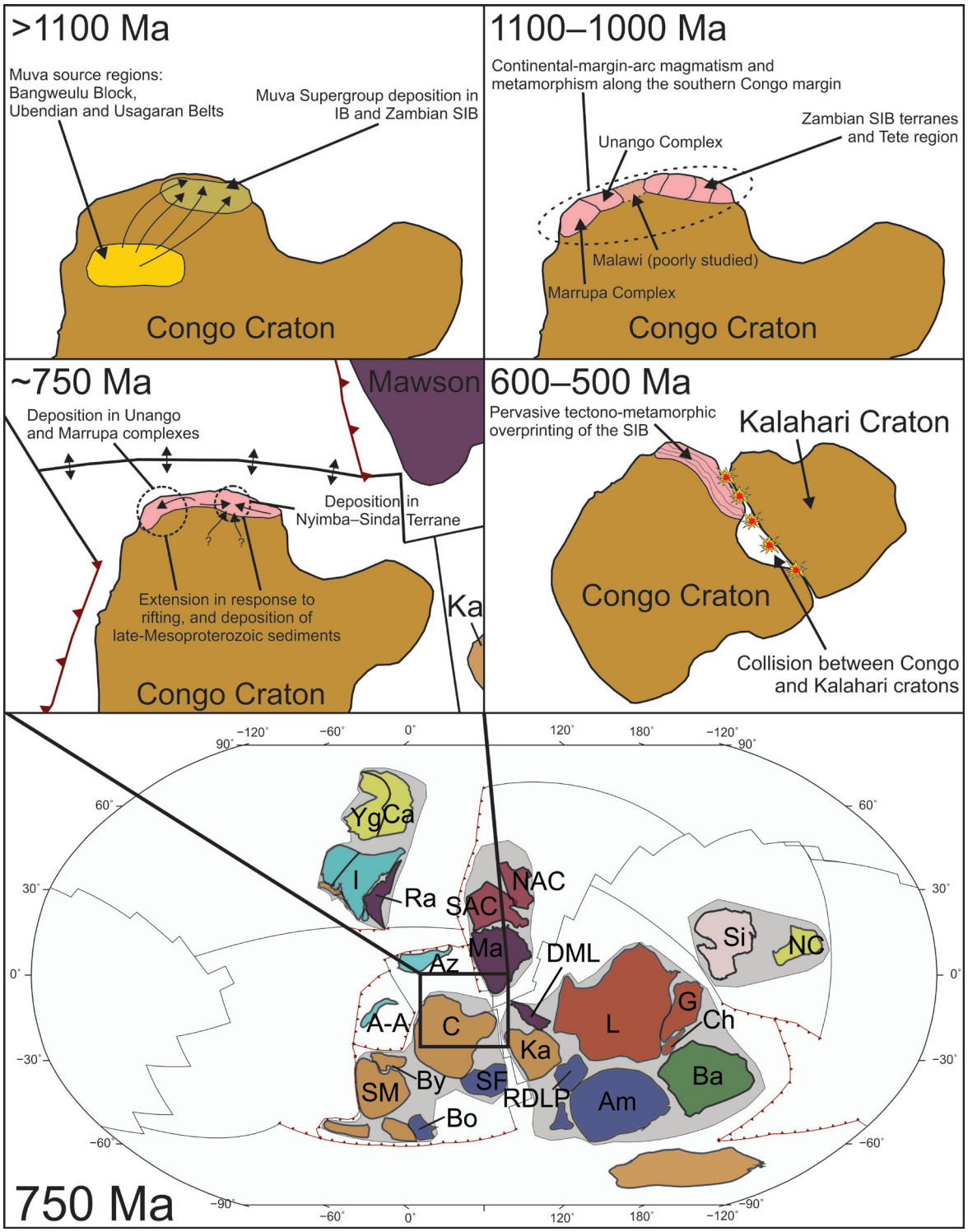

Figure 10. Series of palaeogeographic cartoons showing the interpreted development of the southern Congo margin from *c.* 1100 to 500 Ma. The cartoons depict interpreted sequences of deposition, magmatism, and metamorphism in the SIB, culminating with pervasive overprinting as a result of the collision between the Congo and Kalahari cratons in the later stages of Gondwana amalgamation. The *c.* 750 Ma cartoon is linked to a palaeogeographic reconstruction for the Earth at this time, adapted from Merdith et al. (2017). Yg, Yangtze; Ca, Cathaysia; NC, North China; I, India; Az, Azania; A–A, Afif–Abas; NAC, North Australian Craton; SAC, South Australian Craton; Ma, Mawson; DML, Dronning Maud Land; L, Laurentia; G, Greenland; Ch, Chortis; SM, Sahara Metacraton; By, Bayuda; C, Congo; Ka, Kalahari; Bo, Borborema; SF, São Francisco; RDLP, Rio de la Plata; Am, Amazonia; Ba, Baltica; Si, Siberia.

tions contradict this hypothesis, instead arguing that the SIB collided with the southern Congo margin after forming on the Rushinga microcontinent (Fig. 9; Begg et al., 2009; Johnson et al., 2007b; Johnson et al., 2005). These alternative interpretations cite the likely presence of the Mwembeshi Shear Zone between the two belts (re-activating the suture between the belts), and their contrasting styles of metamorphism. However, rigorous pressure–temperature estimates are not available for most regions in either belt, and recent estimates obtained for the Chipata Terrane instead appear to indicate that both the Irumide and Southern Irumide belts experienced similar pressures of metamorphism during the same period (Karmakar and Schenk, 2016), which may contradict the basis for these interpretations. As such, it remains a plausible scenario that at least the Zambian terranes of the SIB originally formed on the Congo margin and were available for sedimentation from Muva Supergroup sources, similar to sequences in the Irumide Belt (Fig. 10). This suggests that the Palaeoproterozoic basement of the SIB is the same basement to that of the Irumide Belt, and implies the SIB did not form on a discrete micro-continental mass that later collided with the southern Congo margin. The Luangwa Valley (and possibly Mwembeshi Shear Zone) located between the Irumide and Southern Irumide belts may instead reflect the site of thinned continental crust that experienced multiple periods of extension and contraction. We suggest an alternative model where the gap in magmatic ages recorded in the southern Irumide Belt (*c.* 1095–1040 Ma) and Irumide Belt (*c.* 1020 Ma) reflects the magmatic front migrating towards the foreland in response to a shallowing subduction zone. Such a feature is documented in the Andes (Fig. 9; Ramos and Folguera, 2005), with a spatial and temporal gap (~100 km and 40 Ma) in magmatic fronts that is similar to that recorded in the Irumide and Southern Irumide belts. If rifting subsequently separated a micro-continental mass from the southern Congo margin (forming the Rushinga Microcontinent), it would be equivalent to basement located on the southern Congo Craton. The plausibility of these interpretations are dependent on the remaining work to be done to constrain the relationship between the Irumide and Southern Irumide belts.

Detrital zircons from Z14-05 indicate that this sample is part of a cover sequence present within the Nyimba–Sinda terrane that postdates the orogenic events occurring in the SIB and Irumide Belts between *c.* 1095 and 1020 Ma (Johnson et al., 2007b). The extent of this cover sequence is unknown, though it appears to correlate with sedimentary rocks in northeast Mozambique and southern Tanzania, which yield similar age populations and depositional constraints to the analysed sample (Fig. 10; Bingen et al., 2009a; Thomas et al., 2016). This sequence likely includes the extensive carbonates preserved in the Nyimba–Sinda Terrane, with marbles similarly preserved in southern Tanzania. The prominent *c.* 1.0 Ga age peak and isotopic nature of zircons from Z14-05 are consistent with SIB magmatism and possibly crustal melting in the Irumide Belt. Widespread Neoproterozoic gneiss occurs within this terrane, in close association with the potentially rift related volcanic rocks (Barr and Drysdall, 1972; Johnson et al., 2006). This led Johnson et al. (2006) to speculate that this terrane could represent rifting between the Congo and Kalahari cratons. Similarly aged (714 ± 17 Ma) magmatism has been identified in northeast Mozambique (Bjerkgard et al., 2009), which is also interpreted as part of a continental rift related cover sequence (Bingen et al., 2009a). If these sequences do indeed have a rift related origin, then the timing of their formation supports the Neoproterozoic model of Merdith et al. (2017). These authors interpret such rifting along the southern margin of the Congo Craton at this time, occurring as an extension of the spreading system that served to separate the Australian Plate from Laurentia

during the initial breakup of Rodinia (Fig. 10).

CONCLUSIONS

Detrital zircons in metasedimentary rocks of the Chewore–Rufunsa and Kacholola terranes are Palaeoarchaean to Palaeoproterozoic in age and are derived from relatively evolved sources, reflecting the reworking of crustal material. These sedimentary protoliths were deposited between *c.* 1.8 and 1.1 Ga. Similar age peaks and isotopic characteristics of zircon grains from these western terranes of the SIB suggest that they correlate with the Muva Supergroup (or at least share the same sources). Whether the sedimentary protoliths reflect these terranes forming on the edge of the Congo Craton, or instead reflect the deposition of sediments from the same sources on to an advancing Rushinga microcontinent that collided with the Congo Craton, remains unresolved. Further east in the SIB, detrital zircons in metasedimentary rocks of the Nyimba–Sinda Terrane show a marked difference in age, ranging from Palaeoproterozoic to Neoproterozoic. The sedimentary protoliths here were deposited between *c.* 900 and 740 Ma, suggesting that this is a Neoproterozoic cover sequence with correlatives elsewhere within the SIB, in northeast Mozambique and southern Tanzania. Detrital zircons of this terrane display U–Pb ages and εHf(t) values that suggest that they are sourced from *c.* 1095–1040 Ma continental-margin-arc magmatism in the SIB and possibly *c.* 1020 Ma crustal anatexis in the Irumide Belt. Age and depositional constraints indicate that these sedimentary protoliths were deposited after magmatism and metamorphism in the Irumide and Southern Irumide belts. We suggest that this cover sequences, and its correlatives in Mozambique and Tanzania, reflect a history of Neoproterozoic extension that is intermittently recorded throughout the SIB. Such extension is interpreted to reflect rifting occurring on the southern margin of the Congo Craton during initial break up of Rodinia. This study serves to highlight the enigmatic development of much of the SIB, and its relationship to the Irumide Belt. Additional work is required to rigorously constrain the evolution of this region to determine the tectonic implications for the development of the southern Congo Craton and central Gondwana during the Neoproterozoic.

ACKNOWLEDGEMENTS

This paper forms TRaX record #402 and is a contribution to IGCP projects #628 (Gondwana Map) and #648 (Supercontinents and Global Dynamics). This project was funded by Australian Research Council Future Fellowship #FT120100340 to A. Collins. B. Wade, S. Gilbert and A. McFadden of Adelaide Microscopy are thanked for their help with collection of analytical data. B. Alessio is supported by a Research Training Program scholarship. Comments from R. Thomas greatly improved this contribution.

REFERENCES

Agar, R., 1984. Geological Map of the Petauke Area. Geol. Survey Zambia. Government of the United Kingdom (Ordnance Survey).

Archibald, D.B., Collins, A.S., Foden, J.D., Payne, J.L., Macey, P.H., Holden, P., Razakamanana, T., 2017. Stenian–Tonian arc magmatism in west–central Madagascar: the genesis of the Dabolava Suite. Journal of the Geological Society, jgs2017-2028.

Archibald, D.B., Collins, A.S., Foden, J.D., Payne, J.L., Taylor, R., Holden, P., Razakamanana, T., Clark, C., 2015. Towards unravelling the Mozambique Ocean conundrum using a triumvirate of zircon isotopic proxies on the Ambatolampy Group, central Madagascar. Tectonophysics 662, 167-182.

Ashwal, L.D., Tucker, R.D., Zinner, E.K., 1999. Slow cooling of deep crustal granulites and Pb-loss in zircon. Geochimica et Cosmochimica Acta 63, 2839-2851.

Barr, M., Drysdall, A., 1972. The geology of the Sasare area: Explanation of degree sheet 1331, SW Quarter. Government Printer,

South Africa.

Begg, G., Griffin, W., Natapov, L., O'Reilly, S.Y., Grand, S., O'Neill, C., Hronsky, J., Djomani, Y.P., Swain, C., Deen, T., 2009. The lithospheric architecture of Africa: seismic tomography, mantle petrology, and tectonic evolution. Geosphere 5, 23-50.

Bingen, B., Jacobs, J., Viola, G., Henderson, I., Skår, Ø., Boyd, R., Thomas, R., Solli, A., Key, R., Daudi, E., 2009a. Geochronology of the Precambrian crust in the Mozambique belt in NE Mozambique, and implications for Gondwana assembly. Precambrian Research 170, 231-255.

Bingen, B., Jacobs, J., Viola, G., Henderson, I.H.C., Skår, Ø., Boyd, R., Thomas, R.J., Solli, A., Key, R.M., Daudi, E.X.F., 2009b. Geochronology of the Precambrian crust in the Mozambique belt in NE Mozambique, and implications for Gondwana assembly. Precambrian Research 170, 231-255.

Bjerkgard, T., Stein, H., Bingen, B., Henderson, I., Sandstad, J., Moniz, A., 2009. The Niassa Gold Belt, northern Mozambique–A segment of a continental-scale Pan-African gold-bearing structure? Journal of African Earth Sciences 53, 45-58.

Boniface, N., Schenk, V., Appel, P., 2012. Paleoproterozoic eclogites of MORB-type chemistry and three Proterozoic orogenic cycles in the Ubendian Belt (Tanzania): Evidence from monazite and zircon geochronology, and geochemistry. Precambrian Research 192, 16-33.

Boyd, R., Nordgulen, Ø., Thomas, R., Bingen, B., Bjerkgård, T., Grenne, T., Henderson, I., Melezhik, V., Often, M., Sandstad, J., Solli, A., Tveten, E., Viola, G., Key, R., Smith, R., Gonzalez, E., Hollick, L., Jacobs, J., Jamal, D., Motuza, G., Bauer, W., Daudi, E., Feitio, P., Manhica, V., Moniz, A., Rosse, D., 2010. The geology and geochemistry of the East African Orogen in northeastern Mozambique. South African Journal of Geology 113, 87-129.

Brewer, M., Haslam, H., Darbyshire, P., Davis, A., 1979. Rb-Sr Age Determinations in the Bangweulu Block, Luapula Province, Zambia Institute of Geological Sciences, London 79/5.

Burnham, A., Berry, A., 2017. Formation of Hadean granites by melting of igneous crust. Nature Geoscience 10, 457-461.

Collins, A.S., 2003. Structure and age of the northern Leeuwin Complex, Western Australia: constraints from field mapping and U–Pb isotopic analysis. Australian Journal of Earth Sciences 50, 585-599.

Collins, A.S., Pisarevsky, S.A., 2005. Amalgamating eastern Gondwana: the evolution of the Circum-Indian Orogens. Earth-Science Reviews 71, 229-270.

Collins, A.S., Reddy, S.M., Buchan, C., Mruma, A., 2004. Temporal constraints on Palaeoproterozoic eclogite formation and exhumation (Usagaran Orogen, Tanzania). Earth and Planetary Science Letters 224, 175-192.

Collins, A.S., Windley, B.F., 2002. The tectonic evolution of central and northern Madagascar and its place in the final assembly of Gondwana. The Journal of geology 110, 325-339.

Corfu, F., Hanchar, J.M., Hoskin, P.W., Kinny, P., 2003. Atlas of zircon textures. Reviews in mineralogy and geochemistry 53, 469-500.

Cox, R., Armstrong, R.A., Ashwal, L.D., 1998. Sedimentology, geochronology and provenance of the Proterozoic Itremo Group, central Madagascar, and implications for pre-Gondwana palaeogeography. Journal of the Geological Society 155, 1009-1024.

Cox, R., Coleman, D.S., Chokel, C.B., DeOreo, S.B., Wooden, J.L., Collins, A.S., De Waele, B., Kröner, A., 2004. Proterozoic Tectonostratigraphy and Paleogeography of Central Madagascar Derived from Detrital Zircon U-Pb Age Populations. The Journal of geology 112, 379-399.

Cox, R., Rivers, T., Mapani, B., Tembo, D., De Waele, B., 2002. New U-Pb data for the Irumide belt: LAM-ICP-MS results for Lu-

angwa Terrane, 11th IAGOD Quadrennial Symposium and Geocongress, technical meeting IGCP, p. 10.

Daly, M., 1986. The intracratonic Irumide belt of Zambia and its bearing on collision orogeny during the Proterozoic of Africa. Geological Society, London, Special Publications 19, 321-328.

Daly, M., Chakraborty, S., Kasolo, P., Musiwa, M., Mumba, P., Naidu, B., Namateba, C., Ngambi, O., Coward, M., 1984. The Lufilian arc and Irumide belt of Zambia: results of a geotraverse across their intersection. Journal of African Earth Sciences (1983) 2, 311-318.

Daly, M., Unrug, R., 1982. The Muva Supergroup of northern Zambia: a craton to mobile belt sedimentary sequence. Verhandelinge van die Geologiese Vereniging van Suid-Afrika 85, 155-165.

De Waele, B., 2004. The Proterozoic geological history of the Irumide belt, Zambia.

De Waele, B., Fitzsimons, I., 2007. The nature and timing of Palaeoproterozoic sedimentation at the southeastern margin of the Congo Craton; zircon U–Pb geochronology of plutonic, volcanic and clastic units in northern Zambia. Precambrian Research 159, 95-116.

De Waele, B., Fitzsimons, I., Wingate, M., Tembo, F., Mapani, B., Belousova, E., 2009. The geochronological framework of the Irumide Belt: a prolonged crustal history along the margin of the Bangweulu Craton. American Journal of Science 309, 132-187.

De Waele, B., Johnson, S.P., Pisarevsky, S.A., 2008. Palaeoproterozoic to Neoproterozoic growth and evolution of the eastern Congo Craton: Its role in the Rodinia puzzle. Precambrian Research 160, 127-141.

De Waele, B., Kampunzu, A.B., Mapani, B.S.E., Tembo, F., 2006a. The Mesoproterozoic Irumide belt of Zambia. Journal of African Earth Sciences 46, 36-70.

De Waele, B., Liégeois, J.-P., Nemchin, A.A., Tembo, F., 2006b. Isotopic and geochemical evidence of proterozoic episodic crustal reworking within the irumide belt of south-central Africa, the southern metacratonic boundary of an Archaean Bangweulu Craton. Precambrian Research 148, 225-256.

De Waele, B., Mapani, B., 2002. Geology and correlation of the central Irumide belt. Journal of African Earth Sciences 35, 385-397.

De Waele, B., Wingate, M.T., Fitzsimons, I.C., Mapani, B.S., 2003. Untying the Kibaran knot: A reassessment of Mesoproterozoic correlations in southern Africa based on SHRIMP U-Pb data from the Irumide belt. Geology 31, 509-512.

Dhuime, B., Hawkesworth, C., Cawood, P., 2011. When continents formed. Science 331, 154-155.

Finch, R.J., Hanchar, J.M., 2003. Structure and chemistry of zircon and zircon-group minerals. Reviews in mineralogy and geochemistry 53, 1-25.

Fitzsimons, I., Hulscher, B., Collins, A., 2004. Structural, metamorphic and SHRIMP U–Pb age data from the Pan-African of Madagascar: evidence for multi-stage assembly of the East African Orogen, 20th Colloquium of African Geology, BRGM, Orleans, France, p. 164.

Goscombe, B., Armstrong, R., Barton, J., 2000. Geology of the Chewore Inliers, Zimbabwe: constraining the Mesoproterozoic to Palaeozoic evolution of the Zambezi Belt. Journal of African Earth Sciences 30, 589-627.

Griffin, W., Wang, X., Jackson, S., Pearson, N., O'Reilly, S.Y., Xu, X., Zhou, X., 2002. Zircon chemistry and magma mixing, SE China: in-situ analysis of Hf isotopes, Tonglu and Pingtan igneous complexes. Lithos 61, 237-269.

Grimes, C.B., John, B.E., Kelemen, P., Mazdab, F., Wooden, J., Cheadle, M.J., Hanghøj, K., Schwartz, J., 2007. Trace element chemistry of zircons from oceanic crust: A method for distinguishing detrital zircon provenance. Geology 35, 643-646.

Hanson, R., 2003. Proterozoic geochronology and tectonic evolution of southern Africa. Geological Society, London, Special Publications 206, 427-463.

Hauzenberger, C., Tenczer, V., Bauernhofer, A., Fritz, H., Klötzli, U., Košler, J., Wallbrecher, E., Muhongo, S., 2014. Termination of the Southern Irumide Belt in Tanzania: Zircon U/Pb geochronology. Precambrian Research 255, 144-162.

Hawkesworth, C., Kemp, A., 2006. Using hafnium and oxygen isotopes in zircons to unravel the record of crustal evolution. Chemical Geology 226, 144-162.

Hoskin, P., Black, L., 2000. Metamorphic zircon formation by solid-state recrystallization of protolith igneous zircon. Journal of Metamorphic Geology 18, 423-439.

Hoskin, P.W., Ireland, T.R., 2000. Rare earth element chemistry of zircon and its use as a provenance indicator. Geology 28, 627-630.

Hoskin, P.W., Schaltegger, U., 2003. The composition of zircon and igneous and metamorphic petrogenesis. Reviews in mineralogy and geochemistry 53, 27-62.

Jackson, S.E., Pearson, N.J., Griffin, W.L., Belousova, E.A., 2004. The application of laser ablation-inductively coupled plasma-mass spectrometry to in situ U–Pb zircon geochronology. Chemical Geology 211, 47-69.

Johns, C.C., Liyungu, K., Mabuku, S., Mwale, G., Sakungo, F., Tembo, D., Vallance, G., Barr, M.W.C., 1989. The stratigraphic and structural framework of Eastern Zambia: results of a geotraverse. Journal of African Earth Sciences (and the Middle East) 9, 123-136.

Johnson, S., De Waele, B., Evans, D., Banda, W., Tembo, F., Milton, J., Tani, K., 2007a. Geochronology of the Zambezi Supracrustal sequence, southern Zambia: a record of Neoproterozoic divergent processes along the southern margin of the Congo Craton. The Journal of geology 115, 355-374.

Johnson, S., De Waele, B., Liyungu, A., 2006. U-Pb SHRIMP geochronology of granitoid rocks in eastern Zambia: terrane subdivision of the Mesoproterozoic Southern Irumide Belt. Tectonics 25.

Johnson, S.P., De Waele, B., Tembo, F., Katongo, C., Tani, K., Chang, Q., Iizuka, T., Dunkley, D., 2007b. Geochemistry, geochronology and isotopic evolution of the Chewore–Rufunsa Terrane, Southern Irumide Belt: a Mesoproterozoic continental margin arc. Journal of Petrology 48, 1411-1441.

Johnson, S.P., Rivers, T., De Waele, B., 2005. A review of the Mesoproterozoic to early Palaeozoic magmatic and tectonothermal history of south–central Africa: implications for Rodinia and Gondwana. Journal of the Geological Society 162, 433-450.

Karmakar, S., Schenk, V., 2016. Mesoproterozoic UHT metamorphism in the Southern Irumide Belt, Chipata, Zambia: Petrology and in situ monazite dating. Precambrian Research 275, 332-356.

Kirkland, C., Smithies, R., Taylor, R., Evans, N., McDonald, B., 2015. Zircon Th/U ratios in magmatic environs. Lithos 212, 397-414.

Kröner, A., Cordani, U., 2003. African, southern Indian and South American cratons were not part of the Rodinia supercontinent: evidence from field relationships and geochronology. Tectonophysics 375, 325-352.

Ludwig, K., 2004. Users manual for ISOPLOT/EX, version3. 1. A geochronological toolkit for Microsoft Excel. Berkeley Geochronology Center, Special Publication 4.

Maboko, M., 1995. Neodymium isotopic constraints on the protolith ages of rocks involved in Pan-African tectonism in the Mozambique Belt of Tanzania. Journal of the Geological Society 152, 911-916.

Macey, P.H., Thomas, R.J., Grantham, G.H., Ingram, B.A., Jacobs, J., Armstrong, R.A., Roberts, M.P., Bingen, B., Hollick, L., de Kock, G.S., Viola, G., Bauer, W., Gonzales, E., Bjerkgård, T., Henderson, I.H.C., Sandstad, J.S., Cronwright, M.S., Harley, S., Solli, A., Nordgulen, Ø., Motuza, G., Daudi, E.,

Manhiça, V., 2010. Mesoproterozoic geology of the Nampula Block, northern Mozambique: Tracing fragments of Mesoproterozoic crust in the heart of Gondwana. Precambrian Research 182, 124-148.

Mapani, B., Rivers, T., Tembo, F., De Waele, B., Katongo, C., 2004. Growth of the Irumide terranes and slices of Archaean age in eastern Zambia. Geoscience Africa 2004, Abstract 2, 414-415.

Mapani, B., Rivers, T., Tembo, F., Katongo, C., 2001. Terrane mapping in the eastern Irumide and Mozambique belts: implications for the assembly and dispersal of Rodinia, IGCP, pp. 10-11.

McDonough, W.F., Sun, S.-S., 1995. The composition of the Earth. Chemical Geology 120, 223-253.

McGee, B., Halverson, G.P., Collins, A.S., 2012. Cryogenian rift-related magmatism and sedimentation: South-western Congo Craton, Namibia. Journal of African Earth Sciences 76, 34-49.

Merdith, A.S., Collins, A.S., Williams, S.E., Pisarevsky, S., Foden, J.F., Archibald, D., Blades, M.L., Alessio, B.L., Armistead, S., Plavsa, D., 2017. A full-plate global reconstruction of the Neoproterozoic. Gondwana Research.

Möller, A., Appel, P., Mezger, K., Schenk, V., 1995. Evidence for a 2 Ga subduction zone: eclogites in the Usagaran belt of Tanzania. Geology 23, 1067-1070.

Muhongo, S., Kröner, A., Nemchin, A., 2001. Single zircon evaporation and SHRIMP ages for granulite-facies rocks in the Mozambique belt of Tanzania. The Journal of geology 109, 171-189.

Oliver, G., Johnson, S., Williams, I., Herd, D., 1998. Relict 1.4 Ga oceanic crust in the Zambezi Valley, northern Zimbabwe: Evidence for Mesoproterozoic supercontinental fragmentation. Geology 26, 571-573.

Paton, C., Hellstrom, J., Paul, B., Woodhead, J., Hergt, J., 2011. Iolite: Freeware for the visualisation and processing of mass spectrometric data. Journal of Analytical Atomic Spectrometry 26, 2508-2518.

Payne, J.L., Pearson, N.J., Grant, K.J., Halverson, G.P., 2013. Reassessment of relative oxide formation rates and molecular interferences on in situ lutetium–hafnium analysis with laser ablation MC-ICP-MS. Journal of Analytical Atomic Spectrometry 28, 1068-1079.

Pidgeon, R., 1992. Recrystallisation of oscillatory zoned zircon: some geochronological and petrological implications. Contributions to Mineralogy and Petrology 110, 463-472.

Pidgeon, R., Nemchin, A., Hitchen, G., 1998. Internal structures of zircons from Archaean granites from the Darling Range batholith: implications for zircon stability and the interpretation of zircon U-Pb ages. Contributions to Mineralogy and Petrology 132, 288-299.

Plavsa, D., Collins, A.S., Foden, J.D., Clark, C., 2015. The evolution of a Gondwanan collisional orogen: A structural and geochronological appraisal from the Southern Granulite Terrane, South India. Tectonics 34, 820-857.

Plavsa, D., Collins, A.S., Payne, J.L., Foden, J.D., Clark, C., Santosh, M., 2014. Detrital zircons in basement metasedimentary protoliths unveil the origins of southern India. Geological Society of America Bulletin 126, 791-811.

Ramos, V.A., Folguera, A., 2005. Tectonic evolution of the Andes of Neuquén: constraints derived from the magmatic arc and foreland deformation. Geological Society, London, Special Publications 252, 15-35.

Ray, A., 1984. Geological Map of the Rufunsa Area. Geol. Survey Zambia. Government of the United Kingdom (Ordnance Survey).

Reimink, J.R., Davies, J.H., Waldron, J.W., Rojas, X., 2016. Dealing with discordance: a novel approach for analysing U–Pb detrital zircon datasets. Journal of the Geological Society, 2015-2114.

Ring, U., Kröner, A., Toulkeridis, T., 1997. Palaeoproterozoic granulite-facies metamorphism and granitoid intrusions in the Ubendian-Usagaran Orogen of northern Malawi, east-central Africa. Precambrian Research 85, 27-51.

Sarafian, E., Evans, R.L., Abdelsalam, M.G., Atekwana, E., Elsenbeck, J., Jones, A.G., Chikambwe, E., 2018. Imaging Precambrian lithospheric structure in Zambia using electromagnetic methods. Gondwana Research 54, 38-49.

Schandelmeier, H., 1980. Regionale Gliederung des Präkambriums und Aspekte der Krustenentwicklungum Mambwe, Nordost-Zambia. Lenz.

Schandelmeier, H., 1983. The geochronology of post-Ubendian granitoids and dolerites from the Mambwe area, northern province, Zambia. Rep. Inst. Geol. Sci 83, 40-46.

Sláma, J., Košler, J., Condon, D.J., Crowley, J.L., Gerdes, A., Hanchar, J.M., Horstwood, M.S., Morris, G.A., Nasdala, L., Norberg, N., 2008. Plešovice zircon—a new natural reference material for U–Pb and Hf isotopic microanalysis. Chemical Geology 249, 1-35.

Stern, R.J., 2002. Crustal evolution in the East African Orogen: a neodymium isotopic perspective. Journal of African Earth Sciences 34, 109-117.

Thomas, R.J., Bushi, A.M., Roberts, N.M., Jacobs, J., 2014. Geochronology of granitic rocks from the Ruangwa region, southern Tanzania–Links with NE Mozambique and beyond. Journal of African Earth Sciences 100, 70-80.

Thomas, R.J., Spencer, C., Bushi, A.M., Baglow, N., Boniface, N., de Kock, G., Horstwood, M.S., Hollick, L., Jacobs, J., Kajara, S., 2016. Geochronology of the central Tanzania Craton and its southern and eastern orogenic margins. Precambrian Research 277, 47-67.

Tulibonywa, T., Manya, S., Maboko, M.A., 2015. Palaeoproterozoic volcanism and granitic magmatism in the Ngualla area of the Ubendian Belt, SW Tanzania: Constraints from SHRIMP U–Pb zircon ages, and Sm–Nd isotope systematics. Precambrian Research 256, 120-130.

Vavra, G., Schmid, R., Gebauer, D., 1999. Internal morphology, habit and U-Th-Pb microanalysis of amphibolite-to-granulite facies zircons: geochronology of the Ivrea Zone (Southern Alps). Contributions to Mineralogy and Petrology 134, 380-404.

Vayrda, I., 1984. Geological Map of the Chipata Area. Geol. Survey Zambia. Government of the United Kingdom (Ordnance Survey).

Wang, C., Liang, X., Foster, D.A., Fu, J., Jiang, Y., Dong, C., Zhou, Y., Wen, S., Van Quynh, P., 2016. Detrital zircon U–Pb geochronology, Lu–Hf isotopes and REE geochemistry constrains on the provenance and tectonic setting of Indochina Block in the Paleozoic. Tectonophysics 677, 125-134.

Westerhof, A.P., Lehtonen, M.I., Mäkitie, H., Manninen, T., Pekkala, Y., Gustafsson, B., Tahon, A., 2008. The Tete-Chipata Belt: A new multiple terrane element from western Mozambique and southern Zambia. Geological Survey of Finland Special Paper 48, 145-166.

Woodhead, J., Hergt, J., Shelley, M., Eggins, S., Kemp, R., 2004. Zircon Hf-isotope analysis with an excimer laser, depth profiling, ablation of complex geometries, and concomitant age estimation. Chemical Geology 209, 121-135.

CHAPTER 3

This chapter has been published in *The Journal of the Geological Society* as:
Alessio, B.L., Collins, A. S., Clark, C., Glorie, S., Siegfried, P., & Taylor, R. 2019.
Age, origin and palaeogeography of the Southern Irumide Belt, Zambia.

Statement of Authorship

Title of Paper	Age, origin and tectonic geography of the Southern Irumide Belt, Zambia
Publication Status	☑ Published ☐ Accepted for Publication ☐ Submitted for Publication ☐ Unpublished and Unsubmitted w ork w ritten in manuscript style
Publication Details	Alessio, Brandon L., Collins, Alan S., Clark, Chris, Glorie, Stijn, Siegfried, Pete & Taylor, Richard. 2019. Age, origin and tectonic geography of the Southern Irumide Belt, Zambia. Journal of the Geological Society. https://doi.org/10.1144/jgs2018-174

Principal Author

Name of Principal Author (Candidate)	Brandon Luke Alessio		
Contribution to the Paper	Fieldwork, sample preparation, data collection, processing and interpretation, manuscript design and composition, drafting of figures.		
Overall percentage (%)	80		
Certification:	This paper reports on original research I conducted during the period of my Higher Degree by Research candidature and is not subject to any obligations or contractual agreements with a third party that would constrain its inclusion in this thesis. I am the primary author of this paper.		
Signature		Date	07/01/19

Co-Author Contributions

By signing the Statement of Authorship, each author certifies that:

i. the candidate's stated contribution to the publication is accurate (as detailed above);
ii. permission is granted for the candidate in include the publication in the thesis; and
iii. the sum of all co-author contributions is equal to 100% less the candidate's stated contribution.

Name of Co-Author	Alan Collins		
Contribution to the Paper	Fieldwork, guidance in data interpretation and manuscript review.		
Signature		Date	14/01/19

Name of Co-Author	Chris Clark		
Contribution to the Paper	Assistance in data collection and manuscript review.		
Signature		Date	16/01/19

Name of Co-Author	Stijn Glorie		
Contribution to the Paper	Manuscript review.		
Signature		Date	07/01/19

Name of Co-Author	Pete Siegfried		
Contribution to the Paper	Manuscript review.		
Signature		Date	16/01/19

Name of Co-Author	Richard Taylor		
Contribution to the Paper	Assistance in data collection and manuscript review.		
Signature		Date	07/01/19

ABSTRACT

The Southern Irumide Belt (SIB) of Zambia records over one and a half billion years (*c.* 2000 to 500 Ma) of tectonic evolution along the southern Congo Craton margin. To understand this evolution we present U–Pb, Lu–Hf, rare earth element zircon and structural data for the SIB of Zambia, which are used to investigate the formation and evolution of the SIB and its relationship to the Irumide Belt of the southern Congo Craton. Orthogneiss in the Chewore–Rufunsa and Chipata terranes yield ages between *c.* 2040 to 2000 Ma, and are interpreted to represent exposed basement underlying much of the SIB and equivalent to Irumide Belt basement. Detrital zircon data from the Chipata Terrane yield age populations and εHf(t) values that are equivalent to those from other terranes of the SIB and the Irumide Belt. The similarities between basement units and overlying sedimentary sequences in the SIB and Irumide Belt are supportive of the SIB forming on the southern Congo margin, rather than accreting to this margin during the late-Mesoproterozoic. Subsequent structural deformation in this region are attributed to two phases of compression, a N–S directed compression during the late-Neoproterozoic to Cambrian, and a weaker E–W directed compression during the Phanerozoic.

INTRODUCTION

The Southern Irumide Belt (SIB) of Zambia (Fig. 1) consists predominantly of late-Mesoproterozoic igneous rocks that bear a strong Ediacaran–Cambrian overprint, relating to collision between the Congo and Kalahari cratons during Gondwana amalgamation. Located adjacent to the Irumide Belt (sensu stricto; referred to as the Irumide Belt herein) of the Congo Craton, the SIB rocks record over one and a half billion years (*c.* 2000 to 500 Ma) of tectonic evolution of this margin (Collins and Pisarevsky, 2005; De Waele, Johnson and Pisarevsky, 2008; Merdith et al., 2017). This time span included the formation and breakup of Rodinia, as well as the amalgamation of Gondwana. As such, these rocks can be used to understand what role the Congo Craton played in these events (De Waele, Johnson and Pisarevsky, 2008) and in the geodynamic evolution of the Proterozoic (Merdith et al., 2019). In Zambia, the SIB is divided into a series of structurally stacked terranes (Fig, 2), with the western-most terrane (Chewore–Rufunsa) displaying the geochemical and isotopic characteristics of a *c.* 1100–1040 Ma continental-margin-arc (Johnson et al., 2007). The origin and evolution of the other terranes are suggested to be a continuation of this arc, or exotic island arcs that accreted at this time (Mapani et al., 2001; De Waele et al., 2006b; Johnson, De Waele and Liyungu, 2006; Johnson et al., 2007). Johnson et al. (2007) suggest that the SIB formed on a microcontinent that subsequently collided with the Irumide Belt at *c.* 1040 Ma. However, more recent models suggest that the SIB formed as an integral part of the southern Congo margin throughout the Palaeoproterozoic and Mesoproterozoic (Bingen et al., 2009; Alessio et al., 2018). This later model is supported by the correlation of sedimentary sequences located along this margin and within the SIB, which were deposited throughout the Palaeoproterozoic to Mesoproterozoic (Alessio et al., 2018). Understanding the origin and structural history of rocks throughout the SIB can help to validate these models and thereby allow for a better understanding of the evolution of this region. Here, we present new U–Pb, Lu–Hf, rare earth element (REE) zircon and structural data from a transect crossing the Zambian terranes of the SIB, predominantly from the Chewore–Rufunsa and Chipata Terranes. These data are used to (1) understand the internal architecture and evolution of the SIB and (2) compare this to the history of the Irumide Belt.

GEOLOGICAL BACKGROUND

The Congo Craton is defined by De Waele, Johnson and Pisarevsky (2008) as the amalgamated central African landmass at the time of

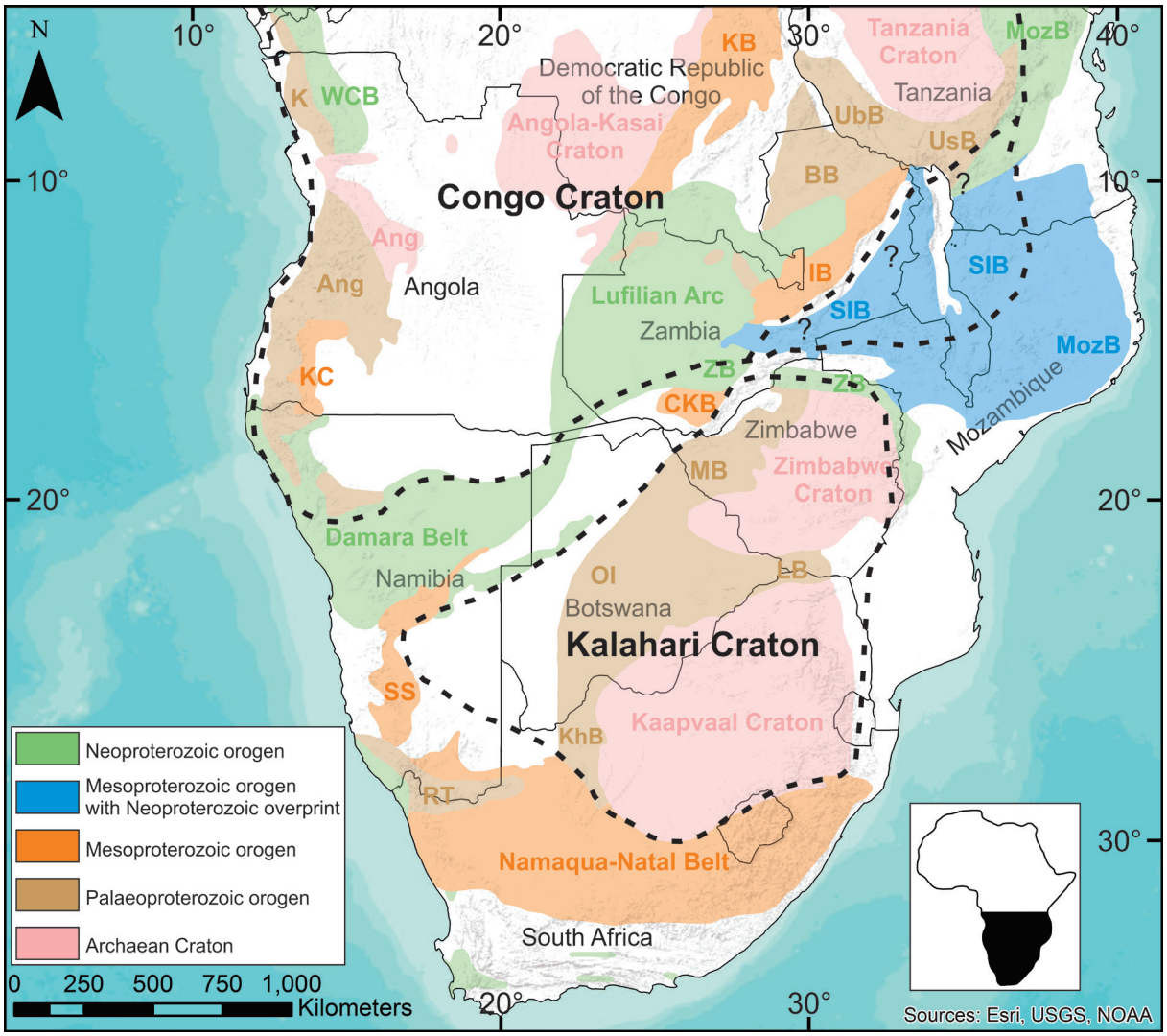

Figure 1. Simplified tectonic map of central Africa adapted from Alessio et al. (2018) following Hanson (2003) and Karmakar and Schenk (2016). The extent of the Congo and Kalahari cratons are denoted by the black dashed lines. Note the two different interpretations for the southern Congo Craton margin between the IB and SIB (see text for further explanation). Abbreviations: ANG, Angola Block; BB, Bangweulu Block; CKB, Choma-Kalomo Block; IB, Irumide Belt; K, Kimezian; KB, Kibaran Belt; KC, Kunene Complex; KhB, Kheis Belt; LB, Limpopo Belt; MB, Magondi Belt; MozB, Mozambique Belt; OI, Okwa Inlier; RT, Richtersveld Terrane; SIB, Southern Irumide Belt; UbB, Ubendian Belt; UsB, Usagaran Belt; WCB, West Congo Belt; ZB, Zambezi Belt.

Gondwana assembly, and contains several Archean to Neoproterozoic tectonic units (Fig. 1). The location of the southern margin of the Congo Craton in Zambia prior to the Neoproterozoic is debated: either it is located between the Irumide Belt and Southern Irumide Belt (e.g. De Waele et al., 2006b; Johnson et al., 2007), or it is located south of the Southern Irumide Belt (Bingen et al., 2009; Alessio et al., 2018, this study; Fig. 1).

Southern Irumide Belt

In Zambia, the SIB comprises four terranes referred to from west to east as: Chewore–Rufunsa, Kacholola, Nyimba–Sinda and Chipata (Fig. 2; Mapani et al., 2004; Johnson, De Waele and Liyungu, 2006; Alessio et al., 2018). These terranes are bound by ductile shear zones of unconstrained age that are suggested to record their imbrication (Johns et al., 1989; Johnson, De Waele and Liyungu, 2006). Subsequent work identified a series of complexes throughout northern Mozambique and South-

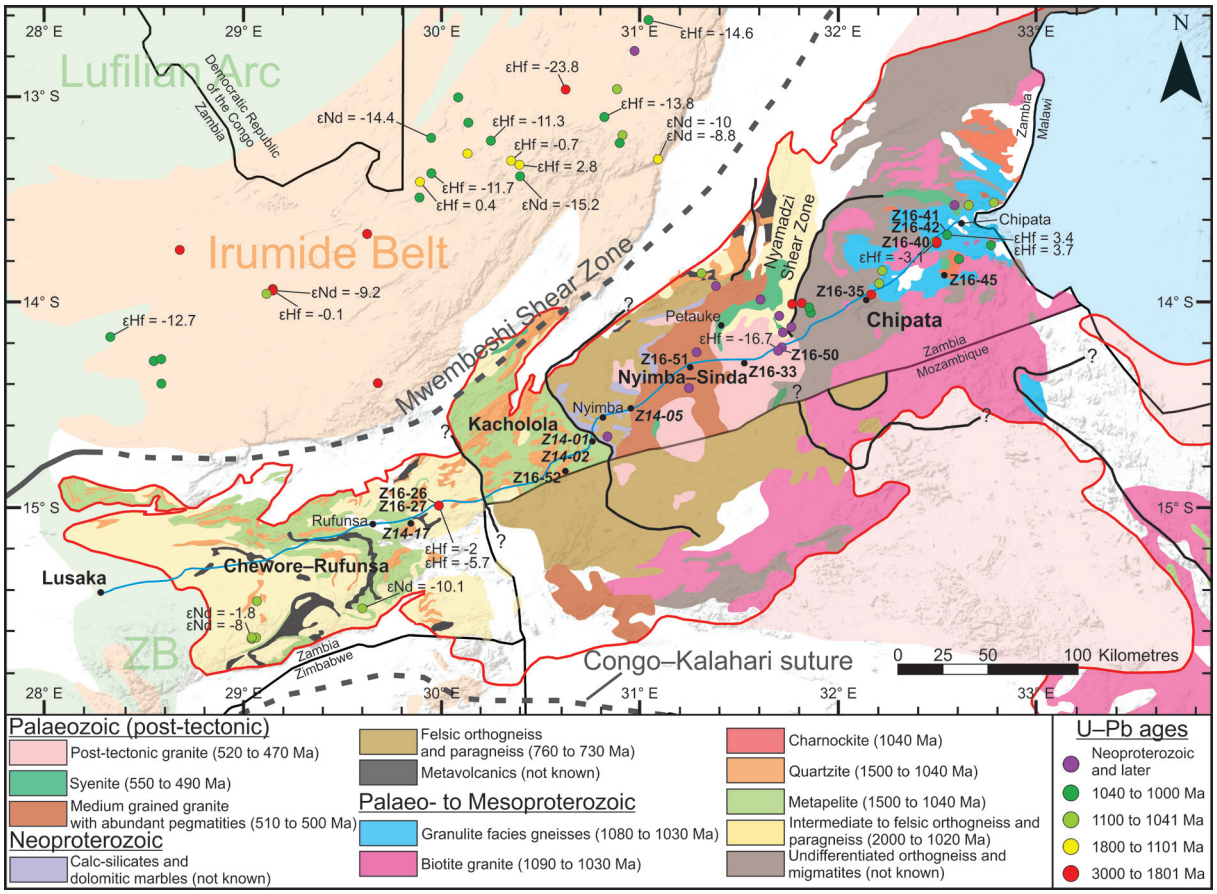

Figure 2. Simplified geological map of eastern Zambia adapted from Alessio et al. (2018) following Johnson, De Waele and Liyungu (2006), with geological units distinguished for the SIB (outlined in red) in Zambia and Mozambique. Samples analysed in this study are located on the map, with samples Z14-01, Z14-02, Z14-05 and Z14-17 from Alessio et al. (2018) also shown in italics. Available age and isotopic data for the Irumide and Southern Irumide belts of Zambia (Johnson, De Waele and Liyungu, 2006; Johnson et al., 2007; De Waele et al., 2009) are also plotted on the map. Lithological data for Zambia are adapted from the Geological Survey of Zambia (Agar, 1984; Ray, 1984; Vayrda, 1984) and Johnson, De Waele and Liyungu (2006). Lithological data for Mozambique is adapted from Westerhof et al. (2008). Shading for Malawi and tectonic units outside of the SIB and Malawi follow the legend in Figure 1. The Great East Road, along which samples and structural measurements were collected, is marked by the blue line.

ern Tanzania that are similar in age and tectonic history to the Zambian terranes, and are likely an extension of the SIB (Bingen et al., 2009; Hauzenberger et al., 2014; Thomas et al., 2016). The rocks within these terranes bear a prominent Ediacaran–Cambrian overprint that reflects collision between the Congo and Kalahari cratons during Gondwana amalgamation at *c.* 550 to 530 Ma (Oliver et al., 1998; Collins and Pisarevsky, 2005; De Waele et al., 2006b; Merdith et al., 2017).

Chewore–Rufunsa

The Chewore–Rufunsa Terrane is largely composed of Mesoproterozoic orthogneiss and metasediments (Fig. 2). Johnson et al. (2007) obtained zircon U–Pb, Lu–Hf, whole-rock REE and Sm–Nd data for meta-igneous rocks in the southern part of the Chewore–Rufunsa Terrane. These data were used to argue that the terrane formed in a continental-margin-arc setting, on a juvenile Palaeoproterozoic basement. Detrital zircon data from a quartzite in this region yields Archaean to Palaeoproterozoic age populations, equivalent to those in the Muva Supergroup found throughout eastern Zambia (Alessio et al., 2018). Rocks throughout this terrane record a late-Mesoproterozoic metamorphic fabric that increases from greenschist in the northern part of the terrane

to granulite facies in the south, and are overprinted by broadly E–W trending Neoproterozoic structural fabrics (Johnson, De Waele and Liyungu, 2006; Johnson et al., 2007). High-pressure metamorphic overprinting is observed in the southern part of this terrane, which can be similarly observed in the adjacent Zambezi Belt and was generated during the late-Neoproterozoic Congo–Kalahari collision (Johnson and Oliver, 1998; John et al., 2004; Alessio and Kelsey, 2018).

Kacholola

The Kacholola Terrane predominantly contains Mesoproterozoic metasediments, with limited exposures of Mesoproterozoic orthogneiss (Fig. 2). Limited data are available from this terrane, though the metasediments here have been shown to be equivalent to that preserved in the adjacent Chewore–Rufunsa Terrane (Johnson, De Waele and Liyungu, 2006; Alessio et al., 2018). Metasediments here are suggested to predominantly record amphibolite facies assemblages, though the timing of this metamorphism is unconstrained. The Kacholola Terrane is suggested to have experienced top to the WNW thrusting over the Chewore–Rufunsa Terrane, though the timing of this event is unknown (Johnson, De Waele and Liyungu, 2006).

Nyimba–Sinda

The Nyimba–Sinda Terrane is distinct from the other Zambian SIB terranes, being comprised of Neoproterozoic gneiss, carbonates, calc-silicates and Cambrian granites (Fig. 2). A metasedimentary rock from this terrane yielded Palaeoproterozoic to Mesoproterozoic detrital zircon populations, suggesting that sediments in this terrane form a rift-related cover sequence that was deposited between *c.* 900 and 740 Ma, and sourced from magmatic units within the SIB (Alessio et al., 2018). Neoproterozoic lithologies in this terrane record late-Neoproterozoic to Cambrian amphibolite facies overprints and NE–SW trending structural fabrics, though the widespread Cambrian granites show little to no evidence of deformation (Johns et al., 1989; Johnson, De Waele and Liyungu, 2006).

Chipata

The Chipata Terrane is predominantly comprised of Mesoproterozoic granite, gneiss and charnockite (Fig. 2). Currently no detrital zircon data are available for this terrane. This terrane records a high-grade, late-Mesoproterozoic tectonometamorphic fabric that reflects pressure–temperature conditions of ~5–6 kbar and 900–1000 °C (Karmakar and Schenk, 2016), likely hotter than the overprints recorded in the other SIB terranes (Johnson, De Waele and Liyungu, 2006). In some areas, this has been overprinted by lower-grade Neoproterozoic metamorphism (Karmakar and Schenk, 2016). Johns et al. (1989) identified a series of deformation events in this region, involving N to NE trending, tight to isoclinal folds. The age of this deformation was suggested to range from Palaeoproterozoic to Cambrian in age, though much of this timing is incompatible with the late–Mesoproterozoic protolith age of rocks in this terrane.

Irumide Belt

The Irumide Belt is located to the north-west of the SIB (Fig. 1), and is a NE–SW trending Mesoproterozoic orogen comprised of Palaeoproterozoic granitic basement, metasedimentary units of the Muva Supergroup, and granitoid intrusions (Daly, 1986; De Waele et al., 2006a; De Waele et al., 2009). Deformation in the belt is interpreted to have occurred at *c.* 1020 Ma and involved amphibolite-facies (7 to 8 kbar and ~650 °C) metamorphism, large-scale structural overprinting, and intrusion of primarily calc-alkaline granitoids (De Waele, 2004; De Waele et al., 2006a). Notably, this belt lacks the pervasive Ediacaran–Cambrian tectonometamorpic overprint recorded in the SIB (De Waele et al., 2009). De Waele et al. (2006b) obtained Sm–Nd isotopic data for granitoids

Table 1. Summary of samples analysed in this study.

Sample number	Latitude (S)	Longitude (E)	Description	Analytical data presented
Chewore-Rufunsa Terrane				
Z16-26	14° 59' 09"	29° 59' 11"	Quartz-K feldspar-Biotite-Garnet gneiss	Zircon U-Pb, Lu-Hf, REE
Z16-27	14° 59' 09"	29° 59' 11"	Plagioclase-Quartz-Biotite gneiss	Zircon U-Pb, Lu-Hf, REE
Kacholola Terrane				
Z16-52	14° 53' 24"	30° 36' 09"	Quartz-K feldspar-Plagioclase gneiss	Zircon REE
Nyimba Sinda Terrane				
Z16-33	14° 18' 06"	31° 32' 09"	Granite	Zircon Lu-Hf and whole-rock geochemistry
Z16-50	14° 14' 08"	31° 41" 48'	Granite	Zircon U-Pb, REE and whole-rock geochemistry
Z16-51	14° 19" 16'	31° 15" 32'	Granite	Whole-rock geochemistry
Chipata Terrane				
Z16-35	13° 59" 38'	32° 08" 04'	Quarzite	Zircon U-Pb, Lu-Hf, REE
Z16-40	13° 42" 25'	32° 29" 21'	Quartz-K feldspar-Plagioclase-Garnet gneiss	Zircon U-Pb, Lu-Hf, REE
Z16-41	13° 40" 23'	32° 32" 57'	Clinopyroxene charnockite	Zircon U-Pb, Lu-Hf, REE
Z16-42	13° 40" 23'	32° 32" 57'	Clinopyroxene-Garnet charnockite	Zircon U-Pb, Lu-Hf, REE
Z16-45	13° 52" 53'	32° 22" 22'	Biotite granite	Zircon REE

across the belt. These authors noted a lack of juvenile material and interpreted this to suggest that the Irumide Belt formed a passive margin prior to *c.* 1040 Ma, and acted as the boundary of the Congo Craton. These authors inferred that the coeval active margin was further to the present-day south and is represented by the SIB.

METHODS

Structural data and samples for geochronology and geochemistry (Table 1) were collected along a W–E transect across all four terranes of the Zambian SIB, predominantly following the Great East Road from Lusaka to Chipata (Fig. 2). Structural data are plotted on lower-hemisphere equal-area stereographic projections. Zircon trace element and isotopic data were acquired at the John de Laeter Centre, Curtin University (Western Australia). Whole-rock geochemical analyses of granite samples Z16-33, Z16-50, and Z16-51 were undertaken using X-ray fluorescence (XRF) at Franklin and Marshall College (United States).

Zircon analysis

Trace element and isotopic data were obtained from separated zircon grains that were extracted from crushed rocks using standard magnetic and heavy liquid techniques. Zircon separates were hand-picked, mounted in epoxy resin and then polished to expose the grains. The grains were imaged on an FEI Quanta 600 Scanning Electron Microscope (SEM) using a Gatan cathodoluminescence (CL) detector to identify compositional domains that were suitable for analysis. Zircon grains were analysed for U–Pb isotopes and trace elements via split stream LA–ICP–MS, using a Resonetics RESOlution laser ablation system connected to an Agilent 7900 quadrupole mass spectrometer and a Nu Instruments Nu Plasma II multi-collector. U–Pb isotopes were measured using MC–ICP–MS, while trace elements were measured in tandem using quadrupole ICP–MS. Ablation of zircon was performed in a He atmosphere with a frequency of 5 Hz. A spot size of 30 μm was used for all analyses. A total acquisition time of 80 seconds was used consisting of 10 seconds of spot pre-ablation, 40 seconds of background acquisition and 30 seconds of sample ablation. The Standard GJ ($^{206}Pb/^{238}U$ = 608.5 ± 0.4 Ma; Jackson et al. (2004)) was used as the primary standard for all zircon analyses, while Plešovice ($^{206}Pb/^{238}U$ = 337.13 ± 0.37 Ma; Sláma et al. (2008)) and 91500 ($^{206}Pb/^{238}U$ = 1065.4 ± 0.6 Ma; Wiedenbeck et al. (1995)) were used as secondary standards. Standard glass NIST SRM 610 was used during trace element analysis as a reference material for corrections to mass bias drift. Throughout this study Plešovice yielded a 95% concordant average $^{206}Pb/^{238}U$ age of 340.1 ± 3.4 Ma (2σ, n = 10), 91500 yielded a 95% concordant average $^{206}Pb/^{238}U$ age of 1061.6 ± 3.4 Ma (2σ, n = 20). Zircon data were reduced using IOLITE (Paton et al., 2011).

Lu–Hf isotope analysis in zircon was conducted using the Nu Plasma II multi-collector, with no split streaming to the quadrupole ICP–MS.

Zircons were ablated in a helium atmosphere, which was mixed with argon upstream of the ablation cell. Individual analyses consisted of two cleaning pulses, followed by 40 seconds of background acquisition and 20 seconds of sample ablation with a 10 Hz repetition rate, and beam intensity of ~2.8 to 3 J/cm^2. A spot size of ~50 μm was used, and was centred over previously ablated U–Pb and trace element spots. Data were normalised to $^{179}Hf/^{177}Hf$ = 0.7325, Yb and Lu isobaric interferences on 176Hf were corrected for following the methodology of Woodhead et al. (2004). Reduction of Lu–Hf data was done using IOLITE (Paton et al., 2011). Known standards were run throughout the analytical session to verify the stability and performance of the instrument. The primary standard used for Hf isotopes was Mud Tank, which yielded a mean $^{176}Hf/^{177}Hf$ ratio of 0.282506 ± 0.00001 (2σ, n = 29). This is within uncertainty of the known value of 0.282507 ± 0.000006 provided by Woodhead and Hergt (2005).

RESULTS

Zircon U–Pb and Lu–Hf isotopes

A series of samples from the Chewore–Rufunsa, Nyimba–Sinda and Chipata terranes of the SIB were analysed for their U–Pb and Lu–Hf isotopes (Table 1; Fig. 2). Attempts were made to obtain similar data from the Kacholola terrane, though the obtained data are poor and as a result are not presented.

Z16-26: Chewore–Rufunsa gneiss

Sample Z16-26 is a felsic orthogneiss obtained from the Chewore–Rufunsa terrane, approximately 40 km NE of Rufunsa along the Great East Road (Fig. 2). From this sample, 23 zircon analyses were obtained. Eleven of them are ≥ 90 % concordant and display variable ages between *c.* 2670 and 2030 Ma (Figure 3a). The six youngest of these appear to display a Pb loss trend with an upper intercept age of 2035 ± 25 Ma (N = 6; MSWD = 7). While there is significant uncertainty in this calculated age due to the high MSWD and relatively few grains used to produce this upper concordia intercept, we interpret these analyses to broadly represent the crystallisation of the igneous protolith to this sample, with the older grains representing inherited grains. Obtained εHf(t) values for this sample are displayed in Figure 4a and are predominantly evolved (reflecting the recycling of crustal material as opposed to being mantle derived) for the grains that are interpreted to have crystallised with the protolith, ranging from approximately –2 to –10. Grains that are interpreted as inherited are plotted at their individual crystallisation ages, and are again isotopically evolved. The oldest analysed grain at *c.* 2.7 Ga is the most juvenile, with an upper error limit of approximately +2.

Z16-27: Chewore–Rufunsa intrusive

Sample Z16-27 is from a granodiorite that intrudes the orthogneiss represented by sample Z16-26. Forty-one analyses were obtained from this sample, with 23 being ≥ 90 % concordant. The concordant analyses are displayed in Figure 3b, and demonstrate a similar range of ages to those recorded in the host gneiss. The five oldest analyses ranging from *c.* 2670 to 2170 Ma are interpreted as inherited, while the younger analyses are likely forming a Pb loss trend that relates to the crystallisation of the rock. The 13 youngest analyses produce an upper intercept age of 2000 ± 9 Ma (N = 13; MSWD = 4.3; Fig 3b). This in interpreted as a broad estimate of the crystallisation age of this rock that is consistent with the context of the rock, which intrudes the older gneiss (Z16-26). εHf(t) values (Fig. 4a) for grains interpreted to have crystallised with the rock range from +4 to –14 and are more variable than those analysed from the host gneiss (Z16-26), extending to more juvenile values. The two oldest inherited grains in this sample are the most juvenile, with εHf(t) values ranging from approximately +11 to +2.

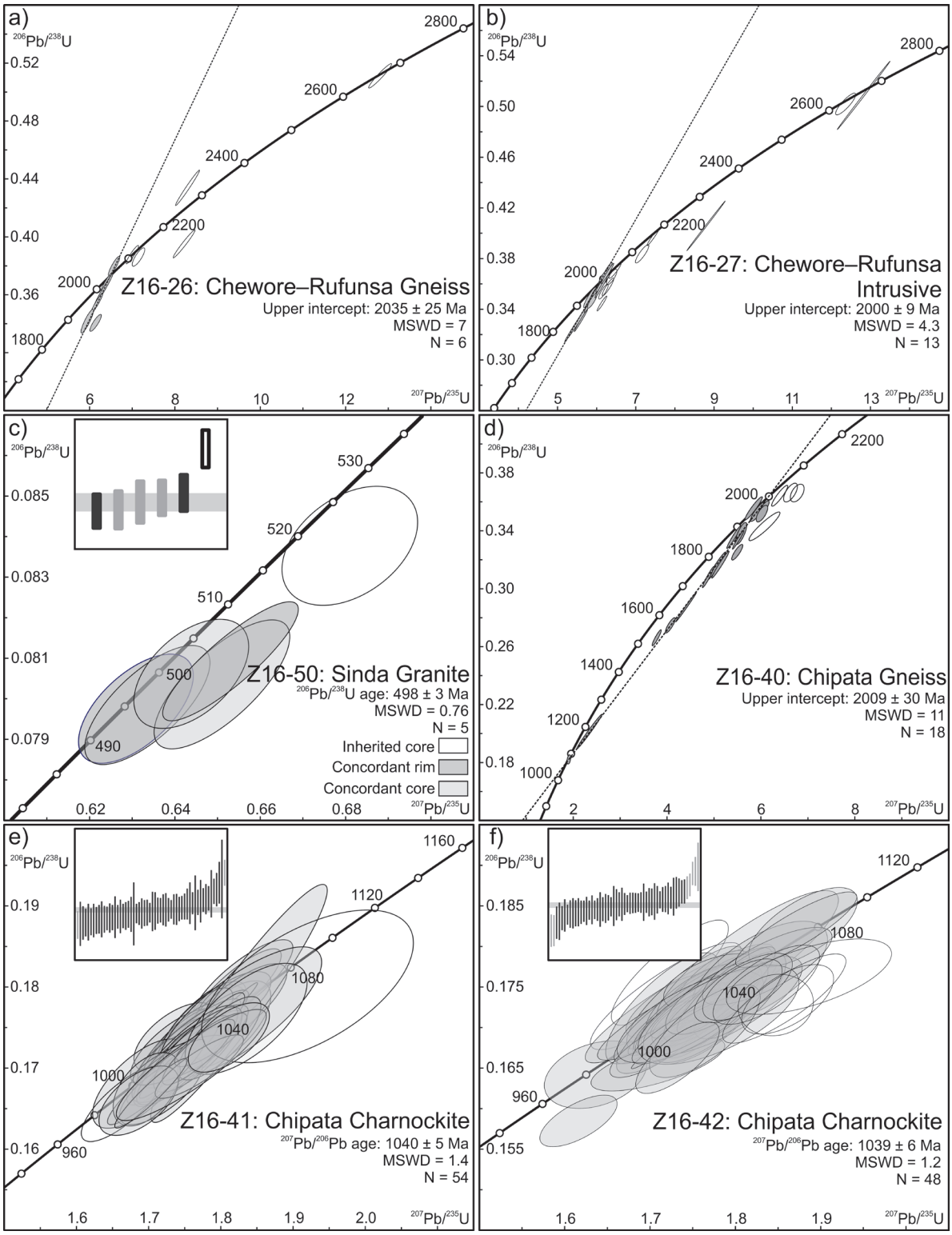

Figure 3. U–Pb concordia diagrams for zircon in samples from the SIB. Only analyses with concordance ≥ 90 % are plotted. Analyses used for final age calculation are shaded in grey, with interpreted Pb loss chord indicated by the dashed line. a) Sample Z16-26 from the Chewore–Rufunsa Terrane. b) Sample Z16-27 from the Chewore-Rufunsa terrane. c) Sample Z16-50 from the Nyimba-Sinda terrane. Inset displays individual $^{206}Pb/^{238}U$ ages, with ages used in final age calculation shaded grey for zircon cores and black for zircon rims. d) Sample Z16-40 from the Nyimba-Sinda terrane. e) Sample Z16-41 from the Chipata terrane. Inset displays $^{207}Pb/^{206}Pb$ ages, with ages used in final age calculation shaded black. d) Sample Z16-42 from the Chipata terrane. Inset displays $^{207}Pb/^{206}Pb$ ages, with ages used in final age calculation shaded black.

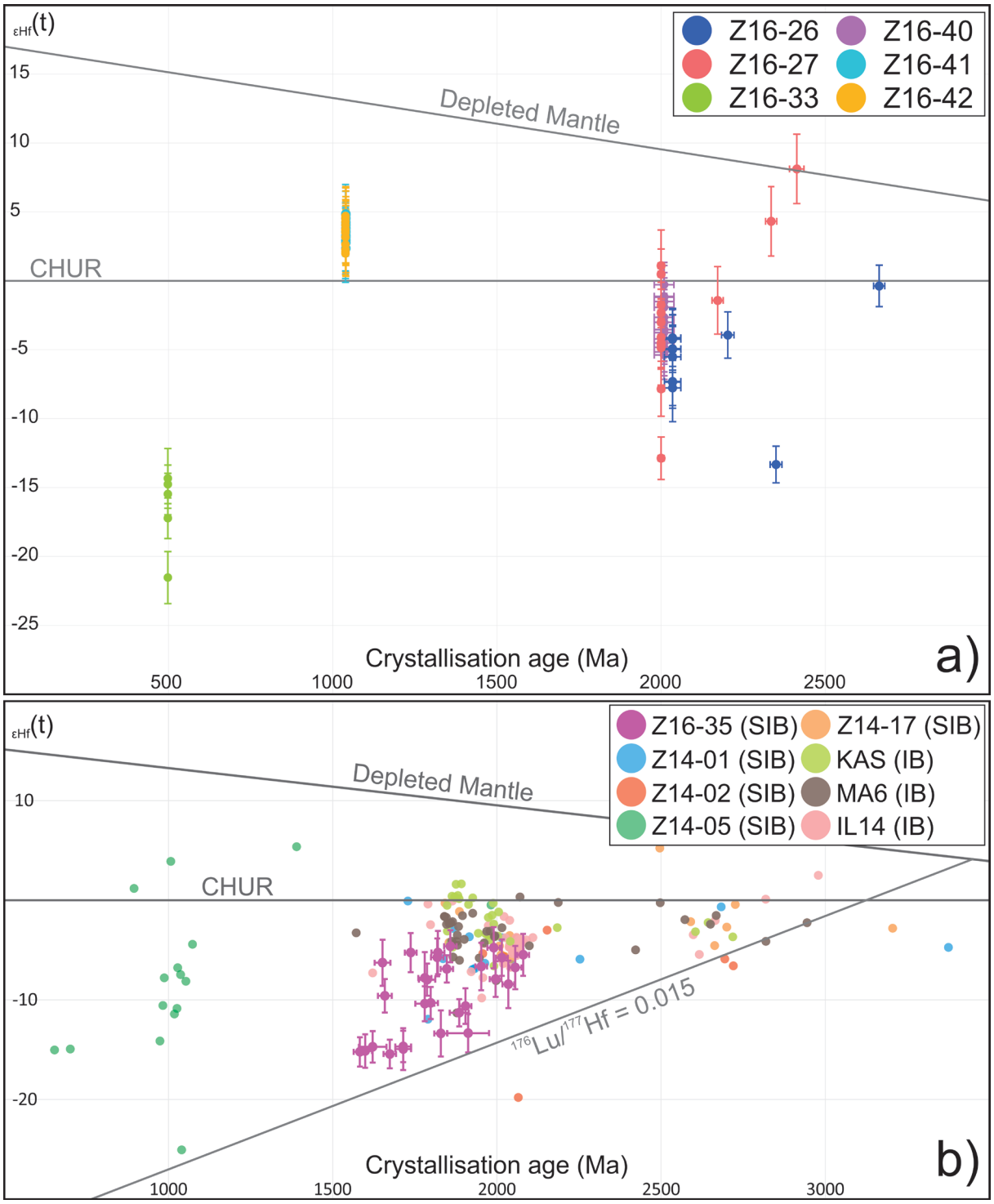

Figure 4. εHf(t) versus U–Pb age plots with uncertainties for age and εHf(t) values are shown at the 2σ level. The depleted mantle curve of Griffin et al. (2002) is plotted. a) εHf(t) versus U–Pb age plot for zircon samples recording crystallisation or protolith ages. εHf(t) values are plotted at the interpreted crystallisation age for each sample, with the exception of grains interpreted as inherited in samples Z16-26 and Z16-27. b) εHf(t) versus U–Pb age plot for detrital zircon sample Z16-35 from the Chipata terrane. Also plotted are additional detrital zircon data obtained by Alessio et al. (2018) from the Irumide Belt (IB) and SIB.

Z16-50 and Z16-33: Sinda Granite

A sample of the post-tectonic Sinda Granite (Z16-50) was obtained from the Nyimba-Sinda terrane, approximately 7 km west of Sinda village (Fig. 2). From 62 obtained analyses, only six were ≥ 90% concordant and are displayed

in Figure 3c. Two of the concordant analyses were obtained from zircon rims that display no discernible age difference to the concordant cores. The oldest of these concordant analyses is interpreted to represent inheritance, and has been excluded from age calculations. The remaining five analyses yield a weighted average $^{206}Pb/^{238}U$ age of 498 ± 3 Ma, with an MSWD of 0.76. Such an age is within error of previous values (504 ± 7 Ma) provided by Johnson, De Waele and Liyungu (2006), and is interpreted as a reliable estimate of the crystallisation age of this sample. An additional sample (Z16-33) of this granite was dated, though yielded insufficient concordant data to produce a rigorous age constraint. Using the calculated age of 497.9 Ma, the εHf(t) values recorded by this sample (Fig. 4a) are the lowest obtained in the study, being highly evolved and ranging from –12 to –23.

Z16-40: Chipata gneiss

Z16-40 was obtained from a felsic orthogneiss within the Chipata terrane, approximately 20 km SW of Chipata along the Great East Road (Fig. 2). Sixty-one analyses were obtained for this sample, with 22 being ≥ 90% concordant. The concordant analyses are plotted in Figure 3d, from these analyses, 18 are interpreted to form a distinct Pb loss trend. The remaining four analyses reflect inheritance between 2140 and 2060 Ma. A calculated upper intercept of the 18 analyses defining the main Pb loss trend yields an age of 2009 ± 30 Ma with an MSWD of 11, which is interpreted as the crystallisation age of the igneous protolith. Lu–Hf data were obtained for zircon grains interpreted to have formed with the protolith (Fig. 4a), and yield broadly evolved εHf(t) values that range from approximately +2 to –7.

Z16-41: Chipata Charnockite

Sample Z16-41 is from a charnockite of the Chipata terrane located approximately 10 km west of Chipata along the Great East Road (Fig. 2). Sixty analyses were obtained from this sample, with 56 being ≥ 90 % concordant (Fig. 3e). The range of individual $^{206}Pb/^{238}U$ grain ages span from 1054 ± 67 Ma to 988 ± 21 Ma. Fifty-four analyses yield a weighted mean $^{206}Pb/^{238}U$ age of 1027 ± 6 Ma (MSWD = 4.2). A $^{207}Pb/^{206}Pb$ age, instead, yields a slightly older age of 1040 ± 5 Ma with a better MSWD of 1.4. This suggests that the zircons may reflect small amounts of modern Pb loss and as such this $^{207}Pb/^{206}Pb$ age is taken as the best estimate of the crystallisation of the charnockite protolith. The obtained εHf(t) values for this sample range from approximately +7 to 0 (Fig. 4a) with most analyses plotting at approximately +4.

Z16-42: Chipata Charnockite

Z16-42 is from a charnockite obtained from the same area as charnockite sample Z16-41. Sixty analyses were obtained for this sample, of which 55 were ≥ 90 % concordant. The concordant analyses are presented in Figure 3f and are similar to those from sample Z16-41. Individual $^{206}Pb/^{238}U$ grain ages in this sample range from 1080 ± 22 Ma to 980 ± 19 Ma, largely overlapping the previous sample. Much like the previous sample a spread of ages is apparent and because of this we consider the $^{207}Pb/^{206}Pb$ to provide a more reliable age estimate. Inspection of the $^{207}Pb/^{206}Pb$ ages resulted in the exclusion of the five oldest and two youngest ages due to being inherited or subjected to Pb loss, respectively. The remaining 48 analyses yield a weighted average $^{207}Pb/^{206}Pb$ age of 1039 ± 6 Ma (MSWD = 1.2), which is taken as the best estimate of a single crystallisation age and is within error of the calculated age for sample Z16-41. εHf(t) values for this sample (Fig. 4a) are nearly identical to the previous charnockite sample, ranging from approximately +7 to 0 and most samples plotting at +3.

Z16-35: Chipata Quartzite

A sample of quartzite was selected approximately 10 km NE of Katete along the Great

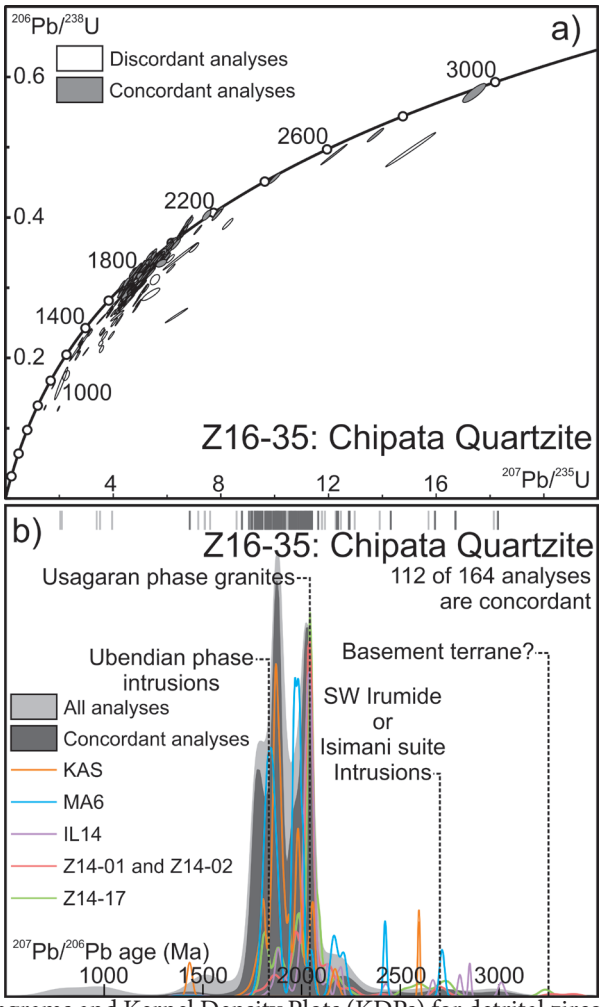

Figure 5. U–Pb concordia diagrams and Kernel Density Plots (KDPs) for detrital zircon in quartzite sample Z16-35 from the Chipata terrane. a) Concordia diagram. Analyses with concordance ≥ 90 % are shaded grey. b) KDPs with 207Pb/206Pb ages plotted for all analyses in light grey and analyses with concordance ≥ 90 % in dark grey. Outlines of detrital zircon data from Alessio et al. (2018) for the Irumide Belt (KAS, MA6 and IL14) and SIB (Z14-01 and Z14-02, Z14-17) are shown by the coloured distributions. Likely sources are indicated by the dashed lines.

East Road within the Chipata Terrane (Fig. 2). U–Pb analyses were performed in 164 detrital zircon cores (Fig. 5a). Amongst them, 112 analyses were ≥ 90 % concordant, and ranging in age from 2992 ± 19 Ma to 1434 ± 22 Ma. The Kernel Density Plot (KDP) for this sample (Fig. 5b) displays prominent peaks at *c.* 2030, 1910 and 1790 Ma. From the analysed grains, the youngest ≤ 10 % discordant analysis yielded a $^{207}Pb/^{206}Pb$ age of 1434 ± 22 Ma (2σ uncertainty) that is interpreted to represent an estimate of the maximum depositional age of this sample. Hafnium data for 30 of the *c.* 2100–1600 Ma analyses are presented in Figure 4b. Obtained εHf(t) values for this sample are all negative with none of the analyses being within error of a positive value. The overall range of εHf(t) values range from approximately –3 to –17.

Geochemistry

Zircon trace element composition

Rare earth element (REE) data were obtained for zircon samples from each terrane of the SIB. Zircons from variably deformed igneous lithologies of the Chewore–Rufunsa, Nyimba–Sinda and Chipata terranes display REE concentrations typical of zircon from a wide range of lithologies and tectonic environments (Hoskin and Ireland, 2000). All samples analysed from these terranes display a general increase in elemental abundance with increas-

ing atomic mass. Sample Z16-50 from the Cambrian Nyimba–Sinda granite additionally includes analyses indicating a negative Sm anomaly that is distinct from all other samples.

Nyimba–Sinda granite

Major and trace element geochemistry were obtained for three samples of granite from the Nyimba–Sinda Terrane, two of which were fine-grained (Z16-33 and Z16-51) and the third being coarser-grained (Z16-50). All samples were identified as A-type granites using the $K_2O + Na_2O$ differentiation scheme of Whalen, Currie and Chappell (1987). All samples display trace element concentrations that indicate decreasing elemental abundance with increasing atomic mass, with the fine-grained samples displaying negative anomalies in Th, Nb, and Y. Z16-51, additionally, displays a unique positive Sr anomaly. The coarse-grained sample displays broadly similar concentrations to the fine-grained samples, though with an overall higher abundance. Notably, this sample displays positive Th and Y anomalies as opposed to the negative anomalies visible in the other samples.

Structural geology

Structural data were obtained from an E–W transect of the SIB in order to constrain the broad-scale structural overprints recorded. Measurements were taken along the Great East Road. Foliation (gneissic and schistose) measurements were largely taken from the Mesoproterozoic orthogneiss and metasediments found throughout the SIB. Original bedding was observed a number of times in psammitic and quartzitic layers of the Mesoproterozoic metasediments, and is generally consistent with nearby foliation. Crenulation cleavages were measured from metapelite layers in the Chewore–Rufunsa Terrane and intersect foliations in these rocks. Recorded lineations are mineral lineations, likely parallel to related fold axes. The data are presented in Figure 6, in conjunction with structural measurements obtained during the mapping campaigns of the GTK consortium (Manninen et al., 2006) and the Geological Survey of Zambia (Agar, 1984; Ray, 1984; Thieme, 1984; Vayrda, 1984). Due to the density of measurements from other studies, representative values have been projected (moved north or south) onto equally spaced E–W lines. Bedding, foliation and cleavage measurements from the Chewore–Rufunsa terrane (Fig. 6c) strike broadly E–W. A significant number of broadly N–S striking foliation measurements were also obtained. Similarly, mineral lineation measurements are dominantly E–W plunging, though a number of SE plunging lineations were recorded. Bedding and foliation measurements from the Kacholola terrane (Fig. 6d) are generally shallow dipping and predominantly E–W striking, though several N–S striking measurements are also recorded. A number of NE to E plunging mineral lineations were recorded in this terrane, in addition to a number of consistently NW plunging measurements and a single SE measurement. Bedding and foliation measurements obtained from the Chipata terrane (Fig. 6e) are broadly similar to those from the Kacholola terrane, though a number of more steeply dipping (> 70°), approximately N–S striking, measurements were also recorded. All recorded mineral lineations from this terrane are approximately north-plunging, often at an angle of ~40°. The obtained data are used to extrapolate bedding and foliation trends throughout the SIB (Fig. 6a), incorporating the previous trends identified by Johns et al. (1989). These trends agree well with structures observed on available satellite imagery and are indicative of two phases of regional folding (Fig. 6b). The first phase (F_1) is identified as series of broadly NE–SW trending folds, which can be interpreted to extend from the Chewore–Rufunsa Terrane across terrane boundaries through to the Chipata terrane and further beyond. In the Chipata Terrane, early work by Johns et al. (1989) described the folds generated in this phase as tight to isocli-

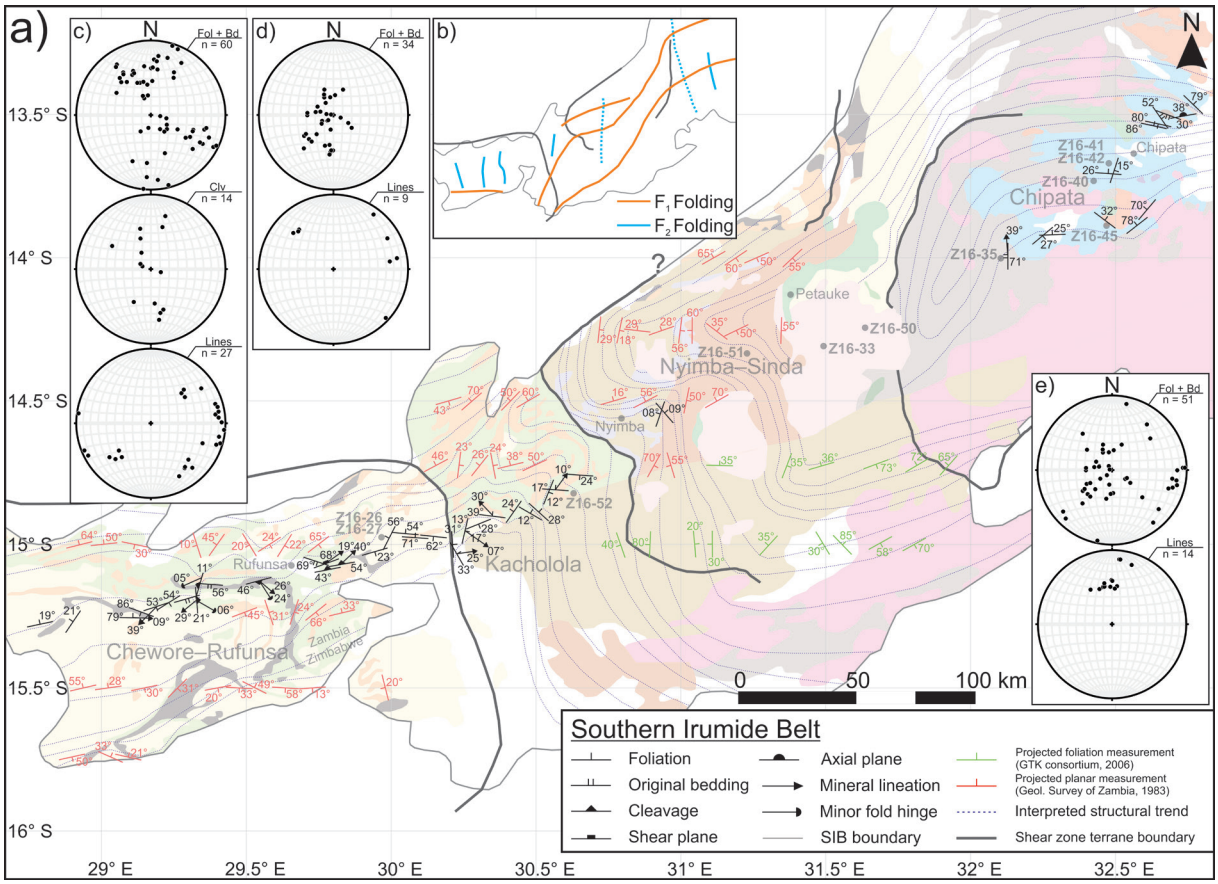

Figure 6. Structural diagram of the Zambian SIB terranes. a) Structural map displaying representative measurements obtained in this study, as well as measurements previously obtained by the Geological Survey of Zambia and GTK mapping consortium (Agar, 1984; Ray, 1984; Thieme, 1984; Vayrda, 1984; Manninen et al., 2006). The dashed blue lines represent foliation strike trends interpreted from the available structural data, satellite imagery and previous interpretations of Johns et al. (1989). b) Interpreted axial plane traces throughout the SIB. The blue lines reflect approximately N–S trending folds, while the orange lines reflect a separate phase of broadly NE–SW trending folds. c) Stereonets displaying structural data (Poles to foliation and bedding, poles to cleavage, mineral lineations) obtained from the Chewore–Rufunsa Terrane during this study. d) Stereonets displaying structural data (Poles to foliation and bedding, mineral lineations) obtained from the Kacholola terrane during this study. e) Stereonets displaying structural data (Poles to foliation and bedding, mineral lineations) obtained from the Chipata Terrane during this study.

nal, which is broadly consistent with the available data for the other terranes that indicate close to tight folding. Structural trends related to these folds agree well between terranes, which are bound by ductile shear zones that in many instances conform to the interpreted structural trend. One exception exists between the southern shear zone between the Nyimba–Sinda and Chipata terranes that continues into Mozambique, though this may reflect the inaccuracy of interpreted shear zones in that region. The second phase of folding (F_2) is indicated by a series of approximately N–S trending folds that do not cross any of the terrane boundaries, though their presence in each terrane suggests that they were formed after their amalgamation. These folds, being open and lower amplitude than those attributed to F_1 folding are suggested to overprint the more prominent NE–SW trending F_1 folds. Both F_1 and F_2 folds are developed in Neoproterozoic gneisses of the Nyimba–Sinda Terrane, implying that these structures post-date the protolith age for the gneiss of *c.* 760–730 Ma.

DISCUSSION

Age and origin of SIB terranes

Chewore–Rufunsa

U–Pb data from an orthogneiss as well as an intruding granodiorite from the Chewore–Rufunsa Terrane yield upper concordia intercepts of 2035 ± 25 Ma and 2000 ± 9 Ma, respectively (Fig. 3a,b). Both obtained ages are interpreted as crystallisation ages and indicate the presence of Palaeoproterozoic basement in this terrane. Similar ages were previously obtained by Johnson et al. (2007) from orthogneiss located in the southern Chewore–Rufunsa Terrane. However, these were interpreted as xenocryst ages and accompanied by analyses yielding crystallisation ages of *c.* 1050 to 1100 Ma. More recently, Palaeoproterozoic detrital cores were also identified in quartzite from the Chewore–Rufunsa and Kacholola terranes (Alessio et al., 2018). As such the dated lithologies could represent exposed Palaeoproterozoic basement in the northern Chewore–Rufunsa Terrane that is broadly equivalent in age to some of the oldest magmatism in the Irumide Belt (De Waele et al., 2006b). Predominantly negative εHf(t) values suggest the analysed rocks to be isotopically evolved (Fig. 4a), similar to the Irumide Belt, and reflect the reworking of existing material with minor mantle input.

Nyimba–Sinda

The Nyimba–Sinda Terrane uniquely contains widespread Neoproterozoic to Cambrian granites and gneiss. While late-Mesoproterozoic and Palaeoproterozoic ages have been obtained from rocks in this terrane, they are far less widespread (Figs. 2, 7). A U–Pb crystallisation age of 498 ± 3 Ma was obtained for the Sinda Granite (Fig. 3c), within error of previous estimates obtained by Johnson, De Waele and Liyungu (2006). Major and trace element geochemistry obtained for the granite confirms it to be an A-type granite that intruded post Congo–Kalahari collision. εHf(t) values (Fig. 4a) suggest little mantle input and that the rock largely reflects the reworking of pre-existing material within the terrane. While the isotopic nature of Palaeoproterozoic basement in this terrane is yet to be identified, the highly evolved εHf(t) values recorded by this sample would be consistent with the reworking of Palaeoproterozoic basement similar to that identified in the Chewore–Rufunsa and Chipata terranes (Fig. 4a).

Chipata

The U–Pb analyses obtained from an orthogneiss within the Chipata Terrane (Fig. 3d) give an upper intercept age of 2009 ± 30 Ma. This obtained age is within error of the protolith ages of the samples from the Chewore–Rufunsa Terrane. Additionally, this age is consistent with previous Palaeoproterozoic ages obtained by Johnson, De Waele and Liyungu (2006) for the Chipata Terrane. As such, this sample may similarly reflect exposed SIB basement within the Chipata Terrane (Fig. 7). εHf(t) values recorded by this sample are broadly equivalent to the similarly aged rocks in the Chewore–Rufunsa Terrane (Fig. 4a). As such, this rock likely reflects crustal reworking with relatively minor mantle input. Obtained U–Pb data for charnockites within the Chipata Terrane yield weighted average ages of *c.* 1040 Ma (Fig. 3e,f). Karmakar and Schenk (2016) speculated that the charnockites may be been coeval with 1031 to 1013 Ma high-temperature to ultra-high-temperature metamorphism recorded in metapelites from this terrane, and if magmatic in origin provided a partial heat source for metamorphism. No association is observed between orthopyroxene and either K-feldspar or biotite, with the latter not being present in the samples, suggesting little textural evidence for the charnockites being metamorphosed (Touret and Huizenga, 2012). As such, we suggest that the obtained data reflect magmatic crystallisation in both samples at *c.* 1040 Ma. Notably, this implies that the charnockites crystallised *c.* 10 m.y. prior to the HT to UHT metamorphism recorded in the Chipata terrane. The charnockites yield positive εHf(t)

values (Fig. 4a) and are suggested to have a juvenile origin, with little crustal input. While a small number of juvenile analyses have been previously obtained from zircons within the SIB, particularly from *c.* 2000 Ma inherited zircons (Johnson, De Waele and Liyungu, 2006; Johnson et al., 2007), these are among the first *c.* 1000 Ma juvenile lithologies reported from the SIB.

The detrital sample from the Chipata Terrane (Fig. 5) yielded a maximum depositional age of 1434 ± 22 Ma. The relationship between this quartzite sample and the granulite facies gneisses within the Chipata Terrane is unclear (Fig. 2). If the sediments forming the paragneisses that are part of this lithological unit share a similar depositional history, then the minimum depositional age of these rocks would be constrained by the age of biotite granites that have been observed to intrude them (Vayrda, 1984). As such, the oldest obtained age of 1058 ± 34 Ma for biotite granites in the Chipata Terrane may provide a broad constraint on the minimum depositional age of the sample. The detrital populations obtained from this terrane correlate well in both age and isotope values with those identified in the Chewore–Rufunsa and Kacholola terranes (Fig. 4b, 5b), which have been recently suggested to be equivalents of the Muva Supergroup that is found throughout eastern Zambia (Fig. 7; Alessio et al., 2018). The data obtained here support a depositional connection between the Irumide and Southern Irumide belts.

Structural evolution

The SIB experienced a major orogenic phase that involved widespread magmatism and metamorphism (M_0) between *c.* 1100–1000 Ma (Fig. 7; Johnson, De Waele and Liyungu, 2006; Johnson et al., 2007; Karmakar and Schenk, 2016). Such an event is likely associated with deformation (D_0), which would have generated foliation planes (S_0) within the Mesoproterozoic lithologies found in the belt. The timing of the N–S trending, terrane bounding ductile shear zones is uncertain. In many cases these shear zones conform to fold structures generated in subsequent deformation phases, suggesting that these were pre-existing features that were deformed. As such, the generation of these shear zones may have occurred during D_0, if not earlier. However, these features bound terranes that share a similar basement and subsequent depositional, magmatic and metamorphic history (Fig. 7). One exception is the predominantly Neoproterozoic Nyimba–Sinda Terrane, though this is suggested to be a superimposed rift-basin, rather than an exotic terrane (Alessio et al., 2018). As these shear zones bound a series of terranes with a very similar history (Fig. 7; and therefore likely not far-travelled relative to each other) their importance appears to be relatively minor in the context of the SIB's evolution.

D_1, a phase of N–S directed compression, is interpreted from the prominent E–W to NE–SW trending folds (F_1) in the region. In many cases the ductile shear zone terrane boundaries conform to these fold structures, suggesting that they were deformed by this folding. These folds are broadly aligned with the late-Neoproterozoic Congo–Kalahari suture (Fig. 7). This collision is interpreted to have been the driving force behind this deformation, which also resulted in metamorphic (M_1) overprinting (John et al., 2004; Johnson, De Waele and Liyungu, 2006; Johnson et al., 2007). It is possible that this event overprinted the S_0 foliation with the S_1 foliation generated in the Neoproterozoic gneiss of the Nyimba–Sinda Terrane at (likely) this time. This S_1 foliation is crosscut by the post-tectonic granites that intrude this terrane (Fig. 2, 6a) and are largely undeformed (Agar, 1984), suggesting that D_1 deformation had ceased by *c.* 500 Ma.

D_2, a phase of E–W directed compression, is interpreted from N–S trending folds (F_2), which are found throughout each terrane. These more open, low amplitude folds weakly refold (and therefore post-date) the more pervasive and tighter F_1 folds. The timing of this event is

uncertain, though restricted to the Phanerozoic. Permian to Triassic rifting was widespread throughout central Africa, with associated rift basins located adjacent the north and south flanks of the SIB in Zambia. In Zimbabwe, Mozambique, and Tanzania, this rifting has been shown to be followed by Permian to Triassic exhumation, interpreted to be associated with the Mauritanian-Variscan and Gondwanide orogenies (Fernandes et al., 2015; Kasanzu et al., 2016; Mackintosh et al., 2018). As such, it is possible that these structures were formed in response to the intra-plate stresses associated with these orogenies (Fig. 7).

Relationship between the Southern Irumide Belt and Irumide Belt

Figure 2 presents available zircon U–Pb and Lu–Hf data, as well as whole rock Sm–Nd for the variably deformed igneous units in the Irumide Belt and Zambian SIB. Late-Mesoproterozoic (1100–1000 Ma) magmatic ages can be observed in both the Irumide and Southern Irumide belts, as can older, 3000–1800 Ma magmatism. The most notable difference between these regions relates to Neoproterozoic magmatism, which is widespread throughout the Southern Irumide Belt and likely a result of the belt being at the forefront of the collision between the Congo and Kalahari cratons (Fig. 7). Available εHf(t) and εNd(t) data for Palaeoproterozoic to Mesoproterozoic magmatic units (Fig. 2) are limited for this region, though suggested magmatic events throughout this period predominantly involved the reworking of crustal material.

The development of the SIB and its relationship to the Irumide Belt is controversial. The original interpretation is that the belts display different geological histories (Johnson, De Waele and Liyungu, 2006; Johnson et al., 2007; De Waele, Johnson and Pisarevsky, 2008). Proponents of this interpretation suggested that distinct differences existed in the timing of magmatism and metamorphism in the Southern Irumide (*c.* 1100–1040 Ma) and Irumide (*c.* 1040–1000 Ma) belts, though this is inconsistent with ages of both ranges having been obtained from either belt (Figs. 2, 7). The suggested timing differences and the presence of a major shear zone (Mwembeshi Shear Zone; Fig. 2), were used to argue for no genetic relationship existing between the Irumide and Southern Irumide belts. On this basis, Johnson et al. (2007) suggested that the SIB did not form on the Congo margin itself but instead developed as a microcontinent that subsequently collided with the Congo margin at *c.* 1040 Ma, which ceased magmatism in the SIB (initiated at c. 1100 Ma) and initiated compression and crustal melting in the Irumide Belt (lasting until *c.* 1000 Ma; Fig. 7).

Bingen et al. (2009) introduced an alternative model to that of the SIB accreting to the southern Congo Margin in the late-Mesoproterozoic. These authors instead suggest that the SIB could have been located along the southern Congo margin prior to the late-Mesoproterozoic and acted as a long-lived, variably compressional active continental margin. The different timing of magmatism in the Irumide Belt and SIB in this scenario is instead ascribed to an advancing magmatic front in response to a shallowing subduction zone located south of the SIB. This model suggests that the *c.* 1100–1040 Ma magmatism recorded in the SIB occurred in a continental-margin-arc setting along the southern Congo margin, which was followed by shallowing of the subducting slab that dipped towards the Irumide Belt. This shallowing caused the section of slab melting to propagate in-land, below the Irumide Belt, initiating subsequent *c.* 1040–1000 Ma magmatism in this region (Fig. 7; Bingen et al., 2009; Alessio et al., 2018). U–Pb monazite ages from Karmakar and Schenk (2016) in the Chipata Terrane of the SIB suggests that both belts experienced similar grades of metamorphism during this time (Fig. 7). The model of the SIB being located along the southern Congo margin prior to the late-Mesoproterozoic is supported by recent work by Alessio et al.

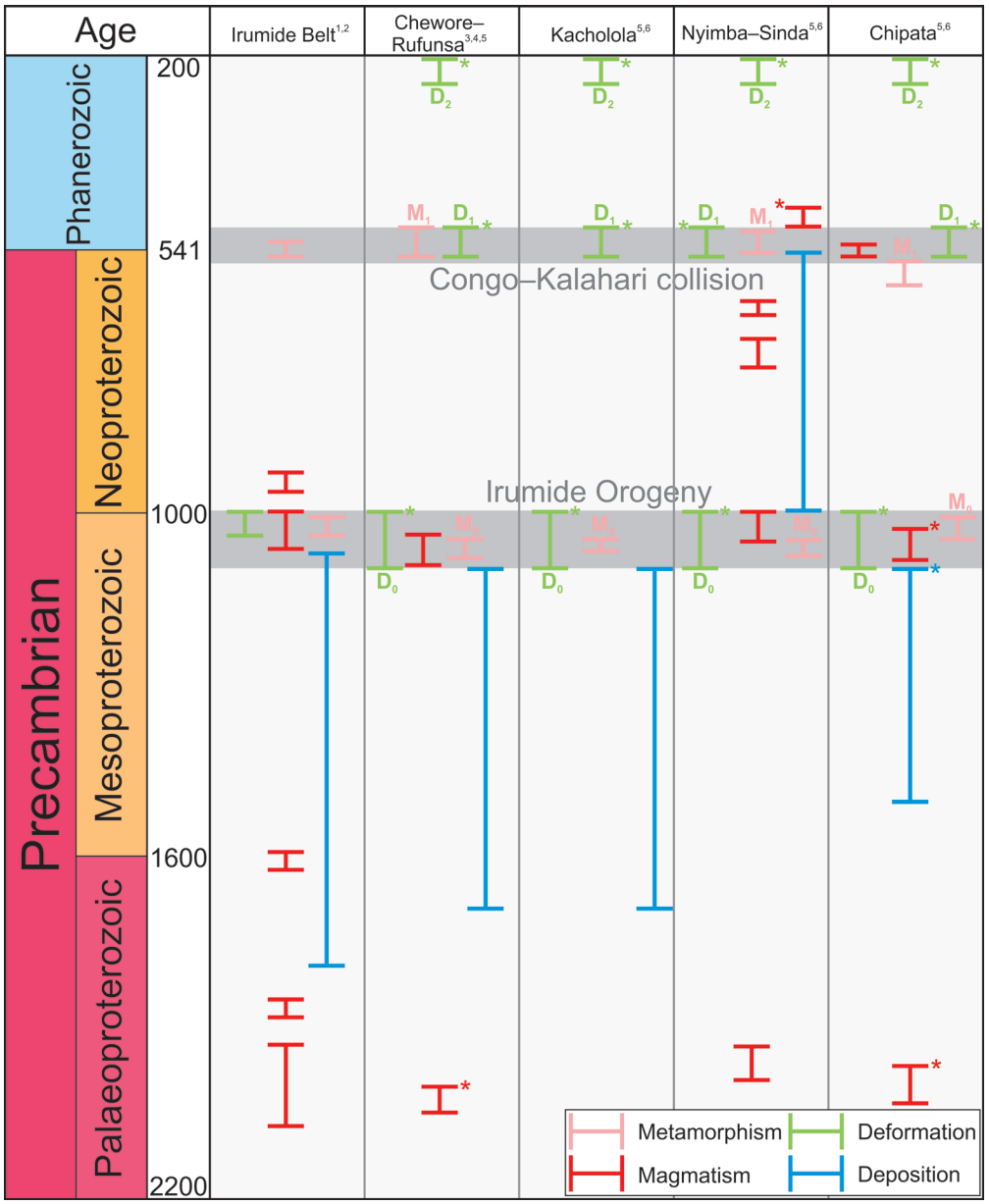

Figure 7. Time-space plot of existing data for the Irumide Belt and SIB, indicating periods of magmatism (red), metamorphism (pink), deformation (green) and deposition (blue) throughout the Precambrian to Phanerozoic. Bars throughout the plot indicate the duration of events defined by the maximum and minimum error ranges of a series of analyses, or interpreted timing in the case of deformation events. Bars with stars indicate constraints that were defined or improved in this study. The timing of key orogenic events (Irumide Orogeny and Congo–Kalahari collision) are denoted by the dark grey bars. References are indicated by the numbers accompanying a given unit's name and are as follows: 1, De Waele et al. (2006b); 2, De Waele et al. (2009); 3, Johnson et al. (2007); 4, Goscombe, Armstrong and Barton (2000); 5, Alessio et al. (2018); 6, Johnson, De Waele and Liyungu (2006); 7, Karmakar and Schenk (2016).

(2018), who obtained U–Pb age populations from detrital zircons in the SIB (Fig. 5b) that are equivalent to those preserved in the Muva Supergroup located in the Irumide Belt and Bangweulu Block (Fig 2; Daly and Unrug, 1982; Daly et al., 1984; Daly, 1986; De Waele and Mapani, 2002), as well as those obtained from the Chipata Terrane in this study. The correlation between sediments in these regions lead to the suggestion that the SIB was depositionally connected to the Congo Craton during the Palaeoproterozoic and, therefore, formed on the Congo margin (Fig. 7; Alessio et al., 2018).

Prior to the current study Lu–Hf and Sm–Nd isotopic data for magmatic rocks and/or zircons were only available from the Chewore–Rufunsa terrane. Johnson et al. (2007) reported negative (–1.8 to –13.5) whole-rock εNd(t) values for *c.* 1090 to 1040 Ma meta-igneous lithologies, while both positive and negative (+2.9 to –3.7) εHf(t) values were reported for *c.* 2200 to 1900 Ma inherited zircons from similar rocks. The obtained εHf(t) values of Johnson et al. (2007) were used by these authors to suggest that the SIB basement is predominantly juvenile and Palaeoproterozoic, as opposed to the evolved Archaean to Palaeoproterozoic basement of the Irumide Belt. However, we herewith document predominantly evolved Palaeoproterozoic basement in both the Chewore–Rufunsa and Chipata terranes (Fig. 4), similar to Palaeoproterozoic basement document in the Irumide Belt (Fig. 2, 7; De Waele et al., 2009). Our results indicate that the entire Zambian portion of the SIB could be floored by predominantly evolved Palaeoproterozoic basement similar to that in the Irumide Belt, which is corroborated by the significantly more evolved εHf(t) values obtained by the post-tectonic granite located between the Chewore–Rufunsa and Chipata terranes. This study also provides εHf(t) data for two charnockite samples from the Chipata Terrane, yielding some of the youngest Mesoproterozoic U–Pb crystallisation ages (*c.* 1040 Ma) recorded in the SIB. While juvenile xenocrystic zircons have been analysed from the SIB, these samples record the only evidence yet of late-Mesoproterozoic juvenile magmatism in this belt. While the majority of magmatism in the SIB reflects crustal reworking, these data indicate that the Chipata Terrane was intruded by mantle derived material while crustal reworking was occurring in the Irumide Belt. Overall, the available data demonstrate that little distinction can be made between the crystallisation ages recorded in the Irumide and Southern Irumide belts, for both the Palaeoproterozoic basement and late Mesoproterozoic magmatism. This common history is supportive of a model whereby the Southern Irumide Belt did not collide with the southern Congo Craton margin subsequent to its formation and instead developed on this margin, prior to the orogenic events recorded during the late-Mesoproterozoic and late-Neoproterozoic (Alessio et al., 2018).

CONCLUSIONS

A suite of U–Pb and Lu–Hf data were acquired for lithologies throughout the Zambian terranes of the SIB. Three samples obtained from the Chewore–Rufunsa and Chipata terranes yield Palaeoproterozoic ages between *c.* 2100 and 2000 Ma, which are equivalent to basement ages interpreted from xenocrysts in the Irumide Belt. These samples yield predominantly evolved εHf(t) values and are interpreted to represent exposed basement rock that underlies (at least) the Zambian terranes of the SIB. A sample of detrital zircon from the Chipata Terrane yielded U–Pb age populations and εHf(t) values that are equivalent to those in sedimentary rocks from the Chewore–Rufunsa and Kacholola terranes, as well as those of the Muva Supergroup within the Irumide Belt. This study also identifies the first instance of late Mesoproterozoic juvenile magmatism in the SIB within the Chipata Terrane, U–Pb dating constrains crystallisation of these rocks at *c.* 1040 Ma, coeval with crustal reworking in the Irumide Belt. Two regional-scale structural overprints were identified within the belt, a N–S directed contraction that was likely the result of Congo–Kalahari collision at *c.* 550 to 530 Ma, and a subsequent E–W directed shortening, possibly occurring during the Permian to Triassic. The presence of equivalent basement material and overlying sedimentary sequences in both the Irumide and Southern Irumide belts opposes hypotheses of the SIB forming on a separate microcontinent, prior to collision with the southern Congo margin during the late-Mesoproterozoic. The obtained data instead support a tectonic model

where the SIB represents an extension of the southern Congo Craton margin since at least the Palaeoproterozoic (*c.* 2000 Ma).

ACKNOWLEDGEMENTS

This paper forms TRaX record #415 and is a contribution to IGCP projects #628 (Gondwana Map) and #648 (Supercontinents and Global Dynamics). B. McDonald of the John de Laeter Centre as well as D. Kelsey of Adelaide Microscopy are thanked for their help with collection of analytical data. B. Alessio is supported by a Research Training Program scholarship. D. Gasser and B. Bingen are thanked for reviews that significantly improved the quality of this submission. This project was funded by Australian Research Council Future Fellowship #FT120100340 to A. Collins.

REFERENCES

Agar, R., 1984. Geological Map of the Petauke Area. Geol. Survey Zambia. Government of the United Kingdom (Ordnance Survey).

Alessio, B.L., Collins, A.S., Siegfried, P., Glorie, S., De Waele, B., Payne, J.L., Archibald, D., 2018. Neoproterozoic tectonic geography of the south-east Congo Craton in Zambia as deduced from the age and composition of detrital zircons. Geoscience Frontiers.

Alessio, B.L., Kelsey, D.E., 2018. On yoderite: Using calculated phase equilibria to investigate its rarity in the geological record of whiteschists. Journal of Metamorphic Geology 36, 297-314.

Bingen, B., Jacobs, J., Viola, G., Henderson, I., Skår, Ø., Boyd, R., Thomas, R., Solli, A., Key, R., Daudi, E., 2009. Geochronology of the Precambrian crust in the Mozambique belt in NE Mozambique, and implications for Gondwana assembly. Precambrian Research 170, 231-255.

Collins, A.S., Pisarevsky, S.A., 2005. Amalgamating eastern Gondwana: the evolution of the Circum-Indian Orogens. Earth-Science Reviews 71, 229-270.

Daly, M., 1986. The intracratonic Irumide belt of Zambia and its bearing on collision orogeny during the Proterozoic of Africa. Geological Society, London, Special Publications 19, 321-328.

Daly, M., Chakraborty, S., Kasolo, P., Musiwa, M., Mumba, P., Naidu, B., Namateba, C., Ngambi, O., Coward, M., 1984. The Lufilian arc and Irumide belt of Zambia: results of a geotraverse across their intersection. Journal of African Earth Sciences (1983) 2, 311-318.

Daly, M., Unrug, R., 1982. The Muva Supergroup of northern Zambia: a craton to mobile belt sedimentary sequence. Verhandelinge van die Geologiese Vereniging van Suid-Afrika 85, 155-165.

De Waele, B., 2004. The Proterozoic geological history of the Irumide belt, Zambia.

De Waele, B., Fitzsimons, I., Wingate, M., Tembo, F., Mapani, B., Belousova, E., 2009. The geochronological framework of the Irumide Belt: a prolonged crustal history along the margin of the Bangweulu Craton. American Journal of Science 309, 132-187.

De Waele, B., Johnson, S.P., Pisarevsky, S.A., 2008. Palaeoproterozoic to Neoproterozoic growth and evolution of the eastern Congo Craton: Its role in the Rodinia puzzle. Precambrian Research 160, 127-141.

De Waele, B., Kampunzu, A.B., Mapani, B.S.E., Tembo, F., 2006a. The Mesoproterozoic Irumide belt of Zambia. Journal of African Earth Sciences 46, 36-70.

De Waele, B., Liégeois, J.-P., Nemchin, A.A., Tembo, F., 2006b. Isotopic and geochemical evidence of proterozoic episodic crustal reworking within the irumide belt of south-central Africa, the southern metacratonic boundary of an Archaean Bangweulu Craton. Precambrian Research 148, 225-256.

De Waele, B., Mapani, B., 2002. Geology and correlation of the central Irumide belt. Journal of African Earth Sciences 35, 385-397.

Goscombe, B., Armstrong, R., Barton, J., 2000.

Geology of the Chewore Inliers, Zimbabwe: constraining the Mesoproterozoic to Palaeozoic evolution of the Zambezi Belt. Journal of African Earth Sciences 30, 589-627.

Griffin, W., Wang, X., Jackson, S., Pearson, N., O'Reilly, S.Y., Xu, X., Zhou, X., 2002. Zircon chemistry and magma mixing, SE China: in-situ analysis of Hf isotopes, Tonglu and Pingtan igneous complexes. Lithos 61, 237-269.

Hanson, R., 2003. Proterozoic geochronology and tectonic evolution of southern Africa. Geological Society, London, Special Publications 206, 427-463.

Hauzenberger, C., Tenczer, V., Bauernhofer, A., Fritz, H., Klötzli, U., Košler, J., Wallbrecher, E., Muhongo, S., 2014. Termination of the Southern Irumide Belt in Tanzania: Zircon U/Pb geochronology. Precambrian Research 255, 144-162.

Hoskin, P.W., Ireland, T.R., 2000. Rare earth element chemistry of zircon and its use as a provenance indicator. Geology 28, 627-630.

Jackson, S.E., Pearson, N.J., Griffin, W.L., Belousova, E.A., 2004. The application of laser ablation-inductively coupled plasma-mass spectrometry to in situ U–Pb zircon geochronology. Chemical Geology 211, 47-69.

John, T., Schenk, V., Mezger, K., Tembo, F., 2004. Timing and PT evolution of whiteschist metamorphism in the Lufilian Arc–Zambezi Belt orogen (Zambia): implications for the assembly of Gondwana. The Journal of geology 112, 71-90.

Johns, C.C., Liyungu, K., Mabuku, S., Mwale, G., Sakungo, F., Tembo, D., Vallance, G., Barr, M.W.C., 1989. The stratigraphic and structural framework of Eastern Zambia: results of a geotraverse. Journal of African Earth Sciences (and the Middle East) 9, 123-136.

Johnson, S., De Waele, B., Liyungu, A., 2006. U-Pb SHRIMP geochronology of granitoid rocks in eastern Zambia: terrane subdivision of the Mesoproterozoic Southern Irumide Belt. Tectonics 25.

Johnson, S., Oliver, G., 1998. A second natural occurrence of yoderite. Journal of Metamorphic Geology 16, 809-818.

Johnson, S.P., De Waele, B., Tembo, F., Katongo, C., Tani, K., Chang, Q., Iizuka, T., Dunkley, D., 2007. Geochemistry, geochronology and isotopic evolution of the Chewore–Rufunsa Terrane, Southern Irumide Belt: a Mesoproterozoic continental margin arc. Journal of Petrology 48, 1411-1441.

Karmakar, S., Schenk, V., 2016. Mesoproterozoic UHT metamorphism in the Southern Irumide Belt, Chipata, Zambia: Petrology and in situ monazite dating. Precambrian Research 275, 332-356.

Manninen, T., Makitie, H., Lehtonen, M., Cune e, G., Lehto, T., Korkiakoski, E., 2006. Geological Map No. 1430/1431. GTK Consortium for Geological Mapping. Ministerio Dos Recursos Minerais, Mozambique.

Mapani, B., Rivers, T., Tembo, F., De Waele, B., Katongo, C., 2004. Growth of the Irumide terranes and slices of Archaean age in eastern Zambia. Geoscience Africa 2004, Abstract 2, 414-415.

Mapani, B., Rivers, T., Tembo, F., Katongo, C., 2001. Terrane mapping in the eastern Irumide and Mozambique belts: implications for the assembly and dispersal of Rodinia, IGCP, pp. 10-11.

Merdith, A.S., Collins, A.S., Williams, S.E., Pisarevsky, S., Foden, J.F., Archibald, D., Blades, M.L., Alessio, B.L., Armistead, S., Plavsa, D., Clark, C., Müller, R.D., 2017. A full-plate global reconstruction of the Neoproterozoic. Gondwana Research 50, 84-134.

Merdith, A.S., Williams, S.E., Brune, S., Collins, A.S., Müller, R.D., 2019. Rift and plate boundary evolution across two supercontinent cycles. Global and Planetary Change 173, 1-14.

Oliver, G., Johnson, S., Williams, I., Herd, D., 1998. Relict 1.4 Ga oceanic crust in the Zambezi Valley, northern Zimbabwe: Evidence for Mesoproterozoic supercontinen-

tal fragmentation. Geology 26, 571-573.
Paton, C., Hellstrom, J., Paul, B., Woodhead, J., Hergt, J., 2011. Iolite: Freeware for the visualisation and processing of mass spectrometric data. Journal of Analytical Atomic Spectrometry 26, 2508-2518.
Ray, A., 1984. Geological Map of the Rufunsa Area. Geol. Survey Zambia. Government of the United Kingdom (Ordnance Survey).
Sláma, J., Košler, J., Condon, D.J., Crowley, J.L., Gerdes, A., Hanchar, J.M., Horstwood, M.S., Morris, G.A., Nasdala, L., Norberg, N., 2008. Plešovice zircon—a new natural reference material for U–Pb and Hf isotopic microanalysis. Chemical Geology 249, 1-35.
Thieme, J., 1984. Geological Map of the Lusaka Area. Geol. Survey Zambia. Government of the United Kingdom (Ordnance Survey).
Thomas, R.J., Spencer, C., Bushi, A.M., Baglow, N., Boniface, N., de Kock, G., Horstwood, M.S., Hollick, L., Jacobs, J., Kajara, S., 2016. Geochronology of the central Tanzania Craton and its southern and eastern orogenic margins. Precambrian Research 277, 47-67.
Touret, J.L.R., Huizenga, J.M., 2012. Charnockite microstructures: From magmatic to metamorphic. Geoscience Frontiers 3, 745-753.
Vayrda, I., 1984. Geological Map of the Chipata Area. Geol. Survey Zambia. Government of the United Kingdom (Ordnance Survey).
Westerhof, A.P., Lehtonen, M.I., Mäkitie, H., Manninen, T., Pekkala, Y., Gustafsson, B., Tahon, A., 2008. The Tete-Chipata Belt: A new multiple terrane element from western Mozambique and southern Zambia. Geological Survey of Finland Special Paper 48, 145-166.
Whalen, J.B., Currie, K.L., Chappell, B.W., 1987. A-type granites: geochemical characteristics, discrimination and petrogenesis. Contributions to Mineralogy and Petrology 95, 407-419.
Wiedenbeck, M., Alle, P., Corfu, F., Griffin, W., Meier, M., Oberli, F.v., Quadt, A.v., Roddick, J., Spiegel, W., 1995. Three natural zircon standards for U-Th-Pb, Lu-Hf, trace element and REE analyses. Geostandards and Geoanalytical Research 19, 1-23.
Woodhead, J., Hergt, J., Shelley, M., Eggins, S., Kemp, R., 2004. Zircon Hf-isotope analysis with an excimer laser, depth profiling, ablation of complex geometries, and concomitant age estimation. Chemical Geology 209, 121-135.
Woodhead, J.D., Hergt, J.M., 2005. A preliminary appraisal of seven natural zircon reference materials for in situ Hf isotope determination. Geostandards and Geoanalytical Research 29, 183-195.

CHAPTER 4

This chapter is published in *The Journal of Metamorphic Geology* as:
Alessio, Brandon L., & Kelsey, David E. 2018. On yoderite: Using calculated phase equilibria to investigate its rarity in the geological record of whiteschists.

Statement of Authorship

Title of Paper	On yoderite: Using calculated phase equilibria to investigate its rarity in the geological record of whiteschists
Publication Status	☑ Published ☐ Accepted for Publication ☐ Submitted for Publication ☐ Unpublished and Unsubmitted w ork w ritten in manuscript style
Publication Details	Alessio, Brandon L., & Kelsey, David E. (2018). On yoderite: Using calculated phase equilibria to investigate its rarity in the geological record of whiteschists. Journal of Metamorphic Geology, 36(3), 297-314. doi: 10.1111/jmg.12293

Principal Author

Name of Principal Author (Candidate)	Brandon Luke Alessio		
Contribution to the Paper	Sample preparation, data collection, processing and interpretation, manuscript design and composition, drafting of figures.		
Overall percentage (%)	60		
Certification:	This paper reports on original research I conducted during the period of my Higher Degree by Research candidature and is not subject to any obligations or contractual agreements with a third party that would constrain its inclusion in this thesis. I am the primary author of this paper.		
Signature		Date	7/1/19

Co-Author Contributions

By signing the Statement of Authorship, each author certifies that:

i. the candidate's stated contribution to the publication is accurate (as detailed above);

ii. permission is granted for the candidate in include the publication in the thesis; and

iii. the sum of all co-author contributions is equal to 100% less the candidate's stated contribution.

Name of Co-Author	David Kelsey		
Contribution to the Paper	Data collection, processing and interpretation, as well as manuscript review.		
Signature		Date	8/1/19

ABSTRACT

We present a new activity–composition model for green (Mn^{3+}-absent) yoderite for use in the latest internally consistent thermodynamic dataset used by THERMOCALC, for calculations primarily in $MgO–Al_2O_3–SiO_2–H_2O–O$ system, where O is a proxy for Fe_2O_3. *P–T* grids calculated with our model in the MASH and MASHO system feature invariant points and univariant reaction bundles that are consistent with existing experimental results. Using this new model we have explored the stability of yoderite in whiteschists, a rare type of high pressure rock that conforms closely to the MASHO system. Using a series of calculated models in which composition varies, we show that yoderite stability is a function of bulk rock SiO_2, MgO, and Al_2O_3, where the most important component for stabilising yoderite is a function of pressure and temperature. The rarity of yoderite in naturally occurring whiteschists is largely related to these compositional factors, with most whiteschists having rock compositions that are too SiO_2-rich and Al_2O_3-poor to allow yoderite formation. However, in addition to compositional factors, the calculated *P–T* stability field of yoderite occurs over thermal gradients that are generally too high to occur in modern-style subduction zones. As nearly all known whiteschist occurrences are Phanerozoic in age, the near complete absence of yoderite in late-Neoproterozoic–Phanerozoic whiteschists may be at least partially due to modern subduction systems failing to produce the hotter thermal gradients needed to stabilize yoderite. The provision of this new *a–x* model for green yoderite allows for more rigorous *P–T–X* investigations of all whiteschists.

INTRODUCTION

Yoderite is a dark blue–purple to green coloured silicate mineral that can occur in the $MgO–Al_2O_3–SiO_2–H_2O–Fe_2O_3$ (MASHO) system. Currently there are only two known localities on the planet that contain the mineral. The first was discovered by McKie (1959) at Mautia Hill (Tanzania), while the second was discovered by Johnson and Oliver (1998) in the Chewore Hills of northern Zimbabwe. At both localities yoderite occurs within whiteschists, a rare type of high pressure to ultrahigh pressure metamorphic rock whose compositions conform very closely to the MASHO system. In terms of mineralogy, these rocks are characterised by the diagnostic assemblage of talc and kyanite, and commonly additionally contain quartz or coesite (Schreyer & Seifert, 1969; Schreyer, 1974; Schreyer, 1977). Whiteschists were suggested to have protoliths that either have a MASHO composition, such as evaporates or bentonites, or igneous rocks that were subjected to extensive metasomatic alteration. Whiteschists are always found in ancient collisional zones where continental rocks were subducted. As a consequence, there is a predominance of whiteschists in HP–UHP terranes (Franz, Romer, & de Capitani, 2013; Johnson, 2011).

Because of their location within ancient collisional zones, whiteschists have the potential to provide quantitative records of the pressure–temperature (*P–T*) conditions experienced during subduction. However, constraining their metamorphic *P–T* evolution is currently hampered by two issues. First, the stability of yoderite as a function of *P–T–X* (where *X* refers to composition) remains uncertain. Experimental studies showed that yoderite has a large stability field (Fockenberg & Schreyer, 1991, 1994). On this basis, one may expect whiteschists containing yoderite to be common. However, yoderite-bearing whiteschists are much rarer than yoderite-absent whiteschists. Therefore, a paradox exists that remains largely unsolved: why is yoderite so rare, even amongst whiteschists? Second, our ability to understand the metamorphic evolution of whiteschists is impeded by the inability to calculate reliable thermodynamic models for rocks with compositions closely approximating the MASHO system, largely because of the absence of an activity–composition (*a–x*) model for yoderite (cf. Franz et al. 2013).

Franz et al. (2013) provide the only existing study to have performed calculations using an *a–x* model for yoderite. In their study they explored controls on yoderite and whiteschist stability, but their yoderite *a–x* model was of a fixed, single composition. In this context, the ability to include solid-solution yoderite in calculated phase-equilibria models and address the question of its rarity is a fundamental step towards furthering our understanding of whiteschists and increasing their utility in tectono-metamorphic research.

In order to quantitatively explore the *P–T–X* controls on yoderite stability in the MASHO system, we present a new *a–x* model for green (Mn^{3+}-absent) yoderite to be used with THERMOCALC. We use calculated *P–T* grids in the MASH and MASHO systems to establish the validity of the yoderite model as such diagrams provide the strongest link to the results of existing experimental studies. We also present calculated *P–X* pseudosections, which are used to explore compositional constraints on yoderite stability, for the purpose of addressing the rarity of yoderite in whiteschists. These transects are based on the geochemistry of a (purely green) yoderite-bearing whiteschist from the Chewore Hills in northern Zimbabwe. The thermodynamic framework is then applied to calculate a model that constrains the *P–T* history of the same Chewore Hills whiteschist. This study presents the first attempt at developing a solid-solution *a–x* model for yoderite that is calibrated on the basis of matching calculated phase equilibria to experimentally-constrained invariant and univariant equilibria, i.e. *P–T* grids (cf. Franz et al., 2013).

PREVIOUS STUDIES OF WHITESCHIST AND YODERITE STABILITY

Early experimental work in the MASHO system determined that the characteristic talc–kyanite assemblages of whiteschists become stable above pressures of ~10 kbar and temperatures of ~670–840 °C (Schreyer & Seifert, 1969). At lower pressures talc–kyanite bearing assemblages were found to be replaced by cordierite-bearing assemblages, whereas at lower temperatures it is replaced by chlorite–quartz assemblages. Subsequent experimental work by Fockenberg and Schreyer (1994) expanded the talc–kyanite stability field as their study determined lower *P–T* values for the stability of talc–kyanite assemblages, showing that it can occur above ~5 kbar and 590 °C. More recently Franz et al. (2013) calculated phase diagrams for rock compositions largely conforming to the MASHO system and determined that stable talc–kyanite assemblages can occur above pressures of ~5 kbar, in agreement with the experimental results of Fockenberg and Schreyer (1994). In naturally occurring whiteschists, *P–T* estimates from talc–kyanite assemblages have been determined via conventional barometry to be stable at 6–8 kbar in the Modum Complex (Norway; Munz, 1990). The Kokchetav Massif (Kazakhstan) contains the highest pressure whiteschists known. Using phengite geobarometry Parkinson (2000) determined that talc–kyanite assemblages remain stable to pressures of 35 kbar. All available temperature estimates of naturally occurring whiteschists fall within the range of ~550–800 °C (Franz et al., 2013), remaining stable at temperatures below that determined by experimental studies.

Yoderite has been found naturally in two forms, with two different chemistries that reflect the presence or absence of Mn^{3+}. The two different chemistries of yoderite result in the mineral having different colours, either green or blue–purple. The green variety is Mn^{3+}-absent and found in the Mautia Hill and Chewore Hills whiteschists, with the approximate formula $Mg_2Al_{5.6}Fe^{3+}_{0.4}Si_4O_{18}(OH)_2$ (Higgins, Ribbe, & Nakajima, 1982). The dark blue to purple variety of yoderite is restricted to Mautia Hill whiteschists, differing from green yoderite by additionally containing Mn^{3+}, with the approximate formula $Mg_2Al_{5.6}Fe^{3+}_{0.34}Mn^{3+}_{0.7}Si_4O_{18}(OH)_2$ (Abu-Eid, Langer, & Seifert, 1978). Schreyer and Yoder Jr (1968) conducted the

first experimental investigation into the stability of yoderite, and synthesized the mineral in the MASH system. They suggested the rarity of yoderite in nature was due to the small *P*–*T* stability field of yoderite + quartz (> ~10 kbar and 675–770 °C), with the assemblage kyanite + talc being more likely to form. The stability of yoderite in the MASH experimental system was later shown to be incorrect by Fockenberg and Schreyer (1991), who argued that yoderite can only form in the presence of Fe_2O_3 (see also Franz et al., 2013). They instead suggested that any previous syntheses of yoderite were due to traces of ferric iron in either the starting mixtures or seeds used in the experiments. Subsequent work also disproved the notion that the rarity of yoderite was the result of a small stability field in *P*–*T* space (Fockenberg & Schreyer, 1991, 1993, 1994). Through experiments notionally in the MASHO system it was determined that yoderite is stable over a wide range of *P*–*T* conditions, between ~6–25 kbar and 590–795 °C. This led Fockenberg and Schreyer (1994) to conclude that stability of yoderite was instead restricted by rock composition, with yoderite only able to occur in rocks rich in MgO, Al_2O_3, SiO_2, H_2O, and containing Fe_2O_3. They also argued that for yoderite to occur, the rocks must also be poor in alkalis and CaO (see also Franz et al., 2013). More recent work by Franz et al. (2013) arrived at the same conclusions and suggested that the presence of CO_2-bearing fluid drastically reduces the stability of whiteschist mineral assemblages, which may in turn affect the stability of yoderite. These authors calculated *P*–*T* pseudosections for a wide variety of potential continental to oceanic protoliths to whiteschists for the purpose of highlighting the size of the whiteschist stability field. Franz et al. (2013) used the predominance of whiteschists in UHP terranes to state that subduction of continental material is a pre-requisite for whiteschist formation as it is only this setting that allows for HP–UHP conditions. Schreyer (1988) stated that the rarity of yoderite was attributed to the stability of yoderite occurring at higher geothermal gradients than those prevailing in subduction zones.

ACTIVITY–COMPOSITION MODEL FOR YODERITE

Our goal in developing the solid-solution green yoderite model was in the first instance to replicate as best possible the experimentally constrained *P*–*T* grids of Fockenberg and Schreyer (1994) and Schreyer (1988). This is because univariant and invariant equilibria provide the backbone of higher-variance equilibria in larger systems (e.g. Kelsey, White, Holland, & Powell, 2004; Powell, Holland, & Worley, 1998; White, Powell, Holland, & Worley, 2000). The activity–composition model presented here is the first attempt at a thermodynamic model for yoderite for use in THERMOCALC. The model is primarily designed for use in the system MASHO and its subsystems. We have not included Mn^{3+} in the model as it is not currently possible to model this valency of Mn in THERMOCALC. Because of this, the provided yoderite model is for the green, Mn^{3+}-absent variety found in the Chewore Hills whiteschist. This variety is also reported to occur at Mautia Hill, though yoderite at this locality is predominantly of the purple, Mn-bearing variety (McKie, 1959, 1966; Jons et al., 2004). The yoderite model was developed entirely through the use of the 'make' command of THERMOCALC *a*–*x* coding. The 'make' facility of THERMOCALC is premised on the symmetric formalism (Powell & Holland, 1993), which, in part, is that the thermodynamic properties of phase end-members can be described by linear combinations of thermodynamic properties of other phases (e.g. Holland & Powell, 1996; Powell & Holland, 1993, 1999; White, Powell, Holland, Johnson, & Green, 2014). This approach allows for the addition of new phase end-memebers in THERMOCALC without compromising the integrity of the internally consistent thermodynamic dataset, provided that the ther-

modynamic data for phases used in the 'make' process are already present in the dataset. In the context of solid-solution yoderite, the 'make' facility was used to construct dependent end-members and their thermodynamics from the chemistry and thermodynamic properties of independent end-members already in the Holland and Powell (2011) internally consistent dataset. The approach we have taken to develop the solid-solution yoderite model is somewhat similar to the new micro-φ approach of Powell, White, Green, Holland, and Diener (2014).

The MASHO solid-solution green yoderite model is characterised by Al–Fe^{3+} cation substitution (e.g. Fockenberg & Schreyer, 1994). We have included a Fe^{2+}-bearing end-member as part of a larger system FMASHO yoderite model, but the thermodynamics of the Fe^{2+}-bearing end-member remain largely unconstrained at present and were not calibrated as part of this study. Therefore, the full solid-solution model displays Al–Fe^{3+} and Fe–Mg cation substitutions (Table 1). Yoderite structure is characterised by four octahedral, three trigonal bipyramid and four tetrahedral coordination sites in which cations reside per formula unit (Higgins et al., 1982). Higgins et al. (1982) suggest Fe^{3+} substitutes into octahedral and trigonal bipyramid coordination sites and therefore as a first approximation we have assumed that the four octahedral and one of the trigonal bipyramid coordination sites, here termed M1 and B1, respectively, involve substitution of the same set of cations—Mg, Fe^{2+}, Al, Fe^{3+}—and that the remaining two trigonal bipyramid sites (here termed B2) involve Al and Fe^{3+} substitution only. The distribution of Fe^{3+} amongst the sites in our model currently displays equipartitioning (cf. Holland & Powell, 2006), but an order–disorder parameter could be introduced. Fe^{2+}–Mg order–disorder is modelled to occur via a parameter, Q(yod). The four end-members chosen to describe solid-solution yoderite in the FMASHO system are myod $[Mg_2Al_6(SiO_4)_4O_2(OH)_2]$, fyod $[Fe_2Al_6(SiO_4)_4O_2(OH)_2]$, yodo $[Mg_2Al_4Fe^{3+}{}_2(SiO_4)_4O_2(OH)_2]$ and fmoy $[MgFeAl_6(SiO_4)_4O_2(OH)_2]$ (Table 1).

Natural yoderite formation at Mautia Hill was ascribed to the end-member reaction yoderite + quartz = talc + kyanite + hematite + H_2O (McKie, 1959; Schreyer & Seifert, 1969). However, trial calculations with myod—the most dominant compositional component of yoderite—defined by this linear combination of end-members did not produce univariant and invariant reaction bundles with topologies consistent with the experimentally constrained *P*–*T* grids of Schreyer (1988) and Fockenberg and Schreyer (1994). By instead making myod and its thermodynamic properties with the linear combination of end-members yoderite + quartz = Tschermaks talc + kyanite, univariant and invariant reaction bundles calculated with topologies consistent with Schreyer (1988) and Fockenberg & Schreyer (1994). End-member yodo and its thermodynamic properties were made by the linear combination yoderite = Tschermaks talc + kyanite + hematite. End-members fyod and fmoy and their thermodynamic properties were made using the linear combination yoderite + quartz = talc + kyanite + hematite + H_2O.

Two compositional and one order–disorder parameters are required to describe the composition of yoderite with end-members shown in Table 1. The compositional variables are defined as:

x(yod) = (3xFe,M1 + xFe,B1)/(3xFe,M1 + xFe,B1 + 3xMg,M1 + xMg,B1),

f(yod) = 2xFe3,B2.

The order–disorder parameter is defined as follows, based on an assumed preference of Fe^{2+} for the B1 site:

Q(yod) = 2(x – xFe,M1).

Q cannot be found directly from cations of Fe and Mg; instead it must be found from the solution of an internal equilibrium. Site fractions in terms of the compositional and order–disorder parameters are:

x(Mg,M1) = (1 – x)(1 – 1/8 f)

Table 1. Yoderite a–x model site distributions.

	M1				B1				B2		
	Mg	Fe	Al	Fe^{3+}	Mg	Fe	Al	Fe^{3+}	Al	Fe^{3+}	
myod	1	0	3	0	1	0	1	0	2	0	$[SiO_4]_4O_2(OH)_2$
fyod	0	1	3	0	0	1	1	0	2	0	$[SiO_4]_4O_2(OH)_2$
yodo	1	0	2.5	0.5	1	0	0.5	0.5	1	1	$[SiO_4]_4O_2(OH)_2$
fmoy	1	0	3	0	0	1	1	0	2	0	$[SiO_4]_4O_2(OH)_2$

x(Fe,M1) = x (1 – 1/8 f)
x(Fe3,M1) = 1/8 f
x(Al,M1) = 1 – 1/8 f
x(Mg,B1) = (1 – x)(1 – ¼ f)
x(Fe,B1) = x (1 – ¼ f)
x(Fe3,B1) = ¼ f
x(Al,B1) = 1 – ¼ f
x(Fe3,B2) = ½ f
x(Al,B2) = 1 – ½ f.

The corresponding end-member proportions are:

pmyod = 1 – x – ½ Q – f
pfyod = x – ½ Q
pyodo = f
pfmoy = Q

Ideal activity expressions for each end-member are:

amyod,ideal = (xMg,M1)1(xAl,M1)3(xMg,B1)1(xAl,B1)1(xAl,B2)2
afyod,ideal = (xFe,M1)1(xAl,M1)3(xFe,B1)1(xAl,B1)1(xAl,B2)2
ayodo,ideal = (xMg,M1)1(xAl,M1)5/2(xFe3,M1)1/2(xMg,B1)1(xAl,B1)1/2(xFe3,B1)1/2(xAl,B2)1(xFe3,B2)1
afmoy,ideal = (xMg,M1)1(xAl,M1)3(xFe,B1)1(xAl,B1)1(xAl,B2)2.

Interaction energy parameters, Wij, expressing non-ideal mixing (Powell & Holland, 1993), and DQF parameters expressing modification to the enthalpy of formation of end-members (e.g. Holland & Powell, 1992, 2003; Powell et al., 2014; White, Powell, Holland, et al., 2014), are effectually unconstrained by existing experimental data but are required for the calibration of thermodynamic data. Nevertheless, the magnitude of energetics associated with Al–Fe^{3+} and Fe-Mg exchange in other minerals may provide a useful analogy for that of yoderite (e.g. Powell et al., 2014). Using this as a guiding basis, Wij and DQF values were constrained such that the *P*–*T* grid of Fockenberg and Schreyer (1994) was effectually replicated by our calculations. However, as the *P*–*T* locations of invariant points in the Fockenberg and Schreyer (1994) experimentally constrained reaction grid carry some uncertainty, our additional goal in constraining Wij and DQF values was to calculate the yoderite + quartz stability field to span a range of thermal gradients that are consistent with those proposed in Schreyer (1988) and Fockenberg & Schreyer (1994). To achieve these goals, the Wij and DQF values for the yoderite model are as follows:

Wmyod,fyod 10 0 –0.02,
Wmyod,yodo 12 0 0,
Wmyod,fmoy 4 0 0,
Wfyod,yodo 16 0 0,
Wfyod,fmoy 4 0 0,
Wyodo,fmoy 12 0 0,

and

DQFmyod –20 0 0,
DQFyodo 30 0 0,

where each are described by the linear relationship a + bT + cP. Overall, the appointed Wij and DQF values, as well as the model overall, result in a topology that is consistent with the proposed topologies in the MASH and MASHO systems (e.g. Fockenberg & Schreyer, 1994; Schreyer & Seifert, 1969; Schreyer, 1988), thus allowing practical calculations for natural low Fe^{2+}-bearing rock compositions involving solid-solution yoderite. The yoderite *a*–*x* model for use with THERMOCALC is located in the supporting information (Table S1).

METHODS

Pressure–temperature–composition calculations

P–T grids and *P–X* models were calculated using the phase equilibria modelling program THERMOCALC v. 3.37 with the internally consistent thermodynamic dataset of Holland and Powell (2011), ds62. Quantitative *P–T* information were calculated for the systems MASH and MASHO, which are preferable to achieve our aims rather than larger, more complex system as MASH and MASHO almost entirely describe the composition of whiteschists, and allow for comparison of our results with the published *P–T* grids and other studies involving yoderite. Activity–composition models for phases other than yoderite are from White, Powell, and Johnson (2014), White, Powell, Holland, et al. (2014) and Powell et al. (2014). The geochemistry of the Chewore Hills yoderite-bearing pod discovered by Johnson and Oliver (1998) was used as a basis for exploring yoderite stability as a function of changing composition, specifically a series of *P–X* models in which the amounts of MgO, Al_2O_3, SiO_2, H_2O and Fe_2O_3 were varied. This Zimbabwean whiteschist composition was used as a basis for our purpose, as whole rock geochemistry for the yoderite bearing whiteschists reported at Mautia Hill is only available for those containing purple Mn^{3+}-bearing yoderite.

PHASE RELATIONS IN MASH AND MASHO

In order to both calibrate and determine the validity of our solid-solution yoderite *a–x* model, *P–T* grids for the MASH and MASHO systems (Figure 1) were calculated. Stable univariant reaction bundles around invariant points were determined through Schreinemakers analysis.

MASH petrogenetic grid

The *P–T* grid calculated for the MASH system is shown in red in Figure 1. Based on petrological relationships involving natural yoderite, arguably the most important univariant reactions that must appear in our calculated *P–T* grids are those that involve yoderite, kyanite, talc, quartz and water (McKie, 1959) and yoderite, kyanite, quartz, chlorite and water (Johnson & Oliver, 1998). In MASH, these two univariant assemblages are the (chl) and (ta) reactions, respectively, that intersect to define invariant point I6 of Schreyer and Seifert (1969). This invariant point calculates as IP6 in our MASH *P–T* grid at 14.2 kbar, 628 °C (Figure 1) compared to ~10.3 kbar, 670 °C in Schreyer and Seifert (1969). In our MASH calculations talc, chlorite and orthopyroxene feature Tschermaks exchange solid solution behaviour, which were not accounted for in the production of the MASH *P–T* grid topology in Schreyer and Seifert (1969). In addition, we included other MASH phases Mg-staurolite (st), Mg-cordierite (cd), pyrope garnet (g) and solid-solution sapphirine (sa) in our calculations. Chiefly for these two reasons, our calculated MASH grid involves a number of different univariant and invariant equilibria to that of Schreyer and Seifert (1969).

The *P–T* grid of Schreyer and Seifert (1969) is based on earlier experimental work notionally in the MASH system. Most notably, this includes the work done by Schreyer and Yoder Jr (1968), who synthesised yoderite in the supposed MASH system. The synthesis of yoderite in these experiments was later shown to be an experimental error (Fockenberg & Schreyer, 1991), and instead suggests that any yoderite bearing equilibria in the Schreyer and Seifert (1969) grid actually relate to the MASHO system. Indeed, previous studies argued it is impossible to produce a yoderite bearing *P–T* grid in the pure MASH system using experimental data due to yoderite stability purportedly being a strong function of Fe^{3+} (Fockenberg & Schreyer, 1991, 1994; Franz et al., 2013). We were able to calculate a *P–T* grid in MASH featuring yoderite as our model allows for Fe^{3+} to be absent. Therefore, calibrating the yoderite model via the MASHO *P–T*

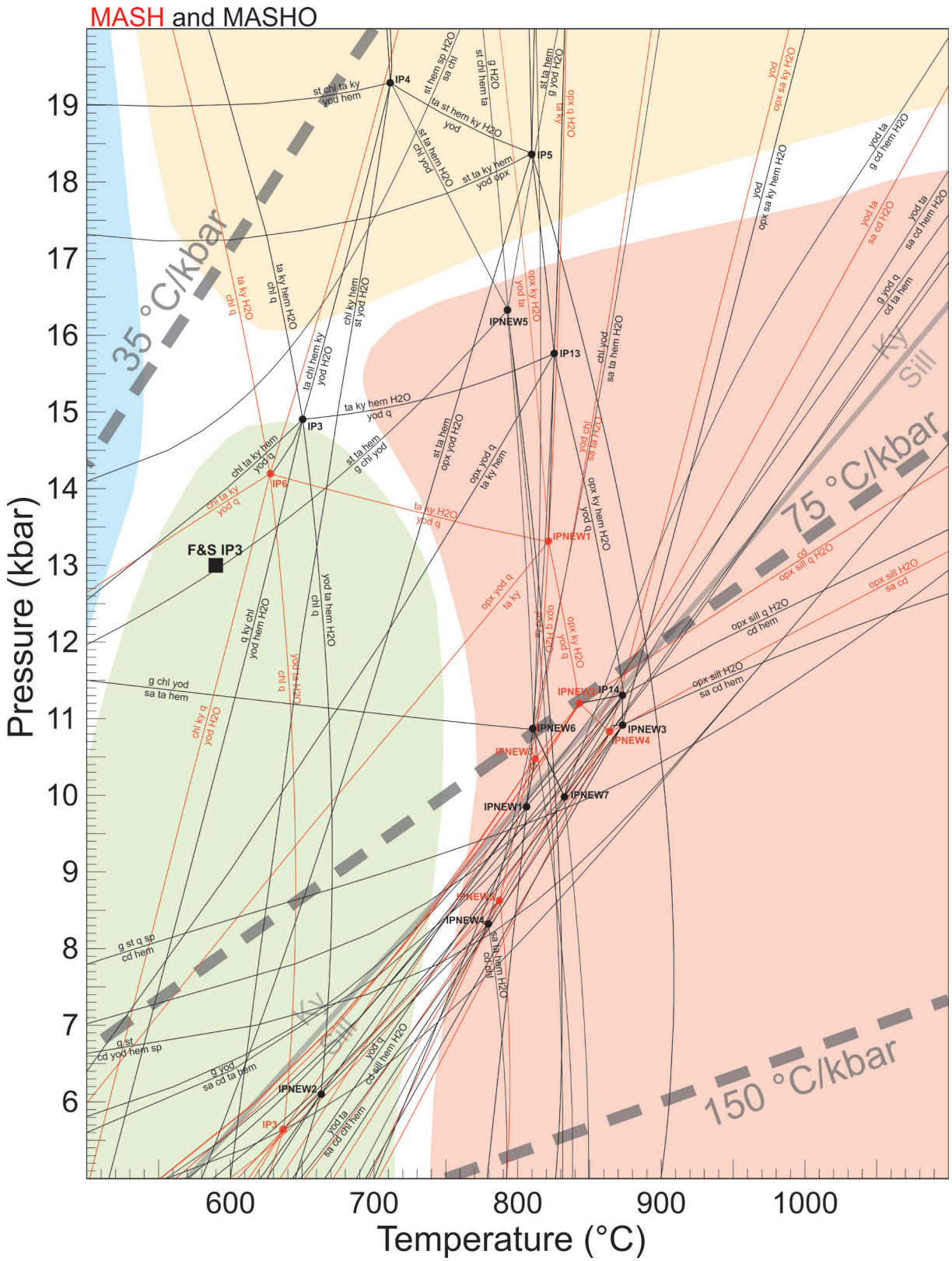

Figure 1. *P–T* grids calculated for the MASH (red) and MASHO (black) chemical systems. Invariant points are marked by circles, univariant reactions are denoted by the lines emanating from each point. Invariant points identical to those in Schreyer and Seifert (1969) and Fockenberg and Schreyer (1994) are given the same labels as those in their published grids. Points that are unique to our calculated grid are labelled as 'IPNEW'. The invariant point from which both known yoderite forming reactions emanate from, IP3, is shown for both this study (~15 kbar and 650

°C) and that by Fockenberg and Schreyer (1994; denoted by black square labelled 'F&S IP3'). The coloured fields behind the calculated grids refer to the different metamorphic facies as shown in Vernon and Clarke (2008), where red = granulite, green = amphibolite, blue = blueschist, yellow = eclogite. A fully labelled version of the calculated MASH and MASHO *P–T* grids can be located in the supplementary material.

grid may ultimately provide a better guide as to where the MASH grid occurs in *P–T* space. For these reasons we consider our calculated MASH *P–T* grid to be a successful result.

MASHO petrogenetic grid

MASH system invariant points represent the termination of hematite-absent univariant reaction lines in the MASHO system. In a direction away from the MASH termination point along each hematite-absent univariant MASHO reaction, the amount of Fe^{3+} in the assemblage increases. When Fe^{3+} reaches saturation in the univariant assemblage hematite appears to produce a MASHO invariant point. Therefore, each MASH invariant point shown in Figure 1 has a corresponding MASHO invariant point. The *P–T* grid calculated for the MASHO system is shown in black in Figure 1. The calculated MASHO grid strongly parallels the calculated MASH grid and occurs to slightly higher temperature. Our calculated MASHO grid resembles well the experimentally constrained *P–T* grid in Fockenberg and Schreyer (1994), with good agreement in the relative topology of invariant points and bundles of univariant reactions around invariant points. Invariant point three (IP3) is of particular note, as it represents the invariant point from which the yoderite forming reactions for both known natural occurrences emanate. With our thermodynamic model we calculate this point at higher *P–T* conditions than in the Fockenberg and Schreyer (1994) grid, at 15 kbar and 650 °C compared to ~13 kbar and 600 °C in their study. Point IP4 calculates at 19.3 kbar and 711 °C compared to ~21 kbar and 650 °C in Fockenberg and Schreyer (1994). Obtaining a large pressure difference between points IP3 and IP4 as well as achieving yoderite stability over a similar apparent thermal gradient span to Fockenberg and Schreyer (1994) were important drivers for our choice of W and DQF values for our yoderite model. More negative DQFmyod, as well as lower DQFyodo and Wmyod,yodo values, reduce the pressure difference between IP3 and IP4. If the W values were slightly higher and less negative, the pressure difference between IP3 and IP4 increases. However, the pressure of point IP3 also increases, moving further away from the location given in Fockenberg and

Table 2. Compositions of the phases at invariant points two, three and four (IP2, IP3 and IP4, respectively). IP3 relates to both known natural yoderite forming reactions, whereas IP2 constrains cordierite stability in whiteschists and IP4 constrains staurolite stability.

Invariant point	IP2	IP3	IP4
Phases present	cd q yod ta chl hem H_2O	ky q yod ta chl hem H_2O	st ky yod ta chl hem H_2O
Pressure (kbar)	6.1	14.9	19.3
Temperature (°C)	663	650.4	711.4
Compositional and order-disorder variables			
y (chl)	0.4	0.38	0.37
f (chl)	0.38	0.36	0.36
QA1 (chl)	0.22	0.26	0.27
f (yod)	0.08	0.06	0.07
y (ta)	0.07	0.06	0.05
f (ta)	0.03	0.03	0.02
v (ta)	0.06	0.07	0.04
f (st)	-	-	0.2
h (cd)	0.81	-	-

Schreyer (1994). Therefore, our chosen DQF and W values are ultimately a compromise that achieves yoderite stability in a location in *P–T* space, and with an overall grid topology that is consistent with constraints from Fockenberg and Schreyer (1994). Calculated compositions of the phases present at IP3, IP4 and IP2 are presented in Table 2. The calculated yoderite forming reactions that apply to Mautia Hill (talc + kyanite + hematite + H_2O > yoderite + quartz) and the Chewore Hills (talc + chlorite + hematite + kyanite > yoderite + H_2O) have identical topology to that in Fockenberg and Schreyer (1994). Seven stable invariant points not present in the experimentally constrained grid of Fockenberg and Schreyer (1994) occur in our calculated grid (labelled with the prefix 'IPNEW'), and a number of points in the Fockenberg and Schreyer (1994) grid were unable to be calculated. This highlights how calculated phase equilibria can provide valuable information about mineral equilibria that the restrictions of experiments (e.g. composition, difficulty of experiments) cannot (e.g. Kelsey, White, & Powell, 2005). Differences between our calculated *P–T* grid and their experimentally constrained *P–T* grid can probably be attributed to the following. First, the Fockenberg and Schreyer (1994) grid is based on experiments that were seeded with reactants and products, and thus were partially biased due to the metastable persistence of seeds. Second is the presence of FeO in their experiments, which was ignored for the construction of their *P–T* grid. This is particularly relevant for point IP5 (Figure 1) and the invariant points of Fockenberg and Schreyer (1994) that were unable to be calculated in our grid as these points contain either kornuperine or pyrope, which in the experimental run products were measured to contain significant FeO. Therefore, due to FeO the variance of many of the assemblages they encountered were trivariant or higher. Third, the Fockenberg and Schreyer (1994) grid doesn't account for Fe^{3+} or Tschermaks substitution in chlorite, talc or orthopyroxene. Overall these factors will have resulted in some uncertainty in the presence and locations of their reactions, which was acknowledged by Fockenberg and Schreyer (1994). Because of this, we consider absolute differences between reaction points and lines in the experimental versus calculated grids to be of minor consequence, and for our calculated *P–T* grid to be valid.

CONTROLS ON YODERITE STABILITY

To explore whether there are any consistent trends in *P–T* conditions or rock chemistry or mineralogy amongst whiteschists versus yoderite-bearing whiteschists and help identify factors controlling yoderite stability, Table 3 provides a summary of all known whiteschist localities with published data. From the data it is possible to observe a number of features that are for the most part restricted to yoderite-bearing whiteschists. The yoderite-bearing localities are almost exclusively the only whiteschist occurrences to contain hematite. The only known exception to this is the Modum Complex (Norway) whiteschist, but this occurrence is distinguishable by a much higher XFe ratio (=$Fe^{2+}/(Fe^{2+} + Mg^{2+})$) of 0.24, as opposed to values of 0 and 0.04 that are among the lowest recorded. The yoderite-bearing localities are also the only two with clear suggestions that Mn may be present in its tri- or tetra-valent state, although we are reluctant to draw any significant conclusions from this due to the lack of available information on the valence state of Mn in the other whiteschists. The majority of whiteschist localities also contain phlogopite or phengite, with some additionally containing feldspar, suggesting that the whiteschists at these locations may have contained enough K_2O and/or Na_2O and/or CaO to prevent yoderite stability. The peak *P–T* conditions experienced by each whiteschist provide further evidence for yoderite being restricted more by composition, as the majority of whiteschists record peak *P–T* conditions that overlap the large yoderite stability field.

From the data in Table 3 it seems that Fe_2O_3 is an important control on yoderite stability, as was recognised previously (Fockenberg & Schreyer, 1993, 1994). Components K_2O, Na_2O, CaO, and CO_2 were argued by previous workers to be factors controlling yoderite stability, due to these components causing stability of minerals such as micas, feldspars and carbonates rather than yoderite (Fockenberg & Schreyer, 1994; Franz et al., 2013). Mn_2O_3 is also stated as affecting yoderite stability but we are unable to perform calculations with this component. As the main question at hand is why yoderite is rare amongst even whiteschists, we will restrict our investigation to the five components that define the key mineralogy of whiteschists, namely H_2O, Al_2O_3, Fe_2O_3, MgO and SiO_2.

Yoderite stability in whiteschists

Figure 2 shows a qualitative MgO–Al_2O_3–SiO_2 compatibility diagram. Plotted on the diagram are whole-rock geochemical data (listed in Table 4) from all known whiteschists where such data is available, and rock compositions obtained from Franz et al. (2013), which are amenable to whiteschist and yoderite-bearing assemblages should the compositions attain appropriate *P*–*T* conditions. The average pelite composition (Ague, 1991) is also plotted. The green and purple shaded areas of the diagram show the crossing tie lines for yoderite-forming reactions at the Chewore Hills and Mautia Hill, respectively. The plotted geochemical data show that whiteschists and whiteschist protoliths are predominantly SiO_2-rich, but extend to more MgO-rich compositions. That is, whiteschist and whiteschist protolith compositions define a trend that is close to parallel

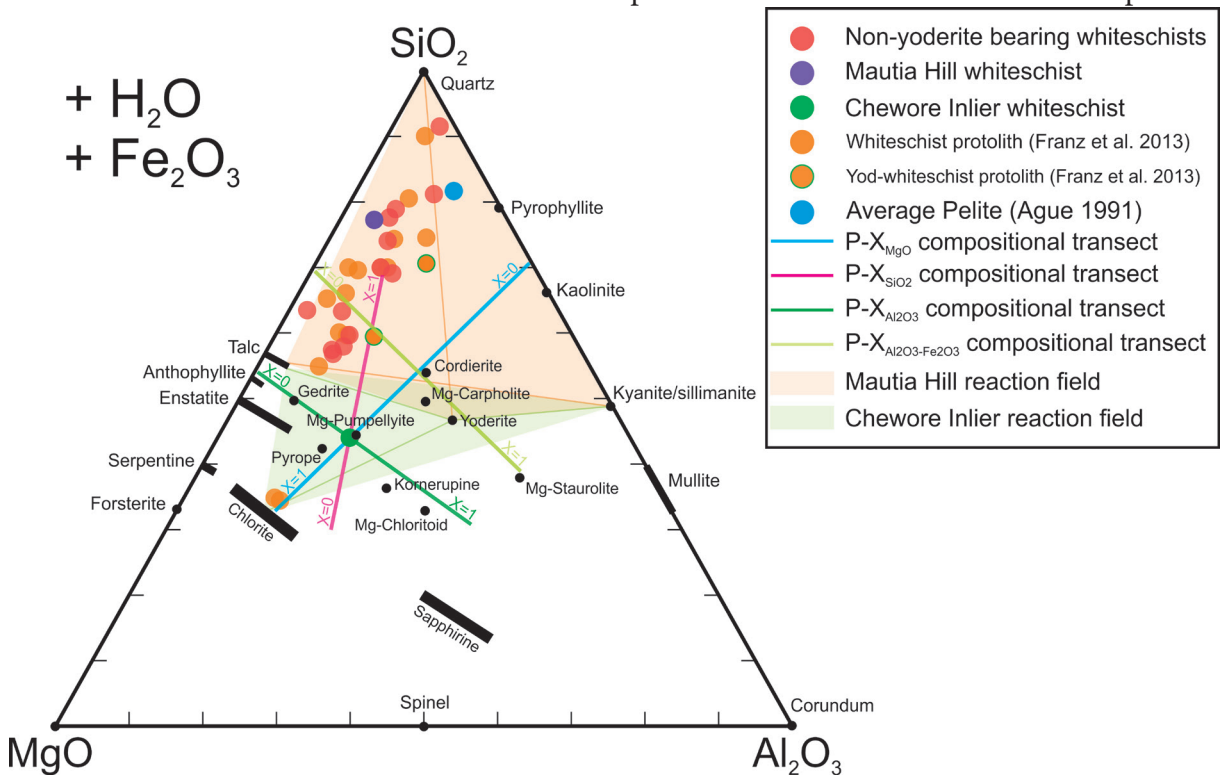

Figure 2. MgO, Al_2O_3, SiO_2 (MAS) compatibility diagram comparing compositions of whiteschists (red), yoderite bearing whiteschists (green, purple) and the average pelite of Ague (1991). Additionally plotted are compositions from Franz et al. (2013), which are labelled as 'whiteschist protolith' (yellow) and yoderite bearing whiteschist (yellow with green outline). The compositions plotted on the diagram are relative mole% oxide amounts. Each apex represents a composition of either 100 mole% MgO, Al_2O_3 or SiO_2. The compositional ranges of the MgO, Al_2O_3, SiO_2, Al_2O_3 and Fe_2O_3 *P*–*X* models marked as thick coloured lines. Also displayed are the crossing tie line reactions (shaded areas) for yoderite forming reactions for Mautia Hill (yoderite + quartz > talc + kyanite + H_2O; orange) and the Chewore Hills (talc + chlorite + kyanite + hematite > yoderite + H_2O; green).

Table 3. Summary of all known whiteschist localities. Abbreviations as follows: g = garnet, ky = kyanite, ph = phengite, ta = talc, q = quartz, coe = coesite, py = pyrope, hem = hematite, chl = chlorite, yod = yoderite, tur = tourmaline, amp = amphibole, phl = phlogopite, ksp = K-feldspar, ep = epidote, omp = omphacite, ru = rutile, ged = gedrite, cd = cordierite, crn = corundum, sa = sapphirine, pl = plagioclase, ab = albite, krn = kornuperine.

Whiteschist locality	Reference	Protolith	Peak Mineral assemblage	Fe–Ti oxide phases	*P–T* conditions	*P–T* conditions overlap yoderite stability?	Molar X_{Fe}	Oxidation state of Mn	Mica present?	Feldspar present?
Kokchetav Massif	(Parkinson, 2000)	Metasomatic mafic	Garnet, kyanite, phengite, talc, quartz, coesite	Rutile	35 kbar, ~780 °C	P no, T yes	Chemistry unavailable	Chemistry unavailable	Phengite	No
Dora Maira Massif	(Ferrando et al., 2009)	Sedimentary	Quartz, kyanite, talc, pyrope, phengite, coesite	Rutile	40–43 kbar, 730 °C	P no, T yes	0.13	Only reported as Mn 2+	Phengite	No
Zambezi Belt	(John, Schenk, Mezger, & Tembo, 2004; Johnson & Oliver, 1998)	Metasomatic mafic	Kyanite, talc, hematite ± chlorite, **yoderite**, quartz, tourmaline	Hematite	>13–21 kbar, 590–650 °C	Yes	0	Not stated but suggested to be oxidised	No	No
Pamirs	(Hubbard, Grew, Hodges, Yates, & Pertsev, 1999)	Sedimentary	Kyanite, talc, amphibole, talc, phlogopite, tourmaline ± K-feldspar	-	7 kbar, 650 °C	Yes	Chemistry unavailable	Chemistry unavailable	Phlogopite	K-feldspar
Dabie Shan	(Rolfo et al., 2000)	Metasomatic felsic	Quartz, epidote, kyanite, talc, omphacite, rutile	Rutile	26–27 kbar, ~710 °C	P no, T yes	0.23	Only reported as Mn 2+	No	No
Mautia Hill	(Jöns & Schenk, 2004; McKie, 1959)	Sedimentary	Quartz, **yoderite**, talc, kyanite, hematite	Hematite	10–11 kbar, 700–720 °C	Yes	0.04	Mn 3+	No	No
Sar-e-Sang	(Faryad, 2002)	Sedimentary	Talc, kyanite, tourmaline, gedrite, cordierite, corundum, sapphirine, plagioclase, phlogopite	Rutile	11 kbar, 650–800 °C	Yes	0.002	Only reported as Mn 2+	Phlogopite	Plagioclase
Val d'Ayas	(Le Bayon et al., 2006)	Metasomatic felsic	Talc, kyanite, phengite, quartz	Rutile	17–20 kbar, 550–600 °C	P no, T yes	0.14	Only reported as Mn 2+	Phengite	No
Lyell Highway	(Chmielowski, 2009)	Sedimentary	Talc, kyanite, garnet, quartz	-	13–20 kbar, 590–800 °C	yes	0.25	Only reported as Mn 2+	No	No
Modum Complex	(Munz, 1990)	Metasomatic mafic	Talc, kyanite, tourmaline, quartz ± gedrite, phlogopite, albite, sapphirine, opx, kornuperine	Hematite	6–8 kbar, 600–750 °C	Yes	0.24	Below detection	Phlogopite	Albite
Central Hoggar	(Adjerid et al., 2015)	Sedimentary or mafic protolith, metasomatised	Talc, kyanite ± quartz, amphibole, phengite	Rutile	>11 kbar, 600–800 °C	Yes	0.02	Not stated but might be oxidised	Phengite	No

Table 4. Geochemical data for whiteschists from all known localities where such data is available.

		Bulk-rock composition (mole %)									
Locality	Reference	H_2O	SiO_2	Al_2O_3	CaO	MgO	FeO*	K_2O	Na_2O	TiO_2	O
Chewore Hills	(Johnson & Oliver, 1998)	20.98	32.8	12.97	0.18	28.06	9.03	0	0.3	0.19	4.51
Zambezi Belt		6.54	65.73	7.57	0.11	16.82	3.49	0.06	0.19	1.11	1.62
Mautia Hill	(Schreyer, 1977)	5.89	70.4	4.52	0	17.36	2.08	0.02	0.13	0.19	0.68
Sar e Sang		10.36	49.87	8.37	0.1	30.3	0.27	0.11	0.52	0.2	0.1
Lyell Highway	(Chmielowski, 2009)	8.2	60.45	7.59	0.59	19.1	6.55	0.27	0.13	0.3	3.28
Dabie Shan	(Rolfo et al., 2000)	0.6	85.49	6.85	3.75	1.44	1.5	0.09	0.65	0.13	0.53
Val d'Ayas	(Le Bayon et al., 2006)	10.95	69.46	8.55	0.32	6.72	1.09	2.75	0.4	0.28	0.54
Dora Maira	(Ferrando et al., 2009)	4.92	71.34	9.23	0.18	10.79	1.6	1.55	0.09	0.28	0.01
Modum Complex	(Munz, 1990)	6.66	66.77	5.71	0.73	14.29	4.61	0.69	1.91	0.95	2.3
Central Hoggar	(Adjerid et al., 2015)	11.85	55.31	1.99	0.04	30.27	0.68	0.06	0.07	0.06	0.34

to the SiO_2–MgO join. Curiously, the natural green yoderite occurrence from Chewore Hills, and the two yoderite-amenable protoliths have rock compositions that are slightly more elevated in Al_2O_3 than most whiteschists and whiteschist protoliths, and may suggest an Al_2O_3 control on yoderite stability. However, this conflicts with the Mn-yoderite sample from Mautia hill, which has a relatively low amount of Al_2O_3 in comparison to most whiteschists. Using these observations as a basis, we now use our fully quantitative solid-solution thermodynamic model for yoderite to explore compositional controls on yoderite stability in whiteschists.

Pressure–composition modelling

P–X models were calculated at 725 °C to explore yoderite stability as a function of varying MgO, Al_2O_3, SiO_2, H_2O and Fe_2O_3 using the composition of the yoderite-bearing Chewore Hill whiteschist sample as the basis (Figure 3). The compositional ranges explored in each model are provided in Table 5. The compositional variation in MgO (Figure 3a), SiO_2 (Figure 3b), and Al_2O_3 (Figure 3c) are shown as coloured lines on the MAS compatibility diagram (Figures 2 and 3f). Figure 3a displays how the stability of yoderite varies with changing MgO. Yoderite is stable across all compositions in the model, suggesting that the amount of MgO is not a significant control on yoderite stability. The model shows that yoderite is generally restricted to pressures between 6.5–15.1 kbar, though its stability expands up-pressure in the absence of quartz to ~19 kbar where it coexists with talc and chlorite. This is in agreement with the work done by Fockenberg and Schreyer (1994), who observed that the stability of yoderite increases from around 15 to 19 kbar in the absence of quartz. At pressures above 15.1 kbar there is a stronger control on yoderite stability, whereby talc–kyanite–quartz assemblages without yoderite occur at low bulk MgO and yoderite stabilises at higher bulk MgO. At lower pressures talc–kyanite assemblages are not stable, and yoderite and quartz can occur in low MgO, high SiO_2 (relative to each other) compositions. In many regards the P–X_{SiO2} model (Figure 3b) mirrors the P–X_{MgO} model (Figure 3a), whereby yoderite is stable across the entire compositional range, depending on pressure, and many of the same assemblage fields occur. Similar to the P–X_{MgO} model, above ~15.1 kbar yoderite assemblages only occur to higher MgO, lower SiO_2

compositions, whereas talc–kyanite–quartz occurs in higher SiO_2 lower MgO compositions. Again, at pressures < ~15.1 kbar where talc–kyanite assemblages are not stable, yoderite and quartz can occur in high SiO_2, lower MgO (relative to each other) compositions.

Figure 3c shows how yoderite stability changes with varying concentrations of Al_2O_3. At low amounts of Al_2O_3, the assemblage chlorite–talc–hematite–water is stable over the entire pressure range of the model. Throughout the majority of the diagram, between X = 0.05 and X = 0.80 yoderite remains stable between ~6.5–18.8 kbar. For Al_2O_3-rich compositions (above X = 0.80) and pressures above 9 kbar, sapphirine-bearing assemblages stabilise at the expense of yoderite. Between 5.5–9.0 kbar, sapphirine and yoderite coexist in compositions from ~X = 0.6 to X = 1.0. Talc–kyanite assemblages do not occur in this model. This is a function of the relatively SiO_2-poor nature of the Chewore Hills whiteschist used as the basis, which plots below the talc–yoderite join (Figure 3f). Therefore, this model is unable to provide insight into yoderite-bearing assemblages versus the diagnostic talc–kyanite–quartz assemblages of whiteschists. However, the model does suggest that Al_2O_3 is perhaps a strong control on yoderite stability given that yoderite-bearing assemblages do not occur in very low Al_2O_3 compositions.

Yoderite formation was previously linked to high fO2 (Fockenberg & Schreyer, 1991, 1994), and as such it may be expected to only remain stable in compositions with a relatively high amount of Fe_2O_3. However, our model shows that for nearly the entire compositional range of the diagram, yoderite remains stable between ~6.5–18.8 kbar and is stable in hematite-absent assemblages in lower Fe_2O_3 compositions. However, it is important to note that yoderite is unstable at all pressures once there is no Fe_2O_3 at X = 0. That yoderite can occur in low-Fe_2O_3, hematite-absent compositions suggests that although the two known natural occurrences of the mineral in low Mn_2O_3 rock compositions are associated with hematite, it should be possible to observe yoderite in whiteschists that do not contain hematite. The provision of a calculated MASH *P*–*T* grid (Figure 1) that contains yoderite implies that at least in theory Fe_2O_3 is not a prerequisite for enabling yoderite stability. Exploring the stability of yoderite with varying amounts of H_2O (Figure 3e) reveals that only ~1 mole% H_2O (at X = 0.04) is required to form the mineral. Throughout the model, yoderite is stable at similar pressure ranges as those of the other models. As free H_2O disappears from the assemblages below ~X = 0.5, garnet and spinel become stable, and are found in the majority of fields < ~X = 0.5.

In order to more fully assess the influence of bulk Al_2O_3 on yoderite stability and its relationship to talc–kyanite assemblages, two further models with varying Al_2O_3 were calculated using a composition with an overall higher SiO_2 content (see light green line on Figure 2). These models were used to address how yoderite stability varies with increasing Al_2O_3 and either increasing (Figure 4a) or decreasing Fe_2O_3 (Figure 4b), in an attempt to further elucidate any Fe_2O_3 control. Both models show the talc–kyanite–quartz assemblage occurring at pressures above ~15.1 kbar, in compositions up to approximately X = 0.45. With higher Al_2O_3 (X > ~0.45) quartz disappears from assemblages in both models, and yoderite bearing assemblages occur. This comparison suggests that above a critical amount of Al_2O_3, yoderite bearing assemblages will form at the expense of typical whiteschist assemblages. That yoderite appears at the same location across the model suggests that Fe_2O_3 has a minor control on yoderite stability and that Al_2O_3 is the more dominant control. However, at pressures < 15.1 kbar yoderite is absent from the most Al_2O_3-poor compositions.

In summary of our investigation into compositional constrains on yoderite stability, we interpret that the relative importance of bulk MgO, SiO_2, and Al_2O_3 on whether yoderite

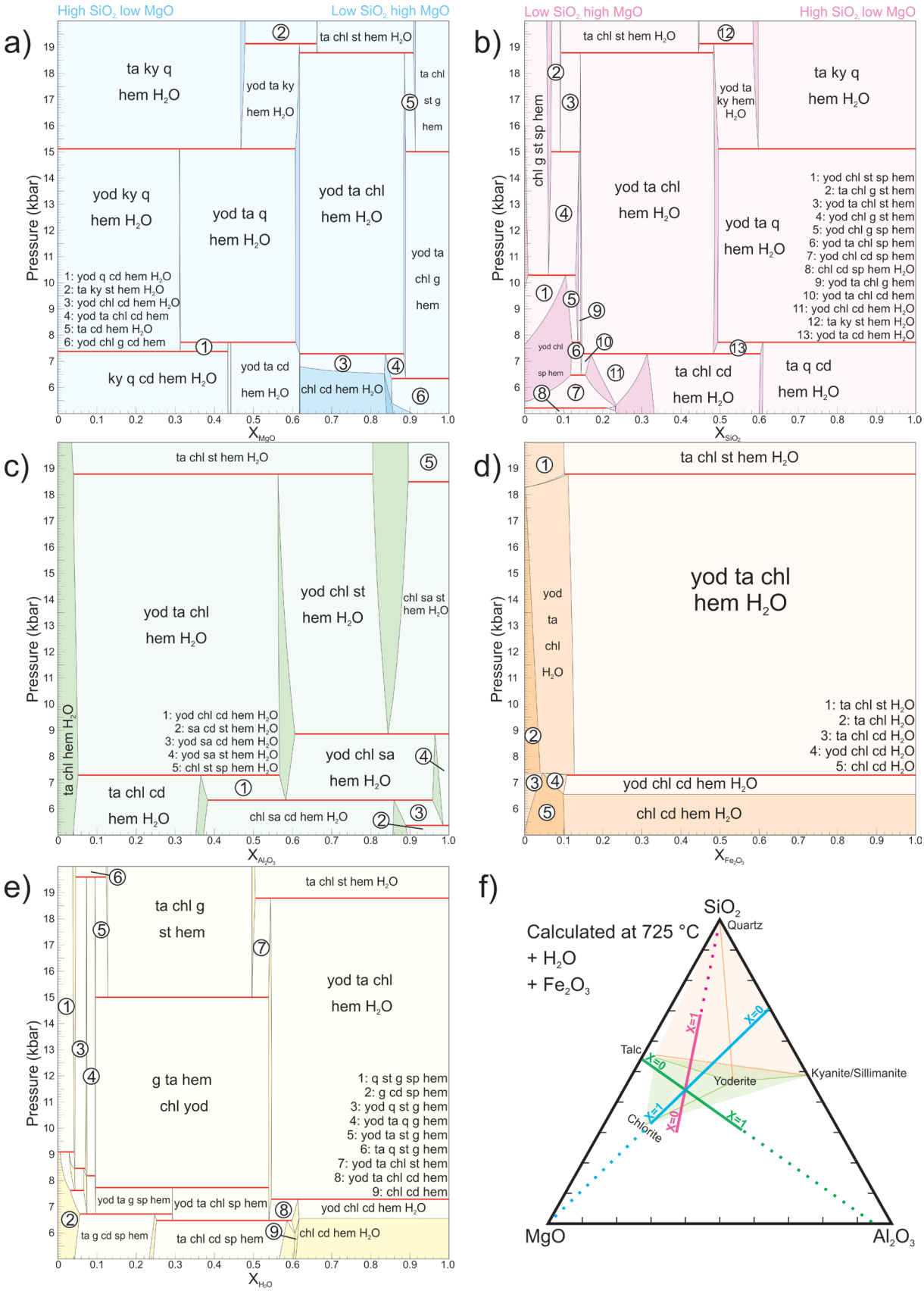

Figure 3. Calculated P–X models for the MASHO system at 725 °C, based on the chemistry of the green yoderite-bearing pod from the Chewore Hills, with the compositional (X) axis showing varying MgO (a), SiO_2 (b), Al_2O_3 (c), Fe_2O_3 (d) and H_2O (e). The exact compositional ranges for each diagram can be found in Table 5. Red hori-

zontal lines in each model denote univariant reactions. Labelled fields in each model have their assemblages listed within the relevant model. Individual, fully labelled diagrams for those presented in this figure can be located in the supplementary material. Compositional transects of the $P–X_{(MgO)}$, $P–X_{(SiO2)}$ and $P–X_{(Al2O3)}$ models are shown in the MAS diagram (f), with the crossing tie line reactions shown for the Mautia Hill (orange shaded) and Chewore Hills (green shaded) yoderite forming reactions. The compositions plotted on the diagram are relative mole% oxide amounts. Each apex represents a composition of either 100 mole% MgO, Al_2O_3 or SiO_2.

versus more typical talc–kyanite whiteschist assemblages occur is strongly a function of *P–T* conditions. At pressures high enough for talc–kyanite assemblages to form, yoderite can only occur if Al_2O_3 and MgO are high enough. In the case of MgO, the bulk composition needs to be more MgO-rich than the talc–kyanite join. At lower pressures where talc–kyanite assemblages are not stable for the conditions we have modelled, yoderite formation is effectively insensitive to bulk MgO and SiO_2 content and is more strongly controlled by bulk Al_2O_3 content. In application to real rock compositions, the importance of the trend on Figure 2 suggests Al_2O_3 is a major control on yoderite stability, but the importance of pressure and temperature conditions is difficult to distinguish from compositional controls.

APPLICATION OF MODEL TO CHEWORE-HILL SAMPLE

To demonstrate the ability of our model to provide quantitative *P–T* information for a specific rock, we present a calculated *P–T* model for yoderite bearing sample SJ.13.128.1 described by Johnson and Oliver (1998). This sample contains the green yoderite variety and was interpreted to record the *P–T* conditions of a metasomatised basalt (Johnson & Oliver, 1998) that may have been located at a depth > 50 km (John, Schenk, & Tembo, 2000). Metamorphism was likely associated with the collision between the Congo and Kalahari Cratons during amalgamation of the Gondwana supercontinent between *c.* 550–530 Ma (Johnson & Oliver, 2002). Figure 5 presents a series of photomicrographs that display the relationships between key minerals in the sample. Yoderite was interpreted by Johnson and Oliver (1998) to result from a reaction involving talc, kyanite, chlorite and hematite (+ H_2O). In thin section coarse-grained yoderite contains inclusions of chlorite (Figures 5b and 5d), kyanite and hematite. Yoderite is in contact with hematite, as well as finer-chlorite that serves to separate yoderite from coarse-grained talc and kyanite (Figures 5a to 5f). A single twin is observed in one of the larger yoderite grains in the sample. Talc grains are generally coarse-grained and elongate, weakly oriented in a similar direction. Talc is in contact with kyanite, yoderite and chlorite (Figure 5f). A small number of

Table 5. Compositional ranges used to calculate the *P–X* models displayed in Figure 3.

Model (Figure 3)		Bulk composition (mole %)					
		H_2O	SiO_2	Al_2O_3	MgO	FeO*	O
MgO (a)	X = 0	26.13	40.85	16.16	0	11.24	5.62
	X = 1	17.77	27.78	10.99	32	7.64	3.82
SiO_2 (b)	X = 0	22.21	20	13.74	29.71	9.56	4.78
	X = 1	12.49	55	7.33	16.71	5.38	2.39
Al_2O_3 (c)	X = 0	21.77	34.04	1	29.13	9.36	4.68
	X = 1	15.39	24.07	30	20.6	6.62	3.31
Fe_2O_3 (d)	X = 0	22.12	34.6	13.68	29.6	0	0
	X = 1	17.15	26.81	10.6	22.94	15	7
H_2O (e)	X = 0	0	37.54	14.85	32.12	10.34	5.17
	X = 1	30	26.28	10.39	22.48	7.24	3.62

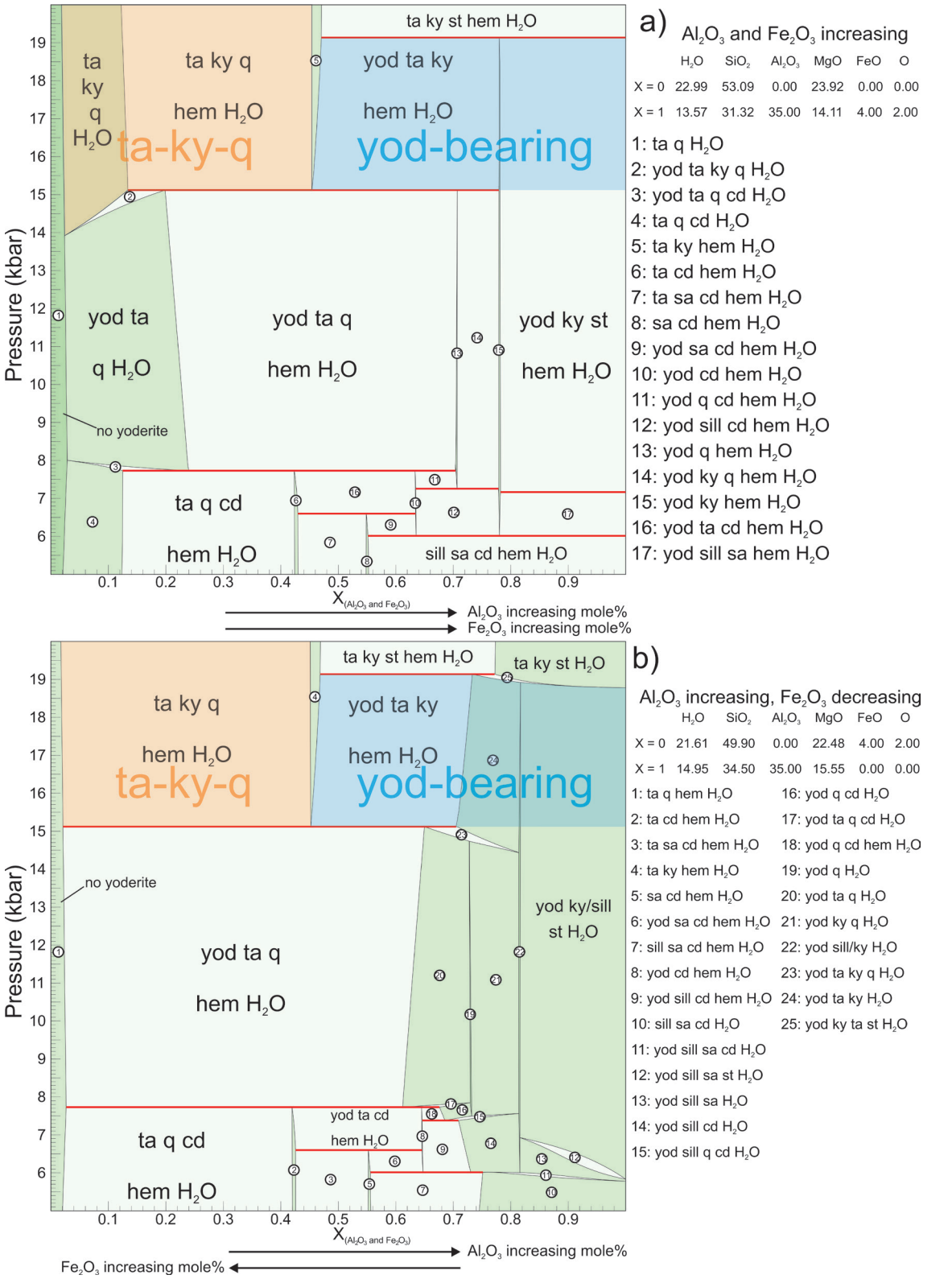

Figure 4. P–X pseudosections calculated in the MASHO system at 725 °C, where Al_2O_3 and Fe_2O_3 vary along the X-axis. In these models, the SiO_2 concentrations is higher than the talc–kyanite join (see light green bold line on Figure 2). This composition allows for a comparison between the stability of talc–kyanite–quartz bearing assemblages and yoderite-bearing assemblages. a) *P–X* model with Al_2O_3 and Fe_2O_3 both increasing from X = 0 to X = 1; b) P–X pseudosection with Al_2O_3 increasing and Fe_2O_3 decreasing from X = 0 to X = 1. Red horizontal lines on both models denote univariant reactions.

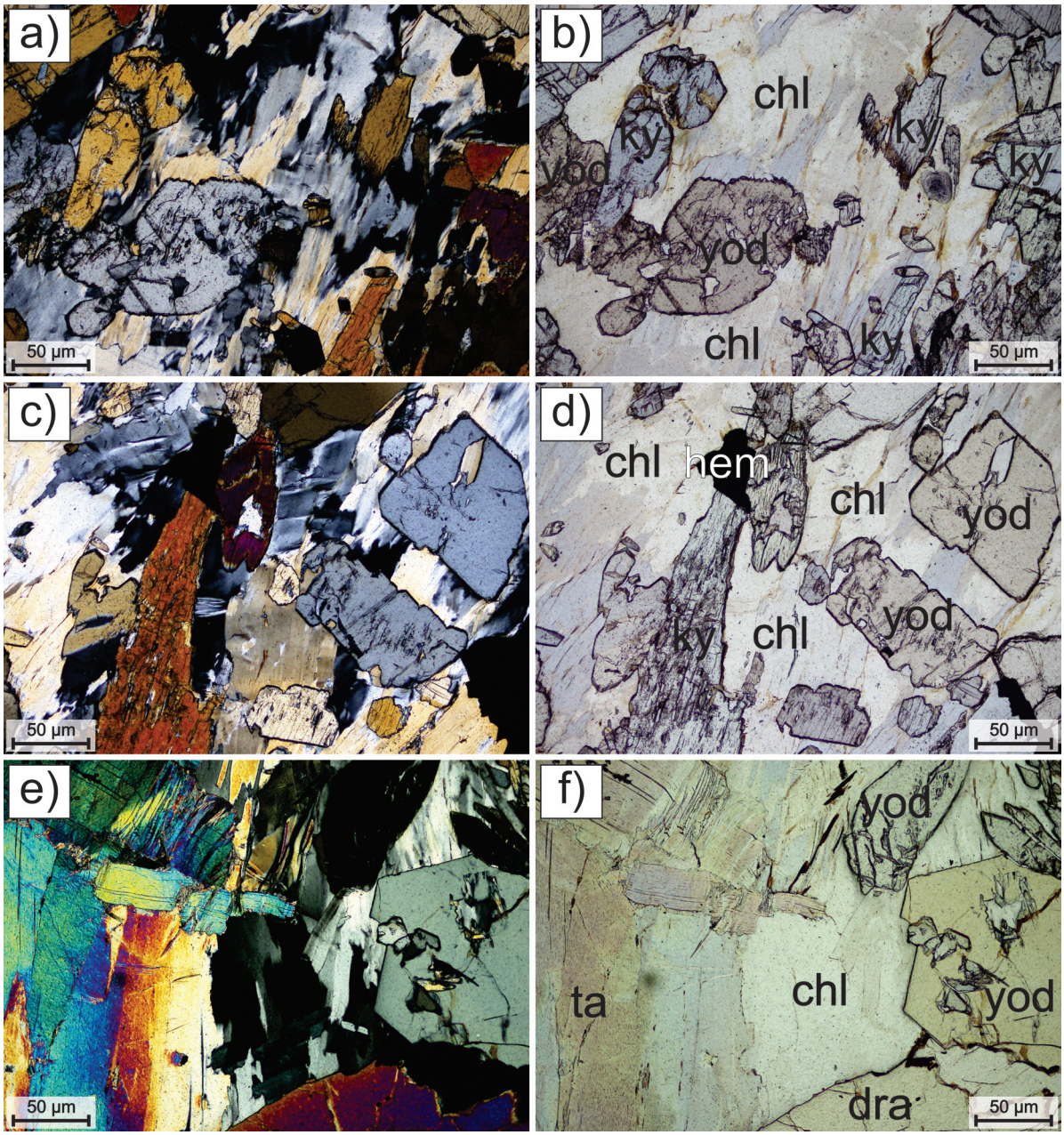

Figure 5. Photomicrographs of yoderite bearing sample SJ.13.128.1 discovered by Johnson and Oliver (1998). Abbreviations as follows: ky = kyanite, yod = yoderite, chl = chlorite, hem = hematite, ta = talc, dra = dravite. a) Cross-polarised image (XPL) of yoderite grains separated by kyanite and chlorite, with kyanite additionally separated by chlorite; b) same field of view as a) in plane polarised light (PPL); c) XPL image of yoderite with chlorite inclusions separated from kyanite with chlorite inclusions by later chlorite. Hematite is also present in the field of view and is in contact with chlorite and kyanite; d) same field of view as c) in PPL; e) XPL image of yoderite and talc in contact with chlorite, which serves to separate the two phases. Dravite is present at the bottom of the image and is in contact with chlorite and yoderite; f) same field of view as e) in PPL.

talc grains contain inclusions of chlorite and kyanite. Kyanite ranges from coarse- to fine-grained in size, and occurs in contact with yoderite, talc and chlorite (Figures 5b and 5d). The finer grains commonly occur as inclusions in yoderite and talc, whereas the coarser grains occur as individual crystals with inclusions of chlorite and very fine hematite. Chlorite is generally fine-grained and occurs in contact with all other minerals in the sample. Chlorite predominantly occurs as a matrix mineral separating the coarser talc, kyanite and yoderite

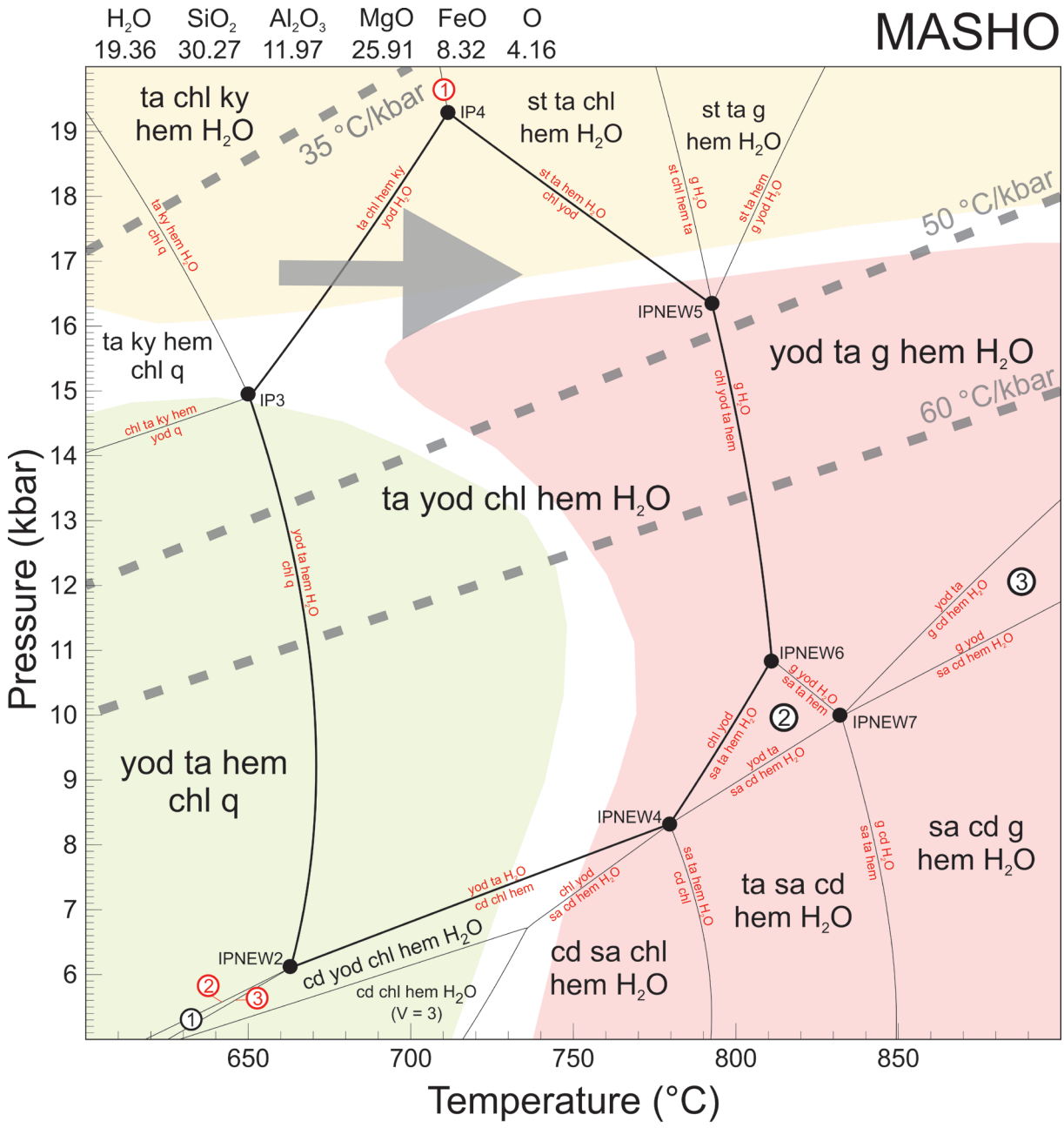

Figure 6. *P–T* pseudosection calculated in the MASHO system for a sample (SJ.13.128.1) of yoderite bearing white-schist from the Chewore Hills (Johnson & Oliver, 1998). Lines with red labels correspond to stable univariant reactions and all fields are divariant unless stated otherwise. The coloured fields behind the calculated grids refer to the different metamorphic facies as shown in Vernon and Clarke (2008), where red = granulite, green = amphibolite, blue = blueschist, yellow = eclogite. The field talc–yoderite–chlorite–hematite–H2O is outlined by bold lines, and corresponds to the peak assemblage displayed by the sample, occurring between ~6–19 kbar and 650–810 °C. Petrological observations of abundant kyanite support that the sample was located in the adjacent talc–kyanite–chlorite–hematite–H2O field during its prograde history. A possible prograde to peak P–T trajectory is denoted by the grey arrow.

grains, although coarser-grained chlorite does occur in the sample and is generally found in sharp contact with elongate talc grains. Dravite is also present within the sample (Figure 5f) and is in contact with kyanite, yoderite and chlorite. Dravite ranges from coarse- to fine-grained in size, with the coarser-grained dravite containing small inclusions of chlorite. From the spatial and textural relationships of grains in the sample, talc, yoderite, chlorite and hematite are interpreted to be part of the peak assemblage. The larger kyanite grains could be interpreted as belonging to the peak assemblage, as these grains are similar to yoderite and talc in terms of their distribution and size. However, kyanite also occurs as inclusions in peak talc and yoderite, indicating its prograde stability. Further to this there are only inclusions of chlorite and hematite in the larger kyanite grains, and not talc or yoderite. For this reason we interpret that all kyanite in this sample is part of the prograde assemblage, which implies the metastable persistence of kyanite during peak metamorphism.

Figure 6 displays the calculated *P*–*T* model, which is comprised almost entirely of divariant fields bound by univariant reactions and invariant points due to the relatively small number of components in the system. Our model ignores dravite present in this sample, as the internally consistent thermodynamic dataset of THERMOCALC does not contain boron. The model shows that the field corresponding to the interpreted peak assemblage talc–yoderite–chlorite–hematite is stable between ~6–19 kbar and ~650–810 °C. Whereas this field is stable over a large range of pressures, it is possible to use petrological relationships and geodynamic constraints to limit the practical size of the field. Johnson and Oliver (1998) determined that the yoderite in this sample formed via the univariant reaction ta + ky + chl + hem > yod + H_2O joining points IP3 and IP4. This suggests that the sample was located at the high pressure, low temperature region of the peak assemblage field for at least part of its metamorphic history, at pressures of 15–19 kbar and temperatures between 650–710 °C. As this whiteschist was interpreted to form during subduction between *c.* 550–530 Ma (Johnson & Oliver, 2002), it is possible to speculate that the geodynamic environment of subduction places thermal gradient restrictions that limit the accessible parts of the peak assemblage field. To highlight this possibility, additionally shown on Figure 6 are thermal gradients corresponding to hot modern-style (50 °C/kbar; Qu et al., 2011) and Proterozoic–Archean (60 °C/kbar; Bousquet et al., 2008) subduction zones. The age of this sample coincides with the proposed transition to modern subduction (Sizova, Gerya, Brown, & Perchuk, 2010) and as such we propose that the gradient of ~50 °C/kbar provides a practical upper limit for the range of *P*–*T* conditions that were possible, thereby halving the pressure range of the peak field. The interpreted metastable persistence of significant (40%) kyanite into the peak field provides a good indication of the sample's prograde trajectory, suggesting that the rock could have reached pressures in excess of 15–20 kbar. We note that in larger chemical systems univariant reactions become fields, and so kyanite would coexist with the interpreted yoderite-bearing peak assemblage in a (narrow?) field in such calculations. Due to the lack of diversity of retrograde minerals in the sample, a detailed cooling trajectory cannot be reliably constrained in this sample. However, if the sample was indeed subducted, the *P*–*T* path is likely to be clockwise, involving cooling with decreasing pressure to reach chlorite stability.

APPLICATION OF MODEL TO MAUTIA HILL

Initial discoveries of both the green and purple varieties of yoderite were reported from Mautia Hill, Tanzania (McKie, 1959, 1966). Petrographic information is only available for purple yoderite at this location, which is interpreted to replace the margins of talc and

kyanite and from via the reaction ta + ky > yod + q (McKie, 1959; Mruma & Basu, 1987). Metamorphism of the Mautia Hill whiteschist likely occurred at *c.* 550 Ma, as a result of collision between the Tanzania Craton and Madagascar-India during Gondwana formation (Cutten, Johnson, & Waele, 2006). Applying our solid-solution yoderite *a–x* model is not directly possible for a green yoderite-bearing rock from this locality, as a rock composition cannot be sourced. However, Jöns and Schenk (2004) report maximum *P–T* conditions of 10–11 kbar and 720 °C based on conventional thermobarometry of metabasite parageneses. The temperatures are consistent with talc–kyanite and yoderite stability in our MASH and MASHO P–T grids. However, in the absence of being able to calculate a *P–T* model based on whole rock geochemistry it is not possible to provide a rigorous analysis of the reported pressures. Suffice it to say that yoderite and quartz, as well as yoderite-bearing quartz-absent assemblages, are stable in our *P–T* grids at 10–11 kbar.

GEODYNAMIC CONTROLS ON YODERITE FORMATION

Many existing studies on whiteschist and yoderite stability focus on rock compositional criteria for explaining their rarity. Whereas this is no doubt an important factor, the geodynamic environment of whiteschist formation, advocated to be subduction, is mostly not considered as an important factor (cf. Schreyer, 1988). The stability field of yoderite as calculated in this study and as shown in (Fockenberg & Schreyer, 1994; Schreyer, 1988) occurs to higher thermal gradient conditions than talc–kyanite assemblages, and for this reason the rarity of yoderite amongst whiteschist may reflect a geodynamic control in addition to compositional factors. With the exception of those found in the Modum Complex and possibly Pamir Mountains, all known whiteschists are proposed to be late Neoproterozoic or Phanerozoic in age (Adjerid, Godard, & Ouzegane, 2015; Chmielowski, 2009; Faryad, 2002; Ferrando, Frezzotti, Petrelli, & Compagnoni, 2009; Jöns & Schenk, 2004; Le Bayon, de Capitani, & Frey, 2006; Parkinson, 2000; Rolfo, Compagnoni, Shutong, & Jiang, 2000). As whiteschists are subduction related and many fall within the definition of a UHP rock (Chopin, 2003), it may be the case that whiteschists require Earth with the cooler ambient upper-mantle temperatures that allowed for the occurrence of modern subduction systems (Brown, 2007; Sizova et al., 2010; Sizova, Gerya, & Brown, 2014). Due to this, the rarity of yoderite in the geologic record could, in part, be the result of modern subduction systems generally failing to produce the warmer geothermal gradients necessary to form yoderite.

SUMMARY

We have presented a new *a–x* model for yoderite, for use in the MASH and MASHO chemical systems, which can be extended to FMASHO. The results of our modelling demonstrate that the stability of yoderite is a function of bulk rock SiO_2, MgO and Al_2O_3 concentration, but which of these is most important is a function of pressure and temperature. With the presence of sufficient Al_2O_3, green-yoderite bearing assemblages will occur at the expense of the typical talc–kyanite–quartz assemblages of whiteschists. Fe_2O_3 and H_2O are not considered to be major controls on yoderite stability. We propose that the rarity of yoderite in nature, even among whiteschists, is due to a combination of rock compositional factors as well as the thermal restrictions imposed by modern-style subduction zones. Talc–kyanite assemblages occur at lower thermal gradients than yoderite and so will be favoured. The provision of an *a–x* model for yoderite provides a platform for more thorough *P–T* constraints in whiteschists, including the impact of addition of other chemical components, thus enhancing the utility of whiteschists in tectonometamorphic research.

ACKNOWLEDGEMENTS

S. Johnson is thanked for providing the authors with a sample of the green-yoderite bearing whiteschist from the Chewore Hills. BLA is supported by a Research Training Program scholarship. This paper forms TRaX record #390.

REFERENCES

Abu-Eid, R.M., Langer, K., & Seifert, F. (1978). Optical absorption and Mössbauer spectra of purple and green yoderite, a kyanite-related mineral. Physics and chemistry of minerals, 3(3), 271-289.

Adjerid, Z., Godard, G., & Ouzegane, K. (2015). High-pressure whiteschists from the Ti-N-Eggoleh area (Central Hoggar, Algeria): A record of Pan-African oceanic subduction. Lithos, 226, 201-216.

Ague, J. J. (1991). Evidence for major mass transfer and volume strain during regional metamorphism of pelites. Geology, 19(8), 855-858.

Bousquet, R., El Mamoun, R., Saddiqi, O., Goffé, B., Möller, A., & Madi, A. (2008). Mélanges and ophiolites during the Pan-African orogeny: the case of the Bou-Azzer ophiolite suite (Morocco). Geological Society, London, Special Publications, 297(1), 233-247.

Brown, M. (2007). Metamorphic conditions in orogenic belts: a record of secular change. International Geology Review, 49(3), 193-234.

Chmielowski, R.M. (2009). The Cambrian metamorphic history of Tasmania. Thesis, University of Tasmania,

Chopin, C. (2003). Ultrahigh-pressure metamorphism: tracing continental crust into the mantle. Earth and Planetary Science Letters, 212(1), 1-14.

Cutten, H., Johnson, S.P., & De Waele, B. (2006). Protolith ages and timing of metasomatism related to the formation of whiteschists at Mautia Hill, Tanzania: implications for the assembly of Gondwana. The Journal of geology, 114(6), 683-698.

Faryad, S.W. (2002). Metamorphic conditions and fluid compositions of scapolite-bearing rocks from the lapis lazuli deposit at Sare Sang, Afghanistan. Journal of Petrology, 43(4), 725-747.

Ferrando, S., Frezzotti, M.L., Petrelli, M., & Compagnoni, R. (2009). Metasomatism of continental crust during subduction: the UHP whiteschists from the Southern Dora-Maira Massif (Italian Western Alps). Journal of Metamorphic Geology, 27(9), 739-756.

Fockenberg, T., & Schreyer, W. (1991). Yoderite, a mineral with essential ferric iron; its lack of occurrence in the system MgO–Al2O3–SiO2–H2O. American mineralogist, 76(5-6), 1052-1060.

Fockenberg, T., & Schreyer, W. (1993). Synthesis and properties of Mn-bearing yoderite and of Mn-bearing kornerupine as by-product. Mineralogy and Petrology, 48(2-4), 115-128.

Fockenberg, T., & Schreyer, W. (1994). Stability of Yoderite in the Absence and in the Presence of Quartz: an Experimental Study in the System MgO–Al2O3–Fe2O3–SiO2–H2O. Journal of Petrology, 35(5), 1341-1375.

Franz, L., Romer, R.L., & de Capitani, C. (2013). Protoliths and phase petrology of whiteschists. Contributions to Mineralogy and Petrology, 166(1), 255-274.

Higgins, J.B., Ribbe, P.H., & Nakajima, Y. (1982). An ordering model for the commensurate antiphase structure of yoderite. American mineralogist, 67(1-2), 76-84.

Holland, T., & Powell, R. (1992). Plagioclase feldspars: Activity-composition relations based upon Darken's quadratic formalism and Landau theory. American mineralogist, 77, 5341.

Holland, T., & Powell, R. (1996). Thermodynamics of order-disorder in minerals: II. Symmetric formalism applied to solid solutions. American mineralogist, 81(11-12),

1425-1437.

Holland, T., & Powell, R. (2003). Activity–composition relations for phases in petrological calculations: an asymmetric multicomponent formulation. Contributions to Mineralogy and Petrology, 145(4), 492-501.

Holland, T., & Powell, R. (2006). Mineral activity–composition relations and petrological calculations involving cation equipartition in multisite minerals: a logical inconsistency. Journal of Metamorphic Geology, 24(9), 851-861.

Holland, T., & Powell, R. (2011). An improved and extended internally consistent thermodynamic dataset for phases of petrological interest, involving a new equation of state for solids. Journal of Metamorphic Geology, 29(3), 333-383.

John, T., Schenk, V., & Tembo, F. (2000). MORB-type geochemical signatures of eclogites from central Zambia: evidence for a Precambrian suture-zone. Journal of African Earth Sciences, 30(4), 42-42.

Johnson, S. (2011). Preliminary investigation of in-situ, high-pressure, high-fO2 metasomatism and metamorphism of meta-basalt to whiteschist. Frontier Research on Earth Evolution, 1.

Johnson, S., & Oliver, G.J.H. (1998). A second natural occurrence of yoderite. Journal of Metamorphic Geology, 16(6), 809-818.

Johnson, S., & Oliver, G.J.H. (2002). High fO2 metasomatism during whiteschist metamorphism, Zambezi belt, northern Zimbabwe. Journal of Petrology, 43(2), 271-290.

Jöns, N., & Schenk, V. (2004). Petrology of whiteschists and associated rocks at Mautia Hill (Tanzania): fluid infiltration during high-grade metamorphism? Journal of Petrology, 45(10), 1959-1981.

Kelsey, D.E., White, R.W., Holland, T., & Powell, R. (2004). Calculated phase equilibria in K2O–FeO–MgO–Al2O3–SiO2–H2O for sapphirine-quartz-bearing mineral assemblages. Journal of Metamorphic Geology, 22(6), 559-578.

Kelsey, D.E., White, R.W., & Powell, R. (2005). Calculated phase equilibria in K2O–FeO–MgO–Al2O3–SiO2–H2O for silica-undersaturated sapphirine-bearing mineral assemblages. Journal of Metamorphic Geology, 23(4), 217-239.

Le Bayon, R., de Capitani, C., & Frey, M. (2006). Modelling phase–assemblage diagrams for magnesian metapelites in the system K2O–FeO–MgO–Al2O3–SiO2–H2O: geodynamic consequences for the Monte Rosa nappe, Western Alps. Contributions to Mineralogy and Petrology, 151(4), 395-412.

McKie, D. (1959). Yoderite, a new hydrous magnesium iron alumino-silicate from Mautia Hill, Tanganyika.

McKie, D. (1966). A green variety of yoderite. Nature, 210, 1148.

Mruma, A.H., & Basu, N.K. (1987). Petrology of the talc-kyanite-yoderite-quartz schist and associated rocks of Mautia Hill, Mpwapwa District, Tanzania. Journal of African Earth Sciences, 6(3), 301-311.

Munz, A. (1990). Whiteschists and orthoamphibole-cordierite rocks and the P–T–t path of the Modum Complex, South Norway. Lithos, 24(3), 181-199.

Parkinson, C.D. (2000). Coesite inclusions and prograde compositional zonation of garnet in whiteschist of the HP-UHPM Kokchetav massif, Kazakhstan: a record of progressive UHP metamorphism. Lithos, 52(1), 215-233.

Powell, R., White, R.W., Green, E.C.R., Holland, T.J.B., & Diener, J.F.A. (2014). On parameterizing thermodynamic descriptions of minerals for petrological calculations. Journal of Metamorphic Geology, 32(3), 245-260.

Powell, R., & Holland, T. (1993). On the formulation of simple mixing models for complex phases. American mineralogist, 78(11-12), 1174-1180.

Powell, R., & Holland, T. (1999). Relating formulations of the thermodynamics of min-

eral solid solutions: activity modeling of pyroxenes, amphiboles, and micas. American mineralogist, 84(1-2), 1-14.

Powell, R., Holland, T., & Worley, B. (1998). Calculating phase diagrams involving solid solutions via non-linear equations, with examples using THERMOCALC. Journal of Metamorphic Geology, 16(4), 577-588.

Qu, J.F., Xiao, W.J., Windley, B.F., Han, C.M., Mao, Q.G., Ao, S.J., & Zhang, J.E. (2011). Ordovician eclogites from the Chinese Beishan: implications for the tectonic evolution of the southern Altaids. Journal of Metamorphic Geology, 29(8), 803-820.

Rolfo, F., Compagnoni, R., Shutong, X.U., & Jiang, L. (2000). First report of felsic whiteschist in the ultrahigh-pressure metamorphic belt of Dabie Shan, China. European Journal of Mineralogy, 12(4), 883-898.

Schreyer, W., & Seifert, F. (1969). Compatibility relations of the aluminum silicates in the systems MgO–Al2O3–SiO2–H2O and K2O–MgO–Al2O3–SiO2–H2O at high pressures. American Journal of Science, 267(3), 371-388.

Schreyer, W., & Yoder Jr, H.S. (1968). Yoderite: synthesis, stability, and interpretation of its natural occurrence. Carnegie Institution of Washington Yearbook, 66, 376-393.

Schreyer, W. (1974). Whiteschist, a new type of metamorphic rock formed at high pressures. Geologische Rundschau, 63(2), 597-609. doi: 10.1007/bf01820834

Schreyer, W. (1977). Whiteschists: their compositions and pressure-temperature regimes based on experimental, field, and petrographic evidence. Tectonophysics, 43(1), 127-144.

Schreyer, W. (1988). Experimental studies on metamorphism of crustal rocks under mantle pressures. Mineralogical Magazine, 52(1), 1-26.

Sizova, E., Gerya, T., Brown, M., & Perchuk, L.L. (2010). Subduction styles in the Precambrian: insight from numerical experiments. Lithos, 116(3), 209-229.

Sizova, E., Gerya, T., & Brown, M. (2014). Contrasting styles of Phanerozoic and Precambrian continental collision. Gondwana Research, 25(2), 522-545.

White, R.W., Powell, R., Holland, T.J.B., Johnson, T.E., & Green, E.C.R. (2014). New mineral activity–composition relations for thermodynamic calculations in metapelitic systems. Journal of Metamorphic Geology, 32(3), 261-286.

White, R.W., Powell, R., Holland, T.J.B., & Worley, B.A. (2000). The effect of TiO2 and Fe2O3 on metapelitic assemblages at greenschist and amphibolite facies conditions: mineral equilibria calculations in the system K2O–FeO–MgO–Al2O3–SiO2–H2O–TiO2–Fe2O3. Journal of Metamorphic Geology, 18(5), 497-512.

White, R.W., Powell, R., & Johnson, T.E. (2014). The effect of Mn on mineral stability in metapelites revisited: New a–x relations for manganese-bearing minerals. Journal of Metamorphic Geology, 32(8), 809-828.

CHAPTER 5

This chapter s prepared for publication to *Gondwana Research* as:
Alessio, B.L., Collins, A. S., Kelsey, D. E., Clark, C., Glorie, S. & Taylor, R. Identifying the tectono-metamorphic overprints of a Gondwana forming collision: a structural and thermobarometric transect of the Southern Irumide and Zambezi belts, Zambia.

Statement of Authorship

Title of Paper	Identifying the tectono-metamorphic overprint of a Gondwana forming collision: a structural and thermobarometric transect of the Southern Irumide and Zambezi belts, Zambia
Publication Status	☐ Published ☐ Accepted for Publication ☐ Submitted for Publication ☑ Unpublished and Unsubmitted w ork w ritten in manuscript style
Publication Details	Alessio, Brandon L., Collins, Alan S., Kelsey, David E., Clark, Chris, Glorie, Stijn, Siegfried, Pete & Taylor, Richard. Identifying the tectono-metamorphic overprint of a Gondwana forming collision: a structural and thermobarometric transect of the Southern Irumide and Zambezi belts, Zambia.

Principal Author

Name of Principal Author (Candidate)	Brandon Luke Alessio		
Contribution to the Paper	Fieldwork, sample preparation, data collection, processing and interpretation, manuscript design and composition, drafting of figures.		
Overall percentage (%)	80		
Certification:	This paper reports on original research I conducted during the period of my Higher Degree by Research candidature and is not subject to any obligations or contractual agreements with a third party that would constrain its inclusion in this thesis. I am the primary author of this paper.		
Signature		Date	07/01/19

Co-Author Contributions

By signing the Statement of Authorship, each author certifies that:

i. the candidate's stated contribution to the publication is accurate (as detailed above);

ii. permission is granted for the candidate in include the publication in the thesis; and

iii. the sum of all co-author contributions is equal to 100% less the candidate's stated contribution.

Name of Co-Author	Alan Collins		
Contribution to the Paper	Fieldwork, guidance in data interpretation and manuscript review.		
Signature		Date	14/01/19

Name of Co-Author	David Kelsey		
Contribution to the Paper	Data collection in addition to guidance in data collection and interpretation, as well as manuscript review.		
Signature		Date	08/01/19

Name of Co-Author	Chris Clark		
Contribution to the Paper	Assistance in data collection and manuscript review.		
Signature		Date	16/01/19

Name of Co-Author	Stijn Glorie		
Contribution to the Paper	Manuscript review.		
Signature		Date	07/01/19

Name of Co-Author	Pete Siegfried		
Contribution to the Paper	Manuscript review.		
Signature		Date	26/01/19

Name of Co-Author	Richard Taylor		
Contribution to the Paper	Assistance in data collection and manuscript review.		
Signature		Date	07/01/19

ABSTRACT

The late-Neoproterozoic collision of the Congo and Kalahari cratons occurred during the final stages of Gondwana amalgamation. In the Southern Irumide and Zambezi belts of southern Zambia, this collision is recorded by pervasive structural overprints and metamorphic overprints that vary significantly, ranging from high-pressure 'whiteschist' mineral assemblages to more conventional amphibolite facies mineral assemblages. This study uses structural and thermobarometric constraints to better understand the contrasting tectono-metamorphic overprints within the Southern Irumide and Zambezi belts, and the implications they have for Gondwana assembly. Additionally, we present U–Pb and Lu–Hf isotopic data for Zambezi Belt supracrustal units, which constrain the evolution of the region and demonstrate their equivalence in age and isotopic composition to units in the Southern Irumide Belt. Thermobarometric calculations for a sample of metapelite from a supracrustal sequence in the Zambezi Belt show it records peak conditions of 4.1–7.9 kbar and 560–670 °C (70–165 °C/kbar). Calculations made for a sample of retrogressed whiteschist from the Chewore–Rufunsa Terrane of the Southern Irumide Belt suggest conditions below 15 kbar and 590 °C (30–90 °C/kbar), further elucidating the pressure–temperature evolution of whiteschists in the region that experienced peak conditions between 9–19 kbar and 650–790 °C (30–90 °C/kbar). Both the metapelite and (retrogressed) whiteschist are interpreted to have formed during Congo–Kalahari collision, and are likely coeval with E–W trending folds identified in both the Southern Irumide and Zambezi belts. However, the amphibolite facies metapelite is interpreted to have formed in a compressional setting proximal to the southern Congo margin, whereas the whiteschist instead formed directly at the site of continental collision, marking the suture zone between the Congo and Kalahari cratons. These data highlight the multiple processes occurring during Congo–Kalahari collision, further elucidating the development of a key suture zone at the centre of Gondwana amalgamation.

INTRODUCTION

The end of the Neoproterozoic Era saw the emergence of complex life (Meert and Lieberman, 2008) and amalgamation of the supercontinent Gondwana (e.g. Merdith et al., 2017). These two events mark critical stages in the development of both the planet and life, and are likely intrinsically related (Meert and Lieberman, 2008). Thus, constraining Neoproterozoic palaeogeography and the amalgamation of Gondwana is a key step towards understanding the inteplay between the evolving continents and wider Earth system. The Congo Craton (Fig. 1) occupied a key position of central Gondwana and is bordered on its southern margin by the Damara–Lufilian–Zambezi orogens, which record collision between the Congo and Kalahari cratons in the final stages of Gondwana amalgamation (e.g. De Waele et al., 2008; John et al., 2004; Merdith et al., 2017). This collision is additionally recorded in the Mesoproterozoic Southern Irumide Belt (SIB), which formed part of the southern Congo margin during the Neoproterozoic (Alessio et al., 2019; Johnson et al., 2006). Together, the SIB and adjacent Zambezi Belt (Fig. 1a, b) provide complementary tectono-metamorphic records that provide first order constraints on the style and dynamics of collision between the Congo and Kalahari cratons. Such constraints provide insights into the development of a major collision zone forming part of central Gondwana, thereby enabling a better understanding of its amalgamation. This study provides new structural and pressure–temperature (*P–T*) constraints for the Chewore–Rufunsa Terrane of the SIB, and supracrustals of the Zambezi Belt. These are compared to pre-existing data in order to constrain the tectono-metamorphic overprints generated during Congo–Kalahari collision. In addition, we provide new U–Pb, Lu–Hf and rare earth element (REE) zircon data for supracrustal lithologies from the Zambezi Belt, which are used

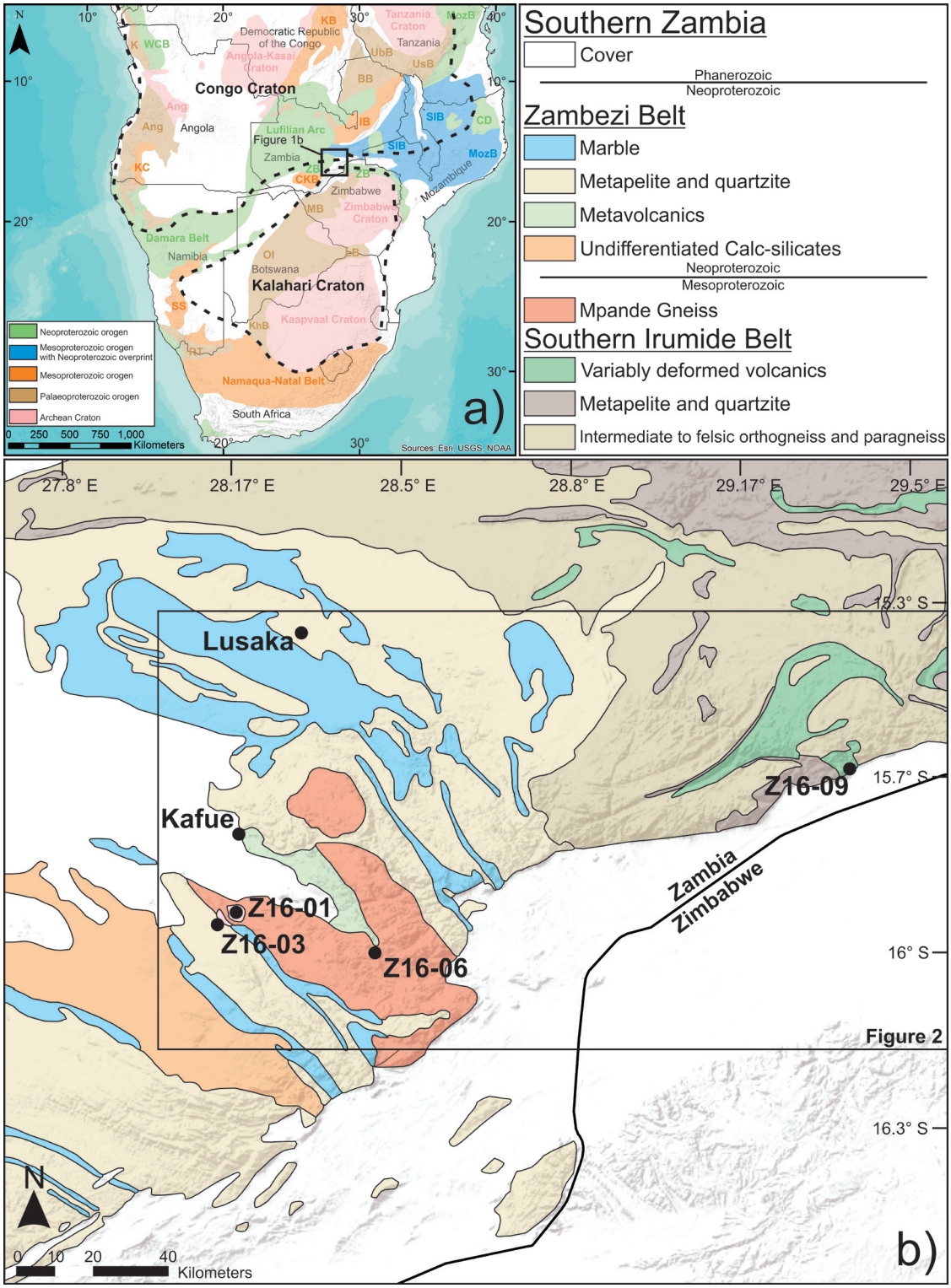

Figure 1. Location maps illustrating the study area and its position relative to tectonic units in central Africa. a) Simplified tectonic map of central Africa adapted from Alessio et al. (2018) and Hanson (2003). Abbreviations: ANG, Angola Block; BW, Bangweulu Block; CD, Cabo Delgado Nappe Complex; CKB, Choma-Kalomo Block; DB, Damara Belt; GAB, Gabon Craton; IB, Irumide Belt; KAP, Kaapvaal Craton; KAS, Kasai Block; KB, Kibaran Belt; LA, Lufilian Arc; LB, Limpopo Belt; LF, Lurio Foreland; MAB, Magondi Belt; MB, Mozambique Belt; NC, NE Congo Block; NKB, NE Kibaran Belt; RUS, Rusizian Belt; SIB, Southern Irumide Belt; TAN, Tanzania Craton; UBB, Ubendian Belt; UG, Uganda Block; USB, Usagaran Belt; WCB, West Congo Belt; ZB, Zambezi Belt; ZIM, Zimbabwe Craton. b) Simplified geological map of the Kafue and Lusaka regions adapted from Johnson et al. (2007a).

to better constrain the development of this belt and its temporal relationship to the SIB.

GEOLOGICAL BACKGROUND

The Congo Craton refers to the amalgamated central African landmass at the time of Gondwana assembly (Fig. 1; De Waele et al., 2008), and comprises a series of Archean to Palaeoproterozoic cratons that formed the nucleus of Gondwana (Merdith et al., 2017). The collision of the Congo and Kalahari cratons occurred between *c.* 550–530 Ma (Johnson et al., 2006; Johnson et al., 2007b), and is reflected in the pervasive tectono-metamorphic overprints preserved in the both the SIB and Damara–Lufilian–Zambezi orogens (Fig. 1b).

The Southern Irumide Belt

In Zambia, the SIB (Fig. 1a, b) is comprised of four structurally stacked, predominantly late-Mesoproterozoic (*c.* 1095–1040 Ma) terranes. These terranes bear a pervasive tectono-metamorphic fabric that overprints earlier Mesoproterozoic deformation relateing to Congo–Kalahari collision and stacking at *c.* 550–520 Ma (Alessio et al., 2019; Johnson et al., 2006; Johnson et al., 2007b). The belt extends from southern Zambia to Malawi, Mozambique, and Tanzania, where numerous studies have identified terranes with similar lithologies and overprints to those in Zambia (Alessio et al., 2018; Bingen et al., 2009; Boyd et al., 2010; Hauzenberger et al., 2014; Westerhof et al., 2008). Earlier interpretations of the SIB considered it to be separate to the Congo Craton prior to the late Mesoproterozoic, instead accreting to the southern Congo Craton margin at this time (Johnson et al., 2007b). However, more recent interpretations suggest the belt to have initially formed on the Congo Craton margin, which is based on the similarity of basement units and overlying sediments in the SIB and the Irumide Belt (sensu stricto; referred to as the Irumide Belt herein) that formed along the Congo margin (Alessio et al., 2019; Alessio et al., 2018; Bingen et al., 2009). Two phases of regional compression have been observed in the Zambian terranes of the SIB, with D_1 being broadly N–S directed and likely coeval with Congo–Kalahari collision (Alessio et al., 2019). D_2 in this region was E–W directed and possibly occurred during the Permian–Triassic in response to intra-plate stresses associated with the Mauritanian–Variscan and Gondwanide orogenies, though the timing of D_2 is uncertain (Alessio et al., 2019).

The Zambezi Belt

The Zambezi belt is primarily located in southern Zambia and northern Zimbabwe, between the Congo and Kalahari cratons (Fig. 1a, b). Previous work suggests a continuity between this belt, the Lufillian Arc, and Damara Belt (e.g. Hanson et al., 1994; Hutchins and Reeves, 1980; Johnson et al., 2007a; Kampunzu and Cailteux, 1999; Mazac, 1974), which together define the suture between the Congo and Kalahari cratons. Peak metamorphism in these belts was constrained to have occurred between *c.* 550–520 Ma, and likely represents the time of this suturing (Johnson et al., 2005). In Zambia, the Zambezi Belt crops out as a series of Neoproterozoic supracrustal lithologies (Fig. 1b). These were previously dated by Johnson et al. (2007a), who suggest this section of the Zambezi Belt to have resided on the southern Congo Craton margin prior to collision with the Kalahari Craton (Johnson et al., 2007a). These authors obtained U–Pb zircon ages of *c.* 880 Ma from volcanoclastic formations and ages of *c.* 820 Ma from granites that intrude sediments yielding detrital ages predominantly between *c.* 1100–1000 Ma. These authors also obtained Nd isotopic data from the volcanics, which are indicative of assimilation and recycling of basement rock that is suggested to have occurred during rifting on the southern Congo Craton margin.

Congo–Kalahari metamorphism

Numerous studies have produced *P–T* estimates for lithologies in close proximity to the

Congo–Kalahari suture. Several of the these estimates were obtained from whiteschists — chemically simple rocks that are suggested to reflect continental subduction (Johnson, 2011) — which are exposed throughout the SIB, Lufillian Arc and Zambezi Belt (Alessio and Kelsey, 2018; John et al., 2004). The earliest estimates of the conditions recorded by these rocks come from the Zambezi Belt and utilise petrogenetic grids that gave peak *P–T* conditions of 13–21 kbar and 590–650 °C (Johnson and Oliver, 1998). Subsequent *P–T* estimates of whiteschists in the SIB and Lufilian Arc were obtained via conventional thermobarometry, and gave conditions of 9–14 kbar and 675–775 °C (John et al., 2004). The most recent work done to constrain the thermobarometric conditions recorded by these whiteschists comes from the Zambezi Belt and utilises calculated phase equilibria modelling, which constrains peak conditions of ~14–19 kbar and 650–770 °C (Alessio and Kelsey, 2018). U–Pb monazite geochronology constrains metamorphism of the whiteschists to have occurred at *c.* 530 Ma (John et al., 2004). In northern Zimbabwe (proximal to the Congo–Kalahari suture), Goscombe et al. (2000) identified 550–500 Ma metamorphic overprints recording peak conditions of ~7–9 kbar and ~590–720 °C for a series of Mesoproterozoic terranes referred to as the Chewore Inliers. The whiteschists investigated by Johnson and Oliver (1998) are part of these inliers, though are considered to be discrete, fault-bound and likely separate to the other terranes here (Goscombe et al., 2000). Whereas P–T information is unavailable from the Zambian portion of the Zambezi Belt, the available geochronological data suggests that the overprints here are contemporaneous with those elsewhere in the Zambezi belt and southern Zambia (Goscombe et al., 2000; John et al., 2004; Johnson et al., 2007a).

METHODS

Samples were collected from the Chewore–Rufunsa Terrane of the Southern Irumide Belt, as well as the Zambezi Belt supracrustal sequences located within the Kafue region of southern Zambia (Fig. 1b). These samples were analysed for geochronology, zircon trace element composition and thermobarometric modelling as described below. An attempt to constrain the thermal evolution of modelled samples via in-situ U–Pb apatite dating was also undertaken, though the obtained data are poor and did not produce a meaningful age. The obtained thermochronological data can be found in the supplementary material. The structural context of the Chewore–Rufunsa Terrane and Kafue region were constrained via transects through both areas. Structural data obtained along these transects are plotted on lower-hemisphere equal-area stereographic projections created with the STEREONET 9 program, based on algorithms described by Cardozo and Allmendinger (2013) and Allmendinger et al. (2011). Zircon trace element and isotopic data were acquired at the John de Laeter Centre, Curtin University (Western Australia).

Thermobarometric modelling

Pressure–temperature models were calculated for metapelite sample Z16-06 from the Zambezi Belt, as well as SIB whiteschist sample Z16-09, which was sourced from the Chowe River (Fig. 1b) in near proximity (< 2 km) to the whiteschist exposure studied by John et al. (2004). Calculations utilised the phase equilibrium modelling program THERMOCALC v.3.37, using the internally consistent dataset of Holland and Powell (2011), ds62. Activity–composition models used are from Powell et al. (2014), White et al. (2014a), White et al. (2014b) as well as Alessio and Kelsey (2018). Quantitative *P–T* information for the metapelite sample was calculated for the Mn-NCKFMASHTO ($MnO–Na_2O–CaO–K_2O–FeO–MgO–Al_2O_3–SiO_2–H_2O–TiO_2–Fe_2O_3$) system. Quantitative *P–T* information for sample Z16-09 was calculated for the NCKFMASHO system, which relates to its relatively

simple bulk-rock chemistry. Due to the uncertainty in Fe_2O_3 versus FeO amounts (i.e. oxidation state) measured during routine whole-rock geochemical analyses and the influence of Fe^{3+} on mineral stability (e.g. Boger et al., 2012), appropriate contents for the modelled pelite Z16-06 were evaluated via the calculation of a $T–X_O$ model. An assumed mole% value of 0.95 = (Fe_2O_3/(FeO + Fe_2O_3)) was used for sample Z16-09, which we consider an appropriate reflection of the oxidation state of the rock given the presence of hematite in the sample and the highly oxidising processes that form whiteschists (Alessio and Kelsey, 2018; Fockenberg and Schreyer, 1994; Franz et al., 2013; Johnson, 2011; Johnson and Oliver, 1998; Schreyer, 1974). All models were calculated with excess H_2O. Modelled bulk-rock compositions for samples Z16-06 and Z16-09 were acquired via X-ray fluorescence (XRF) at Franklin and Marshall College (United States). These compositions can be found in the supplementary material. CaO proportions in sample Z16-09 were recalculated to account for the presence of significant apatite in the sample, which is unable to be considered in thermobarometric calculations. A mineral liberation analysis map and associated EDS data for sample Z16-09 can be found in the supplementary material.

Zircon analysis

Isotope and trace element data were obtained from separated zircon grains that were extracted from crushed rocks using standard magnetic and heavy liquid techniques. Zircon separates were hand-picked, mounted in epoxy resin and then polished to expose the grains. The grains were imaged at Adelaide Microscopy on an FEI Quanta 600 Scanning Electron Microscope (SEM) Zircon grains using a Gatan cathodoluminescence (CL) detector to identify compositional domains that were suitable for analysis. Related CL images for analysed zircon samples are provided in the supplementary material. Zircon grains were analysed for U–Pb isotopes and trace elements via split stream LA–ICP–MS, using a Resonetics RESOlution laser ablation system connected to an Agilent 7900 quadrupole ICP–MS and a Nu Instruments Nu Plasma II multi-collector (MC). U–Pb isotopes were measured using MC–ICP–MS, while trace elements were measured in tandem using quadrupole ICP–MS. Ablation of zircon was performed in a He-ablation atmosphere with a frequency of 5 Hz. A spot size of 30 μm was used for all analyses. A total acquisition time of 80 seconds was used consisting of 10 seconds of spot pre-ablation, 40 seconds of background acquisition and 30 seconds of sample ablation. The Standard GJ ($^{206}Pb/^{238}U$ = 608.5 ± 0.4 Ma; Jackson et al. (2004)) was used as the primary standard for all zircon analyses, while Plešovice ($^{206}Pb/^{238}U$ = 337.13 ± 0.37 Ma; Sláma et al. (2008)) and 91500 ($^{206}Pb/^{238}U$ = 1065.4 ± 0.6 Ma; Wiedenbeck et al. (1995)) were used as secondary standards. Standard glass NIST 610 was used during trace element analysis as a reference material for corrections to mass bias drift. Throughout this study Plešovice yielded a 95% concordant average $^{206}Pb/^{238}U$ age of 340.1 ± 3.4 Ma (2σ, n = 10), 91500 yielded a 95% concordant average $^{206}Pb/^{238}U$ age of 1061.6 ± 3.4 Ma (2σ, n = 20). Zircon data were reduced using IOLITE (Paton et al., 2011). All individual U–Pb zircon analyses can be found in the supplementary material.

Lu–Hf isotope analysis of zircon was conducted using the same Nu Plasma II multi-collector, with no split streaming to the quadrupole ICP–MS. Zircons were ablated in a helium atmosphere, which was mixed with argon upstream of the ablation cell. Individual analyses consisted of two cleaning pulses, followed by 40 seconds of background acquisition and 20 seconds of sample ablation with a 10 Hz repetition rate, and beam intensity of ~2.8 to 3 J/cm^2. A spot size of ~50 μm was used, and was centred over previously ablated U–Pb and trace element spots. Data were normalised to $^{179}Hf/^{177}Hf$ = 0.7325; Yb and Lu isobaric inter-

ferences on ^{176}Hf were corrected for following the methodology of Woodhead et al. (2004). Reduction of Lu–Hf data was done using IOLITE (Paton et al., 2011). Known standards were run throughout the analytical session to verify the stability and performance of the instrument. The primary standard used for Hf isotopes was Mud Tank, which yielded a mean $^{176}Hf/^{177}Hf$ ratio of 0.282506 ± 0.00001 (2σ, n = 29). This is within uncertainty of the known value of 0.282507 ± 0.000006 provided by (Woodhead and Hergt, 2005). All individual zircon Lu–Hf analyses can be found in the supplementary material.

RESULTS

Structure

Structural data were collected from the Kafue region and southern Chewore–Rufunsa Terrane of the SIB to identify dominant structural fabrics and their relationship to the tectono-metamorphic overprints recorded by rocks in these areas. These data supplement that previously obtained by the Geological Survey of Zambia (Thieme, 1984) and are presented in Figure 2a, b. Obtained bedding and foliation measurements from the Kafue region, as well as the southern Chewore–Rufunsa Terrane, are displayed on stereonets in Figure 2b. Bedding and foliation measurements from the Kafue region are predominantly moderate to steeply dipping (> 40°) and strike N–S

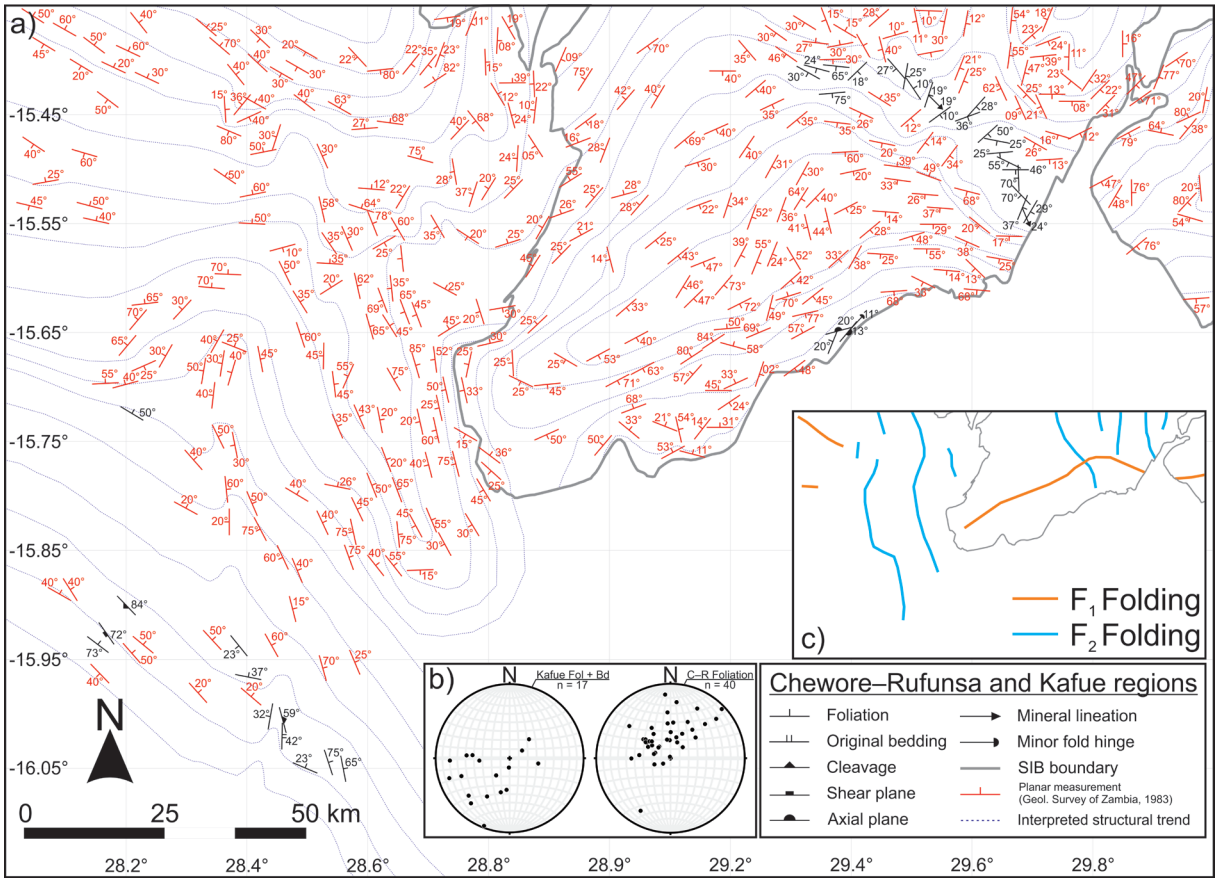

Figure 2. Structural diagram of the Kafue region and southern Chewore–Rufunsa terrane of the SIB. a) Structural map displaying measurements obtained in this study, as well as projected measurements previously obtained by Thieme (1984). The dashed blue lines represent foliation strike trends interpreted from the available structural data. Grid references refer to latitude (S) and longitude (E) in decimal degrees. b) Stereonets displaying poles to bedding and foliation measurements obtained from the Kafue region and southern Chewore–Rufunsa terrane during this study. c) Interpreted fold axial traces. The orange lines reflect a phase of broadly NE–SW trending folds (F1), while the blue lines represent a subsequent phase of N–S directed folding (F2).

to NW–SE, consistent with N–S oriented folds. Foliation measurements obtained from the Chewore–Rufunsa Terrane vary in both dip and orientation. The majority of foliation measurements from this terrane are relatively shallow to moderately dipping (< 50°) and broadly E–W striking, consistent with an E–W trending fold. A number of measurements are more steeply dipping and are broadly NW–SE striking, which may reflect N–S folding. The newly obtained and existing data are used to extrapolate foliation trends in the region (as marked by the dashed blue lines in Fig. 2a), and indicate two phases of compression, one broadly directed N–S (D_1) and the other E–W directed (D_2; Fig. 2c). The first phase is identified from the prominent E–W trending tight to isoclinal fold (F_1) that extends across the entire Chewore–Rufunsa Terrane and is also observed in the western extent of the Kafue region (Fig. 2a, c). The second phase of compression is identified from a series of N–S trending folds (F_2) that can be observed in both the Chewore–Rufunsa Terrane and Kafue region, being more prominent in the latter. These folds range from open to tight and refold the tighter E–W trending F_1 folds (Fig. 2a). Such a relationship is consistent with fold structures observed throughout the entire Zambian portion of the SIB, with E–W trending folds in the terranes further east suggested to be refolded by subsequent N–S folding (Alessio et al., 2019).

Thermobarometric modelling

Two samples were utilised for thermobarometric modelling, which constrain the tectono-metamorphic overprints in the Kafue region and Chewore–Rufunsa Terrane of the SIB. Sample Z16-06 is a metapelitic schist, sourced from the supracrustal sequences of the Zambezi Belt located in the Kafue region of southern Zambia (Fig. 1b). Chlorite–quartz schist sample Z16-09 was sourced from the southern-most extent of the Chewore–Rufunsa Terrane (Fig. 1b), which is part of the white-schist exposures studied by (John et al., 2004).

Z16-06: Kafue metapelite

Petrography

Sample Z16-06 consists of quartz, plagioclase, muscovite, biotite, garnet, staurolite and chlorite as well as minor ilmenite and rutile (Fig. 3a, b). Elongate muscovite and to a lesser extent biotite are present as layers that define a pervasive fabric throughout the sample (Fig. 3a). These layers are separated by layers predominantly comprised of generally equant to rounded quartz and plagioclase. A heterogeneity is observable in these layers, with some layers containing randomly oriented to loosely aligned biotite and a single layer containing abundant garnet that is significantly larger (up to ~150 μm) than the phases it is in contact with. Garnet in this sample is highly poikiloblastic, containing abundant quartz inclusions, and is often flattened to appear rectangular in shape with the long axis parallel to the main fabric. The main fabric can be observed to wrap around these grains in places. Several garnet grains, predominantly those that are more rounded, are in contact with chlorite and biotite that form a sigmoidal taper away from the garnet in alignment with fabric defined by muscovite and biotite. The flattened nature of garnet grains in the sample, associated sigmoidal tapers and deflection of the fabric are indicative of the garnet in this sample forming prior to or synchronous with the main fabric. While sigmoidal tapers are present, the quartz inclusions in the garnet are flattened with the long axis parallel to the main fabric, much like several of the garnet grains, and minor evidence of rolling is observed in these inclusions. Staurolite (Fig. 3a, b) is similar in size to the garnet. The fabric defined by muscovite and biotite is deflected by staurolite, suggesting it pre-dates the main fabric, or at least the most recent fabric to have developed around staurolite. The staurolite is highly poikiloblastic, containing abundant quartz inclusions. While appearing to pre-date the main fabric recorded by the rock, the large grain sizes of garnet and staurolite suggest that these phases remained

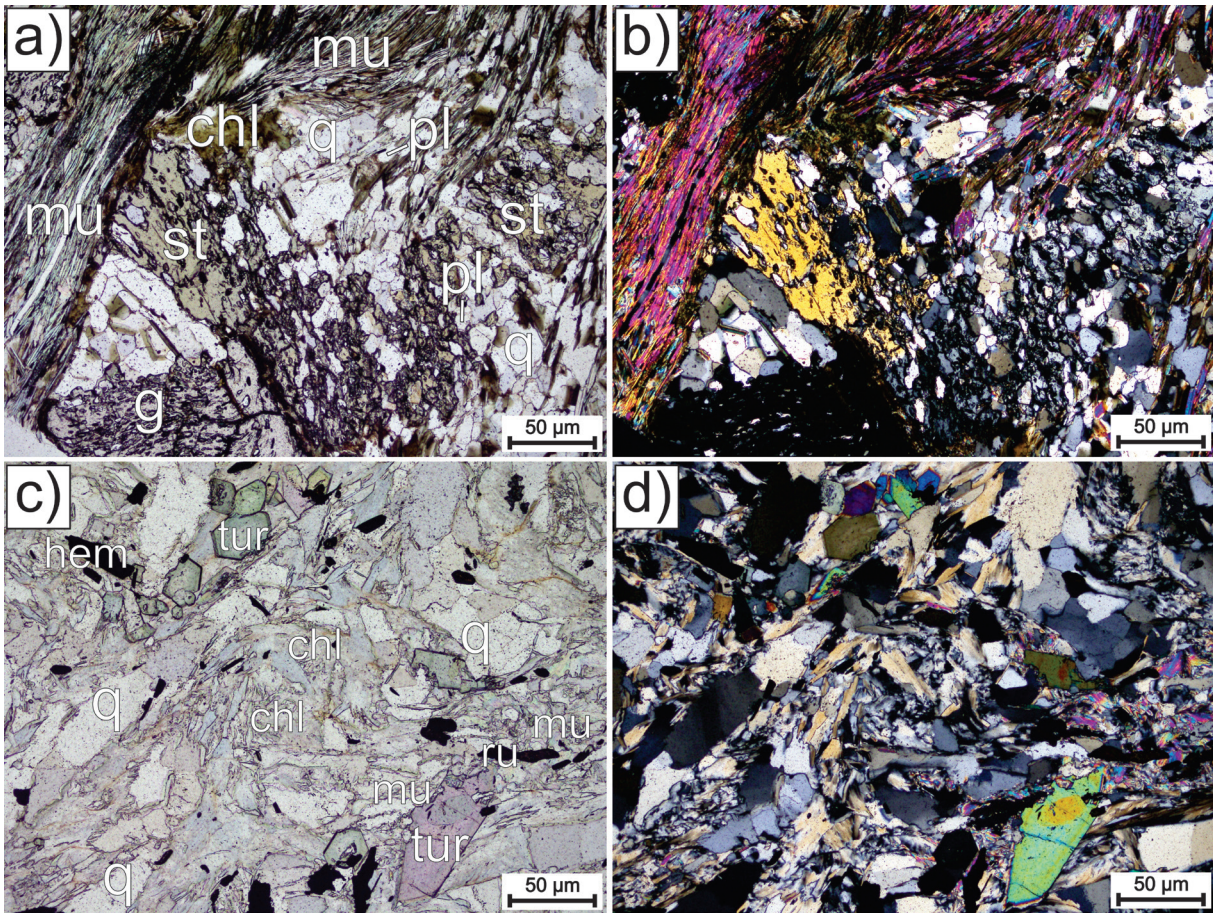

Figure 3. Photomicrographs of samples used for P–T calculations. a) Plane polarised light (PPL) image of metapelite sample Z16-06 displaying poikiloblastic garnet in contact with quartz, muscovite and staurolite. Staurolite is variably poikiloblastic, and is in contact with quartz, muscovite, plagioclase, chlorite and garnet. Muscovite defines a pervasive fabric within the sample. Chlorite is found within the muscovite defined fabric, but is also observed separating staurolite, muscovite and quartz. b) Same field of view as image a), in cross polarised light (XPL). c) PPL image of chlorite–quartz schist sample Z16-09. The sample is predominantly comprised of quartz, muscovite and chlorite, with tourmaline and hematite. Larger tourmaline and quartz grains can be seen to be dispersed by finer chlorite, muscovite and quartz. d) Same field of view as image c) in XPL.

stable during peak-metamorphism. Chlorite in this sample is predominantly found in the quartz dominated layers, and occurs in contact with all other phases in the sample. It is typically unaligned with the fabric, though does form part of the sigmoidal tails observed on garnet grains. Rutile is primarily observed to form in cracks of garnet grains, suggesting that it formed subsequently to the garnet. Whether the rutile formed during peak metamorphism, or a later stage of prograde metamorphism, is uncertain. However, the absence of rutile from the main fabric of the rock and restriction to being retained within prograde–peak garnet grains suggests that it likely reflects prograde metamorphism. It is possible that rutile was a primary inclusion in garnet, with the weakness around these inclusions being exploited by later fractures. Given their abundance and presence in the pervasive fabric of the rock, muscovite, biotite, quartz and plagioclase are interpreted to form part of the stable peak assemblage. Therefore, the interpreted peak assemblage for this sample consists of garnet, staurolite, quartz, plagioclase, muscovite, biotite and ilmenite. Temperature–composition modelling (found in the supplementary material) identifies the presence of ilmenite over magnetite or hematite, as this is only relevant mineral that occurs in the oxidation range allowing for the stability of garnet and staurolite in the peak assemblage without the additional

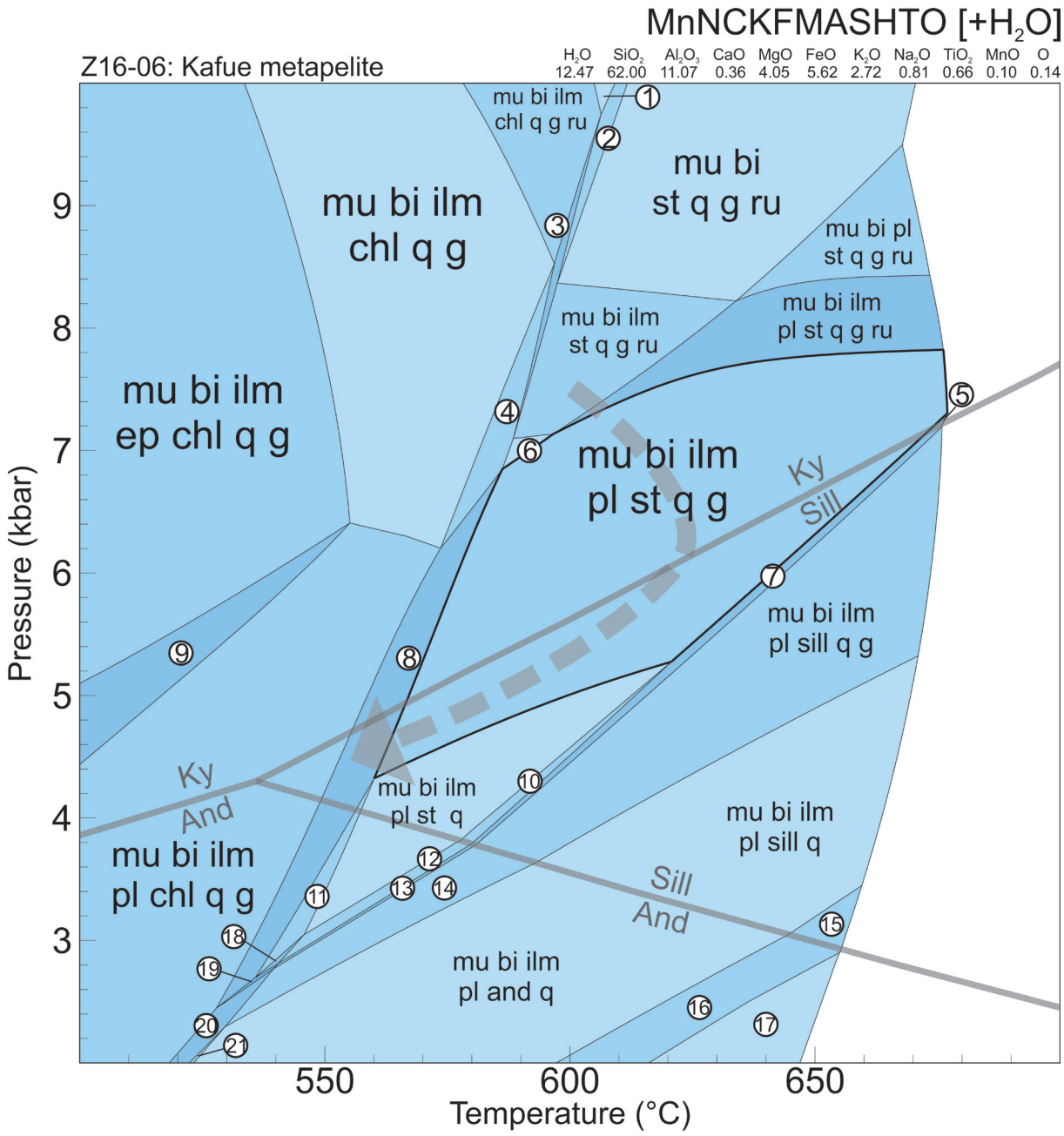

1: mu bi chl q g ru
2: mu bi chl q g ru st
3: mu bi chl q g ru st ilm
4: mu bi chl q g st ilm
5: mu bi ilm pl st q g ky
6: mu bi ilm st q g
7: mu bi ilm pl st q g sill
8: mu bi ilm pl st q g chl
9: mu bi ilm pl chl q g ep
10: mu bi ilm pl st q sill
11: mu bi ilm pl st q chl
12: mu bi ilm pl st q and
13: mu bi ilm pl st q and g
14: mu bi ilm pl q and g
15: mu bi ilm pl sill q ru
16: mu bi ilm pl and q ru
17: mu bi pl and q ru
18: mu bi ilm pl st q chl and
19: mu bi ilm pl st q chl and g
20: mu bi ilm pl q chl and g
21: mu bi ilm pl q chl and

Figure 4. *P–T* pseudosection calculated in the MnNCKFMASHTO system for sample Z16-06, a metapelite from the Zambezi Belt supracrustals. The field muscovite–biotite–ilmenite–plagioclase–staurolite–quartz–garnet–H_2O is outlined in bold lines and corresponds to the peak assemblage recorded by the sample, which is stable between ~4.1–7.9 kbar and 560–670 °C. The interpreted *P–T* path experienced by the sample is marked by the grey dashed line, though is largely illustrative due to the relative lack of petrographic constraints on prograde and retrograde metamorphism.

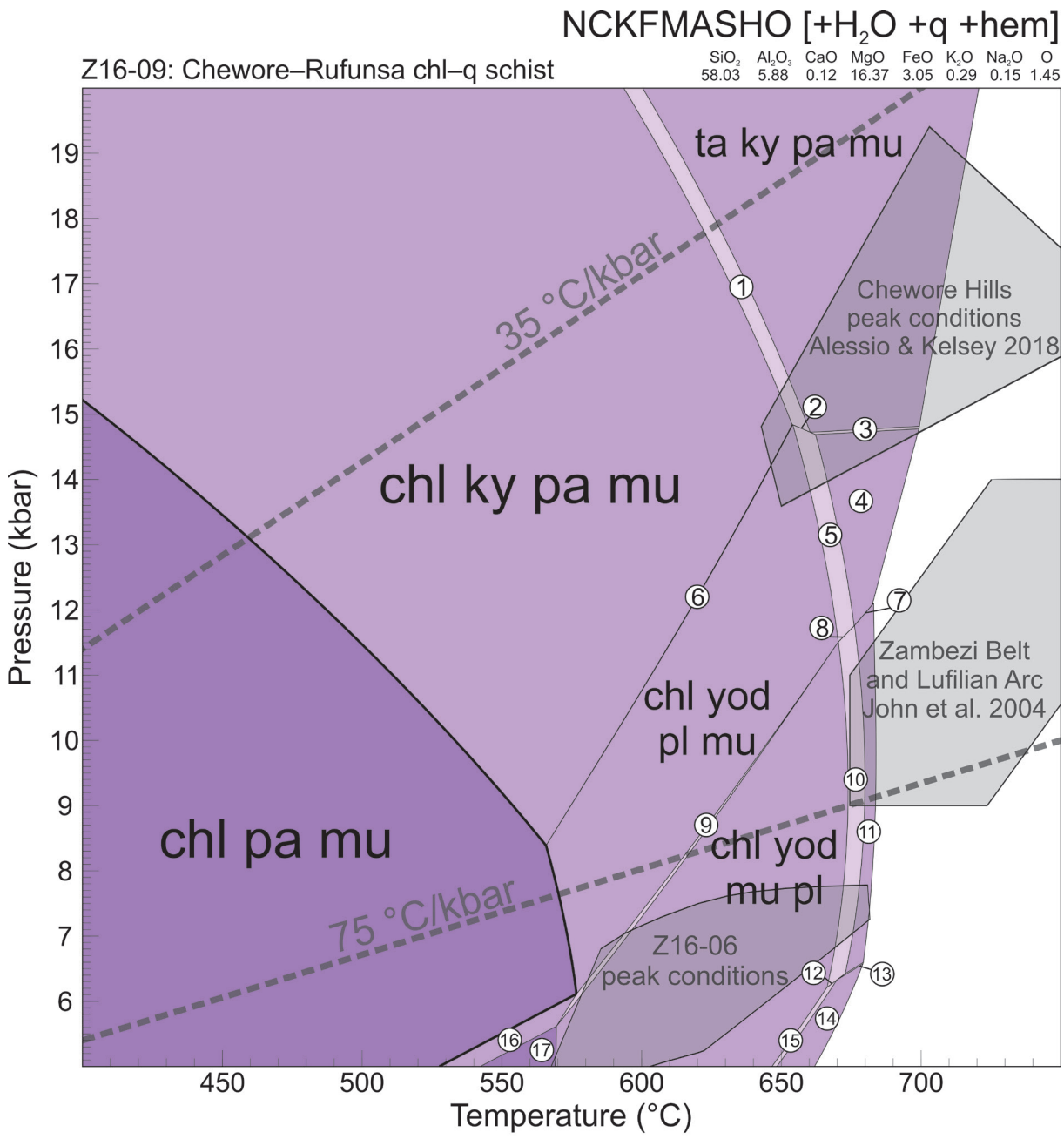

Figure 5. *P–T* pseudosection calculated in the NCKFMASHO system for chlorite–quartz schist sample Z16-09 from the southern Chewore–Rufunsa Terrane. The field corresponding to the equilibrium assemblage of the rock is interpreted as the chl–pa–mu–q–hem–H_2O field, which is outlined by bold lines and (within the diagram) occurs at pressures up to 15 kbar and temperatures up to 570 °C. Superimposed on the diagram in black are the peak conditions calculated by Alessio and Kelsey (2018) for a yoderite bearing whiteschist from the Chewore Hills, the peak conditions calculated by John et al. (2004) for whiteschists collected within 2 km of this sample and of the Lufilian Arc, as well as the peak conditions recorded by sample Z16-06.

stability of chlorite. This range also permits the stability of rutile at higher and lower pressures. Chlorite is interpreted as a retrograde phase, due to its tendency to mantle peak phases and generally being unaligned with the fabric.

P–T modelling

The calculated *P–T* model for sample Z16-06 in the MnNCKFMASHTO system is presented in Figure 4. The muscovite–biotite–ilmenite–plagioclase–staurolite–quartz–garnet–H2O field corresponds to the interpreted peak assemblage recorded by this sample, and is stable between ~4.1–7.9 kbar and 560–670 °C. Such conditions correspond to a thermal gradient of ~80–120 °C/kbar. The interpreted prograde stability of staurolite and garnet, as well as the minor presence of rutile and absence of any aluminosilicate mineral may indicate that the prograde path of the rock passed through the higher pressure, rutile-bearing fields. However, the prograde evolution of the rock beyond these rutile-bearing fields is undefined. The presence of retrograde chlorite and apparent persistence of staurolite and garnet suggests that the cooling trajectory passed through the adjacent muscovite–biotite–ilmenite–plagioclase–staurolite–quartz–garnet–chlorite–H_2O field.

Z16-09: Southern Irumide Belt chlorite schist

Petrography

This sample consists of quartz, chlorite, muscovite, tourmaline, hematite, apatite and minor rutile (Fig. 3c, d). Quartz is abundant throughout the sample, and ranges from ~10–100 μm in size. It is observed in contact with chlorite, tourmaline, and muscovite. Muscovite in this sample ranges from < 10 to ~30 μm in size and is predominantly associated with chlorite, though is also in contact with quartz and tourmaline. Chlorite is in contact with all other phases in the sample and is fine grained (~1–20 μm). The chlorite in this sample does not display pleochroism and is very pale coloured, suggesting it is Fe-poor (confirmed by EDS) and more likely the Mg-rich end-member sheridanite. Hematite is highly variable in size (though never greater than ~50 μm) and shape. It is observed in contact with all other phases in the sample. Textural relationships suggest that the dominant minerals quartz, chlorite and muscovite are in equilibrium and do not separate each other. Apatite and tourmaline grains are larger grained (~20–200 and 30–100 μm, respectively) than the more dominant minerals muscovite and chlorite, though are separated from each other by these phases. We interpret that the sample records an equilibrium assemblage of chlorite–quartz–muscovite–hematite ± tourmaline–apatite

P–T modelling

Figure 5 displays a P–T model calculated for sample Z16-09 in the NCKFMASHO system. The field chlorite–paragonite–muscovite–quartz–hematite–H2O is interpreted to correspond to the interpreted equilibrium assemblage recorded by the sample. We suggest that the occurrence of paragonite (mode = 1.7–2.5%) in this field relates to the presence of Na in dravite in the rock, which cannot be accounted for in phase equilibria calculations. EDS analysis of tourmaline in this sample suggests it to be dravite and accordingly, the Na and Al from this mineral are instead incorporated into paragonite in the model. None the less, the model in Figure 5 provides a broad constraint of the P–T conditions recorded by the sample's equilibrium assemblage. The field best corresponding to this assemblage is large and stable to pressures < 15 kbar (at 400 °C) and temperatures < 580 °C corresponding to thermal gradients between ~30–90 °C/kbar.

Zircon geochronology and chemistry

Attempts were made to constrain the specific metamorphic ages of the samples modelled in this study (Z16-06 and Z16-09), though were unsuccessful due to the paucity of datable accessory phases (e.g. Zircon, Monazite) within these samples. U–Pb data were acquired for

apatite grains within these samples, though were poor and did not produce any meaningful age. Sample Z16-09 was acquired from outcrop in Chowe River, which hosts the whiteschist studied by John et al. (2004) that yields a metamorphic age of *c.* 530 Ma. Goscombe et al. (2000) identified 550–500 Ma amphibolite facies metamorphic overprints in the Zambezi Belt of Zimbabwe. Johnson et al. (2007a) obtained U–Pb zircon ages for basement and overlying sedimentary rocks of the Zambezi supracrustals, indicating that the sedimentary rocks (from which sample Z16-06 is derived) were deposited during the Neoproterozoic, on *c.* 1100 Ma basement. The timing of deposition restricts sample Z16-06 to recording a metamorphic overprint relating to Congo–Kalahari collision, consistent with the metamorphic ages elsewhere in the Zambezi Belt, as opposed to the late-Mesoproterozoic metamorphism that is the only other metamorphic event recorded in this region (Alessio et al., 2019; Goscombe et al., 2000; Johnson et al., 2006; Karmakar and Schenk, 2016). The relationship between the sedimentary rocks that sample Z16-06 is derived from and underlying basement has been further constrained by dating the following samples of the Zambezi

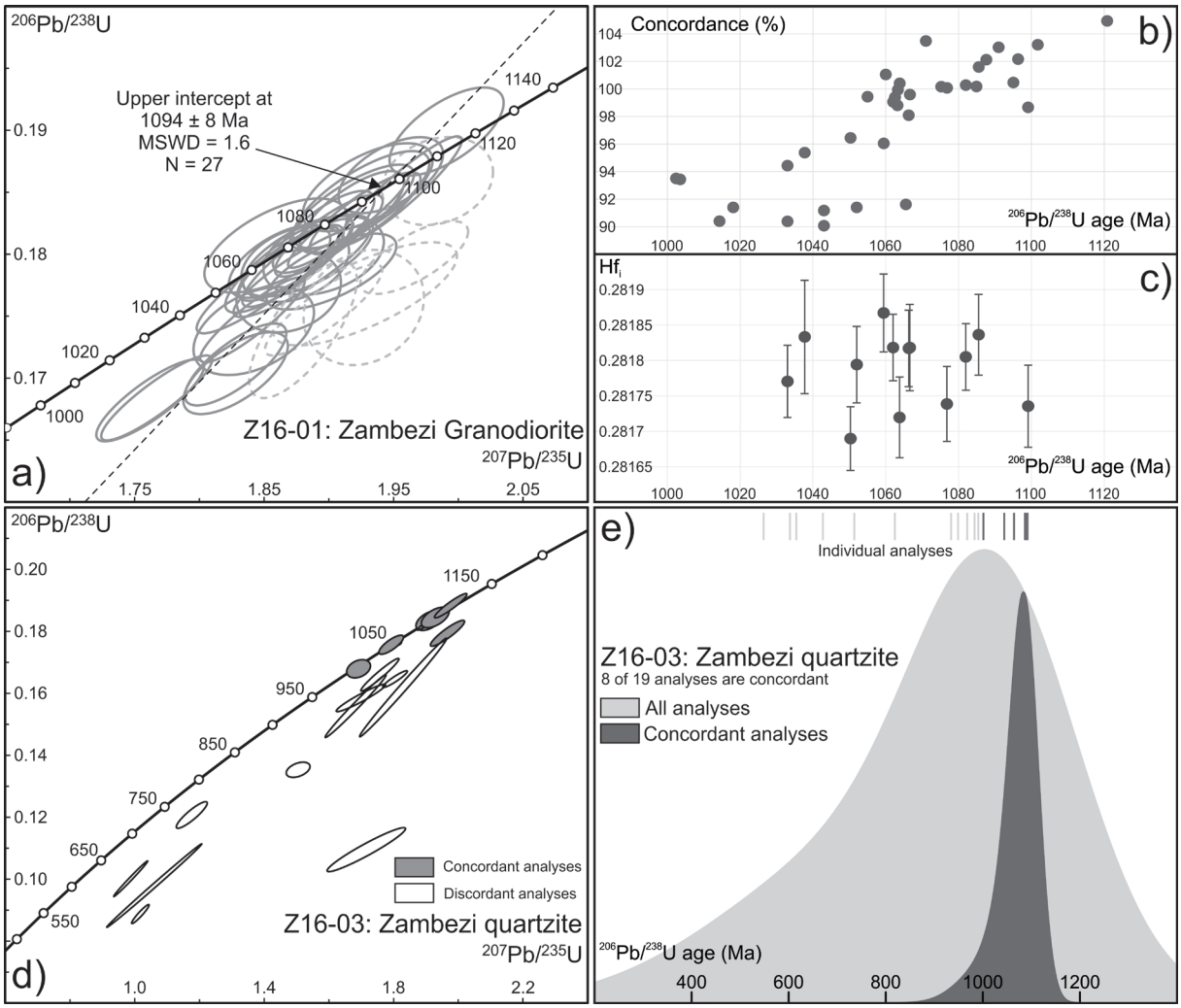

Figure 6. U–Pb concordia diagrams for zircon samples obtained from the Kafue region. a) Concordia diagram displaying ≥90% concordant analyses for granodiorite sample Z16-01, which are used to calculate a crystallisation age for the sample. The interpreted Pb loss chord for the sample is indicated by the dashed line. b) Concordance versus $^{206}Pb/^{238}U$ age plot for sample Z16-01. c) Hf_i versus $^{206}Pb/^{238}U$ age plot for sample Z16-01. d) Concordia diagram for detrital zircon sample Z16-03, ≥ 90% concordant analyses are shaded grey. e) Associated KDPs for Z16-35 with $^{207}Pb/^{206}Pb$ ages plotted for all analyses (light grey) and only ≥ 90% concordant analyses (dark grey).

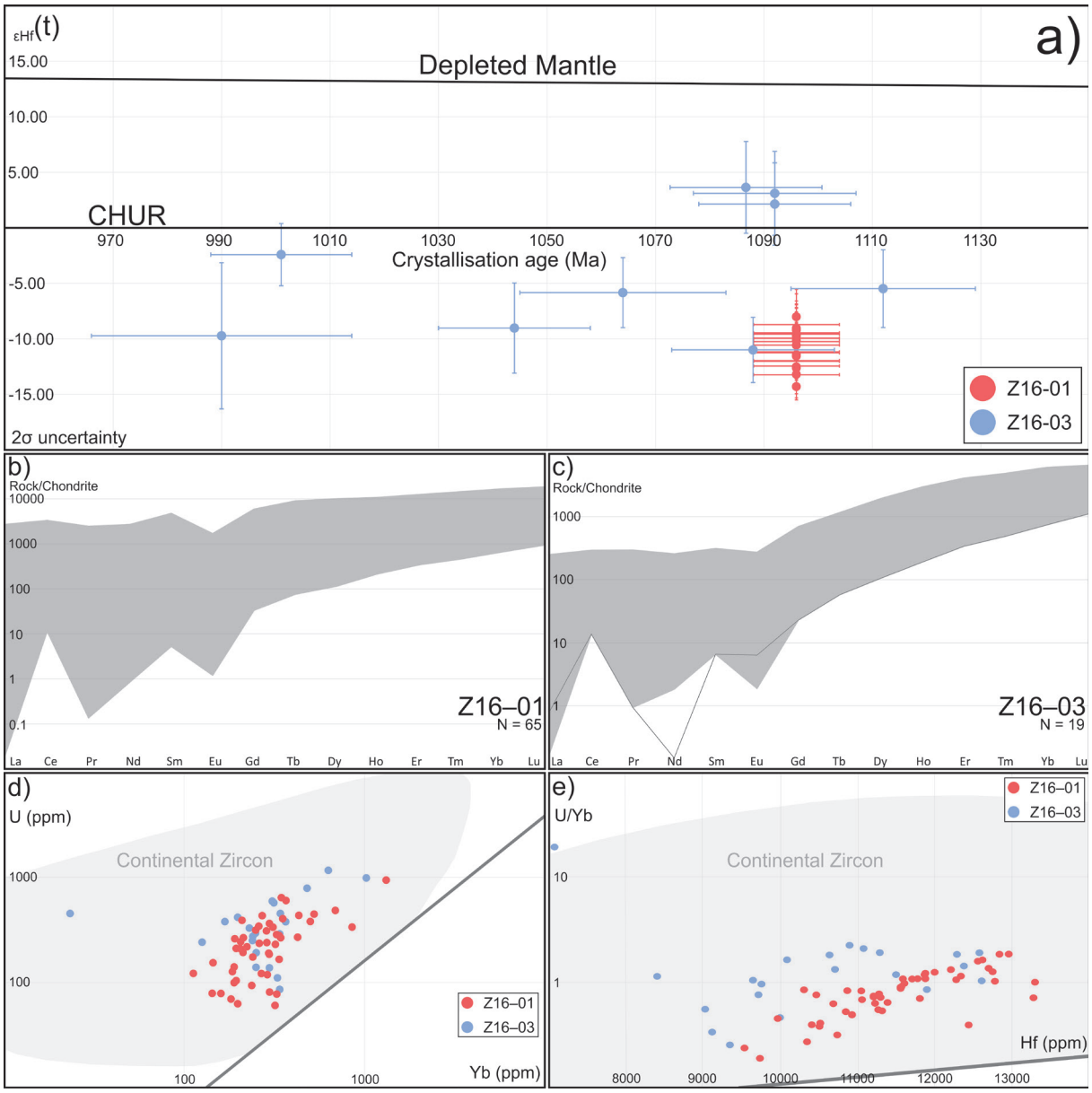

Figure 7. εHf(t) versus U–Pb age plot and trace element diagrams for granodiorite sample Z16-01 and detrital zircon sample Z16-03 from the Kafue region. a) εHf(t) versus U–Pb age plot. εHf(t) values for sample Z16-01 are plotted at the interpreted crystallisation age of 1096 ± 11 Ma for the sample, while values for detrital sample Z16-03 are plotted at the individually obtained age for each grain. The Uncertainty for age and εHf(t) values for the data obtained in this study are shown at the 2σ level. The depleted mantle curve of Griffin et al. (2002) is plotted. b) and c) Rare-earth element diagrams normalised to the average chondrite (McDonough and Sun, 1995) for samples Z16-01 and Z16-03, respectively. d) U (ppm) versus Yb (ppm) diagram for Z16 samples, with the grey field outlining the values for continental zircons (Grimes et al., 2007). e) U/Yb versus Hf (ppm) diagram for Z16 samples, with the grey field outlining the values for continental zircons (Grimes et al., 2007).

supracrustals.

Z16-01: Kafue granodiorite

Sample Z16-01 is a granodiorite collected from the Kafue region, approximately 20 km south of Kafue (Fig. 1b). Zircons extracted from this sample are clear to yellow in hue, between 50 to 200 µm at the long axis and display aspect ratios between 1:2 and 1:5. In CL images, the grains generally exhibit oscillatory zonation, typical of igneous zircon, with inclusions observed in some grains. Sixty-five (65) zircons were analysed from this sample for their U–Pb isotopes, from which 35 are ≥ 90% concord-

ant. These near-concordant analyses are presented in Figure 6a, and form a distinct lead loss line that is corroborated by decrease in concordance with age (Fig. 6b) and broadly identical Hf_i values across grains (Fig. 6c). Eight analyses were removed from age calculations, with these grains possibly containing a common Pb component, with the remaining 27 used to calculate an upper concordia intercept in ISOPLOT that yields an age of 1094 ± 8 Ma (N = 27; MSWD 1.6), which is taken as the best estimate for crystallisation of the granodiorite. Lu–Hf data were obtained for 15 grains from this sample (Fig. 7a) and yield evolved εHf(t) values ranging from approximately –3 to –18. REE data were obtained for all analysed zircons (Fig. 7b), displaying typical concentrations that indicate a general increase of elemental abundance with increasing atomic mass (Hoskin and Ireland, 2000). All grains contain U, Yb and Hf concentrations (Fig. 7d,e) that are consistent with zircon derived from a continental source (Grimes et al., 2007).

Z16-03: Kafue quartzite

A sample of detrital zircons were obtained from a quartzite within the Kafue region, approximately 5 km south-west from sample Z16-01 (Fig. 1b). Nineteen zircons were obtained from the sample, which were clear to yellow-brown and 30 to 70 μm at the long axis with aspect ratios of 1:1 to 1:2. Due to the paucity of zircon obtained from this sample, the associated data and interpretations thereof are noted to be preliminary findings. Oscillatory zonation was observed in most analysed grains, which were rounded and commonly fractured. The 19 grains from this sample were analysed for U–Pb isotopes and are presented in Figure 6d. Eight of the analysed grains are ≥ 90% concordant, and yield $^{206}Pb/^{238}U$ ages that range from 1001 ± 13 Ma to 1112 ± 17 Ma. The Kernel Density Plot (KDP) for this sample indicates the concordant analyses to form a single population at *c.* 1100 Ma (Fig. 6e). Obtained εHf(t) values for this sample are presented in Figure 7a, and display predominantly evolved values from *c.* 1100–1000 Ma. Three samples can be seen to record largely juvenile values, ranging from +8 to –1, while also recording very similar ages (*c.* 1100 Ma). REE data obtained for this sample (Fig. 7c) demonstrate an increasing enrichment in the heavier elements. A single analysis recording a 100% concordant age of 1044 ± 14 Ma demonstrates a distinct negative Nd anomaly, and broadly records the lowest REE concentrations of any analysed zircon. All grains record U, Yb and Hf values that indicate a continental source (Fig. 7d, e).

DISCUSSION

Nature of deformation in southern Zambia

Structures

The fold structures identified in the Kafue region and southern Chewore–Rufunsa Terrane indicate the occurrence of a N–S directed compression (D_1) and a subsequent E–W directed compression (D_2). Such structures were previously identified throughout the SIB and were interpreted to have occurred after the late-Mesoproterozoic orogenic events recorded within (Alessio et al., 2019). This timing is consistent with the structures identified in this study, which are observed in sediments with a maximum depositional age of *c.* 1000 Ma and suggests that, at least in the SIB, these structures overprint earlier structural and metamorphic fabrics (D_0 and M_0; Alessio et al. 2019). D_1 is identified from the prominent E–W trending fold in the Chewore–Rufunsa Terrane, and similar structures within the Zambezi supracrustals (Fig. 2). Given the prominence of these structures and their orientation, parallel to the Congo–Kalahari suture, it is likely that these formed as a result of the collision between the two cratons between *c.* 550–520 Ma. As such, D_1 is likely coeval with the late-Neoproterozoic–Cambrian metamorphic overprint (M_1) recorded in the samples analysed in this

study. The N–S trending folds (F_2) identified in both the Kafue and Chewore–Rufunsa areas are particularly prominent in the Kafue region, and the E–W fold (F_1) identified in the Chewore–Rufunsa Terrane is refolded by these structures (Fig. 2). Given that the tighter E–W directed structures are either deflected or refolded by the N–S directed, predominantly more gently folded structures, it is interpreted that these features reflect a later deformation event (D_2).

Metamorphism

The observed peak assemblage in Kafue region sample Z16-06 (Fig. 3) corresponds to the muscovite–biotite–ilmenite–plagioclase–staurolite–quartz–garnet–H_2O field in the calculated *P–T* model for this sample, suggesting that the sample experienced conditions of 4.1–7.9 kbar and 560–670 °C (Fig. 4). Such conditions correspond to thermal gradients between ~70–165 °C/kbar. The presence of prograde staurolite, garnet and rutile, as well as retrograde chlorite, broadly indicate the sample experienced a clockwise *P–T* path during metamorphism, typical of many collisional environments (England and Richardson, 1977). The observed mineralogical and textural features for SIB sample Z16-09 best correspond the peak field of chlorite–(paragonite)–muscovite–quartz–hematite–H_2O, with paragonite suggested to act as a proxy for the absence of dravite in thermobarometic calculations. This field suggests that the sample experienced *P–T* conditions < 15 kbar (at 400 °C) and < 560 °C (Fig. 5), reflecting thermal gradients ranging from ~30–90 °C/kbar.

SIB sample Z16-09 was sourced from the Chowe River (Fig. 1), in near proximity to the whiteschist samples investigated by John et al. (2004). These authors suggested that these whiteschists, and those of the Lufillian Arc, experienced conditions of 9–14 kbar and 675–775 °C, and that they recorded the initial south-dipping subduction of the Congo Craton beneath the Kalahari Craton during continental collision. Subsequent constraints for a yoderite-bearing whiteschist from the Chewore Inliers of Zimbabwe suggest peak metamorphic conditions of ~15–19 kbar and 650–790 °C (Alessio and Kelsey, 2018). The proximity of the sample Z16-09 to the Chowe River whiteschists, their similar (largely MASHO) compositions, and their dominantly hydrous assemblages, suggest that the sample likely represents largely retrogressed whiteschist. The whiteschists (sensu stricto) in this region suggest that initial subduction of the Congo Craton beneath the Kalahari Craton resulted in peak thermal gradients between ~30–90 °C/kbar, consistent with the retrograde thermal gradient calculated for sample Z16-09. Such gradients are hotter than typical subduction zone metamorphism (Brown, 2007), though consistent with continental subduction, which is the likely mechanism for whiteschist formation (Franz et al., 2013; Johnson, 2011).

The calculated thermal gradient for Zambezi Belt sample Z16-06 (Fig. 4) can be seen to overlap that calculated for SIB sample Z16-09 (Fig. 5). However, it is important to note that these *P–T* conditions relate to peak metamorphism for sample Z16-06 and retrograde metamorphism for Z16-09. Available geochronological data suggests metamorphism in this region occurred as a result of Congo–Kalahari collision, at *c.* 530 Ma (Goscombe et al., 2000; John et al., 2004; Johnson et al., 2007a). Similarly, the whiteschists throughout Zambia and northern Zimbabwe formed during this collision, following earlier eclogite formation during convergence towards the Kalahari Continent at *c.* 600 Ma (John et al., 2004). As such, the contemporaneous metamorphism and minor overlap between thermal gradients suggests that these rocks do not record multiple events, but instead record paired metamorphic overprints relating to different tectonic processes occurring within the same orogenic event (Brown, 2010; Miyashiro, 1961). In this way, the metapelites in the Kafue region may be a record of Congo–Kalahari collision, though

reflecting deformation of the orogenic hinterland instead of the suturing and continental subduction recorded by the whiteschists. It is therefore possible that the whiteschists throughout Zambia and Zimbabwe serve to mark the suture zone between the Congo and Kalahari cratons.

Age constraints and Mesoproterozoic to Phanerozoic evolution of the southern Congo margin

Granodiorite sample Z16-01 yielded a upper concordia intercept of 1094 ± 8 Ma (Fig. 6a), which is within error of previous constraints for this unit provided by Katongo et al. (2004). εHf(t) values obtained from this sample are negative and range from –3 to –18 (Fig. 7a). Therefore, the granodiorite is interpreted to have formed from crustal reworking, with minimal mantle input. The age of this sample indicates that magmatism occurring along this part of the southern Congo margin is broadly coeval with intrusions in the SIB. Magmatism here was suggested to be related to an advancing microcontinent (on which the SIB would have formed) that collided with the southern Congo margin at *c.* 1040 Ma (Johnson et al., 2007b). However, more recently magmatism has been suggested to relate to subduction along the southern Congo margin (where the SIB would have already been located) at this time, which is corroborated by Paleoproterozoic basement and overlying sediment in the Irumide and Southern Irumide belts yielding equivalent U–Pb ages and εHf(t) values (Alessio et al., 2019; Alessio et al., 2018). The detrital zircon sample obtained from a quartzite in the Kafue region yielded a single concordant population at *c.* 1.1 to 1.0 Ga (Fig. 6d, e), with εHf(t) values ranging from approximately +8 to –16 (Fig. 7a). The youngest ≤ 10% discordant grain yielded a $^{206}Pb/^{238}U$ age of 1001 ± 13 Ma (2σ uncertainty). These sediments are intruded by the Gneiss yielding a protolith age of *c.* 820 Ma (Hanson et al., 1994), which is interpreted to constrain the minimum depositional age of the sample. Similar to the detrital sample from this sequence analysed by Johnson et al. (2007a), this sample suggests that the modelled metapelite sample (Z16-06) from this sequence was deposited during the Neoproterozoic, and thus bears a metamorphic overprint relating to Congo–Kalahari collision instead of late-Mesoproterozoic orogenesis. The sediments here broadly record the same ages as the matrix of a basal conglomerate from the same formation, which has been previously interpreted to have sourced its sediments directly from the underlying basement (Johnson et al., 2007a). Another source can be identified in the Southern Irumide Belt, which was similarly located on the southern Congo margin at this time: A Neoproterozoic cover sequence from the Nyimba–Sinda terrane of the SIB yields ages similar to that obtained from these units and was suggested to be derived from the underlying basement or adjacent intrusions within the SIB (Alessio et al., 2018).

Deformation (D_1) of the southern Congo margin occurred around *c.* 550–530 Ma, as a result of collision between the Congo and Kalahari cratons. This collision is recorded by the prominent E–W trending structures (F_1) in the Southern Irumide and Zambezi belts, in addition to the whiteschist and amphibolite facies metamorphic overprints generated at this time (M_1). Subsequent deformation (D_2) was weaker and resulted in the generation of N–S folds (F_1) that refolded the E–W trending F1 folds. The timing of D_2 is largely unconstrained, though restricted to occurring during the Phanerozoic. However, it has been previously noted that this deformation could have occurred during the Permian–Triassic, in response to intra-plate stresses associated with the Mauritanian–Variscan and Gondwanide orogenies (Alessio et al., 2019).

CONCLUSIONS

The Southern Irumide Belt and Kafue region of southern Zambia provide vital records of the tectono-metamorphic processes occurring

as a result of the collision between the Congo and Kalahari cratons during the final stages of Gondwana amalgamation. Thermobarometric modelling indicates that metapelitic amphibolite facies rocks in the Kafue region reached peak conditions of 4.1–7.9 kbar and 560–670 °C, corresponding to thermal gradients of 70–165 °C/kbar. A chlorite–quartz schist sample obtained from the Chewore–Rufunsa Terrane is suggested to be retrogressed whiteschist, which was previously shown to record peak conditions between 9–19 kbar and 650–790 °C, corresponding to thermal gradients of 30–90 °C/kbar. Thermobarometric modelling suggests that these sample Z16-09 experienced retrograde pressures below 15 kbar (at 400 °C) and temperatures below 590 °C, corresponding to thermal gradients between 30–90 °C/kbar. Both the whiteschists and metapelite are interpreted to have occurred as a result of Congo–Kalahari collision and are likely coeval with E–W trending folds seen in both the SIB and Zambezi supracrustals. The differences in *P–T* conditions experienced by the amphibolite facies rocks and the whiteschists are ascribed to their location during collision. The amphibolite facies rocks were located proximal to the suture zone between the Congo and Kalahari cratons, whereas the whiteschists were formed within the suture zone itself, where the Congo Craton subducted beneath the Kalahari Craton.

ACKNOWLEDGEMENTS

This paper f is a contribution to IGCP projects #628 (Gondwana Map) and #648 (Supercontinents and Global Dynamics). This project was funded by Australian Research Council Future Fellowship #FT120100340 to A. Collins and Discovery Project #DP160101006 to D. Kelsey. B. McDonald of the John de Laeter Centre is thanked for help with the collection of analytical data. B. Alessio is supported by a Research Training Program scholarship.

REFERENCES

Alessio, B.L., Collins, A.S., Clark, C., Glorie, S., Siegfried, P.R., Taylor, R., 2019. Age, origin and palaeogeography of the Southern Irumide Belt, Zambia. Journal of the Geological Society, jgs2018-2174.

Alessio, B.L., Collins, A.S., Siegfried, P., Glorie, S., De Waele, B., Payne, J.L., Archibald, D., 2018. Neoproterozoic tectonic geography of the south-east Congo Craton in Zambia as deduced from the age and composition of detrital zircons. Geoscience Frontiers.

Alessio, B.L., Kelsey, D.E., 2018. On yoderite: Using calculated phase equilibria to investigate its rarity in the geological record of whiteschists. Journal of Metamorphic Geology 36, 297-314.

Allmendinger, R.W., Cardozo, N., Fisher, D.M., 2011. Structural geology algorithms: Vectors and tensors. Cambridge University Press.

Bingen, B., Jacobs, J., Viola, G., Henderson, I., Skår, Ø., Boyd, R., Thomas, R., Solli, A., Key, R., Daudi, E., 2009. Geochronology of the Precambrian crust in the Mozambique belt in NE Mozambique, and implications for Gondwana assembly. Precambrian Research 170, 231-255.

Boger, S., White, R., Schulte, B., 2012. The importance of iron speciation (Fe+ 2/Fe+ 3) in determining mineral assemblages: an example from the high-grade aluminous metapelites of southeastern Madagascar. Journal of Metamorphic Geology 30, 997-1018.

Boyd, R., Nordgulen, Ø., Thomas, R., Bingen, B., Bjerkgård, T., Grenne, T., Henderson, I., Melezhik, V., Often, M., Sandstad, J., Solli, A., Tveten, E., Viola, G., Key, R., Smith, R., Gonzalez, E., Hollick, L., Jacobs, J., Jamal, D., Motuza, G., Bauer, W., Daudi, E., Feitio, P., Manhica, V., Moniz, A., Rosse, D., 2010. The geology and geochemistry of the East African Orogen in northeastern Mozambique. South African Journal of Geology 113, 87-129.

Brown, M., 2007. Metamorphic conditions in

orogenic belts: a record of secular change. International Geology Review 49, 193-234.
Brown, M., 2010. Paired metamorphic belts revisited. Gondwana Research 18, 46-59.
Cardozo, N., Allmendinger, R.W., 2013. Spherical projections with OSXStereonet. Computers & Geosciences 51, 193-205.
De Waele, B., Johnson, S.P., Pisarevsky, S.A., 2008. Palaeoproterozoic to Neoproterozoic growth and evolution of the eastern Congo Craton: Its role in the Rodinia puzzle. Precambrian Research 160, 127-141.
England, P.C., Richardson, S., 1977. The influence of erosion upon the mineral facies of rocks from different metamorphic environments. Journal of the Geological Society 134, 201-213.
Fockenberg, T., Schreyer, W., 1994. Stability of Yoderite in the Absence and in the Presence of Quartz: an Experimental Study in the System MgO– Al2O3– Fe2O3– SiO2-H2O. Journal of Petrology 35, 1341-1375.
Franz, L., Romer, R.L., de Capitani, C., 2013. Protoliths and phase petrology of whiteschists. Contributions to Mineralogy and Petrology 166, 255-274.
Goscombe, B., Armstrong, R., Barton, J., 2000. Geology of the Chewore Inliers, Zimbabwe: constraining the Mesoproterozoic to Palaeozoic evolution of the Zambezi Belt. Journal of African Earth Sciences 30, 589-627.
Griffin, W., Wang, X., Jackson, S., Pearson, N., O'Reilly, S.Y., Xu, X., Zhou, X., 2002. Zircon chemistry and magma mixing, SE China: in-situ analysis of Hf isotopes, Tonglu and Pingtan igneous complexes. Lithos 61, 237-269.
Grimes, C.B., John, B.E., Kelemen, P., Mazdab, F., Wooden, J., Cheadle, M.J., Hanghøj, K., Schwartz, J., 2007. Trace element chemistry of zircons from oceanic crust: A method for distinguishing detrital zircon provenance. Geology 35, 643-646.
Hanson, R., 2003. Proterozoic geochronology and tectonic evolution of southern Africa. Geological Society, London, Special Publications 206, 427-463.
Hanson, R.E., Wilson, T.J., Munyanyiwa, H., 1994. Geologic evolution of the Neoproterozoic Zambezi orogenic belt in Zambia. Journal of African Earth Sciences 18, 135-150.
Hauzenberger, C., Tenczer, V., Bauernhofer, A., Fritz, H., Klötzli, U., Košler, J., Wallbrecher, E., Muhongo, S., 2014. Termination of the Southern Irumide Belt in Tanzania: Zircon U/Pb geochronology. Precambrian Research 255, 144-162.
Holland, T., Powell, R., 2011. An improved and extended internally consistent thermodynamic dataset for phases of petrological interest, involving a new equation of state for solids. Journal of Metamorphic Geology 29, 333-383.
Hoskin, P.W., Ireland, T.R., 2000. Rare earth element chemistry of zircon and its use as a provenance indicator. Geology 28, 627-630.
Hutchins, D., Reeves, C., 1980. Regional geophysical exploration of the Kalahari in Botswana. Tectonophysics 69, 201-220.
Jackson, S.E., Pearson, N.J., Griffin, W.L., Belousova, E.A., 2004. The application of laser ablation-inductively coupled plasma-mass spectrometry to in situ U–Pb zircon geochronology. Chemical Geology 211, 47-69.
John, T., Schenk, V., Mezger, K., Tembo, F., 2004. Timing and PT evolution of whiteschist metamorphism in the Lufilian Arc–Zambezi Belt orogen (Zambia): implications for the assembly of Gondwana. The Journal of Geology 112, 71-90.
Johnson, S., 2011. Preliminary investigation of in-situ, high-pressure, high-fO2 metasomatism and metamorphism of meta-basalt to whiteschist. Frontier Research on Earth Evolution 1, 2011.
Johnson, S., De Waele, B., Evans, D., Banda, W., Tembo, F., Milton, J., Tani, K., 2007a. Geochronology of the Zambezi supracrustal sequence, southern Zambia: a record of Neoproterozoic divergent processes along the southern margin of the Congo Craton.

The Journal of Geology 115, 355-374.

Johnson, S., De Waele, B., Liyungu, A., 2006. U-Pb SHRIMP geochronology of granitoid rocks in eastern Zambia: terrane subdivision of the Mesoproterozoic Southern Irumide Belt. Tectonics 25.

Johnson, S., Oliver, G., 1998. A second natural occurrence of yoderite. Journal of Metamorphic Geology 16, 809-818.

Johnson, S.P., De Waele, B., Tembo, F., Katongo, C., Tani, K., Chang, Q., Iizuka, T., Dunkley, D., 2007b. Geochemistry, geochronology and isotopic evolution of the Chewore–Rufunsa Terrane, Southern Irumide Belt: a Mesoproterozoic continental margin arc. Journal of Petrology 48, 1411-1441.

Johnson, S.P., Rivers, T., De Waele, B., 2005. A review of the Mesoproterozoic to early Palaeozoic magmatic and tectonothermal history of south–central Africa: implications for Rodinia and Gondwana. Journal of the Geological Society 162, 433-450.

Kampunzu, A., Cailteux, J., 1999. Tectonic evolution of the lufilian arc (Central Africa Copper Belt) during Neoproterozoic pan African orogenesis. Gondwana Research 2, 401-421.

Karmakar, S., Schenk, V., 2016. Mesoproterozoic UHT metamorphism in the Southern Irumide Belt, Chipata, Zambia: Petrology and in situ monazite dating. Precambrian Research 275, 332-356.

Katongo, C., Koller, F., Kloetzli, U., Koeberl, C., Tembo, F., Waele, B.D., 2004. Petrography, geochemistry, and geochronology of granitoid rocks in the Neoproterozoic-Paleozoic Lufilian–Zambezi belt, Zambia: Implications for tectonic setting and regional correlation. Journal of African Earth Sciences 40, 219-244.

Mazac, O., 1974. Reconnaissance gravity survey of Zambia. Republic of Zambia, Ministry of Mines and Industry.

McDonough, W.F., Sun, S.-S., 1995. The composition of the Earth. Chemical geology 120, 223-253.

Meert, J.G., Lieberman, B.S., 2008. The Neoproterozoic assembly of Gondwana and its relationship to the Ediacaran–Cambrian radiation. Gondwana Research 14, 5-21.

Merdith, A.S., Collins, A.S., Williams, S.E., Pisarevsky, S., Foden, J.F., Archibald, D., Blades, M.L., Alessio, B.L., Armistead, S., Plavsa, D., 2017. A full-plate global reconstruction of the Neoproterozoic. Gondwana Research.

Miyashiro, A., 1961. Evolution of metamorphic belts. Journal of petrology 2, 277-311.

Paton, C., Hellstrom, J., Paul, B., Woodhead, J., Hergt, J., 2011. Iolite: Freeware for the visualisation and processing of mass spectrometric data. Journal of Analytical Atomic Spectrometry 26, 2508-2518.

Powell, R., White, R., Green, E., Holland, T., Diener, J., 2014. On parameterizing thermodynamic descriptions of minerals for petrological calculations. Journal of Metamorphic Geology 32, 245-260.

Schreyer, W., 1974. Whiteschist, a new type of metamorphic rock formed at high pressures. Geologische Rundschau 63, 597-609.

Sláma, J., Košler, J., Condon, D.J., Crowley, J.L., Gerdes, A., Hanchar, J.M., Horstwood, M.S., Morris, G.A., Nasdala, L., Norberg, N., 2008. Plešovice zircon—a new natural reference material for U–Pb and Hf isotopic microanalysis. Chemical Geology 249, 1-35.

Thieme, J., 1984. Geological Map of the Lusaka Area. Geol. Survey Zambia. Government of the United Kingdom (Ordnance Survey).

Westerhof, A.P., Lehtonen, M.I., Mäkitie, H., Manninen, T., Pekkala, Y., Gustafsson, B., Tahon, A., 2008. The Tete-Chipata Belt: A new multiple terrane element from western Mozambique and southern Zambia. Geological Survey of Finland Special Paper 48, 145-166.

White, R., Powell, R., Holland, T., Johnson, T., Green, E., 2014a. New mineral activity–composition relations for thermodynamic calculations in metapelitic systems. Journal

of Metamorphic Geology 32, 261-286.
White, R., Powell, R., Johnson, T., 2014b. The effect of Mn on mineral stability in metapelites revisited: New a–x relations for manganese-bearing minerals. Journal of Metamorphic Geology 32, 809-828.
Wiedenbeck, M., Alle, P., Corfu, F., Griffin, W., Meier, M., Oberli, F.v., Quadt, A.v., Roddick, J., Spiegel, W., 1995. Three natural zircon standards for U-Th-Pb, Lu-Hf, trace element and REE analyses. Geostandards and Geoanalytical Research 19, 1-23.
Woodhead, J., Hergt, J., Shelley, M., Eggins, S., Kemp, R., 2004. Zircon Hf-isotope analysis with an excimer laser, depth profiling, ablation of complex geometries, and concomitant age estimation. Chemical Geology 209, 121-135.
Woodhead, J.D., Hergt, J.M., 2005. A preliminary appraisal of seven natural zircon reference materials for in situ Hf isotope determination. Geostandards and Geoanalytical Research 29, 183-195.

CHAPTER 6

This chapter has been submitted for publication in *Tectonophysics* as:
Alessio, B.L., Glorie, S., Collins, A.S., Jourdan, F., Jepson, G., Nixon, A., Siegfried, P., Clark. C. The tectono-thermal evolution of the southern Congo margin as deterimined from apatite and muscovite thermochronology.

Statement of Authorship

Title of Paper	The tectono-thermal evolution of the southern Congo margin as determined from apatite and muscovite thermochronology
Publication Status	☐ Published ☐ Accepted for Publication ☑ Submitted for Publication ☐ Unpublished and Unsubmitted w ork w ritten in manuscript style
Publication Details	Alessio, Brandon L., Glorie, Stijn, Collins, Alan S., Jourdan, Fred, Jepson, Gilby, Nixon, Angus, Siegfried, Pete, Clark, Chris,. Submitted. The tectono-thermal evolution of the southern Congo margin as determined from apatite and muscovite thermochronology. Tectonophysics.

Principal Author

Name of Principal Author (Candidate)	Brandon Luke Alessio		
Contribution to the Paper	Fieldwork, sample preparation, data collection, processing and interpretation, manuscript design and composition, drafting of figures.		
Overall percentage (%)	80		
Certification:	This paper reports on original research I conducted during the period of my Higher Degree by Research candidature and is not subject to any obligations or contractual agreements with a third party that would constrain its inclusion in this thesis. I am the primary author of this paper.		
Signature		Date	07/01/19

Co-Author Contributions

By signing the Statement of Authorship, each author certifies that:

i. the candidate's stated contribution to the publication is accurate (as detailed above);
ii. permission is granted for the candidate in include the publication in the thesis; and
iii. the sum of all co-author contributions is equal to 100% less the candidate's stated contribution.

Name of Co-Author	Stijn Glorie		
Contribution to the Paper	Fieldwork, guidance in data collection and interpretation, as well as manuscript review.		
Signature		Date	07/01/19

Name of Co-Author	Alan Collins		
Contribution to the Paper	Fieldwork, guidance in data interpretation, as well as manuscript review.		
Signature		Date	10/01/19

Name of Co-Author	Fred Jourdan		
Contribution to the Paper	Data collection and manuscript review.		
Signature		Date	17/01/19

Name of Co-Author	Gilby Jepson		
Contribution to the Paper	Guidance in data collection and interpretation, as well as manuscript review.		
Signature		Date	08/01/19

Name of Co-Author	Angus Nixon		
Contribution to the Paper	Guidance in data collection and interpretation, as well as manuscript review.		
Signature		Date	08/01/19

Name of Co-Author	Pete Siegfried		
Contribution to the Paper	Manuscript review.		
Signature		Date	16/01/19

Name of Co-Author	Chris Clark		
Contribution to the Paper	Manuscript review.		
Signature		Date	16/01/19

ABSTRACT

The Southern Irumide Belt (SIB) of Zambia consists of predominantly Mesoproterozoic terranes that record a pervasive tectono-metamorphic overprint from collision between the Congo and Kalahari cratons in the final stages of Gondwana amalgamation. This study applies multi-method thermochronology to samples throughout southern Zambia to constrain the post-collisional, Phanerozoic thermo-tectonic evolution of the region. U–Pb apatite and $^{40}Ar/^{39}Ar$ muscovite data are used to constrain the cooling history of the region following Congo–Kalahari collision, and reveal ages of *c.* 550–450 Ma. Variations in the recorded cooling ages are interpreted to relate to localised post-tectonic magmatism and the proximity of analysed samples to the Congo–Kalahari suture. Apatite fission track data are used to constrain the low-temperature thermo-tectonic evolution of the region and identify mean central ages of *c.* 320–300, 210–200 and 120–110 Ma. Thermal modelling of these samples identifies a number of thermal events occurring in the region throughout the Phanerozoic. Carboniferous to Permian–Triassic heating is suggested to relate to the development of Karoo rift basins found throughout central Africa and constrain the timing of sedimentation in the basin. Permian to Jurassic cooling is identified in a number of samples, reflecting exhumation as a result of the Mauritanian–Variscan and Gondwanide orogenies. Subsequent cooling of the majority of samples occurs from the Cretaceous and persists until present, reflecting exhumation in response to larger scale rifting associated with the break-up of Gondwana. Each model reveals a later phase of enhanced cooling beginning at *c.* 30 Ma that, if not an artefact of modelling, corresponds to the development of the East African Rift System. The obtained thermochronological data elucidate the previously unconstrained thermal evolution of the SIB, and provides a refined regional framework for constraining the tectonic history of central Africa throughout the Phanerozoic.

INTRODUCTION

The southern margin of the Congo Craton occupied a key position within Gondwana, which amalgamated at the end of the Neoproterozoic Era. In the later stages of amalgamation, the Congo Craton collided with the Kalahari Craton to form the Damara–Lufilian–Zambezi orogen (Collins and Pisarevsky, 2005; Merdith et al., 2017). In southern Zambia, this event resulted in a pervasive tectono-metamorphic fabric not only seen in the Zambezi Belt, but also the Southern Irumide Belt (SIB), a Mesoproterozoic orogen that occupies areas of Zambia, Malawi, Mozambique and Tanzania (Alessio and Kelsey, 2018; Goscombe et al., 2000; John et al., 2004; Johnson et al., 2006). Thus, southern Zambia provides two complementary records that can be used to better understand the evolution of the southern Congo Craton margin. However, while previous work has investigated the tectono-metamorphic overprints in the region, far less work has been undertaken to understand the thermo-tectonic evolution. Thermochronometers such as apatite U–Pb, muscovite ^{40}Ar–^{39}Ar and apatite fission track (AFT) can be used to constrain the post-magmatic thermal history below the relevant closure temperature for each thermochronological method. This information can be used to provide constraints on the temperature range and duration of metamorphism, in addition to subsequent tectonic activity such as sedimentary burial and exhumation/denudation. In the context of southern Zambia, these thermochronometers are applied to provide previously unavailable insights on the thermal evolution of a major collisional zone that formed part of central Gondwana, and how its low-temperature evolution relates to adjacent regions in central Africa (e.g. Fernandes et al., 2015; Kasanzu, 2017; Kasanzu et al., 2016; Mackintosh et al., 2017; Noble, 1997). This study provides apatite U–Pb, AFT and muscovite ^{40}Ar–^{39}Ar thermochronological data for the Southern Irumide and Zambezi belts in southern Zambia (Figs. 1, 2). These data are

used to provide constraints on the thermo-tectonic evolution of the southern Congo margin following collision with the Kalahari Craton during the later stages of Gondwana amalgamation c. 550–530 Ma (Johnson et al., 2006; Johnson et al., 2007b) and the subsequent exhumation history of the region, which is discussed in relation to Karoo rifting, Gondwana break-up, and the development of the East African Rift System (EARS).

BACKGROUND

The Congo Craton is a term used to describe the amalgamated central African landmass at the time of Gondwana assembly (De Waele et al., 2008), and contains a series of Archean to Palaeoproterozoic cratonic units (Fig. 1). This craton forms the nucleus of Gondwana and is bordered on all sides by Ediacaran to Cambrian orogenies, with its southern margin marked by the Damara–Lufilian–Zambezi orogen (Merdith et al., 2017). The Damara–Lufilian–Zambezi orogen developed in response to collision between the Congo and Kalahari Cratons in the later stages of Gondwana amalgamation at c. 550–530 Ma (Johnson et al., 2006; Johnson

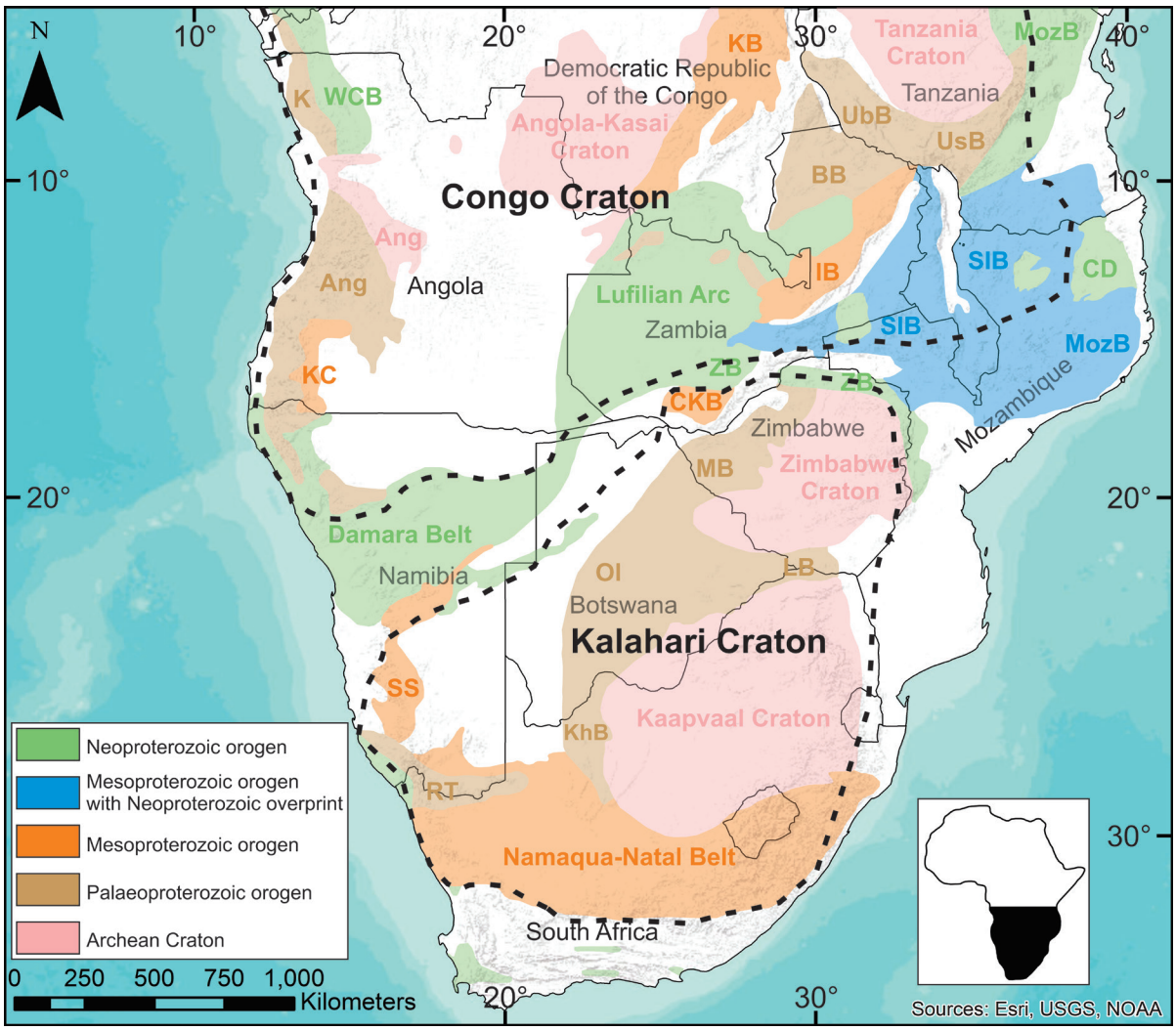

Figure 1. Simplified tectonic map of central Africa adapted from Alessio et al. (2018) following Hanson (2003) and Karmakar and Schenk (2016). Figure 2, relating to the study region, is indicated by the black box. The extent of the Congo and Kalahari cratons are denoted by the black dashed outlines. Abbreviations: ANG, Angola Block; BB, Bangweulu Block; CKB, Choma-Kalomo Block; IB, Irumide Belt; K, Kimezian; KB, Kibaran Belt; KC, Kunene Complex; KhB, Kheis Belt; LB, Limpopo Belt; MB, Magondi Belt; MozB, Mozambique Belt; OI, Okwa Inlier; RT, Richtersveld Terrane; SIB, Southern Irumide Belt; UbB, Ubendian Belt; UsB, Usagaran Belt; WCB, West Congo Belt; ZB, Zambezi Belt.

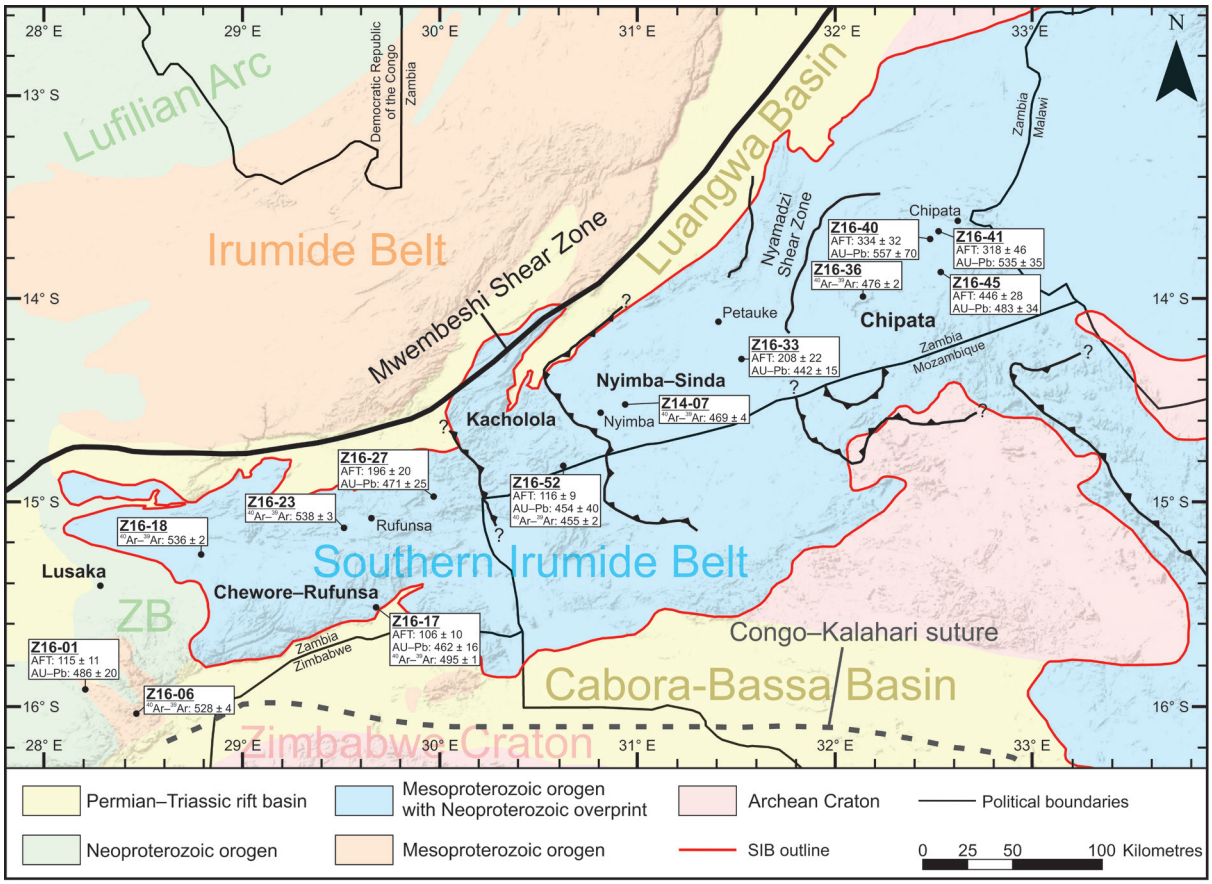

Figure 2. Simplified tectonic map of eastern Zambia and adjacent regions adapted from Alessio et al. (2018), following Johnson et al. (2006). Ages in the legend refer to the predominant tectonic periods in each geological feature. Samples analysed in this study are indicated on the map with their obtained thermochronological ages (in Ma).

et al., 2007b), and records a pervasive tectono-metamorphic fabric from this event that is similarly recorded within the SIB.

Geology and tectonometamorphic evolution of southern Zambia

Southern Zambia contains sections of two major orogens, the Zambezi and Southern Irumide belts (Figs. 1, 2). In Zambia, the SIB consists of structurally stacked, late Mesoproterozoic to Neoproterozoic terranes that formed on a Palaeoproterozoic basement, in a continental-margin-arc setting (Alessio et al., 2019; Johnson et al., 2007b). The SIB likely extends past Malawi, into Mozambique and southern Tanzania where terranes of similar age and tectonic setting have been identified (Fig. 1; Alessio et al., 2018; Bingen et al., 2009; Hauzenberger et al., 2014; Thomas et al., 2016). The Zambezi Belt is a continuation of the Lufilian Arc and Damara Belt to the west (e.g. Hanson et al., 1994; Hutchins and Reeves, 1980; Johnson et al., 2007a; Kampunzu and Cailteux, 1999; Mazac, 1974), which is referred to collectively as the Damara–Lufilian–Zambezi orogen. In southern Zambia, the Zambezi Belt largely crops out as a supracrustal sequence with Neoproterozoic metasedimentary rocks and *c.* 880 Ma volcanoclastic formations intruded by *c.* 820 Ma granites (Johnson et al., 2007a). This orogen marks the suture zone between the Congo Craton and the Kalahari Craton, which comprise the landmass of present day central and southern Africa, respectively. Their collision resulted in the tectono-metamorphic fabric that is recorded in both the Zambezi and Southern Irumide belts (John et al., 2004). Located adjacent to the north of the SIB and south of the Zambezi Belt are the Luangwa and Cabora-Bassa basins, respectively (Fig. 2). These basins belong to a series of 'Karoo' basins found throughout central

and southern Africa, which formed around the late Carboniferous and display a common stratigraphic succession (Fig. 3; Catuneanu et al., 2005). Sedimentation in these Karoo basins occurred from the Carboniferous to Jurassic, reaching burial depths ranging from ~4–12 km (Banks et al., 1995; Catuneanu et al., 2005; Oesterlen and Millsteed, 1994).

The tectonic fabric resulting from Congo–Kalahari collision has previously been interrogated along the southern margin of the SIB, where whiteschists were shown to record peak pressure–temperature (*P–T*) conditions of 12–14 kbar and 725–775 °C (John et al., 2004), consistent with whiteschists located in the Zambezi Belt of northern Zimbabwe (Alessio and Kelsey, 2018). These high-pressure rocks are suggested to record subduction of the Congo Craton beneath the Kalahari Craton in the early stages of collision, and now mark the suture zone between these cratons (John et al., 2004). Thermobarometric estimates for lithologies interpreted to be located proximal to this suture zone record more Barrovian *P–T* conditions, with Goscombe et al. (2000) reporting peak conditions of ~7–9 kbar and ~590–720 °C from a series of reworked basement rocks of the Zambezi Belt in northern Zimbabwe.

Previous studies of the thermal evolution of central Africa

In Zambia, little has been done to constrain the high and low temperature thermo-tectonic evolution. However, several studies elsewhere in central Africa have provided thermochronological constraints. High-temperature thermochronological data for the Zambezi Belt in northern Zimbabwe constrains post Congo–Kalahari collision cooling between *c.* 500–430 Ma. This time range is constrained by a range

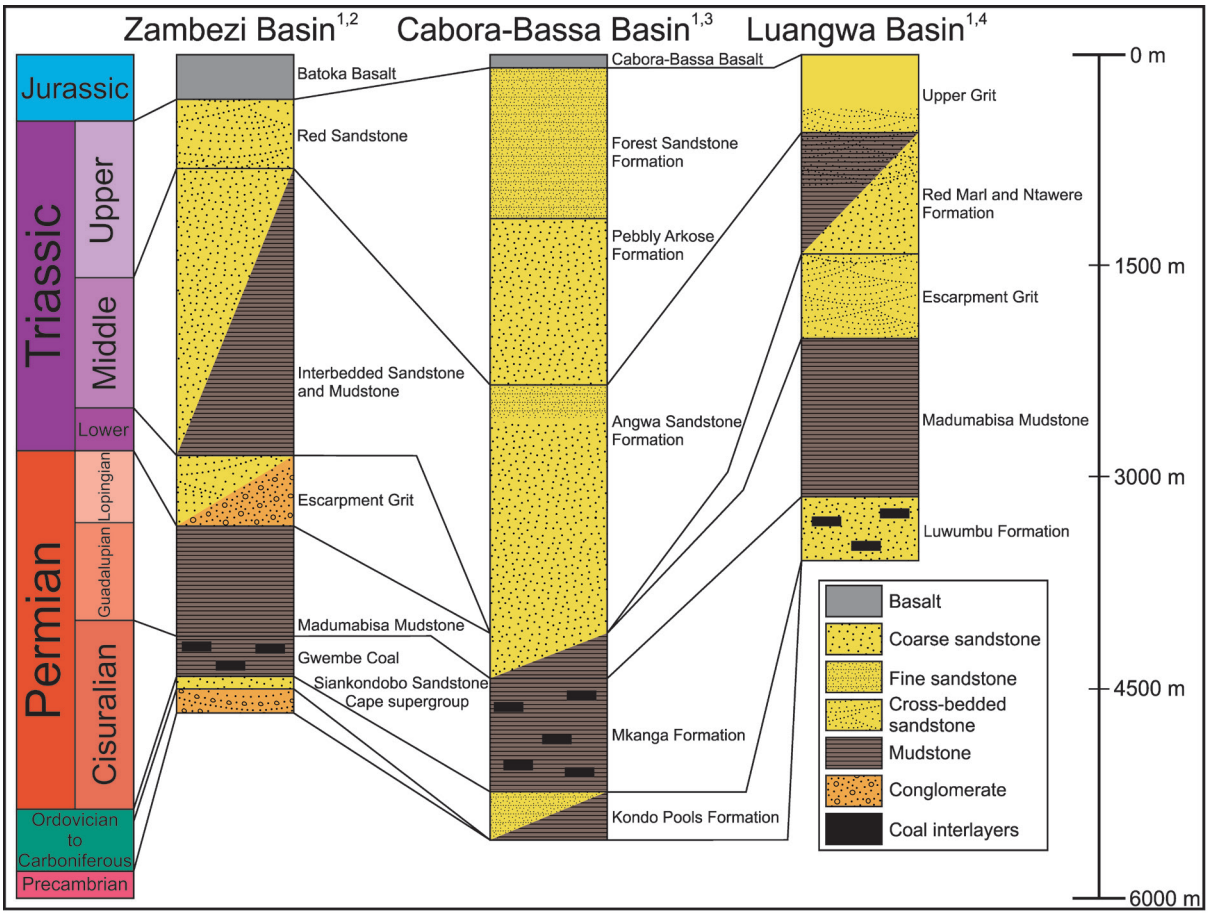

Figure 3. Generalised stratigraphic column for the 'Karoo' Mid-Zambezi, Cabora-Bassa and Luangwa basins. References: 1, Catuneanu et al. (2005); 2, Nyambe and Utting (1997); 3, Oesterlen and Millsteed (1994); 4, Banks et al. (1995).

of thermochronometers, with ages of 492 ± 40 Ma from Rb–Sr muscovite, 491 ± 2 Ma from ^{40}Ar–^{39}Ar hornblende, 464 ± 11 Ma and 451 ± 20 Ma from K–Ar biotite and Muscovite, respectively (Goscombe et al., 2000). In northeast Mozambique, U–Pb monazite dating yielded similar Cambrian−Ordovician ages to those reported from northern Zimbabwe and possibly reflect crystallisation from a cooling magmatic-hydrothermal system (Hurai et al., 2017).

Low temperature thermochronological data for Kenya, Tanzania, Mozambique and Zimbabwe have identified at least four cooling events have occurred in central Africa subsequent to Gondwana amalgamation (Boone et al., 2018a; Boone et al., 2018b; Fernandes et al., 2015; Kasanzu, 2017; Kasanzu et al., 2016; Mackintosh et al., 2019; Mackintosh et al., 2017; Noble, 1997). In Zimbabwe, Mackintosh et al. (2017) identified the initiation of a cooling event at *c.* 500 Ma that terminated with the onset of sedimentation (*c.* 300 Ma) in Karoo rift basins found throughout central and southern Africa. These authors suggest the cooling to reflect denudation caused by stress transmission from orogenesis occurring during Gondwana amalgamation. The second cooling event relates to the formation and development of these Karoo rift basins during the Permian and Triassic. In Tanzania and Zimbabwe, a period of cooling is identified from *c.* 350 to 200 Ma (Kasanzu, 2017; Kasanzu et al., 2016; Mackintosh et al., 2019; Noble, 1997), while ages recorded in Mozambique suggest rapid cooling between *c.* 240 to 230 Ma (Fernandes et al., 2015). These cooling ages are argued to reflect exhumation caused by intra-plate stresses associated with the Mauritanian-Variscan and Gondwanide orogenies (Kasanzu et al., 2016). Thermo-tectonic cooling at *c.* 120–100 Ma is identified in Precambrian basement in Kenya, and is attributed to denudation of the basement, which acted as both a basement high separating adjacent rifts in the region and a source of sediment to these basins (Boone et al., 2018b). Similarly, a period of cooling at c. 100 Ma is identified in Tanzania, thought to be related to the opening of the Indian and South Atlantic oceans during Gondwana break-up (Kasanzu, 2017). Throughout central Africa, a final phase of denudation is observed to occur between the late Cretaceous and Neogene that is suggested to relate to the development of the EARS. In Tanzania, Kasanzu et al. (2016) identified an exhumation event beginning at *c.* 70 Ma, while in Zimbabwe Mackintosh et al. (2017) identified a period of denudation between *c.* 40–25 Ma. These events likely reflect uplift and exhumation in response to plate boundary reorganisation or plume impact beneath the Tanzanian Craton (Koptev et al., 2015; Roberts et al., 2012). Ages relating to denudational cooling in response to active (EARS) rifting are recorded in Kenya and Mozambique, with constraints of *c.* 14 and 6 Ma, respectively (Boone et al., 2018b; Fernandes et al., 2015).

SAMPLING AND METHODS

Thirteen samples from southern Zambia were acquired for thermochronological analysis, with sample locations shown in Figure 2. Apatite and/or muscovite from these samples was extracted and subjected to three thermochronological techniques. (1) Apatite U–Pb dating provides constraints on cooling beneath a closure temperature of ~350–550 °C (Chew and Spikings, 2015), while (2) muscovite ^{40}Ar–^{39}Ar times cooling below a closure temperature of ~355–495 °C (Scibiorski et al., 2015). Finally, (3) AFT uses the retention of spontaneous fission tracks in apatite grains to provide information on a sample's thermal history between temperatures of ~120–60 °C. This temperature range corresponds to the apatite Partial Annealing Zone (APAZ), within which fission tracks are partially retained in an apatite grain (Wagner and Van Den Haute, 1992). Together, our application of multi-method thermochronology can be used to provide detailed constraints on the thermal evolution of the study

region from > 400 °C to < 100 °C.

Sample acquisition

Eleven samples were obtained from the SIB of Zambia, and include both variably deformed igneous and metasedimentary rocks. Intrusions throughout the SIB are predominantly late Mesoproterozoic in age and formed on an isotopically evolved, Palaeoproterozoic basement (Alessio et al., 2019). Samples analysed in this study have been acquired from both the late Mesoproterozoic intrusions and exposures of Palaeoproterozoic basement. A number of the analysed igneous samples lack direct age constraints, and could therefore relate to either period of magmatism. However, either period is significantly older than the thermal events interrogated by the mid- and low-temperature thermochronometers used in this study. A sample of *c.* 500 Ma post-tectonic granite, which is restricted to the Nyimba–Sinda Terrane of the SIB in Zambia, was also analysed. Deposition of the metasedimentary samples interrogated in this study occurred from the Palaeoproterozoic to Mesoproterozoic, with the exception of the sample from the Nyimba–Sinda Terrane that forms part of a rift-related cover sequence that was deposited during the Neoproterozoic (Alessio et al., 2019; Alessio et al., 2018). Two samples were obtained from the Kafue region of southern Zambia, and form a part of a supracrustal sequence of the Zambezi Belt. One sample was taken from a late Mesoproterozoic intrusion, equivalent in age to those from the SIB. The other sample was obtained from a metasedimentary sequence deposited during the Neoproterozoic, similar to the sedimentary rocks of the Nyimba–Sinda Terrane (Johnson et al., 2007a). A table listing each sample, the location it was obtained from, and its likely formation age, can be found in the supplementary material.

Apatite U–Pb

U–Pb data were obtained from eight apatite samples (Table 1) that were extracted using standard magnetic and density separation techniques. Separated apatite grains were then hand-picked, mounted in epoxy resin and polished to expose the internal section of each grain (Glorie et al., 2017b). Apatite grains were analysed for U–Pb isotopes using an Agilent 7900 ICP-MS and NewWave UP213 Laser Ablation System. Ablation was performed in a He-atmosphere with a frequency of 5 Hz. A spot size of 30 μm was used for all analyses. A total acquisition time of 60 seconds was used consisting of 30 seconds of background acquisition followed by 30 seconds of sample ablation. Madagascar apatite (ID-TIMS U–Pb age of 473.5 ± 0.7 Ma; Chew et al. (2014)) was used as the primary standard, while McClure apatite (TIMS U–Pb age of 523.51 ± 1.47 Ma; Schoene and Bowring (2006)) and Durango apatite (^{40}Ar–^{39}Ar age of 31.44 ± 0.18 Ma; McDowell et al. (2005)) were used as secondary standards for accuracy checks. Data were reduced using IOLITE (Paton et al., 2011), following the methodologies of Chew et al. (2011) and Chew et al. (2014). ^{207}Pb corrected overall weighted mean ^{238}U/^{206}Pb ages were calculated for each sample, and accompany the intercept age defined by the isochron regression for a given sample. McClure apatite yielded a weighted mean ^{207}Pb corrected ^{206}Pb/^{238}U age of 522.7 ± 8.4 Ma (MSWD = 0.83) in this study, which is within uncertainty of the reference age provided by Schoene and Bowring (2006). Durango yielded an age of 29.8 ± 1.6 Ma (MSWD = 1.09), consistent with the reference age provided by (McDowell et al., 2005).

Apatite fission track (AFT) analysis and thermal history modelling

The same samples used for apatite U–Pb analysis were additionally utilised for AFT analysis (Table 2). Apatite grain mounts were etched in 5 M HNO3 at 20 ± 1 °C for 20 s to reveal the spontaneous fission tracks within each grain and then imaged with a Zeiss AXIO Imager M2m Autoscan System. Fission track densities and lengths were measured using the Fast-

Tracks software, with at least 1000 tracks across a minimum of 20 grains counted, where possible. Samples with a paucity of confined fission tracks were repolished, irradiated using a Cf source, and reimaged to increase data yield. Given the consistency of the populations, presented confined track length distributions for these samples pool the tracks measured before and after irradiation, with the separate distributions for each sample presented in the supplementary material. Fission track ages were calculated using direct measurements of U (Gillespie et al., 2017; Glorie et al., 2017b; Song et al., 2017), which were obtained during U–Pb LA-ICP-MS analysis of the samples. Zeta age calibration was performed via repeated analysis of Durango apatite standard, using the age equations from Vermeesch (2017). Analytical data were reduced using IOLITE (Paton et al., 2011).

AFT central ages were calculated with RadialPlotter (Vermeesch, 2009), which represent the apparent AFT age of a given sample. For samples with large age dispersion (exceeding 25%) and those failing the chi-squared probability test P(χ^2), multiple AFT age populations may be present, potentially indicating the partial preservation of distinct cooling events (O'Sullivan and Parrish, 1995). The preservation of multiple cooling events in a single sample can be attributed to significant differences in apatite chemistry, particularly Cl and U concentration. Chlorine is known to influence fission track annealing (Green et al., 1986), with increasing concentrations serving to slow annealing. Similarly, increased U concentrations in apatite have been noted to influence fission track annealing (Carpena et al., 1988; Glorie et al., 2017a; Hall et al., 2016; Hendriks and Redfield, 2005; Jepson et al., 2018). This study uses Cl and eU (effective U; eU = U + 0.235Th) concentrations as a discriminator for age populations in radial plots with overdispersed single-grain ages, and discusses the obtained results accordingly.

The inverse thermal history modelling capabilities of the QTQt software package (version 5.5.0) were used for thermal history modelling, which is based on the Bayesian transdimensional Markov Chain Monte Carlo (MCMC) statistical method to derive the most likely temperature–time (T–t) path experienced by a given sample (Gallagher, 2012). For each sample, the MCMC was run for 250,000 iterations, after discarding an initial 50,000 burn-in runs (Gallagher et al., 2009). The AFT age, confined track length data, and Dpar values of each sample were used as input parameters for modelling, and can be referred to in the supplementary material. The fission track annealing model of Ketcham et al. (2007) was used during thermal history modelling, with no c-axis projection of confined fission tracks. Apatite U–Pb ages were used as mid-temperature constraints. Data fit of obtained thermal models was assessed by comparing the ATF ages and confined track length distributions predicted by the model to those observed in

Table 1. Apatite U−Pb data. n is the number of analyses performed on each sample. Each value refers to a mean. A table showing the individual analyses can be found in the supplementary material.

Sample	Lithology	Latitude (S)	Longitude (E)	n	$^{207}Pb/^{235}U$	± 2σ	$^{206}Pb/^{238}U$	± 2σ	$^{207}Pb/^{206}Pb$	± 2σ	Isochron regression age (Ma)	± 2σ	Weighted mean age* (Ma)	± 2σ
Chewore-Rufunsa Terrane														
Z16-17	Felsic Gneiss	15° 32' 17"	29° 41' 09"	40	4.65	0.21	0.11	0.008	0.28	0.01	462	16	461	6
Z16-27	Granodiorite	14° 59' 09"	29° 59' 11"	40	11.87	0.63	0.18	0.013	0.45	0.02	471	25	458	9
Kacholola Terrane														
Z16-52	Felsic Gneiss	14° 53' 24"	30° 36' 09"	31	18.56	0.91	0.23	0.016	0.57	0.02	454	40	466	13
Nyimba Sinda Terrane														
Z16-33	Granite	14° 18' 06"	31° 32' 09"	17	2.21	0.15	0.08	0.006	0.19	0.01	442	15	439	9
Chipata Terrane														
Z16-40	Felsic Gneiss	13° 42' 25"	32° 29' 21"	18	10.36	0.64	0.18	0.013	0.41	0.02	557	70	604	25
Z16-41	Charnockite	13° 40' 23"	32° 32' 57"	30	25.95	2.17	0.29	0.027	0.59	0.04	535	35	559	20
Z16-45	Charnockite	13° 52' 53"	32° 32' 22"	38	40.22	3.26	0.4	0.037	0.71	0.04	483	34	491	18
Zambezi Belt, Kafue region														
Z16-01	Granodiorite	15° 54' 03"	28° 11' 59"	23	5.63	0.55	0.13	0.011	0.28	0.02	486	20	485	13

*^{207} corrected $^{206}Pb/^{238}U$ weighted mean age

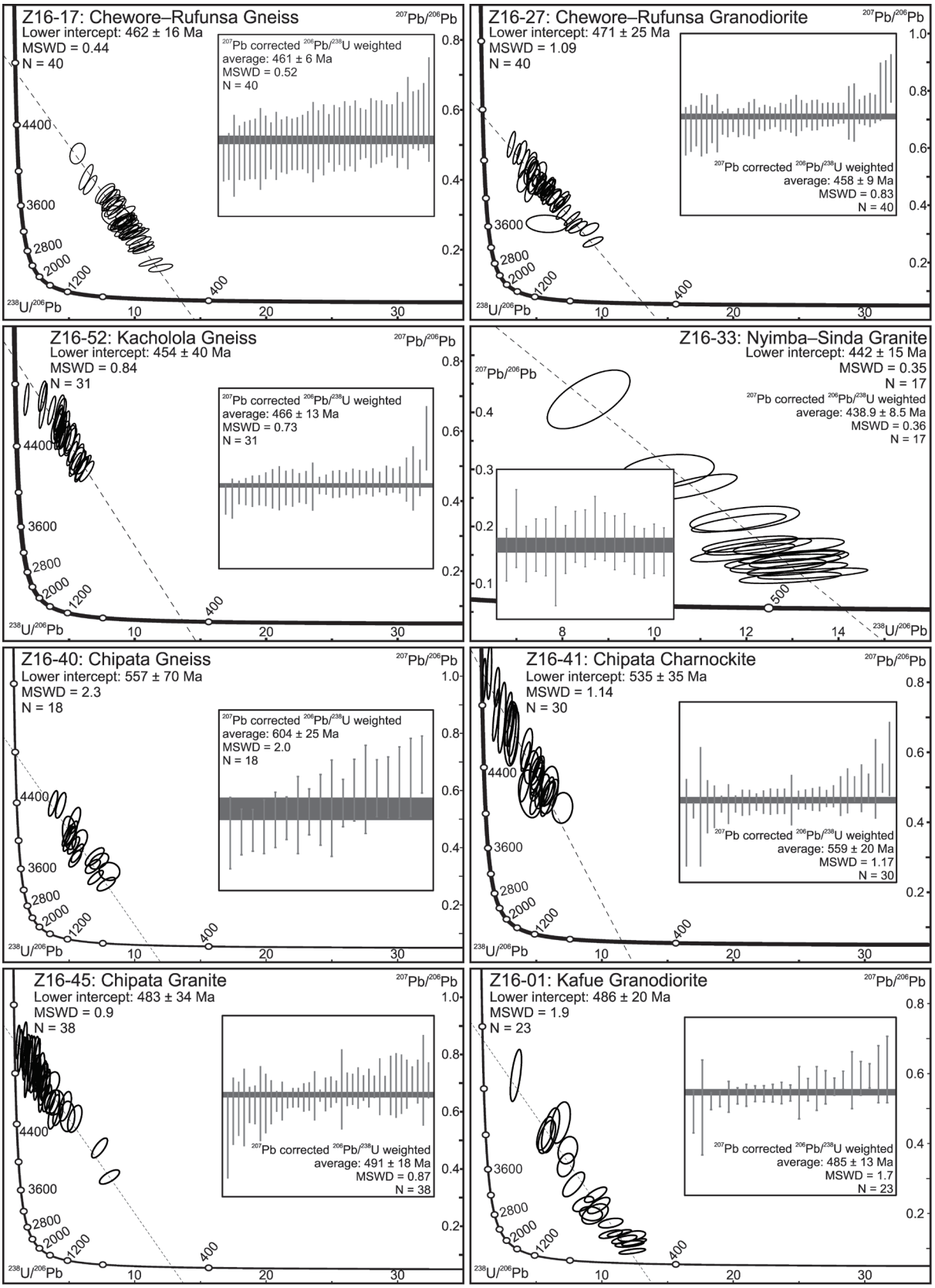

Figure 4. Apatite U–Pb results displayed on Terra–Wasserburg Concordia diagrams. Insets display the weighted mean ^{207}Pb corrected $^{206}Pb/^{238}U$ ages obtained for each sample.

the sample. A detailed report of modelling parameters, constraints, and data fit for each sample can be referred to in the supplementary material. Further information relating to the modelling procedure can be found in Gallagher (2012).

Muscovite ^{40}Ar–^{39}Ar

Seven samples of muscovite were used for ^{40}Ar–^{39}Ar dating (Table 2). Grains separated via paper shaking were hand-picked and range in size from ~80–250 μm, while also being relatively free of inclusions. Sample Z16-36 was the only exception, which instead ranged in size from > 250 μm to ~1 cm and was still inclusion-poor. The picked muscovite samples were sent to the Western Australia Argon Isotope Facility, Curtin University, where they were further picked for the most pristine grains that were used for ^{40}Ar–^{39}Ar dating. Samples were loaded into wells and bracketed by small wells that included Fish Canyon sanidine (FCs) used as a neutron monitor yielding an age of 28.294 ± 0.037 Ma (1σ) using the decay constants of (Renne et al., 2011). Correction factors for interfering isotopes were (^{39}Ar/^{37}Ar)Ca = 7.30x10-4 (± 11%), (^{36}Ar/^{37}Ar)Ca = 2.82x10-4 (± 1%) and (^{40}Ar–^{39}Ar)K = 6.76x10-4 (± 32%). Samples were step heated using a 110W Spectron Laser Systems, with a continuous Nd–YAG (IR: 1064 nm) laser. Ar isotopes were measured in static mode using a MAP 215-50 mass spectrometer, with a Balzers SEV 217 electron multiplier primarily using nine to ten cycles of peak-hopping. Ages obtained from ^{40}Ar–^{39}Ar data are plateau ages, defined as including at least 70% of the released ^{39}Ar and containing at least three consecutive steps that yield the same apparent age within a 95% confidence interval with P ≥ 0.05. The quoted plateau age should agree with each apparent age of the plateau steps within a 2σ confidence interval.

RESULTS

Apatite U–Pb

Terra-Wasserburg and ^{207}Pb corrected weighted mean ^{238}U/^{206}Pb diagrams are presented in Figure 4, with all samples yielding lower concordia intercepts that are within uncertainty of the associated ^{207}Pb corrected weighted mean ^{238}U/^{206}Pb age. All uncertainties are reported and shown at the 2σ level. Summarised results for each sample used for U–Pb analysis can be found in Table 1. Data tables for individual unknown and standard grain analyses can be located in the supplementary material.

Chewore–Rufunsa Terrane

Samples Z16-17 and Z16-27 from the Chewore–Rufunsa Terrane contain variable U concentrations (~6–220 ppm), with average values of 76 and 29 ppm, respectively. All 40 obtained analyses from felsic gneiss sample Z16-17 fall along a well-defined isochron regression line, yielding a lower concordia intercept of 462 ± 16 Ma (MSWD = 0.44; Fig. 4). Similarly, all 40 obtained analyses from granodiorite sample Z16-27 display a well-defined isochron regression line and yield a lower intercept of 471 ± 25 Ma (MSWD = 1.09; Fig. 4) that is consistent with the felsic gneiss. These obtained lower intercepts are taken as the most reliable estimate of cooling below the closure temperature of apatite in these samples.

Kacholola Terrane

Apatite grains obtained from felsic gneiss sample Z16-52 yield U concentrations between ~5–29 ppm. Thirty-one analyses were obtained from this sample, which yield a lower concordia intercept of 454 ± 40 Ma (MSWD = 0.84; Fig. 4) and ^{207}Pb corrected weighted mean ^{238}U/^{206}Pb age of 466 ± 13 Ma (MSWD = 0.73; Fig. 4).

Nyimba–Sinda Terrane

Granite sample Z16-33 yielded apatite grains with U concentrations between ~8–88 ppm, with an average concentration of 55 ppm.

Table 2: Muscovite ^{40}Ar–^{39}Ar data.

Sample	Lithology	Latitude (S)	Longitude (E)	Total ^{39}Ar released (%)	Plateau age (Ma)	± 2σ	MSWD	P
Chewore-Rufunsa Terrane								
Z16-17	Felsic Gneiss	15° 32' 17"	29° 41' 09"	97.8	494.63	1.05	0.72	0.71
Z16-18	Felsic Gneiss	15° 16' 49"	28° 46' 59"	79.3	535.71	1.61	1.37	0.19
Z16-23	Metapelite	15° 07' 38"	29° 32' 25"	91.1	537.58	2.61	1.09	0.36
Kacholola Terrane								
Z16-52	Felsic Gneiss	14° 53' 24"	30° 36' 09"	100	455.43	2.41	0.6	0.83
Nyimba Sinda Terrane								
Z14-07	Psammite	14° 32' 00"	30° 57' 23"	100	469.46	4.29	0.95	0.5
Chipata Terrane								
Z16-36	Quartzite	13° 59' 38"	32° 08' 04"	99.6	475.77	1.52	0.76	0.67
Zambezi Belt, Kafue region								
Z16-06	Metapelite	16° 00' 52"	28° 27' 31"	94.8	528.34	3.65	1.46	0.15

Eighteen analyses were obtained from this sample, with 17 defining an isochron regression that yields a lower concordia intercept of 442 ± 15 Ma (MSWD 0.35; Fig. 4).

Chipata Terrane

Apatite grains were extracted from samples of felsic gneiss, charnockite, and granite (Z16-40, Z16-41, and Z16-45, respectively) in the Chipata Terrane. U concentrations in these samples are the lowest of all obtained samples, between ~1–27 ppm (averages of ~5–12 ppm). As a result, U–Pb ages obtained from these samples are poorly resolved relative to other dated samples. Of the 27 grains analysed for sample Z16-40, 18 analyses define an isochron regression line with a lower concordia intercept of 557 ± 70 Ma (MSWD = 2.3; Fig. 4). Thirty-three grains were analysed from charnockite sample Z16-41, of which 30 fall along a relatively well resolved isochron regression line that yields a lower intercept of 535 ± 35 Ma (MSWD = 1.14; Fig. 4). From 40 analyses obtained for granite sample Z16-45, 38 define an isochron regression trend that yields a lower intercept of 483 ± 34 Ma (MSWD = 0.9; Fig. 4). For samples Z16-40 and Z16-45, these constraints are within uncertainty of the ages obtained from samples in the Chewore–Rufunsa and Kacholola terranes. Notably, sample Z16-41 records an age that is distinctly higher than that recorded by other samples outside of the Chipata Terrane of the SIB.

Kafue region (Zambezi Belt)

Granodiorite sample Z16-01 yielded apatite grains with variable U concentrations between ~3–100 ppm. From 30 analyses, 23 were found to define a consistent isochron regression trend that yields a lower concordia intercept of 486 ± 20 Ma (MSWD = 1.9: Fig. 4). This age is consistent with constraints obtained for the Chewore–Rufunsa, Kacholola, and Chipata terranes of the SIB.

Muscovite ^{40}Ar–^{39}Ar

^{40}Ar–^{39}Ar data were obtained from muscovite grains extracted from a variety of lithologies located throughout the SIB, which are presented in Figure 5 and Table 2. From the Chewore–Rufunsa Terrane, muscovite from felsic gneiss samples Z16-17 and Z16-18, as well as metapelite sample Z16-23 were analysed. Z16-17 and Z16-18 yielded weighted average plateau ages of 494.6 ± 1.1 Ma (MSWD = 0.72; P-value = 0.71) and 535.7 ± 1.6 Ma (MSWD = 1.37; P-value = 0.19), while Z16-23 yielded an age of 537.6 ± 2.6 Ma (MSWD = 1.09; P-value = 0.36). Felsic gneiss sample Z16-52 from the Kacholola Terrane yielded a weighted average plateau age of 455.4 Ma (MSWD = 0.6; P-value = 0.83). Psammite sample Z14-07 from the Nyimba–Sinda Terrane yielded a weighted average plateau age of 469.5 ± 4.3 Ma (MSWD = 0.95; P-value = 0.5). Muscovite obtained from quartzite sample Z16-36, located in the Chipata Terrane, yields a weighted average plateau

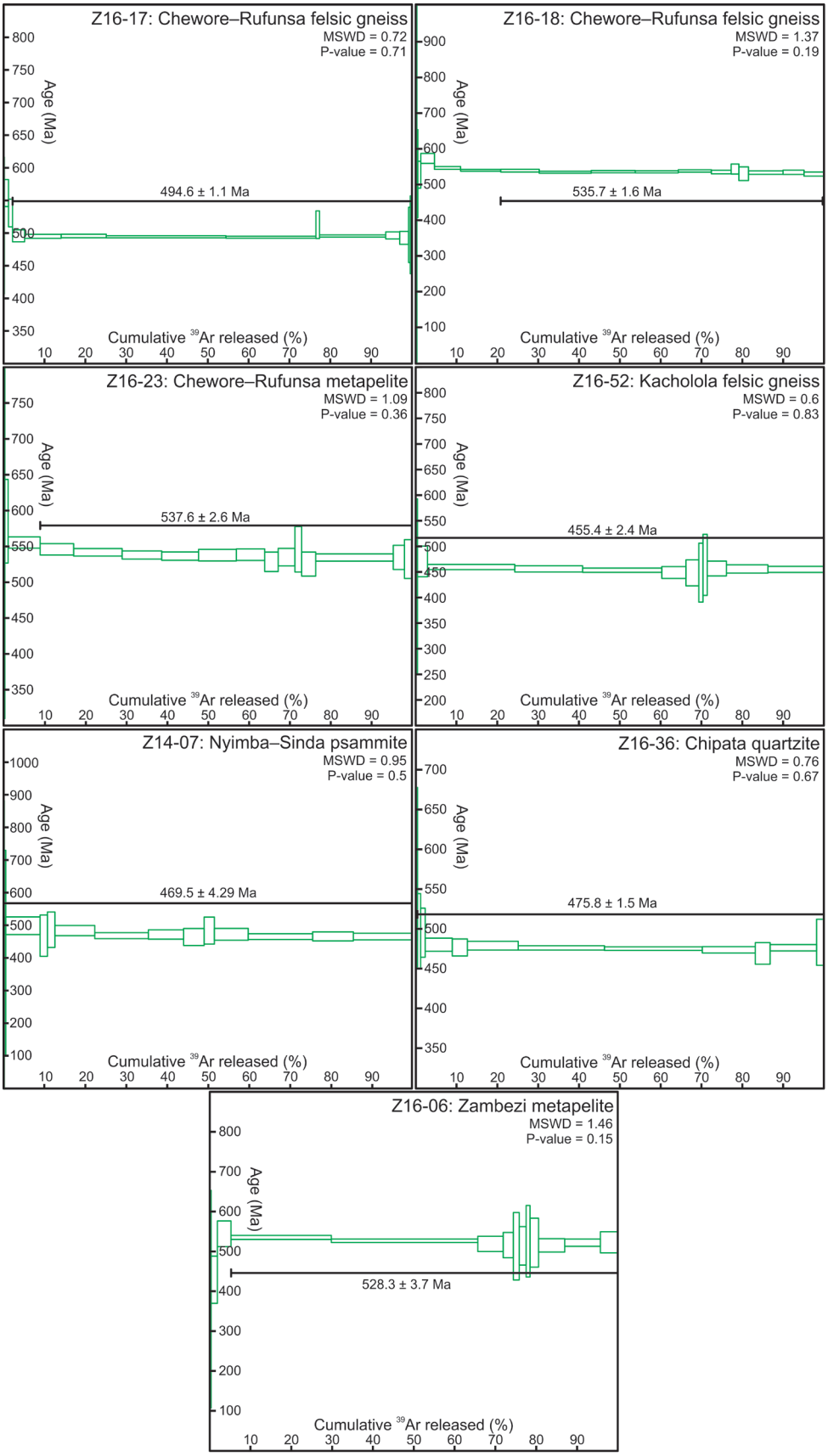

Figure 5. ^{40}Ar–^{39}Ar muscovite results. Plateau sections are marked by the black lines with the accompanying plateau age and 2σ error for the sample.

Table 3: Apatite fission track data: n is the number of grains analysed per sample and # of lengths is the number of confined track lengths idenfied in each sample. Age is the central age calculated for each sample. A table showing the individual analyses can be found in the supplementary material.

Sample	Lithology	Latitude (S)	Longitude (E)	Elevation (m)	n	Age ± 2σ (Ma)	# of lengths	Mean confined length (µm)	± 1σ (µm)
Chewore-Rufunsa Terrane									
Z16-17	Felsic Gneiss	15° 32' 17"	29° 41' 09"	500	34	106 ± 10	81	11.7	1.6
Z16-27	Granodiorite	14° 59' 09"	29° 59' 11"	770	35	196 ± 20	39	11.2	1.5
Kacholola Terrane									
Z16-52	Felsic Gneiss	14° 53' 24"	30° 36' 09"	660	29	116 ± 9	32	11.5	1.3
Nyimba Sinda Terrane									
Z16-33	Granite	14° 18' 06"	31° 32' 09"	1130	15	208 ± 22	53	11.0	1.4
Chipata Terrane									
Z16-40	Felsic Gneiss	13° 42' 25"	32° 29' 21"	980	23	334 ± 32	42	12.1	1.5
Z16-41	Charnockite	13° 40' 23"	32° 32' 57"	1020	23	318 ± 48	20	11.9	1.5
Z16-45	Charnockite	13° 52' 53"	32° 32' 22"	1120	28	446 ± 28	32	10.9	1.7
Zambezi Belt, Kafue region									
Z16-01	Granodiorite	15° 54' 03"	28° 11' 59"	1040	26	115 ± 11	24	11.2	1.8

age of 475.8 ± 1.5 Ma (MSWD = 0.76; P-value = 0.67). Outside of the SIB, a metapelitic schist forming part of a supracrustal sequence in the Zambezi Belt (Z16-06) yielded a weighted average plateau age of 528.3 ± 3.7 Ma (MSWD 1.46; P-value = 0.15).

Apatite fission track thermochronology

AFT results for each sample were plotted using RadialPlotter (Vermeesch, 2009) and are presented on individual radial plots in figures 6 and 7 that are colour coded against eU and log Cl concentration, which were used as chemical discriminators for individual analyses. Associated confined track length distributions are also plotted for each sample. Calculated central age uncertainties are quoted at the 2σ level. Summarised results for each sample used for AFT analysis can be found in Table 1. Data tables for individual standard and unknown analyses can be referred to in the supplementary material.

Chewore–Rufunsa

Felsic gneiss sample Z16-17 (n = 34) and granodiorite sample Z16-27 (n = 35) yield central ages of 106 ± 10 Ma and 196 ± 20 Ma, respectively. Both samples failed the χ^2 test and record relatively high dispersion, with Z16-17 recording 27% dispersion and Z16-27 recording 24% dispersion. The radial plots for sample Z16-17 (Fig. 6) displays a spread of ages ranging from 207–61 Ma. Grains older than *c.* 100 Ma yield relatively lower eU concentrations, suggesting that they are possibly more retentive to annealing than the younger grains and may preserve an earlier thermal event (Fernie et al., 2018; Glorie et al., 2017b; Jepson et al., 2018). In contrast, no relationship between age and Cl concentration can be observed in the sample. Sample Z16-27 (Fig. 6) displays a range of ages between 322–97 Ma. Like sample Z16-17, the older grains in this sample record relatively lower eU concentrations, suggesting they may record an older part of the thermal history. Sample Z16-17 yielded a mean confined fission track length of 11.7 ± 1.6 µm (n = 81), while Z16-27 yielded a mean length of 11.2 ± 1.48 µm (n = 39).

Kacholola

Felsic gneiss sample Z16-52 (n = 29) yielded a central age of 116 ± 9 Ma, passing the χ^2 test (P = 0.36) and recording no significant dispersion. The radial plot for this sample (Fig. 6) displays ages ranging from 152–54 Ma. Uranium and Chlorine concentrations in comparison to AFT age show no distinct relationship. The mean confined track length for this sample is 11.5 ± 1.3 µm (n = 32).

Nyimba–Sinda

Sample Z16-33 (n = 15) from a post-tectonic granite yields a central age of 208 ± 22 Ma, failing the χ^2 test and recording moderate dis-

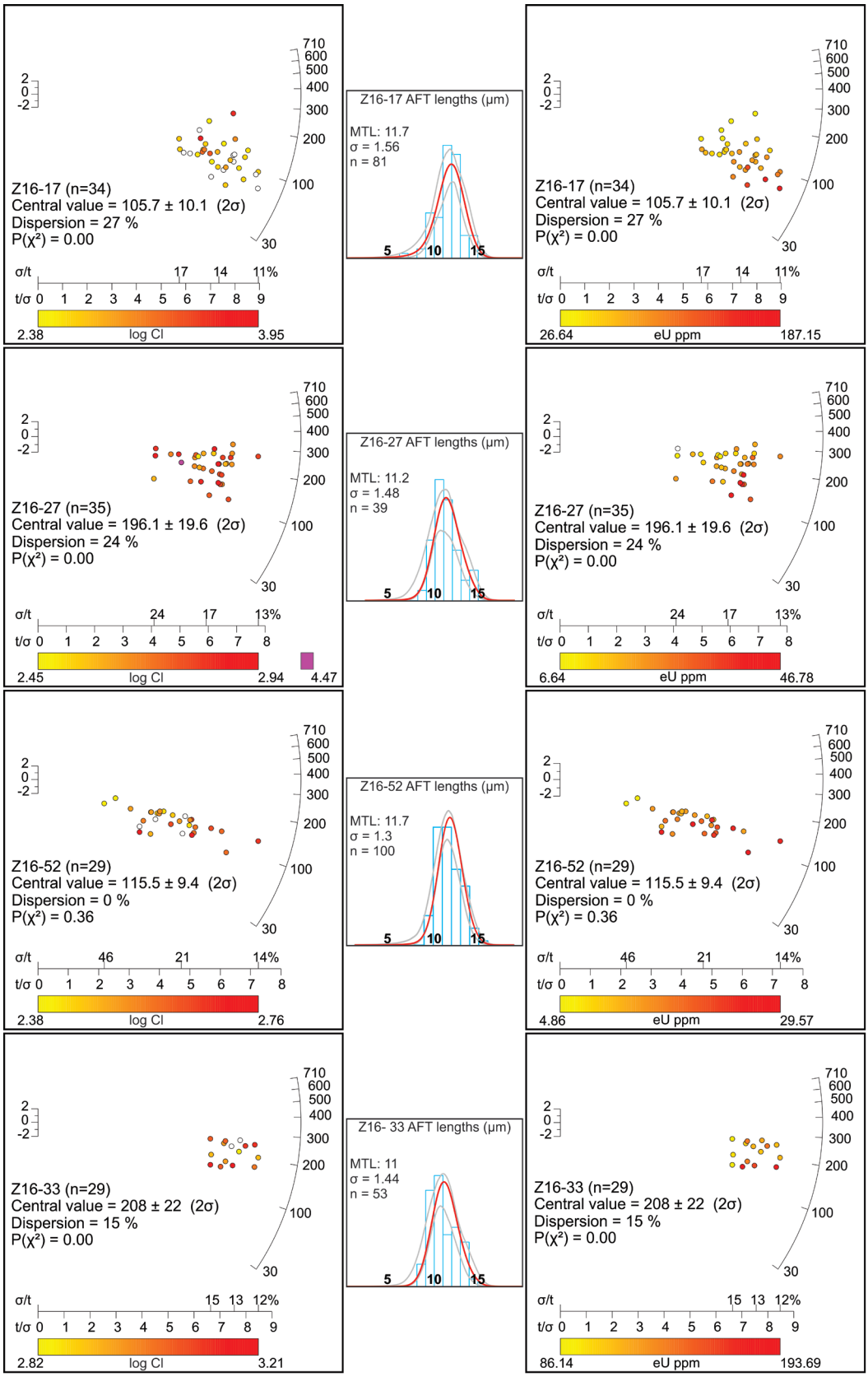

Figure 6. Apatite fission track results for samples Z16-17, Z16-27, Z16-52 and Z16-33, displayed on radial plots drawn using Radialplotter (Vermeesch, 2009). Grain analyses are coloured with respect to relative log Cl (left) and eU (right) concentrations.

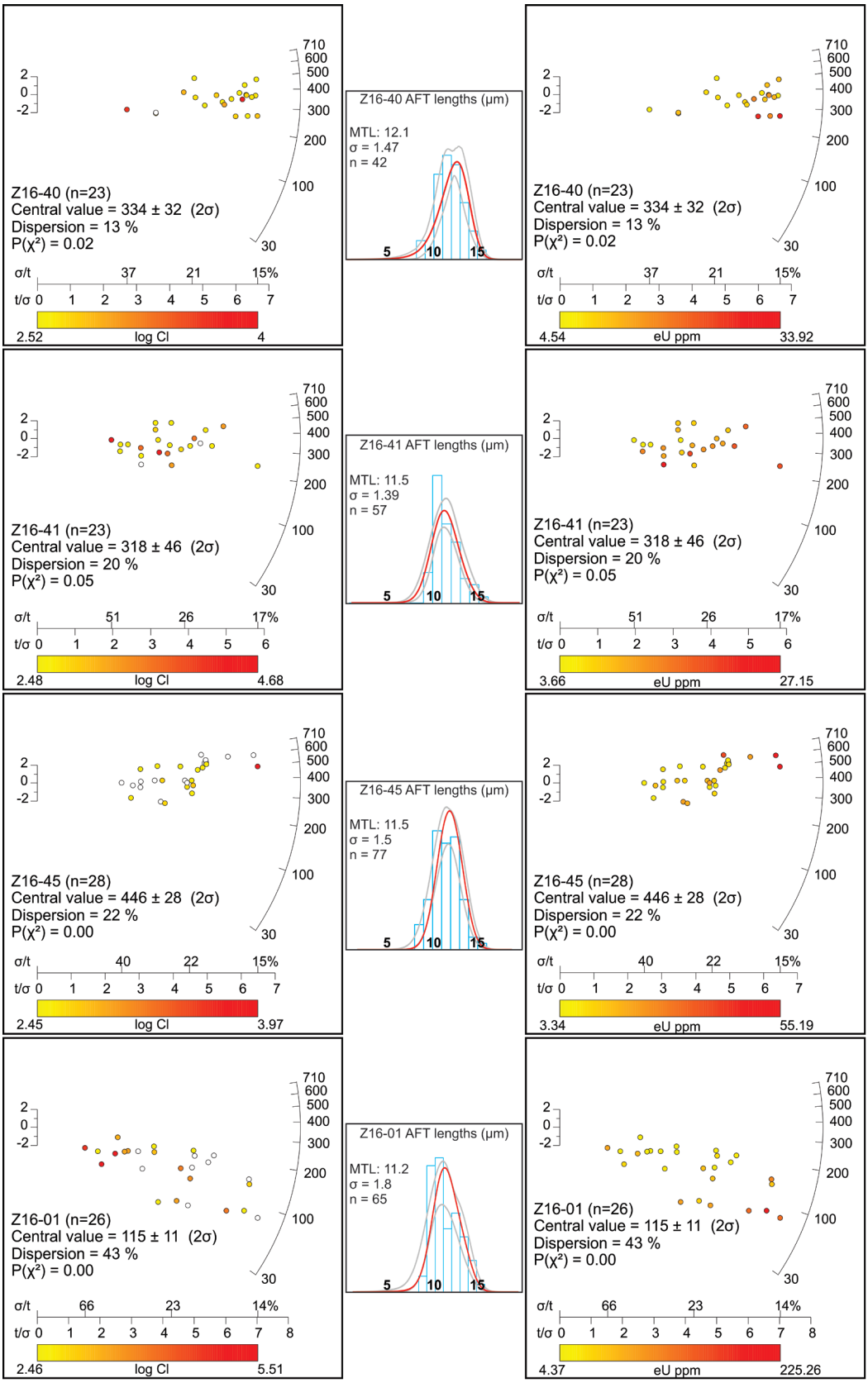

Figure 7. Apatite fission track results for samples Z16-40, Z16-41, Z16-45 and Z16-01, displayed on radial plots drawn using Radialplotter (Vermeesch, 2009). Grain analyses are coloured with respect to relative log Cl (left) and eU (right) concentrations.

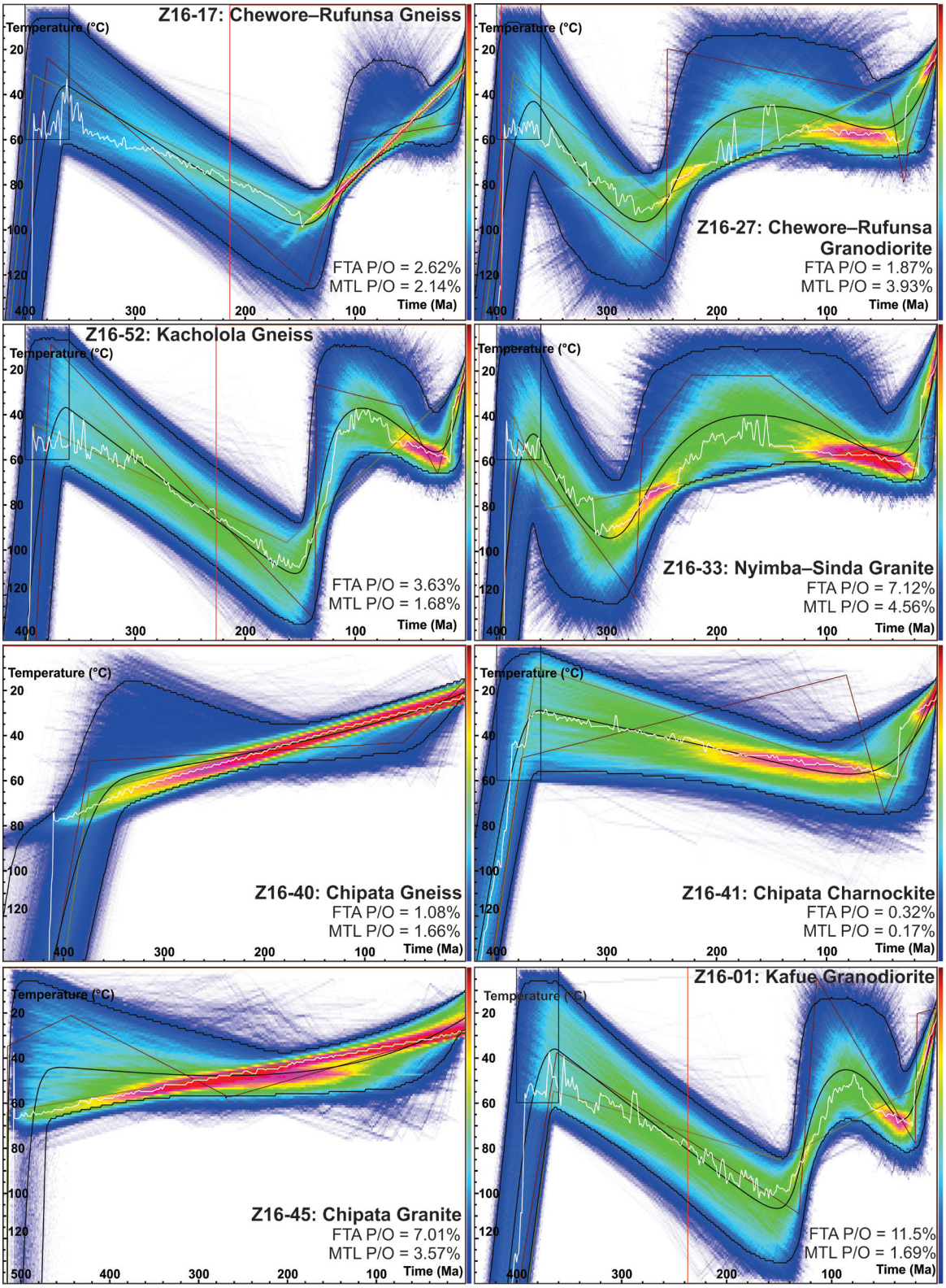

Figure 8. Thermal history models for apatite samples, calculated with the QTQt program. An additional temperature–time modelling constraints of being at surface prior to Carboniferous sedimentation is shown by the black boxes. The red box for each sample shows the temperature–time model space. Light brown paths show the maximum posterior models, dark brown paths show the maximum likelihood models, black paths show the expected models, white lines show the maximum mode models (further information can be found in Gallagher (2012)).

persion (15%). The radial plot (Fig. 6) displays ages ranging between 268–172 Ma, with no discernible relationship between Cl concentration and age. This sample yielded a mean confined track length of 11 ± 1.4 μm (n = 53).

Chipata

Felsic gneiss sample Z16-40, charnockite sample Z16-41, and granite sample Z16-45 yielded central ages of 334 ± 32 Ma, 318 ± 46 Ma, and 446 ± 28 Ma, respectively. Z16-41 passed the χ^2 test and all samples display moderate to little dispersion between analyses. The radial plot for sample Z16-40 (Fig. 7) displays a range of ages from 549–203 Ma with no significant correlation between age and log Cl or eU concentrations. However, three grains with similar ages around c. 250 Ma yield the highest eU concentrations recorded in the sample. Sample Z16-41 (Fig. 7) yields ages between 617–149 Ma. The oldest analyses present in this sample (between c. 617–400 Ma) record generally lower eU concentrations and may preserve an earlier part of the thermal history. Sample Z16-45 displays ages between 709–207 Ma (Fig. 7). No significant relationship between age and Cl concentration can be discerned within the sample. However, it is noted that the highest recorded eU concentrations correspond to some of the oldest grains, contrary to the other analysed samples where high eU concentrations correspond with younger analyses. Sample Z16-40 yielded a mean confined track length of 12.1 ± 1.5 μm (n = 42), while Z16-41 yielded a mean confined track length of 11.9 ± 1.5 μm (n = 20). Z16-45 yielded a mean confined track length of 10.9 ± 1.7 μm (n = 32).

Zambezi Belt (Kafue region)

Sample Z16-01 is a granodiorite obtained from the Kafue region of southern Zambia, within the Zambezi Belt. The sample yielded a central age of 115 ± 11 Ma, failing the χ^2 test and recording high dispersion (43%). The radial plot for the sample (Fig. 7) displays ages ranging between 238–37 Ma. High log Cl concentrations in this sample correlate with older ages, while higher eU concentrations correlate with younger ages, suggesting a compositional control on how the thermal history of this sample is recorded. This sample yielded a mean confined track length of 11.2 ± 1.83 μm (n = 24).

Thermal history modelling

Thermal history models were calculated for each apatite sample and are presented in Figure 8. The calculated models are described below in terms of their expected models, the weighted means of each model's posterior distribution, which represent the most representative thermal history. Additionally displayed on the models are the 95% confidence intervals of the corresponding expected model, and the probability distribution (posterior) of the sampled thermal histories (Gallagher, 2012). For each model, ~400–500 °C constraints were placed at the apatite U–Pb age obtained for that particular sample. A low-temperature constraint for each sample is included at near-surface conditions prior to at least the Carboniferous (0–60 °C, 400–360 Ma). This is interpreted from the unconformity between Precambrian basement and the Carboniferous Kondo Pools Formation recorded in the Cabora-Bassa Basin, in addition to a similar unconformity marked by the Permian Luwumbu Formation in the Luangwa Basin, which suggest that any Karoo-related sedimentation in the SIB occurred after this time (Fig. 3; Banks et al., 1995; Oesterlen and Millsteed, 1994). The calculated thermal models yield predicted AFT ages and mean track lengths that are generally within 4% of the observed values (i.e. predicted/observed = 0.97), with all but one sample displaying good agreement (predicted/observed > 0.9; Wildman et al., 2015) between the predicted and observed values. It is noted that the thermal model for sample Z16-01 yields a predicted AFT age within 11.5% of the observed value, though the calculated thermal history is near-identical to that obtained for samples Z16-17 and Z16-52 and is discussed together with

the more reliable models. High time acceptance rates were obtained for thermal models of samples Z16-40 and Z16-45 (~0.9 and 0.8, respectively) that utilised a 0–60°C, 400–360 Ma constraint. The presented samples were recalculated without this constraint, which reduced the acceptance rate and improved the predicted versus observed data fit for these samples. Models calculated with the additional constraint can be found in the supplementary material, which are noted to display a similar thermal history to the presented models.

The thermal models calculated for samples obtained from the Chipata Terrane (Z16-40, Z16-41, and Z16-45; Fig. 2) display a common thermal history (Fig. 8). Following initial cooling, samples Z16-40 and Z16-45 display expected models that suggest they experienced little to no reheating throughout the Phanerozoic. Sample Z16-41 records gradual reheating from *c.* 360–80 Ma, though likely remaining below the APAZ throughout this time. The thermal models calculated for samples located in the other SIB terranes and Zambezi Belt (Z16-01, 17, 27, 33 and 52; Fig. 2) terranes show similar thermal histories that can be traced from their apatite U–Pb cooling ages to present (Fig. 8). Samples Z16-01, 17 and 52 record heating from *c.* 380 Ma until c. 150 Ma, followed by cooling below the APAZ at c. 110–100 Ma. Samples Z16-01 and Z16-52 record additional reheating from *c.* 80–30 Ma that possibly re-entered the APAZ for Z16-01. Samples Z16-27 and Z16-33 record near identical thermal histories, with reheating occurring from *c.* 380 Ma to *c.* 300–270 Ma, reaching temperatures above the APAZ. Subsequent cooling reaches temperatures of ~40–50 °C at *c.* 180–160 Ma, and though the samples experience minor reheating from this time to *c.* 60–40 Ma, remain below the APAZ until present. The calculated thermal models suggest that every sample, with the exception of samples Z16-40 and Z16-45, experienced a final period of relatively rapid cooling from *c.* 30 Ma to present (Fig. 8).

DISCUSSION

Post-collisional thermal evolution of the southern Congo Craton

Apatite U–Pb dating provides constraints on cooling below temperatures of ~350–550 °C (Chew and Spikings, 2015), while muscovite ^{40}Ar–^{39}Ar dating can constrain cooling below temperatures below ~355–495 °C (Scibiorski et al., 2015). These cooling ages can be used to constrain events of magmatism, metamorphism, and deformation in a given sample. In the context of this study, these thermochronometers are used to provide rigorous constraints on the thermal evolution of the southern Congo Craton margin following its collision with the Kalahari Craton, the last major orogenic event that is interpreted to have occurred in this region (Alessio et al., 2019).

The calculated intercept ages obtained from apatite U–Pb dating range between *c.* 560–440 Ma, while the obtained ^{40}Ar–^{39}Ar ages range between *c.* 540–450 Ma, both consistent with estimates available for northern Zimbabwe and northeast Mozambique (Goscombe et al., 2000; Hurai et al., 2017). The samples obtained from the Kacholola and Nyimba–Sinda terranes can be observed to record the youngest cooling ages (Fig. 2). However, the Nyimba–Sinda Terrane is intruded throughout by post-tectonic granite with a crystallisation age of *c.* 500 Ma (Alessio et al., 2019; Johnson et al., 2006), which may have reheated these samples beyond the closure temperature of medium temperature thermochronometers (> 600 ˚C). The distribution of obtained cooling ages (Fig. 2) highlights a broad spatial variability between older (*c.* 540–530 Ma) and younger (*c.* 500 Ma) ages in the Chewore–Rufunsa Terrane. In the northern Chewore–Rufunsa Terrane, samples Z16-18 and Z16-23 record 40Ar–39Ar ages of c. 540–530 Ma, similar in age to sample Z16-06 (*c.* 530 Ma) from the Kafue region and *c.* 40 Ma older than the age obtained from the southern extent of this terrane. A similar trend is observed in the U–Pb ages obtained for these samples, though the

associated uncertainty makes this relationship less resolvable than using the ^{40}Ar–^{39}Ar ages. This spatial variation in age is consistent with the differences in the style and nature of thermal overprints created during Congo–Kalahari collision. The older samples in the Kafue region and northern Chewore–Rufunsa Terrane experienced Barrovian thermal gradient, amphibolite facies metamorphism. The younger sample, located along the Congo–Kalahari suture instead experienced relatively high thermal gradient, possibly eclogite facies metamorphism (John et al., 2004; Johnson and Oliver, 2002). We interpret that the proximity of this sample to the site of collision between the Congo and Kalahari cratons resulted in it recording younger cooling ages than the samples further away, due to thermal lag prolonging the time this sample resided above the closure temperatures of apatite and muscovite. Apatite U–Pb ages obtained from the Chipata Terrane are generally consistent with the ^{40}Ar–^{39}Ar ages obtained for the Chewore–Rufunsa Terrane, timing cooling at *c.* 560–480 Ma. While equivalent data are not available from the SIB in Mozambique, a nearby Neoproterozoic nappe emplaced during Gondwana amalgamation (The Monapo Klippe; Macey et al., 2010) is interpreted to record a ~300 °C hydrothermal overprint during the late Cambrian–Ordovician (Hurai et al., 2017).

Low temperature thermal evolution of central-east Africa

The obtained low-temperature thermochronological data provide a wide range of cooling ages, spanning from the Cambrian to Cretaceous (~450–100 Ma). While there are no comparable low-temperature thermochronological data available from Zambia, the obtained ages are consistent with numerous studies on the thermal history of neighbouring regions (Boone et al., 2018a; Boone et al., 2018b; Kasanzu, 2017; Kasanzu et al., 2016; Mackintosh et al., 2019; Mackintosh et al., 2017). The thermal models calculated in this study indicate the presence of four major thermal events that are recorded throughout central Africa: Congo–Kalahari collision, Karoo rifting and sedimentation, Gondwana breakup, and EARS development. These ages and thermal events are discussed in relation to the Phanerozoic tectonic history of central Africa, with these interpretations used to produce a model for the region's geodynamic evolution that is presented in Figure 9.

Congo–Kalahari collision

Sample Z16-45 yielded an AFT central age of 446 ± 28 Ma, within error of the obtained U–Pb age of 483 ± 34 Ma for this sample. Given the apparent overlap in ages recorded by these thermochronometers, cooling in this sample occurred rapidly. Notably, this constraint suggests that the SIB, acting as a single tectonic unit, exhumed rapidly following Congo–Kalahari collision. As such, this sample provides a key constraint on the thermo-tectonic evolution of samples from the SIB, and possibly wider southern Zambia, prior to the subsequent thermal events occurring during the Phanerozoic. The thermal history model for this sample (Fig. 8) displays an expected model that suggests minor reheating of the sample occurred following Congo–Kalahari collision. However, it is noted that the 95% confidence intervals for the expected model of this sample could allow for some reheating throughout this time. As such, it is possible that this sample records cooling following Congo–Kalahari collision, and experienced minor thermal disturbance thereafter (Fig. 9).

Karoo rifting

Samples Z16-40 and Z16-41 yielded AFT central ages of 334 ± 32 Ma and 318 ± 46 Ma, respectively. Furthermore, samples Z16-27 and Z16-33 yielded younger central ages of 196 ± 20 Ma and 208 ± 22 Ma, respectively. Both groups of ages have been obtained by previous studies in adjacent regions (Fernandes et al., 2015; Kasanzu et al., 2016; Mackintosh et al.,

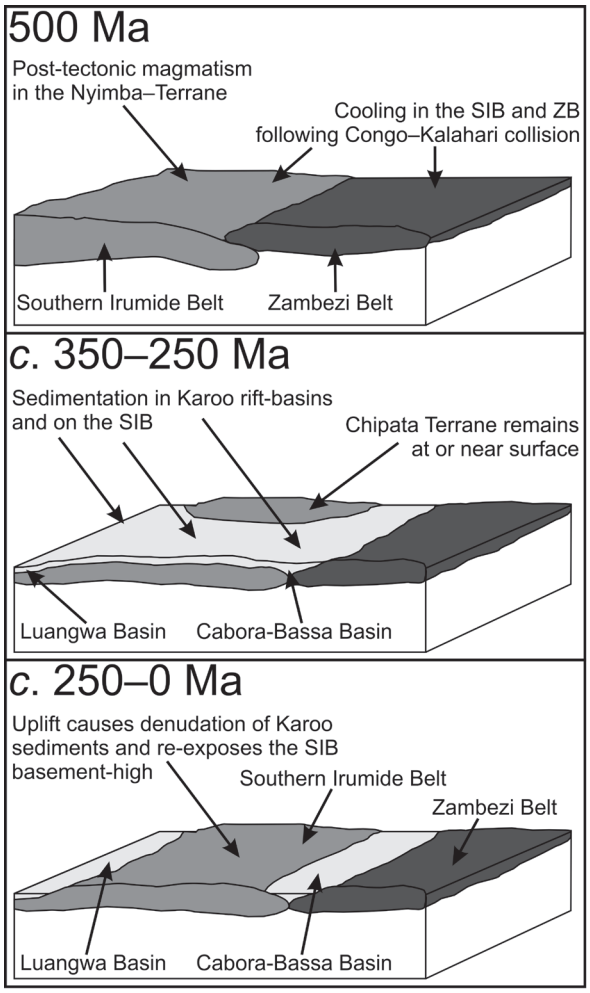

Figure 9. Geodynamic evolution of the study region throughout the Phanerozoic, as interpreted from obtained mid- and low-temperature thermochronological data.

2019; Mackintosh et al., 2017), and are suggested to relate to the development of Karoo rift basins located throughout central Africa. Thermal modelling of the samples with Carboniferous apparent AFT ages (Z16-40 and Z16-41) and the older sample Z16-45 (Fig. 8) produced expected models that indicate, after cooling from Congo–Kalahari collision, samples Z16-41 and possibly Z16-45 were gradually reheated until the Jurassic. Tectonic cooling resumes after this time and persists until present. The expected model for Z16-40 suggests that this sample was not reheated following Congo–Kalahari collision. The 95% confidence intervals obtained for the expected models of these samples allow for the possibility of very minor to increased heating during this time, or conversely, could allow for cooling. Given that the heating predicted by the expected models for these samples coincide with the onset of Karoo sedimentation, and the proximity of these samples to Karoo rift basins (Fig. 2), we interpret the expected models to be representative of the samples thermal history. As such, the reheating of samples Z16-41 and possibly Z16-45 was likely the result of burial, caused by the onset of sedimentation recorded in the Karoo rift basins throughout central and southern Africa (Fig. 9), though this reheating may be more or less pronounced than that predicted by our thermal models (Fig. 8). Thermal history modelling for the younger samples (Z16-27 and Z16-33; Fig. 8) indicates relatively rapid reheating between the Carboniferous and Permian that is similarly consistent with Karoo basin sedimentation. Subsequent cooling in these samples lasts until *c.* 180–160 Ma, likely reaching temperatures

above the APAZ. A period of cooling from *c.* 350–220 Ma has been identified in AFT samples from Tanzania, which is suggested to be the result of exhumation caused by intra-plate stresses associated with the Mauritanian-Variscan and Gondwanide orogenies (Kasanzu, 2017; Kasanzu et al., 2016). We suggest that these same intra-plate stresses resulted in the gradual exhumation of these samples throughout the Triassic and Jurassic (Fig. 9).

Gondwana break-up

Samples Z16-17 and Z16-52 from the SIB, as well as Z16-01 from the Zambezi Belt recorded the youngest AFT central ages from the analysed samples, ranging from *c.* 120–110 Ma. The calculated thermal models for these samples indicate a period of cooling that initiates at *c.* 150–140, persisting to *c.* 100–80 Ma for samples Z16-01 and Z16-52, or to the present day for Z16-01. These thermal models are consistent with those calculated by Kasanzu (2017) for rocks in Tanzania, which indicate a cooling throughout this period, which increases in rate from *c.* 100 Ma. Such a period of enhanced cooling is not inconsistent with the expected thermal model of sample Z16-17, though disagrees with the expected thermal models for samples Z16-01 and Z16-52 that predict reheating at this time. Kasanzu (2017), interprets that the exhumation recorded in this region was in response to the opening of the Indian and South Atlantic oceans at *c.* 160–90 Ma, during Gondwana break-up. The obtained AFT central ages for these samples are coeval with those obtained from Kenya by Boone et al. (2018b), who attributed the cooling ages to a basement high, which served to separate rifts in the region. Given the position of these samples within the SIB that separates the Karoo aged Luangwa and Cabora–Bassa rift basins, it is possible that this region similarly reflects a basement high that was previously located beneath a single Karoo basin (Fig. 9). This interpretation is consistent with stratigraphic correlations between the Luangwa and Cabora–Bassa basins (Fig. 3), in addition to the thermal models calculated for these samples, which indicate burial coeval with sedimentation in the Karoo basins (Fig. 8). Exhumation of this feature is likely a result of intracontinental deformation related to the plate reorganisation occurring during the Jurassic and Cretaceous.

Development of the East African Rift System

Notably, all samples outside of the Chipata Terrane display rapid cooling in their thermal models from *c.* 30 Ma to present. This period of rapid cooling is consistent with thermal models obtained by Kasanzu et al. (2016), Mackintosh et al. (2017), as well as Mackintosh et al. (2019) who identify a phase of denudation occurring at *c.* 40–25 Ma. It is important to note that such a cooling signal in the obtained thermal models may be a modelling artefact, caused by the presence of short (< 10 μm) confined fission tracks in the samples (Fig. 6, 7). However, coeval apatite He dates obtained by Mackintosh et al. (2019) for the Zambezi Belt of northern Zimbabwe are supportive of the existence of this cooling event. Rifting in the EARS initiated at *c.* 30–20 Ma, though uplift and cooling throughout this region has occurred since *c.* 50 Ma as a result of plume impact beneath the Tanzanian Craton (Koptev et al., 2015; Roberts et al., 2012). The synchronous timing of cooling across the region suggests that much of central Africa was subjected to uplift and denudation as a result of this impact. The continued cooling to present day suggests that denudation in these regions continued with the onset of rifting, which is reflected in the Neogene AFT central ages obtained from Kenya and Mozambique (Boone et al., 2018b; Fernandes et al., 2015).

Regional comparison of low-temperature thermochronological data

Figure 10 displays the available AFT central age data for central and eastern Africa. While there is a broad overlap in the obtained ages

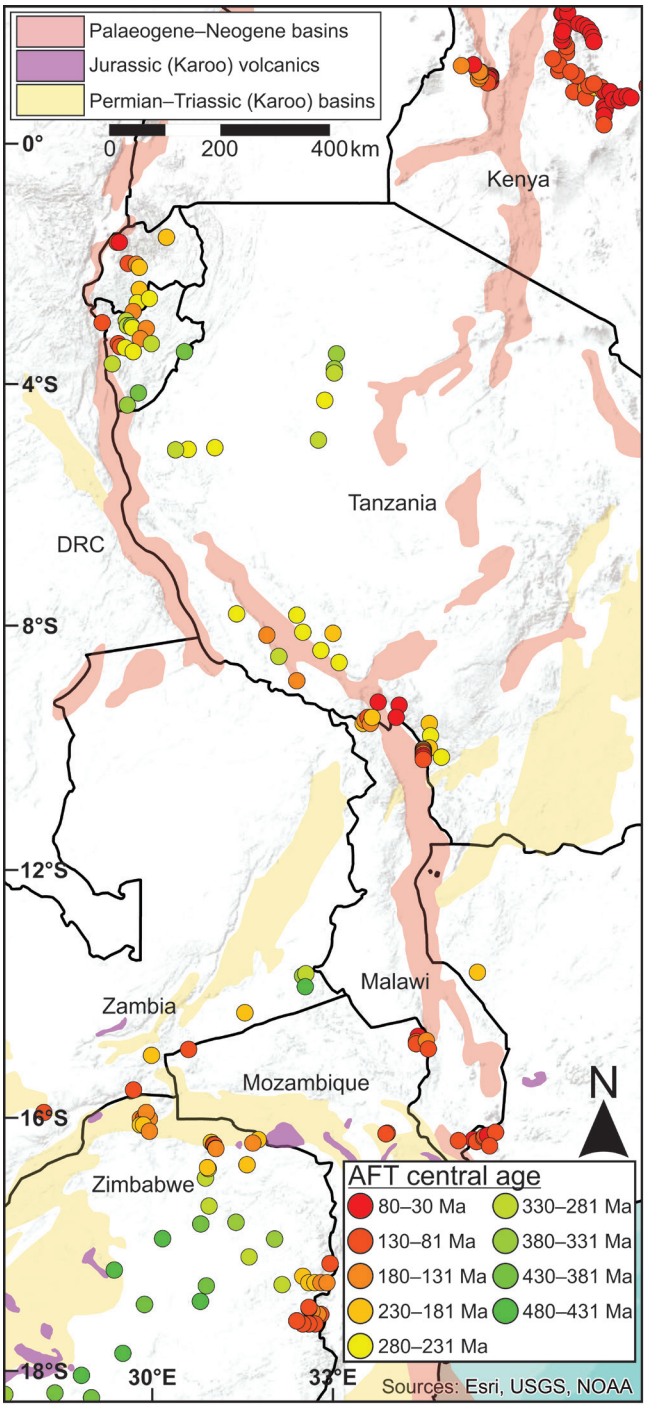

Figure 10. Map of available AFT central age data for Zambia (this study), Zimbabwe (Belton, 2006; Mackintosh et al., 2017, 2019; Noble, 1997), Mozambique (Fernandes et al., 2015), Malawi (Daszinnies et al., 2008; Van der Beek et al., 1998), Tanzania (Kasanzu, 2017; Kasanzu et al., 2016), Kenya (Foster and Gleadow 1992, 1996), Rwanda and Burundi (Van den Haute, 1984). Political boundaries are marked by the solid black lines.

for each region, a general spatial control can be observed between sample ages and their proximity to Permian–Triassic and Palaeogene–Neogene basins found throughout the region. The oldest central ages, relating to cooling after Gondwana amalgamation are clustered together in Tanzania, Burundi, Zambia, and throughout Zimbabwe. The retention of relatively old central ages in an area that experienced multiple subsequent thermal events suggests that these regions were exhumed to shallow levels rapidly following Gondwana

amalgamation, and not subjected to further subsidence or burial. This is consistent with their positions to basins throughout the region, generally being located more distal to these features than the younger samples. Karoo related (*c.* 350–200 Ma) ages can be found dispersed throughout the mapped region (Fig. 10) and likely relates to their proximity to the basins found throughout central Africa. Though notably, the majority of these Karoo aged samples are more closely associated with the flanks of Palaeogene–Neogene basins found throughout the region. In the southern region of the mapped area, a number of these Karoo related ages can also be observed to be proximal to Karoo-related volcanics. However, the relationship between these volcanics and the AFT ages recorded by samples is unclear, as several older (> 300 Ma) samples are located proximal to these features in Zimbabwe. Samples with late-Jurassic to Cretaceous central AFT ages, likely relating to Gondwana rifting, are observed in Zambia, Rwanda and Burundi. In southern Zambia and northern Zimbabwe, these ages are found both within and between the Karoo aged Luangwa and Cabora–Bassa Basins. The positioning of these similar ages supports the interpretation of the SIB in this area acting a basement high that was previously buried by Karoo sediments, suggesting that these two basins were previously connected. These central ages are generally in close association with the youngest available data, which instead relate to the development of the EARS, either in relation to plume impact or subsequent rifting.

CONCLUSIONS

A suite of thermochronological data were collected for samples throughout the Southern Irumide Belt of Zambia, which have been used to constrain the thermal evolution of the belt from the late-Neoproterozoic to the present day. Obtained ^{40}Ar–^{39}Ar muscovite and U–Pb apatite data constrain cooling from high-temperatures generated during Congo–Kalahari collision, and indicate that rocks in the Chewore–Rufunsa and Chipata terranes cooled to temperatures of ~350–500 °C between *c.* 550–480 Ma. Younger U–Pb apatite and ^{40}Ar–^{39}Ar muscovite ages of *c.* 470–450 Ma were obtained from samples in the Kacholola and Nyimba–Sinda terranes, which may relate to the intrusion of post-tectonic granite throughout the Nyimba–Sinda terrane that either prolonged cooling or reset the thermochronometers in these samples. The collected AFT data provides constraints on the low-temperature thermal evolution of the region, and identifies a number of thermal events occurring after Congo–Kalahari collision that are consistent with data obtained throughout central Africa. Obtained central ages of *c.* 330–200 Ma time the evolution of Karoo rifting in southern Zambia, with accompanying thermal models that serve to elucidate the timing of sedimentation within the basin. A number of samples yielded AFT central ages between *c.* 120–110 Ma. Thermal modelling of these samples identifies a period of cooling beginning at *c.* 150 Ma and persisting to the present day, which serves to constrain subsequent denudation in response to the opening of the Indian and South Atlantic oceans during Gondwana break-up. Thermal modelling also reveals a later stage (*c.* 30 Ma to present) of cooling, consistent with the development of the EARS. The results of this study serve to elucidate the previously unknown thermal evolution of a collisional zone at the heart of Gondwana amalgamation, and provides a greater regional framework for understanding the thermo-tectonic evolution of central Africa throughout the Phanerozoic.

ACKNOWLEDGEMENTS

This paper is a contribution to IGCP projects #628 (Gondwana Map) and #648 (Supercontinents and Global Dynamics). This project was funded by Australian Research Council Future Fellowship #FT120100340 to A. Collins. S. Gilbert of Adelaide Microscopy is thanked

for help with the collection of analytical data. B. Alessio is supported by a Research Training Program scholarship.

REFERENCES

Alessio, B.L., Collins, A.S., Clark, C., Glorie, S., Siegfried, P.R., Taylor, R., 2019. Age, origin and palaeogeography of the Southern Irumide Belt, Zambia. Journal of the Geological Society, jgs2018-2174.

Alessio, B.L., Collins, A.S., Siegfried, P., Glorie, S., De Waele, B., Payne, J.L., Archibald, D., 2018. Neoproterozoic tectonic geography of the south-east Congo Craton in Zambia as deduced from the age and composition of detrital zircons. Geoscience Frontiers.

Alessio, B.L., Kelsey, D.E., 2018. On yoderite: Using calculated phase equilibria to investigate its rarity in the geological record of whiteschists. Journal of Metamorphic Geology 36, 297-314.

Banks, N., Bardwell, K., Musiwa, S., 1995. Karoo rift basins of the Luangwa Valley, Zambia. Geological Society, London, Special Publications 80, 285-295.

Bingen, B., Jacobs, J., Viola, G., Henderson, I., Skår, Ø., Boyd, R., Thomas, R., Solli, A., Key, R., Daudi, E., 2009. Geochronology of the Precambrian crust in the Mozambique belt in NE Mozambique, and implications for Gondwana assembly. Precambrian Research 170, 231-255.

Boone, S.C., Kohn, B.P., Gleadow, A.J.W., Morley, C.K., Seiler, C., Foster, D.A., Chung, L., 2018a. Tectono-thermal evolution of a long-lived segment of the East African Rift System: Thermochronological insights from the North Lokichar Basin, Turkana, Kenya. Tectonophysics 744, 23-46.

Boone, S.C., Seiler, C., Kohn, B.P., Gleadow, A.J.W., Foster, D.A., Chung, L., 2018b. Influence of Rift Superposition on Lithospheric Response to East African Rift System Extension: Lapur Range, Turkana, Kenya. Tectonics 37, 182-207.

Carpena, J., Kienast, J.-R., Ouzegane, K., Jehanno, C., 1988. Evidence of the contrasted fission-track clock behavior of the apatites from In Ouzzal carbonatites (northwest Hoggar): The low-temperature thermal history of an Archean basement. Geological Society of America Bulletin 100, 1237-1243.

Catuneanu, O., Wopfner, H., Eriksson, P.G., Cairncross, B., Rubidge, B.S., Smith, R.M.H., Hancox, P.J., 2005. The Karoo basins of south-central Africa. Journal of African Earth Sciences 43, 211-253.

Chew, D., Petrus, J., Kamber, B., 2014. U–Pb LA–ICPMS dating using accessory mineral standards with variable common Pb. Chemical Geology 363, 185-199.

Chew, D.M., Spikings, R.A., 2015. Geochronology and thermochronology using apatite: time and temperature, lower crust to surface. Elements 11, 189-194.

Chew, D.M., Sylvester, P.J., Tubrett, M.N., 2011. U–Pb and Th–Pb dating of apatite by LA-ICPMS. Chemical Geology 280, 200-216.

Collins, A.S., Pisarevsky, S.A., 2005. Amalgamating eastern Gondwana: the evolution of the Circum-Indian Orogens. Earth-Science Reviews 71, 229-270.

De Waele, B., Johnson, S.P., Pisarevsky, S.A., 2008. Palaeoproterozoic to Neoproterozoic growth and evolution of the eastern Congo Craton: Its role in the Rodinia puzzle. Precambrian Research 160, 127-141.

Fernandes, P., Cogné, N., Chew, D.M., Rodrigues, B., Jorge, R.C., Marques, J., Jamal, D., Vasconcelos, L., 2015. The thermal history of the Karoo Moatize-Minjova Basin, Tete Province, Mozambique: An integrated vitrinite reflectance and apatite fission track thermochronology study. Journal of African Earth Sciences 112, 55-72.

Fernie, N., Glorie, S., Jessell, M.W., Collins, A.S., 2018. Thermochronological insights into reactivation of a continental shear zone in response to Equatorial Atlantic rifting (northern Ghana). Scientific reports 8,

16619.

Gallagher, K., 2012. Transdimensional inverse thermal history modeling for quantitative thermochronology. Journal of geophysical research: solid earth 117.

Gallagher, K., Charvin, K., Nielsen, S., Sambridge, M., Stephenson, J., 2009. Markov chain Monte Carlo (MCMC) sampling methods to determine optimal models, model resolution and model choice for Earth Science problems. Marine and Petroleum Geology 26, 525-535.

Gillespie, J., Glorie, S., Xiao, W., Zhang, Z., Collins, A.S., Evans, N., McInnes, B., De Grave, J., 2017. Mesozoic reactivation of the Beishan, southern Central Asian Orogenic Belt: Insights from low-temperature thermochronology. Gondwana Research 43, 107-122.

Glorie, S., Agostino, K., Dutch, R., Pawley, M., Hall, J., Danišík, M., Evans, N.J., Collins, A.S., 2017a. Thermal history and differential exhumation across the Eastern Musgrave Province, South Australia: Insights from low-temperature thermochronology. Tectonophysics 703-704, 23-41.

Glorie, S., Alexandrov, I., Nixon, A., Jepson, G., Gillespie, J., Jahn, B.-M., 2017b. Thermal and exhumation history of Sakhalin Island (Russia) constrained by apatite U-Pb and fission track thermochronology. Journal of Asian Earth Sciences 143, 326-342.

Goscombe, B., Armstrong, R., Barton, J., 2000. Geology of the Chewore Inliers, Zimbabwe: constraining the Mesoproterozoic to Palaeozoic evolution of the Zambezi Belt. Journal of African Earth Sciences 30, 589-627.

Green, P., Duddy, I., Gleadow, A., Tingate, P., Laslett, G., 1986. Thermal annealing of fission tracks in apatite: 1. A qualitative description. Chemical Geology: Isotope Geoscience Section 59, 237-253.

Hall, J.W., Glorie, S., Collins, A.S., Reid, A., Evans, N., McInnes, B., Foden, J., 2016. Exhumation history of the Peake and Denison Inliers: insights from low-temperature thermochronology. Australian Journal of Earth Sciences 63, 805-820.

Hanson, R.E., Wilson, T.J., Munyanyiwa, H., 1994. Geologic evolution of the Neoproterozoic Zambezi orogenic belt in Zambia. Journal of African Earth Sciences 18, 135-150.

Hauzenberger, C., Tenczer, V., Bauernhofer, A., Fritz, H., Klötzli, U., Košler, J., Wallbrecher, E., Muhongo, S., 2014. Termination of the Southern Irumide Belt in Tanzania: Zircon U/Pb geochronology. Precambrian Research 255, 144-162.

Hendriks, B., Redfield, T., 2005. Apatite fission track and (U-Th)/He data from Fennoscandia: An example of underestimation of fission track annealing in apatite. Earth and Planetary Science Letters 236, 443-458.

Hurai, V., Paquette, J.-L., Huraiová, M., Slobodník, M., Hvožďara, P., Siegfried, P., Gajdošová, M., Milovská, S., 2017. New insights into the origin of the Evate apatite-iron oxide-carbonate deposit, Northeastern Mozambique, constrained by mineralogy, textures, thermochronometry, and fluid inclusions. Ore Geology Reviews 80, 1072-1091.

Hutchins, D., Reeves, C., 1980. Regional geophysical exploration of the Kalahari in Botswana. Tectonophysics 69, 201-220.

Jepson, G., Glorie, S., Konopelko, D., Gillespie, J., Danišík, M., Evans, N.J., Mamadjanov, Y., Collins, A.S., 2018. Thermochronological insights into the structural contact between the Tian Shan and Pamirs, Tajikistan. Terra Nova 30, 95-104.

John, T., Schenk, V., Mezger, K., Tembo, F., 2004. Timing and PT evolution of whiteschist metamorphism in the Lufilian Arc–Zambezi Belt orogen (Zambia): implications for the assembly of Gondwana. The Journal of geology 112, 71-90.

Johnson, S., De Waele, B., Evans, D., Banda, W., Tembo, F., Milton, J., Tani, K., 2007a. Geochronology of the Zambezi supracrustal sequence, southern Zambia: a record of

Neoproterozoic divergent processes along the southern margin of the Congo Craton. The Journal of geology 115, 355-374.

Johnson, S., De Waele, B., Liyungu, A., 2006. U-Pb SHRIMP geochronology of granitoid rocks in eastern Zambia: terrane subdivision of the Mesoproterozoic Southern Irumide Belt. Tectonics 25.

Johnson, S., Oliver, G., 2002. High fO2 metasomatism during whiteschist metamorphism, Zambezi belt, northern Zimbabwe. Journal of Petrology 43, 271-290.

Johnson, S.P., De Waele, B., Tembo, F., Katongo, C., Tani, K., Chang, Q., Iizuka, T., Dunkley, D., 2007b. Geochemistry, geochronology and isotopic evolution of the Chewore–Rufunsa Terrane, Southern Irumide Belt: a Mesoproterozoic continental margin arc. Journal of Petrology 48, 1411-1441.

Kampunzu, A., Cailteux, J., 1999. Tectonic evolution of the lufilian arc (Central Africa Copper Belt) during Neoproterozoic pan African orogenesis. Gondwana Research 2, 401-421.

Kasanzu, C.H., 2017. Apatite fission track and (U-Th)/He thermochronology from the Archean Tanzania Craton: Contributions to cooling histories of Tanzanian basement rocks. Geoscience Frontiers 8, 999-1007.

Kasanzu, C.H., Linol, B., Wit, M.J., Brown, R., Persano, C., Stuart, F.M., 2016. From source to sink in central Gondwana: Exhumation of the Precambrian basement rocks of Tanzania and sediment accumulation in the adjacent Congo basin. Tectonics 35, 2034-2051.

Ketcham, R.A., Carter, A., Donelick, R.A., Barbarand, J., Hurford, A.J., 2007. Improved modeling of fission-track annealing in apatite. American mineralogist 92, 799-810.

Koptev, A., Calais, E., Burov, E., Leroy, S., Gerya, T., 2015. Dual continental rift systems generated by plume–lithosphere interaction. Nature Geoscience 8, 388.

Macey, P.H., Thomas, R.J., Grantham, G.H., Ingram, B.A., Jacobs, J., Armstrong, R.A., Roberts, M.P., Bingen, B., Hollick, L., de Kock, G.S., Viola, G., Bauer, W., Gonzales, E., Bjerkgård, T., Henderson, I.H.C., Sandstad, J.S., Cronwright, M.S., Harley, S., Solli, A., Nordgulen, Ø., Motuza, G., Daudi, E., Manhiça, V., 2010. Mesoproterozoic geology of the Nampula Block, northern Mozambique: Tracing fragments of Mesoproterozoic crust in the heart of Gondwana. Precambrian Research 182, 124-148.

Mackintosh, V., Kohn, B., Gleadow, A., Gallagher, K., 2019. Long-term reactivation and morphotectonic history of the Zambezi Belt, northern Zimbabwe, revealed by multi-method thermochronometry. Tectonophysics 750, 117-136.

Mackintosh, V., Kohn, B., Gleadow, A., Tian, Y., 2017. Phanerozoic Morphotectonic Evolution of the Zimbabwe Craton: Unexpected Outcomes From a Multiple Low-Temperature Thermochronology Study. Tectonics 36, 2044-2067.

Mazac, O., 1974. Reconnaissance gravity survey of Zambia. Republic of Zambia, Ministry of Mines and Industry.

McDowell, F.W., McIntosh, W.C., Farley, K.A., 2005. A precise 40Ar–39Ar reference age for the Durango apatite (U–Th)/He and fission-track dating standard. Chemical Geology 214, 249-263.

Merdith, A.S., Collins, A.S., Williams, S.E., Pisarevsky, S., Foden, J.F., Archibald, D., Blades, M.L., Alessio, B.L., Armistead, S., Plavsa, D., Clark, C., Müller, R.D., 2017. A full-plate global reconstruction of the Neoproterozoic. Gondwana Research 50, 84-134.

Noble, W.P., 1997. Post Pan African tectonic evolution of Eastern Africa: an apatite fission track study. La Trobe University.

O'Sullivan, P.B., Parrish, R.R., 1995. The importance of apatite composition and single-grain ages when interpreting fission track data from plutonic rocks: a case study from the Coast Ranges, British Columbia. Earth and Planetary Science Letters 132, 213-224.

Oesterlen, P., Millsteed, B., 1994. Lithostratigraphy, palaeontology, and sedimentary environments of the western Cabora Bassa Basin, lower Zambezi Valley, Zimbabwe. South African Journal of Geology 97, 205-224.

Paton, C., Hellstrom, J., Paul, B., Woodhead, J., Hergt, J., 2011. Iolite: Freeware for the visualisation and processing of mass spectrometric data. Journal of Analytical Atomic Spectrometry 26, 2508-2518.

Renne, P.R., Balco, G., Ludwig, K.R., Mundil, R., Min, K., 2011. Response to the comment by WH Schwarz et al. on "Joint determination of 40 K decay constants and 40 Ar/40 K for the Fish Canyon sanidine standard, and improved accuracy for 40 Ar/39 Ar geochronology" by PR Renne et al.(2010). Geochimica et Cosmochimica Acta 75, 5097-5100.

Roberts, E.M., Stevens, N., O'Connor, P.M., Dirks, P., Gottfried, M.D., Clyde, W., Armstrong, R., Kemp, A., Hemming, S., 2012. Initiation of the western branch of the East African Rift coeval with the eastern branch. Nature Geoscience 5, 289.

Schoene, B., Bowring, S.A., 2006. U–Pb systematics of the McClure Mountain syenite: thermochronological constraints on the age of the 40 Ar/39 Ar standard MMhb. Contributions to Mineralogy and Petrology 151, 615.

Scibiorski, E., Tohver, E., Jourdan, F., 2015. Rapid cooling and exhumation in the western part of the Mesoproterozoic Albany-Fraser Orogen, Western Australia. Precambrian Research 265, 232-248.

Song, D., Glorie, S., Xiao, W., Collins, A.S., Gillespie, J., Jepson, G., Li, Y., 2017. Tectono-thermal evolution of the southwestern Alxa Tectonic Belt, NW China: Constrained by apatite U-Pb and fission track thermochronology. Tectonophysics.

Thomas, R.J., Spencer, C., Bushi, A.M., Baglow, N., Boniface, N., de Kock, G., Horstwood, M.S., Hollick, L., Jacobs, J., Kajara, S., 2016. Geochronology of the central Tanzania Craton and its southern and eastern orogenic margins. Precambrian Research 277, 47-67.

Vermeesch, P., 2009. RadialPlotter: A Java application for fission track, luminescence and other radial plots. Radiation Measurements 44, 409-410.

Vermeesch, P., 2017. Statistics for LA-ICP-MS based fission track dating. Chemical Geology 456, 19-27.

Wagner, G., Van Den Haute, P., 1992. Fission-track Dating. Kluwer Academic Publishers.

Wildman, M., Brown, R., Watkins, R., Carter, A., Gleadow, A., Summerfield, M., 2015. Post break-up tectonic inversion across the southwestern cape of South Africa: New insights from apatite and zircon fission track thermochronometry. Tectonophysics 654, 30-55.

CHAPTER 7

Discussion and Conclusions

The purpose of the studies that form this thesis were to better constrain the tectonic evolution of the SIB as a proxy for the wider southern Congo margin. By better understanding and constraining the palaeogeographic development of this region, it is possible to produce more rigorous plate tectonic models that can be used to understand the relationship between the evolving continents and various components of the wider Earth System. To effectively constrain the evolution of the SIB, and thus wider Congo Craton, the studies in this thesis revolved around three main foci: to determine the extent and evolution of the southern Congo margin during the late-Mesoproterozoic, to constrain the Neoproterozoic evolution of this margin and Congo–Kalahari collision, and to constrain the Phanerozoic thermo-tectonic evolution of the region. Below, the findings of the studies included in this thesis are discussed in the context of these foci, summarising how each of them contributed to our understanding of each research area and their implications in relation to previous studies of the region.

PALAEOPROTEROZOIC TO LATE-MESOPROTEROZOIC EVOLUTION

Johnson et al. (2005) introduced the term 'Southern Irumide Belt' as a way of distinguishing the rocks that comprise it from those in the Irumide Belt (*sensu stricto*). The SIB is considered to be distinct due to the variety of deformed sedimentary, igneous and volcanic units contained within (Johnson et al., 2006; Johnson et al., 2007), as opposed to the monotonous granitoids and metasedimentary Muva Supergroup that largely form the Irumide Belt (Daly, 1986; De Waele and Mapani, 2002). These lithological features, and the presence of the Mwembeshi Shear Zone that runs between these belts (Sarafian et al., 2018), led Johnson et al. (2006) to suggest that no genetic relationship existed between the Irumide and Southern Irumide belts and that the Mwembeshi Shear Zone represents a key suture along the southern Congo margin. Johnson et al. (2007) obtained Lu–Hf and Sm–Nd data for magmatic rocks and zircon grains from the Chewore–Rufunsa Terrane of the SIB, these authors identified that the late-Mesoproterozoic rocks that form much of the exposed SIB is isotopically evolved (εNd(t) values between –1.8 to –13.5). These rocks were suggested to have formed on a juvenile Palaeoproterozoic basement, as opposed to the evolved Archaean to Palaeoproterozoic basement observed in the Irumide Belt, though it should be noted that both positive and negative εHf(t) values (+2.9 to –3.7) were obtained for the basement derived zircons analysed in that study. With these data, the lithological differences, and presence of the Mwembeshi Shear Zone between the Irumide and Southern Irumide belts, Johnson et al. (2007) suggested a tectonic model whereby the SIB did not develop on the Congo Craton, but instead developed in a continental-margin-arc setting on a microcontinent that collided with the southern Congo margin at *c.* 1040 Ma. This collision is interpreted to have ceased magmatism in the SIB, and initiated compression and melting within the Irumide Belt. Bingen et al. (2009) suggested an alternate model for the evolution of the SIB where it instead formed on the southern Congo margin, which acted as a long-lived active margin. Any differences in the timing of magmatism in the Irumide and Southern Irumide belts is suggested by this model to relate to an event of foreland propagation, where a shallowing subducting slab resulted in the migration of the magmatic front inland and beneath the Irumide Belt.

To better constrain the development of the southern Congo margin during the late-Mesoproterozoic and test the competing tectonic models for SIB evolution, this project included two studies that largely looked at basement rock and sedimentary sequences in the SIB. By better constraining the Palaeoproterozoic basement of the SIB, and the sediments that overlie it, these studies developed an improved framework of understanding that was used to

better interpret the late-Mesoproterozoic evolution of the SIB. Chapter 2 used U–Pb and Lu–Hf isotopic data to investigate the provenance of sedimentary rocks from the Chewore–Rufunsa, Kacholola and Nyimba–Sinda terranes, while Chapter 3 provided similar data for a sedimentary rock from the Chipata Terrane. The Nyimba–Sinda Terrane (being largely Neoproterozoic in age) contains predominantly Neoproterozoic sedimentary rocks that are explained further below. The remaining terranes were found to contain sediments that recorded Archaean to Palaeoproterozoic age distributions and largely evolved εHf(t) values, which were identical to the ages and εHf(t) values recorded by detrital zircons from the Muva Supergroup within the Irumide Belt. Chapter 3 primarily used U–Pb and Lu–Hf isotopic data to investigate the age and origin of basement lithologies identified in the Chewore–Rufunsa and Chipata terranes. This study found that basement exposed in these terrane was Palaeoproterozoic and isotopically evolved, similar to Palaeoproterozoic basement in the Irumide Belt (Fig. 1). Furthermore the consistency of basement lithologies in these terranes may reflect a common basement for not only Chewore–Rufunsa and Chipata terranes, but also the Kacholola and Nyimba–Sinda terranes that are located between them. This study also identified the occurrence of *c.* 1040 Ma magmatism in the Chipata Terrane, and conversely highlighted the occurrence of *c.* 1100–1040 Ma magmatism in the Irumide Belt.

The findings of this project show that basement rock in the SIB is equivalent to that found in the Irumide Belt, and also show that the overlying sediments in either belt were derived from the same sources. This suggests that the isotopically evolved, late-Mesoproterozoic intrusions in the Irumide and Southern Irumide belts formed at a broadly similar time (though a general distinction does remain), on evolved Archaean to Palaeoproterozoic basement, and similarly intrude sedimentary sequences of the Palaeoproterozoic Muva Supergroup. Notwithstanding the common basement rocks, the fact that these regions sourced sediments recording a depositional age between *c.* 1500 to 1100 Ma strongly suggests that the SIB was part of the southern Congo margin prior to the late-Mesoproterozoic. Any interpretation to the contrary must account for the transport of such sediment to the microcontinent that SIB would have formed on, which (assuming the same sources as the Muva Supergroup) would need to be transported across an open ocean and variably active subduction zone. As such, the findings of this project strongly support a tectonic model of the SIB forming along the southern Congo margin, with obtained zircon U–Pb data suggesting it has resided along this margin since at least the Palaeoproterozoic (*c.* 2000 Ma).

NEOPROTEROZOIC EVOLUTION AND CONGO−KALAHARI COLLISION

The terranes of the SIB are largely comprised of late-Mesoproterozoic lithologies. However, Johnson et al. (2006) observed that, unlike the other Zambian terranes of the SIB, the Nyimba–Sinda Terrane was predominantly comprised of deformed Neoproterozoic gneiss, carbonates and calc-silicates that were intruded by Cambrian post-tectonic granite. As such, this terrane preserves a vital record for understanding the Neoproterozoic evolution of the region that, until now, had yet to be interrogated. While the Neoproterozoic evolution of the belt has been largely enigmatic, it records a pervasive tectono-metamorphic overprint relating to Congo–Kalahari collision at *c.* 550–530 Ma, which is similarly recorded outside of the SIB and has been the subject of studies investigating the *P–T* evolution of the region. In the Zambezi Belt, Goscombe et al. (2000), obtained conditions of ~7–9 kbar and 590–720 °C for metapelites formed during this collision. In the Lufilian Arc and Zambezi Belt, constraints obtained for whiteschists that were formed in this collision range from 12–21 kbar and 590–775 °C (John et al., 2004; Johnson

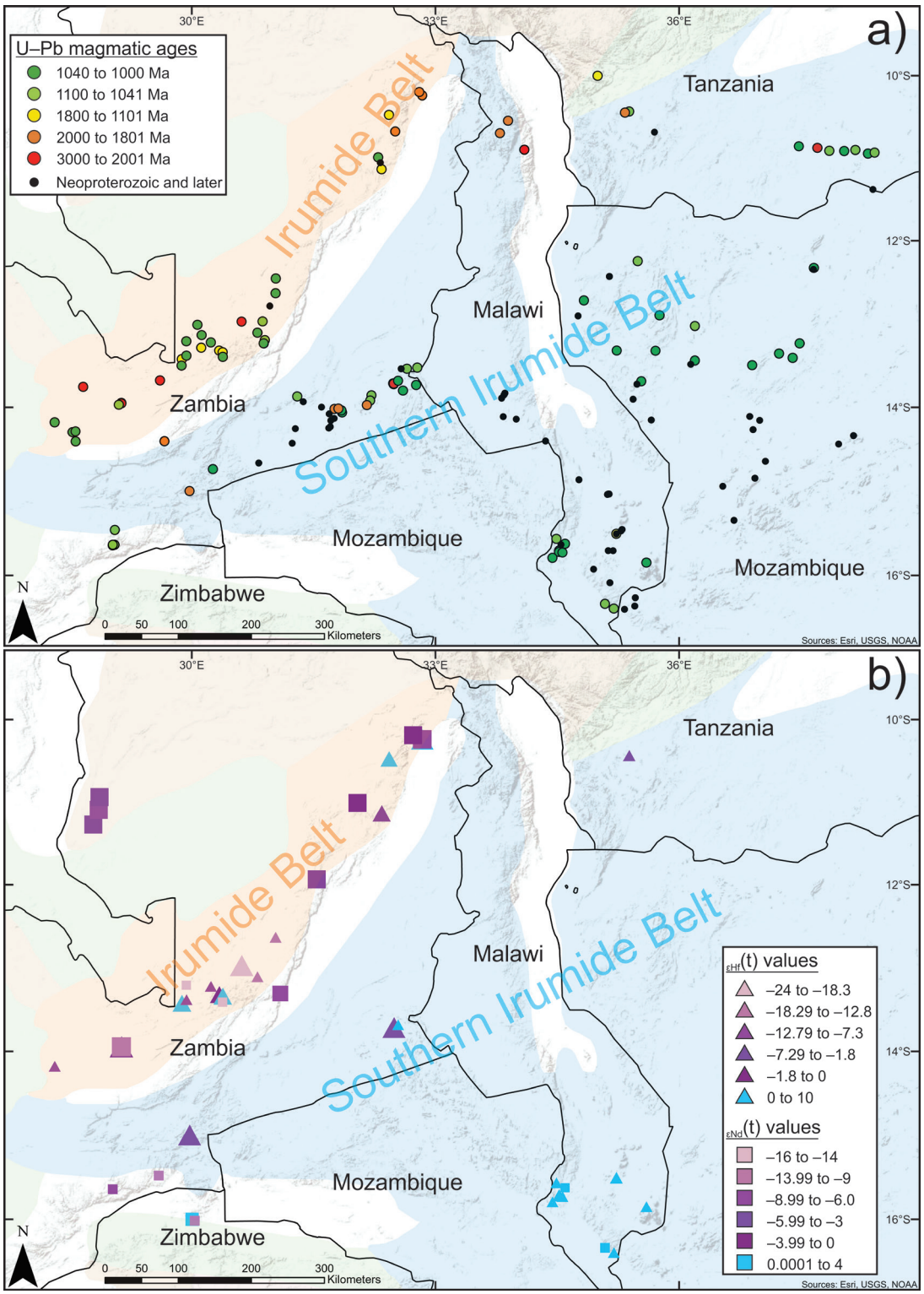

Figure 1. Map of available age and isotopic data for the Irumide and Southern Irumide belts of Zambia (Johnson, De Waele and Liyungu, 2006; Johnson et al., 2007; De Waele et al., 2009), Malawi (Ring, Kröner and Toulkeridis, 1997; Kröner et al., 2001; Manda et al., 2018), northern Mozambique (Bingen et al., 2009) and southern Tanzania (Hauzenberger et al., 2014; Thomas et al., 2016). Tectonic units in this region are shaded in colour following the legend in Figure 1. Political boundaries are marked by the solid black lines. a) Available U–Pb crystallisation ages for the Irumide and Southern Irumide Belts. b) Available εHf(t) and εNd(t) values for the Mesoproterozoic and older magmatic units Irumide and Southern Irumide belts. Symbol sizes relate to the age of the sample, where the larger symbols are record older crystallisation ages.

and Oliver, 1998). The available constraints highlight a significant discrepancy in thermal gradients recorded contemporaneously in the whiteschists and metapelites. John et al. (2004) suggest that the whiteschist metamorphism records subduction of the Congo Craton beneath the Kalahari Craton during their collision, though the relationship of these rocks to the lower grade rocks found throughout the region had not yet been interrogated.

Chapter 2 investigated the provenance of sediments within the Nyimba–Sinda Terrane, with a sample of detrital zircons yielding a prominent late-Mesoproterozoic and minor Archaean to Palaeoproterozoic U–Pb age populations. Depositional constraints for the Nyimba–Sinda sample suggest that it was deposited between *c.* 900–740 Ma, and likely forms a rift-related cover sequence that overlies the Palaeoproterozoic to Mesoproterozoic units seen elsewhere in the SIB. To better understand the relationship between the high-pressure whiteschists, and lower pressure metapelites within the Southern Irumide and Zambezi belts, it was necessary to first create an activity–composition model for the mineral yoderite (for use with *THERMOCALC*), which has been observed in whiteschists from Zimbabwe (Zambezi Belt) and Tanzania (Mautia Hill). The study in Chapter 4 constructed and validated a model for yoderite that was used to improve *P*–*T* constraints of whiteschist metamorphism in the Zambezi Belt. Most importantly, the provision of this model allows for more rigorous constraints of all whiteschists. Yoderite was shown in Chapter 4 to be highly stable within the $MgO–Al_2O_3–SiO_2–H_2O–Fe_2O_3$ chemical system that all whiteschists are largely restricted to, with its absence in these rocks largely related to compositional and possibly geodynamic controls. By being able to constrain stability fields of yoderite stability within samples that do not contain the mineral, it reduces the calculated *P*–*T* stability range of fields that do reflect the evolution of the sample. This was demonstrated by the models for retrogressed whiteschist that were calculated in Chapter 5, where the *P*–*T* stability of fields corresponding to the equilibrium assemblages recorded in these samples were likely reduced by the presence of stable yoderite fields in the models. The models calculated for these samples showed that whiteschist exposed in the Chewore–Rufunsa Terrane of the SIB experienced retrograde conditions that were equivalent to the peak metamorphic conditions recorded in amphibolite facies metapelites elsewhere in the Southern Irumide and Zamebzi belts.

When investigating the Neoproterozoic evolution of the SIB, this project identified that the Nyimba–Sinda Terrane, unique to the other Zambian terranes of the belt, hosted a cover sequence that was likely deposited during the Neoproterozoic. It is interpreted that this cover sequence represents a superimposed rift-basin, which is based on occurrence of *c.* 750–730 Ma rift-related volcanic units that are similarly restricted to the Nyimba–Sinda Terrane. Such interpretations corroborate existing palaeogeographic models that suggest rifting along the southern Congo margin at *c.* 750 Ma, as an extension of the spreading system that served to separate Australia from Laurentia during Rodina break-up. Upon investigating the Neoproterozoic to Cambrian collision between the Congo and Kalahari cratons, this project provided *P*–*T* information for retrogressed whiteschist and showed that it experienced similar conditions to metapelites in the Zambezi Belt (and likely the SIB). Our study into the different metamorphic assemblages recorded in this region agrees with the interpretation of John et al. (2004), that the whiteschists were formed as a result of the Congo Craton subducting beneath the Kalahari Craton during collision. Contrasting this with the amphibolite to granulite facies rocks within the Southern Irumide and Zambezi belts, we suggest that the whiteschists mark the suture zone between the Congo and Kalahari cratons, while the lower-pressure rocks were formed

proximal to the site of collision. As such, the different overprints recorded in this region provide a unique insight into the processes of continental collision.

PHANEROZOIC THERMO-TECTONIC EVOLUTION

The SIB, and Zambia as a whole, has had no significant work done to understand its thermal evolution via the use of low- and mid-temperature thermochronometers such as apatite and muscovite. However, studies in neighbouring regions (such as Zimbabwe, Mozambique, and Tanzania) have shown that, following the Neoproterozoic collision of the Congo and Kalahari cratons, central Africa has experienced multiple thermal events relating to Permian–Triassic 'Karoo' rifting, Gondwana break-up, and the development of the East African Rift System (Fernandes et al., 2015; Kasanzu, 2017; Mackintosh et al., 2017). As such, constraining the thermal evolution of the SIB can further improve our understanding of the Phanerozoic tectonic history of central Africa.

The final study in this project (Chapter 6) used apatite fission track (AFT), U–Pb, and $^{40}Ar/^{39}Ar$ muscovite dating to interrogate the thermal evolution of the SIB, identifying the occurrence of multiple thermal events in the region. The utilisation of mid-temperature thermochronometers (U–Pb apatite, $^{40}Ar/^{39}Ar$ muscovite) showed that after Congo–Kalahari collision, the SIB underwent cooling between *c.* 550–450 Ma. Some spatially controlled variation was observed in these cooling ages that span over 100 m.y., and were attributed to both the presence of post-tectonic magmatism in the Nyimba–Sinda Terrane (investigated in Chapter 3) and the proximity of the analysed samples to the Congo–Kalahari suture. The latter variation likely relating to the different overprints recorded in the SIB that were investigated in Chapter 5. Low-temperature (AFT) thermochronology identified the occurrence of at least three thermal events during the Phanerozoic, occurring in the Carboniferous to Triassic, Permian to Jurassic, and Cretaceous to present. Such periods of thermal activity were shown to be consistent with adjacent regions likewise relating to Karoo rift-basin sedimentation, the Mauritanian–Variscan and Gondwanide orogenies and Gondwana break-up. A final period of cooling was identified to occur from *c.* 30 Ma, though it is uncertain whether this was an artefact of temperature–time modelling. If this cooling is real, it would be consistent with findings elsewhere, and would likely correspond to the development of the East African Rift System (Kasanzu, 2017; Mackintosh et al., 2018).

Our study into the thermal evolution of the SIB was largely consistent with the findings of previous studies in adjacent regions, suggesting that the much of central-east Africa experienced a common thermo-tectonic history during the Phanerozoic. However, beyond providing constraints from a hitherto unstudied part of this region, our study further contributed to understanding the Phanerozoic thermal evolution of central Africa in two ways: The first was by obtaining mid-temperature thermochronological data, which has been a largely underutilised technique in previous studies of adjacent regions. These data provide some of the first robust constrains on the cooling history this region following Congo–Kalahari collision, which reflects the formation of Gondwana and the modern African Plate. The second contribution was to place the data obtained in the study, and those obtained by others, into a regional context that could be better used for understanding the region's evolution as a cohesive unit, as opposed to individual study areas. The final figure in Chapter 6, a map displaying a regional comparison of available low-temperature thermochronological data, is a testament to this. An example of the utility of such a comparison is that it allowed for identification of late-Jurassic to Cretaceous AFT central ages in late-Mesoproterozoic rocks of the SIB, which were identical in age to those in the Phanerozoic sediments of the Karoo

aged Cabora–Bassa Basin located on the belt's southern flank. This identification provided a basis for the interpretation that the SIB formed a basement high that was previously buried by Karoo sediments, suggesting that the Cabora–Bassa Basin was previously connected to the Karoo aged Luangwa Basin that is located on the northern flank of the SIB. Given that Karoo rift-basins are widespread throughout central Africa, this project contributes a foundation for further work attempting to both understand the region's thermal evolution and identify further connections between these basins.

RESEARCH LIMITATIONS AND DIRECTIONS FOR FUTURE RESEARCH

The following points outline a number of the challenges and limitations encountered during the course of this project, as well as suggested directions to both remedy these challenges and produce more robust models for the evolution of the SIB and wider Congo Craton:

1) As this study was constricted to the Zambian terranes of the SIB, any further studies of the belt's evolution would be well suited to investigating the origin and evolution of terranes in Malawi, Mozambique and Tanzania. Better constraints for the evolution of these terranes and their relationship to those that were the focus of this study, in Zambia, will undoubtedly result in more robust and cohesive models for the tectonic evolution of this region.

2) Sampling such a wide area of southern Zambia naturally resulted in sparse sample density. Further sampling in the Kacholola and Nyimba–Sinda terranes would help to identify the presence of any basement exposures, which could be used to test the hypothesis that the Zambian terranes of the SIB are floored a common, isotopically evolved, Palaeoproterozoic basement. Throughout the Chewore–Rufunsa, Kacholola, and Chipata terranes, further sampling of sedimentary lithologies may help to identify the occurrence of any Neoproterozoic sedimentation within these terranes, further supporting the interpretation of rifting along the southern Congo margin during the Neoproterozoic.

3) The activity–composition model created for yoderite was constructed for use within the $MgO–Al_2O3–SiO_2–H_2O–Fe_2O_3$ chemical system. While Chapter 5 showed that it can be used with more complex chemical systems, calculations with this model will effectually be insensitive to other elements present within the modelled system. As such, further work to refine and expand this model for use with more complex chemical systems (such as $FeO–MgO–Al_2O_3–SiO_2–H_2O–Fe_2O_3$), would result in more rigorous *P–T* constraints for any modelled whiteschist.

4) While the pervasive Neoproterozoic tectono-metamorphic overprint throughout the SIB impedes such an effort, attempting to better understand the nature of late-Mesoproterozoic (and possibly older) deformation (D_0) within the belt would improve our understanding of its evolution. One such method may be through a detailed investigation of the terrane bounding shear zones observed in the SIB of Zambia. The structural investigations in this project lead to the interpretation that these shear zones are relatively minor in the context of the regions tectonic evolution, and imply that these 'terranes' might be more accurately referred to as 'terrains'. However, without further study of these features, their significance largely remains the subject of speculation. Similarly, further investigation of the metamorphic overprints recorded in the SIB would assist in understanding the relationships both between terranes and with adjacent belts. Previous work has shown that Mesoproterozoic metamorphic overprints are preserved in parts of the belt, which could be used to better constrain the evolution of the different terrains and relationship to the Irumide Belt and wider Congo Craton. Similarly,

further investigation of the Neoproterozoic metamorphic overprints in the belt could help to better understand the Gondwana forming collision between the Congo and Kalahari cratons.

CONCLUSIONS

The overarching goal of this project, and the studies that comprise it, was to constrain approximately two billion years of the southern Congo Craton's tectonic evolution, spanning from the Palaeoproterozoic to present. To do this, the studies that formed this thesis investigated the tectonic evolution of the Southern Irumide Belt, which since at least the late-Mesoproterozoic onwards, formed a part of this margin and is therefore a useful proxy for the southern Congo Craton's evolution. Systematically, this project investigated the formation of the SIB and its evolution from the Palaeoproterozoic to present, developing a comprehensive framework of understanding for the belt throughout this time.

By studying the age and isotopic nature of basement units in the SIB, it was interpreted that the belt likely formed along the southern Congo margin during the Palaeoproterozoic, and remained in this position until present. This was corroborated by the presence of identical sedimentary sequences in the SIB and Irumide Belt (*sensu stricto*), suggesting that both belts derived the same sediments during the Mesoproterozoic and therefore were unlikely to be separated by an ocean and variably active subduction zones. Such interpretations support models of the Southern Irumide Belt acting as a continental-margin-arc on the Congo Craton during the late-Mesoproterozoic, instead of colliding with this craton as part of a microcontinent at this time. The identification of Neoproterozoic sedimentary rock in the Nyimba–Sinda Terrane were suggested to represent a rift-related cover sequence that was deposited between *c.* 900 and 730 Ma, likely at the lower end of this range due to the presence of *c.* 750–730 Ma rift volcanics in this terrane. This interpretation corroborates plate tectonic models that suggest that the southern Congo margin experienced rifting at this time as an extension of the spreading system that served to separate Australia from Laurentia during Rodina break-up. Investigating the tectono-metamorphic overprint recorded in the SIB from Congo–Kalahari collision in the late stages of Gondwana amalgamation, this project identified that prominent, broadly east–west trending fold structures in the region were likely generated during this event. Thermobarometric models were calculated for a lower-pressure metapelite and retrogressed parts of the higher-pressure whiteschists in the region, with the latter utilising an activity–composition model for yoderite that was created during this project to provide more robust *P*–*T* constraints for whiteschists. These models demonstrated that while the various mineral assemblages in this region were generated at the same time, during the same event, they record vastly different *P*–*T* conditions. The *P*–*T* models show that the peak conditions recorded by amphibolite facies rock in the Zambezi Belt are broadly equivalent to the retrograde conditions experience by whiteschists. As such, the whiteschists in this region are suggested to have formed from the Congo Craton subducting beneath the Kalahari Craton during collision, marking the suture zone between them, whereas the lower grade rocks in this region likely formed proximal to the zone of collision. The thermal evolution of the region following this collision was interrogated through the use of mid- and low-temperature thermochronometers, which constrain its thermo-tectonic evolution throughout the Phanerozoic. Mid-temperature thermochronology constrains cooling from Congo–Kalahari collision in the SIB to between *c.* 550 to 450 Ma, varying based on the presence of post-tectonic granite intrusions and proximity to the Congo–Kalahari suture, where cooling likely occurred at the slowest rate. Low-temperature thermochronology suggests the occurrence of at least

three thermal events during the Phanerozoic. Carboniferous to Triassic heating is suggested to relate to 'Karoo' rift-basin sedimentation, while Permian to Jurassic cooling is suggested to reflect exhumation of the region in response to the Mauritanian–Variscan and Gondwanide orogenies. Late-Cretaceous to present cooling is also observed in the majority of dated samples from the SIB, and likely reflects exhumation in response to Gondwana break-up. Additionally, a final phase of increased cooling is was identified from *c.* 30 Ma to present, and if not an artefact of modelling, would correspond to the development of the East African Rift System.

The above section summarises the findings of this project, and provides an interpretation for the formation and evolution of the SIB over two billion years of Earth's history. As a proxy for the tectonic evolution of the southern Congo margin, and by extension the wider Congo Craton, this project provides a framework of understanding for this region that can contribute to more robust and accurate Palaeogeographic reconstructions. Accordingly, this contribution is a small but fundamental step in understanding the interplay between the evolving continents and wider Earth System.

REFERENCES

Bingen, B., Jacobs, J., Viola, G., Henderson, I., Skår, Ø., Boyd, R., Thomas, R., Solli, A., Key, R., Daudi, E., 2009. Geochronology of the Precambrian crust in the Mozambique belt in NE Mozambique, and implications for Gondwana assembly. Precambrian Research 170, 231-255.

Daly, M., 1986. The intracratonic Irumide belt of Zambia and its bearing on collision orogeny during the Proterozoic of Africa. Geological Society, London, Special Publications 19, 321-328.

De Waele, B., Mapani, B., 2002. Geology and correlation of the central Irumide belt. Journal of African Earth Sciences 35, 385-397.

Fernandes, P., Cogné, N., Chew, D.M., Rodrigues, B., Jorge, R.C., Marques, J., Jamal, D., Vasconcelos, L., 2015. The thermal history of the Karoo Moatize-Minjova Basin, Tete Province, Mozambique: An integrated vitrinite reflectance and apatite fission track thermochronology study. Journal of African Earth Sciences 112, 55-72.

Goscombe, B., Armstrong, R., Barton, J., 2000. Geology of the Chewore Inliers, Zimbabwe: constraining the Mesoproterozoic to Palaeozoic evolution of the Zambezi Belt. Journal of African Earth Sciences 30, 589-627.

John, T., Schenk, V., Mezger, K., Tembo, F., 2004. Timing and PT evolution of whiteschist metamorphism in the Lufilian Arc–Zambezi Belt orogen (Zambia): implications for the assembly of Gondwana. The Journal of geology 112, 71-90.

Johnson, S., De Waele, B., Liyungu, A., 2006. U-Pb SHRIMP geochronology of granitoid rocks in eastern Zambia: terrane subdivision of the Mesoproterozoic Southern Irumide Belt. Tectonics 25.

Johnson, S., Oliver, G., 1998. A second natural occurrence of yoderite. Journal of Metamorphic Geology 16, 809-818.

Johnson, S.P., De Waele, B., Tembo, F., Katongo, C., Tani, K., Chang, Q., Iizuka, T., Dunkley, D., 2007. Geochemistry, geochronology and isotopic evolution of the Chewore–Rufunsa Terrane, Southern Irumide Belt: a Mesoproterozoic continental margin arc. Journal of Petrology 48, 1411-1441.

Johnson, S.P., Rivers, T., De Waele, B., 2005. A review of the Mesoproterozoic to early Palaeozoic magmatic and tectonothermal history of south–central Africa: implications for Rodinia and Gondwana. Journal of the Geological Society 162, 433-450.

Kasanzu, C.H., 2017. Apatite fission track and (U-Th)/He thermochronology from the Archean Tanzania Craton: Contributions to cooling histories of Tanzanian basement rocks. Geoscience Frontiers 8, 999-1007.

Mackintosh, V., Kohn, B., Gleadow, A., Gal-

lagher, K., 2018. Long-term reactivation and morphotectonic history of the Zambezi Belt, northern Zimbabwe, revealed by multi-method thermochronometry. Tectonophysics.

Mackintosh, V., Kohn, B., Gleadow, A., Tian, Y., 2017. Phanerozoic Morphotectonic Evolution of the Zimbabwe Craton: Unexpected Outcomes From a Multiple Low-Temperature Thermochronology Study. Tectonics 36, 2044-2067.

Sarafian, E., Evans, R.L., Abdelsalam, M.G., Atekwana, E., Elsenbeck, J., Jones, A.G., Chikambwe, E., 2018. Imaging Precambrian lithospheric structure in Zambia using electromagnetic methods. Gondwana Research 54, 38-49.

Appendix 1

Supplementary material for: Neoproterozoic tectonic geography of the south-east Congo Craton in Zambia as deduced from the age and composition of detrital zircons.

Table S1. Zircon standard U-Pb analyses.

Z14-17

Analysis	Isotope ratios and 1σ error (absolute) Pb^{207}/U^{235}		Pb^{206}/U^{238}		ρ*	Concordance (%)	Calculated age in Ma and 1σ error (absolute) Pb^{207}/Pb^{206}		Pb^{206}/U^{238}	
STDGJ01	0.93054	0.01687	0.11102	0.00142	0.3936	107	632.1	37.6	678.7	8.22
STDGJ02	0.84321	0.01436	0.10192	0.00128	0.4233	104	604	35.07	625.7	7.5
STDGJ03	0.81479	0.01391	0.09756	0.00123	0.4259	96	624.5	35.01	600.1	7.22
STDGJ04	0.7909	0.01353	0.09636	0.00122	0.4202	101	586.9	35.23	593	7.15
STDGJ05	0.80207	0.01375	0.09421	0.00119	0.4172	87	665.8	34.87	580.4	7.03
STDGJ06	0.79121	0.01342	0.09487	0.0012	0.4318	94	621.5	34.59	584.3	7.06
PLES1	0.38155	0.00763	0.05037	0.00066	0.3536	77	410.1	42.98	316.8	4.04
PLES2	0.37752	0.00623	0.05098	0.00064	0.4475	89	359.3	34.96	320.5	3.92
PLES3	0.38398	0.00666	0.05176	0.00066	0.4295	90	363.3	36.85	325.3	4.03
STDGJ07	0.80332	0.01568	0.09749	0.00133	0.4289	101	594.8	39.8	599.7	7.78
STDGJ08	0.82303	0.01624	0.0973	0.00133	0.4283	92	651.8	39.49	598.6	7.81
STDGJ09	0.81275	0.01616	0.09826	0.00135	0.4199	100	603.5	40.07	604.2	7.91
STDGJ10	0.82336	0.01645	0.09723	0.00134	0.4220	91	654	39.85	598.2	7.86
STDGJ11	0.81505	0.01668	0.09752	0.00135	0.4199	96	625.7	41.12	599.9	7.94
PLES4	0.4144	0.00908	0.05378	0.00076	0.3898	75	447.4	45.63	337.7	4.63
PLES5	0.3986	0.00808	0.05391	0.00074	0.4267	95	355.1	42.4	338.5	4.55
PLES6	0.40158	0.00822	0.05435	0.00075	0.4248	96	353.8	42.77	341.1	4.61
STDGJ12	0.96915	0.01689	0.11576	0.0015	0.4318	112	629.7	35.39	706.1	8.68
STDGJ13	0.87717	0.01507	0.10731	0.00139	0.4388	114	577.8	35.05	657.1	8.07
STDGJ14	0.83123	0.0143	0.10065	0.0013	0.4392	103	600.3	34.97	618.2	7.61
STDGJ15	0.81009	0.01393	0.09702	0.00125	0.4390	96	623.8	34.84	596.9	7.37
STDGJ16	0.79355	0.01373	0.09579	0.00124	0.4364	97	606.8	35.17	589.7	7.29
STDGJ17	0.80122	0.01387	0.09687	0.00125	0.4339	99	603.4	35.2	596.1	7.37
PLES7	0.38924	0.00648	0.05233	0.00067	0.4660	89	368.8	35.03	328.8	4.09
PLES8	0.38093	0.0064	0.05221	0.00067	0.4524	101	325.6	35.42	328.1	4.09
PLES9	0.40819	0.00676	0.05261	0.00067	0.4551	71	462.6	34.35	330.5	4.12
STDGJ18	0.80425	0.01526	0.09718	0.00129	0.3979	99	604.6	39.08	597.9	7.56
STDGJ19	0.81923	0.01554	0.09837	0.0013	0.4047	98	618.2	38.97	604.8	7.65
STDGJ20	0.81299	0.01565	0.09864	0.00131	0.3954	102	595.1	40.33	606.4	7.69

STDGJ21	0.81446	0.01584	0.09803	0.00131	0.3947	98	613	40.15	602.9	7.67
STDGJ22	0.79842	0.01562	0.09619	0.00128	0.3864	97	610.9	40.42	592.1	7.55
PLES10	0.39342	0.00751	0.05316	0.0007	0.3932	93	357.6	41.05	333.9	4.3
PLES11	0.41411	0.00809	0.05354	0.00071	0.3870	74	455.8	41.22	336.2	4.36
PLES12	0.39746	0.008	0.05365	0.00072	0.3764	94	359.8	43.64	336.9	4.39
STDGJ36	1.11316	0.02071	0.13588	0.00168	0.3264	141	583	39.95	821.3	9.56
STDGJ37	0.92571	0.01758	0.1148	0.00143	0.3293	128	548.5	41.04	700.6	8.27
STDGJ38	0.85569	0.01613	0.10314	0.00129	0.3246	104	610.4	40.31	632.8	7.51
STDGJ39	0.80011	0.01511	0.09781	0.00122	0.3313	104	579.9	40.56	601.6	7.16
STDGJ40	0.80073	0.01514	0.0957	0.0012	0.3288	94	628.9	40.27	589.1	7.04
STDGJ41	0.7823	0.01493	0.09403	0.00118	0.3314	94	616.5	40.72	579.3	6.95
PLES19	0.36932	0.00678	0.05093	0.00063	0.3458	103	312.1	40.91	320.2	3.84
PLES20	0.38111	0.00633	0.05244	0.00063	0.3864	104	317.1	36.52	329.5	3.87
PLES21	0.38004	0.00635	0.05207	0.00063	0.3849	100	326.6	36.67	327.2	3.85
STDGJ42	0.81065	0.01624	0.09838	0.00128	0.3595	102	594.9	42.33	604.9	7.53
STDGJ43	0.81618	0.01651	0.09746	0.00128	0.3604	95	630.2	42.06	599.5	7.5
STDGJ44	0.81005	0.01649	0.09746	0.00128	0.3567	98	613.9	42.39	599.5	7.52
STDGJ45	0.80891	0.01663	0.09792	0.00129	0.3603	100	600.7	42.88	602.2	7.58
STDGJ46	0.8043	0.01669	0.09726	0.00129	0.3503	99	602.9	43.24	598.3	7.57
PLES22	0.40081	0.00779	0.05432	0.0007	0.3887	97	350.7	41.72	341	4.3
PLES23	0.40247	0.0079	0.05498	0.00072	0.3929	104	332.7	42.11	345	4.37
PLES24	0.40594	0.00807	0.05492	0.00072	0.3932	97	354.1	42.68	344.7	4.39
STDGJ47	1.21531	0.02215	0.14652	0.00181	0.3490	144	611.6	38.68	881.4	10.16
STDGJ48	1.03512	0.01904	0.1236	0.00153	0.3475	119	632.2	38.95	751.3	8.77
STDGJ49	0.85891	0.01583	0.10485	0.0013	0.3446	110	584.5	39.33	642.7	7.56
STDGJ50	0.80676	0.01496	0.0972	0.0012	0.3428	98	612.8	39.4	598	7.08
STDGJ51	0.78834	0.01469	0.09496	0.00118	0.3373	95	613.1	39.58	584.8	6.94
STDGJ52	0.78586	0.01461	0.09396	0.00117	0.3463	92	629	39.35	578.9	6.88
PLES25	0.39193	0.00625	0.05293	0.00063	0.4149	92	360.5	34.72	332.5	3.86
PLES26	0.42507	0.00674	0.05248	0.00063	0.4096	59	559.3	33.72	329.7	3.84
PLES27	0.38664	0.00626	0.05211	0.00062	0.4014	90	364.9	35.17	327.4	3.82
STDGJ53	0.8044	0.0158	0.09713	0.00125	0.3534	99	606.4	41.24	597.5	7.35
STDGJ54	0.82024	0.01623	0.09887	0.00128	0.3536	100	609.9	41.51	607.8	7.5

STDGJ55	0.8022	0.01604	0.09818	0.00127	0.3430	105	576.9	42.17	603.7	7.48
STDGJ56	0.81867	0.0165	0.09723	0.00127	0.3502	93	641.9	42.07	598.1	7.45
STDGJ57	0.80513	0.01624	0.09722	0.00127	0.3512	99	606.1	42.3	598.1	7.45
PLES28	0.38935	0.00747	0.05336	0.00068	0.3694	103	325.7	41.73	335.1	4.18
PLES29	0.40938	0.00785	0.05475	0.0007	0.3759	90	380.5	41.32	343.6	4.29
PLES30	0.41154	0.00817	0.0556	0.00072	0.3629	97	357.8	43.25	348.8	4.4
STDGJ58	1.21056	0.02052	0.14674	0.00176	0.3603	147	598.5	36.05	882.6	9.88
STDGJ59	1.05691	0.01796	0.12636	0.00152	0.3693	122	628.2	35.97	767.1	8.68
STDGJ60	0.86301	0.01469	0.10438	0.00125	0.3672	106	603.3	36.15	640	7.31
STDGJ61	0.80546	0.01383	0.09749	0.00117	0.3624	100	601.6	36.49	599.7	6.89
STDGJ62	0.80198	0.01377	0.09561	0.00115	0.3570	93	634.2	36.27	588.6	6.79
STDGJ63	0.76976	0.01332	0.09334	0.00113	0.3571	96	597.4	36.75	575.3	6.65
PLES31	0.79344	0.0136	0.09397	0.00114	0.3673	89	648.3	36.05	579	6.7
PLES32	0.38446	0.00566	0.05254	0.00061	0.4443	99	332.4	31.77	330.1	3.75
PLES33	0.3872	0.00567	0.05316	0.00062	0.4362	104	321.8	31.66	333.9	3.79
STDGJ64	0.81182	0.01563	0.09745	0.00125	0.3631	97	618.9	40.27	599.4	7.32
STDGJ65	0.81343	0.01596	0.09893	0.00127	0.3533	103	590.5	41.25	608.1	7.47
STDGJ66	0.79676	0.01579	0.09718	0.00126	0.3510	102	584.3	41.7	597.9	7.38
STDGJ67	0.81574	0.01629	0.09772	0.00127	0.3496	96	623.2	41.73	601.1	7.45
STDGJ68	0.81485	0.01639	0.09759	0.00127	0.3466	96	623.8	42	600.3	7.47
PLES34	0.40879	0.00725	0.05565	0.0007	0.4201	102	340.7	37.83	349.1	4.27
PLES35	0.40917	0.0074	0.05624	0.00071	0.4141	111	318.9	38.79	352.7	4.34
PLES36	0.4268	0.00801	0.05573	0.00071	0.3983	81	434.1	39.27	349.6	4.35
STDGJ68	1.1755	0.02077	0.13932	0.00162	0.2890	130	647.3	38.51	840.8	9.15
STDGJ69	1.01594	0.01794	0.12342	0.00144	0.2937	126	593.8	38.55	750.2	8.25
STDGJ70	0.82461	0.01465	0.0998	0.00117	0.3085	102	601.6	38.68	613.2	6.85
STDGJ71	0.79479	0.01429	0.09559	0.00113	0.3069	96	615.1	38.93	588.5	6.65
PLES37	0.38636	0.00598	0.05327	0.00061	0.3770	107	312.2	34.58	334.6	3.71
PLES38	0.38286	0.00596	0.05246	0.0006	0.3905	101	326.2	34.47	329.6	3.69
PLES39	0.40561	0.0065	0.05231	0.00061	0.3809	71	461.1	34.87	328.7	3.73
STDGJ72	0.8089	0.01695	0.0969	0.00126	0.3337	96	623	43.76	596.2	7.42
STDGJ73	0.80027	0.01727	0.09701	0.00128	0.3449	100	597.6	45.06	596.8	7.53
STDGJ74	0.81313	0.01792	0.09838	0.00132	0.3548	101	601.8	45.72	604.9	7.73

STDGJ75	0.8147	0.0185	0.09809	0.00133	0.3564	98	612.4	46.78	603.2	7.84
PLES40	0.39744	0.0085	0.05574	0.00075	0.4070	128	273.3	45.53	349.7	4.55
PLES41	0.40449	0.00894	0.05692	0.00077	0.4027	134	265.8	46.88	356.9	4.72

Z14-01

	Isotope ratios and 1σ error (absolute)						Calculated age in Ma and 1σ error (absolute)			
Analysis	Pb^{207}/U^{235}		Pb^{206}/U^{238}		ρ*	Concordance (%)	Pb^{207}/Pb^{206}		Pb^{206}/U^{238}	
STDGJ01	0.95705	0.02148	0.11454	0.0016	0.3340	112	623.9	47.04	699	9.26
STDGJ02	0.90075	0.02505	0.10519	0.0016	0.2588	95	676.7	58.94	644.7	9.32
STDGJ03	0.85768	0.02379	0.1007	0.00153	0.2552	93	665.1	58.9	618.5	8.95
STDGJ04	0.81646	0.02261	0.09758	0.00148	0.2625	96	627	59.1	600.2	8.68
STDGJ05	0.78473	0.02214	0.09603	0.00146	0.2486	103	576	60.73	591.1	8.59
STDGJ06	0.78195	0.02206	0.09672	0.00147	0.2507	108	552.6	60.93	595.2	8.64
PLES1	0.37215	0.00816	0.05153	0.00071	0.3523	108	300.8	48.17	323.9	4.36
PLES2	0.38584	0.00844	0.0521	0.00072	0.3485	91	358.1	47.72	327.4	4.41
PLES3	0.37963	0.00842	0.05202	0.00072	0.3435	101	324.7	48.48	326.9	4.42
STDGJ07	0.81081	0.01974	0.0968	0.00141	0.3319	94	630.6	50.49	595.6	8.31
STDGJ08	0.8061	0.02006	0.09739	0.00143	0.3333	99	605	51.9	599.1	8.41
STDGJ09	0.80343	0.02011	0.09676	0.00143	0.3259	97	611.9	52.13	595.4	8.39
STDGJ10	0.81156	0.02041	0.0986	0.00146	0.3295	102	593.3	52.15	606.2	8.55
STDGJ11	0.81501	0.02069	0.09839	0.00146	0.3316	100	606.7	52.89	605	8.57
PLES4	0.39978	0.00954	0.05427	0.00079	0.3621	98	347.4	51.48	340.7	4.82
PLES5	0.40068	0.00964	0.05484	0.0008	0.3605	105	328.9	51.88	344.2	4.88
PLES6	0.40294	0.00984	0.05468	0.0008	0.3444	99	348.3	52.74	343.2	4.9
STDGJ12	0.96941	0.01711	0.11856	0.00154	0.4274	125	578.6	36.06	722.3	8.87
STDGJ13	0.88873	0.01585	0.10647	0.00139	0.4279	105	623.5	36.24	652.2	8.08
STDGJ14	0.83969	0.01491	0.10093	0.00131	0.4298	101	616.1	36.1	619.9	7.69
STDGJ15	0.80403	0.01443	0.09814	0.00128	0.4222	104	583	36.72	603.5	7.51
STDGJ16	0.80307	0.01434	0.0953	0.00124	0.4276	91	643.9	36.16	586.8	7.31
STDGJ17	0.78787	0.01417	0.09588	0.00125	0.4278	100	589.4	36.76	590.2	7.36
PLES7	0.38039	0.00586	0.05227	0.00066	0.5148	103	319.7	31.66	328.5	4.04
PLES8	0.38793	0.00603	0.05315	0.00067	0.5101	102	326.5	31.96	333.8	4.11
PLES9	0.38795	0.00601	0.05303	0.00067	0.5107	100	331.5	31.78	333.1	4.1

STDGJ18	0.81628	0.01693	0.09847	0.00134	0.3728	100	608.3	43.03	605.4	7.85
STDGJ19	0.81536	0.01711	0.09907	0.00135	0.3645	103	593.2	43.27	608.9	7.94
STDGJ20	0.81542	0.01712	0.09775	0.00134	0.3627	97	621.9	43.49	601.2	7.84
STDGJ21	0.79497	0.01706	0.09597	0.00132	0.3555	97	606.6	44.68	590.8	7.76
STDGJ22	0.82193	0.01786	0.09702	0.00134	0.3473	91	655	44.97	596.9	7.87
PLES10	0.4098	0.00757	0.05459	0.00072	0.4326	88	389.5	38.63	342.7	4.42
PLES11	0.40867	0.00816	0.05445	0.00073	0.3987	88	389.2	42.23	341.8	4.48
PLES12	0.41089	0.0084	0.05439	0.00074	0.3856	85	403.7	43.12	341.4	4.51
STDGJ23	1.04206	0.01969	0.12683	0.00162	0.3598	130	590.2	39.83	769.8	9.26
STDGJ24	0.91433	0.01651	0.10958	0.00138	0.3788	108	623.1	37.73	670.3	8.01
STDGJ25	0.83198	0.01506	0.10147	0.00128	0.3707	106	585.2	38.05	623	7.46
STDGJ26	0.81023	0.01477	0.09746	0.00123	0.3717	97	615.2	38.16	599.5	7.21
STDGJ27	0.79707	0.01456	0.09606	0.00121	0.3705	97	610.9	38.28	591.3	7.13
STDGJ28	0.79647	0.01463	0.09537	0.00121	0.3751	94	625	38.45	587.2	7.09
PLES13	0.39176	0.006	0.05319	0.00064	0.4514	96	347.7	32.43	334	3.93
PLES14	0.38767	0.00588	0.05278	0.00064	0.4576	97	341.2	32.13	331.6	3.9
PLES15	0.38812	0.00587	0.05292	0.00064	0.4676	98	338.1	32.01	332.4	3.91
STDGJ29	0.78854	0.01631	0.09688	0.00127	0.3313	105	568.4	44.04	596.1	7.47
STDGJ30	0.82265	0.01696	0.09933	0.0013	0.3281	101	606.2	43.6	610.5	7.65
STDGJ31	0.80766	0.01697	0.09741	0.00129	0.3321	98	608.6	44.49	599.2	7.56
STDGJ32	0.80801	0.01696	0.0975	0.00129	0.3298	99	607.6	44.43	599.7	7.57
STDGJ33	0.80119	0.01682	0.09677	0.00128	0.3284	98	605.3	44.45	595.5	7.51
PLES16	0.3984	0.00729	0.05408	0.00069	0.3887	98	347.1	39.66	339.5	4.2
PLES17	0.3934	0.00725	0.05423	0.00069	0.3887	109	312.1	40.22	340.4	4.22
PLES18	0.3992	0.00743	0.05424	0.00069	0.3760	99	344.8	40.44	340.5	4.23
STDGJ34	1.15124	0.02051	0.13824	0.00167	0.3346	135	619.3	37.94	834.7	9.47
STDGJ35	0.93316	0.0167	0.11217	0.00136	0.3393	111	616.8	38.13	685.4	7.87
STDGJ36	0.84861	0.01534	0.10237	0.00124	0.3313	103	609	38.6	628.3	7.26
STDGJ37	0.78818	0.01453	0.09742	0.00119	0.3343	108	556	39.16	599.3	6.97
STDGJ38	0.80212	0.01456	0.09608	0.00117	0.3347	95	624.1	38.64	591.4	6.88
STDGJ39	0.79586	0.01448	0.09456	0.00115	0.3357	91	641.7	38.62	582.4	6.79
PLES19	0.38555	0.00583	0.05202	0.00061	0.4240	90	361.7	32.92	326.9	3.71
PLES20	0.38477	0.00584	0.05228	0.00061	0.4169	95	345.6	32.99	328.5	3.73

PLES21	0.38699	0.00585	0.05193	0.0006	0.4252	87	373.9	32.84	326.3	3.71
STDGJ40	0.82389	0.01676	0.09784	0.00126	0.3197	94	641.9	42.91	601.7	7.38
STDGJ41	0.80646	0.01677	0.10075	0.0013	0.3197	116	531.3	45.14	618.8	7.62
STDGJ42	0.82598	0.01725	0.09867	0.00128	0.3206	96	629	44.17	606.6	7.51
STDGJ43	0.79475	0.01678	0.09675	0.00126	0.3183	101	588.1	44.94	595.4	7.41
STDGJ44	0.79835	0.01691	0.09778	0.00128	0.3143	105	575	45.16	601.4	7.49
PLES22	0.39308	0.00813	0.05398	0.0007	0.3313	106	320.5	45.61	338.9	4.27
PLES23	0.39909	0.00773	0.05432	0.00069	0.3600	100	340.9	42.33	341	4.21
PLES24	0.3976	0.00782	0.05421	0.00069	0.3472	101	336.8	43.02	340.3	4.22
STDGJ45	1.09867	0.01956	0.13681	0.00161	0.3104	154	537	39.59	826.6	9.14
STDGJ46	1.01609	0.01787	0.12456	0.00146	0.3186	132	571.8	38.27	756.8	8.4
STDGJ47	0.86413	0.01522	0.10317	0.00122	0.3207	101	629	37.98	633	7.11
STDGJ48	0.82883	0.0147	0.09856	0.00117	0.3224	95	637.8	38.16	606	6.84
STDGJ49	0.76899	0.01387	0.09416	0.00112	0.3123	101	574.5	39.21	580.1	6.58
STDGJ50	0.78182	0.01399	0.09518	0.00113	0.3112	100	587.2	38.8	586.1	6.64
PLES25	0.37231	0.00542	0.0514	0.00058	0.3950	105	307.8	32.42	323.1	3.54
PLES26	0.37043	0.00588	0.05086	0.00058	0.3556	100	319.5	35.75	319.8	3.53
PLES27	0.36933	0.00583	0.05096	0.00059	0.3820	104	309	35.26	320.4	3.6
STDGJ51	0.79578	0.0162	0.09725	0.00123	0.3083	103	580	43.71	598.3	7.2
STDGJ52	0.80787	0.01666	0.09689	0.00123	0.3042	96	620.9	43.97	596.1	7.22
STDGJ53	0.8107	0.01674	0.09759	0.00124	0.3133	98	612.9	44.02	600.3	7.28
STDGJ54	0.81368	0.01699	0.09777	0.00125	0.3069	97	616.8	44.49	601.3	7.33
STDGJ55	0.81104	0.01715	0.09858	0.00126	0.3048	102	592.7	44.58	606.1	7.41
PLES28	0.39719	0.00755	0.05412	0.00067	0.3438	100	339	41.77	339.8	4.09
PLES29	0.41003	0.0086	0.05516	0.0007	0.3039	94	367.6	46.5	346.1	4.27
PLES30	0.39811	0.00827	0.05426	0.00069	0.3143	101	338.3	46.03	340.6	4.2
STDGJ56	1.13425	0.02159	0.13687	0.00165	0.2952	136	608.4	41.33	826.9	9.38
STDGJ57	1.03137	0.01839	0.12482	0.00147	0.3007	126	602.5	38.71	758.2	8.42
STDGJ58	0.89592	0.01625	0.10867	0.00128	0.3035	111	597.3	39.46	665	7.46
STDGJ59	0.82244	0.01487	0.09889	0.00117	0.3008	99	616.3	39.22	607.9	6.84
STDGJ60	0.78163	0.0142	0.09403	0.00111	0.3049	94	615.1	39.42	579.3	6.54
STDGJ61	0.77936	0.01417	0.09393	0.00111	0.3033	95	611	39.51	578.7	6.53
PLES33	0.37468	0.00635	0.05045	0.00058	0.3283	87	366.4	38.35	317.3	3.55

STDGJ67	0.96166	0.0172	0.11385	0.00134	0.3098	107	649.5	38.54	695.1	7.78
STDGJ68	0.87184	0.01581	0.10561	0.00125	0.2925	108	599.9	39.45	647.2	7.27
PLES34	0.38924	0.00725	0.05291	0.00062	0.2892	96	344.7	42.3	332.4	3.82
PLES35	0.37598	0.00692	0.05149	0.00061	0.2979	99	328	41.67	323.6	3.72
STDGJ62	0.81839	0.01655	0.09868	0.00121	0.2711	100	609.3	44.02	606.6	7.11
STDGJ63	0.8182	0.0179	0.09832	0.00125	0.2517	98	616.6	47.68	604.5	7.31
STDGJ64	0.78858	0.01657	0.0966	0.0012	0.2601	103	574.8	46.06	594.5	7.07
STDGJ65	0.79755	0.01673	0.09601	0.0012	0.2628	96	612.6	45.7	591	7.03
STDGJ66	0.80343	0.01876	0.09675	0.00126	0.2227	97	612.2	51	595.3	7.42
PLES36	0.39294	0.00809	0.05309	0.00065	0.2592	93	357.6	46.82	333.5	3.99
PLES37	0.39391	0.0081	0.0542	0.00066	0.2549	107	316.5	46.93	340.2	4.06
PLES38	0.38165	0.008	0.05312	0.00066	0.2688	115	290.2	48.1	333.6	4.01
STDGJ69	1.12855	0.02161	0.13935	0.00162	0.2375	150	559.5	42.64	841	9.19
STDGJ70	1.0578	0.02	0.12621	0.00147	0.2513	121	634	41.58	766.2	8.42
STDGJ71	0.93556	0.01786	0.11358	0.00133	0.2506	116	596.1	42.19	693.5	7.67
STDGJ72	0.84906	0.01634	0.10374	0.00121	0.2496	109	582.7	42.63	636.3	7.09
STDGJ73	0.80523	0.01525	0.0966	0.00113	0.2601	96	621.8	41.62	594.5	6.63
STDGJ74	0.77584	0.01507	0.09295	0.0011	0.2581	92	624.9	42.64	573	6.47
PLES39	0.37994	0.00601	0.05204	0.00057	0.3260	100	328.6	36.08	327	3.52
PLES40	0.38734	0.00633	0.05235	0.00058	0.3182	92	358.6	37.26	328.9	3.58
PLES41	0.39455	0.00709	0.05134	0.00059	0.2760	73	443.1	40.09	322.8	3.61
STDGJ75	0.81311	0.0174	0.09834	0.00124	0.2858	100	602.6	45.86	604.7	7.26
STDGJ76	0.84168	0.02596	0.09985	0.00151	0.2188	95	644	65.68	613.5	8.86
STDGJ77	0.8043	0.01749	0.09662	0.00123	0.2833	96	617	46.36	594.6	7.22
STDGJ78	0.79957	0.01751	0.09712	0.00124	0.2884	101	593.3	46.44	597.5	7.27
STDGJ79	0.80518	0.01783	0.09733	0.00125	0.2879	99	603.3	47.13	598.8	7.32
PLES42	0.40814	0.0088	0.05441	0.00069	0.3267	88	387	46.55	341.5	4.23
PLES43	0.3957	0.008	0.05451	0.00068	0.3453	109	313.5	44.4	342.1	4.13
PLES44	0.40072	0.00845	0.0544	0.00068	0.3353	99	346.3	46.13	341.5	4.17

Z14-02

	Isotope ratios and 1σ error (absolute)				Calculated age in Ma and 1σ error (absolute)	
Analysis	Pb^{207}/U^{235}	Pb^{206}/U^{238}	ρ*	Concordance (%)	Pb^{207}/Pb^{206}	Pb^{206}/U^{238}

STDGJ01	0.87771	0.01725	0.108	0.00144	0.3751	117	565.2	41.05	661.1	8.36
STDGJ02	0.84122	0.01753	0.10218	0.00137	0.3399	106	593.8	43.85	627.2	8
STDGJ03	0.80981	0.0169	0.09853	0.00132	0.3389	103	590.2	44.03	605.8	7.75
STDGJ04	0.81596	0.01676	0.09631	0.00129	0.3533	90	655.6	42.8	592.8	7.58
STDGJ05	0.802	0.0167	0.09612	0.00129	0.3474	95	622.9	43.63	591.6	7.59
STDGJ06	0.78131	0.01625	0.09521	0.00128	0.3459	100	586.8	43.81	586.3	7.52
PLES1	0.38351	0.00624	0.05221	0.00066	0.4706	96	341.4	34.08	328.1	4.03
PLES2	0.38312	0.00624	0.05206	0.00066	0.4744	95	345.8	34.04	327.1	4.03
PLES3	0.3752	0.00612	0.05152	0.00065	0.4622	101	322	34.28	323.8	3.99
STDGJ07	0.79441	0.0194	0.09639	0.00138	0.3162	100	595.1	51.86	593.2	8.13
STDGJ08	0.82692	0.02014	0.09702	0.00139	0.3228	89	667.8	50.56	596.9	8.2
STDGJ09	0.81492	0.01726	0.09829	0.00137	0.3918	99	608.5	43.28	604.4	8.03
STDGJ10	0.81407	0.01748	0.09917	0.00139	0.3834	104	587	44.08	609.6	8.12
STDGJ11	0.82093	0.01775	0.09815	0.00138	0.3847	96	627.5	44	603.5	8.09
PLES6	0.40578	0.00754	0.05508	0.00074	0.4723	100	347.3	38.24	345.6	4.54
PLES7	0.40451	0.00754	0.05462	0.00074	0.4704	96	358.9	38.42	342.8	4.51
PLES8	0.40483	0.00769	0.05513	0.00075	0.4535	102	339.8	39.16	345.9	4.57
STDGJ12	0.92095	0.02368	0.11267	0.00162	0.2607	119	577.1	55.49	688.2	9.38
STDGJ13	0.85606	0.02189	0.10254	0.00147	0.2665	101	622.8	54.77	629.3	8.62
STDGJ14	0.81311	0.02108	0.09821	0.00142	0.2633	100	604.8	55.68	603.9	8.33
STDGJ15	0.79432	0.02083	0.09571	0.00139	0.2517	97	610.2	56.29	589.2	8.18
STDGJ16	0.77079	0.01994	0.09369	0.00135	0.2591	98	591.3	55.61	577.3	7.98
PLES9	0.39578	0.00745	0.0538	0.0007	0.3941	98	343.7	40.67	337.8	4.29
PLES10	0.39511	0.00772	0.05414	0.00071	0.3840	104	325.6	42.43	339.9	4.35
PLES11	0.39186	0.00817	0.05395	0.00072	0.3459	107	315.1	45.67	338.7	4.42
STDGJ17	0.82771	0.02427	0.09866	0.00152	0.2458	96	633.9	62.33	606.6	8.94
STDGJ18	0.80924	0.02469	0.0984	0.00154	0.2457	102	590.9	65.33	605	9.06
STDGJ19	0.80408	0.02504	0.09714	0.00154	0.2437	99	605.1	66.5	597.6	9.05
STDGJ20	0.82894	0.02603	0.09719	0.00155	0.2364	89	669.5	66.35	597.9	9.14
STDGJ21	0.80706	0.02577	0.09737	0.00157	0.2418	99	607.9	68.02	599	9.2
PLES12	0.41848	0.01182	0.05531	0.00084	0.2809	85	407.2	60.73	347	5.13
PLES13	0.40674	0.01155	0.05534	0.00084	0.2843	102	342	62.33	347.2	5.15
PLES14	0.40652	0.0117	0.05551	0.00085	0.2890	104	333.9	63.19	348.2	5.2

Z14-05

Analysis	Isotope ratios and 1σ error (absolute) Pb^{207}/U^{235}		Pb^{206}/U^{238}		ρ*	Concordance (%)	Calculated age in Ma and 1σ error (absolute) Pb^{207}/Pb^{206}		Pb^{206}/U^{238}	
STDGJ1	0.83282	0.01636	0.10164	0.00112	0.1686	107	585.4	44.64	624	6.57
STDGJ2	0.79727	0.01569	0.09612	0.00107	0.1679	97	611.8	44.46	591.6	6.28
STDGJ3	0.73727	0.01465	0.08838	0.00099	0.1812	87	624	44.72	545.9	5.85
STDGJ4	0.7138	0.01424	0.08456	0.00095	0.1808	81	649.2	44.64	523.3	5.65
STDGJ5	0.68006	0.01536	0.07956	0.00091	0.1690	73	675.9	49.52	493.5	5.46
PLES1	0.31621	0.00737	0.04251	0.00048	0.1558	72	370.5	53.64	268.4	2.96
STDGJ6	0.87582	0.01783	0.10632	0.00121	0.1849	109	596	45.63	651.4	7.08
STDGJ7	0.84631	0.01711	0.10117	0.00116	0.1916	99	629.2	45.03	621.3	6.78
PLES2	0.37423	0.00714	0.05032	0.00056	0.2059	86	369.7	44.37	316.5	3.42
PLES3	0.37759	0.00711	0.0489	0.00054	0.2193	68	453.6	42.81	307.7	3.33
PLES4	0.35958	0.00709	0.04736	0.00053	0.2117	72	416.2	44.59	298.3	3.29
STDGJ8	0.78546	0.01926	0.0955	0.00128	0.2891	100	590.9	51.84	588	7.53
STDGJ9	0.81072	0.02015	0.09763	0.00132	0.2927	98	611.7	52.21	600.5	7.76
STDGJ10	0.81697	0.0205	0.09693	0.00132	0.2999	93	643.9	52.26	596.4	7.78
STDGJ11	0.8244	0.02097	0.09934	0.00137	0.3081	100	610.4	53.06	610.5	8.02
STDGJ12	0.79857	0.02072	0.09746	0.00136	0.3071	103	583	54.23	599.5	7.97
PLES5	0.38641	0.00943	0.05264	0.00071	0.3440	97	339.3	52.3	330.7	4.35
PLES6	0.40004	0.00986	0.05419	0.00074	0.3567	97	351.8	52.52	340.2	4.51
PLES7	0.39467	0.00983	0.05332	0.00073	0.3640	94	357.8	52.76	334.9	4.48
STDGJ13	1.20274	0.03191	0.14642	0.00209	0.3393	150	588.6	54.23	880.9	11.78
STDGJ14	1.04843	0.02848	0.12937	0.00187	0.3432	140	559.4	55.66	784.3	10.69
STDGJ15	0.99027	0.02704	0.11927	0.00174	0.3501	119	612	55.18	726.4	10.02
STDGJ23	1.15612	0.03204	0.14037	0.00207	0.3610	142	594.4	56.11	846.8	11.7
STDGJ23-2	0.85432	0.0138	0.10472	0.00115	0.2874	112	574.9	35.78	642	6.74
STDGJ24	0.84625	0.01361	0.10079	0.00111	0.2971	97	637.1	35.25	619	6.53
STDGJ25	0.78392	0.01268	0.09454	0.00105	0.3030	95	610	35.56	582.3	6.17
STDGJ16	0.76046	0.01235	0.09154	0.00102	0.2964	92	614	35.64	564.7	6.01
STDGJ17	0.73171	0.01198	0.08883	0.00099	0.3084	92	595.2	36.57	548.6	5.87
PLES8	0.35373	0.00549	0.04852	0.00053	0.3190	94	324.9	35.47	305.4	3.26

PLES9	0.3604	0.00564	0.04767	0.00052	0.3125	74	407	35.04	300.2	3.23
PLES10	0.40635	0.00611	0.04811	0.00053	0.3390	47	649.8	32.52	302.9	3.25
STDGJ18	0.82572	0.01547	0.09953	0.00121	0.3346	100	610.1	39.68	611.7	7.09
STDGJ19	0.81932	0.01549	0.09889	0.00121	0.3321	100	607	39.98	607.9	7.08
STDGJ20	0.79577	0.01526	0.0955	0.00117	0.3316	95	619.3	40.43	588	6.9
STDGJ21	0.80521	0.01535	0.0976	0.0012	0.3504	100	597.8	40.16	600.3	7.04
STDGJ22	0.8072	0.01561	0.09504	0.00118	0.3485	89	660.3	40.3	585.3	6.92
PLES11	0.38073	0.00728	0.05194	0.00064	0.3621	97	335.6	41.69	326.4	3.91
PLES12	0.3899	0.00738	0.05244	0.00064	0.3682	90	367.7	41.08	329.5	3.94
PLES13	0.3959	0.00755	0.05235	0.00065	0.3627	81	405.4	40.63	329	3.96
STDGJ23	0.9811	0.01605	0.11931	0.00125	0.2343	122	594.6	37.4	726.6	7.22
STDGJ24	0.92069	0.01563	0.11021	0.00118	0.2214	107	629	38.17	674	6.84
STDGJ25	0.79209	0.01315	0.09549	0.00101	0.2394	96	613.5	37.35	587.9	5.97
STDGJ26	0.75175	0.01184	0.09072	0.00095	0.2482	92	611.1	35.36	559.8	5.63
STDGJ27	0.72228	0.01151	0.08756	0.00093	0.2612	90	601.4	35.73	541.1	5.48
PLES14	0.33587	0.00579	0.04559	0.00049	0.2454	82	351	40.23	287.4	3.02
PLES15	0.34264	0.00593	0.04636	0.0005	0.2399	82	358.2	40.27	292.1	3.08
PLES16	0.34168	0.00547	0.04669	0.0005	0.2830	88	335.8	37.06	294.2	3.05
STDGJ28	0.78802	0.0152	0.09581	0.00119	0.3890	100	591.2	39.46	589.8	7.03
STDGJ29	0.81484	0.01594	0.09649	0.00122	0.3965	92	648	39.48	593.8	7.15
STDGJ30	0.80861	0.01613	0.0985	0.00125	0.3926	103	586.9	40.49	605.6	7.35
STDGJ31	0.83903	0.01686	0.09996	0.00128	0.4097	97	634.5	40.21	614.2	7.52
STDGJ32	0.81338	0.01676	0.09924	0.00129	0.4090	105	582.9	41.45	610	7.55
PLES17	0.42202	0.00798	0.05364	0.00068	0.4655	68	492.7	37.53	336.8	4.17
PLES18	0.3889	0.00759	0.05272	0.00068	0.4734	95	349.1	39.39	331.2	4.14
PLES20	0.55926	0.01115	0.06681	0.00087	0.4707	66	627.9	38.3	416.9	5.27
PLES21	0.59304	0.01191	0.0652	0.00086	0.4748	51	804.2	37.19	407.2	5.2
STDGJ33	1.0894	0.01764	0.13206	0.00143	0.2708	133	599.3	36.11	799.6	8.15
STDGJ34	0.9761	0.01672	0.11677	0.00129	0.2607	113	627.8	38.03	712	7.44
STDGJ35	0.83176	0.01417	0.10112	0.00111	0.2553	105	593.2	37.6	621	6.52
STDGJ36	0.77622	0.01348	0.0939	0.00104	0.2606	96	603.4	38.65	578.6	6.14
STDGJ37	0.75556	0.01315	0.09053	0.00101	0.2515	89	624.2	38.59	558.6	5.95
STDGJ43	0.86678	0.01466	0.10474	0.00116	0.2751	106	605.6	37.55	642.2	6.75

STDGJ44	0.82842	0.01446	0.10021	0.00112	0.2549	102	603.4	38.74	615.6	6.55
STDGJ45	0.79636	0.01396	0.09549	0.00107	0.2609	94	622.3	38.76	587.9	6.29
PLES22	0.36398	0.00586	0.04959	0.00054	0.2810	92	340	37.08	312	3.3
PLES23	0.35684	0.00563	0.04884	0.00053	0.3025	93	329.6	36.36	307.4	3.24
PLES24	0.46324	0.00766	0.04774	0.00053	0.2758	32	940	34.81	300.7	3.27
STDGJ38	0.87162	0.01588	0.10442	0.00122	0.2956	103	622	39.28	640.3	7.15
STDGJ39	0.84889	0.01573	0.10211	0.0012	0.2984	102	613.1	39.99	626.8	7.05
STDGJ40	0.80679	0.01505	0.09682	0.00115	0.2997	96	618	40.18	595.8	6.74
STDGJ41	0.75255	0.01417	0.09236	0.0011	0.3049	100	569.3	40.82	569.5	6.47
STDGJ42	0.74267	0.01412	0.0906	0.00108	0.2986	96	582.3	41.07	559.1	6.39
PLES25	0.36151	0.00702	0.04921	0.00059	0.2993	91	339.3	43.62	309.7	3.61
PLES26	0.36883	0.00756	0.0493	0.0006	0.2837	82	380.1	45.79	310.2	3.69
PLES27	0.36457	0.00722	0.05006	0.0006	0.2951	99	319.2	44.49	314.9	3.7
STDGJ46	1.14836	0.01988	0.1368	0.00154	0.2735	130	637.5	38.18	826.5	8.72
STDGJ47	1.00613	0.01744	0.1213	0.00136	0.2692	121	611.7	38.36	738	7.84
STDGJ48	0.83912	0.01466	0.10028	0.00113	0.2650	98	630.5	38.52	616.1	6.63
STDGJ49	0.77954	0.01372	0.09473	0.00107	0.2630	98	594.3	39.13	583.5	6.3
STDGJ50	0.75653	0.01255	0.09063	0.00101	0.2839	89	625.4	36.47	559.2	5.96
STDGJ56	0.9615	0.01594	0.11654	0.0013	0.2955	118	600	36.52	710.6	7.51
STDGJ57	0.88538	0.01438	0.10797	0.0012	0.3070	113	586.7	35.79	661	6.98
PLES28	0.38756	0.00633	0.05355	0.00059	0.2993	109	309.4	37.61	336.3	3.62
PLES29	0.3864	0.00912	0.05231	0.00065	0.1958	92	355.5	54.37	328.7	3.99
PLES30	0.35844	0.00643	0.04955	0.00056	0.2674	101	308.1	41.29	311.8	3.45
STDGJ51	0.78519	0.01491	0.09442	0.00115	0.3286	94	615.8	40.21	581.6	6.78
STDGJ52	0.79753	0.01537	0.09631	0.00118	0.3285	98	606.6	40.83	592.7	6.94
STDGJ53	0.82071	0.01589	0.10012	0.00123	0.3328	105	584.4	41.07	615.1	7.22
STDGJ54	0.82912	0.01627	0.09971	0.00124	0.3352	100	615.3	41.36	612.7	7.24
STDGJ55	0.81039	0.01604	0.0971	0.00121	0.3391	96	623.2	41.57	597.4	7.1
PLES31	0.39547	0.00851	0.05101	0.00065	0.3103	70	461	47.1	320.7	3.98
PLES32	0.37731	0.00777	0.05156	0.00065	0.3255	98	332.2	45.2	324.1	3.96
STDGJ58	1.25047	0.03062	0.15074	0.00198	0.2070	149	608.2	53.88	905.1	11.1
STDGJ59	1.02656	0.02531	0.12442	0.00164	0.1954	127	596.5	54.35	756	9.39
STDGJ60	0.85422	0.02114	0.10174	0.00134	0.1977	98	634.2	54.22	624.6	7.86

STDGJ61	0.81034	0.01989	0.09709	0.00128	0.1983	96	621.4	53.85	597.3	7.51
STDGJ62	0.77152	0.01914	0.09438	0.00125	0.2020	101	576.4	54.74	581.4	7.34
PLES34	0.35841	0.00824	0.04865	0.00061	0.2238	89	345.8	52.63	306.2	3.78
PLES35	0.36905	0.00845	0.04957	0.00063	0.2265	84	369.3	52.02	311.9	3.85
PLES36	0.37058	0.00854	0.04907	0.00062	0.2324	77	401.7	51.77	308.8	3.83
STDGJ63	0.79513	0.01884	0.09719	0.00131	0.3043	103	579.5	49.94	597.9	7.7
STDGJ64	0.81612	0.01948	0.09794	0.00133	0.3118	97	619.5	49.86	602.3	7.79
STDGJ65	0.815	0.01973	0.09887	0.00135	0.3153	102	596.1	50.66	607.8	7.92
STDGJ66	0.80987	0.01987	0.09654	0.00133	0.3199	94	634.2	50.96	594.1	7.81
STDGJ67	0.81063	0.02004	0.09765	0.00135	0.3141	98	611.7	51.38	600.6	7.93
PLES37	0.38709	0.00943	0.05289	0.00072	0.3387	100	332.9	52.68	332.3	4.44
PLES38	0.39125	0.00972	0.05352	0.00074	0.3289	102	330.5	53.66	336.1	4.53
PLES39	0.39557	0.01025	0.05368	0.00076	0.3195	97	348.7	56.07	337.1	4.63
STDGJ68	1.26705	0.02404	0.15214	0.00178	0.2600	148	618.8	41.77	912.9	9.98
STDGJ69	1.09258	0.02095	0.13099	0.00154	0.2500	128	622.1	42.15	793.5	8.79
STDGJ70	0.86434	0.01654	0.10455	0.00123	0.2611	106	602.9	42.15	641	7.18
STDGJ71	0.82019	0.01559	0.09819	0.00116	0.2566	97	625	41.66	603.8	6.79
STDGJ72	0.79336	0.01524	0.09617	0.00114	0.2650	99	598	42.21	591.9	6.69
STDGJ73	0.76293	0.01489	0.09205	0.0011	0.2546	93	608.1	42.77	567.7	6.48
PLES40	0.36721	0.00666	0.04967	0.00057	0.2880	88	355.4	41.34	312.5	3.53
PLES41	0.36355	0.00661	0.05021	0.00058	0.2926	102	308.1	41.55	315.8	3.57
PLES42	0.36001	0.00651	0.04981	0.00058	0.3023	103	304	41.22	313.4	3.55
STDGJ74	0.79636	0.01592	0.09645	0.00121	0.3366	99	599.6	42.1	593.6	7.14
STDGJ75	0.82838	0.01679	0.09872	0.00125	0.3426	96	634.4	42.32	606.9	7.36
STDGJ76	0.81371	0.01677	0.09864	0.00126	0.3400	101	597.8	43.21	606.4	7.41
STDGJ77	0.80898	0.0169	0.09864	0.00127	0.3376	104	585.2	43.76	606.4	7.46
STDGJ78	0.80488	0.01724	0.09623	0.00125	0.3405	94	627.8	44.51	592.3	7.38
PLES43	0.38162	0.00797	0.0531	0.00068	0.3638	114	291.4	45.44	333.5	4.19
PLES44	0.46596	0.0096	0.0543	0.0007	0.3770	50	682.6	41.76	340.9	4.3
PLES45	0.44833	0.00946	0.05516	0.00072	0.3781	61	565.7	43.49	346.1	4.41

* ρ denotes error correlation between ratios used to produce concordia diagram

Table S2. Individual unknown U-Pb analytical data.

Z14-17

Analysis	Isotope ratios and 1σ error (absolute) Pb^{207}/U^{235}		Pb^{206}/U^{238}		ρ*	Concordance (%)	Calculated age in Ma and 1σ error (absolute) Pb^{207}/Pb^{206}		Pb^{206}/U^{238}	
Z14-17-01	13.26699	0.18444	0.51145	0.00635	0.5547	98	2726.4	20.42	2662.8	27.09
Z14-17-02	6.89469	0.09688	0.37213	0.00462	0.5492	95	2156.4	21.89	2039.4	21.7
Z14-17-03	7.49444	0.11175	0.39356	0.00502	0.5202	97	2204.2	23.6	2139.3	23.22
Z14-17-04	5.65671	0.09065	0.32514	0.00426	0.4807	89	2045.9	26.4	1814.8	20.73
Z14-17-05	6.10712	0.0901	0.35247	0.00446	0.5277	95	2038.7	23.54	1946.4	21.25
Z14-17-06	4.55126	0.07214	0.30187	0.00391	0.4928	95	1789.1	26.66	1700.6	19.36
Z14-17-07	4.67668	0.08377	0.30863	0.00421	0.4325	96	1798.2	31.02	1734	20.73
Z14-17-08	2.27505	0.03366	0.13575	0.00172	0.5326	41	1979.5	23.67	820.6	9.74
Z14-17-09	4.91337	0.075	0.3073	0.00393	0.5223	91	1895.4	24.79	1727.4	19.39
Z14-17-10	6.2318	0.09921	0.36114	0.00472	0.5004	98	2031.4	25.77	1987.6	22.34
Z14-17-100	5.50603	0.08968	0.33658	0.00418	0.4363	97	1936.3	27.58	1870.2	20.15
Z14-17-101	5.0576	0.07832	0.31795	0.00391	0.4229	94	1886.2	27.05	1779.7	19.14
Z14-17-102	5.15456	0.07562	0.32961	0.00396	0.4487	99	1855.5	25.36	1836.5	19.2
Z14-17-103	5.15707	0.0734	0.33212	0.00394	0.4704	100	1842.6	24.42	1848.7	19.08
Z14-17-104	3.58013	0.05048	0.22606	0.00267	0.4763	70	1878.1	24.02	1313.8	14.05
Z14-17-105	5.24484	0.0739	0.30858	0.00365	0.4781	86	2004.5	23.57	1733.7	18
Z14-17-106	3.14713	0.04456	0.18665	0.00221	0.4733	55	1990.3	23.72	1103.2	12.01
Z14-17-107	0.72002	0.01086	0.04518	0.00055	0.4412	15	1889.5	26.05	284.8	3.37
Z14-17-108	5.54967	0.07993	0.32476	0.00388	0.4774	90	2014	24.05	1813	18.86
Z14-17-109	0.94911	0.01399	0.05971	0.00072	0.4651	20	1884.8	25.14	373.8	4.35
Z14-17-11	10.83665	0.16778	0.46267	0.00602	0.5200	96	2556.9	23.42	2451.3	26.53
Z14-17-110	5.89155	0.0901	0.35343	0.00432	0.4521	99	1969.9	25.9	1951	20.59
Z14-17-111	6.06431	0.09064	0.35132	0.00425	0.4637	96	2031.9	24.92	1940.9	20.28
Z14-17-112	4.7742	0.08791	0.31626	0.00419	0.3709	99	1791.1	32.9	1771.4	20.51
Z14-17-113	6.33232	0.09809	0.36839	0.00452	0.4544	100	2024.4	25.94	2021.8	21.3
Z14-17-114	6.35267	0.09873	0.3677	0.00451	0.4565	99	2033.3	25.95	2018.6	21.27
Z14-17-115	3.16778	0.0657	0.21792	0.00304	0.3273	74	1722	37.93	1270.9	16.07
Z14-17-116	6.34021	0.10215	0.37069	0.00461	0.4422	101	2015.4	27.07	2032.7	21.7
Z14-17-117	5.04109	0.08124	0.28825	0.00348	0.3902	79	2054.7	27.81	1632.8	17.42

Z14-17-118	5.2348	0.08272	0.30621	0.00365	0.4101	85	2014.4	27.03	1722.1	18.02	
Z14-17-119	6.24998	0.10449	0.36527	0.00448	0.4023	100	2015.9	28.63	2007.1	21.16	
Z14-17-12	0.3753	0.00603	0.02904	0.00038	0.4983	12	1503.1	27.7	184.5	2.35	
Z14-17-120	6.34438	0.10821	0.37143	0.00459	0.4027	101	2012.8	29.02	2036.1	21.59	
Z14-17-121	6.23422	0.10808	0.3667	0.00455	0.4139	100	2004.5	29.27	2013.9	21.48	
Z14-17-13	5.86934	0.09183	0.35232	0.00455	0.5230	99	1968.9	25.08	1945.7	21.71	
Z14-17-14	3.36162	0.06392	0.22694	0.00316	0.4143	75	1756.8	33.12	1318.5	16.61	
Z14-17-15	2.57161	0.04283	0.14911	0.00197	0.4862	44	2030.4	27.09	896	11.07	
Z14-17-16	6.03026	0.09574	0.34006	0.00442	0.5244	91	2079.5	25	1887	21.25	
Z14-17-17	6.05178	0.09943	0.34448	0.00454	0.5057	92	2063	26.18	1908.2	21.77	
Z14-17-18	4.59104	0.08107	0.2931	0.00397	0.4692	89	1858.2	29.46	1657	19.8	
Z14-17-19	9.49657	0.16825	0.4061	0.00563	0.4716	86	2554	27.46	2197.1	25.81	
Z14-17-20	11.4758	0.21225	0.44937	0.00644	0.4557	89	2700.4	28.6	2392.5	28.65	
Z14-17-21	6.12262	0.08963	0.35906	0.00458	0.5330	98	2010.1	23.47	1977.7	21.72	
Z14-17-22	1.06845	0.01806	0.07294	0.00097	0.4393	26	1736.2	29.43	453.8	5.81	
Z14-17-23	5.76228	0.08316	0.35025	0.00443	0.5407	99	1946.3	23.13	1935.8	21.16	
Z14-17-24	13.09867	0.18558	0.5132	0.0065	0.5574	99	2699.5	20.84	2670.3	27.68	
Z14-17-25	2.44997	0.03652	0.17091	0.00217	0.5202	60	1696.4	24.96	1017.1	11.96	
Z14-17-26	5.14629	0.07865	0.31148	0.00402	0.5102	89	1953.9	24.94	1748	19.75	
Z14-17-28	4.71385	0.06692	0.2745	0.00344	0.5556	77	2022.6	22.36	1563.6	17.4	
Z14-17-29	5.31698	0.11294	0.34883	0.0052	0.3560	107	1808.7	37.94	1929	24.83	
Z14-17-30	9.39319	0.15266	0.48183	0.00644	0.4821	113	2244.5	26.15	2535.2	28.03	
Z14-17-31	6.42373	0.09889	0.37727	0.00487	0.5104	103	2007.5	25	2063.5	22.79	
Z14-17-32	4.55337	0.06844	0.29129	0.00371	0.5193	89	1854.3	24.63	1648	18.5	
Z14-17-33	4.74908	0.07214	0.30146	0.00385	0.5161	91	1868.4	24.93	1698.5	19.06	
Z14-17-34	22.58755	0.35186	0.6469	0.00862	0.5092	100	3205.3	22.64	3216.1	33.74	
Z14-17-35	5.84493	0.09171	0.3412	0.00441	0.4957	94	2018.2	25.59	1892.4	21.2	
Z14-17-36	6.12173	0.09578	0.35917	0.00463	0.4991	98	2009.2	25.47	1978.3	21.96	
Z14-17-38	3.8419	0.05968	0.22608	0.00289	0.4998	66	2004	25.22	1313.9	15.2	
Z14-17-39	3.49256	0.0644	0.23923	0.00326	0.4123	80	1729.9	32.42	1382.7	16.97	
Z14-17-40	5.40413	0.10286	0.32578	0.00457	0.4037	93	1961	32.77	1817.9	22.22	
Z14-17-61	10.92103	0.15899	0.45719	0.00557	0.4617	94	2589.9	23.16	2427.1	24.65	
Z14-17-62	5.85918	0.08439	0.34447	0.00412	0.4666	95	2006.1	24.22	1908.1	19.77	

Z14-17-63	5.7759	0.08559	0.33948	0.00411	0.4539	94	2006.6	25.05	1884.2	19.79
Z14-17-64	5.95391	0.08803	0.35011	0.00424	0.4583	96	2005.8	24.92	1935.1	20.23
Z14-17-65	4.60838	0.07593	0.30922	0.0039	0.4129	98	1768.1	29.21	1736.9	19.19
Z14-17-66	10.11681	0.14708	0.44781	0.00541	0.4760	96	2496.4	23.06	2385.5	24.07
Z14-17-67	5.64647	0.08442	0.32895	0.00399	0.4587	91	2022.3	25.06	1833.3	19.37
Z14-17-68	6.17885	0.09481	0.35786	0.0044	0.4529	97	2032.7	25.8	1972	20.87
Z14-17-69	6.41412	0.10288	0.37023	0.00465	0.4328	100	2038.6	27.17	2030.5	21.86
Z14-17-70	5.80591	0.08717	0.33754	0.00409	0.4640	93	2025.9	24.99	1874.8	19.73
Z14-17-71	12.20481	0.18038	0.48896	0.0059	0.4777	96	2662.9	22.86	2566.2	25.54
Z14-17-72	7.90144	0.1194	0.37677	0.00458	0.4701	87	2370.2	24.15	2061.2	21.46
Z14-17-73	5.87749	0.09191	0.34324	0.00423	0.4531	94	2017.8	26.17	1902.3	20.28
Z14-17-74	5.1052	0.08231	0.29851	0.00372	0.4436	84	2015.6	27.14	1683.9	18.48
Z14-17-75	5.73206	0.08957	0.33299	0.00409	0.4636	91	2027.1	25.93	1852.9	19.76
Z14-17-76	5.10185	0.0833	0.32414	0.00405	0.4404	97	1867	27.85	1809.9	19.71
Z14-17-77	6.24251	0.10484	0.35647	0.00452	0.4284	96	2057.4	28.15	1965.4	21.5
Z14-17-78	4.72693	0.07777	0.27562	0.00345	0.4411	78	2020.4	27.52	1569.3	17.42
Z14-17-79	6.16851	0.10073	0.36029	0.00448	0.4489	98	2017.4	27.15	1983.6	21.24
Z14-17-80	5.56427	0.09765	0.33586	0.00433	0.4174	95	1958.9	29.79	1866.7	20.87
Z14-17-81	4.58495	0.07906	0.3051	0.00392	0.3873	96	1783.9	30.87	1716.6	19.36
Z14-17-82	5.80971	0.0844	0.33137	0.00398	0.4636	90	2060.2	24.3	1845	19.26
Z14-17-83	5.78078	0.08534	0.34719	0.00419	0.4584	98	1968.6	25	1921.2	20.05
Z14-17-84	6.91857	0.09821	0.37515	0.00446	0.4799	96	2148.9	23.29	2053.6	20.91
Z14-17-85	4.93685	0.07334	0.29151	0.00353	0.4574	83	1998.7	25.08	1649.1	17.6
Z14-17-86	5.94406	0.09218	0.34476	0.00426	0.4367	94	2030.4	26.3	1909.5	20.41
Z14-17-87	5.08446	0.08607	0.2958	0.0038	0.3989	82	2025	29.27	1670.4	18.92
Z14-17-88	4.53098	0.06602	0.26492	0.00317	0.4686	75	2016	24.33	1515	16.17
Z14-17-89	6.3108	0.09444	0.36152	0.00438	0.4592	97	2052.2	24.98	1989.4	20.75
Z14-17-90	6.11942	0.09445	0.35229	0.00433	0.4459	95	2043.4	25.95	1945.5	20.64
Z14-17-91	5.65086	0.08545	0.34684	0.00421	0.4609	99	1929.4	25.57	1919.5	20.15
Z14-17-92	6.07562	0.09444	0.34575	0.00426	0.4473	93	2063.7	26.04	1914.3	20.38
Z14-17-93	3.97237	0.05924	0.23037	0.00277	0.4651	66	2030.3	24.77	1336.4	14.53
Z14-17-94	1.29343	0.01991	0.06343	0.00077	0.4472	17	2322.1	25.07	396.5	4.7
Z14-17-95	5.38238	0.08536	0.31284	0.00387	0.4405	87	2026.2	26.69	1754.6	19

Z14-17-96	6.47855	0.11757	0.36272	0.00483	0.3849	95	2092.2	31.14	1995.1	22.85
Z14-17-97	5.0429	0.07918	0.32268	0.00395	0.4531	97	1854.2	26.76	1802.8	19.26
Z14-17-98	5.65742	0.09561	0.32972	0.00419	0.4155	91	2021.2	28.77	1837	20.33
Z14-17-99	6.47995	0.10764	0.37354	0.0047	0.4285	100	2040.7	27.98	2046	22.08

Z14-01

	Isotope ratios and 1σ error (absolute)						Calculated age in Ma and 1σ error (absolute)			
Analysis	Pb^{207}/U^{235}		Pb^{206}/U^{238}		ρ*	Concordance (%)	Pb^{207}/Pb^{206}		Pb^{206}/U^{238}	
Z14-01-01	6.11097	0.10833	0.35427	0.0047	0.4542	96	2029.6	29.19	1955	22.39
Z14-01-02	3.26148	0.07397	0.22181	0.00331	0.3339	74	1742.2	40.75	1291.4	17.45
Z14-01-03	6.29152	0.11651	0.36777	0.00499	0.4341	100	2015	30.87	2018.9	23.51
Z14-01-04	5.79152	0.10539	0.33324	0.00447	0.4450	91	2043	30.03	1854.1	21.62
Z14-01-05	4.14612	0.0761	0.23737	0.00319	0.4373	67	2051.9	30.32	1373	16.63
Z14-01-06	6.45623	0.12991	0.36824	0.00523	0.4009	98	2058.6	33.94	2021.1	24.62
Z14-01-07	5.75058	0.11123	0.31499	0.00436	0.4168	83	2129.7	32.04	1765.2	21.36
Z14-01-08	5.91694	0.1104	0.3433	0.00464	0.4381	94	2028.5	30.87	1902.5	22.24
Z14-01-09	4.38039	0.08182	0.26349	0.00355	0.4394	77	1964.4	31.09	1507.7	18.11
Z14-01-10	6.38868	0.12286	0.37559	0.00514	0.4263	103	2005.2	32.06	2055.7	24.07
Z14-01-100	4.51936	0.0938	0.26468	0.00343	0.3060	75	2012.1	36.5	1513.8	17.5
Z14-01-101	5.91022	0.10088	0.3422	0.0041	0.3108	93	2034.5	30.76	1897.3	19.7
Z14-01-102	5.54746	0.09275	0.33656	0.00409	0.3490	96	1949.8	29.84	1870.1	19.73
Z14-01-103	3.65229	0.05279	0.24154	0.00275	0.3904	78	1794.6	26.14	1394.7	14.29
Z14-01-104	6.72404	0.10742	0.36182	0.00432	0.3511	92	2161.9	28	1990.8	20.47
Z14-01-105	5.33081	0.08387	0.30658	0.00354	0.3632	84	2044.8	27.68	1723.9	17.46
Z14-01-106	5.09396	0.08377	0.30185	0.00364	0.3689	85	1991.9	28.89	1700.5	18.04
Z14-01-107	5.89342	0.09149	0.34213	0.00402	0.3785	94	2028.4	27.21	1896.9	19.31
Z14-01-108	4.87104	0.08265	0.28377	0.00337	0.3114	80	2022.7	30.54	1610.3	16.94
Z14-01-109	5.85935	0.09416	0.33923	0.00403	0.3653	93	2033.1	28.2	1883	19.38
Z14-01-11	4.58057	0.08851	0.29591	0.00404	0.4226	91	1836.2	32.85	1671	20.09
Z14-01-110	6.17461	0.09672	0.35966	0.0042	0.3734	98	2022.4	27.49	1980.5	19.92
Z14-01-111	5.64266	0.09296	0.34316	0.00397	0.3261	98	1946	29.72	1901.9	19.03
Z14-01-112	5.90771	0.1068	0.34679	0.00429	0.3247	96	2008.2	32.09	1919.2	20.56
Z14-01-113	6.12586	0.09535	0.35389	0.00411	0.3624	96	2036.9	27.48	1953.2	19.58

Z14-01-114	5.8179	0.09725	0.34812	0.00421	0.3387	98	1974.5	29.91	1925.6	20.12
Z14-01-115	2.56129	0.06686	0.17574	0.00252	0.1873	60	1727.4	49.29	1043.7	13.82
Z14-01-116	7.73996	0.1529	0.39777	0.00516	0.3054	96	2241.4	34.3	2158.8	23.82
Z14-01-117	3.77637	0.06747	0.22434	0.00272	0.3200	66	1987.2	31.76	1304.7	14.32
Z14-01-118	6.14994	0.12443	0.35541	0.00438	0.2522	96	2036.5	36.48	1960.4	20.82
Z14-01-119	6.20745	0.11452	0.35668	0.00435	0.2902	96	2046.2	33.07	1966.4	20.68
Z14-01-12	2.94004	0.05795	0.18444	0.00254	0.4159	58	1889.2	33.46	1091.2	13.81
Z14-01-120	6.23401	0.12803	0.3587	0.00443	0.2482	97	2044.1	36.93	1976	21.04
Z14-01-121	4.96749	0.08797	0.2984	0.00348	0.2778	86	1967.6	32.35	1683.4	17.27
Z14-01-122	5.13668	0.08645	0.30732	0.00356	0.2940	87	1974.9	30.62	1727.5	17.53
Z14-01-123	5.76676	0.08707	0.3384	0.00379	0.3469	93	2009.7	27.06	1879	18.23
Z14-01-124	5.67571	0.09289	0.33032	0.00388	0.3526	91	2024.5	28.86	1839.9	18.8
Z14-01-125	5.74916	0.09376	0.33338	0.00381	0.3373	91	2031.2	28.82	1854.7	18.41
Z14-01-126	15.56403	0.25165	0.51158	0.00604	0.3376	89	2986	26.32	2663.4	25.77
Z14-01-127	6.85713	0.12384	0.37378	0.00463	0.3154	96	2140.2	31.8	2047.1	21.75
Z14-01-128	6.70265	0.1263	0.359	0.00458	0.2995	91	2170.6	33.36	1977.4	21.74
Z14-01-129	5.60943	0.09733	0.32136	0.00382	0.3139	88	2051.8	30.91	1796.3	18.65
Z14-01-13	6.25219	0.13131	0.36604	0.00524	0.3861	100	2012.7	35.6	2010.7	24.72
Z14-01-130	4.97577	0.07872	0.31442	0.00364	0.3634	94	1877.2	28.36	1762.4	17.88
Z14-01-131	6.23635	0.13083	0.35005	0.00447	0.2863	93	2087.1	36.81	1934.8	21.33
Z14-01-132	5.63998	0.12262	0.32303	0.0043	0.2975	88	2053.3	38.11	1804.5	20.96
Z14-01-133	3.12942	0.06251	0.20174	0.00252	0.3048	64	1841.7	35.91	1184.7	13.54
Z14-01-134	5.07402	0.09237	0.30143	0.00371	0.3404	85	1987.7	32.01	1698.4	18.36
Z14-01-135	5.63914	0.10799	0.34542	0.00435	0.3210	99	1933	34.03	1912.7	20.82
Z14-01-136	5.80696	0.14329	0.34821	0.00515	0.2575	98	1970.9	44.33	1926.1	24.65
Z14-01-137	6.22026	0.10824	0.36001	0.00432	0.3590	97	2033.8	30.16	1982.2	20.5
Z14-01-138	4.38052	0.08944	0.29449	0.00367	0.2927	94	1764.4	37.07	1663.9	18.29
Z14-01-139	5.09715	0.09589	0.2923	0.00359	0.3456	81	2050	32.46	1653	17.9
Z14-01-14	5.3626	0.11528	0.33144	0.00478	0.3776	96	1916.1	36.96	1845.4	23.14
Z14-01-140	6.31646	0.12749	0.36391	0.00449	0.3065	98	2041.6	35.18	2000.7	21.2
Z14-01-15	4.43053	0.12434	0.29357	0.00496	0.2801	93	1790.3	50.95	1659.3	24.71
Z14-01-16	5.95982	0.12168	0.34324	0.00478	0.4085	93	2041.9	34.06	1902.3	22.93
Z14-01-17	3.92886	0.08379	0.24978	0.00355	0.3835	77	1865.4	36.67	1437.4	18.3

Z14-01-18	5.60258	0.11528	0.32039	0.00445	0.4039	87	2054.5	34.2	1791.6	21.71
Z14-01-19	6.80222	0.14533	0.37149	0.00527	0.3880	95	2135.4	35.46	2036.4	24.79
Z14-01-20	8.77825	0.18934	0.41182	0.00588	0.3865	93	2397.5	34.84	2223.3	26.85
Z14-01-21	6.22366	0.09186	0.36029	0.00456	0.5308	98	2033.2	23.54	1983.6	21.63
Z14-01-22	6.16473	0.09795	0.35433	0.00461	0.5004	96	2045.9	25.73	1955.3	21.92
Z14-01-23	5.78785	0.09046	0.33814	0.00438	0.4988	93	2017.1	25.48	1877.7	21.11
Z14-01-24	6.19697	0.11031	0.35884	0.00473	0.4177	97	2032.5	30.11	1976.7	22.44
Z14-01-25	6.17684	0.0948	0.35458	0.00459	0.5152	96	2048	24.65	1956.4	21.82
Z14-01-26	5.75714	0.08927	0.34393	0.00446	0.5113	96	1977.3	25.18	1905.5	21.37
Z14-01-27	6.08127	0.09737	0.34629	0.00447	0.4964	93	2062.3	25.82	1916.9	21.41
Z14-01-28	6.14637	0.10663	0.35734	0.00475	0.4505	97	2025.7	28.76	1969.5	22.56
Z14-01-29	1.27347	0.02335	0.11371	0.0015	0.4054	57	1227.6	34.33	694.2	8.71
Z14-01-30	5.82391	0.09843	0.33325	0.00437	0.4708	90	2053.7	27.65	1854.1	21.11
Z14-01-31	4.08753	0.06744	0.25072	0.00323	0.4676	75	1930.2	27.46	1442.2	16.66
Z14-01-32	6.11351	0.10996	0.34314	0.00459	0.4475	91	2087.7	29.53	1901.8	22.04
Z14-01-33	5.85796	0.10222	0.34791	0.00464	0.4488	97	1987.8	29.13	1924.6	22.18
Z14-01-34	6.95987	0.11906	0.37767	0.00502	0.4736	96	2146.7	27.59	2065.4	23.5
Z14-01-35	6.16578	0.10605	0.34792	0.00459	0.4586	93	2078.4	28.26	1924.7	21.93
Z14-01-36	4.76043	0.09022	0.27652	0.00371	0.3876	78	2027.4	32.36	1573.8	18.73
Z14-01-37	1.27324	0.0308	0.09341	0.00137	0.3115	36	1603.2	44.21	575.7	8.07
Z14-01-38	5.90579	0.10939	0.34441	0.00454	0.4004	94	2020.3	31.42	1907.8	21.75
Z14-01-39	6.0377	0.09979	0.3505	0.00455	0.4848	96	2028.2	26.88	1937	21.7
Z14-01-40	4.55301	0.09323	0.27453	0.0038	0.3930	80	1960.7	34.75	1563.8	19.23
Z14-01-41	5.29057	0.08558	0.3043	0.00379	0.4168	84	2045	27.6	1712.6	18.71
Z14-01-42	4.69149	0.07429	0.27777	0.00348	0.4596	79	1994	26.47	1580.1	17.57
Z14-01-43	8.59038	0.12478	0.35769	0.0044	0.4874	76	2598.8	22.69	1971.2	20.91
Z14-01-44	6.19848	0.09844	0.35977	0.00454	0.4504	98	2029.2	26.62	1981.1	21.52
Z14-01-45	4.94686	0.07868	0.29637	0.00368	0.4335	85	1972.5	27.18	1673.3	18.28
Z14-01-46	2.21311	0.03974	0.16296	0.00208	0.3628	61	1596.6	32.91	973.2	11.51
Z14-01-47	4.66962	0.07862	0.27911	0.00349	0.3998	80	1976.6	29.11	1586.9	17.6
Z14-01-48	4.64672	0.0739	0.27875	0.00343	0.4288	80	1970.1	27.16	1585.1	17.31
Z14-01-49	4.81054	0.08257	0.28482	0.00362	0.4104	81	1993.7	29.25	1615.6	18.14
Z14-01-50	2.23244	0.03582	0.15736	0.00195	0.4334	56	1677.4	28.19	942.1	10.86

Z14-01-51	4.77946	0.08696	0.3076	0.00408	0.3983	94	1844.1	31.84	1728.9	20.09
Z14-01-52	6.18973	0.10725	0.35837	0.00463	0.4223	97	2033.4	29.22	1974.5	21.98
Z14-01-53	5.78858	0.11153	0.33803	0.00456	0.3877	93	2018.1	32.9	1877.2	21.95
Z14-01-54	9.64813	0.1609	0.4064	0.00516	0.4311	85	2579.5	26.5	2198.5	23.66
Z14-01-55	5.17113	0.08918	0.32854	0.00418	0.4021	98	1866.9	30.09	1831.3	20.28
Z14-01-56	5.18331	0.11204	0.30799	0.00438	0.3405	87	1987.7	37.7	1730.8	21.57
Z14-01-57	5.96225	0.11826	0.34937	0.00471	0.3430	96	2011.6	34.74	1931.6	22.51
Z14-01-58	6.17163	0.10189	0.35436	0.00448	0.4294	95	2047.6	27.79	1955.4	21.3
Z14-01-59	6.20036	0.12771	0.36233	0.00478	0.3180	99	2016.2	36.17	1993.2	22.62
Z14-01-60	8.01605	0.14544	0.40916	0.00545	0.3924	98	2253.1	30.44	2211.1	24.94
Z14-01-61	6.16939	0.09091	0.35393	0.00416	0.4276	95	2049.2	25.19	1953.3	19.81
Z14-01-62	3.18821	0.04757	0.16916	0.002	0.4207	46	2186.1	25.27	1007.5	11.05
Z14-01-63	6.18496	0.0953	0.35477	0.00429	0.4371	95	2050.3	26.07	1957.3	20.41
Z14-01-64	5.39933	0.08096	0.31892	0.00374	0.4195	89	1997.4	25.79	1784.5	18.3
Z14-01-65	4.66915	0.06578	0.28196	0.0033	0.4658	82	1958.2	23.83	1601.2	16.58
Z14-01-66	6.07149	0.08733	0.34903	0.00412	0.4598	94	2045.7	24.2	1930	19.68
Z14-01-67	6.23855	0.09808	0.35931	0.00434	0.4101	97	2042	27.01	1978.9	20.6
Z14-01-68	4.47318	0.07206	0.2754	0.00333	0.4158	82	1924	27.72	1568.2	16.85
Z14-01-69	21.99294	0.33528	0.60764	0.00739	0.4335	94	3261.9	23.13	3060.6	29.65
Z14-01-70	12.60202	0.2218	0.49863	0.00657	0.3857	97	2683.6	28.6	2607.9	28.24
Z14-01-71	4.32975	0.07498	0.28247	0.00358	0.3842	88	1819.3	30.64	1603.8	17.99
Z14-01-72	6.21839	0.10622	0.35723	0.00443	0.3865	96	2046.8	29.4	1969	21.02
Z14-01-73	6.06277	0.10079	0.35264	0.0044	0.4093	96	2025.1	28.46	1947.2	20.97
Z14-01-74	6.05498	0.09111	0.35131	0.00418	0.4487	96	2029	25.3	1940.9	19.94
Z14-01-75	5.51317	0.0941	0.31738	0.00393	0.3949	87	2043.1	29.15	1776.9	19.23
Z14-01-76	5.57037	0.09454	0.33381	0.00413	0.4005	94	1971.9	29.19	1856.8	19.95
Z14-01-77	5.81611	0.10354	0.33893	0.00429	0.3845	93	2021.5	30.64	1881.5	20.65
Z14-01-78	6.92878	0.14487	0.38237	0.00495	0.3080	99	2116.8	36.26	2087.3	23.07
Z14-01-79	5.77879	0.09703	0.34788	0.00432	0.4047	98	1963.3	28.86	1924.5	20.66
Z14-01-80	6.22701	0.10927	0.34598	0.00429	0.3841	91	2105	29.8	1915.4	20.53
Z14-01-81	4.92189	0.07632	0.31377	0.00366	0.3709	95	1859.4	27.92	1759.2	17.98
Z14-01-82	6.18137	0.08565	0.36111	0.00409	0.4295	99	2015.9	24.02	1987.4	19.38
Z14-01-83	6.13795	0.08774	0.35202	0.00405	0.4277	95	2048.8	24.51	1944.3	19.3

Z14-01-84	5.66115	0.07585	0.30944	0.00349	0.4521	81	2133.3	22.6	1738	17.17
Z14-01-85	2.43639	0.0361	0.16914	0.00194	0.3933	59	1704.4	26.9	1007.4	10.71
Z14-01-86	25.13351	0.37701	0.64532	0.00748	0.3940	95	3375.9	23.05	3209.9	29.29
Z14-01-87	5.27668	0.07936	0.31074	0.00365	0.4192	87	2002.3	25.87	1744.4	17.95
Z14-01-88	3.4985	0.05416	0.22271	0.00264	0.4001	70	1862.7	27.34	1296.2	13.91
Z14-01-89	4.9246	0.06919	0.29453	0.00336	0.4370	84	1974.6	24.13	1664.2	16.75
Z14-01-90	3.92557	0.06559	0.26903	0.00326	0.3846	89	1728.9	29.91	1535.9	16.56
Z14-01-91	2.08348	0.04007	0.1442	0.00185	0.3227	51	1710.9	35.26	868.4	10.4
Z14-01-92	3.36178	0.05181	0.17693	0.00208	0.3958	48	2199.5	26.27	1050.2	11.39
Z14-01-93	6.09247	0.09254	0.32373	0.00376	0.4029	83	2182.9	25.75	1807.9	18.3
Z14-01-94	5.66672	0.10654	0.34817	0.00443	0.3379	100	1926.8	33.36	1925.8	21.19
Z14-01-95	5.70935	0.09241	0.3362	0.00399	0.3824	93	2002.4	28.18	1868.4	19.24
Z14-01-96	4.80367	0.08829	0.28474	0.00349	0.3390	81	1990.4	32.18	1615.2	17.5
Z14-01-97	5.69858	0.11664	0.34232	0.00445	0.2925	96	1966.9	36.58	1897.8	21.35
Z14-01-98	5.41908	0.0874	0.31944	0.00384	0.3958	89	2000.8	27.83	1787	18.75
Z14-01-99	5.97148	0.10769	0.3507	0.00433	0.3470	97	2007.3	31.54	1937.9	20.67

Z14-02

	Isotope ratios and 1σ error (absolute)						Calculated age in Ma and 1σ error (absolute)			
Analysis	Pb^{207}/U^{235}		Pb^{206}/U^{238}		ρ*	Concordance (%)	Pb^{207}/Pb^{206}		Pb^{206}/U^{238}	
Z14-02-01	6.32955	0.1005	0.34853	0.00451	0.4826	91	2121.6	25.77	1927.6	21.56
Z14-02-02	5.68745	0.09712	0.32681	0.00433	0.4554	89	2046.5	28.32	1822.9	21.03
Z14-02-04	5.65549	0.0975	0.28904	0.00381	0.4487	73	2251.3	27.94	1636.7	19.06
Z14-02-05	4.64094	0.07251	0.19184	0.00245	0.4956	43	2611	23.88	1131.3	13.25
Z14-02-06	6.28262	0.11312	0.35275	0.00478	0.4411	93	2087.3	29.8	1947.7	22.8
Z14-02-07	5.72974	0.10406	0.32213	0.00438	0.4266	86	2085	30.32	1800.1	21.35
Z14-02-08	5.97217	0.09549	0.33314	0.00428	0.4937	88	2098.9	25.7	1853.6	20.69
Z14-02-09	4.29051	0.08039	0.24105	0.0033	0.4150	67	2086.2	31.36	1392.1	17.15
Z14-02-10	2.84572	0.05038	0.16443	0.00221	0.4446	48	2036.5	29.37	981.4	12.22
Z14-02-11	4.54346	0.08381	0.25925	0.00357	0.4592	72	2059.1	30.05	1486	18.25
Z14-02-12	5.84628	0.11223	0.32457	0.00438	0.4011	86	2107.4	32.17	1812	21.32
Z14-02-13	2.67168	0.04886	0.09024	0.00123	0.4580	19	2942.1	27.31	557	7.29
Z14-02-14	4.86161	0.09667	0.21299	0.00291	0.3885	50	2513.9	31.99	1244.7	15.46

Z14-02-15	5.71779	0.10928	0.32215	0.00438	0.4230	87	2080.9	31.62	1800.2	21.37
Z14-02-16	5.03808	0.09237	0.29366	0.00392	0.4354	82	2021	30.52	1659.8	19.56
Z14-02-17	7.12069	0.12482	0.37546	0.00493	0.4662	94	2197	28.07	2055	23.11
Z14-02-18	13.28407	0.23974	0.51406	0.0069	0.4502	98	2720	27.65	2673.9	29.38
Z14-02-19	6.26343	0.11587	0.35695	0.00479	0.4393	95	2060.8	30.42	1967.7	22.76
Z14-02-20	4.52207	0.09772	0.25338	0.00358	0.3740	70	2090.6	36.33	1455.9	18.4
Z14-02-21	4.46114	0.08993	0.2646	0.00368	0.3712	76	1989.7	34.86	1513.3	18.76
Z14-02-22	6.49192	0.14	0.36898	0.00537	0.3492	98	2065.3	37.24	2024.6	25.28
Z14-02-23	4.13462	0.07782	0.25513	0.00337	0.4091	76	1919.2	32.05	1464.9	17.32
Z14-02-24	11.7936	0.23149	0.46353	0.00632	0.3951	91	2694.1	31.03	2455.1	27.82
Z14-02-25	5.85477	0.12041	0.35378	0.00487	0.3756	100	1956.7	35.29	1952.6	23.18
Z14-02-26	5.39323	0.10928	0.19154	0.0026	0.3840	39	2860.3	31.55	1129.7	14.06
Z14-02-27	5.75642	0.12215	0.27199	0.00377	0.3671	65	2385.4	34.77	1550.9	19.11
Z14-02-28	5.50741	0.12155	0.29778	0.00419	0.3558	78	2153	37.18	1680.3	20.83

Z14-05

	Isotope ratios and 1σ error (absolute)						Calculated age in Ma and 1σ error (absolute)			
Analysis	Pb^{207}/U^{235}		Pb^{206}/U^{238}		ρ*	Concordance (%)	Pb^{207}/Pb^{206}		Pb^{206}/U^{238}	
Z14-05-01	1.62952	0.02873	0.15393	0.00174	0.2550	83	1116.4	36.22	923	9.72
Z14-05-02	1.81817	0.03264	0.16982	0.00194	0.2544	89	1138.8	36.66	1011.1	10.71
Z14-05-03	1.45538	0.02471	0.11622	0.00131	0.2749	49	1443.6	33.23	708.8	7.59
Z14-05-04	1.58679	0.03251	0.15505	0.00188	0.2294	89	1048.3	42.3	929.2	10.49
Z14-05-05	1.65485	0.02516	0.15747	0.0017	0.3295	86	1101.4	30.64	942.7	9.48
Z14-05-06	1.58639	0.03984	0.15653	0.00211	0.1926	91	1028.3	51.96	937.5	11.75
Z14-05-07	1.26174	0.03217	0.12498	0.00169	0.1904	74	1020.5	52.79	759.2	9.68
Z14-05-08	1.615	0.04733	0.15525	0.0023	0.1627	86	1080.7	60.1	930.3	12.83
Z14-05-09	1.66624	0.03597	0.15914	0.00201	0.2392	87	1093.7	43.82	952	11.17
Z14-05-10	1.24362	0.02488	0.12395	0.0015	0.2748	75	1007.7	40.83	753.3	8.62
Z14-05-100	1.9953	0.0342	0.17551	0.0021	0.3730	83	1257.2	32.59	1042.4	11.53
Z14-05-101	0.95237	0.02043	0.10194	0.00129	0.2509	73	859.9	44.96	625.8	7.57
Z14-05-102	0.84804	0.01617	0.09752	0.00118	0.2933	85	709.4	40.5	599.9	6.92
Z14-05-103	1.17458	0.03973	0.1236	0.002	0.1477	84	895.3	71.07	751.2	11.45
Z14-05-104	1.65182	0.02852	0.1597	0.00189	0.3479	89	1067.8	34.24	955.1	10.49

Z14-05-105	1.70049	0.03248	0.16544	0.00203	0.3137	94	1055	38.53	986.9	11.24	
Z14-05-106	1.68963	0.03332	0.1656	0.00206	0.3029	95	1040.4	39.6	987.8	11.4	
Z14-05-107	1.64665	0.03203	0.16201	0.00201	0.3114	94	1032.8	38.97	967.9	11.14	
Z14-05-108	1.5195	0.03034	0.15448	0.00193	0.3059	96	966.2	40.4	926	10.8	
Z14-05-109	1.48533	0.0295	0.14476	0.00181	0.3120	83	1051.9	39.58	871.5	10.21	
Z14-05-11	1.55177	0.03552	0.15265	0.00198	0.2388	89	1034.2	46.7	915.8	11.08	
Z14-05-110	1.6301	0.03214	0.16066	0.00201	0.3177	93	1029.3	39.26	960.5	11.15	
Z14-05-111	1.70208	0.03404	0.16804	0.00212	0.3248	98	1026	39.79	1001.3	11.68	
Z14-05-112	1.62412	0.03219	0.16043	0.00201	0.3321	94	1025	39.3	959.2	11.19	
Z14-05-113	1.55349	0.02924	0.12117	0.0015	0.3544	50	1486.9	34.77	737.3	8.6	
Z14-05-114	1.67918	0.03385	0.16531	0.00209	0.3293	96	1031.9	39.75	986.2	11.58	
Z14-05-115	1.60512	0.03296	0.15575	0.00199	0.3263	88	1061.2	40.3	933.1	11.1	
Z14-05-116	1.65979	0.03449	0.16306	0.00209	0.3333	94	1036.4	40.84	973.7	11.61	
Z14-05-117	1.00039	0.05092	0.10288	0.00228	0.1056	67	943.3	105.64	631.3	13.33	
Z14-05-118	1.60845	0.03619	0.15933	0.00212	0.3133	93	1019.8	44.48	953	11.79	
Z14-05-119	1.63257	0.03673	0.16124	0.00215	0.3187	94	1025.8	44.3	963.7	11.93	
Z14-05-12	1.47386	0.03231	0.14694	0.00187	0.2519	88	1007.1	44.68	883.8	10.5	
Z14-05-120	1.66698	0.03618	0.16424	0.00216	0.3414	95	1030.9	42.32	980.3	11.94	
Z14-05-121	1.56598	0.03475	0.15902	0.00207	0.2443	98	969.9	45.96	951.3	11.49	
Z14-05-122	1.66875	0.03511	0.16194	0.00208	0.2553	91	1061.7	42.9	967.6	11.52	
Z14-05-123	1.55903	0.03021	0.15246	0.00189	0.2840	87	1046.2	39.34	914.7	10.56	
Z14-05-124	1.61758	0.03367	0.16132	0.00206	0.2674	96	1006.5	42.57	964.1	11.41	
Z14-05-125	4.526	0.08107	0.27525	0.00348	0.3304	81	1945.3	32.16	1567.4	17.6	
Z14-05-126	5.54175	0.09455	0.33003	0.00408	0.3609	93	1982.6	30.17	1838.5	19.77	
Z14-05-127	4.87697	0.0795	0.30551	0.00367	0.3810	91	1892.2	28.79	1718.6	18.11	
Z14-05-128	1.08959	0.02223	0.11885	0.0015	0.2934	88	822	42.45	724	8.64	
Z14-05-129	1.63627	0.03204	0.16188	0.00204	0.3171	95	1022.7	39.3	967.2	11.3	
Z14-05-13	1.69806	0.03616	0.16383	0.00207	0.2763	91	1073.2	42.75	978	11.47	
Z14-05-130	1.13648	0.02061	0.11784	0.00144	0.3469	77	926.9	36.48	718.1	8.28	
Z14-05-131	1.48546	0.03116	0.14945	0.00193	0.2997	91	988.6	42.31	897.9	10.84	
Z14-05-132	0.80611	0.01524	0.09311	0.00115	0.3488	82	701.5	39.24	573.9	6.78	
Z14-05-133	1.6529	0.03289	0.16788	0.00214	0.3323	103	969.3	39.71	1000.4	11.79	
Z14-05-14	1.84516	0.04318	0.16183	0.00217	0.2455	77	1262	45.9	967	12.07	

Z14-05-15	1.55026	0.02959	0.14904	0.0018	0.3272	83	1080.2	37.54	895.6	10.12
Z14-05-16	1.25719	0.02955	0.12419	0.00165	0.2576	74	1025.6	47.39	754.6	9.45
Z14-05-17	1.64086	0.03349	0.15972	0.002	0.3182	91	1055	40.45	955.2	11.11
Z14-05-18	0.96214	0.02006	0.10922	0.00137	0.3281	91	738	42.91	668.2	7.94
Z14-05-19	1.68172	0.03622	0.16273	0.0021	0.3245	91	1067.2	42.16	971.9	11.63
Z14-05-20	1.08251	0.02408	0.11664	0.00151	0.3107	84	847.4	44.93	711.2	8.73
Z14-05-21	1.53399	0.02493	0.14908	0.0017	0.3196	85	1059.8	33.11	895.8	9.56
Z14-05-22	1.74307	0.02357	0.16255	0.00177	0.3935	85	1142.4	26.76	971	9.79
Z14-05-23	1.19679	0.01579	0.12292	0.00133	0.4130	79	947.6	26.73	747.3	7.61
Z14-05-24	1.55492	0.02511	0.15426	0.00177	0.3328	91	1018.2	32.9	924.8	9.87
Z14-05-25	1.57603	0.02272	0.15486	0.00172	0.3788	89	1037.6	28.95	928.1	9.59
Z14-05-26	1.39377	0.01909	0.14017	0.00154	0.4116	85	990.4	27.46	845.6	8.68
Z14-05-27	1.53426	0.02496	0.15173	0.00175	0.3352	89	1024.5	32.65	910.6	9.79
Z14-05-28	1.44062	0.02379	0.14397	0.00167	0.3384	86	1003.3	33.51	867.1	9.4
Z14-05-29	1.40366	0.02047	0.14005	0.00157	0.3973	84	1006.4	29.14	845	8.86
Z14-05-30	4.38858	0.06232	0.28097	0.00317	0.4124	86	1853.7	25.19	1596.2	15.93
Z14-05-31	1.59771	0.02768	0.1609	0.0019	0.3269	97	987.5	35.06	961.8	10.57
Z14-05-32	1.05895	0.01934	0.11137	0.00134	0.3053	76	898.6	37.66	680.7	7.75
Z14-05-33	1.58395	0.02931	0.15614	0.0019	0.3087	91	1030.8	37.37	935.3	10.59
Z14-05-34	1.3496	0.02311	0.13207	0.00157	0.3468	76	1045.5	34.21	799.7	8.91
Z14-05-35	1.62565	0.03071	0.15869	0.00195	0.3078	90	1050.4	37.94	949.5	10.85
Z14-05-36	1.47985	0.02443	0.1463	0.00172	0.3694	86	1024.7	32.43	880.2	9.66
Z14-05-37	3.34244	0.04935	0.21053	0.0024	0.4240	65	1882.8	25.56	1231.6	12.8
Z14-05-38	1.87398	0.03294	0.16884	0.00204	0.3492	83	1209.8	34.02	1005.7	11.26
Z14-05-39	1.47976	0.02616	0.14926	0.0018	0.3542	91	983.6	35.22	896.8	10.08
Z14-05-41	1.50656	0.02074	0.15101	0.00158	0.3367	91	999.3	28.53	906.6	8.84
Z14-05-42	1.53275	0.02077	0.15023	0.00157	0.3519	86	1044.4	27.75	902.3	8.81
Z14-05-43	1.63553	0.02678	0.16174	0.0018	0.2935	94	1026.3	33.79	966.5	10.01
Z14-05-44	1.03193	0.01746	0.11094	0.00124	0.2806	79	855.1	35.75	678.2	7.21
Z14-05-45	1.41326	0.02247	0.1388	0.00154	0.3189	81	1039.9	32.47	837.9	8.73
Z14-05-46	1.54832	0.02195	0.15159	0.00163	0.3685	87	1046.2	28.51	909.9	9.14
Z14-05-47	0.92578	0.01276	0.10259	0.0011	0.3935	80	791.3	28.55	629.6	6.42
Z14-05-48	1.58303	0.02405	0.15707	0.00174	0.3668	92	1018.9	30.54	940.5	9.7

Z14-05-49	1.39875	0.02274	0.14097	0.0016	0.3382	86	987.3	32.65	850.1	9.05	
Z14-05-50	1.08088	0.02261	0.11875	0.00147	0.2617	89	808.8	44.06	723.4	8.47	
Z14-05-51	1.56451	0.02701	0.15444	0.00181	0.3390	90	1028.9	34.56	925.8	10.08	
Z14-05-52	3.09974	0.04366	0.18938	0.0021	0.4409	58	1938.5	24.12	1118	11.37	
Z14-05-53	1.58932	0.02756	0.15654	0.00185	0.3497	91	1033	34.35	937.5	10.31	
Z14-05-54	1.62036	0.02592	0.1595	0.00184	0.3947	92	1034.1	31.09	954	10.23	
Z14-05-55	1.10753	0.02781	0.11599	0.00157	0.2374	78	907.6	51.76	707.4	9.08	
Z14-05-56	1.72537	0.02858	0.17028	0.002	0.4090	99	1028.5	31.95	1013.7	11.04	
Z14-05-57	1.57192	0.03071	0.15494	0.00194	0.3400	90	1030.9	38.46	928.6	10.83	
Z14-05-58	1.6749	0.03024	0.16757	0.00205	0.3934	100	1000.6	35.02	998.7	11.3	
Z14-05-59	0.86292	0.02435	0.102	0.00146	0.2215	96	652.5	60.23	626.1	8.57	
Z14-05-60	1.76085	0.03273	0.17288	0.00215	0.4020	99	1038.4	35.52	1027.9	11.82	
Z14-05-61	3.03828	0.04372	0.20224	0.00224	0.3415	67	1782.7	26.96	1187.4	11.99	
Z14-05-62	1.67959	0.02499	0.16472	0.0018	0.3305	94	1040.8	30.59	983	9.96	
Z14-05-63	1.31613	0.02298	0.13476	0.00155	0.2758	86	953.2	36.56	815	8.79	
Z14-05-64	1.31211	0.02081	0.13488	0.0015	0.3109	86	945	33.09	815.6	8.52	
Z14-05-65	1.58261	0.02296	0.15547	0.00169	0.3383	90	1037.2	29.69	931.5	9.43	
Z14-05-66	1.59523	0.02796	0.15557	0.0018	0.2753	89	1051.8	36.07	932.1	10.07	
Z14-05-67	1.48089	0.02258	0.14921	0.00165	0.3343	91	985.7	31.43	896.5	9.25	
Z14-05-68	1.14101	0.01616	0.11918	0.00129	0.3599	80	911.9	29.34	725.8	7.42	
Z14-05-69	1.53531	0.02172	0.14957	0.00162	0.3619	85	1053.3	28.97	898.5	9.1	
Z14-05-70	1.35506	0.02847	0.13733	0.00171	0.2317	85	973.5	43.79	829.5	9.68	
Z14-05-71	0.9043	0.01495	0.09975	0.00113	0.3112	77	798.2	35.03	613	6.61	
Z14-05-72	1.14418	0.03178	0.10864	0.00155	0.1640	60	1104.9	57.03	664.9	9.04	
Z14-05-73	1.50606	0.02361	0.14842	0.00167	0.3388	87	1030.1	31.85	892.1	9.36	
Z14-05-74	1.36067	0.02565	0.13512	0.00162	0.2793	81	1014.5	38.77	817	9.19	
Z14-05-75	4.99523	0.07009	0.30309	0.00332	0.3878	88	1948.8	24.87	1706.6	16.44	
Z14-05-76	1.49714	0.02345	0.14885	0.00168	0.3509	88	1012	31.71	894.5	9.4	
Z14-05-77	5.88113	0.09421	0.33554	0.00395	0.3511	91	2058	28.38	1865.2	19.05	
Z14-05-78	1.52104	0.03056	0.15226	0.00188	0.2679	92	997.9	41.31	913.6	10.52	
Z14-05-79	1.51167	0.02402	0.15306	0.00173	0.3528	94	974.6	32.17	918.1	9.7	
Z14-05-81	0.83256	0.01368	0.09626	0.00109	0.3042	84	701.2	35.41	592.5	6.38	
Z14-05-82	1.45728	0.02564	0.14982	0.00175	0.2858	95	946.3	36.58	900	9.82	

Z14-05-83	2.64674	0.03607	0.21753	0.00237	0.3932	91	1389.7	26.01	1268.8	12.56
Z14-05-84	1.30392	0.02114	0.13372	0.00152	0.3226	85	951.3	33.43	809.1	8.66
Z14-05-85	1.48446	0.02713	0.14495	0.00173	0.2792	83	1050.8	37.37	872.6	9.76
Z14-05-86	1.57257	0.02698	0.15386	0.0018	0.3095	88	1046.8	34.9	922.6	10.06
Z14-05-87	1.558	0.02325	0.15591	0.00174	0.3646	93	1001.2	30.15	934	9.73
Z14-05-88	1.20405	0.01809	0.12341	0.00138	0.3646	79	952.4	30.52	750.1	7.94
Z14-05-89	2.58768	0.0372	0.19354	0.00217	0.3947	73	1568.3	26.62	1140.5	11.71
Z14-05-90	0.93534	0.01759	0.1034	0.00124	0.2865	80	795.5	39.66	634.3	7.25
Z14-05-91	1.56666	0.03392	0.14749	0.00192	0.2493	79	1123.8	43.86	886.9	10.78
Z14-05-92	1.36576	0.0257	0.13702	0.00167	0.3027	83	995.7	38.41	827.8	9.45
Z14-05-93	1.03752	0.01814	0.10994	0.0013	0.3226	76	883.5	35.99	672.4	7.54
Z14-05-94	1.36971	0.02404	0.13777	0.00164	0.3350	84	990.4	35.48	832	9.29
Z14-05-95	1.56041	0.02786	0.15578	0.00187	0.3339	93	1005.5	35.98	933.3	10.43
Z14-05-96	1.36378	0.03165	0.13628	0.00182	0.2411	82	1003.4	47.6	823.6	10.33
Z14-05-98	1.3106	0.02403	0.12598	0.00153	0.3248	71	1081.6	36.41	764.9	8.79
Z14-05-99	1.46495	0.02713	0.14887	0.00182	0.3329	92	969.1	37.27	894.6	10.19

* ρ denotes error correlation between ratios used to produce concordia diagram

Table S3. Individual Lu-Hf analytical data.

Sample	Hf^{176}/Hf^{177}	2σ error	Lu^{176}/Hf^{177}	Yb^{176}/Hf^{177}	U/Pb AGE	Hf_i	ε(Hf)	1σ error	T(DM) (Ga)	T(DM) (crustal)
Z14-01-03	0.28144	3.335E-05	0.00133	0.04648	2015	0.281392506	-3.8	1.2	2.55	2.84
Z14-01-11	0.28147	2.332E-05	0.00070	0.02229	1836	0.281449371	-5.9	0.8	2.47	2.83
Z14-01-70	0.28108	3.058E-05	0.00083	0.02789	2683	0.281042358	-0.7	1.1	3.00	3.18
Z14-01-79	0.28138	2.382E-05	0.00074	0.02417	1963	0.281354177	-6.3	0.8	2.60	2.96
Z14-01-81	0.28151	2.599E-05	0.00081	0.02567	1859	0.281482051	-4.2	0.9	2.43	2.75
Z14-01-86	0.28050	2.707E-05	0.00043	0.01355	3375	0.280469425	-4.7	0.9	3.75	3.97
Z14-01-90	0.28173	3.541E-05	0.00146	0.04925	1729	0.281681901	-0.1	1.2	2.16	2.40
Z14-01-94	0.28140	2.621E-05	0.00099	0.03510	1926	0.281360961	-6.9	0.9	2.59	2.97
Z14-01-120	0.28133	2.660E-05	0.00077	0.02682	2044	0.28129812	-6.4	0.9	2.67	3.03
Z14-01-135	0.28140	3.226E-05	0.00123	0.03987	1933	0.28135879	-6.8	1.1	2.60	2.97
Z14-01-14	0.28148	2.350E-05	0.00056	0.01618	1916	0.281459508	-3.7	0.8	2.45	2.76
Z14-01-15	0.28133	2.403E-05	0.00062	0.01960	1790	0.281308104	-11.9	0.8	2.66	3.16
Z14-01-55	0.28153	2.734E-05	0.00042	0.01220	1866	0.2815159	-2.8	1.0	2.37	2.67
Z14-01-60	0.28120	2.850E-05	0.00052	0.01462	2253	0.281176614	-5.9	1.0	2.83	3.16
Z14-01-69	0.28092	4.473E-05	0.00037	0.01137	3261	0.280898112	7.8	1.6	3.19	3.15
Z14-02-16	0.28138	3.356E-05	0.00122	0.04156	2021	0.281335199	-5.7	1.2	2.63	2.96
Z14-02-18	0.28088	2.565E-05	0.00060	0.01921	2720	0.280851583	-6.6	0.9	3.26	3.56
Z14-02-19	0.28142	3.814E-05	0.00158	0.05633	2060	0.281361694	-3.8	1.3	2.60	2.88
Z14-02-22	0.28097	3.708E-05	0.00167	0.05584	2065	0.28090869	-19.8	1.3	3.22	3.83
Z14-02-24	0.28097	3.708E-05	0.00167	0.05584	2694	0.280888264	-5.9	1.3	3.22	3.50
Z14-02-25	0.28142	2.587E-05	0.00103	0.03923	1957	0.281385259	-5.4	0.9	2.56	2.90
Z14-02-28	0.28137	2.872E-05	0.00115	0.03988	2153	0.281323915	-3.0	1.0	2.64	2.91
Z14-05-06	0.28195	1.853E-05	0.00047	0.01568	1028	0.281943639	-6.8	0.6	1.80	2.27
Z14-05-13	0.28199	1.805E-05	0.00052	0.01784	1073	0.281981308	-4.4	0.6	1.75	2.16
Z14-05-24	0.28183	1.670E-05	0.00039	0.01274	1018	0.281818904	-11.4	0.6	1.97	2.54
Z14-05-25	0.28193	2.109E-05	0.00059	0.01919	1037	0.281918241	-7.5	0.7	1.84	2.32
Z14-05-30	0.28158	3.558E-05	0.00101	0.03315	1853	0.281540805	-2.2	1.2	2.35	2.63
Z14-05-31	0.28195	1.612E-05	0.00047	0.01577	987	0.281941095	-7.8	0.6	1.81	2.30
Z14-05-39	0.28188	1.736E-05	0.00053	0.01798	983	0.281865434	-10.6	0.6	1.91	2.46

Z14-05-43	0.28184	2.105E-05	0.00066	0.02146	1026	0.281829629	-10.9	0.7	1.96	2.51
Z14-05-59	0.28196	1.641E-05	0.00053	0.01755	653	0.281949177	-15.0	0.6	1.80	2.49
Z14-05-62	0.28143	1.988E-05	0.00066	0.02153	1040	0.281420207	-25.0	0.7	2.52	3.38
Z14-05-69	0.28191	2.006E-05	0.00124	0.04143	1053	0.281889298	-8.1	0.7	1.89	2.37
Z14-05-77	0.28207	2.028E-05	0.00081	0.02004	2058	0.282035758	20.1	0.7	1.66	1.44
Z14-05-79	0.28178	2.072E-05	0.00062	0.01932	974	0.281770497	-14.1	0.7	2.04	2.67
Z14-05-81	0.28193	1.856E-05	0.00061	0.01991	701	0.281921254	-14.9	0.6	1.84	2.52
Z14-05-83	0.28207	1.833E-05	0.00048	0.01652	1390	0.282054107	5.4	0.6	1.65	1.80
Z14-05-103	0.28226	2.081E-05	0.00048	0.01573	895	0.28225305	1.2	0.7	1.38	1.67
Z14-05-124	0.28227	1.899E-05	0.00076	0.02563	1007	0.282258144	3.9	0.7	1.37	1.59
Z14-05-126	0.28154	2.213E-05	0.00088	0.02765	1982	0.281506413	-0.5	0.8	2.39	2.62
Z14-17-01	0.28104	2.490E-05	0.00042	0.01273	2726	0.28102087	-0.4	0.9	3.03	3.20
Z14-17-24	0.28103	2.940E-05	0.00113	0.03892	2700	0.280973891	-2.7	1.0	3.10	3.32
Z14-17-31	0.28142	2.667E-05	0.00118	0.03777	2008	0.281373947	-4.6	0.9	2.57	2.89
Z14-17-32	0.28152	2.484E-05	0.00092	0.02880	1854	0.281483635	-4.2	0.9	2.43	2.75
Z14-17-34	0.28069	2.717E-05	0.00083	0.02674	3205	0.280636672	-2.8	1.0	3.54	3.72
Z14-17-61	0.28111	2.863E-05	0.00088	0.02773	2590	0.281061648	-2.2	1.0	2.98	3.20
Z14-17-66	0.28139	2.777E-05	0.00133	0.04334	2496	0.281331122	5.2	1.0	2.62	2.69
Z14-17-69	0.28141	2.569E-05	0.00081	0.02546	2039	0.281382935	-3.5	0.9	2.56	2.85
Z14-17-71	0.28097	2.319E-05	0.00056	0.01717	2663	0.280946422	-4.5	0.8	3.13	3.40
Z14-17-99	0.28135	2.656E-05	0.00087	0.03028	2041	0.281314924	-5.9	0.9	2.65	2.99
Z14-17-101	0.28158	2.919E-05	0.00085	0.02619	1886	0.281550318	-1.1	1.0	2.33	2.59
Z14-17-103	0.28163	3.040E-05	0.00079	0.02372	1842	0.281602697	-0.3	1.1	2.26	2.50
Z14-17-113	0.28138	3.047E-05	0.00117	0.03653	2024	0.281333757	-5.6	1.1	2.63	2.96
Z14-17-116	0.28137	2.857E-05	0.00100	0.03117	2015	0.281332555	-5.9	1.0	2.63	2.97
Z14-17-120	0.28137	2.193E-05	0.00063	0.02093	2013	0.281345901	-5.5	0.8	2.60	2.95
MA6_04	0.28146	1.806E-05	0.00058	0.02133	1969	0.281440505	-3.1	0.6	2.48	2.77
MA6_06	0.28159	2.351E-05	0.00073	0.02776	1841	0.28156512	-1.6	0.8	2.31	2.58
MA6_38	0.28119	3.142E-05	0.00135	0.04743	2928.3	0.281114583	7.7	1.1	2.90	2.89
MA6_44	0.28143	1.915E-05	0.00062	0.02369	1994.3	0.281411387	-3.6	0.7	2.52	2.82
MA6_45	0.28172	1.661E-05	0.00079	0.03159	1571.6	0.281693458	-3.3	0.6	2.14	2.47

MA6_47	0.28151	1.640E-05	0.00087	0.03313	1862.8	0.281481415	-4.1	0.6	2.43	2.75
MA6_51	0.28156	2.437E-05	0.00078	0.02959	1854.6	0.281537144	-2.3	0.9	2.35	2.63
MA6_54	0.28151	1.065E-04	0.00281	0.11947	1886.1	0.281412479	-6.0	3.7	2.55	2.88
MA6_55	0.28091	2.249E-05	0.00143	0.06118	2944.4	0.28082492	-2.3	0.8	3.30	3.48
MA6_56	0.28155	2.365E-05	0.00117	0.04512	1883.1	0.281509732	-2.6	0.8	2.39	2.68
MA6_58	0.28149	1.901E-05	0.00064	0.02376	1877.3	0.281471331	-4.1	0.7	2.44	2.76
MA6_59	0.28148	2.787E-05	0.00127	0.04992	1866.3	0.281434481	-5.7	1.0	2.50	2.85
MA6_60	0.28141	2.457E-05	0.00079	0.02721	1946.2	0.28138005	-5.8	0.9	2.56	2.91
MA6_62	0.28156	2.448E-05	0.00069	0.02655	1865	0.281535096	-2.2	0.9	2.35	2.63
MA6_63	0.28130	2.018E-05	0.00044	0.01623	1997.5	0.281282638	-8.1	0.7	2.69	3.09
MA6_64	0.28156	2.514E-05	0.00089	0.03355	1895.3	0.28153263	-1.5	0.9	2.36	2.62
MA6_65	0.28090	2.231E-05	0.00078	0.02935	2819.1	0.280855256	-4.1	0.8	3.25	3.49
MA6_67	0.28149	1.917E-05	0.00054	0.01938	2070.3	0.281471631	0.3	0.7	2.43	2.64
MA6_69	0.28153	3.018E-05	0.00198	0.07594	1879.9	0.281459123	-4.5	1.1	2.47	2.79
MA6_70	0.28154	2.760E-05	0.00202	0.07708	1900.7	0.281462186	-3.9	1.0	2.47	2.77
MA6_71	0.28119	1.947E-05	0.00032	0.01225	2497.2	0.281176116	-0.2	0.7	2.82	3.01
MA6_72	0.28159	2.021E-05	0.00078	0.02970	1840.1	0.281566236	-1.6	0.7	2.31	2.58
MA6_74	0.28143	2.081E-05	0.00111	0.04686	2186.8	0.281380161	-0.2	0.7	2.56	2.77
MA6_75	0.28112	2.213E-05	0.00080	0.03211	2572.5	0.281078939	-1.9	0.8	2.96	3.17
MA6_76	0.28157	3.449E-05	0.00113	0.04183	1860	0.281534705	-2.3	1.2	2.36	2.64
MA6_77	0.28131	3.231E-05	0.00128	0.04934	1878.1	0.281268849	-11.3	1.1	2.73	3.19
MA6_78	0.28156	2.401E-05	0.00101	0.03748	1926.5	0.281519037	-1.3	0.8	2.38	2.63
MA6_79	0.28146	2.098E-05	0.00071	0.02822	1979.3	0.281434545	-3.1	0.7	2.49	2.78
MA6_80	0.28106	2.658E-05	0.00091	0.03563	2650.2	0.281014957	-2.4	0.9	3.04	3.26
MA6_81	0.28153	2.503E-05	0.00152	0.05775	1857.6	0.281471728	-4.6	0.9	2.45	2.77
MA6_82	0.28112	2.314E-05	0.00069	0.02814	2422.4	0.281092232	-5.0	0.8	2.94	3.23
MA6_83	0.28132	1.999E-05	0.00016	0.00710	2098.8	0.281315341	-4.6	0.7	2.64	2.96
MA6_84	0.28159	3.700E-05	0.00099	0.03869	1846	0.281559777	-1.7	1.3	2.32	2.59
MA6_85	0.28105	1.863E-05	0.00042	0.01460	2667.7	0.281028007	-1.5	0.7	3.02	3.22
MA6_86	0.28157	2.796E-05	0.00082	0.03154	1846.8	0.281539406	-2.4	1.0	2.35	2.63
MA6_87	0.28154	3.196E-05	0.00148	0.04514	1879.4	0.28148787	-3.5	1.1	2.43	2.72
MA6_88	0.28143	2.135E-05	0.00063	0.02398	1992.1	0.281410275	-3.7	0.7	2.52	2.82
MA6_89	0.28144	1.830E-05	0.00060	0.02271	1961.2	0.281412892	-4.3	0.6	2.51	2.83

MA6_90	0.28145	2.018E-05	0.00075	0.02885	2015.3	0.281420559	-2.8	0.7	2.51	2.79
IL14-03	0.28138	2.856E-05	0.00097	0.03380	2081.4	0.281336852	-4.2	1.0	2.62	2.92
IL14-04	0.28145	2.229E-05	0.00055	0.01798	2038.9	0.281426196	-2.0	0.8	2.49	2.76
IL14-05	0.28141	2.423E-05	0.00052	0.01556	2025.9	0.281385471	-3.8	0.8	2.55	2.85
IL14-06	0.28140	1.994E-05	0.00087	0.02833	2041.6	0.281365042	-4.1	0.7	2.58	2.89
IL14-07	0.28161	3.993E-05	0.00124	0.03561	1797.8	0.281570309	-2.5	1.4	2.31	2.60
IL14-08	0.28145	4.511E-05	0.00095	0.03374	1959.6	0.28141139	-4.4	1.6	2.52	2.84
IL14-09	0.28139	2.994E-05	0.00081	0.02655	1921.6	0.281357112	-7.2	1.0	2.59	2.98
IL14-10	0.28137	2.029E-05	0.00072	0.02370	2059.5	0.281338695	-4.6	0.7	2.61	2.93
IL14-13	0.28131	2.371E-05	0.00119	0.03930	1953.6	0.281262094	-9.8	0.8	2.73	3.16
IL14-15	0.28102	2.967E-05	0.00142	0.04995	2978.8	0.280935848	2.5	1.0	3.14	3.23
IL14-16	0.28131	2.819E-05	0.00046	0.01264	2041	0.281291846	-6.7	1.0	2.67	3.04
IL14-17	0.28134	2.184E-05	0.00046	0.01471	2071.8	0.281321386	-5.0	0.8	2.63	2.96
IL14-18	0.28137	1.921E-05	0.00052	0.01703	2073.3	0.281351946	-3.9	0.7	2.59	2.90
IL14-19	0.28135	2.499E-05	0.00098	0.03324	2019.3	0.281316334	-6.4	0.9	2.65	3.00
IL14-20	0.28138	2.231E-05	0.00089	0.02668	2040.5	0.281347487	-4.8	0.8	2.61	2.93
IL14-21	0.28135	2.892E-05	0.00077	0.02809	2023.3	0.281316869	-6.3	1.0	2.65	3.00
IL14-22	0.28163	3.143E-05	0.00101	0.03023	1864.1	0.281594005	-0.1	1.1	2.27	2.51
IL14-24	0.28109	2.323E-05	0.00028	0.00883	2937.9	0.281075231	6.5	0.8	2.95	2.97
IL14-25	0.28139	3.212E-05	0.00072	0.02258	2059.6	0.281364706	-3.7	1.1	2.58	2.88
IL14-26	0.28138	2.955E-05	0.00111	0.03426	2089.5	0.281337874	-4.0	1.0	2.62	2.92
IL14-27	0.28139	2.984E-05	0.00082	0.02878	2038.2	0.281356872	-4.5	1.0	2.59	2.91
IL14-28	0.28136	1.917E-05	0.00050	0.01636	2056.9	0.281342992	-4.5	0.7	2.61	2.92
IL14-29	0.28147	1.995E-05	0.00058	0.01592	1973.9	0.281453197	-2.6	0.7	2.46	2.74
IL14-30	0.28136	2.752E-05	0.00096	0.03275	2068.9	0.281324799	-4.9	1.0	2.64	2.96
IL14-31	0.28150	2.632E-05	0.00139	0.04279	2021.8	0.281447894	-1.6	0.9	2.48	2.72
IL14-32	0.28138	2.817E-05	0.00172	0.05755	1957.4	0.281317156	-7.8	1.0	2.66	3.04
IL14-33	0.28167	3.107E-05	0.00107	0.03557	1789.9	0.281633725	-0.4	1.1	2.22	2.47
IL14-34	0.28140	2.996E-05	0.00109	0.03599	2065.6	0.281354911	-3.9	1.0	2.60	2.89
IL14-35	0.28137	2.840E-05	0.00101	0.03141	2109.4	0.28133158	-3.7	1.0	2.63	2.92
IL14-37	0.28158	2.154E-05	0.00108	0.03745	1621.6	0.281548051	-7.3	0.8	2.35	2.75
IL14-38	0.28103	1.949E-05	0.00016	0.00599	2598.1	0.281019707	-3.5	0.7	3.03	3.28

IL14-40	0.28139	1.754E-05	0.00101	0.03280	2053.9	0.281348993	-4.4	0.6	2.61	2.91
IL14-41	0.28106	2.234E-05	0.00078	0.02227	2664.9	0.281015806	-2.0	0.8	3.04	3.25
IL14-42	0.28138	2.525E-05	0.00067	0.02330	2037.1	0.281351453	-4.7	0.9	2.60	2.92
IL14-43	0.28137	2.209E-05	0.00065	0.02086	2058.7	0.281340324	-4.6	0.8	2.61	2.93
IL14-44	0.28135	2.732E-05	0.00101	0.03433	2060.8	0.281312653	-5.5	1.0	2.65	2.99
IL14-56	0.28137	2.712E-05	0.00076	0.02607	2063.9	0.281344662	-4.3	0.9	2.61	2.92
IL14-57	0.28137	2.134E-05	0.00093	0.03050	2047.6	0.281333299	-5.1	0.7	2.63	2.95
IL14-58	0.28137	2.155E-05	0.00104	0.03460	2046.7	0.281327088	-5.3	0.8	2.64	2.96
IL14-89	0.28097	2.044E-05	0.00044	0.01608	2616.4	0.280951831	-5.4	0.7	3.12	3.41
IL14-90	0.28102	2.415E-05	0.00087	0.02603	2818.5	0.280974541	0.1	0.8	3.09	3.25
KAS-02	0.28148	2.454E-05	0.00096	0.03715	1990.4	0.281447167	-2.4	0.9	2.47	2.74
KAS-03	0.28166	2.089E-05	0.00096	0.03604	1891.7	0.281624833	1.6	0.7	2.23	2.42
KAS-06	0.28166	1.924E-05	0.00078	0.02872	1875.4	0.281634185	1.6	0.7	2.22	2.41
KAS-07	0.28135	2.090E-05	0.00053	0.02019	1990.8	0.281328283	-6.6	0.7	2.63	3.00
KAS-08	0.28153	2.909E-05	0.00161	0.06154	2005.4	0.28147159	-1.2	1.0	2.45	2.68
KAS-09	0.28164	2.342E-05	0.00081	0.03066	1863.1	0.281608528	0.4	0.8	2.25	2.48
KAS-12	0.28150	2.219E-05	0.00130	0.04901	1943.4	0.281451591	-3.3	0.8	2.47	2.76
KAS-13-14	0.28146	2.040E-05	0.00074	0.02720	1973	0.281428127	-3.5	0.7	2.50	2.79
KAS-16	0.28162	2.298E-05	0.00070	0.02470	1848.2	0.281592043	-0.5	0.8	2.27	2.52
KAS-17	0.28151	2.342E-05	0.00091	0.03530	1973.9	0.28147639	-1.7	0.8	2.43	2.69
KAS-18	0.28162	2.569E-05	0.00154	0.06035	1926.3	0.281562915	0.2	0.9	2.32	2.54
KAS-19	0.28162	2.234E-05	0.00070	0.02708	1872.3	0.281598315	0.3	0.8	2.27	2.49
KAS-20	0.28162	1.791E-05	0.00051	0.01827	1881	0.281598857	0.5	0.6	2.26	2.49
KAS-21	0.28152	2.504E-05	0.00117	0.04385	1856.8	0.281476367	-4.4	0.9	2.44	2.76
KAS-22	0.28156	3.286E-05	0.00110	0.04167	1849.1	0.281518978	-3.1	1.2	2.38	2.68
KAS-24	0.28138	2.339E-05	0.00048	0.01781	2040.8	0.281365429	-4.1	0.8	2.58	2.89
KAS-26	0.28157	2.059E-05	0.00056	0.01979	1913.5	0.281552476	-0.4	0.7	2.33	2.57
KAS-28	0.28150	2.416E-05	0.00116	0.04233	1865	0.281462813	-4.7	0.8	2.46	2.79
KAS-30	0.28134	2.007E-05	0.00062	0.02249	2183.9	0.281310837	-2.8	0.7	2.65	2.92
KAS-33	0.28103	1.732E-05	0.00013	0.00637	2643	0.281024318	-2.2	0.6	3.02	3.25
KAS-35	0.28143	1.824E-05	0.00062	0.02238	1976.7	0.281410957	-4.0	0.6	2.52	2.83
KAS-36	0.28097	1.947E-05	0.00061	0.02367	2718.3	0.280934537	-3.7	0.7	3.15	3.39

KAS-44	0.28151	2.357E-05	0.00087	0.02787	1985.4	0.281475232	-1.5	0.8	2.43		2.69
KAS-46	0.28145	2.788E-05	0.00114	0.04330	2003.3	0.2814049	-3.6	1.0	2.53		2.83
KAS-47	0.28163	2.187E-05	0.00088	0.03290	1871	0.281601731	0.4	0.8	2.26		2.49
KAS-48	0.28146	2.240E-05	0.00066	0.02451	1966	0.28143564	-3.4	0.8	2.48		2.78
KAS-54	0.28159	3.974E-05	0.00225	0.08458	1988.8	0.281507185	-0.3	1.4	2.40		2.62
KAS-56	0.28162	2.002E-05	0.00093	0.03320	1885	0.281587355	0.2	0.7	2.28		2.51
KAS-57	0.28104	1.655E-05	0.00029	0.01475	2604.5	0.281023851	-3.2	0.6	3.02		3.27
KAS-De-01	0.28103	1.487E-05	0.00007	0.00374	2592	0.281025952	-3.4	0.5	3.02		3.27
KAS-De-03	0.28145	2.463E-05	0.00108	0.04057	1974	0.281409293	-4.1	0.9	2.53		2.83
KAS-De-05	0.28182	2.336E-05	0.00118	0.04744	1434	0.281783344	-3.2	0.8	2.03		2.36
KAS-De-07	0.28139	2.500E-05	0.00072	0.02806	2059	0.281362359	-3.8	0.9	2.58		2.88
KAS-De-10	0.28162	3.957E-05	0.00108	0.04388	1800	0.281583284	-1.9	1.4	2.29		2.57
KAS-De-11	0.28139	1.936E-05	0.00062	0.02335	2037	0.281369433	-4.1	0.7	2.57		2.88
KAS-De-12	0.28164	1.923E-05	0.00067	0.02517	1886	0.281616287	1.2	0.7	2.24		2.45
KAS-De-13	0.28142	2.215E-05	0.00071	0.02728	1984	0.28139095	-4.5	0.8	2.55		2.87
KAS-De-15	0.28162	3.024E-05	0.00089	0.03454	1917	0.281583421	0.8	1.1	2.29		2.50

Table S4. Individual zircon trace and rare earth element analyses.

Source file	Zr CPS	Zr CPS 2σ	P	P 2σ	La	La 2σ	Ce	Ce 2σ	Pr	Pr 2σ	Nd	Nd 2σ	Sm	Sm 2σ	Eu	Eu 2σ	Gd	Gd 2c	Tb	Tb 2σ	Dy	Dy 2σ	Ho	Ho 2σ	Er	Er 2σ	Tm	Tm 2σ	Yb	Yb 2σ	Lu	Lu 2σ	Hf	Hf 2σ
Z16-05-06-10	1.98E+08	4.30E+06	229	15	0.011	0.006	8.82	0.21	0.06	0.013	1.09	0.17	2.43	0.3	0.24	0.031	13.4	1	4.72	0.28	57.3	3	21.6	1	94.3	3.8	19.82	0.83	177.6	6.4	35.7	1.3	9610	240
Z16-05-13-11	1.96E+08	4.10E+06	204	15	0.002	0.003	9.19	0.23	0.03	0.0095	0.78	0.12	2.12	0.22	0.2	0.034	10.78	0.4	4.06	0.16	48.08	0.87	18.6	0.33	83.9	1.8	17.61	0.39	161	4.1	32.43	0.92	10490	240
Z16-05-30-13	1.96E+08	4.30E+06	330	20	0.000	0.000	9.2	1	0.04	0.014	0.73	0.14	2.08	0.31	0.34	0.073	14.8	1.2	5.94	0.41	77.5	4.7	32.1	1.7	153.7	8.2	33.6	1.9	322	17	68.7	3.8	10330	250
Z16-05-31-14	1.37E+08	3.10E+06	646	35	0.560	0.160	16.6	0.67	0.23	0.051	1.64	0.28	2.21	0.21	0.25	0.041	13.43	0.8	4.65	0.19	56.5	1.9	22.2	0.48	97.6	2.4	21.13	0.53	191.3	4.3	38.43	0.72	10060	180
Z16-05-43-15	2.04E+08	5.10E+06	565	31	20.900	3.000	97.4	7.6	11	1.2	63.9	5.5	36.4	3.6	11.9	1.2	88.9	8	23.3	1.8	225	18	71.7	5.4	282	20	53.5	3.7	464	30	86	5.7	10040	340
Z16-05-59-16	1.90E+08	4.20E+06	216	22	0.005	0.004	10.3	0.43	0.04	0.013	0.788	0.097	1.85	0.22	0.2	0.045	11.6	0.7	4.34	0.17	55.2	1.7	21.72	0.64	98.8	2.9	21.5	0.83	199.7	7.1	40.1	1.3	10160	310
Z16-05-62-17	1.36E+08	1.90E+06	327	21	0.003	0.004	16.1	0.4	0.04	0.016	0.8	0.14	2.66	0.29	0.37	0.056	16.5	0.8	6.28	0.29	75.5	1.9	29.44	0.74	131.3	2.5	26.78	0.58	238.2	4.7	48.51	0.94	9760	160
Z16-05-69-18	1.97E+08	4.00E+06	660	30	15.800	1.400	44.1	2.7	7.17	0.79	41.7	4.5	25.7	3.1	8.7	1.3	70.6	6.3	21.4	1.8	219	16	72.4	3.8	301	14	61.2	2.6	544	23	104.6	4.2	10860	290
Z16-05-77-19	1.86E+08	3.70E+06	172	14	0.450	0.160	10.4	0.34	0.29	0.061	1.96	0.36	2.25	0.29	0.44	0.084	11.68	0.6	4.12	0.19	51	1.6	19.63	0.44	90.5	2.2	19.53	0.49	184.8	5.8	38	1.2	10880	360
Z16-05-79-20	1.40E+08	2.70E+06	445	25	0.170	0.130	12.2	1.2	0.09	0.055	0.88	0.28	1.9	0.25	0.19	0.039	10.71	0.7	4.52	0.2	61	2	26.47	0.86	133.5	2.9	31.24	0.77	312.7	6.5	67.9	1.6	12950	290
Z16-05-81-21	1.81E+08	4.50E+06	229	20	0.960	0.280	16.4	0.94	0.36	0.074	1.93	0.39	2.04	0.28	0.13	0.029	10.82	0.7	4.14	0.2	50.9	1.3	19.76	0.47	91.6	2.4	19.86	0.67	181.4	5.1	36.4	1.2	10670	250
Z16-05-85-22	1.91E+08	4.00E+06	211	15	0.044	0.012	11.2	0.38	0.12	0.025	2.08	0.34	4.59	0.47	0.37	0.054	24.4	1.9	8.22	0.54	98.2	5.3	36.2	1.6	156.9	7.3	32	1.4	283	11	55.1	2.1	9840	230
Z16-05-103-32	1.29E+08	2.30E+06	275	23	0.035	0.016	8.81	0.27	0.04	0.013	0.93	0.15	1.97	0.25	0.24	0.05	12.07	0.5	4.53	0.18	57.6	1.2	23.44	0.44	110.4	1.9	24.19	0.46	233.6	4.1	47.29	0.98	9970	160
Z16-05-124-33	1.80E+08	5.90E+06	198	14	0.015	0.009	7.08	0.31	0.03	0.0074	0.67	0.11	1.73	0.28	0.14	0.028	11.6	1.2	4.16	0.37	52.3	4.8	20.9	1.8	95.8	7.3	20.7	1.6	200	15	39.6	2.7	10100	230
Z16-05-126-34	1.85E+08	3.80E+06	475	21	0.008	0.005	6.68	0.19	0.03	0.0098	0.98	0.16	3.17	0.34	0.47	0.067	21.83	0.7	8.24	0.27	107.3	2.3	42.71	0.84	197.5	4.2	41.8	1.2	386	12	78.7	2.4	10660	260
Z16-05-129-35	1.81E+08	3.10E+06	212	16	1.300	1.000	7.1	1.5	0.29	0.2	1.75	0.74	1.83	0.23	0.14	0.028	10.29	0.5	3.62	0.13	45.62	0.91	17.66	0.35	82.4	1.9	17.95	0.53	167.6	3.6	33.73	0.76	9360	180
Z16-17-01-36	1.73E+08	3.70E+06	224	21	0.185	0.044	12.1	0.54	0.18	0.034	1.57	0.24	2.39	0.22	0.59	0.078	13.05	0.7	4.58	0.17	53.8	1.9	21.5	0.74	100.9	2.9	22.6	0.65	219.5	6.8	47.2	1.3	9710	230
Z16-17-24-37	1.78E+08	3.00E+06	195	18	0.017	0.008	6.52	0.25	0.04	0.014	0.78	0.13	1.9	0.25	0.24	0.045	12.08	0.9	4.5	0.31	55.9	3	22.6	1.1	103.3	4.8	21.84	0.97	199.5	7.8	39.1	1.7	9600	170
Z16-17-31-38	1.80E+08	3.70E+06	746	27	0.007	0.005	0.76	0.06	0.05	0.011	0.78	0.11	3.3	0.25	0.14	0.03	26.9	1.1	11.4	0.39	151.6	5.6	61.9	2	284.4	9.7	60.1	2.1	545	19	108.5	3.6	11120	170
Z16-17-32-39	1.82E+08	3.60E+06	396	21	1.540	0.110	91	2.6	1.36	0.086	10.96	0.61	11.95	0.48	4.09	0.22	49.5	1.8	15.7	0.49	172.2	4	60.9	1.2	266.6	4.8	55.5	1.1	505	10	95.9	2	10080	190
Z16-17-34-40	1.23E+08	2.10E+06	573	26	0.003	0.004	6.47	0.29	0.06	0.012	1.16	0.16	3.14	0.29	0.2	0.045	19.87	0.9	7.48	0.2	92.6	2.5	34.85	0.88	155.6	3.9	32.44	0.96	296	8.4	60.2	1.7	10550	190
Z16-17-120-41	1.70E+08	3.20E+06	383	18	0.003	0.004	3.29	0.18	0.02	0.0082	0.431	0.08	1.62	0.19	0.23	0.041	11.82	0.6	4.93	0.19	57.6	2	20.8	1	87.1	4.7	17.7	1.1	154.4	9.5	29.6	1.9	11650	280
Z16-17-61-51	1.64E+08	3.40E+06	108	13	0.068	0.015	25.1	0.99	0.39	0.049	5.69	0.48	7.73	0.68	3.56	0.33	27.9	2	7.36	0.5	71.5	4.8	23.3	1.6	93.1	6.1	18.8	1.1	172	10	33.9	2.2	8570	200
Z16-17-66-52	1.62E+08	4.70E+06	316	43	0.192	0.079	5.1	1	0.17	0.068	1.84	0.42	2.53	0.44	0.55	0.18	17.9	1.3	5.77	0.37	53.5	6.3	13.9	3.1	48	15	9.1	3.2	78	29	15.2	5.9	12490	340
Z16-17-69-53	1.71E+08	4.00E+06	654	32	0.049	0.017	9.22	0.45	0.41	0.052	7.14	0.6	12.95	0.75	1.69	0.18	53.5	2.2	14.9	0.38	155	4.8	53.3	1.4	225.1	5.7	43.6	1.2	382	10	74	1.8	9910	210
Z16-17-71-54	1.25E+08	2.60E+06	284	24	1.530	0.630	15.2	1.5	0.45	0.16	2.34	0.65	1.44	0.19	0.08	0.024	7.89	0.8	3.1	0.15	40.8	1.3	16.63	0.53	82.1	2.6	18.84	0.64	176.8	5.4	35.8	1.1	11000	260
Z16-17-99-55	1.23E+08	2.30E+06	690	44	0.074	0.026	2.51	0.86	0.08	0.022	1.36	0.27	3.98	0.41	0.23	0.058	27.1	1.4	10.6	0.45	120.3	7	40.4	3.9	166	21	32.4	4.2	282	40	55.8	8.6	11700	300
Z16-17-101-56	1.69E+08	2.20E+06	183	21	0.103	0.024	24.3	2	0.08	0.013	0.84	0.15	1.35	0.21	0.44	0.061	8.7	1	3.4	0.34	46.9	4.1	18.9	1.5	97.4	7.8	23.4	1.6	243	15	54.7	2.7	12100	220
Z16-17-103-57	1.79E+08	4.00E+06	750	170	0.350	0.110	13.8	0.74	0.59	0.15	5.2	1.3	5.64	0.93	0.44	0.063	21.9	1.9	7.05	0.42	82.6	3.2	31.51	0.89	142.6	3.7	30.24	0.74	278.2	6	55	1.4	9580	180
Z16-17-113-58	1.32E+08	2.10E+06	629	27	0.173	0.041	8.9	1	0.18	0.023	2.69	0.22	4.88	0.39	0.55	0.064	30	1.5	10.6	0.41	132.8	5.2	51.2	1.8	230.3	9.2	47.1	2	421	18	84.4	3.4	9180	170
Z16-17-116-59	1.86E+08	3.80E+06	500	23	0.925	0.096	24.7	2.7	0.72	0.079	5.92	0.62	8.27	0.58	2.66	0.29	37.4	1.5	11.8	0.44	113.3	3.6	33.3	1.4	121.5	6	22.2	1.2	187.6	9.7	32.6	1.8	11500	220

Z16-01-03-69	1.57E+08	5.90E+06	595	42	0.600	0.440	4.81	0.97	0.55	0.092	4.33	0.48	6.35	0.72	1.64	0.14	34.5	2.2	11.1	0.58	130	4.8	47.8	2.2	210	11	42	2	381	21	73.9	3.7	10730	470
Z16-01-11-70	1.61E+08	2.60E+06	217	17	0.162	0.062	32	0.73	0.11	0.03	1.26	0.19	2.43	0.22	0.69	0.078	13.17	0.6	4.58	0.14	56.5	1.3	22.26	0.43	110	2.2	25.28	0.64	248.2	5.8	52.4	1.2	10890	230
Z16-01-13-71	1.72E+08	3.90E+06	396	30	0.001	0.003	11.7	0.39	0.09	0.016	2.19	0.3	4.79	0.44	0.9	0.079	26.5	1.7	8.94	0.44	107.5	4.2	42.8	1.8	198.9	7.5	41.5	1.5	382	13	78.2	2.7	9060	230
Z16-01-14-72	1.71E+08	3.90E+06	292	24	0.106	0.044	7.58	0.26	0.09	0.034	1.01	0.19	2.46	0.34	0.73	0.23	16.7	1.4	5.83	0.36	67.1	3.3	25.25	0.89	113.8	3.5	24.61	0.69	235.9	6.7	47.8	1.4	11120	270
Z16-01-55-73	1.53E+08	4.90E+06	214	32	1.450	0.210	22.4	1.3	1.08	0.18	6.7	1.1	4.68	0.71	1.23	0.17	14.2	1.3	4.18	0.3	40.6	2.3	14.08	0.72	60.4	1.9	13.19	0.58	129.5	6.4	26.26	0.98	8940	280
Z16-01-60-74	1.12E+08	2.70E+06	235	29	0.000	0.000	25.5	0.72	0.05	0.012	1.04	0.22	2.36	0.3	0.49	0.11	10.59	0.8	3.69	0.21	43.7	1.7	16.89	0.81	79.1	2.9	18.09	0.65	173.5	7.6	36.1	1.4	10800	370
Z16-01-69-75	1.64E+08	3.70E+06	106	19	0.037	0.025	8.06	0.41	0.06	0.027	0.58	0.17	0.94	0.17	0.64	0.17	4.59	0.7	1.37	0.19	12.9	1.1	4.93	0.47	21.9	1.7	5.38	0.4	55.2	2.5	13.88	0.6	10250	300
Z16-01-70-76	1.16E+08	2.80E+06	251	22	0.017	0.011	14.5	0.57	0.33	0.049	6.45	0.58	11.15	0.7	1.74	0.15	48	1.9	13.8	0.4	143.3	3.2	48.15	0.97	197.7	5.2	38.3	1.3	329	12	61.2	1.9	8630	260
Z16-01-79-77	1.73E+08	5.20E+06	571	33	0.197	0.070	4.48	0.25	0.24	0.043	2.42	0.3	3.45	0.51	0.25	0.063	17.61	0.8	5.78	0.25	72	2.7	27.19	0.79	123	2.7	25.21	0.92	226.3	7.8	44	1.6	10490	360
Z16-01-81-78	1.28E+08	3.30E+06	426	33	1.220	0.750	29.7	2.6	0.38	0.15	3.23	0.87	4.62	0.65	2.64	0.61	28.1	5	7.59	0.87	77.5	5.8	26.3	1.5	119.5	4.6	27.8	1.1	293	11	62.2	2.4	10350	310
Z16-01-86-88	1.73E+08	3.00E+06	166	15	0.050	0.021	27.2	1.7	0.05	0.014	0.99	0.2	1.75	0.22	0.74	0.08	9.22	0.6	3.15	0.17	37.6	1.5	14.71	0.51	70.9	1.9	16.5	0.44	166.8	5.3	36.1	1.2	9670	170
Z16-01-90-89	1.76E+08	3.90E+06	317	18	1.770	0.150	19.9	0.55	0.83	0.068	5.59	0.41	6.11	0.48	1.81	0.17	34.1	1.4	11.6	0.23	136.4	3.8	52.1	1.2	235.6	4.6	48.6	1.1	432.9	8.3	85.7	2.1	9540	190
Z16-01-94-90	1.59E+08	3.80E+06	753	30	1.820	0.210	14.7	0.77	1.81	0.18	12.8	1.2	14.9	1.2	6.8	0.5	60.8	2.6	16.4	0.87	154.4	6.6	48.4	2.2	197.5	7.2	39	1.8	333	14	61.5	2.5	10310	320
Z16-01-120-91	1.69E+08	3.90E+06	552	26	0.089	0.037	1.93	0.41	0.14	0.044	1.61	0.34	3.53	0.37	0.3	0.086	22	1.1	8.55	0.34	103.6	3.5	35.7	1.3	152	6	30.3	1.3	266	10	51.3	1.9	11260	250
Z16-01-135-92	1.79E+08	3.50E+06	644	25	0.000	0.000	0.98	0.05	0.04	0.0093	0.96	0.13	3.06	0.26	0.13	0.025	23.48	0.8	10.2	0.29	139.3	2.5	56.6	1.3	261.3	5.6	54	1.3	475	10	91.1	2.1	10930	230

Data are quoted as ppm unless stated otherwise

Appendix 2

Supplementary material for: Age, origin and palaeogeography of the Southern Irumide Belt, Zambia.

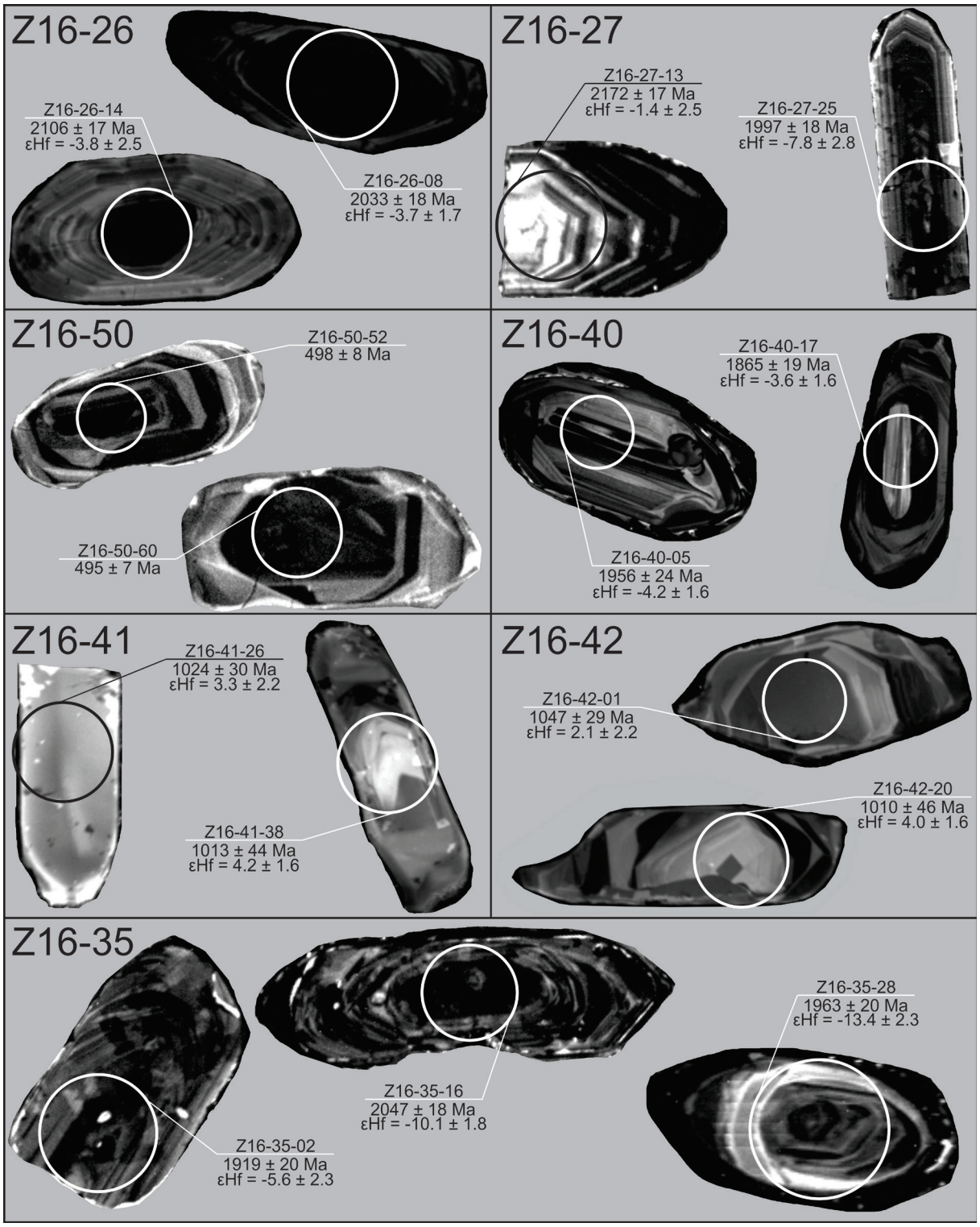

Figure S1. Representative cathodoluminescence images for zircon samples analysed in this study.

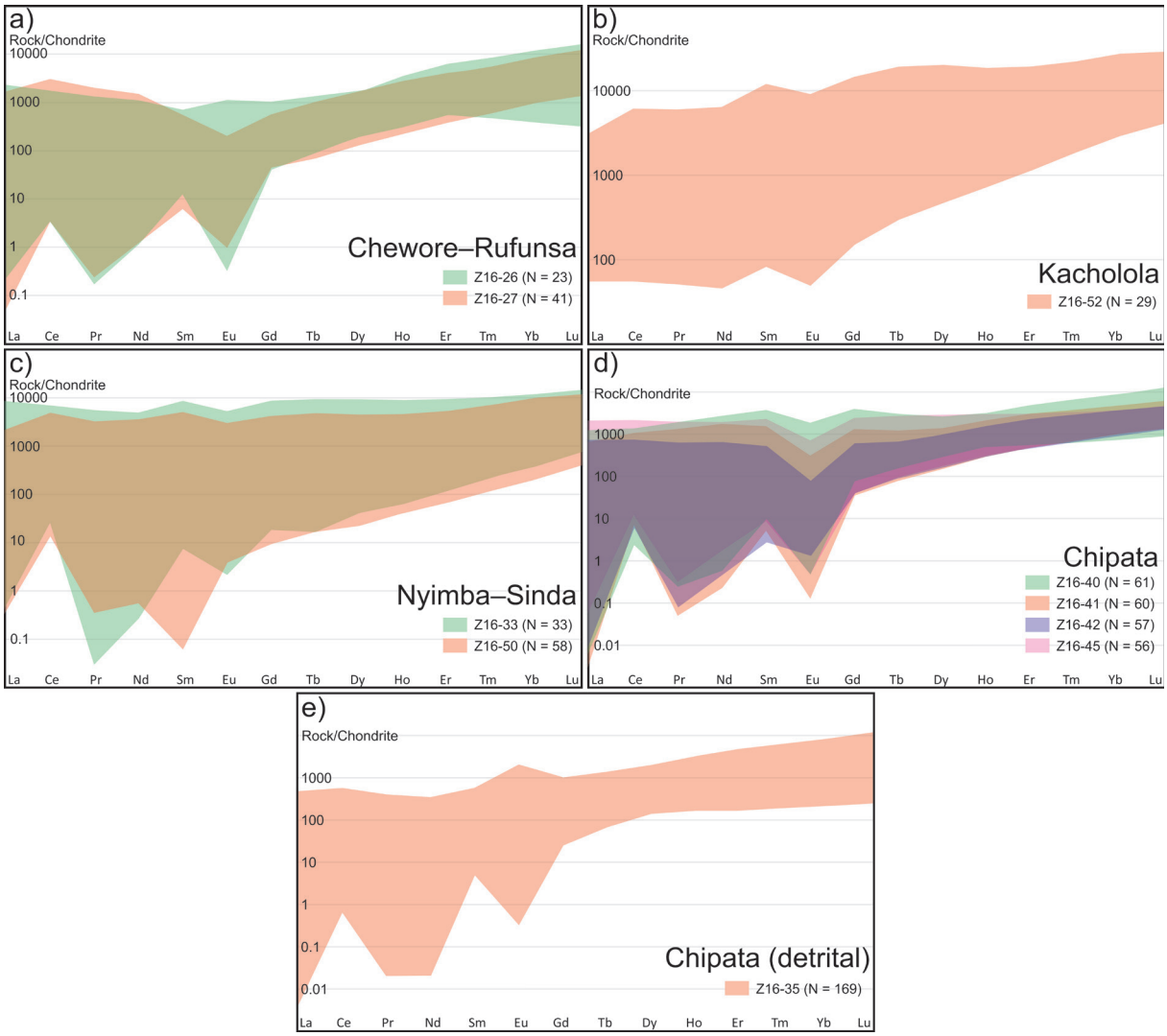

Figure S2. Zircon trace and rare earth element distributions for samples analysed in this study.

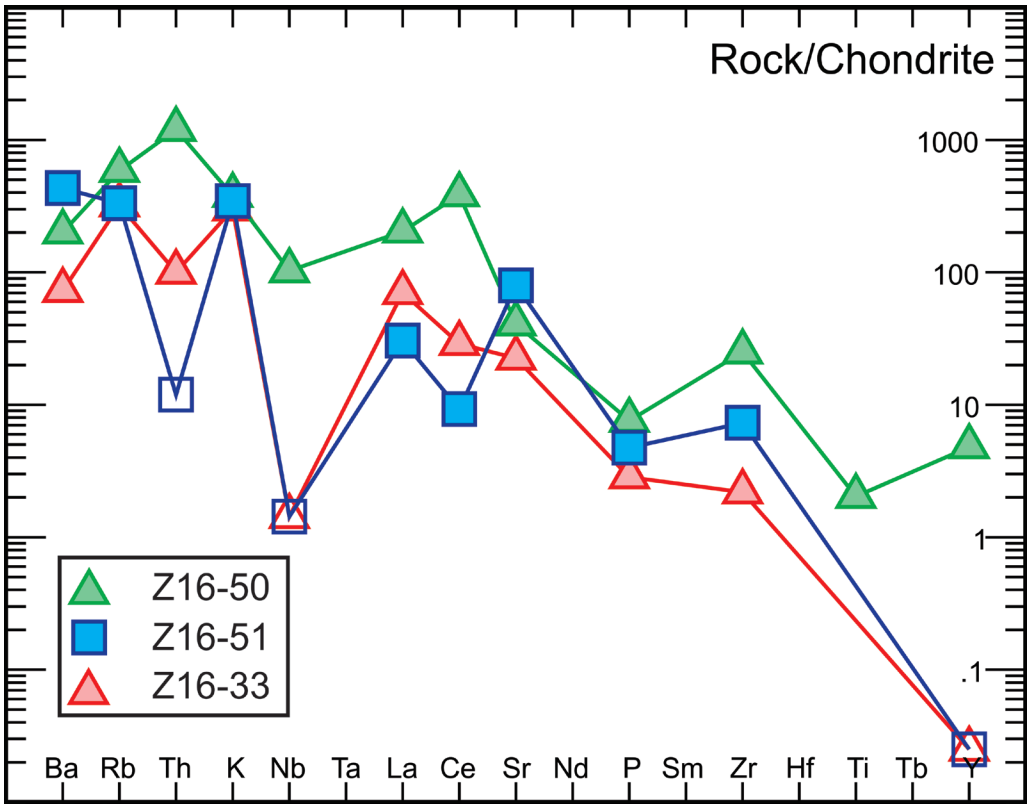

Figure S3. Whole-rock trace element geochemistry patters for Nyimba-Sinda granite samples.

Table S1. Descriptions of analysed zircon samples.

Sample number	GPS coordinates (Deg° Min' Sec")		Southern Irumide Belt terrane	Description	Zircon description			
	Latitude (S)	Longitude (E)			Colour	Aspect ratios	General long axis length of grains	CL characteristics
Z16-26	14 59 09	29 59 11	Chewore-Rufunsa	Felsic gneiss - Quartz (30%), Biotite (20%), Muscovite (5%), Plagioclase (10%), Garnet (5%), K-feldspar (30%)	Clear to brown	1:1 to 1:3	40 to 100 µm	Generally dark in CL. Oscillatory zonation oberserved in all analysed grains. Inclusions observed in the core of a single (Z16-26-04) grain.
Z16-27	14 59 09	29 59 11	Chewore-Rufunsa	Intermediate intrusive - loosely aligned Biotite (10%) and Muscovite (minor), Plagioclase (70%), Quartz (15%), K-feldspar (5%), Amphibole (Minor)	yellow to brown	1:1 to 1:5	60 to 200 µm	Oscillatory zonation observed in most grains. Variable CL brightness observed in the cores and rims, though many grains display brighter cores than rims.
Z16-50	14 14 08	31 41 48	Nyimba-Sinda	Granite - Quartz (40%), K-Feldspar (40%), Plagioclase (20%), Opaque (minor)	Clear	1:1 to 1:3	50 to 200 µm	Oscillatory zoned grains. In many cases zonation patterns in the rims are disturbed, with similar disturbances observed in a number of cores. Some grains display apparent separate, more simple (few alternating zones) rims.
Z16-40	13 42 25	32 29 21	Chipata	Felsic gneiss - Quartz (30%), Plagioclase (15%), K-feldspar (40%), Garnet (5%), Chlorite (5%), Biotite (5%), Opaque (Minor)	Mostly clear - some very light brown	1:1 to 1:5	50 to 200 µm	Predominantly oscillatory zoned grains, inclusions present in many grains. A number of zircon cores are relatively dark in CL, while displaying bright rims.
Z16-41	13 40 23	32 32 57	Chipata	Charnockite - Clinopyroxene (15%), Orthopyroxene (5%), Quartz (20%), Plagioclase (40%), Perthite (20%)	Clear to yellow-brown	1:2 to 1:5	60 to 300 µm	Faint oscillatory zonation preserved in some grains, in many cases the zonation is poorly preserved, with zircon cores surrounded by minimal zonation. A smaller number of grains preserve almost no zonation.
Z16-42	13 40 23	32 32 57	Chipata	Charnockite - Clinopyroxene (20%), Orthopyroxene (5%), Quartz (15%), Plagioclase (30%), Perthite (30%), Garnet, Opaque	yellow to brown - some clear	1:2 to 1:5	60 to 300 µm	Faint oscillatory zonation preserved in some grains, in many cases the zonation is poorly preserved, with zircon cores surrounded by minimal zonation. A smaller number of grains preserve almost no zonation.
Z16-35	13 59 38	32 08 04	Chipata	Quartzite - Small inclusions of biotite and muscovite within quartz grains	Mostly clear - some brown	1:1 to 1:4	50 to 200 µm	Most grains display rounding, with many also being fragmented. Oscillatory zoning is observed in most grains.

Table S2. Individual standard and unknown zircon U-Pb analytical data.

	Isotope ratios and 1σ error (absolute)								Calculated age in Ma and 2σ error (absolute)						Total Isotope counts (PPM) and 2σ error (absolute)					
Analysis	$^{207}Pb/^{206}Pb$		$^{206}Pb/^{238}U$		$^{207}Pb/^{235}U$		ρ*	Concordance (%)	$^{207}Pb/^{206}Pb$		$^{206}Pb/^{238}U$		$^{207}Pb/^{235}U$		U		Th		Pb	
Z16-52 - 19	0.0839	0.0018	0.1545	0.0014	1.805	0.0415	0.04409	72	1282	80	926	16	1209	31	2956	73	27.46	0.64	374	41
Z16-52 - 11	0.08655	0.0005	0.148	0.00115	1.78	0.017	0.4422	66	1349	22	889.8	13	1258	17	3578	74	45.9	2	718	46
Z16-52 - 27	0.0849	0.0009	0.1433	0.00225	1.682	0.02	0.79602	66	1311	40	863	25	1472	53	3220	400	49.8	5	1227	56
Z16-52 - 1	0.1016	0.0018	0.1625	0.0013	2.292	0.05	0.92302	59	1650	63	970.8	14	1574.4	15	3600	190	40.1	3.3	1486	50
Z16-52 - 16	0.1035	0.0011	0.1649	0.00215	2.35	0.022	0.7739	58	1686	37	984	24	1006	42	17170	520	1990	190	3810	170
Z16-52 - 6	0.0998	0.0016	0.1434	0.0015	1.983	0.023	-0.7202	53	1617	59	864	17	1110	16	2769	69	29.8	1.1	306	29
Z16-52 - 8	0.102	0.0018	0.1462	0.00185	1.68	0.21	0.99129	53	1657	64	879	21	1840	21	2740	280	28.3	3.2	1880	190
Z16-52 - 17	0.0837	0.001	0.1045	0.0023	1.211	0.023	0.8894	50	1283	44	641	27	1137	26	4100	2400	82	37	287	81
Z16-52 - 2	0.131	0.0013	0.13503	0.001	2.452	0.0285	0.39634	39	2110	35	816.5	11	-2.26	0.13	1920	140	25.5	2.4	-0.8105	0.000041
Z16-52 - 15	0.147	0.0018	0.1398	0.0027	2.875	0.047	0.81396	37	2309	43	851	27	1476	26	3240	530	49.9	8.5	1200	190
Z16-52 - 4	0.1822	0.0011	0.1472	0.0011	3.714	0.0345	0.16119	33	2672	19	885	12	1038.1	12	5050	160	46.8	2	272.2	5.2
Z16-52 - 14	0.199	0.0028	0.1444	0.0011	3.99	0.075	0.42687	31	2816	45	869.7	13	2415	24	3790	130	151	17	5930	170
Z16-52 - 20	0.294	0.0065	0.175	0.005	7.07	0.105	0.583	30	3435	69	1037	57	1238	19	3810	300	30.7	4.1	909	99
Z16-52 - 13	0.1522	0.004	0.114	0.0024	2.385	0.032	-0.2736	29	2358	92	695	28	1630	30	1750	190	43	12	798	51
Z16-52 - 21	0.1594	0.0031	0.115	0.00225	2.55	0.095	0.96972	29	2445	61	701	26	1375	25	3050	290	36.4	3.5	848	51
Z16-52 - 7	0.2452	0.0038	0.1494	0.0026	5.123	0.065	-0.1547	28	3168	56	897	29	1227.6	13	2840	170	33	5.1	381	28
Z16-52 - 24	0.4457	0.0046	0.1946	0.0014	11.95	0.14	-0.5451	28	4069	31	1146.4	15	805	21	4520	420	189	25	232	29
Z16-52 - 10	0.193	0.0075	0.124	0.0055	3.28	0.055	0.45578	27	2750	130	753	62	1876	77	2300	400	108	35	1840	480
Z16-52 - 18	0.282	0.0195	0.142	0.00395	5.41	0.23	-0.8773	26	3310	220	855	45	1046	29	5300	130	28	3	297	70
Z16-52 - 12	0.4406	0.0024	0.1603	0.002	9.79	0.125	0.94255	24	4053.1	16	959	22	2120	26	5260	230	40.6	3.7	5020	340
Z16-52 - 3	0.214	0.0014	0.1104	0.00415	3.27	0.11	0.9994	23	2935	20	674	48	1282	50	3520	520	97	30	1150	240
Z16-52 - 25	0.3919	0.0046	0.1111	0.0028	5.91	0.075	0.56917	18	3877	35	679	32	1608	40	3080	240	55.5	5.7	1850	190
Z16-52 - 29	0.5077	0.0045	0.11159	0.00085	7.85	0.085	0.44091	16	4263	26	681.9	10	1209.6	15	5960	140	68.1	8.5	1763	34
Z16-52 - 26	0.2397	0.0043	0.0751	0.0031	2.51	0.07	0.91552	15	3115	55	467	37	2600	22	2610	240	57.2	7.8	4620	370
Z16-52 - 22	0.3651	0.0028	0.077	0.00145	3.88	0.095	0.96561	13	3770	23	478	17	1962	22	4944	97	157	11	4100	110
Z16-52 - 23	0.2689	0.0049	0.0616	0.00125	2.291	0.0245	0.43329	12	3298	56	385	15	1274	39	5350	320	47.2	2.5	1714	52
Z16-52 - 5	0.26621	0.0014	0.0459	0.0014	1.7	0.055	0.97926	9	3283.1	16	289	17	1002	15	3160	110	54.4	4	161	20
Z16-52 - 28	0.4074	0.0035	0.0495	0.0012	2.85	0.09	0.98371	8	3936	25	311	14	1366	45	10260	180	126	12	4210	120
Z16-52 - 50**	0.05713	0.0004	0.07976	0.00055	0.631	0.0055	0.60329	100	495	27	494.7	6.5	485.1	11	2740	130	1170	280	225	55

Z16-50 - 58	0.05756	0.0003	0.08062	0.00055	0.644	0.0055	0.50163	98	512	26	499.8	6.7	562.8	8.2	2081	89	2620	190	548	40					
Z16-50 - 14**	0.05809	0.0003	0.08093	0.0006	0.6532	0.0065	0.87148	94	532	26	501.7	7	523	11	860	130	990	210	129	19					
Z16-50 - 49	0.05896	0.0004	0.08378	0.0006	0.6812	0.0065	0.39666	92	564	29	518.7	7.2	480.3	8.1	775	37	1094	43	244.5	5.8					
Z16-50 - 52	0.0584	0.0004	0.08036	0.00065	0.6512	0.0065	0.74025	92	544	27	498.2	8	541	15	1096	41	324	6.1	80.7	5.6					
Z16-50 - 9	0.05909	0.0005	0.082	0.00055	0.674	0.0075	0.53048	89	568	36	508	6.8	522	18	626	25	774	24	166.8	2.1					
Z16-50 - 6	0.05798	0.0004	0.07537	0.0006	0.6049	0.0065	0.75969	89	528	31	468.4	7.4	506	27	599	65	830	130	169	19					
Z16-50 - 2	0.0586	0.0004	0.07647	0.00055	0.622	0.0055	0.71298	86	551	29	475	6.8	522.8	9.1	862	56	259.8	9.8	68	5.7					
Z16-50 - 15	0.0588	0.0004	0.07678	0.00055	0.6261	0.0055	0.80929	85	558	26	476.9	6.6	836	22	830	31	347.5	7.9	183.9	9.7					
Z16-50 - 36	0.05884	0.0004	0.07706	0.00055	0.6319	0.006	0.72332	85	560	28	478.6	6.6	505.2	6.8	861	58	525	48	126	11					
Z16-50 - 48	0.05955	0.0005	0.0788	0.0008	0.6504	0.0065	0.78789	84	585	34	489	9.7	534.8	8.9	709	79	2196	87	91.3	7.1					
Z16-50 - 33	0.05959	0.0004	0.0759	0.0008	0.628	0.0085	0.8879	80	587	30	471.6	9.5	522	21	547	25	548	36	131.4	3.1					
Z16-50 - 45	0.05972	0.0006	0.07428	0.000485	0.619	0.0075	0.21484	78	591	41	461.9	5.9	510.4	7.9	1287	44	727	23	173	11					
Z16-50 - 32	0.06036	0.0003	0.07611	0.00055	0.6385	0.0055	0.7151	77	615	25	472.8	6.7	493.7	6.8	791	31	242	13	51.5	4.6					
Z16-50 - 19	0.05936	0.0005	0.0705	0.0016	0.583	0.0105	0.97514	76	578	36	439	20	687	31	1479	72	8800	2200	329	37					
Z16-50 - 47	0.061	0.0006	0.07645	0.0006	0.647	0.008	0.22702	75	636	42	474.9	7	646.8	10	1725	48	590	110	312	15					
Z16-50 - 13	0.062	0.0018	0.07833	0.00065	0.673	0.0175	-0.2284	74	660	110	486.1	8	479	12	549	25	212	6.7	49.2	1.5					
Z16-50 - 46	0.0604	0.001	0.0745	0.002	0.628	0.009	0.90525	73	634	75	463	24	466	14	723	61	263.6	7.8	51	1.3					
Z16-50 - 21	0.06146	0.0006	0.0764	0.001	0.6573	0.0055	0.61996	72	654	40	474	12	762	18	1561	93	7490	120	700	16					
Z16-50 - 12	0.06261	0.0004	0.0797	0.0008	0.6935	0.0075	0.86419	71	694	26	494.1	9.8	512.9	6.9	3357	78	3886	73	839	28					
Z16-50 - 1	0.0611	0.0004	0.0723	0.0009	0.613	0.0085	0.89313	70	647	27	449.8	11	709	13	992	56	2360	500	200	26					
Z16-50 - 30	0.06082	0.0004	0.07028	0.00055	0.5929	0.0065	0.79713	69	631	28	437.8	6.7	659	35	1108	70	5700	2300	333	54					
Z16-50 - 62	0.06252	0.0005	0.0757	0.00075	0.6587	0.0065	0.72299	68	690	31	470.5	8.7	630	13	1365	25	2320	210	424	51					
Z16-50 - 11	0.0624	0.0004	0.0743	0.0005	0.6447	0.0055	0.89247	67	687	26	462	6.1	521	17	380	35	372	72	88	13					
Z16-50 - 34	0.0641	0.0015	0.07753	0.00065	0.687	0.0155	0.50532	66	734	87	481.4	7.5	470.6	8.3	638	35	377	18	88.3	2.3					
Z16-50 - 7	0.0639	0.0012	0.07582	0.00055	0.673	0.015	0.75141	64	731	78	471.1	6.6	394.9	8.8	123.6	2.1	50.6	1.7	10.33	0.16					
Z16-50 - 3	0.0655	0.0012	0.07739	0.0006	0.704	0.0125	-0.2143	61	786	77	480.5	7.1	524	12	2630	270	3450	250	373	35					
Z16-50 - 26	0.06294	0.0004	0.0676	0.00085	0.5898	0.0065	0.92904	60	704	30	421.4	10	404.1	6.9	553	12	456	11	62.5	1.5					
Z16-50 - 18	0.06333	0.0004	0.0686	0.0008	0.602	0.0095	0.77751	60	718	30	427.5	9.5	472.6	8	494	40	404	17	52.3	1.8					
Z16-50 - 28	0.0654	0.0006	0.0744	0.0009	0.675	0.01	0.61803	59	786	35	462.4	11	535	22	995	33	462	18	122.9	7.3					
Z16-50 - 39	0.0676	0.0011	0.0795	0.00065	0.74	0.0105	-0.4061	58	848	67	493.1	7.5	501.4	7	898	34	272	47	43.9	7.3					
Z16-50 - 56	0.0659	0.0009	0.07179	0.0006	0.657	0.0105	0.35893	56	800	57	446.9	7.3	494.9	11	462	18	378	21	52.2	1.4					
Z16-50 - 8	0.0662	0.0021	0.07015	0.00055	0.63	0.015	0.60595	55	800	120	437.1	6.9	530	18	594	12	246.8	4.4	67.9	4					
Z16-50 - 44	0.0679	0.0009	0.0746	0.0008	0.6994	0.006	-0.0569	54	859	57	463.6	9.6	635.9	10	1582	51	1542	44	267.6	8.3					

Z16-50 - 25	0.0692	0.0021	0.07	0.00085	0.671	0.0145	-0.4812	50	880	130	436	10	497.3	7.4	772	21	316	14	59.7	4.3				
Z16-50 - 51	0.06953	0.0005	0.07252	0.00055	0.6988	0.006	0.15723	49	913	28	451.3	6.8	513.5	7.6	1143	87	356	12	110.6	3.3				
Z16-50 - 24	0.0748	0.0012	0.08275	0.00065	0.859	0.012	-0.5235	48	1058	63	512.5	7.9	533	27	1540	160	8700	2600	176	37				
Z16-50 - 29	0.06415	0.0005	0.05468	0.00043	0.4889	0.005	0.37824	46	745	31	343.2	5.2	562	12	798	54	1130	200	236	32				
Z16-50 - 37	0.0702	0.001	0.0677	0.0008	0.6583	0.006	-0.5365	45	929	57	422	9.6	624.5	12	622	30	255	16	100.6	4.8				
Z16-50 - 53	0.08	0.0023	0.0817	0.00085	0.907	0.0315	0.69591	43	1190	100	506.2	9.9	623	13	1663	37	6700	1400	510	61				
Z16-50 - 4	0.0754	0.0027	0.0711	0.00245	0.7407	0.007	-0.1127	41	1080	140	442	29	567	22	565	31	1173	95	81.8	5.3				
Z16-50 - 27	0.0659	0.0009	0.0519	0.00065	0.476	0.0065	0.56451	41	799	53	326.3	7.8	703	17	2330	68	5720	510	495	5.5				
Z16-50 - 55	0.0802	0.0015	0.0764	0.00085	0.852	0.011	-0.8453	39	1214	77	474.6	9.9	538.4	7.5	1000	51	760	250	123	27				
Z16-50 - 5	0.0754	0.0022	0.0654	0.0015	0.674	0.0095	-0.2831	39	1060	110	409	18	489.1	9.2	506	10	307	20	69.1	3.6				
Z16-50 - 41	0.086	0.0026	0.0727	0.0009	0.847	0.0115	-0.5036	34	1330	110	452.2	11	494.4	11	1230	80	1250	180	254	27				
Z16-50 - 40	0.0863	0.0014	0.0702	0.00075	0.85	0.0105	-0.0223	32	1354	58	437.3	8.8	506.3	9.8	1011	26	586	32	144	11				
Z16-50 - 35	0.08812	0.0007	0.07143	0.00055	0.871	0.0095	0.67142	32	1384	27	444.8	6.6	508.7	8	1070	22	431	41	103.1	8.6				
Z16-50 - 54	0.112	0.005	0.08185	0.00065	1.26	0.055	-0.3069	28	1780	190	507.1	7.7	527.5	7.6	377	23	337	12	55	1.9				
Z16-50 - 42	0.0878	0.0019	0.06063	0.00046	0.741	0.0175	0.45297	27	1388	88	379.5	5.6	670.7	12	1540	100	1410	160	245.8	9.3				
Z16-50 - 10	0.1143	0.0016	0.0805	0.00075	1.28	0.025	0.85241	27	1866	49	499	9.2	538.1	7.1	941	57	1165	41	131.7	4.6				
Z16-50 - 61	0.1029	0.003	0.07157	0.00065	1.029	0.036	0.72099	27	1670	110	445.6	7.8	509.2	7.8	2650	45	2310	130	562	14				
Z16-50 - 43	0.1051	0.0017	0.06846	0.000485	0.998	0.0165	-0.3273	25	1714	60	426.8	5.9	654	33	900	120	1370	170	310.4	7.1				
Z16-50 - 31	0.0899	0.0022	0.05584	0.0005	0.695	0.0185	0.36915	25	1412	94	350.3	6.1	838	49	924	29	1457	55	318	16				
Z16-50 - 23	0.111	0.0075	0.0635	0.00225	0.918	0.033	-0.8544	23	1710	260	397	27	625.4	12	968	45	1291	43	197.7	7.4				
Z16-50 - 50	0.1074	0.0014	0.0636	0.0006	0.936	0.011	0.32106	23	1754	46	397.5	7	512	13	993	29	489	80	88	11				
Z16-50 - 38	0.107	0.0075	0.0505	0.0024	0.68	0.019	-0.3323	19	1640	250	317	29	643	17	2070	120	423	39	271	16				
Z16-50 - 22	0.1213	0.0044	0.0603	0.00165	1.011	0.013	-0.7291	19	1980	130	377	20	504.8	6.6	777	66	236	18	60.8	4				
Z16-50 - 17	0.1186	0.0046	0.0535	0.0026	0.891	0.0095	0.49405	18	1920	140	336	32	496.7	6.9	360	29	215.4	4.7	50.3	1.2				
Z16-50 - 57	0.1217	0.0017	0.0529	0.00125	0.884	0.016	0.63855	17	1978	48	332	15	498.4	7.4	773	31	67	3.1	16.69	0.88				
Z16-50 - 16	0.1325	0.0048	0.05294	0.0005	0.971	0.0305	-0.3698	16	2140	140	332.6	6.1	717	36	962	62	9900	2000	218	20				
Z16-50 - 20	0.17261	0.0009	0.0467	0.0008	1.119	0.0195	0.99579	11	2582.3	17	294.1	9.8	513.8	8	811	12	325.6	6.8	82.3	2.5				
Z16-45 - 21	0.07423	0.0005	0.184	0.0025	1.894	0.0265	0.93042	104	1047	27	1089	27	1087	15	275	25	144.9	9.9	74.8	5.3				
Z16-45 - 9	0.07382	0.0004	0.181	0.00135	1.852	0.016	0.7013	104	1035	23	1072.5	15	1067	16	1261	57	556	15	335.2	6.7				
Z16-45 - 6	0.07381	0.0004	0.1804	0.00135	1.848	0.017	0.85937	103	1035.1	22	1069	15	1054	16	674	60	328	40	175	21				
Z16-45 - 45	0.0738	0.0005	0.1811	0.0014	1.857	0.0165	0.63432	103	1040	23	1072.9	16	1055	16	260	13	215	12	118.3	5.9				
Z16-45 - 36	0.07377	0.0005	0.17979	0.0012	1.842	0.018	0.85714	103	1034	24	1065.8	13	1174.6	12	640	16	195	12	165	6				

Z16-45 - 22	0.07425	0.0005	0.18118	0.00125	1.865	0.0165	0.44138	103	1047	25	1073.4	14	1045.9	14	658	31	294	20	149	8		
Z16-45 - 11**	0.07376	0.0004	0.1788	0.00205	1.825	0.022	0.97085	103	1034	22	1060	22	1099	19	431	46	146.7	2.9	95.7	5.1		
Z16-45 - 41	0.07456	0.0005	0.1824	0.00135	1.882	0.0185	0.77531	102	1056	26	1080	15	1050.7	12	384	28	327	20	174.9	8.6		
Z16-45 - 17	0.07396	0.0005	0.1787	0.0013	1.845	0.0185	0.74996	102	1039	27	1059.6	14	1049.1	14	353	12	350	15	201.3	7.1		
Z16-45 - 60	0.07423	0.0004	0.1795	0.0013	1.858	0.0175	0.49969	102	1046.8	22	1064.2	14	1074.2	12	932	56	196	12	135.6	4.8		
Z16-45 - 59	0.07389	0.0005	0.1776	0.00125	1.822	0.017	0.61782	101	1042	22	1053.8	14	1172	59	203	18	94.3	8.8	71.2	4.6		
Z16-45 - 30	0.07467	0.0004	0.1807	0.0013	1.874	0.0165	0.5909	101	1059	22	1070.7	14	1079	22	163	21	191	23	104.8	9.4		
Z16-45 - 19	0.07453	0.0004	0.1798	0.0012	1.855	0.017	0.68048	101	1055	22	1065.9	13	1056.1	12	222	15	138.7	6.9	74.2	3		
Z16-45 - 4	0.0739	0.0005	0.1763	0.00145	1.811	0.0195	0.88303	101	1038	25	1047	16	1061.4	13	202	10	110.8	5.7	65.1	2.1		
Z16-45 - 48	0.07396	0.0004	0.1765	0.0015	1.811	0.0185	0.78715	101	1039	24	1048	17	1066.2	12	411.6	8	236.1	4.8	150.1	7.5		
Z16-45 - 18	0.07418	0.0004	0.1773	0.00165	1.826	0.0225	0.95432	101	1045	23	1052	18	1046.9	14	367	17	185	12	107.7	8.3		
Z16-45 - 2	0.07421	0.0004	0.1774	0.0013	1.83	0.017	0.72028	101	1046	23	1052.8	14	1283	16	147.8	6.7	115.8	6.1	74.3	2.8		
Z16-45 - 10	0.07406	0.0005	0.1766	0.00185	1.814	0.023	0.98392	101	1042	25	1048	20	1065	12	220	11	142.9	7.5	86.4	2.9		
Z16-45 - 55	0.07427	0.0005	0.1772	0.0015	1.823	0.021	0.79623	100	1047	28	1052	17	1049.1	14	340	27	252	24	143	12		
Z16-45 - 7	0.07448	0.0006	0.1783	0.0017	1.839	0.0195	0.73052	100	1053	29	1058	18	1065.9	12	515	58	380	40	227	22		
Z16-45 - 34	0.07396	0.0005	0.1756	0.00125	1.803	0.017	0.59611	100	1039	26	1042.7	14	1050	17	351	30	265	22	158	10		
Z16-45 - 29	0.07392	0.0004	0.1753	0.0013	1.796	0.0175	0.85578	100	1038	23	1041.4	14	1294	25	177.6	8.3	158.8	3.7	98.4	5.7		
Z16-45 - 20	0.07475	0.0004	0.1791	0.0013	1.861	0.0185	0.89823	100	1061	23	1062.1	14	1100	18	1203	74	577	28	374	15		
Z16-45 - 38	0.07408	0.0005	0.1756	0.0015	1.804	0.019	0.85804	100	1042	25	1043	16	1060.4	13	321	10	168.8	5.6	104.3	3.3		
Z16-45 - 33	0.07396	0.0005	0.1749	0.0013	1.794	0.018	0.66526	100	1039	27	1039.3	14	1109.9	12	815	97	180.7	7.8	118.9	4.3		
Z16-45 - 39	0.0744	0.0004	0.1771	0.0014	1.833	0.0175	0.88334	100	1054.3	25	1051.3	15	1064.1	11	368	38	148	17	90.1	7.4		
Z16-45 - 53	0.07509	0.0005	0.1796	0.00145	1.872	0.017	0.66474	100	1070	26	1065	16	1046.6	12	189.4	9.6	178	15	96.1	6.1		
Z16-45 - 58**	0.07426	0.0004	0.1755	0.00165	1.801	0.0185	0.95919	100	1047	22	1042	18	1079	19	256	15	114	20	65	14		
Z16-45 - 44	0.07427	0.0004	0.1756	0.0013	1.815	0.017	0.72098	100	1048	23	1042.8	14	1300	150	254.5	7.1	197	26	169	31		
Z16-45 - 26	0.07443	0.0005	0.1761	0.00155	1.816	0.0205	0.81882	99	1052	27	1045	17	1040	21	299	10	183.8	3.8	107.3	2.1		
Z16-45 - 54	0.07442	0.0004	0.1757	0.00135	1.815	0.0175	0.81005	99	1052	23	1043.2	15	1053.5	12	271.3	7.7	163.4	3.4	101.9	1.8		
Z16-45 - 43	0.07364	0.0005	0.1717	0.00125	1.759	0.0175	0.8627	99	1030	25	1021.3	14	1050.7	12	677	22	207	11	107.3	9.2		
Z16-45 - 23	0.0741	0.0004	0.17393	0.0012	1.786	0.0155	0.8122	99	1043.3	22	1033.7	13	1084.8	13	1097	33	564	6.2	332	11		
Z16-45 - 15	0.07585	0.0004	0.1816	0.0019	1.916	0.0215	0.93226	99	1090	23	1076	21	1073	11	312	17	190.8	9.3	104	3.5		
Z16-45 - 56	0.07504	0.0005	0.1775	0.00135	1.86	0.022	0.88772	99	1068	26	1053.3	15	1086	30	256	20	184	19	117.1	9.6		
Z16-45 - 12	0.07496	0.0004	0.1772	0.00165	1.845	0.018	0.9281	99	1066	23	1051	18	1061.4	13	604	96	391	67	222	37		
Z16-45 - 35	0.07452	0.0004	0.17499	0.00115	1.8066	0.015	0.88186	99	1054.7	21	1039.6	13	1074.8	13	212.7	6.9	116.8	4.4	72.9	2		
Z16-45 - 51	0.07445	0.0004	0.1737	0.0012	1.787	0.0155	0.58126	98	1053	22	1032.6	13	1040.4	11	362	25	175	13	96.3	4.7		

Z16-45 - 37	0.07404	0.0004	0.17057	0.0012	1.757	0.0155	0.67126	97	1042	22	1015.2	13	1009.5	11	889	42	250.6	4.4	132.1	2.6
Z16-45 - 13**	0.07473	0.0004	0.1734	0.00135	1.783	0.019	0.90486	97	1060	24	1030.6	15	1047.8	11	1079	28	227.8	6.3	113.4	3.7
Z16-45 - 3	0.0775	0.0005	0.1812	0.00205	1.953	0.028	0.98219	95	1133	24	1073	23	1057.2	13	293	19	229	18	120.4	6.4
Z16-45 - 28	0.07556	0.0005	0.1722	0.0016	1.8	0.0175	0.90516	95	1082	24	1024	17	1043.2	13	324	24	278	21	149.4	8.8
Z16-45 - 1	0.0789	0.0007	0.1809	0.0018	1.984	0.0175	0.50905	92	1167	34	1076	18	1107	41	359	12	302	11	175.1	7.1
Z16-45 - 25	0.07484	0.0004	0.16383	0.00115	1.7025	0.0145	0.43151	92	1063.3	21	978	13	1123	17	316.6	9.7	211.8	9.4	118.3	2.9
Z16-45 - 16	0.0771	0.0005	0.1713	0.0013	1.827	0.0175	0.81093	91	1123	26	1019.3	14	1062.8	12	392	15	145	12	81.6	4.5
Z16-45 - 5	0.0783	0.0007	0.176	0.00325	1.917	0.044	0.90565	91	1154	37	1045	35	1088.9	13	1086	13	611.8	8.4	353.1	6.2
Z16-45 - 50	0.0783	0.0007	0.1758	0.0016	1.911	0.018	0.24129	90	1154	34	1044	18	1029.5	11	751	36	331	13	193.3	6
Z16-45 - 46	0.0803	0.0013	0.1753	0.00145	1.956	0.0265	0.68051	87	1200	63	1041	16	1068.6	12	378	28	131	5.6	73.6	2.6
Z16-45 - 14	0.0818	0.0008	0.17877	0.00125	2.023	0.0255	0.49922	86	1237	40	1060.2	14	1067.2	13	389.8	8.7	212.2	5.3	116.5	4.1
Z16-45 - 32	0.0783	0.0008	0.165	0.0014	1.788	0.029	0.89402	85	1153	40	985	16	1030.4	13	226	14	143.2	8.5	72.4	2.9
Z16-45 - 8	0.0788	0.0005	0.1657	0.0013	1.799	0.0195	0.63714	85	1166	26	988.2	14	1043.9	13	131.9	5.5	94.5	3.5	49.2	1.2
Z16-45 - 47	0.08021	0.0006	0.1686	0.0014	1.88	0.017	0.57407	84	1201	26	1005	15	1039.1	14	523	33	387	11	185.3	3.5
Z16-45 - 42	0.0883	0.0033	0.1776	0.0015	2.19	0.095	0.83222	78	1360	140	1057	18	1045.1	14	307	15	186.9	8.5	84.6	4.2
Z16-45 - 57	0.0855	0.0028	0.1655	0.00135	1.98	0.06	0.21012	75	1320	120	987.1	15	1051	15	376.4	8.4	301.7	8.5	160.3	2.8
Z16-45 - 52	0.0851	0.0009	0.1615	0.00335	1.897	0.031	0.85256	73	1315	40	965	37	1040.7	11	289	14	135.7	7.6	65.5	2.6
Z16-45 - 31	0.0863	0.0027	0.1614	0.00405	1.923	0.019	0.56433	72	1330	120	964	45	1053	15	155.8	7.4	121.3	8.6	59.8	4.9
Z16-45 - 40	0.09801	0.0007	0.1854	0.0014	2.538	0.028	0.53249	69	1585	26	1096.4	15	1059.4	14	237.1	9	189.7	4.8	92	2.4
Z16-45 - 24	0.099	0.0011	0.1875	0.002	2.578	0.0435	0.78022	69	1615	34	1108	22	1045.3	13	419	13	158.9	8.6	80.5	2.6
Z16-45 - 27	0.105	0.0095	0.1816	0.00255	2.66	0.285	0.99566	65	1650	310	1075	28	1071.2	12	246	12	205	11	100.9	3
Z16-45 - 49	0.11041	0.0007	0.1408	0.00115	2.18	0.0195	0.47675	47	1805	21	849	13	1055.3	13	256	17	225	14	103.7	5.2
Z16-42 - 26	0.0714	0.0008	0.1768	0.00265	1.723	0.028	0.83629	109	966	44	1049	29	1048	17	57.9	1.5	50.3	1.1	24.04	0.82
Z16-42 - 28	0.0714	0.0008	0.1739	0.0027	1.718	0.036	0.86886	107	966	46	1034	30	1035	17	80	5.8	34.3	2	14.89	0.59
Z16-42 - 24	0.0723	0.001	0.173	0.003	1.734	0.045	0.90679	104	993	53	1028	33	1017	18	43	4.8	18.2	2.3	9.01	0.78
Z16-42 - 14	0.0736	0.0009	0.1786	0.0034	1.814	0.0435	0.85907	103	1027	49	1059	37	1011	24	36.7	2	20.4	1.7	9.64	0.28
Z16-42 - 37	0.0744	0.0007	0.1824	0.002	1.879	0.026	0.66595	103	1049	38	1080	22	1005	23	30.4	1.6	14.53	0.79	8.03	0.6
Z16-42 - 44	0.0727	0.0006	0.1727	0.0016	1.723	0.021	0.74381	102	1002	34	1027	18	1038	28	17.27	0.64	8.18	0.75	3.5	0.14
Z16-42 - 52	0.07298	0.0005	0.1745	0.00145	1.765	0.0205	0.77246	102	1012	28	1037	16	1032	25	32.5	3.3	14.9	1.2	6.99	0.47
Z16-42 - 19	0.0731	0.0007	0.1737	0.0026	1.741	0.028	0.84412	102	1014	39	1032	28	1017	15	138.4	3.8	112.5	4.3	51.2	2.3
Z16-42 - 39	0.0732	0.0007	0.1739	0.0016	1.769	0.022	0.56094	102	1016	37	1034	17	1094	33	20.4	1.4	13.14	0.81	6.4	0.31
Z16-42 - 13	0.07335	0.0006	0.1752	0.00155	1.78	0.0205	0.8149	102	1022	30	1040	17	1049	31	23.81	0.82	10.6	1.2	5.05	0.11

Z16-42 - 55	0.07349	0.0005	0.1755	0.00165	1.773	0.018	0.7053	102	1026	26	1043	18	1027	17	55	2.8	21.1	1.2	10.08	0.23				
Z16-42 - 8	0.0748	0.0006	0.1821	0.0019	1.871	0.029	0.8688	102	1061	31	1078	21	1033	16	39.4	2	26.6	1.6	12.78	0.49				
Z16-42 - 20	0.0729	0.0009	0.1724	0.0028	1.714	0.027	0.78635	101	1010	46	1025	31	1017	21	37.7	1.5	21.8	3	10.9	1.2				
Z16-42 - 41	0.0736	0.0008	0.1757	0.0014	1.772	0.023	0.54983	101	1030	41	1043.5	15	976	14	63.8	2	24	1.1	10.73	0.21				
Z16-42 - 40	0.0741	0.0009	0.1769	0.00255	1.828	0.0325	0.64518	101	1042	47	1050	28	1041	17	83.8	5.5	35.9	1.9	15.9	1.1				
Z16-42 - 25	0.07323	0.0006	0.1723	0.0023	1.747	0.0275	0.88569	100	1019	33	1024	26	1048.2	14	68.7	3.5	59.7	3.4	27.7	1				
Z16-42 - 45	0.0733	0.0008	0.1718	0.00255	1.736	0.032	0.86916	100	1019	40	1022	28	1037	18	39	2.8	30	3.2	14.2	1.4				
Z16-42 - 34	0.0734	0.0008	0.1725	0.00255	1.766	0.022	0.74984	100	1023	40	1026	28	1025	20	71.8	6.7	29.5	1.9	12.64	0.74				
Z16-42 - 23	0.07352	0.0006	0.1733	0.00185	1.751	0.023	0.73719	100	1027	32	1030	20	1021	23	23.4	3	13.5	1.8	5.98	0.59				
Z16-42 - 30	0.0732	0.0008	0.171	0.00205	1.719	0.033	0.87535	100	1016	43	1017	22	1020	15	56.2	3.6	30.2	2.5	13.7	1.1				
Z16-42 - 59	0.0736	0.0006	0.1725	0.0019	1.749	0.0245	0.80438	100	1028	34	1026	21	1025.7	13	75.2	1.8	43.9	1.4	20.53	0.77				
Z16-42 - 33	0.0748	0.0009	0.1776	0.00195	1.837	0.031	0.76308	100	1059	45	1054	21	1055	24	34.6	2.7	21.3	1.3	10.55	0.52				
Z16-42 - 50	0.0722	0.0008	0.1642	0.0017	1.636	0.0245	0.31791	99	989	46	980	19	1016.1	13	91.4	2.2	54.1	1.6	24.01	0.95				
Z16-42 - 1	0.07425	0.0006	0.1745	0.0022	1.788	0.0225	0.82238	99	1047	29	1037	24	1032	19	26.4	1.2	14.46	0.95	7.01	0.21				
Z16-42 - 46	0.0735	0.0008	0.1706	0.00255	1.734	0.03	0.84294	99	1026	41	1015	28	1047	16	49.5	1.8	26.8	4.5	13	2				
Z16-42 - 29	0.0738	0.0008	0.1729	0.00255	1.766	0.034	0.86673	99	1041	44	1028	28	1025.8	14	76.3	1.2	28.7	0.6	12.87	0.25				
Z16-42 - 10	0.07344	0.0005	0.17	0.0014	1.723	0.02	0.86622	99	1025	27	1012	16	1028	18	56.3	3.4	26.2	2.1	12.41	0.78				
Z16-42 - 58	0.0743	0.0008	0.174	0.0022	1.805	0.022	0.72847	99	1048	40	1034	24	1058	22	38.3	2.2	25.1	1.8	12.02	0.55				
Z16-42 - 12	0.07453	0.0005	0.1746	0.0022	1.789	0.0235	0.8837	98	1055	24	1037	24	1034	16	51.3	4.4	19.5	1.9	8.92	0.54				
Z16-42 - 35	0.07419	0.0006	0.1726	0.0016	1.77	0.0215	0.74546	98	1045	30	1026	18	1035	17	85.2	3.6	68.3	2.8	28.2	1.1				
Z16-42 - 53	0.07427	0.0006	0.1729	0.00185	1.773	0.0235	0.84139	98	1048	30	1028	20	1021	22	58.9	2.7	44.4	2.5	21.01	0.65				
Z16-42 - 22	0.0744	0.001	0.1727	0.0025	1.785	0.038	0.7622	98	1048	53	1027	28	1015	25	48.5	3.1	39.3	3.6	17.9	1.5				
Z16-42 - 38	0.0738	0.0005	0.1701	0.00135	1.721	0.0165	0.71813	98	1035	27	1012.5	15	984	19	66.8	5.1	47.7	5.8	22.2	2.3				
Z16-42 - 16	0.07424	0.0005	0.172	0.00135	1.747	0.019	0.82203	98	1047	26	1022.8	15	1028	23	30.7	1.3	18.5	1.4	8.5	0.22				
Z16-42 - 47	0.0741	0.0009	0.1737	0.00185	1.778	0.0245	0.72058	98	1057	37	1032	20	1015	27	51.2	3.5	33.5	2	16.4	0.49				
Z16-42 - 56	0.07421	0.0005	0.1709	0.0013	1.746	0.018	0.64817	97	1046	28	1017.3	15	1009	15	62.1	3	43	1.6	19.65	0.43				
Z16-42 - 48	0.0741	0.0006	0.17	0.00185	1.759	0.024	0.70509	97	1042	34	1012	20	1360	51	36.2	1.2	34.2	1.5	19	1.1				
Z16-42 - 51	0.0745	0.001	0.1713	0.0023	1.747	0.035	0.72231	97	1050	52	1019	25	1021	17	105.1	9.2	59.4	2.6	25.9	1.5				
Z16-42 - 21	0.0751	0.0007	0.1749	0.00175	1.809	0.0235	0.68667	97	1076	40	1039	19	1062.1	13	103.2	4.5	41.1	1.7	21.11	0.76				
Z16-42 - 5	0.07422	0.0006	0.1696	0.0016	1.76	0.022	0.76244	97	1046	29	1010	18	1058	18	63.2	1	38.7	1.3	19.5	0.33				
Z16-42 - 27	0.07413	0.0004	0.1691	0.0017	1.733	0.0225	0.98083	96	1044	24	1007	19	1037	28	21	1.8	13.9	1.1	6.64	0.69				
Z16-42 - 32	0.0754	0.0007	0.1747	0.00155	1.808	0.019	0.6182	96	1078	33	1038	17	1075	28	45.7	7	23.4	4.3	11.7	1.6				
716-47 - 17	0.0741	0.0013	0.1716	0.0025	1.78	0.0385	0.64828	96	1064	54	1021	28	1034	16	38.9	1.8	23.7	1.4	10.89	0.4				

Z16-42 - 7	0.0746	0.0007	0.1702	0.00155	1.754	0.024	0.881	96	1056	35	1013	17	1065	21	34.3	1.1	20.4	1.6	9.92	0.74			
Z16-42 - 4	0.0746	0.0007	0.1697	0.0017	1.746	0.0275	0.83501	96	1055	39	1010	19	1025	25	30.4	1.7	22.3	1.3	10.06	0.43			
Z16-42 - 36	0.07411	0.0006	0.1674	0.00145	1.703	0.0205	0.78165	96	1043	31	998	16	1014	20	49.6	2.4	37.5	1.7	16.93	0.58			
Z16-42 - 2	0.0759	0.0006	0.1753	0.002	1.836	0.0255	0.70899	96	1090	32	1041	22	1067	16	49.4	4.2	34.9	3.7	17.3	1.7			
Z16-42 - 6	0.0739	0.0011	0.1655	0.00135	1.709	0.032	0.69389	95	1037	57	987	15	1017	16	68.5	2.6	27.7	1.1	12.47	0.35			
Z16-42 - 54	0.07617	0.0006	0.1736	0.00225	1.857	0.0295	0.83429	94	1098	32	1032	25	1073	19	33.1	2.4	18.6	1.5	9.88	0.53			
Z16-42 - 11	0.0754	0.0009	0.1696	0.00235	1.764	0.0265	0.7212	94	1075	45	1010	26	1031	16	44.7	2.1	30.8	1.2	14.31	0.37			
Z16-42 - 49	0.0755	0.0007	0.1663	0.0018	1.732	0.02	0.74516	92	1079	34	992	20	1030	18	46.9	2.7	35.2	1.3	15.84	0.49			
Z16-42 - 42	0.0737	0.0007	0.1585	0.0013	1.616	0.0185	0.66623	92	1032	36	948.5	14	1041	16	47.9	4.9	21.4	3.6	10.7	1.1			
Z16-42 - 18	0.0774	0.0007	0.1735	0.00175	1.861	0.022	0.59547	91	1131	33	1032	19	1020	34	41.1	1.2	28.6	3.3	14.7	1.2			
Z16-42 - 3	0.0783	0.0014	0.1763	0.0019	1.886	0.0395	0.60776	91	1150	69	1047	21	1035	19	26.2	1.5	16.7	1.6	7.66	0.44			
Z16-42 - 57	0.0773	0.0007	0.1728	0.00155	1.847	0.018	0.09429	90	1137	41	1028	17	1032	16	58	2.2	22.64	0.85	11.49	0.17			
Z16-42 - 43	0.0756	0.0009	0.1616	0.0029	1.69	0.0295	0.90077	89	1082	48	966	32	1033	15	74.6	4.3	58.7	4.4	28.7	1.8			
Z16-42 - 60	0.0776	0.0012	0.1652	0.00235	1.772	0.0255	0.34547	87	1131	60	985	26	1038	15	70.5	1.2	57.4	2.7	25.7	1.2			
Z16-42 - 9	0.0773	0.0007	0.164	0.002	1.723	0.0235	0.68991	87	1127	34	979	22	1070	21	32.9	2.7	16.2	1.4	7.83	0.5			
Z16-42 - 15	0.0809	0.0017	0.1751	0.00225	1.943	0.0475	0.65951	86	1209	79	1040	25	1035.4	13	77.7	2.3	47.5	2.2	22.2	1.2			
Z16-42 - 31	0.1129	0.0038	0.1819	0.0021	2.84	0.095	0.08993	59	1830	130	1077	23	1027	18	58.6	3.1	45	2.8	19.61	0.93			
Z16-41 - 38	0.0731	0.0008	0.1829	0.00275	1.841	0.0305	0.74445	107	1013	44	1082	30	1036	16	71.8	4.2	37.2	2.8	17.8	1.5			
Z16-41 - 20	0.0738	0.0014	0.1851	0.00395	1.882	0.048	0.71338	106	1033	76	1095	43	1009	16	197.9	3.7	160.1	6.4	73.5	3			
Z16-41 - 40	0.07317	0.0006	0.1796	0.0021	1.82	0.026	0.84245	105	1017	32	1064	23	1073	23	99.8	1.6	44.79	0.91	21.35	0.77			
Z16-41 - 35	0.07408	0.0005	0.1806	0.00215	1.83	0.0285	0.81189	103	1043	28	1070	24	1056	20	52.2	6.2	44.1	3.8	21.7	1.5			
Z16-41 - 11	0.07353	0.0006	0.177	0.00135	1.794	0.017	0.44727	102	1028	29	1050.8	15	1033	18	55	7.6	34.4	2.4	16.1	1.5			
Z16-41 - 6	0.07276	0.0006	0.1725	0.002	1.749	0.024	0.78306	102	1006	33	1026	22	1025.5	12	166	6.5	109.8	4.3	50.2	1.1			
Z16-41 - 54	0.0734	0.0007	0.1757	0.00205	1.776	0.024	0.75334	102	1023	35	1043	23	1035	17	29.3	1.7	20.9	1.8	10.24	0.49			
Z16-41 - 31	0.0732	0.0007	0.1738	0.00175	1.737	0.0235	0.61088	102	1017	40	1033	19	1027	19	54.3	3.1	25.67	0.97	12.94	0.46			
Z16-41 - 57	0.07309	0.0006	0.1732	0.00135	1.753	0.02	0.64574	102	1014	32	1029.9	15	1026	18	67.4	5.8	37.7	1.6	18.38	0.75			
Z16-41 - 25	0.0735	0.0009	0.1754	0.0022	1.808	0.025	0.65283	102	1025	50	1041	24	1004.4	15	70.7	3.8	24.4	1	11.2	0.24			
Z16-41 - 28	0.0741	0.0007	0.1785	0.0014	1.818	0.021	0.64064	101	1043	37	1058.6	15	1139.7	14	44.1	2.4	19.8	1.1	11.54	0.39			
Z16-41 - 2	0.073	0.0007	0.1726	0.00195	1.737	0.0255	0.71774	101	1011	40	1026	21	1054	33	23.2	4.1	14.4	3.7	7.7	1.7			
Z16-41 - 10	0.074	0.0009	0.1774	0.00225	1.818	0.03	0.78834	101	1039	47	1053	25	1023	15	57.5	2.4	34	4.4	16.1	2			
Z16-41 - 26	0.07342	0.0006	0.1738	0.00165	1.754	0.0205	0.86916	101	1024	30	1033	18	1012	21	89	16	53	11	24.1	4.8			
Z16-41 - 36	0.07376	0.0005	0.1756	0.00165	1.783	0.0225	0.87322	101	1034	27	1043	18	1003	17	67.8	4.9	26.6	2.5	11.52	0.9			

Z16-41 - 32	0.0735	0.0005	0.1733	0.0017	1.752	0.02	0.73082	100	1026	28	1030	18	1016.7	14	84.3	4.6	27	1.4	13.45	0.67				
Z16-41 - 17	0.0733	0.0006	0.1717	0.00255	1.732	0.0255	0.8619	100	1020	34	1021	28	1044	17	55.2	2.5	28.7	2.1	13.99	0.93				
Z16-41 - 27	0.07357	0.0006	0.1731	0.00145	1.761	0.0205	0.62875	100	1028	33	1029	16	1046.4	14	168	13	126.2	9.1	62.9	7				
Z16-41 - 19	0.07428	0.0005	0.1764	0.0017	1.803	0.0195	0.98249	100	1048	28	1047	18	1052	19	36.6	2.6	27.4	2	12.12	0.72				
Z16-41 - 30	0.074	0.0008	0.1749	0.00205	1.764	0.0215	0.78044	100	1040	45	1039	23	1032	16	28.8	2.3	19.2	3	9.7	1.3				
Z16-41 - 55	0.07328	0.0006	0.1711	0.00145	1.736	0.021	0.62944	100	1020	32	1018	16	1043.3	12	166.9	3.7	108.8	3.9	48.5	2.3				
Z16-41 - 53	0.07386	0.0006	0.1738	0.00195	1.76	0.0275	0.87654	100	1036	31	1033	21	1031	15	42.8	4.3	25.1	3.3	11.5	1.1				
Z16-41 - 39	0.0747	0.0009	0.178	0.006	1.825	0.05	0.94922	100	1059	50	1054	67	1049	17	28.4	1.3	18.2	0.92	8.67	0.21				
Z16-41 - 12	0.073	0.001	0.1681	0.00225	1.687	0.0265	0.6742	99	1009	53	1001	25	1022	19	42.2	3.2	26.1	2.8	12.63	0.97				
Z16-41 - 3	0.0748	0.0012	0.1769	0.0033	1.827	0.046	0.7652	99	1060	66	1050	36	1026	20	42.6	1.4	28.12	0.6	13.28	0.36				
Z16-41 - 13	0.07405	0.0006	0.1732	0.0025	1.774	0.024	0.91167	99	1041	31	1030	27	1022	18	51.2	3	32	3.1	15	1.6				
Z16-41 - 7	0.0738	0.0007	0.172	0.0017	1.752	0.026	0.86025	99	1034	36	1023	19	1048	18	49.5	4.1	18.8	2.1	7.99	0.71				
Z16-41 - 1	0.07364	0.0005	0.1719	0.0014	1.746	0.0165	0.79932	99	1034	23	1022.3	16	1040	15	75.9	1.6	28.6	1	12.78	0.31				
Z16-41 - 5	0.07409	0.0006	0.1731	0.00165	1.775	0.022	0.86526	99	1042	29	1029	18	1028	15	64.9	4.7	26.1	1.9	12.7	0.74				
Z16-41 - 49	0.0742	0.0007	0.1733	0.00185	1.773	0.0265	0.82098	99	1044	36	1030	20	1015	18	38.7	2.1	24.2	1.7	11.37	0.73				
Z16-41 - 34	0.0741	0.0007	0.1715	0.00255	1.751	0.0295	0.8383	99	1043	40	1029	32	1034	25	35.1	3.1	26.1	2.1	12.49	0.95				
Z16-41 - 16	0.07332	0.0005	0.1692	0.0014	1.722	0.0185	0.69526	99	1022	28	1007.4	15	1003	20	32.8	1.4	19	1.2	9.27	0.59				
Z16-41 - 58	0.07418	0.0006	0.1732	0.0013	1.766	0.019	0.72014	99	1045	29	1029.7	14	1054	37	60.1	5.7	23	2.3	9.9	2.1				
Z16-41 - 45	0.07383	0.0006	0.171	0.00225	1.748	0.0265	0.85545	98	1035	31	1017	25	1032	16	73	3	31.4	1.9	14.8	1.2				
Z16-41 - 56	0.07383	0.0004	0.1707	0.0018	1.741	0.022	0.95758	98	1036	23	1016	20	1052	15	45.4	4	26	2.3	12.22	0.78				
Z16-41 - 37	0.0733	0.0008	0.1672	0.0017	1.717	0.0235	0.72472	98	1020	43	997	19	1052	22	36.6	2	23.9	1.3	11.98	0.36				
Z16-41 - 51	0.07299	0.0006	0.1656	0.0019	1.664	0.0235	0.78071	98	1012	33	988	21	1058	25	73.9	7.7	58.9	6.2	26.3	2.7				
Z16-41 - 18	0.07438	0.0006	0.1723	0.00215	1.768	0.025	0.79514	98	1051	31	1025	24	1034	15	81.6	5.6	24.1	1.6	11.3	0.33				
Z16-41 - 60	0.0741	0.0007	0.171	0.00125	1.743	0.0265	0.77822	97	1044	37	1017.8	14	1060	22	21.4	1.3	11.4	1.1	5	0.2				
Z16-41 - 9	0.07476	0.0006	0.1737	0.0021	1.798	0.0235	0.77435	97	1061	30	1032	23	1030	31	75.1	9.4	36.4	1.6	15.26	0.52				
Z16-41 - 14	0.07373	0.0006	0.1683	0.00215	1.71	0.0275	0.92875	97	1032	32	1003	24	1074	34	71	6.2	25.6	3.9	11.9	1.4				
Z16-41 - 52	0.0735	0.0007	0.1674	0.00185	1.697	0.019	0.49562	97	1027	40	998	21	1020	19	48.5	3.3	24.1	1.6	10.62	0.48				
Z16-41 - 23	0.07498	0.0005	0.1735	0.00135	1.786	0.0205	0.82559	97	1067	28	1031.5	15	1098	20	40.9	2	27.5	1.5	14.24	0.49				
Z16-41 - 4	0.0756	0.0011	0.1761	0.0028	1.835	0.0345	0.65188	97	1082	57	1046	31	995	18	47.2	3.7	21	1.3	9.96	0.31				
Z16-41 - 41	0.07469	0.0005	0.172	0.00165	1.769	0.0205	0.86781	97	1059	26	1023	18	1044	22	62.1	9.9	46	9.6	21	4				
Z16-41 - 24	0.0737	0.0008	0.166	0.00175	1.686	0.0225	0.57589	96	1032	42	990	20	1058	23	44.3	3	22.2	1.2	11.42	0.4				
Z16-41 - 47	0.0747	0.0007	0.1702	0.0016	1.77	0.025	0.84382	96	1057	37	1013	18	1085	40	23.09	0.98	14.75	0.88	8.05	0.93				
Z16-41 - 42	0.0759	0.0016	0.1801	0.00385	1.92	0.06	0.56812	95	1118	95	1067	42	1022	16	58.1	3.6	31.3	2.2	14.3	1.2				

Z16-41 - 22	0.07412	0.0004	0.1669	0.00175	1.703	0.0205	0.94037	95	1044	22	995	19	1042	15	59.9	1.2	23.8	1.1	10.96	0.27
Z16-41 - 46	0.0749	0.001	0.1704	0.0028	1.759	0.0425	0.88036	95	1064	51	1014	31	1034	18	54	2.8	43.5	2	19.26	0.65
Z16-41 - 43	0.0756	0.0009	0.1738	0.00175	1.811	0.023	0.61839	95	1092	40	1033	19	1031	20	66.9	2.1	25.9	1.2	12.52	0.34
Z16-41 - 44	0.07579	0.0006	0.1729	0.0018	1.797	0.03	0.89972	94	1088	30	1028	20	1007	14	135.1	4.2	104.2	2.6	47.6	1.3
Z16-41 - 21	0.0763	0.001	0.1761	0.002	1.838	0.032	0.65577	94	1109	50	1045	22	1037	18	78.4	3.8	32.4	2.5	14.14	0.83
Z16-41 - 29	0.0751	0.0007	0.1681	0.0015	1.74	0.021	0.68195	94	1069	36	1002	17	1035	19	64.3	1.7	64.6	1.5	29.62	0.65
Z16-41 - 8	0.0775	0.0006	0.1768	0.00235	1.879	0.0335	0.98425	93	1133	31	1050	26	1024	16	160	33	140	34	63	14
Z16-41 - 15	0.07513	0.0006	0.1636	0.0015	1.683	0.0175	0.63789	91	1071	29	977	17	1172	53	15.7	1.5	13.2	2.7	7.17	0.93
Z16-41 - 48**	0.0811	0.0008	0.1751	0.00155	1.95	0.0285	0.725	85	1222	38	1040	17	1028	15	68.4	1.8	31.1	3	14.6	1.5
Z16-41 - 50	0.087	0.0029	0.1848	0.00405	2.18	0.08	0.67515	83	1340	130	1107	51	1117	24	100.9	6.8	53.4	5.2	30.5	2.4
Z16-41 - 33	0.0852	0.0007	0.1766	0.00165	2.073	0.0215	0.676	80	1318	31	1048	18	1032.9	14	84.6	5.5	60.8	3.6	29.4	1.2
Z16-41 - 59	0.0866	0.0009	0.1666	0.00185	2.007	0.035	0.52371	73	1365	49	994	20	1030	15	93.5	1.7	35.4	1.1	16.34	0.45
Z16-40 - 50	0.11914	0.0007	0.3558	0.00325	5.84	0.075	0.94863	101	1942	21	1962	31	1725	23	172	10	50.5	2.9	41.7	2.2
Z16-40 - 32	0.07546	0.0004	0.1822	0.0013	1.901	0.016	0.39989	100	1080	23	1078.8	14	1624	18	547	11	120.2	3.3	119.1	9.8
Z16-40 - 24	0.12105	0.0006	0.3538	0.0029	5.907	0.06	0.96348	99	1970.9	18	1953	28	1982.3	14	298.7	4.4	254.1	7.3	240	11
Z16-40 - 57	0.12187	0.0007	0.3535	0.00275	5.932	0.065	0.87419	98	1983	21	1951	26	1860	31	270	18	89.8	3.5	118.2	7
Z16-40 - 45	0.1232	0.0006	0.3552	0.00235	6.045	0.05	0.84245	98	2002.2	18	1959.2	23	2031	20	147.8	5.3	231.8	6.2	231.1	4.1
Z16-40 - 2	0.11693	0.0006	0.3357	0.00315	5.415	0.06	0.96892	98	1908.9	19	1866	31	1952	22	135	11	157	6.7	135.3	5.2
Z16-40 - 42	0.12735	0.0008	0.3644	0.00295	6.394	0.07	0.91736	97	2061	20	2003	28	1757	54	342	34	76.4	2.8	92.9	6.4
Z16-40 - 55	0.1237	0.0007	0.3521	0.00235	6.016	0.05	0.6981	97	2009.3	19	1944.7	22	2237	38	463	19	334	13	528	20
Z16-40 - 27	0.12	0.0008	0.3384	0.0031	5.573	0.049	0.76769	96	1956	24	1879	30	1622.8	14	293	20	59.5	4.3	47.6	3.2
Z16-40 - 31	0.13117	0.0008	0.3666	0.00265	6.625	0.06	0.64892	95	2113	20	2013	25	1714	26	1460	150	3700	2500	1900	1100
Z16-40 - 5	0.11978	0.0006	0.334	0.00265	5.51	0.05	0.97529	95	1952.1	18	1858	26	1895	18	475	11	283	14	284.7	8.2
Z16-40 - 4	0.1334	0.0009	0.3663	0.0025	6.768	0.06	0.50443	94	2142	23	2012.1	23	1587	17	753	39	60.7	2.3	51.8	1.5
Z16-40 - 25	0.1157	0.0008	0.3159	0.00395	5.05	0.08	0.97156	94	1890	24	1769	39	1412	38	907	18	81.8	6.5	73.9	4.2
Z16-40 - 3	0.11325	0.0006	0.3082	0.00295	4.871	0.05	0.96464	94	1851.4	20	1732	29	1745	26	657	55	50.2	2.6	327	12
Z16-40 - 58	0.11762	0.0007	0.3168	0.0038	5.13	0.075	0.9787	92	1919	20	1774	38	2255	42	146	20	216	17	243	17
Z16-40 - 23	0.1289	0.0017	0.3433	0.00405	6.07	0.135	0.93001	92	2064	29	1902	39	1806	47	176	33	86.2	3.4	111.5	6.6
Z16-40 - 14	0.084	0.0019	0.2015	0.0049	2.34	0.11	0.9901	92	1287	85	1183	52	1841	25	210	12	167	12	149	10
Z16-40 - 29	0.11197	0.0008	0.2977	0.00385	4.61	0.075	0.98454	92	1831	23	1680	38	2349	24	1371	59	66.3	2.1	1780	180
Z16-40 - 37	0.12188	0.0007	0.3254	0.0022	5.489	0.048	0.85419	92	1983.1	19	1816.1	21	1364	27	595	31	62.2	4.1	113.2	9.1
Z16-40 - 18**	0.1099	0.0009	0.2875	0.00415	4.4	0.09	0.99569	91	1796	28	1638	44	1978.1	15	306	15	154	3.2	147.9	2.8

Z16-40 - 38	0.10267	0.0006	0.2663	0.00225	3.773	0.0395	0.93203	91	1672.1	20	1522	23	1966	18	117.2	8.1	191	14	180	10				
Z16-40 - 19	0.10702	0.0007	0.2749	0.00215	4.064	0.043	0.85411	90	1748	22	1565	22	1748	32	269.5	9.6	159	18	167.8	7.3				
Z16-40 - 46	0.11235	0.0007	0.2894	0.0033	4.472	0.06	0.96187	89	1837	22	1638	33	1898.8	15	237	7.4	89.1	1.5	86.2	1				
Z16-40 - 17	0.11412	0.0006	0.2923	0.00215	4.607	0.041	0.94311	89	1865.2	19	1653	22	1912	99	425	39	120.8	2.8	310	30				
Z16-40 - 47	0.10635	0.0006	0.2694	0.00185	3.945	0.0345	0.7766	89	1736.8	20	1537.9	19	2065	37	186.1	6	159	14	194.7	7.9				
Z16-40 - 8	0.10773	0.0006	0.2714	0.00215	4.041	0.0395	0.87803	88	1760	21	1548	22	1889	23	278	10	107.3	2.2	130	10				
Z16-40 - 7	0.13024	0.0007	0.3292	0.00225	5.931	0.05	0.7662	87	2100.4	19	1834.6	22	2220	60	226	12	99.6	4.9	231	18				
Z16-40 - 11	0.1446	0.0027	0.3617	0.0026	7.22	0.15	0.31634	87	2279	63	1990	25	1081.3	11	830	40	36.9	1.1	23.3	1.4				
Z16-40 - 30	0.1417	0.0025	0.3489	0.00345	6.84	0.175	0.96833	86	2242	61	1929	33	2062.6	16	122.7	7.9	66.7	4.4	73.1	2.5				
Z16-40 - 6**	0.1146	0.0012	0.2824	0.00375	4.47	0.095	0.95039	86	1871	36	1603	38	2087	45	226	17	238	13	274.4	6				
Z16-40 - 35	0.14058	0.0008	0.342	0.007	6.66	0.14	0.97418	85	2233	20	1895	69	1749	28	400	17	74	3.7	61.4	3.7				
Z16-40 - 48	0.1269	0.0008	0.3104	0.0026	5.464	0.06	0.76137	85	2055	22	1743	25	2089	41	85	11	100	16	103	16				
Z16-40 - 26	0.121	0.0008	0.2898	0.00225	4.855	0.0425	0.63573	83	1970	23	1641	22	1911.8	15	160	14	190	16	162	14				
Z16-40 - 22	0.12628	0.0007	0.3002	0.0021	5.232	0.0465	0.69085	83	2046	20	1692.3	21	1794.4	15	251	19	143	15	132.7	8.3				
Z16-40 - 28**	0.146	0.0045	0.3409	0.00405	6.85	0.155	0.68264	83	2290	100	1891	39	1827	27	377	39	87	18	73	12				
Z16-40 - 56	0.1187	0.0011	0.2797	0.0047	4.6	0.085	0.88301	82	1935	32	1589	47	1962	18	672	25	90.2	5.7	90.7	6.5				
Z16-40 - 12	0.124	0.0042	0.2916	0.00395	5	0.225	0.9269	82	2010	120	1649	39	1983	36	385	12	221	17	237	25				
Z16-40 - 61	0.10454	0.0006	0.2407	0.00195	3.468	0.037	0.93676	82	1705	22	1390	21	1857.8	15	779	33	264	20	281	13				
Z16-40 - 52	0.0983	0.0011	0.2227	0.00335	3.03	0.075	0.98405	82	1590	42	1296	35	2119	19	183.3	5.1	230	11	274.1	6.4				
Z16-40 - 51	0.1626	0.0042	0.3671	0.0029	8.22	0.19	0.58902	81	2478	85	2016	27	1292.2	14	936	28	104.2	3.1	102.9	2.5				
Z16-40 - 59	0.1115	0.0012	0.258	0.0022	3.949	0.043	0.05288	81	1822	39	1480	23	1647	17	116.6	7.4	150.2	9.9	111.9	5.3				
Z16-40 - 20	0.09201	0.0005	0.2022	0.00145	2.571	0.0235	0.93824	81	1466.6	21	1186.9	15	1709	34	218	11	68.9	3.4	52.8	2.3				
Z16-40 - 34	0.1314	0.0021	0.3027	0.0021	5.43	0.075	0.00459	81	2112	53	1704.5	21	1750.5	15	396	30	120	7.6	99.7	4.8				
Z16-40 - 40	0.1227	0.003	0.2745	0.00285	4.66	0.15	0.95815	79	1992	84	1564	29	1906	51	840	140	68	12	530	110				
Z16-40 - 21	0.1528	0.0012	0.3351	0.00355	7.06	0.075	0.83835	78	2376	26	1863	34	1644	71	461	18	104.7	6.4	184	33				
Z16-40 - 60	0.158	0.0028	0.3356	0.00285	7.32	0.15	0.5166	76	2441	56	1866	27	1222	64	466	21	55	20	38	14				
Z16-40 - 44	0.1317	0.0013	0.2857	0.00435	5.25	0.095	0.70909	76	2120	32	1619	44	1821	43	722	19	49.3	6.6	305	31				
Z16-40 - 41	0.1334	0.0018	0.2677	0.00455	4.94	0.135	0.94346	71	2141	46	1529	46	1816	76	1100	29	136	16	247	62				
Z16-40 - 9	0.1033	0.0012	0.2046	0.00185	2.921	0.055	0.97321	71	1681	42	1200	20	2138	36	217	15	217.6	9.7	261	17				
Z16-40 - 15	0.1232	0.0044	0.2394	0.0025	4.09	0.18	0.97687	70	1980	120	1383	26	2750	150	720	120	13.7	1.9	1610	280				
Z16-40 - 49	0.105	0.0017	0.1956	0.0014	2.833	0.05	0.92613	67	1712	57	1151.4	15	1386	28	680	28	54.8	5.1	72.7	5.9				
Z16-40 - 33	0.1847	0.0047	0.3108	0.00295	7.94	0.26	0.984	65	2688	87	1745	29	1642.3	16	155.8	8.9	203.1	6.8	149.5	2.5				
Z16-40 - 1	0.16257	0.0008	0.2622	0.0034	5.88	0.085	0.96715	60	2481.8	17	1501	35	1965.7	15	275.2	9.5	108.1	5.6	105.9	2.5				

Z16-40 - 39	0.1398	0.003	0.2291	0.00315	4.41	0.07	0.34318	60	2221	73	1329	33	1724	35	240	34	168	14	147.8	9
Z16-40 - 43	0.1994	0.0036	0.2932	0.00235	8.07	0.175	0.60335	59	2818	58	1658	23	1904.1	18	172.1	7.6	246	12	224.4	7
Z16-40 - 13	0.154	0.003	0.2352	0.0025	4.95	0.145	0.59874	57	2386	65	1362	26	2081.5	16	143.5	5	219.7	6.7	212.3	3.3
Z16-40 - 36	0.173	0.0065	0.2368	0.00495	5.74	0.33	0.97996	53	2560	130	1369	52	1797	18	221	14	158.4	5.9	129.7	4.4
Z16-40 - 53	0.1571	0.0017	0.2124	0.00245	4.58	0.07	0.71882	51	2423	36	1242	26	1887	19	316	16	106.6	2.7	88.4	1.8
Z16-40 - 16	0.193	0.0075	0.2009	0.0049	5.56	0.165	0.4145	43	2750	130	1179	52	1966	17	428	41	186.3	7.3	332.2	8.1
Z16-40 - 10	0.529	0.04	0.1939	0.00145	14.2	1.05	0.23324	27	4300	240	1142.3	16	2156	34	194.4	7.1	309	15	301	13
Z16-40 - 54	0.403	0.013	0.1655	0.0043	9.11	0.12	0.46103	25	3909	96	987	48	1520	17	360	32	83.2	4.1	99.7	4.1
Z16-35 - 57	0.12632	0.0007	0.3946	0.0027	6.82	0.06	0.80163	105	2046.5	19	2144.2	25	1932	24	590	18	1046	34	899	44
Z16-35 - 52	0.1144	0.0006	0.3497	0.0025	5.499	0.048	0.89934	103	1869.6	19	1933	24	1887	26	118	11	117	14	106	11
Z16-35 - 46	0.12509	0.0007	0.385	0.0075	6.62	0.13	0.99258	103	2029.1	19	2097	69	1833	18	302	17	346	18	301	13
Z16-35 - 160	0.11429	0.0006	0.3471	0.00235	5.395	0.049	0.90752	103	1867.9	19	1920.6	23	2025.9	15	581	34	387	26	356	14
Z16-35 - 162	0.11439	0.0006	0.3456	0.00225	5.361	0.0435	0.87262	102	1869.5	18	1913.5	21	1952.1	15	770	35	748	38	692	20
Z16-35 - 61	0.12607	0.0007	0.3831	0.0028	6.635	0.06	0.93023	102	2043	18	2091	26	1872	25	204.2	6.4	82.6	3.2	68.2	1.9
Z16-35 - 26	0.10867	0.0006	0.3257	0.0027	4.869	0.05	0.93353	102	1776.3	19	1818	26	2029	18	300.5	9.8	90.6	7.7	90	4.9
Z16-35 - 92	0.10844	0.0006	0.3241	0.00225	4.81	0.0405	0.76272	102	1772.5	20	1809.8	22	1878.7	14	794.2	8.8	1002	14	847	25
Z16-35 - 8	0.12634	0.0007	0.3808	0.00325	6.619	0.065	0.94872	102	2046.9	18	2080	31	1536.2	14	247	20	254	23	188	13
Z16-35 - 163	0.11461	0.0007	0.3428	0.0024	5.344	0.048	0.68227	101	1872.9	20	1900	23	1908	21	682	45	363	50	318	16
Z16-35 - 67	0.11159	0.0006	0.3312	0.0033	5.052	0.055	0.97205	101	1824.6	19	1844	32	1989.1	17	414	16	335	11	297	10
Z16-35 - 122	0.10413	0.0006	0.3041	0.0026	4.324	0.0465	0.95061	101	1698.1	20	1712	26	2009	15	613	23	672	28	580	24
Z16-35 - 167	0.10873	0.0006	0.3197	0.0022	4.696	0.04	0.72945	101	1777.3	20	1788.3	22	1746	30	697	18	89	12	60.9	5.9
Z16-35 - 78	0.11465	0.0006	0.3397	0.0033	5.339	0.06	0.96428	101	1873.5	19	1885	32	1992	18	310	12	229	12	206.1	8.1
Z16-35 - 9	0.1087	0.0008	0.3194	0.0038	4.79	0.065	0.90957	101	1777	25	1787	37	2022	19	141	4.2	130.2	3.4	130.4	3.6
Z16-35 - 36	0.12626	0.0007	0.3756	0.00255	6.526	0.055	0.73647	100	2045.6	19	2055.6	24	1820	33	52.2	2.1	61.9	2.6	53.1	2.2
Z16-35 - 12	0.12493	0.0006	0.3712	0.00305	6.384	0.06	0.97518	100	2027.1	18	2035	29	2813	50	662	16	230.3	5	237	10
Z16-35 - 165	0.13611	0.0007	0.4034	0.0029	7.472	0.065	0.71851	100	2177.4	18	2185	27	1729	16	250	13	291	59	228	19
Z16-35 - 147	0.1102	0.0008	0.3237	0.00485	4.81	0.1	0.98503	100	1802	25	1807	48	1736	18	278	17	368	23	296	11
Z16-35 - 81	0.12651	0.0007	0.373	0.00315	6.464	0.065	0.96966	100	2049.2	18	2044	30	1996	18	599	12	46.8	2.9	59.1	2.2
Z16-35 - 118	0.1163	0.0008	0.3414	0.00425	5.41	0.08	0.95401	100	1898	24	1893	41	1785	18	570	39	212	15	170.2	8.6
Z16-35 - 135	0.11546	0.0006	0.3386	0.0023	5.31	0.0465	0.82176	100	1886.3	18	1879.9	22	1840.1	15	326.6	6.4	319.6	7.1	266.3	3.3
Z16-35 - 127	0.1116	0.0007	0.3254	0.0024	4.946	0.047	0.81491	100	1825	21	1816	23	1708	23	210	8.4	444.6	9.7	332	10
Z16-35 - 146	0.12367	0.0007	0.3632	0.0032	6.092	0.065	0.96425	99	2009	18	1997	30	1840	17	108.2	2.9	128.6	4	110	1.6

Z16-35 - 89	0.12578	0.0007	0.3693	0.00285	6.375	0.065	0.96313	99	2038.9	20	2026	27	1969	20	144.4	8.6	92.2	8.7	89.9	8.4					
Z16-35 - 38	0.12678	0.0007	0.3723	0.0029	6.492	0.06	0.97625	99	2053	18	2040	27	1663	39	200	18	52.9	5.6	57.4	8.4					
Z16-35 - 70	0.11285	0.0007	0.3287	0.0024	5.067	0.045	0.79034	99	1844.8	20	1832	23	1919	31	335	14	59.8	2.5	56.5	2.3					
Z16-35 - 79	0.11512	0.0006	0.3358	0.0023	5.287	0.048	0.83514	99	1880.9	19	1866.6	22	1783	36	140.2	6.2	116.7	6.4	94.3	4.9					
Z16-35 - 100	0.1124	0.0009	0.3266	0.0055	5.02	0.095	0.96835	99	1836	27	1821	52	1853.2	16	369	21	107.5	9.1	84.3	4.4					
Z16-35 - 69	0.12581	0.0007	0.3682	0.00255	6.354	0.055	0.89086	99	2039.4	18	2020.8	24	1839	17	159	3.2	207.6	4.6	172.9	5.5					
Z16-35 - 85	0.11447	0.0006	0.3329	0.003	5.21	0.055	0.92055	99	1870.7	19	1852	29	2022	47	476.2	9.2	80.5	2.3	77.9	1.1					
Z16-35 - 149	0.11223	0.0007	0.3254	0.0036	4.94	0.065	0.98535	99	1835	21	1816	35	1352	20	608	47	153.2	6.8	157.4	5					
Z16-35 - 44	0.1596	0.0008	0.4563	0.0031	10	0.085	0.92729	99	2450.6	17	2423	28	1717	18	516	11	610	190	433	84					
Z16-35 - 31	0.11505	0.0006	0.3342	0.00235	5.291	0.0465	0.70387	99	1879.8	19	1858.6	23	1804.6	14	636	23	1124	38	945	17					
Z16-35 - 145	0.10711	0.0006	0.3079	0.0022	4.473	0.044	0.84302	99	1750	21	1730.2	22	1900.4	15	382	30	372	36	359	21					
Z16-35 - 90	0.10705	0.0007	0.3077	0.00265	4.495	0.048	0.77655	99	1749	22	1729	26	1883.9	16	258	14	463	25	432	18					
Z16-35 - 6	0.12582	0.0007	0.3669	0.003	6.363	0.065	0.97853	99	2039.6	18	2015	28	1953.6	16	118.5	6.9	294	17	257	11					
Z16-35 - 42	0.10797	0.0006	0.3101	0.00255	4.608	0.05	0.96237	99	1765	21	1741	25	1976	26	124.1	3.8	83.4	2	78.6	1.5					
Z16-35 - 27	0.1247	0.0007	0.3629	0.00265	6.233	0.055	0.94411	99	2023.8	18	1996	25	1730	18	73.4	3.8	136.6	6	113.5	3.2					
Z16-35 - 34	0.11465	0.0006	0.3317	0.00255	5.23	0.05	0.92262	99	1873.5	19	1847	25	1839.9	16	694	50	304.1	9.1	240	16					
Z16-35 - 137	0.12591	0.0007	0.3662	0.0025	6.264	0.055	0.71871	99	2040.7	19	2011.4	23	1993.7	15	350	21	208	14	193.1	7.6					
Z16-35 - 21	0.12447	0.0007	0.3618	0.00355	6.204	0.07	0.93425	98	2020.4	19	1990	34	1830	41	447	13	137.8	7.7	41.5	1.1					
Z16-35 - 59	0.14101	0.0008	0.4079	0.00325	7.911	0.075	0.89043	98	2238.8	19	2205	30	918	14	1440	44	122	12	54	2.9					
Z16-35 - 50	0.12095	0.0007	0.3509	0.0026	5.808	0.055	0.92723	98	1969.5	19	1939	25	1713	22	325	12	254	14	199	14					
Z16-35 - 134	0.12415	0.0007	0.3602	0.00265	6.093	0.06	0.97067	98	2015.8	18	1983	25	1323	22	795	48	95	18	69.4	4.1					
Z16-35 - 144	0.11519	0.0008	0.3327	0.00275	5.209	0.05	0.82697	98	1882	23	1851	27	1842.2	17	294	17	178.6	4.9	152	4.2					
Z16-35 - 53	0.1136	0.0007	0.3273	0.0024	5.127	0.05	0.84472	98	1857	22	1825	23	1993.6	17	255.5	4.5	113.6	2.3	123.6	4.1					
Z16-35 - 158	0.12315	0.0007	0.3567	0.00345	5.957	0.07	0.94819	98	2001.5	19	1967	33	1900.6	16	361	28	122.8	7.8	104.9	4.5					
Z16-35 - 143	0.2217	0.0013	0.5777	0.0055	17.41	0.175	0.855	98	2992	19	2939	43	1947.4	16	183	11	132.6	7.6	121.8	4.6					
Z16-35 - 43	0.12414	0.0007	0.3595	0.0024	6.125	0.05	0.92214	98	2015.7	18	1979.7	23	2112	19	205	15	88.5	6.3	104.6	3.8					
Z16-35 - 2	0.11737	0.0007	0.3389	0.00335	5.49	0.07	0.97603	98	1916	20	1881	32	1741	37	117.3	6.9	99.6	8.9	84.4	9.1					
Z16-35 - 114	0.12194	0.0007	0.3522	0.0028	5.86	0.055	0.89113	98	1983.9	19	1945	27	1197	31	666	60	185	20	130	20					
Z16-35 - 111	0.11393	0.0007	0.3273	0.00295	5.083	0.055	0.92349	98	1862.2	20	1825	29	1546	16	313.7	9.2	276.5	7.9	165	7.7					
Z16-35 - 136	0.11445	0.0006	0.3279	0.00255	5.118	0.05	0.89091	98	1870.4	19	1828	25	1751	18	301	26	394	33	339	22					
Z16-35 - 107	0.12393	0.0007	0.3568	0.0042	6.01	0.09	0.98534	98	2012.7	20	1967	40	1853	20	306.1	4.6	446.7	7.9	316.7	9.1					
Z16-35 - 104	0.10966	0.0006	0.312	0.0023	4.669	0.0425	0.89481	98	1792.9	19	1750	23	1690	19	101.5	7.7	108.2	6.1	86.3	2.8					
Z16-35 - 58	0.14131	0.0008	0.4042	0.0033	7.854	0.075	0.94227	98	2242.5	18	2188	30	1759	22	316	16	227	12	152.4	7.1					

Z16-35 - 35	0.11166	0.0007	0.3181	0.0024	4.89	0.0465	0.91642	97	1826	20	1780	23	1958	23	455	21	189.5	6.3	201.1	7.1					
Z16-35 - 139	0.11101	0.0007	0.3156	0.0025	4.801	0.045	0.80088	97	1815	22	1768	24	1713.2	15	1193	15	385	78	137.2	2.9					
Z16-35 - 23	0.10793	0.0006	0.3041	0.0023	4.54	0.0415	0.86455	97	1764	21	1712	23	1337.6	14	658	46	136.2	3.6	73.2	3					
Z16-35 - 94	0.19425	0.001	0.5178	0.004	13.74	0.125	0.96807	97	2777.7	16	2690	34	1683	31	460	26	44.2	1.1	37.5	2.7					
Z16-35 - 126	0.12301	0.0008	0.3498	0.0025	5.849	0.055	0.65926	97	1999	22	1933	24	1868.8	14	175.6	4.3	260.9	6.9	166.4	5.1					
Z16-35 - 41	0.11462	0.0006	0.3242	0.0023	5.124	0.0445	0.82223	97	1873	19	1810	23	1040	20	1425	25	268	19	119.8	3.2					
Z16-35 - 17	0.1199	0.001	0.3398	0.0047	5.62	0.11	0.9928	97	1953	29	1885	45	1866.7	16	307	12	311.7	6.6	286.4	5.4					
Z16-35 - 10	0.11549	0.0007	0.3263	0.00305	5.203	0.06	0.99176	96	1886.6	20	1820	30	1898	22	419	12	267	14	241	20					
Z16-35 - 88	0.10614	0.0006	0.2959	0.00225	4.307	0.0385	0.77365	96	1733.4	19	1671	23	1542	15	648	27	89	6.8	54.6	3					
Z16-35 - 112	0.1824	0.0012	0.49	0.006	12.2	0.2	0.99478	96	2674	22	2568	52	1975	16	791	22	117.5	3.9	102.7	2.3					
Z16-35 - 33	0.12559	0.0007	0.3538	0.0024	6.111	0.055	0.95039	96	2036.3	18	1952.5	23	1620	19	747	31	621	19	490	12					
Z16-35 - 51	0.11524	0.0006	0.323	0.0025	5.138	0.05	0.91616	96	1882.7	19	1804	24	1747.8	16	166.7	3.5	144.1	4.5	116.1	3.4					
Z16-35 - 95	0.11352	0.0006	0.3174	0.00225	4.914	0.041	0.82917	96	1855.7	19	1776.8	22	2169.6	15	147	6.8	172.6	8.1	179.2	5.2					
Z16-35 - 130	0.12263	0.0007	0.3445	0.0032	5.771	0.055	0.91344	96	1993.9	20	1908	31	2049.3	15	275	14	118.6	6.1	112.9	3.9					
Z16-35 - 159	0.129	0.0008	0.3622	0.00315	6.328	0.07	0.9056	96	2083	22	1992	30	1831	20	195	17	243	29	219	24					
Z16-35 - 73	0.12093	0.0007	0.3392	0.0026	5.613	0.055	0.97413	96	1969.1	18	1883	25	1698	22	631	20	237.4	9.9	182.1	6.5					
Z16-35 - 115	0.13668	0.0007	0.3827	0.00275	7.143	0.06	0.97512	96	2184.8	17	2089	25	1785	17	546	15	280.1	6.2	209.6	6.6					
Z16-35 - 82	0.1094	0.0009	0.3032	0.00465	4.52	0.095	0.98959	96	1787	29	1707	46	1842	29	267	18	204	17	142	10					
Z16-35 - 63	0.1195	0.001	0.335	0.007	5.49	0.15	0.99419	95	1947	29	1859	67	1942	17	341	13	216.1	9.9	187.5	9.3					
Z16-35 - 5	0.11129	0.0006	0.3093	0.0024	4.746	0.045	0.97194	95	1819.7	18	1737	24	2129.3	16	963	62	738	28	743	23					
Z16-35 - 74	0.1087	0.0009	0.2992	0.00285	4.465	0.055	0.80154	95	1777	29	1687	29	2259	18	114.6	4.8	103.9	2.7	102.8	1.9					
Z16-35 - 140	0.10794	0.0006	0.2965	0.0023	4.339	0.039	0.92824	95	1764.1	19	1674	23	1636	17	1315	55	3630	230	2065	66					
Z16-35 - 7	0.10676	0.0007	0.292	0.00255	4.286	0.0495	0.89629	95	1744	24	1651	25	2013.4	15	306.9	6.3	183.1	3.1	167.7	6.4					
Z16-35 - 54	0.1098	0.0006	0.3008	0.0026	4.528	0.049	0.97828	94	1795.1	20	1695	26	1942	17	476	45	217	25	155	11					
Z16-35 - 65	0.12287	0.0008	0.3389	0.00375	5.69	0.075	0.95029	94	1997	22	1881	36	1773.2	16	330	12	81.2	6.4	63.9	3.8					
Z16-35 - 99**	0.12509	0.0007	0.3451	0.00405	5.89	0.08	0.97667	94	2029.2	18	1911	39	1148	68	260	14	95	5.3	64.2	2.2					
Z16-35 - 109	0.10912	0.0006	0.2974	0.00285	4.429	0.0485	0.9448	94	1783.8	20	1678	29	2029.9	17	333	14	144.8	4.3	129.5	2.9					
Z16-35 - 66	0.12076	0.0007	0.3318	0.0025	5.501	0.05	0.94523	94	1966.7	19	1847	24	1403	23	822	49	232.1	6.7	194.23	0.97					
Z16-35 - 138	0.1226	0.0009	0.337	0.0047	5.62	0.105	0.98547	94	1994	24	1872	45	2434.7	16	449	17	172.7	7.8	200.4	5.4					
Z16-35 - 71	0.12454	0.0007	0.342	0.0023	5.838	0.049	0.81169	94	2021.4	18	1896.1	22	1784.9	16	86.5	3.9	164.4	6.6	127	3.4					
Z16-35 - 128	0.1193	0.0008	0.3273	0.00355	5.32	0.08	0.97654	94	1946	23	1825	34	1991.8	15	696	18	354	32	310	33					
Z16-35 - 32	0.10838	0.0006	0.2934	0.0032	4.381	0.06	0.98326	94	1771	21	1658	32	1726	45	435	18	466	24	119.3	5.3					
Z16-35 - 64	0.116	0.0015	0.3163	0.0023	5.05	0.07	0.01133	94	1893	45	1772	22	1359	17	417	19	135	15	34.64	0.96					

Z16-35 - 14	0.12128	0.0006	0.3316	0.0024	5.546	0.0485	0.93923	93	1974.4	18	1846	23	2060	36	274	50	149	19	138	11			
Z16-35 - 103	0.12032	0.0007	0.3282	0.0025	5.397	0.05	0.95794	93	1960.2	19	1830	24	2027	17	449	13	113.6	2.5	101.1	2.1			
Z16-35 - 166	0.11931	0.0007	0.3251	0.0025	5.28	0.0495	0.92895	93	1945.1	19	1815	24	1678	24	2499	52	2730	370	1048	38			
Z16-35 - 28	0.12055	0.0007	0.3282	0.00425	5.45	0.085	0.99442	93	1963	20	1829	41	1442	18	462.3	4.9	238	19	197	14			
Z16-35 - 16	0.12636	0.0007	0.3436	0.00265	5.995	0.055	0.9118	93	2047.2	18	1904	25	1551	17	708	63	189	13	116.2	7.6			
Z16-35 - 11	0.1173	0.001	0.3181	0.004	5.15	0.095	0.99688	93	1915	29	1780	39	1734	47	404	13	92	12	62	12			
Z16-35 - 120	0.12469	0.0007	0.3386	0.00275	5.745	0.065	0.97241	93	2023.6	18	1880	27	1885	21	538	10	89.1	1.5	72.9	2.5			
Z16-35 - 117	0.1116	0.0007	0.3001	0.0023	4.593	0.0455	0.88904	93	1825	21	1692	23	2005	19	231.3	9.8	164.3	5.1	140.7	3.5			
Z16-35 - 123	0.12437	0.0007	0.3367	0.0036	5.71	0.08	0.98907	93	2019	20	1871	35	1892	27	343	13	98	6	78.3	5.1			
Z16-35 - 48	0.11248	0.0006	0.3015	0.0028	4.661	0.05	0.98624	92	1838.9	18	1699	28	1945	23	1025	91	1023	87	1034	89			
Z16-35 - 152	0.1169	0.0008	0.314	0.006	4.98	0.115	0.99678	92	1908	24	1761	57	1785	21	546	15	270	19	290	23			
Z16-35 - 3	0.11885	0.0006	0.317	0.0023	5.204	0.047	0.93038	92	1938.1	18	1775	23	1722	52	462	14	211	18	205	23			
Z16-35 - 168	0.11707	0.0007	0.311	0.00325	4.938	0.06	0.95932	91	1911	21	1745	32	1662.9	16	582	16	459	10	351.8	8.6			
Z16-35 - 151	0.1195	0.0008	0.3168	0.0042	5.15	0.09	0.98369	91	1948	24	1774	41	2220.8	17	166	5.2	207.9	7.2	219.2	6.1			
Z16-35 - 49	0.1121	0.0009	0.2953	0.0046	4.57	0.105	0.91006	91	1832	28	1667	46	1955.3	16	342.2	7.9	148	4.7	130.2	6.4			
Z16-35 - 56	0.09045	0.0005	0.2241	0.0023	2.787	0.038	0.99303	91	1434	22	1304	24	1698	18	225.1	8.7	375	16	248.7	8.8			
Z16-35 - 113	0.1267	0.0014	0.33511	0.0022	5.79	0.08	0.53325	91	2051	37	1863.1	21	1918	35	340	24	195.1	4.3	175.2	4.4			
Z16-35 - 80	0.1156	0.001	0.305	0.006	4.83	0.125	0.98076	91	1888	32	1713	61	1814	25	132	10	163	13	135.9	9.2			
Z16-35 - 22	0.11504	0.0007	0.3028	0.00255	4.801	0.055	0.96242	91	1879.6	20	1705	25	1854	18	82.3	2.4	124.9	3.1	113.5	2.6			
Z16-35 - 129	0.1149	0.001	0.3023	0.0037	4.73	0.09	0.97787	91	1877	31	1702	37	1859.5	16	176	7.1	180.3	7.2	149.8	2.9			
Z16-35 - 25	0.1219	0.0008	0.3217	0.0028	5.405	0.065	0.96055	91	1983	22	1798	27	1694.7	15	653.1	6.2	585	32	433	25			
Z16-35 - 124	0.11441	0.0007	0.299	0.0026	4.658	0.06	0.98867	90	1870	21	1686	26	1808	27	400	23	324	16	260	7.9			
Z16-35 - 164	0.1101	0.001	0.2847	0.0037	4.25	0.08	0.99619	90	1799	32	1615	37	1918	17	396	22	87	8.3	80.5	6.7			
Z16-35 - 119	0.13164	0.0008	0.3418	0.0024	6.124	0.06	0.86623	89	2119	20	1895.3	23	1740.6	12	147	12	172	12	129.7	6.7			
Z16-35 - 29	0.1176	0.0008	0.3047	0.00365	4.94	0.08	0.98115	89	1919	24	1714	36	1786.6	14	305.4	9.2	378	12	344.2	7.1			
Z16-35 - 161	0.1074	0.0013	0.2746	0.0046	4.01	0.105	0.9827	89	1755	43	1564	46	1830.6	15	312.9	9	301	16	258	18			
Z16-35 - 132	0.11616	0.0007	0.2998	0.0023	4.734	0.046	0.94904	89	1897	20	1690	23	2044.7	16	270	13	205.9	9.5	193.7	5.4			
Z16-35 - 142	0.1545	0.0008	0.3912	0.0032	8.255	0.08	0.93463	89	2395.5	18	2128	29	1750	40	226	17	331	35	243	32			
Z16-35 - 116	0.11292	0.0007	0.2874	0.00295	4.406	0.06	0.95594	88	1846	21	1628	30	2041	73	350	10	56.9	1.7	61.4	3.3			
Z16-35 - 4	0.11108	0.0007	0.2813	0.00275	4.31	0.05	0.96291	88	1816	21	1598	27	1761.6	15	230	17	340	27	286	17			
Z16-35 - 20	0.1361	0.0025	0.345	0.008	6.5	0.265	0.99583	88	2175	64	1912	79	1342	94	192	53	54.1	2.3	40.9	1.1			
Z16-35 - 156	0.1026	0.001	0.2556	0.003	3.56	0.07	0.98935	88	1670	34	1467	31	1828	23	669	64	588	86	564	60			
Z16-35 - 84	0.1209	0.0008	0.306	0.006	5.08	0.12	0.99653	88	1968	23	1722	59	1613	18	321	13	58.9	2	40.81	0.59			

Z16-35 - 30	0.1203	0.0008	0.3047	0.0028	5.049	0.06	0.88435	87	1960	24	1714	28	2733.7	19	264.1	2.8	96.8	1.1	133	3.6
Z16-35 - 24	0.2192	0.0016	0.497	0.01	15.05	0.38	0.99446	87	2974	23	2600	88	1600.8	16	292	22	239	18	222	12
Z16-35 - 19	0.11725	0.0007	0.2963	0.0023	4.801	0.0485	0.89323	87	1913.9	19	1673	23	2040.8	17	248	16	230	22	218	18
Z16-35 - 91**	0.09718	0.0007	0.2358	0.002	3.138	0.0375	0.91092	87	1570	24	1365	21	1634	44	790	16	716	65	493	49
Z16-35 - 108	0.1435	0.001	0.3576	0.00285	7.004	0.07	0.86938	87	2269	23	1971	27	1843	32	638	13	168	13	136.6	9.8
Z16-35 - 13	0.1147	0.0014	0.286	0.005	4.54	0.13	0.99566	87	1873	42	1621	51	1800.4	16	334	12	167.4	7	137.2	3.3
Z16-35 - 153	0.10778	0.0007	0.2661	0.00205	3.896	0.043	0.96179	86	1761	23	1521	21	2063.9	16	278	17	217.7	3.2	217.2	7.1
Z16-35 - 60**	0.1182	0.0008	0.2947	0.00245	4.802	0.06	0.9625	86	1928	23	1665	25	1810	16	130.2	1.9	109.7	3.2	88.8	3.4
Z16-35 - 110	0.1079	0.0008	0.2663	0.00325	3.875	0.0475	0.97667	86	1763	25	1522	33	1907.7	15	788	46	267	17	275	17
Z16-35 - 98	0.12251	0.0007	0.3057	0.0021	5.123	0.047	0.96948	86	1992.2	20	1719.6	21	1808	21	205.5	8.1	185.3	6.6	161.3	6.2
Z16-35 - 83	0.0925	0.0018	0.219	0.0095	2.79	0.17	0.99598	86	1472	74	1270	100	1814	40	305.9	8.1	167.5	4.5	139.4	4.5
Z16-35 - 87	0.10714	0.0006	0.2624	0.00205	3.839	0.0385	0.96474	86	1750	21	1502	21	1541	31	766	14	234	23	182	14
Z16-35 - 96	0.11527	0.0007	0.284	0.007	4.49	0.12	0.9925	86	1883	23	1612	70	1865.5	16	275	10	179.5	7	159	4.3
Z16-35 - 45	0.11423	0.0006	0.2795	0.0026	4.405	0.039	0.97778	85	1866.9	19	1589	26	1608	20	596	77	66.9	4.5	51.6	3.5
Z16-35 - 131	0.09415	0.0005	0.2192	0.0019	2.815	0.031	0.95424	85	1510.3	20	1278	20	1808.7	16	907	38	360	29	197.7	8.5
Z16-35 - 47	0.11033	0.0007	0.2643	0.00215	4.011	0.043	0.95629	84	1804	21	1512	22	2618	31	279	10	154	12	195	12
Z16-35 - 141	0.11502	0.0007	0.2767	0.0028	4.329	0.06	0.96992	84	1879	22	1574	28	1760	19	283.2	6.6	401	8.9	321	5.5
Z16-35 - 77	0.11258	0.0006	0.2682	0.00255	4.144	0.0395	0.95585	83	1840.6	20	1531	26	1725.8	16	220	11	202.1	9.9	158	4.6
Z16-35 - 93	0.116	0.0013	0.279	0.0065	4.47	0.145	0.97912	83	1907	45	1586	63	1875.9	15	483	10	490	19	473	15
Z16-35 - 72	0.1305	0.0014	0.3118	0.003	5.55	0.07	0.47468	83	2103	38	1749	30	1703.4	18	450	28	495	39	412	26
Z16-35 - 150	0.13785	0.0008	0.3278	0.00265	6.141	0.065	0.97009	83	2199.6	19	1828	26	2214.2	17	158	11	71.8	4.7	76.1	3.7
Z16-35 - 76	0.1185	0.001	0.2823	0.00345	4.59	0.085	0.98782	83	1932	28	1603	34	1854	17	75.2	4.5	115.7	5.8	98.5	3.7
Z16-35 - 55	0.12556	0.0007	0.2989	0.0026	5.206	0.05	0.90705	83	2035.9	19	1686	26	1566	19	559	45	260	24	102.2	1.8
Z16-35 - 86	0.09406	0.0005	0.2118	0.0018	2.734	0.026	0.98271	82	1508.4	19	1238	19	1642	21	626	26	103.2	4	68.8	3.1
Z16-35 - 1	0.12544	0.0007	0.2938	0.00485	5.08	0.085	0.98581	82	2034.1	20	1660	48	1833	28	282	32	449	66	391	57
Z16-35 - 39**	0.12573	0.0007	0.2823	0.00355	4.89	0.065	0.99179	79	2038.3	18	1603	36	1884.3	16	332	21	159.8	5.8	141	4.2
Z16-35 - 106	0.08119	0.0005	0.161	0.00195	1.785	0.027	0.98615	79	1225	24	962	21	1783	24	139.4	9	121	11	95	10
Z16-35 - 102	0.1165	0.0017	0.2604	0.00315	4.15	0.1	0.97553	78	1901	51	1492	32	1775.2	16	535	21	455	15	353	10
Z16-35 - 40	0.09546	0.0006	0.2037	0.0027	2.684	0.04	0.95654	78	1536.1	21	1195	29	1795	18	935	28	560	17	301	14
Z16-35 - 15	0.10959	0.0007	0.2381	0.0021	3.585	0.037	0.90548	77	1792	21	1377	22	2090.1	17	185	11	55.3	1.7	54.95	0.79
Z16-35 - 37	0.129	0.0007	0.2782	0.00235	4.938	0.047	0.96856	76	2083.5	18	1582	24	1884	43	453.8	6.3	233.8	4.1	103.9	6.1
Z16-35 - 101	0.1357	0.002	0.2908	0.00365	5.4	0.135	0.86923	76	2171	51	1645	36	1695	20	518	23	60.3	2.5	44	1.1
Z16-35 - 68	0.11142	0.0007	0.236	0.00185	3.609	0.039	0.9572	75	1822	21	1366	19	1870.5	15	429.9	9.8	412	15	338	18

Z16-35 - 155	0.11845	0.0008	0.2511	0.0026	4.04	0.05	0.95249	75	1932	23	1444	27	1893	47	215.7	7.3	138	27	113	18					
Z16-35 - 75	0.12088	0.0007	0.2547	0.00355	4.22	0.06	0.9839	74	1968.4	20	1463	36	2957	19	254	12	181.1	7.7	242.2	8.4					
Z16-35 - 105	0.1304	0.0008	0.2724	0.00305	4.86	0.055	0.98114	74	2102	22	1553	31	2062	18	273	11	73.1	2.7	66.5	2.5					
Z16-35 - 133**	0.10458	0.0007	0.2094	0.00235	2.982	0.0445	0.99074	72	1706	23	1226	25	1800	23	1188	91	531	37	384	13					
Z16-35 - 121	0.11652	0.0007	0.2319	0.00255	3.677	0.043	0.89553	71	1902.6	20	1344	27	1797	17	282	12	269.2	7.5	220.4	3					
Z16-35 - 18	0.095	0.002	0.1751	0.00295	2.254	0.05	0.51301	68	1521	77	1040	32	1787	45	208	23	39.2	4.7	32.9	4.2					
Z16-35 - 97	0.12367	0.0007	0.2324	0.00245	3.932	0.047	0.95303	67	2009	19	1347	26	1766.5	14	219.8	8.1	288.1	4.6	244.7	3.9					
Z16-35 - 148	0.11786	0.0007	0.221	0.00155	3.54	0.0315	0.53272	67	1923	22	1287.3	17	1853.4	17	237	13	436	31	269	29					
Z16-35 - 169	0.0952	0.0015	0.164	0.0095	2.07	0.1	0.97063	64	1528	58	980	100	1875	19	201.9	3.2	995	14	888	20					
Z16-35 - 157	0.1234	0.0009	0.2129	0.00205	3.566	0.033	0.73003	62	2005	25	1244	22	1930	22	192	17	123.6	9.1	120.5	7.2					
Z16-35 - 125	0.08344	0.0005	0.1295	0.0014	1.47	0.017	0.90091	61	1279	23	785	16	1827	20	377	35	301	54	264	34					
Z16-35 - 154	0.1791	0.0022	0.2607	0.00425	6.35	0.17	0.99204	56	2643	40	1493	43	1105.1	13	919	52	543	29	93.3	4.8					
Z16-35 - 62	0.112	0.0008	0.1281	0.0015	1.97	0.019	0.91261	42	1832	26	777	17	1772	32	242.8	6.7	86.4	2	67.1	1.8					
Z16-33 - 22	0.05703	0.0004	0.07822	0.0006	0.6219	0.006	0.71542	99	491	28	485.5	7	842	47	965	16	1610	450	195	28					
Z16-33 - 7	0.05963	0.0004	0.08133	0.0006	0.6759	0.007	0.44564	86	589	31	504.1	7.1	582	32	705	45	129.6	8.7	53	11					
Z16-33 - 27	0.0594	0.0008	0.078	0.0006	0.644	0.011	0.78839	84	577	58	484.1	7.1	675	29	909	37	1173	31	275.1	8.1					
Z16-33 - 35	0.05982	0.0004	0.07857	0.00055	0.653	0.0075	0.75034	82	595	32	487.6	6.6	803.6	11	1417	97	693	70	266	17					
Z16-33 - 21	0.0617	0.001	0.08076	0.0006	0.693	0.0105	-0.4644	76	658	59	500.7	7.4	1004	30	806	35	381	37	205	11					
Z16-33 - 24	0.06212	0.0004	0.07705	0.0006	0.6666	0.007	0.87598	71	677	27	478.5	7.3	535.3	11	979	42	236.1	9.1	58.9	3.1					
Z16-33 - 2	0.0681	0.0023	0.08166	0.00065	0.775	0.0285	0.50694	59	860	130	506	7.6	524.2	8.6	672	23	81.3	2.7	24.5	1					
Z16-33 - 8	0.0648	0.0017	0.0714	0.0009	0.648	0.0135	-0.7446	59	760	100	444.7	11	507	16	976	42	162	10	41	5.9					
Z16-33 - 6	0.0663	0.001	0.07525	0.0006	0.694	0.0095	-0.4693	58	810	62	467.7	7.4	1326	41	2000	81	680	69	830	69					
Z16-33 - 28	0.0711	0.0045	0.08401	0.0006	0.83	0.05	-0.538	52	1000	260	520	7.1	1181	18	1207	67	2280	170	510	19					
Z16-33 - 25	0.07167	0.0005	0.08162	0.00055	0.816	0.0085	0.34468	52	975	30	505.8	6.4	750	52	683	32	147	17	88	12					
Z16-33 - 14	0.071	0.0008	0.0724	0.00075	0.715	0.0135	0.91754	47	954	44	450.6	9	861	14	1630	190	720	180	352	49					
Z16-33 - 23	0.0775	0.0012	0.07656	0.00065	0.829	0.0175	0.72642	42	1128	63	475.5	8	699	55	474	93	177.3	8.6	67.1	3.7					
Z16-33 - 20	0.07146	0.0006	0.06394	0.0005	0.6409	0.006	0.03452	41	969	30	399.5	6.1	547	16	762	41	123	11	40.1	4.6					
Z16-33 - 29	0.0696	0.0007	0.05915	0.00042	0.576	0.0065	-0.334	41	914	39	370.4	5.1	1160	18	1670	120	756	59	577	17					
Z16-33 - 13	0.0845	0.0042	0.0852	0.001	1	0.06	0.96589	40	1330	190	527	12	724	42	3480	270	10300	1500	1050	170					
Z16-33 - 34	0.094	0.008	0.08338	0.0007	1.09	0.1	0.95253	37	1380	320	516.3	8.6	847	19	1431	90	468	47	267.2	9.1					
Z16-33 - 3	0.0883	0.0033	0.0775	0.00085	0.947	0.0285	-0.9014	35	1360	140	481	9.9	839	43	871	30	810	120	197	18					
Z16-33 - 32	0.096	0.0018	0.0744	0.00095	0.981	0.0135	0.30265	30	1544	69	462.9	11	524.7	10	759	28	790	130	91.3	6.8					

Z16-33 - 4	0.1095	0.0008	0.07927	0.00055	1.207	0.012	-0.2017	27	1791	27	491.8	6.5	502.8	7.6	995	48	221	12	56.6	2.6
Z16-33 - 19	0.0858	0.0018	0.0563	0.00135	0.677	0.0085	-0.4248	27	1326	76	353	16	535	12	981	75	75.6	4.2	27.5	2.8
Z16-33 - 11	0.1105	0.0049	0.0717	0.0007	1.1	0.055	0.87212	25	1780	150	446.3	8.3	491	7.7	367	20	232.5	5.4	48.8	1.6
Z16-33 - 31	0.135	0.006	0.08192	0.00055	1.53	0.065	-0.2526	24	2120	150	507.5	6.8	613	19	4540	420	610	100	347	11
Z16-33 - 17	0.1229	0.0011	0.0766	0.0011	1.305	0.0215	0.85549	24	1998	32	476	13	518.6	8.8	567	7.8	942	23	225.9	3.4
Z16-33 - 1	0.13	0.0075	0.0726	0.0014	1.3	0.055	-0.9779	22	2050	210	452	17	605.7	9.3	1374	67	315	19	94.2	3.1
Z16-33 - 18	0.131	0.0055	0.07091	0.00055	1.293	0.0485	-0.591	21	2080	150	441.6	6.8	1880	100	1560	350	39000	15000	1370	190
Z16-33 - 16	0.12	0.0085	0.0618	0.00205	1.049	0.0435	-0.913	19	1990	260	387	25	505	14	449	19	293	10	66.2	1.8
Z16-33 - 5	0.1599	0.0044	0.07597	0.0007	1.691	0.04	-0.6345	19	2447	91	472	8.1	610	54	474	17	1426	30	330	12
Z16-33 - 30	0.1752	0.0023	0.07861	0.0006	1.906	0.023	0.27753	19	2606	43	487.8	7.1	461.8	8.5	885	22	777	38	190.3	6.4
Z16-33 - 9	0.235	0.0075	0.0823	0.00075	2.7	0.075	-0.478	17	3082	98	510	8.7	1083	16	1328	42	1514	83	468	41
Z16-33 - 10	0.2195	0.0017	0.072	0.0008	2.2	0.0275	0.86712	15	2976	24	448.3	9.8	937	53	741	45	1483	44	363	16
Z16-33 - 12	0.1631	0.0048	0.0593	0.00175	1.335	0.0155	0.11112	15	2473	97	371	21	694	14	989	36	252	57	116	8.5
Z16-33 - 26	0.452	0.006	0.089	0.0055	5.53	0.31	0.9835	13	4089	39	547	66	1202	27	1429	66	1710	540	554	10
Z16-33 - 15	0.2492	0.0018	0.0621	0.001	2.134	0.0275	0.95804	12	3179	22	389	12	735	95	780	22	436.3	7.9	166	30
Z16-33 - 33	0.2829	0.0029	0.0585	0.00105	2.269	0.042	0.81534	11	3377	32	366	13	510.5	9.2	682	28	107	14	28.4	2.8
Z16-27 - 29	0.12194	0.0006	0.3706	0.0027	6.256	0.055	0.95001	102	1984.8	16	2032	25	-9.21	0.35	522	11	514	30	-0.8322	0.000082
Z16-27 - 17	0.12201	0.0007	0.3653	0.0026	6.174	0.055	0.83695	101	1984.9	19	2007	25	-1.58	0.14	2910	250	3610	230	-0.8357	0.000057
Z16-27 - 27	0.12336	0.0007	0.3684	0.0033	6.271	0.065	0.97731	101	2004.5	19	2022	31	2130.9	17	259	16	88.7	4	93.8	2.4
Z16-27 - 2	0.1782	0.0009	0.5022	0.0035	12.36	0.105	0.86675	100	2635.4	17	2623	30	1854	18	526	21	188	14	188	16
Z16-27 - 33	0.12607	0.0007	0.3709	0.0026	6.463	0.065	0.91698	100	2043	20	2033	24	1952.8	15	446.2	7.1	231	14	229	18
Z16-27 - 13	0.13569	0.0007	0.3974	0.00285	7.44	0.065	0.97299	99	2172.1	17	2157	26	1991	18	1029	43	185	11	215.7	6.4
Z16-27 - 25	0.12285	0.0006	0.3599	0.00255	6.108	0.055	0.95274	99	1997.3	18	1982	24	1834.9	17	2060	110	484	37	532	37
Z16-27 - 21	0.18237	0.001	0.509	0.011	12.82	0.275	0.99932	99	2673.8	17	2651	97	1978.8	15	1012	18	771	29	702	40
Z16-27 - 41	0.12256	0.0006	0.3569	0.00275	6.021	0.055	0.96371	99	1993	18	1967	26	1972	29	1150	110	99.8	5.8	192	9.6
Z16-27 - 6	0.12037	0.0007	0.3495	0.0033	5.818	0.065	0.924	99	1961	20	1932	31	2315	43	1680	170	347	24	546	21
Z16-27 - 37	0.12376	0.0007	0.3576	0.00345	6.108	0.065	0.9844	98	2010.3	18	1971	33	1972.9	17	184.4	5.8	192	4.5	188.6	4.6
Z16-27 - 5	0.12255	0.0007	0.3538	0.0026	5.981	0.06	0.85349	98	1992.8	20	1953	25	1949	19	574	41	707	61	737	46
Z16-27 - 39**	0.12675	0.0007	0.3656	0.0025	6.378	0.055	0.79126	98	2052.5	18	2008.8	23	2147	31	805	17	558.4	7.6	578	21
Z16-27 - 34	0.12168	0.0006	0.3472	0.00235	5.843	0.05	0.93556	97	1980.2	18	1921.3	23	1823.5	15	1086	68	162.5	6.9	186.8	2.9
Z16-27 - 9	0.13524	0.0007	0.3839	0.00295	7.156	0.07	0.88006	97	2166.3	19	2094	28	2029.1	15	336	13	336	22	337	21
Z16-27 - 38	0.12298	0.0007	0.3468	0.0024	5.881	0.05	0.86538	96	1999	18	1919.1	23	1813	30	3830	140	713	90	625	72

Z16-27 - 16	0.12244	0.0007	0.3449	0.00295	5.83	0.065	0.97265	96	1991	20	1910	28	2165.7	16	1299	81	335	12	356	10					
Z16-27 - 36	0.12597	0.0007	0.3541	0.0024	6.167	0.05	0.8613	96	2041.6	18	1954	23	2631	35	468	12	274	6	404	11					
Z16-27 - 3	0.12742	0.0007	0.3578	0.00285	6.283	0.06	0.91535	96	2061.9	19	1972	27	2014	19	290.5	7.5	103.6	2.5	111.5	4.4					
Z16-27 - 4	0.1207	0.0011	0.334	0.008	5.59	0.17	0.99542	95	1964	33	1858	79	1999.7	15	346	29	203	17	212	13					
Z16-27 - 22	0.12205	0.0007	0.3312	0.0036	5.59	0.07	0.9911	93	1985.6	19	1844	35	1914	21	270	17	191	12	205.5	6.1					
Z16-27 - 20	0.12863	0.0007	0.3447	0.0024	6.128	0.05	0.96409	92	2078.6	18	1909.4	23	2632	16	157.9	6.5	95.2	2.4	131.4	2.2					
Z16-27 - 19	0.1561	0.001	0.406	0.008	8.79	0.2	0.99925	91	2413	22	2197	72	1958.4	15	1600	110	339	22	345	12					
Z16-27 - 24	0.11864	0.0007	0.3033	0.00495	4.97	0.09	0.99519	88	1935	19	1707	49	1697	17	2460	180	299	12	362.3	8.2					
Z16-27 - 14	0.11985	0.0007	0.2981	0.00215	4.958	0.045	0.93291	86	1953.1	19	1682	21	2015.9	17	376.9	9	248.5	5.4	281.8	8.4					
Z16-27 - 8	0.09624	0.0005	0.2282	0.0024	3.016	0.0335	0.97287	85	1551.6	19	1325	25	1950	20	1395	83	461	41	517	26					
Z16-27 - 12	0.1257	0.0008	0.307	0.0085	5.32	0.145	0.99144	84	2038	22	1721	83	1812	15	1790	100	652	15	697	16					
Z16-27 - 10	0.11424	0.0006	0.2738	0.00235	4.32	0.0435	0.97805	84	1867	19	1560	24	2012.2	15	1004	72	336	31	401	22					
Z16-27 - 28**	0.12401	0.0007	0.2971	0.00265	5.094	0.05	0.98193	83	2013.9	18	1677	26	1868	47	652	23	296	25	335	25					
Z16-27 - 23	0.12354	0.0007	0.2941	0.00235	5.025	0.045	0.95165	83	2007.2	18	1662	23	1744	67	880	150	297	26	357	29					
Z16-27 - 7	0.2236	0.0013	0.463	0.0075	14.31	0.26	0.98608	82	3006.1	19	2452	68	1734	46	1284	87	820	120	559	31					
Z16-27 - 26	0.1377	0.0009	0.3126	0.00445	5.93	0.105	0.98591	80	2197	21	1753	44	2040.6	17	273	18	205	19	227	12					
Z16-27 - 40	0.13013	0.0007	0.2881	0.0033	5.211	0.055	0.94373	78	2098.9	20	1632	33	1909	55	221	14	144	21	155	19					
Z16-27 - 35	0.15674	0.0009	0.337	0.006	7.29	0.13	0.9912	77	2420	18	1872	59	1991.4	15	614	49	241	15	232	11					
Z16-27 - 18	0.12684	0.0008	0.258	0.006	4.53	0.125	0.99857	72	2054	21	1479	63	1415	19	2880	150	249	14	277.2	7.4					
Z16-27 - 11	0.12776	0.0007	0.256	0.0105	4.52	0.175	0.99954	71	2066.4	20	1470	110	2768	35	145.2	5.3	67.3	3.4	115.4	2.8					
Z16-27 - 30	0.2281	0.0025	0.3943	0.00375	12.38	0.225	0.88124	71	3036	36	2143	35	1489	83	2260	440	49	14	161	36					
Z16-27 - 15	0.11903	0.0006	0.205	0.0105	3.37	0.17	0.99987	62	1940.9	18	1200	110	2665	43	1020	170	459	74	770	86					
Z16-27 - 1	0.151	0.0017	0.148	0.005	3.03	0.065	0.99852	38	2356	39	890	57	2000.7	15	185.7	3.8	77.4	3.3	81.9	2.1					
Z16-27 - 31	0.6175698	0.003	-1.82E-05	0.0000008	-0.00155	0.00007	0.99848	0	4549.237	14	-0.117	0.01	1994.2	15	941	23	821	30	874	39					
Z16-27 - 32	0.618492	0.0031	-0.000106	1.95E-06	-0.00903	0.000175	0.99999	0	4551.399	14	-0.682	0.025	1426	38	2820	160	1353	58	972	14					
Z16-26 - 23	0.1382	0.0008	0.434	0.005	8.29	0.115	0.98602	105	2203.9	19	2324	46	2020	25	275	72	112	16	113	14					
Z16-26 - 16	0.1251	0.0007	0.38	0.00275	6.568	0.055	0.89581	102	2029.4	18	2076	26	1928.2	15	329	16	102.5	7.2	97.8	3.6					
Z16-26 - 14	0.13062	0.0007	0.3879	0.0026	6.997	0.06	0.93592	100	2105.5	17	2113.1	24	1585	69	635	91	143	11	160	13					
Z16-26 - 20	0.18138	0.0009	0.5114	0.00345	12.805	0.11	0.96011	100	2664.7	17	2662.5	29	1995.4	15	420.3	8.7	184.7	3.4	158.4	7.7					
Z16-26 - 8	0.12537	0.0007	0.369	0.0026	6.397	0.055	0.94349	100	2033.3	18	2025	24	1999	18	303.5	8.6	120.8	5.2	118.9	5.7					
Z16-26 - 13	0.13347	0.0007	0.3862	0.0026	7.141	0.06	0.82005	98	2143.2	18	2105.3	24	2031.9	15	661	28	171	10	167.9	7.8					
Z16-26 - 10	0.12559	0.0007	0.3635	0.00455	6.32	0.09	0.98587	98	2036.3	19	1998	43	1540	75	1330	74	193	14	191	18					

Z16-26 - 5	0.12571	0.0007	0.3541	0.003	6.162	0.06	0.95636	96	2038	18	1954	28	1927	77	261	17	144	40	132	25
Z16-26 - 12	0.12477	0.0008	0.3419	0.00335	5.94	0.06	0.89397	93	2028	23	1896	32	1842	18	462	91	51	3.1	51	2.5
Z16-26 - 18	0.1504	0.0008	0.3953	0.00395	8.21	0.105	0.97793	91	2349.7	18	2147	36	1945	17	284	6	98.3	2.4	130.6	4.3
Z16-26 - 11	0.13028	0.0007	0.3407	0.0024	6.136	0.055	0.86918	90	2100.9	19	1890	23	1704	70	560	19	184	17	215.1	5.7
Z16-26 - 3	0.1254	0.0009	0.327	0.0145	5.71	0.255	0.98185	89	2034	25	1820	140	1966.9	17	199	38	99	22	95	20
Z16-26 - 6	0.12568	0.0007	0.3268	0.00225	5.68	0.049	0.88339	89	2037.5	19	1822.6	22	2129.1	15	304.9	9	115	2.4	118.1	2
Z16-26 - 21	0.13698	0.0008	0.3301	0.0033	6.267	0.07	0.96179	84	2188	20	1839	32	2111	15	922	28	385	14	397	11
Z16-26 - 1	0.12398	0.0007	0.2997	0.0025	5.139	0.055	0.92185	84	2013	20	1690	25	1759	29	1465	82	96.4	2.2	112.4	2.3
Z16-26 - 19	0.11997	0.0006	0.283	0.0065	4.7	0.11	0.99865	82	1955	18	1605	66	2055	15	323	27	217	21	231	15
Z16-26 - 22	0.12407	0.0008	0.282	0.0085	4.83	0.135	0.9976	79	2015	21	1600	84	1978	22	1026	73	127.9	7.8	211	15
Z16-26 - 15	0.12249	0.0007	0.2756	0.0047	4.66	0.08	0.99692	79	1992	18	1569	48	2254	23	1041	68	426	18	595	25
Z16-26 - 9	0.13902	0.0007	0.3017	0.00265	5.793	0.06	0.96006	77	2214.3	18	1699	26	1763	40	1111	33	186	21	187	17
Z16-26 - 17	0.1425	0.001	0.3047	0.00305	5.98	0.085	0.94634	76	2257	23	1714	30	2665.4	16	767	44	470	20	671	15
Z16-26 - 2	0.1377	0.0012	0.232	0.011	4.41	0.185	0.99312	61	2196	31	1340	120	2014	19	651	27	234	28	256	21
Z16-26 - 7	0.1288	0.0011	0.214	0.011	3.8	0.17	0.99892	60	2080	31	1250	120	1807	36	2010	200	1760	110	1700	30
Z16-26 - 4	0.13	0.0014	0.196	0.0115	3.53	0.175	0.99984	55	2096	36	1150	120	2263	25	850	100	750	180	840	140
Z16-17 - 5	0.1862	0.001	0.1375	0.00215	3.55	0.06	0.99712	31	2708.1	17	830	25	1537	27	1351	82	238	12	236.6	9.7
Z16-17 - 3	0.11484	0.0007	0.0561	0.00165	0.893	0.026	0.99245	19	1876	21	352	20	647	28	2640	340	113	14	102.9	6.6
Z16-17 - 4	0.3632	0.005	0.00542	0.00013	0.2716	0.0037	0.9765	1	3761	41	34.9	1.7	243.9	5.9	23950	690	2270	140	1002	27
Z16-17 - 1	0.673176	0.0033	-2.35E-06	1.15E-07	-0.00022	1.15E-05	0.99088	0	4675.79	15	-0.0151	0.0015	-0.22	0.023	20400	2400	14720	760	-0.7954	0.000037
Z16-17 - 2	0.66942	0.0033	-3.2E-06	8E-08	-0.0003	7.5E-06	1	0	4667.31	15	-0.0206	0.001	-0.301	0.015	15420	320	5851	83	-0.7974	0.000048
Z_GJ1_1	0.06042	0.0007	0.09675	0.0013	0.8057	0.015	0.74792	96	621	22	595.3	7.7	600	8.4	403	16	11.16	0.79	2.803	0.087
Z_GJ1_2	0.06018	0.0008	0.09739	0.0014	0.8063	0.016	0.50345	98	609	28	599.1	8	600.4	9	456.8	5.9	12.72	0.93	3.18	0.13
Z_GJ1_3	0.05978	0.0007	0.09573	0.0014	0.7902	0.013	0.57722	99	594	25	589.3	8.1	591.3	7.6	405	19	10.96	0.78	2.81	0.14
Z_GJ1_4	0.06011	0.0007	0.09605	0.0013	0.7935	0.014	0.57667	98	606	25	591.2	7.5	593.1	8	398	18	10.6	1.2	2.807	0.064
Z_GJ1_5	0.0603	0.0007	0.09702	0.0013	0.8059	0.014	0.45473	97	613	26	596.9	7.5	600.1	8.1	426	22	11.7	1.2	2.98	0.12
Z_GJ1_6	0.0596	0.0007	0.09622	0.0013	0.7921	0.014	0.63038	101	588	24	593.1	8.5	592.3	8.1	405	20	10.62	0.84	2.89	0.1
Z_GJ1_7	0.05995	0.0007	0.09763	0.0014	0.8049	0.014	0.56334	100	600	26	600.5	8.1	599.6	8.1	393	21	11.31	0.63	2.83	0.11
Z_GJ1_8	0.06018	0.0007	0.09718	0.0013	0.8066	0.014	0.57418	98	609	25	597.9	7.5	600.5	7.9	406	17	12.2	1	2.782	0.086
Z_GJ1_9	0.05997	0.0007	0.09764	0.0013	0.8092	0.014	0.37171	100	601	27	600.6	7.7	602	7.9	408	23	11.3	1.4	2.79	0.14
Z_GJ1_10	0.06	0.0007	0.09579	0.0013	0.7955	0.014	0.53567	98	602	25	589.7	7.6	594.2	8.2	424	19	11.68	0.95	2.83	0.13

Z_GI1_11	0.06012	0.0007	0.09868	0.0014	0.8226	0.014	0.51044	100	607	27	606.7	7.9	609.5	8	413	21	9.84	0.77	2.88	0.15			
Z_GI1_12	0.0595	0.0007	0.09771	0.0013	0.8086	0.015	0.66857	103	584	25	601	7.9	601.7	8.2	434	20	9.3	1.1	3.12	0.12			
Z_GI1_13	0.05999	0.0008	0.09614	0.0013	0.8029	0.014	0.29904	98	602	28	591.7	7.8	598.4	8.2	383	23	9.9	1.1	2.62	0.11			
Z_GI1_14	0.06003	0.0009	0.09779	0.0013	0.8191	0.016	0.2665	100	603	31	601.4	7.8	607.5	8.8	392	20	9.5	1.1	2.81	0.14			
Z_GI1_15	0.05987	0.0007	0.09814	0.0013	0.8176	0.015	0.53106	101	598	26	603.5	7.6	606.7	8.4	391	20	10.37	0.93	2.76	0.12			
Z_GI1_16	0.05993	0.0008	0.09527	0.0014	0.7922	0.015	0.52145	98	599	30	586.6	8.1	592.4	8.5	375	25	10.1	1.4	2.57	0.14			
Z_GI1_17	0.05973	0.0008	0.09835	0.0014	0.8135	0.015	0.58738	102	592	28	604.8	8	604.4	8.5	385	24	9.88	0.68	2.59	0.13			
Z_GI1_18	0.05966	0.0008	0.09784	0.0014	0.8126	0.015	0.37853	102	590	29	601.7	8.1	603.9	8.2	391	19	9.9	1.2	2.806	0.082			
Z_GI1_19	0.06	0.0008	0.09784	0.0013	0.8143	0.016	0.53582	100	602	28	601.7	7.9	604.8	8.8	404	17	10.3	1	2.784	0.075			
Z_GI1_20	0.0598	0.0007	0.09777	0.0013	0.809	0.015	0.63372	100	599	28	601.3	7.8	601.8	8.4	401	19	10.82	0.88	2.693	0.092			
Z_GI1_21	0.05999	0.0007	0.09746	0.0013	0.8107	0.014	0.5959	100	602	24	599.5	7.7	602.8	7.8	391	17	10.1	1.3	2.656	0.088			
Z_GI1_22	0.06028	0.0007	0.09821	0.0014	0.8176	0.015	0.64996	99	612	25	603.9	7.9	606.7	8.2	408	23	9.9	1	2.97	0.11			
Z_GI1_23	0.05966	0.0007	0.09719	0.0013	0.8014	0.016	0.75665	101	590	27	597.9	7.8	597.6	8.8	431	19	10.3	0.93	3.07	0.11			
Z_GI1_24	0.06026	0.0007	0.09737	0.0014	0.8092	0.015	0.52969	98	611	26	599	8	602	8.2	395	17	10.2	1.2	2.673	0.065			
Z_GI1_25	0.06005	0.0008	0.09672	0.0013	0.8009	0.014	0.30606	99	604	28	595.1	7.7	597.3	8	395	19	11.05	0.98	2.65	0.1			
Z_GI1_26	0.06001	0.0008	0.09706	0.0013	0.8005	0.016	0.68883	99	602	28	597.1	7.7	597	8.8	398	24	10.5	1.3	2.81	0.11			
Z_GI1_27	0.06014	0.0008	0.09668	0.0013	0.7965	0.015	0.58296	98	607	28	594.9	7.9	594.8	8.6	415	24	10.2	1	3.03	0.12			
Z_GI1_28	0.06041	0.0007	0.09746	0.0013	0.8049	0.014	0.32306	97	617	25	599.5	7.6	599.6	7.8	427	20	11.9	1.2	3.031	0.091			
Z_GI1_29	0.05987	0.0007	0.09732	0.0013	0.7928	0.014	0.49782	100	597	26	598.7	7.7	592.7	8	413	14	11.6	1.1	2.92	0.12			
Z_GI1_30	0.06021	0.0008	0.09349	0.0013	0.7647	0.015	0.68887	94	610	29	576.2	7.7	577.9	8.2	409	21	10.8	1.1	2.894	0.087			
Z_Plesovice_1	0.05337	0.0006	0.05145	0.00067	0.3794	0.0066	0.02421	94	343	27	323.45	4.1	326.6	4.8	1084	43	138.5	3.8	20.78	0.23			
Z_Plesovice_2	0.05314	0.0006	0.05377	0.00073	0.3938	0.007	0.69769	101	333	26	337.6	4.5	337.1	5.1	776	35	80.3	3.6	11.82	0.27			
Z_Plesovice_3	0.05292	0.0006	0.05434	0.00072	0.3996	0.0069	0.36791	105	324	26	341.1	4.4	341.4	5	1142	26	115.9	3	21.15	0.43			
Z_Plesovice_4	0.05295	0.0007	0.055	0.00072	0.4057	0.0071	0.13922	106	325	28	345.1	4.4	345.8	5.2	973	40	112	3	17.06	0.49			
Z_Plesovice_5	0.05345	0.0006	0.05426	0.00073	0.4038	0.007	0.63314	98	346	26	340.6	4.5	344.4	5.1	947	53	99.9	5.4	15.96	0.54			
Z_Plesovice_6	0.05326	0.0006	0.05475	0.00073	0.4034	0.007	0.29219	101	339	25	343.6	4.4	344.1	5	810	43	91.3	5.2	14.28	0.51			
Z_Plesovice_7	0.05335	0.0006	0.05486	0.00072	0.4062	0.0073	0.51354	100	343	26	344.3	4.4	346.1	5.3	891	52	93.2	4.9	14.76	0.53			
Z_Plesovice_8	0.05325	0.0007	0.05382	0.0007	0.3977	0.0069	0.2391	100	338	29	337.9	4.3	340	5	650	45	61.7	4	9.39	0.42			
Z_Plesovice_9	0.05345	0.0007	0.05463	0.00076	0.4032	0.0082	0.62546	99	346	31	342.9	4.6	343.9	5.9	789	42	72.5	3.9	12.65	0.33			
Z_Plesovice_1	0.05321	0.0006	0.05232	0.0007	0.3832	0.0067	0.59253	98	337	27	328.7	4.3	329.4	4.9	939	62	115.8	9.4	17.2	1.1			
Z_Plesovice_1	0.05302	0.0007	0.0545	0.00074	0.3968	0.0073	0.47537	104	328	28	342.1	4.5	339.3	5.3	1061	42	128	6.4	19.98	0.61			
Z_Plesovice_1	0.05291	0.0006	0.05462	0.00072	0.3931	0.0067	0.39881	106	324	26	342.8	4.4	336.6	4.9	1084	71	140	11	20.6	1.1			

Z_Plesovice_1	0.0532	0.0007	0.05474	0.00078	0.3946	0.007	0.52408	102	336	30	343.5	4.8	337.7	5.1	1153	47	142.1	7.2	23.04	0.75
Z_91500_1	0.07525	0.0009	0.1797	0.0026	1.865	0.038	0.74391	99	1074	24	1065.1	14	1068.6	13	81.9	3.5	31.4	1.6	15.53	0.34
Z_91500_2	0.07475	0.0012	0.1792	0.003	1.843	0.041	0.67442	100	1060	31	1063	16	1063	16	76	3.9	28.4	1.3	14.14	0.36
Z_91500_3	0.07397	0.0011	0.1782	0.0027	1.822	0.036	0.33595	102	1039	30	1057.1	15	1053.2	13	80.9	3.2	31.7	1.1	15.22	0.33
Z_91500_4	0.07586	0.001	0.1784	0.003	1.851	0.041	0.77031	97	1090	27	1058	17	1066	16	80.3	2.8	30	1.3	15.01	0.25
Z_91500_5	0.07436	0.001	0.1805	0.0026	1.85	0.035	0.6784	102	1050	26	1069.7	14	1063.4	12	79.5	2.8	29.7	1.1	14.99	0.29
Z_91500_6	0.07503	0.001	0.1785	0.0025	1.837	0.035	0.51512	99	1068	26	1058.7	14	1058.8	13	80.6	4.8	31.6	1.8	15.02	0.54
Z_91500_7	0.0754	0.001	0.1782	0.0029	1.865	0.039	0.69728	98	1078	27	1057.3	16	1068.5	14	80.5	3.6	32.1	1.9	15.02	0.39
Z_91500_8	0.07494	0.001	0.1789	0.0029	1.851	0.038	0.7173	100	1065	27	1061	16	1063.7	14	78.6	3.9	31.4	1.4	14.92	0.36
Z_91500_9	0.0749	0.001	0.1787	0.0029	1.845	0.039	0.70565	99	1069	26	1059.9	16	1061.5	14	82.4	4.1	32.1	1.8	15.09	0.29
Z_91500_10	0.0746	0.0013	0.1794	0.0029	1.855	0.047	0.68752	101	1055	35	1064	16	1065	17	78.7	3.9	26.9	1.4	14.93	0.39
Z_91500_11	0.07421	0.0011	0.1796	0.0028	1.846	0.036	0.30176	102	1046	29	1064.9	15	1062.1	13	79.4	4.1	24.9	1.8	14.85	0.46
Z_91500_12	0.07474	0.0011	0.1795	0.0028	1.859	0.038	0.7252	100	1060	29	1064.3	15	1066.5	13	80.7	3.1	29.8	1.6	15.12	0.33
Z_91500_13	0.07424	0.0012	0.1787	0.0028	1.845	0.039	0.70274	101	1046	31	1059.6	15	1061.5	14	79.9	3.8	29.9	1.6	14.94	0.44
Z_91500_14	0.0753	0.0014	0.1808	0.0029	1.904	0.042	0.45525	99	1080	34	1071.5	16	1082	15	79.5	4.6	29.2	1.9	14.97	0.49
Z_91500_15	0.07547	0.0009	0.1793	0.0028	1.878	0.04	0.82708	98	1080	25	1063.1	15	1073	14	80.6	4.3	30	1.5	15.14	0.54
Z_91500_16	0.07471	0.0011	0.1766	0.0029	1.825	0.04	0.51215	99	1059	30	1048.5	16	1054.4	14	79.2	5.6	27	2	14.79	0.64
Z_91500_17	0.07389	0.0009	0.181	0.0028	1.85	0.036	0.69505	103	1037	25	1072.4	15	1063.3	13	80	4.9	28.7	1.7	15.04	0.6
Z_91500_18	0.0745	0.0009	0.1769	0.0029	1.836	0.036	0.77122	100	1054	23	1049.9	16	1058.4	13	79.9	5.5	30.7	2	15.01	0.59
Z_91500_19	0.07513	0.001	0.18	0.0027	1.871	0.038	0.75091	99	1075	28	1067.1	14	1070.7	13	80.4	4.3	31.3	2	15.03	0.44
Z_91500_20	0.07531	0.0011	0.1797	0.0028	1.869	0.038	0.66322	99	1080	27	1065.1	15	1070.1	14	80.4	4.6	27.9	1.8	15.04	0.45
Z_91500_21	0.07503	0.001	0.1785	0.0027	1.852	0.038	0.69951	99	1068	27	1058.9	15	1064	14	78.6	5	26.5	2	14.7	0.67
Z_91500_22	0.07477	0.0011	0.1777	0.0032	1.83	0.046	0.86672	99	1061	30	1055	17	1056	16	80.2	4.5	30.9	1.3	15.08	0.49
Z_91500_23	0.07512	0.0012	0.1797	0.0028	1.86	0.042	0.62032	100	1070	31	1065.5	15	1067	15	80.5	2.7	32.1	1	15.02	0.21
Z_91500_24	0.07502	0.0009	0.1798	0.0028	1.848	0.035	0.55645	100	1068	25	1065.7	15	1062.7	13	78.8	4.1	29.3	1.6	14.84	0.47
Z_91500_25	0.075	0.0012	0.1797	0.0029	1.841	0.045	0.57707	100	1067	33	1065.2	16	1060	16	81.4	5.4	30.7	2.3	15.31	0.72
Z_91500_26	0.0755	0.0015	0.1801	0.0029	1.871	0.044	0.42772	99	1080	39	1067.4	16	1071	16	79.2	4.2	28.9	1.5	14.88	0.45
Z_91500_27	0.07516	0.001	0.1773	0.0027	1.818	0.038	0.47873	98	1071	28	1052.4	15	1051.7	14	80.7	4.6	33	1.6	15.15	0.58
Z_91500_28	0.07485	0.0012	0.1806	0.0034	1.833	0.042	0.68555	101	1063	31	1070	18	1057	15	79.9	3.9	29.3	1.3	14.98	0.45

* ρ denotes error correlation between $^{206}Pb/^{238}U$ and $^{207}Pb/^{235}U$ used to produce concordia diagram

** Signifies rim analyses not included in concordia or age calculations unless otherwise stated

Table S3. Individual zircon Lu-Hf analytical data

Grain number	Hf^{176}/Hf^{177}	2σ error	Lu^{176}/Hf^{177}	Yb^{176}/Hf^{177}	U-Pb AGE	Hf_i	εHf	2σ error	T(DM)	T(DM) - Crustal
Z16_26_5	0.28136	7E-05	0.00242	0.0312	2090	0.281264	-6.6	2.5	2.74	3.07
Z16_26_6	0.281443	5E-05	0.00191	0.02937	2090	0.281367	-2.9	1.6	2.59	2.85
Z16_26_8	0.281375	5E-05	0.00074	0.01182	2090	0.281346	-3.7	1.7	2.6	2.9
Z16_26_10	0.281404	5E-05	0.00321	0.0473	2090	0.281276	-6.2	1.8	2.74	3.05
Z16_26_11	0.281368	5E-05	0.00232	0.0345	2090	0.281276	-6.2	1.9	2.73	3.05
Z16_26_12	0.281477	6E-05	0.00287	0.0556	2090	0.281363	-3.1	2.2	2.61	2.86
Z16_26_13	0.281423	6E-05	0.00141	0.02548	2090	0.281367	-2.9	2.1	2.58	2.85
Z16_26_14	0.281407	7E-05	0.00160	0.02772	2090	0.281343	-3.8	2.5	2.62	2.9
Z16_26_16	0.281417	6E-05	0.00225	0.0357	2090	0.281328	-4.3	2.2	2.65	2.94
Z16_26_18	0.281044	4E-05	0.00311	0.0661	2350	0.280905	-13.3	1.3	3.25	3.67
Z16_26_20	0.281222	4E-05	0.00312	0.0652	2664	0.281063	-0.4	1.5	3	3.15
Z16_26_23	0.28132	5E-05	0.00131	0.02874	2203	0.281265	-3.9	1.7	2.72	3
Z16_27_2	0.281606	8E-05	0.00438	0.0971	2335	0.281411	4.3	2.7	2.53	2.61
Z16_27_3	0.281519	5E-05	0.00454	0.0998	2056	0.281342	-4.6	1.8	2.67	2.93
Z16_27_4	0.281441	5E-05	0.00089	0.0205	2056	0.281406	-2.3	1.7	2.53	2.79
Z16_27_6	0.281511	7E-05	0.00396	0.0874	2056	0.281356	-4.1	2.3	2.64	2.9
Z16_27_9	0.281524	5E-05	0.00099	0.02103	2056	0.281485	0.5	1.8	2.42	2.62
Z16_27_13	0.281461	7E-05	0.00254	0.0548	2172	0.281356	-1.4	2.5	2.61	2.83
Z16_27_16	0.281494	5E-05	0.00381	0.0794	2056	0.281345	-4.5	1.8	2.66	2.92
Z16_27_17	0.281456	5E-05	0.00176	0.04011	2056	0.281387	-3.0	1.7	2.56	2.83
Z16_27_19	0.281605	7E-05	0.00300	0.069	2413	0.281467	8.1	2.5	2.44	2.45
Z16_27_20	0.281627	7E-05	0.00318	0.06576	2056	0.281503	1.1	2.6	2.42	2.59
Z16_27_22	0.281406	5E-05	0.00176	0.0399	3006	0.281305	16.3	1.8	2.63	2.44
Z16_27_25	0.281415	6E-05	0.00419	0.0984	2056	0.281251	-7.8	2	2.8	3.12
Z16_27_27	0.281497	5E-05	0.00191	0.03386	2056	0.281422	-1.7	1.6	2.52	2.76
Z16_27_29	0.2812	4E-05	0.00232	0.0543	2056	0.281109	-12.9	1.5	2.96	3.42
Z16_27_34	0.281466	8E-05	0.00334	0.0621	2056	0.281335	-4.8	2.7	2.66	2.94
Z16_33_22	0.282067	4E-05	0.00136	0.01198	498	0.282054	-14.8	1.4	1.69	2.36
Z16_33_7	0.282016	4E-05	0.00334	0.0372	498	0.281985	-17.2	1.5	1.85	2.51
Z16_33_21	0.282048	4E-05	0.00146	0.01435	498	0.282034	-15.5	1.5	1.72	2.4
Z16_33_24	0.282114	6E-05	0.00509	0.0588	498	0.282067	-14.3	2.2	1.8	2.33
Z16_33_26	0.28192	5E-05	0.00609	0.072	498	0.281863	-21.5	1.9	2.16	2.77
Z16_35_2	0.281478	7E-05	0.00140	0.03194	1881	0.281428	-5.6	2.3	2.51	2.85
Z16_35_3	0.281355	5E-05	0.00179	0.04326	1775	0.281295	-12.8	1.8	2.71	3.2
Z16_35_4	0.28136	5E-05	0.00059	0.015	1598	0.281342	-15.1	1.7	2.62	3.2
Z16_35_5	0.281587	6E-05	0.00171	0.03432	1737	0.281531	-5.3	2	2.38	2.72
Z16_35_6	0.281443	5E-05	0.00279	0.0619	2015	0.281336	-5.8	1.8	2.65	2.96
Z16_35_7	0.281594	7E-05	0.00117	0.02329	1651	0.281558	-6.3	2.3	2.33	2.71
Z16_35_8	0.28142	6E-05	0.00299	0.0632	2080	0.281302	-5.5	2.1	2.7	3

Z16_35_9	0.281491	5E-05	0.00205	0.03637	1787	0.281422	-8.0	1.6	2.53	2.92
Z16_35_10	0.281554	6E-05	0.00223	0.04	1820	0.281477	-5.3	2.2	2.46	2.78
Z16_35_11	0.281433	5E-05	0.00221	0.04	1780	0.281358	-10.4	1.8	2.63	3.06
Z16_35_12	0.28138	7E-05	0.00342	0.0552	2035	0.281248	-8.4	2.4	2.79	3.14
Z16_35_13	0.281372	5E-05	0.00107	0.02098	1621	0.281339	-14.7	1.6	2.63	3.2
Z16_35_16	0.281374	5E-05	0.00284	0.0507	1904	0.281271	-10.6	1.8	2.76	3.17
Z16_35_17	0.281413	4E-05	0.00415	0.06257	1885	0.281265	-11.3	1.4	2.8	3.19
Z16_35_19	0.281348	4E-05	0.00198	0.03582	1673	0.281285	-15.4	1.4	2.73	3.28
Z16_35_20	0.281264	6E-05	0.00205	0.03294	1912	0.28119	-13.3	1.9	2.85	3.34
Z16_35_21	0.281453	6E-05	0.00192	0.02887	1990	0.28138	-4.8	2.1	2.58	2.89
Z16_35_25	0.281468	5E-05	0.00350	0.05566	1798	0.281349	-10.3	1.6	2.67	3.07
Z16_35_26	0.281594	5E-05	0.00375	0.0521	1818	0.281465	-5.7	1.9	2.5	2.81
Z16_35_27	0.281423	5E-05	0.00357	0.0483	1996	0.281288	-7.9	1.8	2.74	3.08
Z16_35_28	0.281372	7E-05	0.00373	0.0434	1829	0.281243	-13.4	2.3	2.83	3.27
Z16_35_29	0.281376	6E-05	0.00318	0.0361	1714	0.281273	-14.9	2.1	2.78	3.28
Z16_35_30	0.281422	5E-05	0.00437	0.0546	1714	0.28128	-14.7	1.6	2.81	3.27
Z16_35_31	0.281557	5E-05	0.00246	0.0352	1858	0.28147	-4.6	1.6	2.47	2.77
Z16_35_32	0.28167	5E-05	0.00670	0.0858	1658	0.28146	-9.6	1.7	2.61	2.92
Z16_35_33	0.281453	7E-05	0.00272	0.03697	1952	0.281352	-6.7	2.4	2.63	2.97
Z16_35_34	0.281495	4E-05	0.00233	0.03123	1847	0.281413	-6.9	1.4	2.55	2.9
Z16_35_35	0.281496	7E-05	0.00192	0.02218	1780	0.281431	-7.8	2.6	2.52	2.91
Z16_35_36	0.281428	6E-05	0.00375	0.0467	2056	0.281281	-6.8	2.2	2.75	3.06
Z16_35_37	0.281446	4E-05	0.00321	0.03755	1582	0.28135	-15.2	1.5	2.68	3.2
Z16_40_2	0.281533	5E-05	0.00191	0.06419	2009	0.28146	-1.5	1.7	2.47	2.71
Z16_40_5	0.281439	5E-05	0.00145	0.05186	2009	0.281384	-4.2	1.6	2.57	2.87
Z16_40_7	0.281412	6E-05	0.00144	0.0413	2009	0.281357	-5.2	2	2.6	2.92
Z16_40_8	0.281457	6E-05	0.00103	0.03842	2009	0.281418	-3.0	2	2.51	2.8
Z16_40_12	0.281454	5E-05	0.00230	0.0853	2009	0.281366	-4.8	1.8	2.6	2.9
Z16_40_14	0.28153	5E-05	0.00160	0.0603	2009	0.281469	-1.2	1.8	2.45	2.69
Z16_40_17	0.281454	5E-05	0.00136	0.052	2009	0.281402	-3.6	1.6	2.54	2.83
Z16_40_23	0.281521	6E-05	0.00132	0.05119	2009	0.281471	-1.1	2.2	2.44	2.68
Z16_40_24	0.281555	4E-05	0.00280	0.1115	2009	0.281448	-1.9	1.3	2.49	2.73
Z16_40_25	0.281548	5E-05	0.00140	0.0524	2009	0.281494	-0.3	1.6	2.41	2.63
Z16_40_27	0.281413	4E-05	0.00098	0.04244	2009	0.281375	-4.5	1.5	2.57	2.88
Z16_40_29	0.281472	5E-05	0.00181	0.0801	2009	0.281403	-3.5	1.8	2.54	2.83
Z16_40_31	0.2814	4E-05	0.00129	0.0551	2009	0.281351	-5.4	1.5	2.61	2.94
Z16_40_37	0.281488	5E-05	0.00157	0.0736	2009	0.281428	-2.6	1.7	2.51	2.77
Z16_40_45	0.281474	6E-05	0.00203	0.0955	2009	0.281397	-3.8	2.1	2.56	2.84
Z16_41_20	0.282213	6E-05	0.00100	0.0525	1040	0.282193	2.4	2.0	1.47	1.71
Z16_41_21	0.282238	7E-05	0.00052	0.02483	1040	0.282228	3.6	2.3	1.41	1.64
Z16_41_23	0.282227	6E-05	0.00053	0.025	1040	0.282217	3.2	2.0	1.43	1.66
Z16_41_24	0.282216	5E-05	0.00055	0.02397	1040	0.282205	2.8	1.6	1.45	1.69

Z16_41_26	0.282234	6E-05	0.00073	0.0367	1040	0.28222	3.3	2.2	1.43	1.66
Z16_41_27	0.282274	5E-05	0.00059	0.0316	1040	0.282262	4.8	1.7	1.37	1.56
Z16_41_28	0.282219	5E-05	0.00046	0.02287	1040	0.28221	2.9	1.7	1.44	1.68
Z16_41_29	0.282237	5E-05	0.00052	0.0289	1040	0.282227	3.5	1.6	1.42	1.64
Z16_41_30	0.282224	7E-05	0.00036	0.02342	1040	0.282217	3.2	2.6	1.43	1.66
Z16_41_33	0.282276	5E-05	0.00062	0.0419	1040	0.282264	4.9	1.9	1.36	1.56
Z16_41_34	0.282252	5E-05	0.00054	0.03608	1040	0.282241	4.1	1.8	1.40	1.61
Z16_41_35	0.282246	5E-05	0.00059	0.0418	1040	0.282235	3.8	1.8	1.41	1.62
Z16_41_36	0.28226	5E-05	0.00026	0.01818	1040	0.282255	4.5	1.6	1.37	1.58
Z16_41_37	0.28227	6E-05	0.00038	0.02634	1040	0.282263	4.8	2.0	1.36	1.56
Z16_41_38	0.282253	5E-05	0.00032	0.02187	1040	0.282247	4.2	1.6	1.39	1.60
Z16_42_1	0.282199	6E-05	0.00062	0.04557	1039	0.282187	2.1	2.2	1.47	1.73
Z16_42_2	0.282238	5E-05	0.00040	0.02809	1039	0.28223	3.6	1.8	1.41	1.63
Z16_42_3	0.28224	4E-05	0.00038	0.0271	1039	0.282233	3.7	1.5	1.41	1.63
Z16_42_4	0.282203	5E-05	0.00058	0.03837	1039	0.282192	2.3	1.8	1.46	1.72
Z16_42_5	0.282265	7E-05	0.00048	0.03393	1039	0.282256	4.5	2.5	1.37	1.58
Z16_42_6	0.28226	7E-05	0.00058	0.0401	1039	0.282249	4.3	2.5	1.39	1.59
Z16_42_7	0.282247	5E-05	0.00069	0.0462	1039	0.282234	3.8	1.9	1.41	1.63
Z16_42_8	0.282236	6E-05	0.00050	0.03144	1039	0.282226	3.5	2.2	1.42	1.64
Z16_42_9	0.28219	5E-05	0.00033	0.0184	1039	0.282184	2.0	1.8	1.47	1.74
Z16_42_10	0.282241	6E-05	0.00040	0.0264	1039	0.282233	3.7	1.9	1.41	1.63
Z16_42_16	0.282273	5E-05	0.00064	0.0446	1039	0.28226	4.7	1.8	1.37	1.57
Z16_42_18	0.28221	6E-05	0.00040	0.0234	1039	0.282202	2.6	1.9	1.45	1.70
Z16_42_20	0.282248	5E-05	0.00033	0.01756	1039	0.282242	4.0	1.6	1.39	1.61
Z16_42_21	0.282228	4E-05	0.00055	0.0348	1039	0.282217	3.2	1.3	1.43	1.66
Z16_42_23	0.28223	8E-05	0.00067	0.0415	1039	0.282217	3.2	2.7	1.43	1.66

Table S4. Individual zircon trace and rare earth element analyses.

Sample	Zr (CPS)	Zr 2SE (CPS)	Si	Si 2SE	P	P 2SE	Ti	Ti 2SE	Y	Y 2SE	Zr	Zr 2SE	Nb	Nb 2SE	La	La 2SE	Ce	Ce 2SE
Z16-40 - 1	3.06E+07	7.60E+05	1.62E+05	1.10E+04	230	170	21.8	8.7	1963	56	4.31E+05	1.10E+04	3.82	0.5	5.8	1.4	46.4	6.2
Z16-40 - 2	2.85E+07	1.10E+06	1.59E+05	1.10E+04	260	200	7.8	6.1	2716	53	4.24E+05	1.40E+04	1.93	0.49	B.D.	0.031	5.3	1.1
Z16-40 - 3	2.70E+07	1.50E+06	1.71E+05	1.40E+04	270	140	12.5	3	1257	52	4.23E+05	1.00E+04	1.7	0.33	B.D.	0.063	16.2	1.4
Z16-40 - 4	2.95E+07	1.50E+06	1.57E+05	1.00E+04	240	140	14.1	5.4	1802	33	4.26E+05	8.90E+03	1.54	0.35	B.D.	0.023	14.3	1.3
Z16-40 - 5	2.76E+07	1.70E+06	1.61E+05	1.40E+04	220	240	5.8	3.8	1821	33	4.24E+05	1.00E+04	1.52	0.29	B.D.	0.055	15.45	0.84
Z16-40 - 6	2.19E+07	1.10E+06	1.67E+05	1.60E+04	B.D.	330	9.9	7.7	1217	27	4.25E+05	9.50E+03	1.98	0.43	1.41	0.35	20.7	2.7
Z16-40 - 7	2.90E+07	1.30E+06	1.60E+05	1.10E+04	B.D.	150	10.5	3.1	1414	60	4.35E+05	1.20E+04	1.26	0.22	0.15	0.1	7.14	0.99
Z16-40 - 8	2.85E+07	1.50E+06	1.64E+05	8.30E+03	90	140	9.3	5.6	1588	46	4.30E+05	1.20E+04	1.79	0.5	0.127	0.071	13.7	1.2
Z16-40 - 9	2.50E+07	8.40E+05	1.73E+05	2.00E+04	160	390	8.3	4.7	1119	54	4.16E+05	1.60E+04	2.89	0.44	0.97	0.46	9.4	1.8
Z16-40 - 10	7.93E+06	5.70E+05	1.48E+05	4.30E+04	930	660	57	34	2340	460	4.44E+05	2.50E+04	18.8	2.4	76	26	420	130
Z16-40 - 11	2.62E+07	9.60E+05	1.76E+05	1.90E+04	250	220	8.8	5.1	1880	71	4.20E+05	1.50E+04	2.23	0.43	1.17	0.47	21.6	1.7
Z16-40 - 12	3.14E+07	9.60E+05	1.65E+05	8.70E+03	290	170	14.5	2.6	3480	160	4.34E+05	1.60E+04	3.07	0.48	1.44	0.52	7.4	2
Z16-40 - 13	2.62E+07	1.70E+06	1.71E+05	1.30E+04	90	190	540	190	1127	95	4.34E+05	7.90E+03	1.73	0.42	7.5	1.6	47.9	9
Z16-40 - 14	2.68E+07	1.60E+06	1.76E+05	1.40E+04	320	210	6.7	3.6	2280	250	4.34E+05	1.50E+04	2.65	0.78	0.06	0.12	7.2	1.6
Z16-40 - 15	2.75E+07	1.80E+06	1.64E+05	7.90E+03	250	160	13.3	5	2050	150	4.17E+05	1.00E+04	2.55	0.54	2.9	1.6	28	12
Z16-40 - 16	3.49E+07	1.50E+06	1.54E+05	2.30E+04	310	280	5.9	7	782	63	4.24E+05	1.80E+04	1.9	0.64	1.3	1.6	18	12
Z16-40 - 17	2.66E+07	1.50E+06	1.64E+05	1.40E+04	110	210	6.5	4.5	1875	53	4.42E+05	7.90E+03	2.41	0.53	0.13	0.14	6.06	0.94
Z16-40 - 18	2.69E+07	1.30E+06	1.54E+05	1.10E+04	30	200	10.7	5.7	1658	26	4.25E+05	8.70E+03	1.26	0.2	B.D.	0.05	3.99	0.59
Z16-40 - 19	2.75E+07	1.10E+06	1.63E+05	1.20E+04	140	140	8.6	3.9	1337	44	4.31E+05	9.00E+03	1.42	0.38	0.09	0.091	9.8	1.1
Z16-40 - 20	3.03E+07	1.30E+06	1.65E+05	1.10E+04	210	270	9.5	2.7	1505	33	4.20E+05	8.30E+03	2.37	0.38	1.89	0.34	16.3	1.9
Z16-40 - 21	2.73E+07	1.50E+06	1.67E+05	1.00E+04	260	190	16.8	5.6	1774	66	4.26E+05	1.10E+04	2.38	0.43	11.2	1.9	46.7	2.5
Z16-40 - 22	3.03E+07	1.20E+06	1.47E+05	1.00E+04	350	170	10.3	4.6	4780	130	4.39E+05	1.30E+04	2.64	0.35	3.74	0.48	35	2.9
Z16-40 - 23	2.83E+07	1.30E+06	1.70E+05	1.00E+04	370	110	20	12	2730	46	4.28E+05	8.00E+03	2	0.29	1.64	0.3	20.2	1.7
Z16-40 - 24	2.79E+07	9.20E+05	1.62E+05	9.30E+03	350	150	4.1	3.9	3660	170	4.29E+05	1.10E+04	2.45	0.5	0.19	0.14	3.07	0.71
Z16-40 - 25	3.02E+07	1.50E+06	1.65E+05	8.80E+03	290	190	5.4	2.8	2300	320	4.37E+05	1.10E+04	1.75	0.38	0.025	0.073	6.4	2.4
Z16-40 - 26	2.89E+07	1.20E+06	1.59E+05	1.30E+04	510	320	8.1	4.5	2017	96	4.37E+05	9.60E+03	1.56	0.28	1.04	0.36	18.4	1.8
Z16-40 - 27	2.76E+07	1.40E+06	1.60E+05	9.80E+03	10	160	9.2	4.4	1930	120	4.27E+05	9.20E+03	1.37	0.25	0.002	0.051	14.4	1.1
Z16-40 - 28	2.69E+07	1.50E+06	1.68E+05	1.10E+04	50	170	15.7	5.5	989	69	4.28E+05	1.10E+04	1.37	0.26	0.5	0.28	12.6	2.1
Z16-40 - 29	3.30E+07	1.60E+06	1.51E+05	1.50E+04	400	260	7.4	2.9	3196	95	4.20E+05	1.10E+04	2.02	0.27	B.D.	0.084	1.53	0.74
Z16-40 - 30	2.26E+07	2.00E+06	1.86E+05	1.40E+04	140	280	28.1	5.7	1945	43	4.23E+05	1.10E+04	2.21	0.53	1.37	0.48	23.4	2
Z16-40 - 31	2.59E+07	1.40E+06	1.70E+05	1.60E+04	240	210	11.5	2.2	2238	72	4.32E+05	7.80E+03	1.17	0.48	0.85	0.32	9.7	1.1

Z16-40 - 32	3.15E+07	1.20E+06	1.61E+05	1.40E+04	250	190	11	5.4	1902	40	4.34E+05	1.50E+04	2.04	0.47	0.036	0.064	3.1	0.65					
Z16-40 - 33	2.49E+07	1.30E+06	1.70E+05	1.50E+04	B.D.	140	10.6	6	2191	42	4.31E+05	1.30E+04	2	0.38	2.23	0.41	22.4	2.3					
Z16-40 - 34	2.59E+07	1.30E+06	1.75E+05	1.10E+04	120	180	10.3	4.4	1710	110	4.27E+05	1.30E+04	1.74	0.35	1.65	0.72	18.7	4.7					
Z16-40 - 35	2.75E+07	1.90E+06	1.60E+05	9.40E+03	470	420	28	12	1289	44	4.38E+05	6.90E+03	2.71	0.38	0.81	0.43	17.4	2.5					
Z16-40 - 36	2.96E+07	1.30E+06	1.63E+05	8.30E+03	220	160	17.4	5.8	1550	39	4.16E+05	9.80E+03	2.29	0.29	9.75	0.69	44.7	4.1					
Z16-40 - 37	2.80E+07	1.40E+06	1.76E+05	1.10E+04	250	140	11	3.3	1891	34	4.34E+05	1.10E+04	1.1	0.3	0.62	0.17	9.8	1					
Z16-40 - 38	2.96E+07	1.20E+06	1.59E+05	1.20E+04	230	170	8.7	4.9	2755	48	4.27E+05	1.00E+04	2.44	0.34	0.032	0.069	2.14	0.46					
Z16-40 - 39	2.47E+07	1.50E+06	1.77E+05	1.20E+04	730	270	15.1	8.4	3290	140	4.29E+05	8.40E+03	2.83	0.45	280	200	580	370					
Z16-40 - 40	2.59E+07	1.50E+06	1.71E+05	8.20E+03	30	230	66	26	1916	73	4.27E+05	1.40E+04	1.45	0.36	1.2	1	7.8	1.4					
Z16-40 - 41	2.67E+07	1.40E+06	1.64E+05	1.20E+04	20	210	11.6	3.5	1033	20	4.35E+05	9.30E+03	1.57	0.31	1.08	0.39	13.7	1.6					
Z16-40 - 42	2.74E+07	1.50E+06	1.76E+05	1.20E+04	270	170	10.3	3.2	1900	43	4.35E+05	1.10E+04	1.64	0.28	0.238	0.096	17.9	1.2					
Z16-40 - 43	3.08E+07	1.20E+06	1.57E+05	1.40E+04	420	170	15.1	4.3	2616	62	4.41E+05	1.60E+04	2.63	0.34	7.2	1.3	65.4	9.5					
Z16-40 - 44	2.55E+07	1.30E+06	1.59E+05	7.90E+03	440	310	10.8	6	1927	88	4.35E+05	1.10E+04	1.5	0.4	6.1	1.2	30.1	4.4					
Z16-40 - 45	2.76E+07	1.70E+06	1.65E+05	1.40E+04	540	230	11	4.8	4480	310	4.26E+05	6.20E+03	1.8	0.42	0.49	0.24	14	1.6					
Z16-40 - 46	2.89E+07	1.60E+06	1.69E+05	1.20E+04	270	140	9	3.1	1498	39	4.23E+05	1.00E+04	0.81	0.2	0.051	0.063	3.38	0.61					
Z16-40 - 47	2.94E+07	1.50E+06	1.54E+05	9.40E+03	430	170	4.4	3.3	2648	44	4.33E+05	8.00E+03	1.29	0.22	0.004	0.065	3.84	0.62					
Z16-40 - 48	2.86E+07	1.40E+06	1.60E+05	1.10E+04	340	180	9.8	5.4	2414	57	4.20E+05	1.10E+04	1.64	0.32	0.52	0.26	16.6	2.1					
Z16-40 - 49	2.58E+07	9.20E+05	1.66E+05	1.20E+04	250	220	9.7	3.6	1120	80	4.29E+05	1.00E+04	3.72	0.6	4.54	0.57	36.6	2.7					
Z16-40 - 50	2.80E+07	1.30E+06	1.58E+05	8.60E+03	300	170	10.1	4.5	1159	66	4.30E+05	1.00E+04	1.75	0.33	0.005	0.077	14.6	1					
Z16-40 - 51	2.12E+07	2.10E+06	1.98E+05	1.50E+04	0	270	29	10	2890	120	4.37E+05	1.70E+04	3.29	0.68	3.02	0.66	37.4	2.9					
Z16-40 - 52	2.64E+07	9.20E+05	1.47E+05	1.10E+04	220	320	11.9	5	2510	230	4.23E+05	1.40E+04	4.15	0.63	0.71	0.26	8.4	1.7					
Z16-40 - 53	3.17E+07	1.80E+06	1.59E+05	1.20E+04	280	350	12.5	6.2	1202	41	4.33E+05	1.50E+04	5.42	0.5	6.6	1.4	44.7	4.4					
Z16-40 - 54	3.19E+07	1.30E+06	1.53E+05	1.60E+04	420	160	65	10	4680	610	4.15E+05	1.00E+04	4.98	0.59	108	19	800	160					
Z16-40 - 55	3.13E+07	1.80E+06	1.48E+05	9.20E+03	270	200	13.5	5.3	2149	70	4.29E+05	1.20E+04	1.56	0.36	0.5	0.23	10	1.7					
Z16-40 - 56	2.85E+07	1.60E+06	1.57E+05	1.10E+04	260	200	11.2	4.4	1279	60	4.21E+05	7.60E+03	1.67	0.27	1.83	0.63	18.4	1.7					
Z16-40 - 57	2.73E+07	1.20E+06	1.57E+05	8.50E+03	40	240	9.4	3.7	1635	44	4.29E+05	1.20E+04	1.12	0.28	0.072	0.087	12.5	1.3					
Z16-40 - 58	3.16E+07	1.80E+06	1.56E+05	1.30E+04	330	260	9.2	3.9	1646	49	4.16E+05	9.50E+03	1.97	0.39	0.33	0.21	12.32	0.99					
Z16-40 - 59	3.08E+07	1.20E+06	1.44E+05	9.90E+03	350	230	10.2	7.5	2458	98	4.35E+05	1.40E+04	2.41	0.52	1.15	0.55	9.4	2.4					
Z16-40 - 60	3.27E+07	1.40E+06	1.47E+05	7.90E+03	180	270	9.8	5.2	2055	77	4.19E+05	6.10E+03	2.11	0.58	3.4	1.2	39.3	8.2					
Z16-40 - 61	3.11E+07	1.70E+06	1.62E+05	1.00E+04	520	160	7.2	4.8	899	26	4.25E+05	7.90E+03	2.98	0.42	0.98	0.23	10.96	0.98					
Z16-41 - 1	2.65E+07	1.20E+06	1.72E+05	9.80E+03	140	240	12.1	6.6	2123	52	4.32E+05	1.30E+04	4.92	0.6	0.05	0.13	17.6	1.9					
Z16-41 - 2	2.89E+07	1.60E+06	1.54E+05	1.00E+04	80	240	9.6	4.6	1768	61	4.25E+05	8.20E+03	2.02	0.3	0.078	0.074	9.82	0.89					

Z16-41 - 3	2.86E+07	1.40E+06	1.69E+05	8.40E+03	160	290	11.6	5.1	1450	120	4.25E+05	6.50E+03	1.46	0.28	0.031	0.081	7.2	1.2
Z16-41 - 4	3.22E+07	1.30E+06	1.64E+05	1.20E+04	370	250	5.8	4.4	1650	180	4.37E+05	1.60E+04	1.66	0.33	B.D.	0.07	10.4	2.1
Z16-41 - 5	3.11E+07	9.70E+05	1.51E+05	9.20E+03	20	230	5.4	5.1	618	36	4.22E+05	1.30E+04	2.88	0.53	0.048	0.088	7.3	1.6
Z16-41 - 6	3.08E+07	1.70E+06	1.51E+05	8.80E+03	240	250	6.3	4.2	800	63	4.25E+05	1.10E+04	2.39	0.5	0.087	0.096	7.9	1.1
Z16-41 - 7	2.66E+07	1.30E+06	1.71E+05	1.10E+04	B.D.	340	7	5.7	912	21	4.25E+05	9.40E+03	2.87	0.45	0.072	0.07	7.5	1.1
Z16-41 - 8	2.28E+07	6.90E+05	1.65E+05	1.40E+04	470	350	0.8	3.7	1137	26	4.28E+05	6.60E+03	3.81	0.67	B.D.	0.046	9.89	0.82
Z16-41 - 9	3.28E+07	9.20E+05	1.60E+05	8.20E+03	510	280	7.3	4.1	657	23	4.22E+05	1.00E+04	2.44	0.36	0.083	0.095	7.5	1.1
Z16-41 - 10	3.18E+07	1.50E+06	1.69E+05	1.60E+04	360	350	4.7	2.5	846	75	4.31E+05	1.70E+04	2.42	0.46	B.D.	0.047	7.3	1.3
Z16-41 - 11	3.29E+07	2.20E+06	1.53E+05	1.60E+04	520	330	1.1	2.1	1886	80	4.30E+05	1.30E+04	4.11	0.54	0.038	0.073	16.1	1.3
Z16-41 - 12	2.66E+07	1.20E+06	1.56E+05	1.10E+04	60	260	23.2	5.6	984	74	4.24E+05	8.50E+03	1.52	0.33	0.009	0.065	5.7	1.1
Z16-41 - 13	2.88E+07	1.50E+06	1.59E+05	9.00E+03	310	350	12.3	5.1	1448	27	4.30E+05	7.20E+03	1.81	0.34	0.048	0.062	7.7	1.1
Z16-41 - 14	2.91E+07	1.00E+06	1.55E+05	8.50E+03	730	600	6.7	5.5	1680	68	4.26E+05	1.20E+04	2.51	0.68	18	20	54	49
Z16-41 - 15	3.01E+07	1.10E+06	1.56E+05	1.00E+04	190	370	9.5	3.3	490	12	4.22E+05	9.60E+03	2.82	0.37	B.D.	0.02	6.93	0.73
Z16-41 - 16	3.22E+07	8.60E+05	1.54E+05	1.70E+04	430	530	8.2	3.4	651	45	4.31E+05	1.40E+04	3.4	0.44	0.016	0.059	9.6	1.9
Z16-41 - 17	2.72E+07	1.10E+06	1.70E+05	1.00E+04	720	590	11.4	4.9	943	74	4.26E+05	7.10E+03	1.83	0.28	0.002	0.074	6.13	0.99
Z16-41 - 18	2.91E+07	1.70E+06	1.52E+05	9.60E+03	790	450	7.3	3.4	1210	160	4.25E+05	7.40E+03	2.47	0.33	0.002	0.075	9.4	1.4
Z16-41 - 19	2.79E+07	1.20E+06	1.81E+05	9.90E+03	670	420	1.3	3.4	2920	140	4.34E+05	8.20E+03	3.89	0.67	0.001	0.081	19.7	1.7
Z16-41 - 20	2.71E+07	1.10E+06	1.61E+05	9.80E+03	1.90E+03	1.30E+03	4	3.3	3200	400	4.38E+05	1.00E+04	5.59	0.91	80	58	230	150
Z16-41 - 21	2.80E+07	1.40E+06	1.59E+05	7.50E+03	1100	890	6.4	3.6	1021	43	4.26E+05	8.00E+03	2.16	0.28	31	13	104	40
Z16-41 - 22	2.84E+07	1.20E+06	1.56E+05	8.80E+03	550	440	670	190	3100	170	4.25E+05	7.90E+03	5.6	0.93	6.2	2.4	36.1	9.1
Z16-41 - 23	2.88E+07	1.30E+06	1.53E+05	8.00E+03	490	440	5.3	4.4	550	16	4.23E+05	7.00E+03	3.04	0.55	0.074	0.06	7.92	0.69
Z16-41 - 24	2.87E+07	1.10E+06	1.63E+05	9.50E+03	680	630	6.5	3.3	650	20	4.28E+05	8.30E+03	2.42	0.33	0.087	0.083	6.77	0.85
Z16-41 - 25	2.85E+07	1.60E+06	1.54E+05	1.40E+04	B.D.	660	7.6	4.4	712	43	4.25E+05	1.10E+04	2.83	0.44	B.D.	0.0036	8.8	1.4
Z16-41 - 26	3.04E+07	1.40E+06	1.43E+05	1.20E+04	210	490	6	2.8	745	43	4.29E+05	1.10E+04	2.72	0.33	B.D.	0.058	7.58	0.9
Z16-41 - 27	2.78E+07	1.20E+06	1.54E+05	1.40E+04	280	960	5.5	2.9	988	44	4.26E+05	6.80E+03	1.97	0.32	B.D.	0.045	7.03	0.99
Z16-41 - 28	3.18E+07	8.30E+05	1.46E+05	7.90E+03	690	930	5.4	3.3	863	22	4.20E+05	9.90E+03	2.43	0.48	B.D.	0.055	9.4	1
Z16-41 - 29	2.78E+07	1.50E+06	1.59E+05	1.40E+04	400	1100	5.9	4.3	1518	70	4.30E+05	1.30E+04	2.29	0.59	0.003	0.09	10.2	1.1
Z16-41 - 30	2.93E+07	1.30E+06	1.61E+05	8.90E+03	B.D.	690	5	4	662	11	4.28E+05	6.60E+03	2.2	0.23	0.069	0.073	8.7	1
Z16-41 - 31	2.90E+07	1.50E+06	1.58E+05	8.20E+03	990	740	8.7	4.1	1480	110	4.29E+05	9.30E+03	1.8	0.34	B.D.	0.031	7.8	1.2
Z16-41 - 32	2.88E+07	1.20E+06	1.59E+05	7.60E+03	460	960	5.2	4.4	608	15	4.29E+05	1.30E+04	3.45	0.35	0.041	0.06	7.5	1.1
Z16-41 - 33	2.32E+07	1.30E+06	1.59E+05	1.00E+04	4.00E+04	3.50E+03	6.9	4.4	1646	36	4.33E+05	1.00E+04	2.61	0.41	145.7	7.2	632	26
Z16-41 - 34	2.77E+07	1.30E+06	1.55E+05	9.20E+03	B.D.	1000	5.6	3.1	1340	120	4.21E+05	9.60E+03	1.76	0.3	0.038	0.059	7.4	0.8
Z16-41 - 35	2.82E+07	1.40E+06	1.60E+05	1.10E+04	1.70E+03	1.10E+03	4.3	4.4	1661	39	4.28E+05	1.00E+04	2.54	0.51	0.008	0.055	10.6	1.5

Z16-41 - 36	2.82E+07	1.20E+06	1.58E+05	9.30E+03	B.D.	1200	11.8	4.7	544	11	4.28E+05	8.30E+03	2.56	0.37	B.D.	0.023	6.67	0.73				
Z16-41 - 37	3.12E+07	1.10E+06	1.47E+05	1.00E+04	B.D.	1.30E+03	3.7	3.1	673	21	4.18E+05	1.10E+04	3.2	1.3	B.D.	0.051	7.07	0.79				
Z16-41 - 38	2.89E+07	1.40E+06	1.55E+05	7.10E+03	700	1300	14.5	3.7	590	11	4.17E+05	7.50E+03	1.51	0.3	0.016	0.047	4.82	0.73				
Z16-41 - 39	2.80E+07	1.40E+06	1.59E+05	9.30E+03	2.70E+03	2.30E+03	9	4.4	1803	83	4.22E+05	9.30E+03	2.93	0.61	0.55	0.67	13.9	2				
Z16-41 - 40	2.95E+07	1.50E+06	1.53E+05	8.60E+03	B.D.	3.40E+03	6.7	4	1300	42	4.20E+05	7.20E+03	1.95	0.29	0.003	0.046	7.85	0.72				
Z16-41 - 41	2.98E+07	1.70E+06	1.53E+05	1.00E+04	2.40E+03	3.00E+03	3.2	2.3	493	14	4.25E+05	8.30E+03	3.31	0.35	0.023	0.051	6.47	0.88				
Z16-41 - 42	3.31E+07	1.40E+06	1.47E+05	7.90E+03	0	5100	4.3	4.7	609	27	4.28E+05	1.90E+04	2.41	0.44	B.D.	0.056	9	1.7				
Z16-41 - 43	2.93E+07	1.60E+06	1.52E+05	7.90E+03	3.30E+03	5.00E+03	4.1	3.6	1108	35	4.27E+05	9.60E+03	1.48	0.3	2.9	4	20	16				
Z16-41 - 44	2.66E+07	1.40E+06	1.56E+05	9.80E+03	B.D.	6.30E+03	7.6	7.6	1470	200	4.17E+05	1.20E+04	2.85	0.63	0.048	0.085	9.8	2.3				
Z16-41 - 45	2.84E+07	1.10E+06	1.54E+05	7.00E+03	7.80E+03	5.90E+03	8.1	3.9	908	46	4.23E+05	1.00E+04	2.31	0.29	0.005	0.049	6.9	0.82				
Z16-41 - 46	3.41E+07	6.80E+05	1.41E+05	1.10E+04	9.90E+03	9.00E+03	4.5	7.5	772	41	4.23E+05	2.80E+03	2.83	0.51	0.04	0.082	8	1.7				
Z16-41 - 47	2.91E+07	1.60E+06	1.48E+05	7.00E+03	200	2800	17.1	4.6	1628	24	4.31E+05	7.70E+03	1.65	0.2	0.2	0.22	9.5	1.3				
Z16-41 - 48	2.91E+07	1.60E+06	1.60E+05	1.00E+04	5.40E+03	4.60E+03	25.4	6.8	1155	24	4.23E+05	9.70E+03	2.14	0.32	1	0.46	11	1.2				
Z16-41 - 49	2.67E+07	9.70E+05	1.56E+05	8.80E+03	6.20E+03	5.80E+03	8	4.5	2377	27	4.28E+05	8.70E+03	2.01	0.57	0.049	0.085	11.9	1.3				
Z16-41 - 50	2.67E+07	1.20E+06	1.69E+05	1.20E+04	4.50E+04	2.10E+04	8.5	6.6	1040	110	4.27E+05	1.10E+04	1.18	0.22	150	100	380	200				
Z16-41 - 51	2.92E+07	1.40E+06	1.49E+05	1.20E+04	600	6100	6.9	4.8	621	70	4.23E+05	1.00E+04	2.72	0.47	0.035	0.06	7.01	0.86				
Z16-41 - 52	2.89E+07	1.40E+06	1.56E+05	8.90E+03	7.10E+03	6.30E+03	1.2	5.3	2379	85	4.24E+05	1.60E+04	2.86	0.46	0.1	0.11	15.8	1.7				
Z16-41 - 53	3.20E+07	1.40E+06	1.58E+05	1.70E+04	B.D.	5.10E+03	6	4.5	749	51	4.33E+05	1.70E+04	2.37	0.6	0.004	0.061	7.36	0.85				
Z16-41 - 54	3.19E+07	1.40E+06	1.46E+05	9.70E+03	700	3200	3.8	4.2	689	31	4.20E+05	1.00E+04	2.31	0.43	0.061	0.09	7.22	0.97				
Z16-41 - 55	2.64E+07	1.50E+06	1.67E+05	1.60E+04	B.D.	5100	5.4	3.8	1410	120	4.23E+05	1.00E+04	1.85	0.35	B.D.	0.081	7.39	0.8				
Z16-41 - 56	3.24E+07	1.60E+06	1.51E+05	1.30E+04	2.70E+03	3.30E+03	6.4	4.1	1150	410	4.38E+05	1.40E+04	3.9	1.7	0.128	0.077	15.2	4.7				
Z16-41 - 57	3.06E+07	1.20E+06	1.41E+05	1.00E+04	B.D.	5.00E+03	9.7	5.2	657	54	4.25E+05	1.10E+04	2.75	0.41	0.017	0.079	7.81	0.97				
Z16-41 - 58	2.79E+07	1.40E+06	1.72E+05	6.40E+03	3.10E+03	5.80E+03	3.2	4.7	1668	44	4.22E+05	8.80E+03	2.82	0.46	0.005	0.066	11.54	0.99				
Z16-41 - 59	2.75E+07	9.80E+05	1.57E+05	1.30E+04	B.D.	3100	11	11	1175	70	4.23E+05	9.10E+03	4.66	0.63	1.7	1.7	17.6	3.4				
Z16-41 - 60	2.83E+07	1.40E+06	1.63E+05	1.10E+04	1.60E+03	3.00E+03	8.8	4.9	751	16	4.29E+05	9.70E+03	3.45	0.5	B.D.	0.047	11.3	1.5				
Z16-42 - 1	2.90E+07	1.40E+06	1.64E+05	9.90E+03	2.50E+03	3.00E+03	7.5	2.6	1779	38	4.23E+05	8.50E+03	1.66	0.3	B.D.	0.028	8.5	0.91				
Z16-42 - 2	2.89E+07	1.10E+06	1.59E+05	8.20E+03	B.D.	2100	4.6	3.5	1166	67	4.31E+05	8.70E+03	2.34	0.28	B.D.	0.039	10	1				
Z16-42 - 3	2.84E+07	1.20E+06	1.68E+05	1.10E+04	4.10E+03	3.50E+03	10.6	5.7	708	46	4.19E+05	9.20E+03	2.3	0.53	B.D.	0.017	6.74	0.54				
Z16-42 - 4	2.91E+07	1.50E+06	1.63E+05	6.80E+03	0	1900	7.5	3	1689	98	4.32E+05	7.10E+03	1.82	0.34	0.062	0.061	10.92	0.74				
Z16-42 - 5	2.79E+07	1.40E+06	1.55E+05	1.00E+04	1.90E+03	2.70E+03	1.6	3.8	956	40	4.22E+05	1.00E+04	3.45	0.52	0.139	0.09	13.7	1.4				
Z16-42 - 6	3.22E+07	2.10E+06	1.53E+05	1.10E+04	2.50E+03	2.50E+03	9.1	4.3	785	30	4.25E+05	1.00E+04	2.39	0.4	0.026	0.057	7.97	0.96				
Z16-42 - 7	2.99E+07	1.40E+06	1.57E+05	7.40E+03	6.00E+03	1.70E+03	8.9	3.5	1689	69	4.18E+05	8.00E+03	2.73	0.43	46.7	7	119	14				

Z16-42 - 8	2.98E+07	1.80E+06	1.55E+05	9.80E+03	0	1400	5.9	4.2	1280	110	4.22E+05	7.40E+03	3.64	0.44	0.047	0.058	11.4	1.3					
Z16-42 - 9	2.90E+07	1.40E+06	1.60E+05	1.00E+04	1.20E+03	1.10E+03	9.7	4.6	713	50	4.35E+05	1.30E+04	2.68	0.36	B.D.	0.041	6.9	1					
Z16-42 - 10	2.97E+07	1.80E+06	1.49E+05	8.80E+03	1.10E+03	1.20E+03	21.2	5.1	614	51	4.15E+05	1.00E+04	1.28	0.22	B.D.	0.04	4.05	0.71					
Z16-42 - 11	3.12E+07	1.00E+06	1.50E+05	8.80E+03	800	1500	14.2	4.7	735	60	4.26E+05	9.50E+03	2.32	0.39	B.D.	0.054	7.02	0.88					
Z16-42 - 12	2.93E+07	1.40E+06	1.54E+05	1.00E+04	1.00E+03	1.40E+03	16.2	5.5	718	31	4.22E+05	5.30E+03	1.89	0.32	B.D.	0.03	6.2	0.86					
Z16-42 - 13	2.90E+07	1.20E+06	1.57E+05	1.20E+04	100	1100	5.2	3.6	2510	120	4.25E+05	8.80E+03	3.21	0.47	1.01	0.55	16.4	1.6					
Z16-42 - 14	1.97E+07	9.90E+05	1.51E+05	1.60E+04	B.D.	1.90E+03	7.1	5	785	38	4.19E+05	9.00E+03	3.1	0.48	B.D.	0.07	9.27	0.79					
Z16-42 - 15	2.81E+07	1.40E+06	1.60E+05	7.70E+03	B.D.	1100	19.2	5.6	864	18	4.30E+05	7.60E+03	1.41	0.32	0.081	0.084	6.95	0.86					
Z16-42 - 16	2.60E+07	9.10E+05	1.75E+05	1.60E+04	300	1800	7.2	4.3	1540	110	4.32E+05	1.30E+04	1.73	0.53	0.04	0.11	8.2	1.3					
Z16-42 - 17	2.59E+07	1.10E+06	1.69E+05	1.30E+04	300	1700	5.6	5.4	2089	63	4.21E+05	1.20E+04	2.58	0.63	1.16	0.69	14.5	1.4					
Z16-42 - 18	2.76E+07	1.60E+06	1.64E+05	7.00E+03	B.D.	1500	13.8	6.1	551	10	4.21E+05	8.10E+03	1.2	0.39	0.045	0.085	5.24	0.79					
Z16-42 - 19	3.23E+07	1.30E+06	1.37E+05	1.30E+04	B.D.	950	2.9	6.4	725	18	4.21E+05	1.40E+04	2.73	0.53	0.028	0.067	8	1.2					
Z16-42 - 20	3.02E+07	1.30E+06	1.50E+05	9.20E+03	90	620	4.9	3	747	32	4.20E+05	8.70E+03	2.32	0.33	B.D.	0.051	7.75	0.73					
Z16-42 - 21	3.17E+07	1.40E+06	1.47E+05	8.20E+03	630	900	9.9	5.1	670	65	4.25E+05	9.50E+03	2.69	0.66	0.07	0.1	8.06	0.66					
Z16-42 - 22	2.78E+07	1.40E+06	1.43E+05	8.80E+03	140	860	10	4.2	612	24	4.28E+05	8.20E+03	2.99	0.51	0.012	0.06	7.56	0.67					
Z16-42 - 23	2.88E+07	1.30E+06	1.51E+05	8.40E+03	220	890	7.6	3.5	990	80	4.25E+05	7.60E+03	1.33	0.28	0.032	0.049	4.93	0.39					
Z16-42 - 24	2.86E+07	1.30E+06	1.53E+05	7.90E+03	B.D.	1000	9.2	4.4	970	45	4.18E+05	8.40E+03	2.05	0.29	0.072	0.071	6.9	0.58					
Z16-42 - 25	2.91E+07	1.70E+06	1.48E+05	8.90E+03	B.D.	660	3.3	3.8	773	57	4.27E+05	7.50E+03	2.72	0.29	0.023	0.052	9.45	0.82					
Z16-42 - 26	3.07E+07	1.30E+06	1.51E+05	8.30E+03	330	890	9.7	3.2	522	21	4.21E+05	8.00E+03	2.32	0.33	0.023	0.048	8.2	0.99					
Z16-42 - 27	2.60E+07	1.50E+06	1.51E+05	1.20E+04	2.90E+03	1.30E+03	5.4	5.4	748	36	4.14E+05	1.00E+04	2.29	0.46	39	13	116	28					
Z16-42 - 28	2.92E+07	1.60E+06	1.46E+05	8.40E+03	960	900	6.2	4.2	919	70	4.25E+05	7.20E+03	2.56	0.41	0.033	0.049	12.1	1.4					
Z16-42 - 29	2.87E+07	1.30E+06	1.50E+05	9.60E+03	B.D.	670	8.9	3.5	648	21	4.31E+05	1.10E+04	3.39	0.48	B.D.	0.04	8.76	0.79					
Z16-42 - 30	2.93E+07	1.40E+06	1.58E+05	6.20E+03	1020	930	5.1	3.8	635	11	4.19E+05	8.70E+03	2.62	0.31	B.D.	0.052	8.41	0.95					
Z16-42 - 31	1.57E+07	6.10E+05	1.64E+05	1.90E+04	2.12E+05	1.40E+04	19	13	6830	480	4.21E+05	1.20E+04	3.49	0.76	2180	190	6380	560					
Z16-42 - 32	2.71E+07	1.10E+06	1.60E+05	7.80E+03	B.D.	1000	1.4	3.7	1019	43	4.25E+05	1.00E+04	2.38	0.49	0.066	0.098	8.34	0.96					
Z16-42 - 33	2.63E+07	1.00E+06	1.54E+05	1.60E+04	B.D.	1500	8.3	6.3	1664	87	4.24E+05	1.60E+04	2.4	0.56	0.003	0.056	9.1	1.4					
Z16-42 - 34	3.08E+07	1.40E+06	1.41E+05	1.10E+04	1000	1100	6.8	4.2	577	37	4.22E+05	1.20E+04	1.89	0.55	0.06	0.13	9.6	1.6					
Z16-42 - 35	3.19E+07	1.00E+06	1.60E+05	1.30E+04	930	590	4.4	4.7	1900	130	4.17E+05	1.30E+04	1.89	0.35	B.D.	0.033	10.8	1.4					
Z16-42 - 36	2.57E+07	4.00E+05	1.43E+05	8.60E+03	0	1100	15.6	4.7	1480	20	4.26E+05	7.00E+03	2.66	0.39	0.14	0.11	9.66	0.98					
Z16-42 - 37	3.00E+07	1.20E+06	1.51E+05	9.70E+03	170	700	11.3	3.2	1652	30	4.25E+05	7.90E+03	1.88	0.36	0.021	0.042	8.6	1					
Z16-42 - 38	2.91E+07	1.50E+06	1.53E+05	1.10E+04	1310	830	18.6	4.9	1160	47	4.18E+05	7.20E+03	2.02	0.31	0.017	0.046	6.9	0.66					
Z16-42 - 39	2.84E+07	1.80E+06	1.61E+05	9.70E+03	1.50E+03	1.20E+03	38	19	1015	78	4.28E+05	8.20E+03	1.54	0.33	3.7	2.5	19.4	8.5					
Z16-42 - 40	2.80E+07	1.00E+06	1.64E+05	9.30E+03	1.70E+03	1.20E+03	10.5	3.4	1771	96	4.14E+05	8.10E+03	1.99	0.43	0.058	0.069	9.7	1.3					

.6-42 - 41	2.65E+07	9.60E+05	1.68E+05	1.30E+04	1.50E+03	1.80E+03	11.9	4	1794	64	4.22E+05	1.10E+04	1.96	0.33	B.D.	0.036	11.5	1.5					
.6-42 - 42	3.09E+07	1.10E+06	1.65E+05	1.70E+04	600	1600	13.8	6.5	1340	140	4.30E+05	1.50E+04	1.96	0.5	B.D.	0.051	8.6	1.6					
.6-42 - 43	3.15E+07	1.20E+06	1.32E+05	1.20E+04	200	1300	8.9	6.6	593	44	4.31E+05	1.20E+04	2.48	0.57	1.02	0.88	10.2	2.1					
.6-42 - 44	2.51E+07	1.10E+06	1.48E+05	1.20E+04	B.D.	1700	4.5	7	1870	140	4.33E+05	1.00E+04	1.95	0.71	0.007	0.082	12.9	1.3					
.6-42 - 45	2.86E+07	1.40E+06	1.46E+05	7.70E+03	B.D.	1200	16.8	3.4	1286	21	4.23E+05	6.90E+03	1.31	0.26	0.016	0.048	6.31	0.87					
.6-42 - 46	2.63E+07	1.60E+06	1.54E+05	1.10E+04	B.D.	1500	11.4	3.8	526	14	4.11E+05	7.60E+03	2.79	0.5	0.005	0.09	7.83	0.85					
.6-42 - 47	3.09E+07	1.50E+06	1.47E+05	9.50E+03	900	1500	7.1	3.8	916	57	4.31E+05	1.10E+04	1.59	0.41	0.041	0.089	5.51	0.63					
.6-42 - 48	2.68E+07	1.80E+06	1.65E+05	8.00E+03	100	1700	2.5	3.8	1290	110	4.11E+05	1.10E+04	1.89	0.42	B.D.	0.092	9.2	1.2					
.6-42 - 49	2.66E+07	1.20E+06	1.54E+05	1.30E+04	B.D.	1100	B.D.	4	863	44	4.20E+05	1.50E+04	1.8	0.36	0.01	0.067	6.48	0.71					
.6-42 - 50	2.67E+07	1.60E+06	1.55E+05	9.40E+03	1.30E+03	1.80E+03	18.4	6.1	1307	43	4.21E+05	1.10E+04	1.64	0.39	B.D.	0.037	7.46	0.99					
.6-42 - 51	2.58E+07	1.30E+06	1.59E+05	1.20E+04	0	2000	10.5	4.4	1224	72	4.27E+05	9.30E+03	1.62	0.5	0.048	0.094	6.94	0.68					
.6-42 - 52	2.85E+07	1.20E+06	1.58E+05	1.00E+04	2.20E+03	1.50E+03	3.8	3.1	1298	59	4.30E+05	9.60E+03	2.41	0.37	0.033	0.055	8.9	1.2					
.6-42 - 53	2.88E+07	1.80E+06	1.68E+05	1.00E+04	5.50E+03	2.80E+03	7.5	3.7	807	43	4.19E+05	8.60E+03	3.25	0.45	28	15	106	49					
.6-42 - 54	2.66E+07	9.50E+05	1.67E+05	9.70E+03	2.10E+03	2.50E+03	7.8	6.6	688	64	4.15E+05	1.40E+04	2.03	0.3	1.2	2	10	4.1					
.6-42 - 55	2.88E+07	1.40E+06	1.55E+05	8.80E+03	1.80E+03	1.80E+03	10.6	3.3	1614	61	4.17E+05	9.30E+03	1.47	0.31	0.089	0.077	7.02	0.96					
.6-42 - 56	2.63E+07	1.50E+06	1.48E+05	1.50E+04	2.19E+04	5.60E+03	6.8	5.1	1800	120	4.24E+05	9.50E+03	1.71	0.38	169	20	443	52					
.6-42 - 57	2.90E+07	1.40E+06	1.52E+05	1.20E+04	0	2700	10.6	4.3	1295	76	4.22E+05	7.20E+03	1.97	0.28	B.D.	0.043	7.85	0.87					
.6-42 - 58	2.71E+07	1.50E+06	1.54E+05	1.20E+04	2.40E+03	2.40E+03	10	4.3	1570	130	4.19E+05	1.30E+04	1.91	0.51	0.07	0.11	7.1	1.1					
.6-42 - 59	3.15E+07	1.70E+06	1.42E+05	1.40E+04	1.80E+03	4.20E+03	3.9	2.7	705	23	4.29E+05	1.70E+04	2.24	0.25	B.D.	0.068	7.9	1.4					
.6-42 - 60	2.83E+07	1.60E+06	1.49E+05	8.40E+03	1.42E+04	6.90E+03	26.3	6	808	33	4.27E+05	6.00E+03	1.62	0.33	370	160	660	280					
.6-45 - 1	3.17E+07	1.10E+06	1.45E+05	1.50E+04	3.50E+03	3.70E+03	8.8	2.5	1799	68	4.29E+05	1.40E+04	2.17	0.48	75.6	5.2	62.3	3.7					
.6-45 - 2	2.98E+07	1.40E+06	1.54E+05	1.20E+04	1.06E+04	7.80E+03	12.3	5.3	1363	92	4.23E+05	1.10E+04	1.22	0.26	12.8	9	64	33					
.6-45 - 3	2.94E+07	1.60E+06	1.56E+05	1.00E+04	4.70E+03	3.70E+03	5.1	3.6	782	35	4.21E+05	8.40E+03	7.83	0.65	0.82	0.44	14.4	2.8					
.6-45 - 4	2.79E+07	1.60E+06	1.63E+05	9.80E+03	1.03E+04	5.80E+03	8.4	4.6	1171	53	4.13E+05	1.20E+04	1.28	0.26	B.D.	0.075	15.3	2.3					
.6-45 - 5	2.94E+07	1.70E+06	1.47E+05	9.30E+03	3.80E+03	4.80E+03	7	2.9	1210	110	4.18E+05	7.70E+03	1.27	0.2	0.056	0.067	9.99	0.87					
.6-45 - 6	2.97E+07	1.50E+06	1.52E+05	7.10E+03	500	5800	3.2	3.4	774	18	4.16E+05	6.50E+03	1.93	0.29	0.049	0.075	8.15	0.83					
.6-45 - 7	2.64E+07	1.30E+06	1.64E+05	1.10E+04	5.00E+04	1.30E+04	3.6	5	1708	86	4.18E+05	8.00E+03	1.62	0.28	22	15	69	36					
.6-45 - 8	2.94E+07	1.10E+06	1.48E+05	1.10E+04	4.30E+03	7.30E+03	39	14	1059	84	4.07E+05	8.90E+03	5.62	0.52	192	84	75	22					
.6-45 - 9	3.31E+07	1.80E+06	1.62E+05	1.10E+04	1.50E+04	1.40E+04	6.3	3.9	1650	110	4.29E+05	9.90E+03	2.17	0.35	0.23	0.2	24.3	2.6					
.6-45 - 10	2.89E+07	1.30E+06	1.57E+05	9.40E+03	2.60E+04	1.50E+04	12.6	4.1	715	12	4.19E+05	9.90E+03	1.5	0.28	0.032	0.059	13.2	1					
.6-45 - 11	2.97E+07	1.70E+06	1.62E+05	9.30E+03	6.00E+04	2.00E+04	6.9	3.5	838	18	4.19E+05	8.70E+03	2.17	0.34	B.D.	0.051	14.8	1.2					
.6-45 - 12	2.78E+07	1.20E+06	1.63E+05	9.50E+03	2.20E+05	6.00E+04	4.6	2.8	959	17	4.19E+05	7.80E+03	3.39	0.47	25.1	9.4	115	36					

Z16-45 - 13	2.90E+07	1.60E+06	1.54E+05	9.80E+03	3.72E+05	8.30E+04	3.7	4	575	13	4.19E+05	1.00E+04	4.03	0.38	23.1	1.8	91.9	6.6
Z16-45 - 14	2.62E+07	9.30E+05	1.72E+05	7.50E+03	5.50E+05	8.20E+05	250	70	1358	25	4.20E+05	7.60E+03	2.92	0.34	436	99	910	210
Z16-45 - 15	2.76E+07	1.60E+06	1.55E+05	1.10E+04	4.00E+05	1.90E+05	7.3	4.8	1085	46	4.22E+05	1.30E+04	5.74	0.61	1.92	0.5	20.8	2.1
Z16-45 - 16	2.93E+07	1.70E+06	1.59E+05	8.40E+03	5.00E+04	4.90E+04	5.3	3.4	603	45	4.25E+05	7.60E+03	3.17	0.33	0.15	0.12	14.3	1.8
Z16-45 - 17	3.27E+07	1.20E+06	1.38E+05	8.00E+03	B.D.	3.10E+04	11.7	6	756	38	4.18E+05	1.20E+04	8.53	0.97	3.17	0.28	29.4	3
Z16-45 - 18	3.14E+07	1.40E+06	1.45E+05	6.80E+03	2.00E+04	4.10E+04	9.5	4.8	1859	62	4.16E+05	9.90E+03	1.51	0.28	0.031	0.09	17.8	2.6
Z16-45 - 19	2.95E+07	1.70E+06	1.42E+05	7.70E+03	3.90E+04	2.40E+04	16.3	6.2	731	41	4.15E+05	9.30E+03	6.59	0.68	1.51	0.56	23.9	3.7
Z16-45 - 20	2.82E+07	1.20E+06	1.59E+05	9.60E+03	4.10E+05	1.10E+05	6	2.9	892	63	4.33E+05	5.80E+03	3.45	0.39	41	12	176	44
Z16-45 - 21	2.56E+07	7.90E+05	1.41E+05	1.30E+04	5.90E+05	1.90E+05	10.4	4.8	2670	130	4.17E+05	1.10E+04	5.18	0.59	214	90	630	250
Z16-45 - 22	3.33E+07	2.10E+06	1.43E+05	1.30E+04	5.00E+04	2.70E+04	40	16	1710	110	4.12E+05	1.50E+04	11.7	2	36.6	7.3	198	52
Z16-45 - 23	2.76E+07	1.50E+06	1.65E+05	1.10E+04	7.00E+04	1.50E+04	4.7	3.4	770	41	4.20E+05	1.30E+04	2.13	0.52	0	0.11	16.7	1.5
Z16-45 - 24	3.31E+07	1.20E+06	1.47E+05	1.20E+04	1.20E+04	1.70E+04	15.2	4.2	988	21	4.22E+05	9.20E+03	9.87	0.72	38	8.5	337	20
Z16-45 - 25	2.76E+07	1.10E+06	1.67E+05	1.30E+04	7.30E+03	7.60E+03	8.1	4.9	1760	130	4.32E+05	1.00E+04	1.79	0.39	0.019	0.068	21.6	1.4
Z16-45 - 26	2.65E+07	1.30E+06	1.68E+05	8.30E+03	9.10E+03	7.50E+03	5.2	3.2	1720	81	4.19E+05	9.70E+03	2.19	0.36	0.3	0.13	18	1.6
Z16-45 - 27	2.85E+07	1.40E+06	1.58E+05	7.70E+03	3.00E+04	1.00E+04	8.9	5.6	1128	49	4.16E+05	5.50E+03	2.47	0.42	330	210	650	310
Z16-45 - 28	2.83E+07	1.60E+06	1.40E+05	9.50E+03	B.D.	5.50E+03	4.7	3.4	903	15	4.16E+05	8.10E+03	3	0.37	B.D.	0.037	22	1.5
Z16-45 - 29	2.71E+07	1.30E+06	1.58E+05	1.10E+04	2.00E+03	5.10E+03	6.4	6	813	15	4.14E+05	9.50E+03	2.29	0.34	1.4	1.5	21.6	3.6
Z16-45 - 30	2.91E+07	1.20E+06	1.58E+05	1.30E+04	1.70E+03	2.30E+03	8.6	3.9	1046	26	4.22E+05	8.80E+03	6.48	0.68	3.6	3.4	34.4	8.8
Z16-45 - 31	3.14E+07	1.60E+06	1.58E+05	7.50E+03	7.30E+03	4.00E+03	47	10	2860	270	4.19E+05	1.20E+04	9.7	1.2	53.9	3.9	436	33
Z16-45 - 32	2.94E+07	1.20E+06	1.63E+05	8.40E+03	600	2300	30	15	1344	73	4.21E+05	1.00E+04	2.78	0.49	66	14	168	30
Z16-45 - 33	2.83E+07	1.70E+06	1.55E+05	8.00E+03	B.D.	2.40E+03	8.9	3.8	832	16	4.21E+05	8.90E+03	1.85	0.31	0.069	0.064	12.4	1.1
Z16-45 - 34	2.84E+07	1.60E+06	1.60E+05	1.10E+04	1.70E+03	1.80E+03	124	22	960	18	4.15E+05	7.40E+03	2.29	0.39	1.89	0.29	22.7	2
Z16-45 - 35	2.75E+07	1.70E+06	1.63E+05	9.90E+03	B.D.	3000	5.7	3.8	2010	82	4.13E+05	9.00E+03	3.33	0.45	1.13	0.23	20.1	1.7
Z16-45 - 36	3.16E+07	1.60E+06	1.46E+05	8.80E+03	3.00E+03	1.80E+03	6.2	3.1	1900	270	4.20E+05	1.10E+04	4.35	0.64	5.9	0.97	51.4	7.4
Z16-45 - 37	2.71E+07	1.20E+06	1.65E+05	1.10E+04	1.90E+03	2.50E+03	4	2.5	604	28	4.23E+05	9.20E+03	3.05	0.46	B.D.	0.0027	13.4	1.5
Z16-45 - 38	2.69E+07	1.50E+06	1.60E+05	6.70E+03	3.60E+03	2.80E+03	6.2	5.6	1574	80	4.23E+05	8.20E+03	2.22	0.31	33	25	99	62
Z16-45 - 39	2.88E+07	1.60E+06	1.49E+05	8.80E+03	800	1300	7.1	3.4	866	77	4.19E+05	9.00E+03	6.78	0.53	1.01	0.36	18.2	1.5
Z16-45 - 40	1.09E+07	9.30E+05	1.70E+05	2.70E+04	5.76E+05	6.00E+04	9	8.7	7350	480	4.11E+05	1.10E+04	10.2	1.5	2970	220	7820	560
Z16-45 - 41	2.55E+07	9.00E+05	1.57E+05	1.20E+04	B.D.	1.80E+03	0.9	3.6	1648	97	4.08E+05	1.50E+04	2.38	0.65	6.8	1.1	32.6	4.8
Z16-45 - 42	2.63E+07	1.20E+06	1.57E+05	9.90E+03	200	1900	8.3	4.6	832	61	4.22E+05	1.20E+04	3.38	0.66	4.19	0.59	24.8	2.3
Z16-45 - 43	2.61E+07	1.10E+06	1.70E+05	1.30E+04	1.50E+03	1.70E+03	1	5.8	1840	130	4.24E+05	1.90E+04	1.76	0.39	B.D.	0.0026	23.1	2.1
Z16-45 - 44	3.20E+07	9.20E+05	1.47E+05	7.50E+03	B.D.	1200	6.9	5.6	1500	180	4.21E+05	1.70E+04	1.63	0.37	0.12	0.16	19.7	3.3
Z16-45 - 45	2.63E+07	1.70E+06	1.58E+05	1.50E+04	700	1000	31.8	6.2	957	60	4.22E+05	1.10E+04	7	1	8.1	1.2	34.8	3.1

Z16-45 - 46	3.07E+07	1.30E+06	1.62E+05	1.10E+04	2200	970	15.4	5	2280	340	4.15E+05	1.00E+04	10.3	2.4	31	12	136	39						
Z16-45 - 47	2.57E+07	1.20E+06	1.55E+05	9.50E+03	B.D.	560	16.7	7.1	882	71	4.22E+05	9.30E+03	6.75	0.93	9.8	3.2	43	13						
Z16-45 - 48	2.73E+07	1.60E+06	1.67E+05	9.40E+03	430	770	10.3	4	1400	110	4.19E+05	1.00E+04	2.39	0.83	0.06	0.11	10.28	0.98						
Z16-45 - 49	2.16E+07	5.70E+05	1.66E+05	7.70E+03	5.80E+04	7.30E+03	680	120	5200	170	4.14E+05	1.10E+04	19.5	1.9	218	15	819	55						
Z16-45 - 50	2.68E+07	1.60E+06	1.47E+05	9.20E+03	6.60E+03	2.00E+03	30	14	995	60	4.11E+05	7.40E+03	3.1	0.66	102	20	277	53						
Z16-45 - 51	2.78E+07	1.40E+06	1.59E+05	8.40E+03	1020	920	5.5	3.9	908	57	4.19E+05	9.70E+03	12.06	0.93	0.077	0.083	9.4	1.3						
Z16-45 - 52	3.47E+07	1.40E+06	1.44E+05	1.60E+04	2050	850	14.2	7	1145	57	4.04E+05	1.60E+04	14.6	1.8	13.1	1.1	71.8	2.2						
Z16-45 - 53	2.72E+07	1.60E+06	1.66E+05	1.00E+04	900	1000	47	16	2540	140	4.24E+05	1.20E+04	5.5	1	15.4	6.6	98	35						
Z16-45 - 54	2.94E+07	1.60E+06	1.75E+05	1.50E+04	1620	960	13	6.3	1793	35	4.16E+05	1.00E+04	1.71	0.37	0.05	0.095	13.2	1.4						
Z16-45 - 55	2.82E+07	1.90E+06	1.43E+05	8.00E+03	430	910	2.7	3.4	1440	120	4.23E+05	9.00E+03	3.24	0.77	64	62	122	98						
Z16-45 - 56	2.42E+07	1.30E+06	1.64E+05	9.70E+03	B.D.	1700	3.5	4.4	954	66	4.13E+05	6.80E+03	1.51	0.41	0.04	0.13	16.6	2.9						
Z16-45 - 57	2.60E+07	1.20E+06	1.50E+05	1.20E+04	900	1300	17	10	1720	100	4.10E+05	1.10E+04	2.61	0.6	13	15	43	11						
Z16-45 - 58	2.67E+07	1.30E+06	1.67E+05	1.60E+04	320	640	5.3	5.9	903	18	4.17E+05	8.60E+03	2.78	0.36	0.017	0.079	19.5	1.6						
Z16-45 - 59	2.76E+07	1.40E+06	1.61E+05	1.40E+04	900	1000	2.1	3.1	1777	53	4.11E+05	9.30E+03	1.78	0.24	0.03	0.1	25.9	2.7						
Z16-45 - 60	2.16E+07	1.30E+06	1.67E+05	2.10E+04	2.79E+04	2.60E+03	5.3	7.6	1890	180	4.16E+05	8.80E+03	2.22	0.48	484	28	1289	60						
Z16-01 - 1	2.96E+07	7.60E+05	1.64E+05	9.30E+03	1000	800	73	13	2590	200	4.22E+05	1.00E+04	16.6	2.3	18.4	2.5	98	12						
Z16-01 - 2	3.06E+07	2.20E+06	1.68E+05	1.60E+04	2560	930	1436	73	17010	790	4.19E+05	1.30E+04	126.6	8.5	488	28	2024	96						
Z16-01 - 3	2.96E+07	2.10E+06	1.56E+05	1.60E+04	850	640	216	21	3780	230	4.16E+05	1.40E+04	37.5	2.2	54.3	7.6	268	23						
Z16-01 - 4	2.67E+07	1.40E+06	1.61E+05	8.60E+03	B.D.	700	11.3	5.6	1597	33	4.26E+05	6.90E+03	2.55	0.43	0.028	0.061	18.5	1.8						
Z16-01 - 5	2.82E+07	1.10E+06	1.51E+05	1.30E+04	380	590	9	6.2	1729	64	4.23E+05	6.60E+03	3.16	0.38	0.033	0.062	11.7	1.2						
Z16-01 - 6	2.70E+07	1.50E+06	1.53E+05	8.20E+03	2340	650	28.6	5.7	1548	83	4.19E+05	7.60E+03	6.58	0.75	26.4	3.7	109	11						
Z16-01 - 7	2.90E+07	1.40E+06	1.45E+05	1.10E+04	B.D.	520	4.5	3	426	8	4.16E+05	8.30E+03	2	0.39	B.D.	0.025	9.23	0.79						
Z16-01 - 8	2.88E+07	1.20E+06	1.51E+05	9.40E+03	810	510	19.7	5.5	1932	69	4.23E+05	7.80E+03	6.5	1.6	2.5	2	8.3	2.4						
Z16-01 - 9	2.89E+07	1.50E+06	1.57E+05	8.10E+03	510	700	17.6	4	927	18	4.23E+05	8.60E+03	2.76	0.36	0.73	0.41	17.6	1.9						
Z16-01 - 10	2.83E+07	1.20E+06	1.58E+05	1.00E+04	40	450	13	3.9	1280	46	4.10E+05	1.00E+04	4.63	0.58	3.9	1.1	38.9	5.4						
Z16-01 - 11	3.21E+07	1.90E+06	1.50E+05	1.10E+04	420	660	106	19	2157	97	4.14E+05	1.50E+04	10.6	1.3	53.2	6.1	168	14						
Z16-01 - 12	3.09E+07	1.10E+06	1.48E+05	1.60E+04	510	490	109	78	1156	50	4.17E+05	1.50E+04	7.3	2.1	10.2	3	48.9	5.2						
Z16-01 - 13	2.89E+07	1.60E+06	1.54E+05	9.10E+03	B.D.	490	17.3	3.7	516.9	7	4.20E+05	6.70E+03	2.02	0.3	0.053	0.089	9.5	0.81						
Z16-01 - 14	2.97E+07	1.40E+06	1.54E+05	1.30E+04	1760	980	558	48	7610	400	4.10E+05	1.60E+04	64.7	5.2	166.8	8.6	544	32						
Z16-01 - 15	2.63E+07	1.00E+06	1.64E+05	9.60E+03	B.D.	780	23.2	9.5	1130	140	4.18E+05	1.30E+04	2.16	0.36	0.4	0.31	13.5	1.9						
Z16-01 - 16	2.41E+07	9.70E+05	1.74E+05	1.30E+04	B.D.	690	390	190	1750	78	4.20E+05	8.40E+03	12.3	1.8	16.3	2.5	82.1	8.1						
Z16-01 - 17	2.03E+07	6.30E+05	2.12E+05	1.20E+04	530	920	4180	620	1328	76	4.11E+05	9.20E+03	30.8	4.3	6.36	0.72	25	2.1						

Z16-01 - 18	2.74E+07	1.30E+06	1.48E+05	8.90E+03	450	540	33	20	1162	41	4.20E+05	1.10E+04	2.12	0.35	5.2	2.4	21.3	5						
Z16-01 - 19	2.81E+07	1.50E+06	1.67E+05	7.60E+03	710	900	38.3	9.8	772	21	4.18E+05	1.40E+04	3.49	0.4	643	96	910	150						
Z16-01 - 20	2.97E+07	1.50E+06	1.42E+05	1.00E+04	270	550	14.9	5.5	512	11	4.16E+05	7.80E+03	1.34	0.24	0.032	0.057	10.35	0.84						
Z16-01 - 21	2.51E+07	9.40E+05	1.69E+05	1.30E+04	3.50E+03	2.30E+03	122	57	730	110	4.09E+05	1.00E+04	5.2	1.4	15	13	36	18						
Z16-01 - 22	3.07E+07	1.60E+06	1.41E+05	1.20E+04	480	670	14.1	6	980	29	4.07E+05	8.70E+03	1.54	0.39	0.16	0.12	7	1.1						
Z16-01 - 23	2.90E+07	1.40E+06	1.56E+05	9.50E+03	200	570	22	4.2	816	17	4.21E+05	7.10E+03	1.17	0.25	0.005	0.046	9.17	0.89						
Z16-01 - 24	2.81E+07	1.60E+06	1.50E+05	9.30E+03	B.D.	410	18.7	4.6	734	30	4.23E+05	8.50E+03	1.98	0.23	0.02	0.071	15	1.8						
Z16-01 - 25	2.95E+07	1.70E+06	1.58E+05	1.20E+04	390	640	20.5	6.6	977	44	4.09E+05	1.00E+04	3.42	0.47	3.9	2.3	24.5	5.6						
Z16-01 - 26	2.79E+07	1.60E+06	1.55E+05	9.10E+03	B.D.	720	42.6	7.7	1484	46	4.18E+05	8.30E+03	1.28	0.24	0.37	0.25	13.1	1.2						
Z16-01 - 27	2.91E+07	1.50E+06	1.48E+05	9.20E+03	B.D.	640	13.8	3.9	687	24	4.19E+05	9.50E+03	1.65	0.27	0.008	0.047	10.48	0.96						
Z16-01 - 28	2.86E+07	1.30E+06	1.59E+05	1.10E+04	B.D.	860	32.3	6.5	905	16	4.18E+05	7.70E+03	2.54	0.37	7.4	3	34.5	5.5						
Z16-01 - 29	2.81E+07	1.50E+06	1.56E+05	1.10E+04	300	650	9.7	3.8	1126	37	4.13E+05	7.50E+03	2.44	0.44	3.1	1.7	27.9	7						
Z16-01 - 30	2.90E+07	1.40E+06	1.62E+05	1.30E+04	40	790	29.2	6.5	1230	47	4.20E+05	8.20E+03	10.5	1	5.48	0.78	48.9	4.2						
Z16-01 - 31	2.89E+07	1.50E+06	1.59E+05	1.10E+04	440	570	17.3	5	970	27	4.14E+05	7.40E+03	2.76	0.23	1.35	0.44	19.4	1.6						
Z16-01 - 32	2.67E+07	8.70E+05	1.66E+05	1.40E+04	510	610	13.1	6.8	757	57	4.26E+05	1.00E+04	4.03	0.7	0.7	0.31	20	2.3						
Z16-01 - 33	3.16E+07	1.40E+06	1.48E+05	1.50E+04	730	660	34.5	5.2	1494	57	4.11E+05	1.00E+04	1.52	0.28	15	10	46	17						
Z16-01 - 34	2.91E+07	1.50E+06	1.58E+05	1.00E+04	90	700	18.4	3.5	743	27	4.21E+05	7.20E+03	2.89	0.44	2.64	0.52	25.4	1.5						
Z16-01 - 35	2.69E+07	1.50E+06	1.76E+05	1.10E+04	1.30E+03	1.10E+03	14.8	4.7	1393	19	4.17E+05	8.50E+03	2.91	0.49	5.58	0.85	38.2	3.2						
Z16-01 - 36	3.14E+07	1.50E+06	1.56E+05	2.00E+04	B.D.	2700	14.8	5.8	1520	130	4.26E+05	1.90E+04	4.06	0.51	2.8	1.8	42	4.4						
Z16-01 - 37	3.19E+07	8.50E+05	1.40E+05	8.40E+03	B.D.	1200	10.2	5.1	794	27	4.03E+05	1.40E+04	3.26	0.46	8.1	4.1	38	11						
Z16-01 - 38	3.13E+07	9.80E+05	1.47E+05	1.30E+04	B.D.	690	12.4	5.9	2351	52	4.17E+05	7.10E+03	2.55	0.47	0.187	0.079	18.9	1.4						
Z16-01 - 39	2.96E+07	1.30E+06	1.55E+05	9.00E+03	B.D.	860	22.9	6	833	16	4.16E+05	7.70E+03	3.29	0.44	9.2	2.2	16.7	2.2						
Z16-01 - 40	3.00E+07	1.70E+06	1.53E+05	9.80E+03	1.60E+03	1.20E+03	16.7	3.9	1191	44	4.17E+05	8.90E+03	4.58	0.63	2.47	0.45	27.3	2.3						
Z16-01 - 41	2.50E+07	6.60E+05	1.67E+05	1.40E+04	B.D.	1700	148	64	979	35	4.11E+05	8.10E+03	9	1.3	23	7.2	84	20						
Z16-01 - 42	3.09E+07	1.30E+06	1.55E+05	8.20E+03	1.40E+03	1.50E+03	23	4.6	1249	27	4.18E+05	1.30E+04	1.99	0.35	2.94	0.69	22.1	2						
Z16-01 - 43	2.79E+07	1.20E+06	1.55E+05	1.70E+04	3.95E+04	6.70E+03	127	58	2933	71	4.10E+05	1.10E+04	6.7	1.1	32.6	6.1	179	16						
Z16-01 - 44	3.11E+07	9.80E+05	1.49E+05	1.30E+04	100	1500	12.3	6.7	1385	35	4.12E+05	8.00E+03	1.8	0.44	0.011	0.054	14.5	1.2						
Z16-01 - 45	2.67E+07	1.60E+06	1.66E+05	1.40E+04	B.D.	1400	11.2	5.7	375.6	9.7	4.12E+05	1.20E+04	1.64	0.38	0.014	0.067	8.55	0.6						
Z16-01 - 46	1.34E+07	1.40E+06	3.18E+05	4.60E+04	B.D.	4300	57	10	1700	85	4.19E+05	1.30E+04	8.48	0.99	25.9	1.5	129.2	9.3						
Z16-01 - 47	2.83E+07	1.50E+06	1.54E+05	8.90E+03	B.D.	2000	26	4.5	1326	22	4.16E+05	8.70E+03	1.17	0.22	B.D.	0.039	12.3	1.4						
Z16-01 - 48	2.91E+07	1.10E+06	1.48E+05	1.10E+04	B.D.	1.50E+03	9.8	3.9	705	16	4.12E+05	7.00E+03	3.24	0.39	0.26	0.13	15.5	1.4						
Z16-01 - 49	3.34E+07	1.10E+06	1.52E+05	9.60E+03	4.30E+03	2.90E+03	7.4	6.2	849	22	4.12E+05	1.10E+04	2.73	0.63	0.059	0.058	12.7	1.5						
Z16-01 - 50	2.89E+07	1.60E+06	1.55E+05	1.90E+04	1.25E+04	3.60E+03	228	38	3760	430	4.15E+05	2.10E+04	49.2	7.2	54	4.9	305	36						

Z16-01 - 51	2.83E+07	1.40E+06	1.50E+05	9.80E+03	8.00E+04	1.40E+04	8.7	5.8	7130	570	4.19E+05	1.10E+04	3.06	0.47	10.2	1.4	59	4.3						
Z16-01 - 52	3.16E+07	1.40E+06	1.45E+05	8.10E+03	B.D.	3.80E+03	20.9	5.4	783	56	4.10E+05	1.20E+04	1.36	0.27	0.03	0.062	11.1	1.4						
Z16-01 - 53	2.61E+07	9.20E+05	1.58E+05	1.00E+04	1.30E+03	9.80E+03	5.8	4.3	680	16	4.17E+05	1.00E+04	1.74	0.38	0.044	0.08	8.6	1.2						
Z16-01 - 54	3.43E+07	9.20E+05	1.48E+05	8.10E+03	4.10E+03	6.90E+03	10	3.8	674	14	4.07E+05	2.10E+04	2.27	0.32	0.19	0.14	10.3	1.2						
Z16-01 - 55	3.15E+07	1.40E+06	1.57E+05	1.40E+04	9.00E+03	8.30E+03	27.9	6.2	1403	49	4.08E+05	1.10E+04	6.59	0.72	6.62	0.92	36.1	5.3						
Z16-01 - 56	2.67E+07	1.50E+06	1.67E+05	9.50E+03	1.70E+04	1.40E+04	9.4	5.8	815	17	4.12E+05	7.10E+03	2.57	0.52	0.062	0.094	15	1.6						
Z16-01 - 57	3.20E+07	1.00E+06	1.51E+05	8.80E+03	7.00E+04	2.90E+04	18.7	8.7	957	79	4.12E+05	7.30E+03	1.4	0.3	0.05	0.1	11.5	1.4						
Z16-01 - 58	2.71E+07	1.30E+06	1.50E+05	1.30E+04	B.D.	4.70E+04	72.7	9.8	1654	73	4.19E+05	1.30E+04	17.5	2.2	12.4	2.1	86.6	8						
Z16-01 - 59	2.64E+07	1.50E+06	1.60E+05	7.80E+03	B.D.	2.90E+04	16.4	5.3	656	27	4.15E+05	7.70E+03	2.05	0.44	1.68	0.64	15.2	1.9						
Z16-01 - 60	2.80E+07	1.60E+06	1.54E+05	9.20E+03	B.D.	1.60E+03	33.1	4.6	1320	110	4.14E+05	7.80E+03	4.54	0.49	3.67	0.65	30.7	4.8						
Z16-01 - 61	3.30E+07	1.40E+06	1.44E+05	1.50E+04	B.D.	3.30E+03	27	10	3297	96	4.15E+05	1.20E+04	9.3	1.8	29	11	101	15						
Z16-01 - 62	9.10E+06	1.40E+06	4.01E+05	6.60E+04	6.70E+03	8.20E+03	30	10	527	19	4.14E+05	1.30E+04	4.69	0.88	1.8	0.75	14.3	2.2						
Z16-01 - 63	2.81E+07	1.10E+06	1.51E+05	1.10E+04	1.30E+03	1.40E+03	23.3	5.7	507	10	4.18E+05	7.60E+03	1.66	0.26	B.D.	0.044	8.74	0.92						
Z16-01 - 64	3.13E+07	1.50E+06	1.34E+05	1.50E+04	B.D.	1.50E+03	17.5	7.2	3220	390	4.14E+05	8.60E+03	3.55	0.57	4.6	3.2	30	12						
Z16-01 - 65	3.01E+07	1.70E+06	1.49E+05	1.20E+04	B.D.	2.10E+03	27.9	8.5	1118	45	4.15E+05	9.80E+03	3.93	0.46	6.47	0.83	48.9	4.4						
Z16-33 - 1	2.78E+07	1.70E+06	1.51E+05	1.00E+04	B.D.	1400	142	36	3700	970	4.10E+05	1.00E+04	35.6	7.6	139	43	620	160						
Z16-33 - 2	3.21E+07	9.00E+05	1.41E+05	9.60E+03	B.D.	1.80E+03	193	50	1230	280	4.27E+05	1.40E+04	14.7	1.9	47	13	313	84						
Z16-33 - 3	3.07E+07	1.50E+06	1.41E+05	1.40E+04	710	920	99	24	1520	160	4.15E+05	1.40E+04	8.1	1.6	27.6	6.7	175	23						
Z16-33 - 4	2.86E+07	1.50E+06	1.55E+05	9.40E+03	B.D.	1.70E+03	14.1	5.3	1720	110	4.09E+05	1.30E+04	6.07	0.7	82	6.3	508	60						
Z16-33 - 5	3.21E+07	1.60E+06	1.40E+05	8.60E+03	B.D.	940	25.4	7.1	1760	230	4.03E+05	1.30E+04	16.8	2.4	172	24	612	94						
Z16-33 - 6	3.14E+07	8.30E+05	1.56E+05	7.70E+03	B.D.	1100	11.6	4.8	535	62	4.16E+05	1.30E+04	11.7	1.4	11.4	2.4	88	12						
Z16-33 - 7	2.67E+07	1.40E+06	1.51E+05	1.10E+04	1.60E+03	2.10E+03	1.1	4.5	137.7	8.5	4.08E+05	1.00E+04	2.74	0.39	0.68	0.48	17.1	2.2						
Z16-33 - 8	3.32E+07	9.50E+05	1.49E+05	9.40E+03	170	700	18	11	450	130	4.02E+05	1.20E+04	15.5	1.8	13.5	5.2	62	21						
Z16-33 - 9	2.25E+07	2.10E+06	1.92E+05	1.30E+04	B.D.	2.00E+03	444	37	3720	150	4.12E+05	1.70E+04	22.8	2.2	213.1	6.6	1083	37						
Z16-33 - 10	2.94E+07	1.20E+06	1.56E+05	1.40E+04	B.D.	1.40E+03	90	11	5320	350	4.27E+05	2.10E+04	19.7	2.7	301	55	1820	140						
Z16-33 - 11	3.17E+07	1.30E+06	1.48E+05	1.20E+04	B.D.	1.50E+03	71	65	654	77	4.16E+05	2.20E+04	4.92	0.24	30.8	5.6	144	28						
Z16-33 - 12	3.32E+07	1.50E+06	1.48E+05	2.60E+04	B.D.	290	510	46	6980	930	4.31E+05	3.00E+03	88	18	367	35	1507	66						
Z16-33 - 13	3.29E+07	7.90E+05	1.46E+05	1.60E+04	990	820	4.7	2.9	382	53	4.11E+05	1.90E+04	9	2.1	1.8	1.3	34.7	3.6						
Z16-33 - 14	2.93E+07	8.40E+05	1.49E+05	1.50E+04	B.D.	1200	29.9	6.8	634	71	4.22E+05	1.30E+04	11.5	1.1	20.3	3.4	166	18						
Z16-33 - 15	2.87E+07	1.50E+06	1.65E+05	1.50E+04	B.D.	1.50E+03	969	58	11970	260	4.23E+05	9.50E+03	174.9	9.5	497	19	1930	100						
Z16-33 - 16	3.04E+07	1.90E+06	1.50E+05	1.20E+04	B.D.	1200	131	25	4710	500	4.06E+05	6.90E+03	104	14	332	94	1200	180						
Z16-33 - 17	2.29E+07	1.70E+06	1.65E+05	1.40E+04	300	1200	111	16	2650	160	4.18E+05	1.50E+04	24.3	2.2	283	30	755	77						

Z16-33 - 18	3.05E+07	1.10E+06	1.54E+05	8.00E+03	B.D.	1500	79	23	1440	230	4.02E+05	1.40E+04	11.8	1.8	131	34	280	40						
Z16-33 - 19	2.42E+07	9.50E+05	1.62E+05	1.30E+04	B.D.	2.80E+03	29.9	6.8	1170	99	4.06E+05	9.90E+03	17.6	1.8	489	51	1130	110						
Z16-33 - 20	2.73E+07	1.30E+06	1.51E+05	1.30E+04	420	830	24.6	5.3	841	36	4.08E+05	8.30E+03	9.9	1	28.7	3.3	169.5	8.9						
Z16-33 - 21	3.31E+07	1.10E+06	1.33E+05	1.80E+04	200	1300	4.9	6	297	65	4.05E+05	1.40E+04	4.59	0.92	14.8	6.5	68	28						
Z16-33 - 22	2.92E+07	1.40E+06	1.51E+05	6.00E+03	40	700	6	2.9	410.3	9.1	4.17E+05	8.90E+03	6.55	0.53	0.19	0.11	29.6	1.7						
Z16-33 - 23	1.93E+07	1.70E+06	1.92E+05	1.60E+04	B.D.	1100	44	8.7	2290	130	4.05E+05	1.00E+04	101.1	3.6	245	20	1080	110						
Z16-33 - 24	3.27E+07	1.70E+06	1.37E+05	1.60E+04	B.D.	630	15.3	4.4	2480	110	4.10E+05	1.70E+04	14.4	1.2	31.1	2.9	178.3	9.7						
Z16-33 - 25	2.61E+07	1.70E+06	1.74E+05	1.40E+04	350	900	13.4	4.9	873	52	4.09E+05	1.20E+04	8.85	0.64	97.8	9.3	190	23						
Z16-33 - 26	1.06E+07	4.70E+05	2.30E+05	4.50E+04	B.D.	6.60E+03	2210	230	5730	550	4.01E+05	3.90E+04	59.3	5	1960	130	4120	130						
Z16-33 - 27	2.86E+07	1.10E+06	1.50E+05	1.10E+04	B.D.	680	13	6.3	361.2	9.2	4.13E+05	9.90E+03	9.2	0.87	0.12	0.11	32.9	2.3						
Z16-33 - 28	3.20E+07	1.20E+06	1.35E+05	1.40E+04	880	840	8.6	4.9	1978	85	4.01E+05	1.20E+04	4.31	0.34	6.7	2.9	101.6	6.5						
Z16-33 - 29	2.70E+07	1.10E+06	1.69E+05	1.30E+04	B.D.	1200	31.9	5	1018	48	4.14E+05	1.30E+04	13.8	1.1	43.5	5.6	168	16						
Z16-33 - 30	2.98E+07	7.10E+05	1.52E+05	1.10E+04	B.D.	680	200	22	4370	170	4.18E+05	1.90E+04	69.7	3.8	144.3	8.3	691	48						
Z16-33 - 31	3.25E+07	9.90E+05	1.46E+05	1.80E+04	470	950	67	10	1643	77	4.13E+05	9.00E+03	9.9	1.2	47.3	3.2	405	24						
Z16-33 - 32	2.88E+07	1.50E+06	1.66E+05	1.10E+04	B.D.	640	102	13	1109	87	4.18E+05	1.00E+04	10.4	1.1	40	4.9	271	28						
Z16-33 - 33	2.00E+07	1.30E+06	1.85E+05	6.80E+03	B.D.	740	1128	70	7760	510	4.14E+05	2.10E+04	59.6	5.2	720	190	2770	180						
Z16-33 - 34	2.85E+07	1.50E+06	1.57E+05	1.00E+04	270	520	49	32	498	54	4.11E+05	8.70E+03	7.2	1.7	6.6	2.5	76	11						
Z16-33 - 35	2.91E+07	1.30E+06	1.55E+05	8.30E+03	280	660	5.5	4.3	146	18	4.06E+05	8.80E+03	2.81	0.44	0.95	0.48	19.8	4.6						
Z16-50 - 1	3.12E+07	1.00E+06	1.54E+05	1.30E+04	B.D.	600	27.1	6.7	2380	110	4.22E+05	1.10E+04	107	12	79.8	8.8	414	34						
Z16-50 - 2	2.96E+07	1.60E+06	1.54E+05	7.80E+03	200	500	2.1	1.8	82.5	4.8	4.07E+05	1.00E+04	2.02	0.36	0.097	0.081	20.5	2.3						
Z16-50 - 3	2.53E+07	1.50E+06	1.68E+05	1.70E+04	B.D.	950	1.4	6.2	659	44	4.14E+05	1.30E+04	21.3	2.1	15.3	2.1	130.3	7.9						
Z16-50 - 4	2.99E+07	1.40E+06	1.59E+05	1.00E+04	B.D.	270	173	20	5330	320	4.10E+05	1.00E+04	440	42	332	30	1100	88						
Z16-50 - 5	3.12E+07	1.30E+06	1.40E+05	7.30E+03	B.D.	750	19	19	1570	420	4.12E+05	2.20E+04	51	15	32	12	420	260						
Z16-50 - 6	2.67E+07	1.10E+06	1.54E+05	1.30E+04	B.D.	620	12.8	4.6	980	130	4.12E+05	1.20E+04	15.2	2.9	23.9	8.8	209	70						
Z16-50 - 7	3.24E+07	1.00E+06	1.32E+05	1.20E+04	410	560	10.3	5.6	1239	98	4.20E+05	1.70E+04	30.5	4.5	12.9	4.6	128	38						
Z16-50 - 8	2.46E+07	1.50E+06	1.60E+05	2.00E+04	B.D.	810	13.1	7.2	1238	56	4.19E+05	1.10E+04	50.7	9.2	26.5	7.8	168	16						
Z16-50 - 9	3.24E+07	9.80E+05	1.36E+05	1.60E+04	B.D.	530	3.5	3	396	13	4.19E+05	1.00E+04	6.7	1.3	0.76	0.16	39	4.9						
Z16-50 - 10	2.87E+07	1.40E+06	1.58E+05	9.30E+03	B.D.	390	85	16	960	180	4.07E+05	6.00E+03	41.8	5.3	17.1	4.9	277	91						
Z16-50 - 11	3.11E+07	1.50E+06	1.46E+05	1.10E+04	B.D.	510	91.6	8.3	3790	200	4.22E+05	1.10E+04	284	18	172	16	1160	120						
Z16-50 - 12	2.65E+07	1.70E+06	1.62E+05	1.00E+04	B.D.	530	29.3	6.7	1094	70	4.12E+05	5.50E+03	131	16	22.3	1.9	191	13						
Z16-50 - 13	2.72E+07	1.90E+06	1.60E+05	1.50E+04	B.D.	420	19	8.5	592	15	4.04E+05	8.00E+03	12.2	1.9	1.98	0.51	78.1	5.4						
Z16-50 - 14	3.14E+07	1.20E+06	1.49E+05	1.10E+04	B.D.	330	8.6	3.7	411	26	4.10E+05	7.90E+03	6.4	1.1	5.5	2.5	92	17						

Z16-50 - 15	2.91E+07	1.30E+06	1.51E+05	1.10E+04	B.D.	300	9.3	3.6	667	36	4.08E+05	8.50E+03	26.3	2.1	17.3	1.5	91.3	8					
Z16-50 - 16	2.16E+07	2.00E+06	1.85E+05	1.20E+04	B.D.	770	310	150	5740	460	4.05E+05	1.30E+04	494	28	512	90	2930	350					
Z16-50 - 17	3.15E+07	2.00E+06	1.39E+05	1.40E+04	B.D.	1.20E+03	930	180	8.60E+03	1.50E+03	4.00E+05	1.80E+04	880	180	1060	320	2620	610					
Z16-50 - 18	3.04E+07	8.80E+05	1.63E+05	8.50E+03	B.D.	380	15.3	4	294	32	4.11E+05	6.60E+03	19.1	3.3	5.8	1.7	133	26					
Z16-50 - 19	3.14E+07	1.80E+06	1.49E+05	1.50E+04	B.D.	320	7	3.7	452	61	4.22E+05	1.00E+04	23.2	4.9	5.7	1.1	97	23					
Z16-50 - 20	2.20E+07	1.30E+06	1.57E+05	1.50E+04	B.D.	1.20E+03	59	15	12070	390	4.22E+05	1.90E+04	33.9	8.6	1485	52	10090	560					
Z16-50 - 21	2.52E+07	1.70E+06	1.59E+05	1.00E+04	B.D.	460	61	16	3390	180	4.10E+05	1.50E+04	89.4	7.1	174	27	840	100					
Z16-50 - 22	3.13E+07	1.60E+06	1.42E+05	1.10E+04	B.D.	530	60	22	2480	570	4.01E+05	1.40E+04	136	53	148	44	1190	350					
Z16-50 - 23	3.23E+07	1.10E+06	1.55E+05	1.70E+04	B.D.	390	39.8	8.3	1540	130	4.16E+05	1.00E+04	94	22	32	10	220	39					
Z16-50 - 24	2.39E+07	1.90E+06	1.69E+05	7.60E+03	B.D.	470	132	13	2690	150	4.15E+05	1.20E+04	252	14	58.1	4	516	28					
Z16-50 - 25	3.00E+07	1.90E+06	1.50E+05	1.90E+04	170	500	64	50	656	70	4.12E+05	1.50E+04	15.6	5.8	1.73	0.89	61	11					
Z16-50 - 26	3.30E+07	7.60E+05	1.42E+05	1.20E+04	B.D.	400	32	11	616	55	4.02E+05	8.20E+03	38	9.3	8.6	3.2	107	22					
Z16-50 - 27	1.10E+07	5.90E+05	1.71E+05	2.40E+04	430	620	38	26	187	22	4.04E+05	7.20E+03	32.8	3.8	4.13	0.99	46.2	4.7					
Z16-50 - 28	2.32E+07	1.40E+06	1.63E+05	1.30E+04	B.D.	430	192	30	3460	200	4.15E+05	1.20E+04	327	27	152	14	757	52					
Z16-50 - 29	2.68E+07	1.00E+06	1.50E+05	1.30E+04	B.D.	390	20.3	5.7	648	22	4.04E+05	1.80E+04	45.4	2.4	18.4	2.4	95	5.5					
Z16-50 - 30	2.65E+07	1.40E+06	1.60E+05	5.40E+03	220	310	13.2	4.6	475	13	4.08E+05	8.30E+03	27.6	2.3	10.7	1.1	74.1	4.2					
Z16-50 - 31	2.81E+07	1.50E+06	1.57E+05	1.20E+04	B.D.	200	25.6	3.6	1407	61	4.14E+05	9.00E+03	59.9	4	30.3	4.3	374	33					
Z16-50 - 32	2.81E+07	1.30E+06	1.68E+05	1.40E+04	130	270	12.3	6.3	516	26	4.09E+05	8.10E+03	41.7	3.2	2.36	0.65	56.1	8.3					
Z16-50 - 33	2.96E+07	8.70E+05	1.50E+05	8.10E+03	B.D.	270	7.8	4.1	317.3	7	4.13E+05	6.90E+03	14.2	1.9	1.2	0.38	42.8	4.3					
Z16-50 - 34	3.19E+07	8.50E+05	1.46E+05	9.90E+03	B.D.	360	6.1	5.6	570	14	4.02E+05	1.10E+04	7	1	0.43	0.24	24.1	2.5					
Z16-50 - 35	3.08E+07	1.10E+06	1.51E+05	1.40E+04	B.D.	290	34	5.4	2900	140	4.02E+05	1.10E+04	70.9	9.6	216	23	1265	71					
Z16-50 - 36	2.66E+07	1.30E+06	1.61E+05	1.20E+04	B.D.	300	23	8.5	750	63	4.19E+05	9.40E+03	27	3.2	12.5	2	135	21					
Z16-50 - 37	3.13E+07	1.10E+06	1.46E+05	1.30E+04	B.D.	470	42.1	8.5	1650	150	4.08E+05	1.30E+04	118	25	128	15	430	50					
Z16-50 - 38	3.10E+07	6.40E+06	1.40E+05	2.30E+04	B.D.	820	143	31	7.50E+03	1.50E+03	3.72E+05	4.70E+04	313	72	341	93	4200	700					
Z16-50 - 39	3.17E+07	1.30E+06	1.35E+05	1.50E+04	B.D.	410	26	11	2360	170	4.12E+05	1.90E+04	63.2	7.2	160	11	952	89					
Z16-50 - 40	3.11E+07	1.70E+06	1.48E+05	9.70E+03	B.D.	250	12.1	6.3	1180	120	4.05E+05	1.40E+04	24.8	2.7	101	16	740	120					
Z16-50 - 41	2.90E+07	1.40E+06	1.60E+05	1.20E+04	B.D.	240	66	13	2740	220	4.11E+05	1.30E+04	191	13	162	29	702	63					
Z16-50 - 42	2.71E+07	1.10E+06	1.55E+05	9.30E+03	110	340	13.4	5	512	25	4.18E+05	1.30E+04	49.3	3.7	22.1	1.8	312	18					
Z16-50 - 43	3.20E+07	1.80E+06	1.44E+05	1.40E+04	B.D.	560	46	12	5500	390	4.02E+05	1.70E+04	98	22	544	55	2520	260					
Z16-50 - 44	3.11E+07	1.70E+06	1.57E+05	1.20E+04	B.D.	280	16.3	7.9	1940	250	4.05E+05	9.10E+03	48	11	71	13	790	160					
Z16-50 - 45	2.93E+07	1.20E+06	1.57E+05	9.90E+03	B.D.	200	7.3	2.9	416	18	4.08E+05	6.70E+03	13.4	1	3.71	0.49	64.7	3.7					
Z16-50 - 46	3.18E+07	9.10E+05	1.58E+05	5.20E+03	B.D.	250	8.6	5.5	1236	96	4.12E+05	9.20E+03	11.7	2.9	7.1	4.1	90	16					
Z16-50 - 47	3.10E+07	1.20E+06	1.51E+05	1.80E+04	90	180	17.6	5	790	52	4.20E+05	1.90E+04	23.6	1.9	17.5	2.5	122.5	9.9					

Z16-50 - 48	2.84E+07	1.30E+06	1.68E+05	9.20E+03	B.D.	150	8.5	3.9	723	80	4.09E+05	8.70E+03	22.8	4.9	25.3	7.4	185	44						
Z16-50 - 49	2.77E+07	1.20E+06	1.64E+05	5.90E+03	B.D.	290	10.1	5.1	247.7	6.9	4.13E+05	1.00E+04	3.05	0.54	1.22	0.25	78.3	7.2						
Z16-50 - 50	2.39E+07	2.60E+06	1.69E+05	1.80E+04	B.D.	440	68	11	3870	530	4.18E+05	1.40E+04	438	52	416	84	1290	170						
Z16-50 - 51	3.16E+07	8.60E+05	1.60E+05	7.00E+03	B.D.	260	69	14	2610	150	4.11E+05	9.50E+03	189	14	74	13	582	31						
Z16-50 - 52	2.61E+07	1.70E+06	1.62E+05	1.50E+04	170	240	6.7	6.1	1770	230	4.14E+05	1.10E+04	23	5.1	2.7	1.4	104	16						
Z16-50 - 53	3.27E+07	1.30E+06	1.47E+05	9.40E+03	B.D.	410	79	11	2620	690	4.17E+05	1.90E+04	168	38	199	84	740	260						
Z16-50 - 54	2.31E+07	9.80E+05	1.70E+05	1.00E+04	B.D.	220	610	440	2100	220	4.00E+05	1.20E+04	211	32	147	56	330	84						
Z16-50 - 55	2.92E+07	1.50E+06	1.53E+05	1.10E+04	B.D.	220	112	16	1461	81	4.04E+05	8.10E+03	163	15	62.5	6.7	411	29						
Z16-50 - 56	2.67E+07	1.80E+06	1.54E+05	8.80E+03	B.D.	320	12.8	4.5	1600	240	4.04E+05	1.10E+04	48.3	3.5	125	38	680	180						
Z16-50 - 57	2.96E+07	1.70E+06	1.54E+05	1.10E+04	B.D.	430	141	26	5300	640	4.11E+05	1.30E+04	284	41	479	63	2130	250						
Z16-50 - 58	2.78E+07	1.40E+06	1.63E+05	1.20E+04	30	190	5.3	4.4	503	37	4.09E+05	1.00E+04	18	1.1	2.27	0.66	39	3.6						
Z16-50 - 59	2.80E+07	1.20E+06	1.60E+05	1.00E+04	70	160	B.D.	2.6	307	15	4.02E+05	8.80E+03	5.96	0.68	0.48	0.11	29.5	1.2						
Z16-50 - 60	2.80E+07	1.30E+06	1.60E+05	1.30E+04	B.D.	170	3.8	2.9	480	9.5	4.07E+05	9.60E+03	33.9	1.4	0.13	0.12	8.9	0.92						
Z16-50 - 61	2.29E+07	2.10E+06	1.81E+05	1.70E+04	B.D.	500	626	89	3830	650	4.01E+05	9.20E+03	140	27	204	25	1960	410						
Z16-50 - 62	2.93E+07	1.50E+06	1.58E+05	6.70E+03	B.D.	76	22.1	5.8	615	61	3.99E+05	6.80E+03	32.5	5.6	23.3	4	95	12						
Z16-52 - 1	2.89E+07	1.60E+06	1.66E+05	8.50E+03	B.D.	190	11.6	4.4	1320	38	4.08E+05	8.10E+03	5.93	0.51	16.4	1.5	62.1	5.2						
Z16-52 - 2	3.05E+07	1.10E+06	1.63E+05	1.10E+04	B.D.	240	56	12	3270	320	4.08E+05	8.80E+03	110	13	83	7.1	441	43						
Z16-52 - 3	2.00E+07	2.30E+06	2.06E+05	2.50E+04	B.D.	1.20E+03	86	14	1.25E+04	1.60E+03	4.04E+05	1.50E+04	143	11	448	60	1200	170						
Z16-52 - 4	3.15E+07	1.20E+06	1.65E+05	1.10E+04	B.D.	190	58	10	4170	360	4.03E+05	1.00E+04	119	11	94	10	362	40						
Z16-52 - 5	2.55E+07	2.00E+06	1.93E+05	1.80E+04	B.D.	280	348	58	5590	210	4.15E+05	2.20E+04	32.1	6.1	311	25	740	33						
Z16-52 - 6	2.57E+07	1.70E+06	1.75E+05	1.30E+04	B.D.	130	24.7	5.9	1972	82	4.03E+05	1.30E+04	7.87	0.73	31.4	2.9	111.4	8.9						
Z16-52 - 7	2.78E+07	1.80E+06	1.73E+05	1.70E+04	B.D.	310	35	11	3140	310	3.98E+05	1.40E+04	103	17	71	13	260	50						
Z16-52 - 8	3.16E+07	8.40E+05	1.52E+05	1.10E+04	B.D.	150	29.1	6.7	1417	66	4.10E+05	7.50E+03	5.3	1	14.4	2.1	34.4	5.8						
Z16-52 - 9	1.64E+07	1.60E+06	2.09E+05	2.80E+04	B.D.	580	65.2	9.1	4830	240	4.03E+05	9.60E+03	32.1	2.5	177.9	8.9	648	45						
Z16-52 - 10	2.24E+07	1.60E+06	1.77E+05	1.30E+04	B.D.	270	19.1	8	2290	250	4.16E+05	2.10E+04	23.9	4.9	58	11	116	18						
Z16-52 - 11	2.94E+07	1.40E+06	1.80E+05	1.10E+04	B.D.	150	90.3	6.9	3440	200	4.09E+05	1.00E+04	51.2	3.7	65.4	6.5	363	25						
Z16-52 - 12	2.89E+07	2.40E+06	1.56E+05	1.80E+04	B.D.	190	196	16	14550	800	4.01E+05	1.50E+04	340	15	405	45	2110	210						
Z16-52 - 13	2.99E+07	1.50E+06	1.49E+05	1.00E+04	B.D.	260	80	11	7530	950	4.09E+05	1.00E+04	178	25	202	17	697	82						
Z16-52 - 14	1.78E+07	1.20E+06	2.06E+05	2.50E+04	B.D.	480	41	12	5700	460	3.94E+05	1.30E+04	55.4	8.8	180	12	508	55						
Z16-52 - 15	2.76E+07	2.00E+06	1.88E+05	1.30E+04	B.D.	340	53	9.9	5670	230	4.11E+05	1.30E+04	48.4	5.6	234	15	472	17						
Z16-52 - 16	2.48E+07	1.50E+06	1.69E+05	1.80E+04	B.D.	210	34	10	2570	180	4.04E+05	1.00E+04	11.4	1.5	21.7	2.9	95	14						
Z16-52 - 17	3.17E+07	1.10E+06	1.59E+05	1.70E+04	B.D.	190	66	14	5300	380	4.07E+05	1.00E+04	124.9	5.6	93	12	271	21						

Z16-52 - 18	2.08E+07	1.80E+06	2.03E+05	1.80E+04	B.D.	510	93	30	7.60E+03	2.10E+03	4.08E+05	1.10E+04	51	16	134	45	730	240						
Z16-52 - 19	3.03E+07	1.10E+06	1.61E+05	1.10E+04	B.D.	130	10.6	5.5	1750	200	4.06E+05	1.10E+04	24.9	6.1	25	11	100	46						
Z16-52 - 20	3.04E+07	1.50E+06	1.65E+05	1.20E+04	B.D.	330	37	11	5740	250	4.18E+05	1.40E+04	83	26	229	32	379	38						
Z16-52 - 21	2.77E+07	1.30E+06	1.58E+05	1.30E+04	B.D.	280	11.5	5.4	8690	910	4.03E+05	1.40E+04	41.6	5.3	379	78	1200	120						
Z16-52 - 22	2.61E+07	1.30E+06	1.90E+05	1.80E+04	B.D.	300	229	37	1.19E+04	1.60E+03	3.99E+05	1.70E+04	712	71	399	56	1630	260						
Z16-52 - 23	2.47E+07	2.20E+06	1.76E+05	1.80E+04	B.D.	440	283	29	1.41E+04	1.20E+03	4.08E+05	1.80E+04	444	39	586	38	1710	150						
Z16-52 - 24	2.02E+07	2.10E+06	1.78E+05	1.50E+04	B.D.	520	130	16	1.31E+04	1.20E+03	4.29E+05	2.20E+04	55.3	7.3	255	40	1000	130						
Z16-52 - 25	2.06E+07	1.60E+06	1.78E+05	1.50E+04	B.D.	230	116	33	8320	730	4.04E+05	9.70E+03	296	52	172	18	652	55						
Z16-52 - 26	1.97E+07	1.80E+06	1.77E+05	1.20E+04	B.D.	560	238	32	1.47E+04	1.20E+03	4.12E+05	1.50E+04	475	55	612	61	1460	190						
Z16-52 - 27	3.16E+07	1.60E+06	1.49E+05	1.90E+04	B.D.	190	28	11	1830	200	3.90E+05	1.40E+04	17.1	4.4	13.3	2.5	44.5	9.8						
Z16-52 - 28	2.14E+07	2.30E+06	1.85E+05	2.10E+04	B.D.	1.00E+03	435	63	2.24E+04	2.30E+03	4.07E+05	2.80E+04	650	120	648	90	2220	320						
Z16-52 - 29	2.33E+07	1.90E+06	1.66E+05	2.00E+04	B.D.	620	241	30	2.82E+04	1.60E+03	4.10E+05	3.00E+04	1600	130	729	46	3680	250						
Z16-03 - 1	2.92E+07	1.80E+06	1.58E+05	9.50E+03	B.D.	120	11.5	5.1	1222	51	4.07E+05	5.70E+03	2.48	0.26	B.D.	0.026	17.8	1.2						
Z16-03 - 2	2.81E+07	1.10E+06	1.51E+05	8.30E+03	B.D.	140	6	3.4	338	6.2	4.08E+05	8.10E+03	1.95	0.37	0.2	0.23	8.43	0.79						
Z16-03 - 3	2.71E+07	1.50E+06	1.66E+05	8.70E+03	B.D.	190	5.5	5.3	952	36	4.12E+05	9.50E+03	2.61	0.62	31.7	4.7	89	11						
Z16-03 - 4	2.89E+07	1.50E+06	1.49E+05	1.10E+04	0	150	39.8	7	1379	34	4.08E+05	7.80E+03	6.82	0.63	1.91	0.41	32.1	3.9						
Z16-03 - 5	2.70E+07	1.60E+06	1.51E+05	1.10E+04	130	180	20	4.3	961	48	3.99E+05	9.70E+03	1.53	0.34	5.6	0.58	32.1	2.2						
Z16-03 - 6	2.85E+07	1.40E+06	1.59E+05	9.70E+03	B.D.	160	12.3	3.5	565	11	4.09E+05	7.20E+03	4.18	0.38	1.95	0.35	30.2	2.1						
Z16-03 - 7	3.01E+07	1.50E+06	1.58E+05	9.50E+03	B.D.	160	21.5	3.8	893	42	4.12E+05	7.90E+03	3.28	0.32	1.97	0.57	23.6	2.4						
Z16-03 - 8	2.65E+07	1.40E+06	1.64E+05	1.40E+04	50	160	4.9	5	1093	35	4.01E+05	8.70E+03	4.65	0.38	2.31	0.55	30	2.5						
Z16-03 - 9	3.36E+07	1.50E+06	1.38E+05	1.70E+04	B.D.	100	6.8	5.6	1115	30	4.01E+05	1.70E+04	4.73	0.46	3.31	0.47	36.5	1.9						
Z16-03 - 10	2.50E+07	1.40E+06	1.54E+05	1.20E+04	B.D.	230	49	16	1830	150	4.04E+05	9.20E+03	4.09	0.53	35	12	139	29						
Z16-03 - 11	2.83E+07	1.40E+06	1.60E+05	1.30E+04	B.D.	170	4.7	4.2	926	21	4.04E+05	1.00E+04	2.45	0.4	B.D.	0.041	8.6	1						
Z16-03 - 12	3.36E+07	1.20E+06	1.43E+05	7.40E+03	B.D.	240	7.3	4	1094	39	4.01E+05	1.60E+04	2.18	0.56	0.4	0.34	11.4	3.1						
Z16-03 - 13	2.66E+07	1.50E+06	1.62E+05	1.20E+04	50	190	8.8	6.2	637	16	4.07E+05	1.50E+04	4.24	0.57	1.66	0.54	18.2	2						
Z16-03 - 14	3.22E+07	1.00E+06	1.41E+05	1.30E+04	B.D.	180	7.6	6	862	68	4.08E+05	1.10E+04	2.52	0.38	0.042	0.088	10.4	1.6						
Z16-03 - 15	3.04E+07	1.30E+06	1.60E+05	9.40E+03	B.D.	150	9.7	3.5	1244	26	4.15E+05	1.20E+04	1.18	0.26	1.4	0.33	14	2.5						
Z16-03 - 16	2.63E+07	1.70E+06	1.64E+05	6.40E+03	B.D.	170	17	6.2	1357	48	4.05E+05	1.20E+04	2.44	0.39	8.12	0.9	76.2	4.1						
Z16-03 - 17	2.72E+07	1.50E+06	1.59E+05	1.10E+04	110	210	14.9	8.6	872	39	4.03E+05	9.10E+03	1.94	0.45	0.28	0.2	29.1	4.9						
Z16-03 - 18	2.64E+07	1.50E+06	1.56E+05	1.40E+04	B.D.	240	16.8	4.5	4600	200	4.03E+05	1.30E+04	27	1.9	7.6	1.4	69.3	5.5						
Z16-03 - 19	2.10E+07	1.70E+06	1.91E+05	1.20E+04	B.D.	270	22.5	6.9	1903	91	4.09E+05	1.60E+04	4.42	0.76	59.4	6.8	179	21						

Z16-17 - 1	88	96	no value	NAN	no value	NAN	no value	NAN	no value	NAN	no value	NAN	no value	NAN	no value	NAN	no value	NAN
Z16-17 - 2	2.77E+04	3.50E+03	1.35E+07	7.00E+06	B.D.	8.40E+06	1.40E+03	2.50E+03	4.60E+08	5.30E+07	4.20E+05	3.10E+04	69	86	2.86E+04	2.60E+03	2.83E+05	2.70E+04
Z16-17 - 3	2.43E+07	1.60E+06	1.54E+05	1.40E+04	B.D.	390	66	14	2660	140	4.12E+05	8.60E+03	10.3	1.3	33.4	3.2	203	18
Z16-17 - 4	2.98E+07	1.90E+06	1.22E+05	1.10E+04	B.D.	560	545	36	14790	720	4.03E+05	3.10E+04	70.2	5.7	407	24	2400	160
Z16-17 - 5	2.58E+07	1.80E+06	1.68E+05	1.50E+04	B.D.	350	37	7.1	909	29	4.03E+05	9.30E+03	3.63	0.47	22.7	1.3	134.1	9.8
Z16-26 - 1	2.70E+07	1.30E+06	1.57E+05	8.10E+03	60	270	9.3	5.7	765	42	4.03E+05	8.60E+03	1.11	0.38	25.5	1.8	83.2	4.9
Z16-26 - 2	2.69E+07	1.50E+06	1.58E+05	9.70E+03	B.D.	330	30.4	9.2	1850	49	3.97E+05	9.90E+03	1.63	0.27	24	3.8	152	20
Z16-26 - 3	3.05E+07	8.60E+05	1.40E+05	1.00E+04	20	240	15	5.9	1230	190	4.10E+05	1.20E+04	1.48	0.42	0.38	0.21	12.1	2
Z16-26 - 4	2.97E+07	1.10E+06	1.50E+05	1.10E+04	B.D.	520	41	13	897	53	4.06E+05	1.10E+04	1.86	0.31	24.6	5	167	43
Z16-26 - 5	2.92E+07	1.30E+06	1.59E+05	1.20E+04	B.D.	310	5.5	3.5	1216	33	4.07E+05	8.80E+03	1.42	0.27	3.17	0.37	21.5	1.7
Z16-26 - 6	2.91E+07	1.30E+06	1.58E+05	1.40E+04	B.D.	500	19.4	7.5	993	34	4.15E+05	1.40E+04	1.05	0.25	11.1	5	41.8	6.5
Z16-26 - 7	2.72E+07	1.20E+06	1.63E+05	1.30E+04	B.D.	460	24	8.7	1380	170	4.00E+05	1.20E+04	1.47	0.34	20	6.9	101	37
Z16-26 - 8	2.92E+07	1.60E+06	1.53E+05	7.30E+03	B.D.	330	11.4	4.6	1563	71	3.99E+05	1.20E+04	1.66	0.26	0.056	0.067	2.18	0.35
Z16-26 - 9	2.74E+07	1.50E+06	1.57E+05	9.90E+03	B.D.	390	9.7	5.6	1976	49	3.93E+05	1.20E+04	1	0.23	2.11	0.29	10.7	1.2
Z16-26 - 10	2.69E+07	1.40E+06	1.62E+05	1.10E+04	B.D.	560	4.2	5.2	2065	79	4.07E+05	9.80E+03	0.65	0.19	0.12	0.1	2.92	0.7
Z16-26 - 11	2.71E+07	1.00E+06	1.53E+05	1.00E+04	B.D.	740	16.5	5.1	863	30	3.88E+05	1.00E+04	1.63	0.49	14.2	1.2	85	6.3
Z16-26 - 12	3.06E+07	1.40E+06	1.39E+05	8.40E+03	B.D.	540	12.8	5.8	5480	270	4.01E+05	1.40E+04	2.1	0.29	2.38	0.63	16.4	1.5
Z16-26 - 13	2.71E+07	1.30E+06	1.53E+05	8.90E+03	470	560	2.6	3.8	569	10	4.09E+05	1.10E+04	2.25	0.33	B.D.	0.041	11.61	0.86
Z16-26 - 14	2.86E+07	1.50E+06	1.56E+05	8.60E+03	B.D.	730	3.3	3.8	902	23	4.07E+05	5.70E+03	3.98	0.71	0.92	0.28	20.4	2.2
Z16-26 - 15	2.98E+07	1.00E+06	1.41E+05	9.90E+03	B.D.	970	54	19	1540	66	4.07E+05	9.40E+03	1.16	0.28	31.2	5.4	136	15
Z16-26 - 16	2.86E+07	1.50E+06	1.56E+05	6.70E+03	B.D.	600	4.2	3.8	844	31	4.02E+05	6.60E+03	1.57	0.27	B.D.	0.039	14	1.2
Z16-26 - 17	2.76E+07	1.80E+06	1.61E+05	7.90E+03	B.D.	1.30E+03	18.8	5.1	938	32	3.96E+05	8.20E+03	4.2	0.36	33.2	2.8	139	14
Z16-26 - 18	3.07E+07	1.60E+06	1.45E+05	1.30E+04	B.D.	5.90E+03	71	15	2590	170	3.96E+05	1.00E+04	7.28	0.99	3.65	0.88	29.8	3.4
Z16-26 - 19	3.25E+07	1.60E+06	1.47E+05	1.40E+04	B.D.	3.00E+05	8.9	3.9	1378	45	3.99E+05	9.40E+03	1.23	0.22	7.2	2.6	34	11
Z16-26 - 20	2.85E+07	1.70E+06	1.55E+05	9.60E+03	2.00E+03	4.20E+03	173	37	2069	53	4.01E+05	1.10E+04	20.1	1.1	1	0.26	32.7	2
Z16-26 - 21	2.13E+07	9.60E+05	1.87E+05	1.40E+04	700	4700	16.4	7.3	801	35	3.99E+05	1.10E+04	1.19	0.34	13.2	1.2	75.8	4.6
Z16-26 - 22	3.24E+07	1.40E+06	1.42E+05	1.10E+04	1.09E+04	4.20E+03	13	4.2	3610	360	4.08E+05	6.60E+03	2.9	0.63	96	11	598	83
Z16-26 - 23	2.27E+07	1.60E+06	1.54E+05	1.60E+04	1.92E+04	3.90E+03	180	100	875	67	4.05E+05	1.00E+04	2.39	0.46	530	320	1050	610
Z16-27 - 1	2.48E+07	1.50E+06	1.68E+05	1.10E+04	2.80E+03	1.20E+03	30.3	6.6	3030	160	3.92E+05	1.60E+04	8.1	1.3	77	17	439	83
Z16-27 - 2	2.56E+07	1.80E+06	1.55E+05	7.60E+03	1.30E+03	1.00E+03	50	15	4444	74	4.05E+05	1.00E+04	4.7	1	16	2.3	113	15
Z16-27 - 3	2.63E+07	1.40E+06	1.66E+05	1.30E+04	2280	950	6.8	4.5	2890	310	4.01E+05	1.10E+04	5.97	0.89	0.92	0.49	17.8	1.8

Z16-27 - 4	2.50E+07	1.40E+06	1.60E+05	1.30E+04	1.60E+03	1.60E+03	3.8	4.4	914	63	4.05E+05	8.90E+03	1.55	0.3	B.D.	0.057	8.1	1.2					
Z16-27 - 5	2.45E+07	1.50E+06	1.70E+05	1.10E+04	B.D.	670	3.4	3.6	770	63	4.03E+05	1.20E+04	1.74	0.36	8.7	6.9	26.2	9					
Z16-27 - 6	2.76E+07	1.60E+06	1.57E+05	8.10E+03	2050	780	3.7	3.6	2533	62	4.08E+05	9.80E+03	3.28	0.42	1.13	0.52	21.7	4.6					
Z16-27 - 7	2.65E+07	1.30E+06	1.57E+05	1.10E+04	610	620	12.4	5.6	905	31	3.98E+05	9.10E+03	1.61	0.29	13.1	2.4	102	16					
Z16-27 - 8	3.12E+07	1.10E+06	1.62E+05	1.10E+04	1420	610	79	37	2540	100	4.10E+05	6.50E+03	12.04	0.83	30	14	135	56					
Z16-27 - 9	2.88E+07	1.30E+06	1.47E+05	1.10E+04	20	490	4.5	3.8	699	40	4.00E+05	7.40E+03	2.42	0.33	4.9	1.1	80.1	7.9					
Z16-27 - 10	2.81E+07	1.80E+06	1.57E+05	8.20E+03	410	460	9.9	3.7	1615	75	4.01E+05	1.00E+04	9.23	0.89	23.5	4.4	153	36					
Z16-27 - 11	2.83E+07	1.50E+06	1.69E+05	1.60E+04	780	610	20.1	8.8	2740	110	4.12E+05	1.40E+04	6.8	1.3	17.3	5.1	113	22					
Z16-27 - 12	1.66E+07	1.10E+06	1.48E+05	1.70E+04	140	680	24.2	7.9	2870	250	4.06E+05	7.80E+03	5.21	0.74	41.7	9	183	68					
Z16-27 - 13	2.62E+07	1.90E+06	1.58E+05	2.00E+04	B.D.	210	93	53	1070	140	4.03E+05	1.10E+04	4.27	0.7	0.013	0.066	16.8	2.2					
Z16-27 - 14	3.17E+07	1.40E+06	1.35E+05	1.10E+04	310	350	20.7	5.9	3974	96	4.01E+05	7.40E+03	18.2	1.3	64.3	3.5	281	20					
Z16-27 - 15	2.84E+07	1.70E+06	1.61E+05	1.10E+04	580	530	153	21	1650	150	4.12E+05	2.00E+04	7.9	1.5	394	47	1830	180					
Z16-27 - 16	2.66E+07	1.10E+06	1.56E+05	1.20E+04	910	450	8.1	5.3	2548	60	4.09E+05	1.40E+04	3.88	0.61	0.88	0.24	18.4	2.2					
Z16-27 - 17	2.81E+07	1.20E+06	1.53E+05	1.10E+04	390	370	19.6	4.7	1507	51	4.00E+05	7.40E+03	1.76	0.34	1.16	0.56	19.8	2.6					
Z16-27 - 18	2.10E+07	1.70E+06	1.89E+05	1.40E+04	630	370	28	11	4020	930	3.95E+05	1.80E+04	20.2	2.6	40.2	6.1	267	14					
Z16-27 - 19	2.82E+07	1.40E+06	1.51E+05	9.00E+03	440	300	39	22	1794	42	4.03E+05	7.10E+03	3.62	0.47	2.17	0.64	33.6	4					
Z16-27 - 20	2.56E+07	1.10E+06	1.59E+05	1.60E+04	120	370	3.8	5.6	2221	50	4.04E+05	5.70E+03	1.89	0.35	0.15	0.17	12.7	1.3					
Z16-27 - 21	2.96E+07	7.70E+05	1.47E+05	1.70E+04	520	270	246	50	2170	190	4.04E+05	2.30E+04	9.6	1.5	15	3.7	81	13					
Z16-27 - 22	3.26E+07	9.40E+05	1.43E+05	1.40E+04	170	220	7.9	4.4	637	16	4.03E+05	8.50E+03	3.16	0.58	0.67	0.3	13.9	2.4					
Z16-27 - 23	3.08E+07	1.10E+06	1.41E+05	1.20E+04	170	240	25.6	9.1	1262	65	4.12E+05	1.40E+04	97.5	4.7	17.1	2.6	112	20					
Z16-27 - 24	3.32E+07	1.10E+06	1.37E+05	1.80E+04	890	430	12.7	3.6	3140	120	3.97E+05	2.00E+04	23.7	3	18.3	1.7	99	6					
Z16-27 - 25	2.72E+07	1.40E+06	1.63E+05	1.10E+04	490	360	10.5	5.9	2118	51	4.13E+05	9.00E+03	10.92	0.9	1.9	0.95	81.4	6.1					
Z16-27 - 26	2.56E+07	1.80E+06	1.62E+05	1.00E+04	240	300	73	24	1881	90	4.01E+05	9.00E+03	3.5	0.41	32.3	2.9	198	22					
Z16-27 - 27	2.93E+07	1.60E+06	1.51E+05	8.30E+03	290	280	7.7	3.2	1420	56	4.04E+05	7.60E+03	1.86	0.3	0.017	0.049	18.2	1.7					
Z16-27 - 28	3.11E+07	9.00E+05	1.52E+05	8.50E+03	1080	280	177	69	3810	150	4.16E+05	2.00E+04	18.1	1.8	70	11	310	38					
Z16-27 - 29	2.71E+07	1.20E+06	1.50E+05	1.00E+04	B.D.	320	6	5.1	441	15	3.94E+05	1.10E+04	0.82	0.22	B.D.	0.059	12	1.3					
Z16-27 - 30	2.71E+07	1.40E+06	1.56E+05	9.70E+03	80	260	333	97	1692	49	4.02E+05	9.70E+03	7.02	0.81	13.9	1.2	90.8	7.2					
Z16-27 - 31	3.11E+07	2.80E+06	1.57E+05	1.30E+04	450	380	65.7	8.9	2044	72	4.06E+05	1.50E+04	32.8	2.1	88	14	226	39					
Z16-27 - 32	3.04E+07	1.40E+06	1.51E+05	9.90E+03	210	260	94	70	1990	200	4.03E+05	1.50E+04	4.5	1.1	4.4	1	77.6	4.3					
Z16-27 - 33	2.69E+07	1.20E+06	1.62E+05	1.10E+04	190	270	10	5.4	752	23	4.00E+05	1.20E+04	1.12	0.38	0.083	0.089	2.23	0.54					
Z16-27 - 34	2.80E+07	1.70E+06	1.53E+05	9.20E+03	410	290	7.1	3.5	1281	58	4.08E+05	9.10E+03	1.44	0.3	0.71	0.44	10	1.7					
Z16-27 - 35	2.56E+07	1.30E+06	1.66E+05	1.20E+04	280	260	34.1	5.2	1347	69	4.04E+05	1.00E+04	6.35	0.77	47.4	4.6	314	21					
Z16-27 - 36	3.05E+07	1.20E+06	1.46E+05	1.10E+04	450	350	2.7	3.8	1351	61	4.08E+05	9.00E+03	2.86	0.47	1.99	0.45	26.7	1.8					

Z16-27 - 37	2.67E+07	1.70E+06	1.40E+05	1.10E+04	470	310	16.1	4.8	1303	36	4.01E+05	9.60E+03	0.94	0.25	0.035	0.083	26.2	1.8					
Z16-27 - 38	3.15E+07	1.60E+06	1.36E+05	8.80E+03	1250	530	6.4	3.7	2781	64	4.06E+05	9.60E+03	5.07	0.85	9.07	0.82	54.7	6.3					
Z16-27 - 39	3.29E+07	1.60E+06	1.49E+05	1.20E+04	810	310	4.6	3.4	3370	100	4.05E+05	7.20E+03	7.7	1.1	10.7	2.9	55	15					
Z16-27 - 40	3.10E+07	1.40E+06	1.52E+05	1.30E+04	230	320	14.3	6.2	1600	130	4.06E+05	1.10E+04	2.59	0.51	12.9	2.3	107	18					
Z16-27 - 41	3.07E+07	1.10E+06	1.55E+05	1.20E+04	540	360	6.4	4	3220	140	4.08E+05	1.10E+04	4.92	0.63	0.29	0.14	38.6	2.5					
Z16-35 - 1	2.53E+07	1.70E+06	1.60E+05	1.10E+04	10	370	16.1	7.3	1962	99	4.02E+05	8.70E+03	1.27	0.27	0.037	0.087	25.1	2					
Z16-35 - 2	2.59E+07	1.70E+06	1.58E+05	1.20E+04	0	370	6.4	3.1	1132	71	3.93E+05	1.20E+04	2.02	0.53	0	0.13	14.1	2.1					
Z16-35 - 3	2.84E+07	1.50E+06	1.54E+05	1.70E+04	B.D.	440	6.4	4.3	1725	32	4.03E+05	8.20E+03	1.18	0.24	0.8	0.25	7.85	0.83					
Z16-35 - 4	2.60E+07	1.30E+06	1.52E+05	1.10E+04	180	400	3.4	4.8	1110	20	4.03E+05	9.10E+03	0.52	0.16	B.D.	0.052	1.11	0.42					
Z16-35 - 5	3.27E+07	8.60E+05	1.38E+05	6.40E+03	450	180	3.3	4.2	699.8	8.7	4.03E+05	1.20E+04	2.57	0.45	1.64	0.44	37.6	2.9					
Z16-35 - 6	2.57E+07	1.60E+06	1.55E+05	1.40E+04	1140	580	B.D.	4.8	2720	77	4.00E+05	7.30E+03	0.76	0.37	B.D.	0.083	1.79	0.54					
Z16-35 - 7	2.75E+07	1.70E+06	1.56E+05	9.80E+03	200	320	9.8	7.3	556	16	4.00E+05	1.20E+04	1.36	0.31	B.D.	0.054	28.5	1.2					
Z16-35 - 8	3.26E+07	1.60E+06	1.27E+05	1.20E+04	730	530	7.6	5.1	1900	110	4.04E+05	7.70E+03	1.05	0.57	0.1	0.12	2.05	0.53					
Z16-35 - 9	3.08E+07	7.80E+05	1.48E+05	1.40E+04	20	650	11.6	4.5	981	80	4.05E+05	1.10E+04	3.12	0.76	0.36	0.12	38.3	4.7					
Z16-35 - 10	2.73E+07	1.10E+06	1.56E+05	8.90E+03	B.D.	460	15.1	5.3	1007	18	3.97E+05	6.30E+03	2.37	0.4	2.18	0.8	42	2.7					
Z16-35 - 11	2.58E+07	8.20E+05	1.56E+05	9.30E+03	1130	730	7.1	7.7	1095	34	4.00E+05	6.10E+03	1.69	0.52	0.03	0.11	5.82	0.87					
Z16-35 - 12	2.63E+07	1.50E+06	1.41E+05	1.20E+04	620	500	5.4	7.3	2638	94	3.96E+05	7.80E+03	1.32	0.25	B.D.	0.089	1.54	0.45					
Z16-35 - 13	2.83E+07	1.30E+06	1.51E+05	1.10E+04	290	660	B.D.	4	1160	150	4.00E+05	1.30E+04	0.97	0.48	0.34	0.26	4.8	2					
Z16-35 - 14	2.48E+07	1.00E+06	1.58E+05	1.20E+04	560	960	8.7	6.9	1436	43	4.08E+05	1.30E+04	3.69	0.47	3.6	1.1	44	6.5					
Z16-35 - 15	2.63E+07	1.50E+06	1.51E+05	8.70E+03	470	660	8.6	4.5	927	35	3.99E+05	1.00E+04	3.3	0.55	4.79	0.7	69.6	4.4					
Z16-35 - 16	2.89E+07	1.70E+06	1.44E+05	8.90E+03	380	460	6.9	3.9	2467	41	3.98E+05	8.40E+03	2.69	0.5	0.48	0.24	5.7	1.3					
Z16-35 - 17	2.87E+07	1.20E+06	1.51E+05	8.60E+03	730	530	12.9	5.3	1816	75	4.05E+05	6.50E+03	1.3	0.3	1.7	1.8	7.6	2.3					
Z16-35 - 18	3.34E+07	1.50E+06	1.32E+05	1.10E+04	200	1400	14.1	3.5	838	22	4.04E+05	1.10E+04	1.03	0.34	2.4	1.1	21.6	4.4					
Z16-35 - 19	2.86E+07	1.60E+06	1.49E+05	8.40E+03	1580	630	20.6	4.5	1741	66	4.03E+05	8.40E+03	1.05	0.28	3.64	0.46	15.3	1.3					
Z16-35 - 20	3.23E+07	1.20E+06	1.47E+05	1.50E+04	2.50E+03	1.00E+03	5.3	5.5	1799	35	4.08E+05	1.00E+04	0.91	0.26	0.001	0.071	0.69	0.39					
Z16-35 - 21	2.90E+07	1.30E+06	1.52E+05	9.90E+03	400	620	5.8	2.2	785	10	4.07E+05	8.40E+03	1.8	0.21	0.029	0.086	13.1	1.3					
Z16-35 - 22	2.78E+07	1.60E+06	1.56E+05	8.10E+03	60	640	6.3	4.2	1191	25	3.98E+05	9.20E+03	1.36	0.3	B.D.	0.056	5.89	0.79					
Z16-35 - 23	3.13E+07	9.70E+05	1.44E+05	1.30E+04	320	770	16.9	5.4	1179	41	4.04E+05	1.20E+04	1.79	0.34	0.15	0.16	23.5	2.5					
Z16-35 - 24	2.75E+07	1.10E+06	1.59E+05	1.20E+04	900	1000	9	4.6	746	18	3.92E+05	7.90E+03	1.85	0.21	0.37	0.21	8	1.4					
Z16-35 - 25	2.75E+07	1.30E+06	1.58E+05	8.50E+03	2670	990	8.5	3.5	2122	43	4.07E+05	7.70E+03	1.32	0.28	0.015	0.049	1	0.27					
Z16-35 - 26	2.50E+07	1.20E+06	1.55E+05	9.80E+03	B.D.	1800	2.6	7.4	1453	53	4.02E+05	1.00E+04	6.3	1.1	0.144	0.092	58.7	4.9					
Z16-35 - 27	2.83E+07	1.50E+06	1.60E+05	1.10E+04	800	1100	9.2	4.5	1700	39	3.97E+05	9.50E+03	3.44	0.49	0.35	0.16	39.5	2.4					

Z16-35 - 28	3.08E+07	9.90E+05	1.36E+05	1.40E+04	2.40E+03	1.30E+03	6.8	3.9	1773	25	4.29E+05	3.70E+04	0.73	0.16	0.028	0.06	1.19	0.31					
Z16-35 - 29	2.86E+07	1.60E+06	1.49E+05	7.10E+03	2.40E+03	1.20E+03	8.4	4.6	2133	46	4.02E+05	7.60E+03	1.83	0.36	0.07	0.072	22.8	1.3					
Z16-35 - 30	2.47E+07	1.10E+06	1.56E+05	8.70E+03	3.00E+03	3.90E+03	235	60	2270	220	3.99E+05	1.10E+04	2.9	0.82	0.42	0.41	15.5	2.4					
Z16-35 - 31	2.56E+07	9.40E+05	1.47E+05	7.60E+03	2.30E+03	2.80E+03	10.2	4.1	1169	35	4.01E+05	6.20E+03	1.64	0.34	0.67	0.21	25.9	1.6					
Z16-35 - 32	2.83E+07	1.30E+06	1.49E+05	8.50E+03	5.10E+03	2.30E+03	13.6	4.5	4556	76	3.96E+05	9.10E+03	2.6	0.45	0.46	0.17	93.6	3.2					
Z16-35 - 33	2.64E+07	9.70E+05	1.46E+05	8.00E+03	5.70E+03	4.30E+03	8.1	4.3	2752	69	3.97E+05	9.80E+03	3.46	0.66	0.18	0.17	33.5	3					
Z16-35 - 34	2.87E+07	1.30E+06	1.43E+05	8.50E+03	B.D.	2.10E+03	11.2	3.4	866	14	4.06E+05	7.10E+03	2.72	0.35	0.042	0.051	41.7	2.4					
Z16-35 - 35	2.86E+07	1.60E+06	1.47E+05	9.70E+03	B.D.	3000	14.3	5.3	506	12	4.01E+05	9.70E+03	6.11	0.58	0.075	0.066	36.9	1.7					
Z16-35 - 36	2.87E+07	1.50E+06	1.48E+05	1.00E+04	B.D.	2600	2.2	3.3	1418	26	3.97E+05	9.90E+03	2.79	0.28	0.042	0.051	2.77	0.48					
Z16-35 - 37	2.83E+07	1.50E+06	1.47E+05	9.30E+03	4.50E+03	2.70E+03	18.4	5.6	1397	63	4.05E+05	8.20E+03	1.93	0.4	4.47	0.87	60.2	7.8					
Z16-35 - 38	2.88E+07	1.60E+06	1.48E+05	9.40E+03	2.10E+03	3.40E+03	10.7	4.3	938	18	4.04E+05	9.00E+03	2.7	0.37	0.053	0.078	22.9	1.6					
Z16-35 - 39	3.18E+07	1.40E+06	1.47E+05	9.40E+03	2.60E+03	4.40E+03	25.4	7.5	2180	130	4.01E+05	8.40E+03	5.41	0.68	15.8	2	338	41					
Z16-35 - 40	3.18E+07	8.10E+05	1.46E+05	1.20E+04	4.50E+03	4.00E+03	28.5	8.7	1574	78	3.92E+05	1.20E+04	1.06	0.25	14.5	4.7	87	21					
Z16-35 - 41	2.60E+07	1.40E+06	1.66E+05	9.40E+03	B.D.	2300	8.2	5.4	1171	30	4.16E+05	1.30E+04	1.81	0.33	0.09	0.1	26	2.5					
Z16-35 - 42	2.50E+07	1.20E+06	1.61E+05	8.40E+03	1.20E+03	3.90E+03	9.4	6.5	1261	62	3.97E+05	1.60E+04	3.17	0.67	0.52	0.75	54.8	6.1					
Z16-35 - 43	2.84E+07	1.40E+06	1.54E+05	1.10E+04	6.10E+03	3.10E+03	5.3	4.2	1185	40	4.00E+05	7.00E+03	2.08	0.24	0.078	0.096	13	1.4					
Z16-35 - 44	2.75E+07	1.50E+06	1.48E+05	8.30E+03	2.40E+03	2.90E+03	9.6	5.9	1174	21	3.94E+05	7.10E+03	15.25	0.97	B.D.	0.032	18	1.4					
Z16-35 - 45	2.68E+07	1.80E+06	1.59E+05	1.00E+04	4.40E+03	2.20E+03	7	5.6	1494	40	4.00E+05	7.00E+03	1.52	0.45	1.83	0.61	19.4	3.1					
Z16-35 - 46	2.61E+07	1.30E+06	1.51E+05	1.50E+04	6.00E+03	4.20E+03	9.9	6.3	1510	130	4.02E+05	9.60E+03	1.49	0.38	0.36	0.22	10.3	2.9					
Z16-35 - 47	2.84E+07	2.00E+06	1.60E+05	7.70E+03	4.90E+03	1.90E+03	40.8	5.3	5131	79	4.10E+05	7.70E+03	16.7	1.2	25.6	6.4	218	19					
Z16-35 - 48	2.87E+07	1.50E+06	1.55E+05	1.10E+04	2.20E+03	1.80E+03	10.6	4.3	1894	50	4.03E+05	8.80E+03	4.06	0.67	2.11	0.36	73.8	3.3					
Z16-35 - 49	3.20E+07	1.00E+06	1.39E+05	1.50E+04	B.D.	1900	6.9	5.1	779	72	4.06E+05	1.50E+04	0.94	0.33	1.45	0.34	44.6	2.4					
Z16-35 - 50	2.68E+07	1.10E+06	1.54E+05	1.20E+04	2.60E+03	2.50E+03	6.7	5.2	808	13	4.02E+05	1.20E+04	2.53	0.44	B.D.	0.031	25.7	2.1					
Z16-35 - 51	2.92E+07	7.60E+05	1.53E+05	1.30E+04	3.20E+03	2.30E+03	6.1	7.3	778	36	4.03E+05	1.90E+04	3.73	0.67	B.D.	0.029	32.9	2.4					
Z16-35 - 52	2.85E+07	1.30E+06	1.52E+05	9.30E+03	500	1900	2.5	3.4	792	46	3.98E+05	7.40E+03	2.55	0.53	0.017	0.061	31.3	2.6					
Z16-35 - 53	3.01E+07	1.10E+06	1.46E+05	9.70E+03	0	1800	10.4	2.8	790	19	4.06E+05	1.10E+04	2.3	0.43	B.D.	0.059	31.4	2					
Z16-35 - 54	2.62E+07	1.30E+06	1.58E+05	1.10E+04	200	2200	12.6	4.8	1191	30	3.98E+05	9.00E+03	2.28	0.65	B.D.	0.073	40.7	2.4					
Z16-35 - 55	2.53E+07	1.00E+06	1.53E+05	1.50E+04	700	1500	16.6	5.5	1870	190	3.94E+05	1.20E+04	2.95	0.56	0.54	0.18	66.8	5.9					
Z16-35 - 56	3.27E+07	1.50E+06	1.32E+05	1.60E+04	1.50E+03	1.50E+03	3.7	4.7	1189	78	4.03E+05	1.30E+04	2.74	0.43	0.38	0.25	21.8	2.7					
Z16-35 - 57	2.72E+07	1.40E+06	1.58E+05	8.30E+03	1.80E+03	1.40E+03	6.5	4.1	1086	25	4.11E+05	9.00E+03	0.7	0.22	0.07	0.11	1.04	0.3					
Z16-35 - 58	2.87E+07	1.60E+06	1.42E+05	8.40E+03	1.30E+03	1.50E+03	6.7	2.5	682	18	3.98E+05	8.80E+03	1.25	0.22	0.025	0.062	5.99	0.88					
Z16-35 - 59	2.68E+07	1.20E+06	1.55E+05	1.00E+04	800	2700	15.6	6.8	631	14	3.93E+05	1.00E+04	1.75	0.37	10.3	3.3	58.5	8					
Z16-35 - 60	2.70E+07	9.40E+05	1.60E+05	1.30E+04	500	1400	4.1	4.7	502	10	3.98E+05	1.00E+04	2.21	0.4	B.D.	0.05	32.1	2.4					

Z16-35 - 61	3.02E+07	7.50E+05	1.44E+05	9.80E+03	900	1400	9.5	4.2	1543	50	4.03E+05	1.10E+04	1.06	0.2	0.01	0.076	8	1.5						
Z16-35 - 62	2.42E+07	1.20E+06	1.44E+05	1.40E+04	4.90E+03	2.60E+03	23.2	6.7	1411	51	3.92E+05	9.50E+03	1.38	0.37	10.8	1.3	123.1	8.5						
Z16-35 - 63	2.54E+07	1.00E+06	1.54E+05	7.60E+03	700	1300	4.5	4.4	906	53	3.96E+05	9.30E+03	1.82	0.52	0.24	0.18	13.51	0.87						
Z16-35 - 64	2.44E+07	9.90E+05	1.52E+05	1.70E+04	2.50E+03	1.80E+03	39	12	2322	76	4.03E+05	1.10E+04	14.8	1.6	59	60	180	120						
Z16-35 - 65	2.78E+07	1.60E+06	1.50E+05	7.10E+03	900	1500	69	20	1196	32	3.91E+05	1.00E+04	1.28	0.22	0.04	0.068	13.5	1.1						
Z16-35 - 66	3.23E+07	6.70E+05	1.40E+05	1.00E+04	2.60E+03	3.20E+03	7.2	6.9	2475	67	3.97E+05	9.70E+03	1.11	0.42	B.D.	0.041	1.46	0.32						
Z16-35 - 67	2.91E+07	1.50E+06	1.52E+05	8.10E+03	1.70E+03	1.20E+03	12.1	4.1	1675	83	3.98E+05	7.20E+03	2.41	0.34	0.15	0.13	26.4	2.2						
Z16-35 - 68	2.58E+07	1.50E+06	1.56E+05	1.10E+04	1.70E+03	2.30E+03	15.1	4.2	1027	26	4.00E+05	1.20E+04	1.73	0.43	4.12	0.38	22.1	2.4						
Z16-35 - 69	2.74E+07	1.20E+06	1.58E+05	8.50E+03	B.D.	1200	2.6	2.7	1215	26	4.00E+05	9.30E+03	2.98	0.56	0.039	0.069	7.3	1.2						
Z16-35 - 70	3.13E+07	6.00E+05	1.36E+05	1.50E+04	600	1400	4.4	5.1	820	27	4.06E+05	1.30E+04	3.69	0.68	3.2	3.6	50.1	7.6						
Z16-35 - 71	2.66E+07	1.10E+06	1.57E+05	1.30E+04	1.10E+03	2.20E+03	9.8	4.6	1212	25	4.00E+05	9.20E+03	0.67	0.17	0.16	0.18	31	3						
Z16-35 - 72	2.54E+07	8.80E+05	1.62E+05	4.90E+03	1.30E+03	2.10E+03	121	29	1700	110	3.90E+05	1.30E+04	2.4	1	4.8	1	26.9	3						
Z16-35 - 73	2.95E+07	1.40E+06	1.52E+05	9.20E+03	2.70E+03	1.50E+03	3.8	2.9	2005	59	3.93E+05	8.50E+03	1.17	0.23	0.018	0.052	2.51	0.31						
Z16-35 - 74	2.40E+07	1.20E+06	1.65E+05	1.30E+04	5.90E+03	2.20E+03	154	37	1230	51	4.06E+05	1.20E+04	3.13	0.38	110	110	310	270						
Z16-35 - 75	3.10E+07	1.10E+06	1.51E+05	1.50E+04	5.00E+03	1.10E+03	91	20	3450	190	4.04E+05	1.40E+04	12	1.4	87	70	290	110						
Z16-35 - 76	2.70E+07	1.50E+06	1.47E+05	9.80E+03	600	1900	6.2	4.6	609	23	4.03E+05	8.50E+03	0.63	0.23	0.23	0.18	2.53	0.49						
Z16-35 - 77	2.87E+07	1.50E+06	1.50E+05	7.10E+03	1.90E+03	1.60E+03	15	3.9	2392	60	4.01E+05	7.10E+03	3.54	0.65	3.71	0.54	110.7	4.6						
Z16-35 - 78	2.92E+07	1.70E+06	1.54E+05	8.00E+03	B.D.	1.10E+03	8.1	2.8	1013	41	4.04E+05	9.90E+03	1.09	0.26	0.15	0.1	20.9	1.9						
Z16-35 - 79	2.70E+07	1.40E+06	1.56E+05	1.10E+04	400	3000	2.2	3.3	1286	27	4.02E+05	6.60E+03	3.72	0.41	0.026	0.082	61.8	3.6						
Z16-35 - 80	2.59E+07	1.60E+06	1.59E+05	1.10E+04	2.20E+03	6.10E+03	4.2	5	790	110	3.90E+05	9.90E+03	0.5	0.16	B.D.	0.062	0.81	0.37						
Z16-35 - 81	2.85E+07	1.50E+06	1.60E+05	1.20E+04	9.50E+03	3.90E+03	3.7	3.2	1473	74	3.97E+05	9.20E+03	2.06	0.39	0.054	0.057	24.1	1.9						
Z16-35 - 82	2.85E+07	1.50E+06	1.48E+05	7.10E+03	1.10E+03	8.40E+03	12.9	3.7	565	60	4.03E+05	8.50E+03	1.14	0.25	0.096	0.081	18.7	1.5						
Z16-35 - 83	3.02E+07	1.30E+06	1.38E+05	1.20E+04	9.00E+04	3.20E+04	8.5	3.2	890	110	4.02E+05	9.00E+03	1.11	0.27	0.2	0.15	8.8	1.3						
Z16-35 - 84	2.62E+07	1.20E+06	1.56E+05	8.40E+03	B.D.	6.10E+04	9.3	6.1	1503	86	4.04E+05	6.80E+03	0.64	0.22	2.04	0.39	26.2	4.5						
Z16-35 - 85	2.90E+07	1.30E+06	1.55E+05	9.20E+03	B.D.	1.10E+04	33	8.1	1424	29	3.92E+05	1.10E+04	1.39	0.29	0.057	0.065	29.3	1.8						
Z16-35 - 86	2.59E+07	1.60E+06	1.52E+05	8.80E+03	B.D.	5.10E+03	63	46	1030	54	3.89E+05	9.30E+03	3.31	0.47	1.86	0.59	13.2	1.9						
Z16-35 - 87	3.14E+07	1.30E+06	1.52E+05	1.20E+04	B.D.	5.00E+03	5.1	4.6	1035	30	4.03E+05	1.20E+04	2.15	0.34	B.D.	0.044	32.1	2						
Z16-35 - 88	3.19E+07	1.20E+06	1.44E+05	1.40E+04	B.D.	4000	6.2	5	1804	95	4.10E+05	1.40E+04	2.85	0.84	0.116	0.093	26.1	2.4						
Z16-35 - 89	3.11E+07	1.10E+06	1.45E+05	7.70E+03	B.D.	2700	6.3	5.6	835	38	3.98E+05	9.70E+03	0.68	0.19	0.012	0.052	3.4	0.89						
Z16-35 - 90	2.65E+07	1.10E+06	1.55E+05	1.00E+04	B.D.	2.00E+03	6.9	6.4	1308	59	3.91E+05	1.10E+04	1.17	0.28	B.D.	0.059	34.1	3.1						
Z16-35 - 91	3.18E+07	1.30E+06	1.46E+05	1.20E+04	B.D.	2.30E+03	10	3	1148	38	3.99E+05	1.30E+04	4.1	0.49	0.1	0.16	50.8	4.4						
Z16-35 - 92	2.67E+07	1.50E+06	1.54E+05	1.00E+04	B.D.	1700	9.1	5.6	1911	51	3.91E+05	1.10E+04	5.57	0.65	0.005	0.071	82.5	4.6						
Z16-35 - 93	2.82E+07	6.80E+05	1.57E+05	1.10E+04	500	1200	85	31	1430	100	3.84E+05	1.00E+04	4.31	0.62	0.22	0.14	10.7	1.3						

Z16-35 - 94	2.63E+07	1.50E+06	1.50E+05	1.40E+04	B.D.	2.50E+03	5.7	5.2	852	25	4.00E+05	8.40E+03	5.25	0.75	2.7	1.2	23.6	3.4				
Z16-35 - 95	2.62E+07	8.40E+05	1.50E+05	1.10E+04	B.D.	1.30E+03	14.2	4.6	2170	130	4.05E+05	1.20E+04	5.65	0.8	0.42	0.39	90.6	7.7				
Z16-35 - 96	1.67E+07	1.10E+06	1.76E+05	1.20E+04	B.D.	1.90E+03	42	14	1300	250	3.92E+05	6.80E+03	3.75	0.97	1.26	0.36	18.3	3				
Z16-35 - 97	2.74E+07	1.60E+06	1.51E+05	6.90E+03	B.D.	870	14.9	5.9	2270	110	4.05E+05	1.10E+04	2.92	0.62	6.5	1.7	110	14				
Z16-35 - 98	2.40E+07	1.30E+06	1.63E+05	2.20E+04	B.D.	1.10E+03	9.9	5.4	2101	56	3.95E+05	1.30E+04	1.81	0.62	3.53	0.69	45.1	5.2				
Z16-35 - 99	2.92E+07	1.40E+06	1.50E+05	1.10E+04	B.D.	800	10.2	3	1447	27	3.96E+05	1.10E+04	2.04	0.4	0.27	0.13	3.75	0.76				
Z16-35 - 100	2.86E+07	1.30E+06	1.54E+05	9.50E+03	B.D.	540	41.9	7.3	754	15	3.99E+05	8.40E+03	1.23	0.2	0.063	0.054	20.8	1.5				
Z16-35 - 101	3.16E+07	7.90E+05	1.33E+05	7.70E+03	B.D.	760	10.2	7	2640	360	3.93E+05	7.80E+03	0.67	0.31	1.87	0.61	12.7	1.6				
Z16-35 - 102	2.66E+07	1.00E+06	1.64E+05	8.20E+03	B.D.	610	24.7	4.5	1083	55	4.02E+05	9.80E+03	0.73	0.27	0.021	0.072	0.8	0.26				
Z16-35 - 103	2.85E+07	1.60E+06	1.50E+05	9.20E+03	B.D.	550	1.5	3.3	1582	33	3.97E+05	8.20E+03	0.83	0.25	0.031	0.06	1.69	0.42				
Z16-35 - 104	2.56E+07	1.20E+06	1.49E+05	1.80E+04	B.D.	1300	10.1	6.1	2824	77	3.95E+05	1.60E+04	3.63	0.63	B.D.	0.074	65.4	2.7				
Z16-35 - 105	2.66E+07	1.60E+06	1.61E+05	1.50E+04	B.D.	1100	29.1	8.9	2221	71	3.93E+05	9.00E+03	1.6	0.53	5.5	1.3	72	13				
Z16-35 - 106	3.31E+07	6.80E+05	1.45E+05	1.80E+04	B.D.	850	17.8	5.5	1190	120	3.90E+05	1.30E+04	1.67	0.46	5.95	0.51	35.6	2.4				
Z16-35 - 107	2.94E+07	1.30E+06	1.52E+05	1.10E+04	B.D.	410	5.8	2.7	442.6	7.2	3.93E+05	7.80E+03	1.77	0.27	0.032	0.034	22.5	1.3				
Z16-35 - 108	2.84E+07	1.40E+06	1.54E+05	9.40E+03	B.D.	460	26	16	664	13	4.00E+05	9.40E+03	1.12	0.29	4.6	1.1	27.2	3.9				
Z16-35 - 109	2.86E+07	1.10E+06	1.52E+05	8.60E+03	B.D.	350	7.3	4	764	21	4.04E+05	8.40E+03	2.65	0.34	65	55	190	130				
Z16-35 - 110	3.20E+07	1.00E+06	1.45E+05	8.40E+03	B.D.	380	3.3	5.8	1340	64	4.01E+05	1.10E+04	0.7	0.24	0.005	0.057	0.6	0.28				
Z16-35 - 111	2.71E+07	1.40E+06	1.65E+05	1.60E+04	B.D.	430	5.9	3.8	1070	28	3.95E+05	8.30E+03	1.66	0.38	0.11	0.14	34.7	1.5				
Z16-35 - 112	2.78E+07	1.30E+06	1.52E+05	1.10E+04	B.D.	440	2.9	5.8	1086	71	3.89E+05	1.10E+04	3.76	0.71	0.023	0.071	8.1	1.4				
Z16-35 - 113	3.45E+07	1.90E+06	1.41E+05	9.60E+03	B.D.	400	14.9	4.3	1800	100	3.87E+05	1.50E+04	4.42	0.83	0.4	0.23	71.5	4.9				
Z16-35 - 114	2.91E+07	1.50E+06	1.48E+05	6.90E+03	B.D.	340	3.3	4.3	1224	86	4.03E+05	1.00E+04	1.27	0.34	0.079	0.079	2.88	0.57				
Z16-35 - 115	2.71E+07	1.70E+06	1.54E+05	1.20E+04	B.D.	540	9.4	2.9	1589	36	3.98E+05	7.60E+03	3.29	0.58	1.1	0.29	49	2.6				
Z16-35 - 116	2.66E+07	1.30E+06	1.58E+05	7.80E+03	B.D.	460	17.3	4.7	699	77	4.07E+05	9.10E+03	2.25	0.33	0.2	0.14	29.1	2.2				
Z16-35 - 117	2.88E+07	1.30E+06	1.48E+05	9.50E+03	B.D.	200	4.6	3.4	709	25	4.00E+05	5.70E+03	0.87	0.24	0.029	0.061	24.4	2				
Z16-35 - 118	2.60E+07	1.40E+06	1.62E+05	9.40E+03	B.D.	390	10.5	5.3	647	49	4.02E+05	7.20E+03	2.49	0.55	0.056	0.07	28.8	2.6				
Z16-35 - 119	2.76E+07	1.20E+06	1.53E+05	5.60E+03	B.D.	400	6.9	3	1413	86	3.94E+05	8.00E+03	0.85	0.26	0.4	0.13	5.56	0.87				
Z16-35 - 120	2.59E+07	1.30E+06	1.61E+05	7.50E+03	B.D.	530	4.7	2.7	1719	59	4.02E+05	9.10E+03	2.67	0.48	1.47	0.32	20.3	2.6				
Z16-35 - 121	2.74E+07	1.30E+06	1.57E+05	1.20E+04	B.D.	470	27.5	7.8	1088	53	3.98E+05	9.10E+03	1.4	0.35	3.63	0.54	32.8	3.5				
Z16-35 - 122	3.08E+07	1.20E+06	1.44E+05	1.10E+04	B.D.	220	10.1	4	1722	59	4.05E+05	1.20E+04	2.05	0.3	0.37	0.18	50.5	3.4				
Z16-35 - 123	3.22E+07	8.10E+05	1.47E+05	9.90E+03	B.D.	320	22.3	7.5	3620	120	4.01E+05	1.10E+04	5.8	0.82	0.11	0.12	70.5	6				
Z16-35 - 124	2.90E+07	1.50E+06	1.59E+05	1.20E+04	B.D.	310	4.9	2.7	1095	20	4.00E+05	5.90E+03	2.17	0.32	0.8	0.25	28.9	2.6				
Z16-35 - 125	2.71E+07	1.70E+06	1.66E+05	1.30E+04	B.D.	490	11.2	6.8	1262	65	3.94E+05	1.10E+04	1.22	0.39	8.4	1.1	168	18				
Z16-35 - 126	3.09E+07	1.80E+06	1.43E+05	1.20E+04	B.D.	270	6	5.3	2380	86	3.99E+05	1.70E+04	1.51	0.24	0.017	0.059	4.35	0.7				

Z16-35 - 127	2.82E+07	1.40E+06	1.51E+05	1.10E+04	B.D.	350	6.2	2.8	732	29	3.95E+05	6.30E+03	1.45	0.23	B.D.	0.045	20.6	1.5					
Z16-35 - 128	2.84E+07	1.60E+06	1.59E+05	6.80E+03	B.D.	290	10.2	4.5	1500	26	3.96E+05	7.70E+03	0.92	0.18	B.D.	0.046	3.54	0.52					
Z16-35 - 129	2.76E+07	1.20E+06	1.50E+05	1.40E+04	B.D.	530	9.8	5	1454	26	3.98E+05	8.50E+03	0.8	0.2	0.028	0.073	1.48	0.39					
Z16-35 - 130	2.94E+07	1.20E+06	1.52E+05	8.20E+03	B.D.	340	2.4	3.1	872	17	3.96E+05	1.20E+04	2.3	0.41	0.006	0.037	15.1	1.3					
Z16-35 - 131	2.65E+07	1.30E+06	1.61E+05	1.30E+04	B.D.	500	12	6.1	994	18	4.04E+05	1.20E+04	1.1	0.37	3.57	0.69	15.7	2.1					
Z16-35 - 132	2.91E+07	1.50E+06	1.55E+05	9.80E+03	B.D.	410	4.6	3.5	1637	67	3.91E+05	7.60E+03	0.93	0.24	B.D.	0.035	1.21	0.41					
Z16-35 - 133	3.27E+07	1.40E+06	1.49E+05	9.20E+03	B.D.	330	7.2	3.4	1105	66	3.90E+05	8.10E+03	1.74	0.43	8	1.6	81	12					
Z16-35 - 134	2.90E+07	7.80E+05	1.45E+05	1.10E+04	10	530	4.7	5.7	1146	22	3.99E+05	9.60E+03	5.37	0.72	B.D.	0.051	51.4	3					
Z16-35 - 135	2.64E+07	1.60E+06	1.49E+05	1.60E+04	230	550	8.6	4.6	1880	150	3.85E+05	7.20E+03	5.78	0.56	0.04	0.11	81.6	8.8					
Z16-35 - 136	2.88E+07	1.40E+06	1.44E+05	1.00E+04	B.D.	470	10.7	3.9	928	39	4.01E+05	9.20E+03	1.8	0.37	B.D.	0.057	31.9	2.3					
Z16-35 - 137	3.16E+07	1.10E+06	1.43E+05	1.20E+04	B.D.	590	7.4	4.9	1968	55	3.92E+05	1.00E+04	2.01	0.4	13	12	47	35					
Z16-35 - 138	2.62E+07	1.50E+06	1.53E+05	9.20E+03	B.D.	590	9	4.1	1820	100	4.00E+05	1.00E+04	0.91	0.29	0.34	0.14	3.08	0.59					
Z16-35 - 139	2.91E+07	1.20E+06	1.49E+05	9.10E+03	B.D.	390	9.6	2.8	1330	27	3.92E+05	6.10E+03	3.14	0.33	0.22	0.11	53.9	2.4					
Z16-35 - 140	3.10E+07	1.10E+06	1.46E+05	1.30E+04	120	490	11.5	6	1091	30	3.97E+05	1.20E+04	2.41	0.3	0.051	0.069	39.2	2					
Z16-35 - 141	3.07E+07	1.30E+06	1.36E+05	1.40E+04	B.D.	930	11.6	7.3	3310	260	4.01E+05	1.40E+04	1.29	0.47	7.8	1.5	57	11					
Z16-35 - 142	2.87E+07	1.20E+06	1.53E+05	6.80E+03	B.D.	580	8	4.4	686	20	3.97E+05	1.10E+04	0.98	0.23	0.025	0.064	14.45	0.88					
Z16-35 - 143	3.04E+07	8.00E+05	1.43E+05	1.30E+04	B.D.	700	B.D.	2	1106	22	3.93E+05	1.00E+04	1.83	0.37	0.017	0.08	19.1	1.2					
Z16-35 - 144	2.69E+07	1.30E+06	1.51E+05	1.20E+04	B.D.	840	17	4.4	896	17	3.93E+05	7.60E+03	1.3	0.23	0.128	0.084	34.8	2.5					
Z16-35 - 145	3.13E+07	9.30E+05	1.32E+05	1.10E+04	B.D.	850	8.6	5.2	986	20	3.93E+05	1.30E+04	2.7	0.23	0.039	0.066	28.1	2.1					
Z16-35 - 146	2.70E+07	1.20E+06	1.50E+05	1.00E+04	B.D.	1500	6	4.7	770	12	3.91E+05	7.40E+03	2.35	0.41	B.D.	0.063	25	2.1					
Z16-35 - 147	3.13E+07	9.90E+05	1.41E+05	1.00E+04	B.D.	900	5.2	4.5	634	14	3.93E+05	1.00E+04	1.16	0.23	B.D.	0.052	17.2	1.2					
Z16-35 - 148	2.56E+07	1.40E+06	1.45E+05	9.10E+03	700	1400	16.2	5.8	1453	43	3.96E+05	7.90E+03	1.77	0.49	1.4	0.31	35.9	2.8					
Z16-35 - 149	2.88E+07	1.50E+06	1.41E+05	1.20E+04	B.D.	1100	16.7	4.4	915	28	3.91E+05	7.00E+03	1.99	0.26	B.D.	0.038	31.6	1.6					
Z16-35 - 150	2.72E+07	1.20E+06	1.50E+05	8.20E+03	B.D.	1.80E+03	17.4	5.4	864	22	4.00E+05	8.90E+03	1.5	0.23	0.67	0.17	14.9	1.3					
Z16-35 - 151	2.68E+07	1.30E+06	1.43E+05	1.10E+04	B.D.	1.90E+03	8.2	5.2	1618	72	4.04E+05	6.20E+03	2.29	0.42	0.41	0.16	15.3	1.1					
Z16-35 - 152	2.75E+07	9.10E+05	1.45E+05	8.60E+03	B.D.	3.30E+03	4.2	4.9	707	17	3.95E+05	1.10E+04	1.26	0.29	0.01	0.074	14.2	1.4					
Z16-35 - 153	2.77E+07	1.30E+06	1.46E+05	6.10E+03	B.D.	3500	3.8	3.5	296.8	5	3.94E+05	9.90E+03	0.61	0.2	B.D.	0.08	0.72	0.36					
Z16-35 - 154	2.99E+07	7.90E+05	1.36E+05	1.40E+04	4.90E+03	8.70E+03	8.1	5.2	1253	43	3.98E+05	1.00E+04	1.54	0.45	19	1.7	57.9	7.9					
Z16-35 - 155	2.99E+07	1.30E+06	1.37E+05	8.70E+03	B.D.	1.90E+04	1.4	5.9	579	20	3.99E+05	8.80E+03	0.59	0.17	0.89	0.34	16.3	3					
Z16-35 - 156	2.54E+07	1.30E+06	1.71E+05	1.50E+04	8.20E+03	6.90E+03	6	6.7	1910	110	3.88E+05	1.20E+04	1.42	0.3	0.72	0.36	7.2	1.5					
Z16-35 - 157	3.14E+07	1.20E+06	1.49E+05	1.20E+04	6.60E+03	4.10E+03	18.6	9.3	1737	98	3.94E+05	1.50E+04	0.89	0.44	11.6	1.9	112	14					
Z16-35 - 158	2.78E+07	1.40E+06	1.47E+05	1.10E+04	4.80E+03	1.70E+03	4.9	4.5	1005	18	3.99E+05	8.60E+03	0.57	0.17	B.D.	0.0036	5.33	0.96					
Z16-35 - 159	2.84E+07	1.40E+06	1.42E+05	6.60E+03	480	940	31	13	784	13	3.91E+05	8.40E+03	2.24	0.28	0.32	0.18	23.5	1.6					

Z16-35 - 160	2.85E+07	1.70E+06	1.41E+05	6.10E+03	100	1200	9	3.6	2498	41	3.92E+05	7.70E+03	2.97	0.47	0.064	0.073	97.8	3.3					
Z16-35 - 161	2.69E+07	2.00E+06	1.58E+05	1.20E+04	100	1000	11	4.3	1118	37	3.97E+05	9.20E+03	3.65	0.52	5.53	0.95	67.9	5.3					
Z16-35 - 162	3.12E+07	7.50E+05	1.42E+05	1.50E+04	B.D.	1200	2.6	4.6	1252	26	3.96E+05	9.50E+03	2.94	0.84	0.021	0.05	49.7	3.2					
Z16-35 - 163	2.87E+07	1.20E+06	1.50E+05	8.50E+03	320	400	8.4	5.2	1162	56	3.95E+05	8.40E+03	3.76	0.44	0.02	0.062	39.4	2					
Z16-35 - 164	2.85E+07	1.40E+06	1.50E+05	9.70E+03	230	480	7.3	4.4	493	98	3.97E+05	1.20E+04	0.41	0.29	B.D.	0.062	0.42	0.27					
Z16-35 - 165	2.70E+07	1.40E+06	1.47E+05	1.10E+04	B.D.	670	13.7	4.1	1020	11	3.96E+05	4.70E+03	0.78	0.25	B.D.	0.045	22	1.6					
Z16-35 - 166	2.71E+07	1.20E+06	1.46E+05	1.10E+04	B.D.	680	12	4.7	1227	18	3.92E+05	1.00E+04	2.68	0.41	0.046	0.06	14.9	1					
Z16-35 - 167	2.97E+07	9.60E+05	1.43E+05	9.60E+03	440	470	14	6.8	2344	48	3.97E+05	1.20E+04	3.93	0.38	0.023	0.07	54.6	2.4					
Z16-35 - 168	3.10E+07	1.40E+06	1.40E+05	1.00E+04	150	480	7.5	2.7	674	27	3.98E+05	1.10E+04	2.53	0.31	0.24	0.12	36.2	2					
Z16-35 - 169	3.26E+07	1.40E+06	1.23E+05	1.10E+04	B.D.	460	7	4.9	595	19	3.92E+05	7.60E+03	2.16	0.58	0.04	0.15	15.7	2.9					
Nist610 - 1	2.42E+04	1.80E+03	3.22E+05	1.70E+04	330	170	424	20	441	18	417	37	409	17	446	21	436	22					
Nist610 - 2	2.15E+04	1.70E+03	3.16E+05	1.80E+04	420	280	424	25	440	24	404	46	414	25	452	28	443	26					
Nist610 - 3	2.07E+04	1.30E+03	3.38E+05	2.70E+04	B.D.	2700	442	24	448	23	451	51	418	19	460	26	445	19					
Nist610 - 4	2.23E+04	1.40E+03	3.12E+05	2.30E+04	7000	1300	416	18	431	22	458	45	402	17	437	20	429	21					
Nist610 - 5	2.15E+04	2.00E+03	3.23E+05	2.20E+04	17000	58000	428	25	448	23	433	42	415	26	457	28	446	29					
Nist610 - 6	2.12E+04	1.40E+03	3.23E+05	1.60E+04	490	770	427	28	440	18	441	45	414	19	449	20	441	22					
Nist610 - 7	2.06E+04	1.30E+03	3.14E+05	1.90E+04	1600	8500	427	30	437	26	427	56	403	26	446	31	431	26					
Nist610 - 8	2.09E+04	1.30E+03	3.29E+05	1.80E+04	310	590	438	28	448	19	445	39	418	18	453	15	446	16					
Nist610 - 9	2.13E+04	1.40E+03	3.13E+05	2.10E+04	280	320	407	31	429	22	426	43	397	22	436	20	424	23					
Nist610 - 10	2.11E+04	1.70E+03	3.22E+05	1.90E+04	390	160	433	36	452	21	441	54	419	20	453	21	443	18					
Nist610 - 11	2.33E+04	1.70E+03	3.18E+05	1.80E+04	450	250	423	18	438	11	433	35	408	16	445	18	438	20					
Nist610 - 12	2.08E+04	1.10E+03	3.27E+05	1.60E+04	B.D.	2000	429	22	449	18	414	48	416	18	455	20	443	16					
Nist610 - 13	2.23E+04	1.60E+03	3.14E+05	1.90E+04	1500	2600	431	31	436	19	434	48	406	18	441	21	432	20					
Nist610 - 14	2.17E+04	1.60E+03	3.20E+05	1.90E+04	550	460	415	35	444	24	429	39	411	23	453	24	445	26					
Nist610 - 15	2.13E+04	1.70E+03	3.25E+05	2.60E+04	420	430	427	25	441	22	423	46	412	22	447	24	439	17					
GJ1 - 1	3.03E+07	1.30E+06	1.55E+05	1.20E+04	70	170	2.6	4.4	258.3	7.2	4.27E+05	6.90E+03	1.55	0.47	B.D.	0.069	15	1.7					
GJ1 - 2	3.10E+07	9.90E+05	1.64E+05	9.30E+03	30	200	7.7	6.2	265.6	7.3	4.31E+05	1.30E+04	1.7	0.31	B.D.	0.0019	15.1	1.6					
GJ1 - 3	3.01E+07	1.30E+06	1.53E+05	1.20E+04	B.D.	130	11.6	3.4	262.6	5.5	4.38E+05	7.10E+03	1.79	0.3	B.D.	0.025	14.2	1.2					
GJ1 - 4	2.90E+07	1.20E+06	1.57E+05	1.10E+04	B.D.	140	3.7	4.3	255	6.4	4.21E+05	1.50E+04	1.72	0.31	B.D.	0.024	14.4	1.2					
GJ1 - 5	3.19E+07	1.00E+06	1.54E+05	1.70E+04	B.D.	140	9.8	3.4	254.9	8	4.33E+05	1.10E+04	1.52	0.33	0.038	0.073	12.3	2					
GJ1 - 6	2.98E+07	1.50E+06	1.57E+05	1.10E+04	B.D.	230	6.1	4.3	250.3	7.6	4.32E+05	1.10E+04	1.5	0.41	0.001	0.05	14.4	1.4					

GJ1 - 7	3.05E+07	1.60E+06	1.61E+05	9.60E+03	200	1700	3.7	3.8	252	4.4	4.27E+05	8.00E+03	1.59	0.31	B.D.	0.04	14.07	0.53					
GJ1 - 8	3.04E+07	6.90E+05	1.42E+05	1.10E+04	200	3100	0.2	4	253.1	9.5	4.36E+05	2.70E+04	1.39	0.27	0.029	0.068	14.8	1.6					
GJ1 - 9	3.03E+07	1.30E+06	1.52E+05	1.30E+04	B.D.	770	2.9	4.8	260.3	7.3	4.25E+05	1.10E+04	1.41	0.39	B.D.	0.0029	14.4	1.6					
GJ1 - 10	2.93E+07	1.30E+06	1.59E+05	1.40E+04	2.10E+03	2.30E+03	1.4	3.5	262	8	4.24E+05	1.20E+04	1.73	0.28	0.022	0.084	14.4	1.5					
GJ1 - 11	2.76E+07	1.60E+06	1.51E+05	1.20E+04	B.D.	3.40E+04	4.4	3.1	251.1	7	4.19E+05	6.30E+03	1.59	0.3	B.D.	0.049	14.6	1.1					
GJ1 - 12	2.89E+07	1.10E+06	1.60E+05	1.10E+04	550	820	0.5	3.9	261.6	8.5	4.24E+05	9.40E+03	1.69	0.5	B.D.	0.02	14.3	1.2					
GJ1 - 13	2.94E+07	1.80E+06	1.37E+05	1.10E+04	B.D.	460	4.6	3.9	253.1	5.4	4.11E+05	5.00E+03	1.45	0.28	0.015	0.039	13.55	0.9					
GJ1 - 14	2.81E+07	1.40E+06	1.56E+05	8.80E+03	130	730	8.6	4.4	249.6	6.1	4.16E+05	9.30E+03	1.41	0.24	0.036	0.047	14.6	1.3					
GJ1 - 15	2.90E+07	9.30E+05	1.56E+05	1.30E+04	B.D.	8.40E+03	2.3	4	245.8	6.2	4.05E+05	1.10E+04	1.67	0.54	B.D.	0.052	14	1.5					
GJ1 - 16	2.75E+07	1.80E+06	1.54E+05	1.00E+04	690	790	1.5	3.3	249.6	6.4	4.20E+05	1.10E+04	1.17	0.3	0	0.051	13.5	1.3					
GJ1 - 17	2.81E+07	1.60E+06	1.43E+05	9.90E+03	370	380	4.4	4.6	243.6	4.7	4.15E+05	7.00E+03	1.66	0.35	B.D.	0.004	13.68	0.93					
GJ1 - 18	2.75E+07	1.40E+06	1.59E+05	9.40E+03	420	300	6.6	3.3	252.5	5.5	4.07E+05	9.30E+03	1.37	0.3	0.08	0.1	14.53	0.98					
GJ1 - 19	2.78E+07	1.50E+06	1.47E+05	8.20E+03	170	200	4.7	3.4	255.3	5.1	4.11E+05	6.50E+03	1.39	0.31	0.004	0.041	13.29	0.95					
GJ1 - 20	2.92E+07	1.60E+06	1.54E+05	9.20E+03	B.D.	94	3.5	3.1	247.5	4.8	3.97E+05	6.30E+03	1.47	0.31	0.049	0.063	14.4	1					
GJ1 - 21	2.88E+07	1.40E+06	1.53E+05	8.10E+03	B.D.	180	0.4	3.1	256	4.9	4.03E+05	7.50E+03	1.52	0.26	0.054	0.051	14.5	0.89					
GJ1 - 22	2.80E+07	1.70E+06	1.54E+05	1.10E+04	B.D.	3000	5.4	5.3	254	6.5	4.04E+05	9.40E+03	1.66	0.32	0.032	0.056	13.9	1.1					
GJ1 - 23	2.83E+07	1.60E+06	1.53E+05	1.10E+04	210	330	5	3.3	254.3	6	3.99E+05	9.50E+03	1.48	0.25	B.D.	0.056	13.5	1.2					
GJ1 - 24	2.81E+07	1.60E+06	1.46E+05	1.00E+04	170	340	4.4	3	257	5.8	4.08E+05	9.00E+03	1.41	0.28	0.047	0.069	14	1.1					
GJ1 - 25	2.87E+07	1.50E+06	1.55E+05	7.00E+03	B.D.	1.20E+03	2.6	3.4	246.3	4.7	3.98E+05	8.10E+03	1.43	0.34	0.003	0.043	13.2	1.1					
GJ1 - 26	2.81E+07	1.50E+06	1.48E+05	8.80E+03	1.20E+03	2.20E+03	4.6	3.5	256.6	7	4.01E+05	6.80E+03	1.67	0.31	0.024	0.076	13.9	1.3					
GJ1 - 27	2.90E+07	1.70E+06	1.51E+05	1.10E+04	B.D.	1.30E+03	1.3	4.1	254.4	3.9	3.93E+05	9.80E+03	1.39	0.22	B.D.	0.042	14.6	1.2					
GJ1 - 28	2.93E+07	1.70E+06	1.54E+05	1.00E+04	70	680	2.3	3.4	251.9	7.5	3.91E+05	9.60E+03	1.58	0.26	0.01	0.061	14.05	0.89					
GJ1 - 29	2.88E+07	1.20E+06	1.54E+05	1.20E+04	B.D.	340	2.1	3.1	255.9	6	4.01E+05	6.80E+03	1.63	0.29	B.D.	0.051	12.65	0.97					
GJ1 - 30	2.85E+07	1.70E+06	1.36E+05	6.60E+03	B.D.	280	4.2	3.3	250.3	6.4	3.95E+05	9.70E+03	1.4	0.2	B.D.	0.044	13.1	1.2					
Ples - 1	3.11E+07	1.20E+06	1.52E+05	1.20E+04	165	79	66.6	7	502	10	4.23E+05	1.10E+04	4.53	0.55	B.D.	0.019	2.49	0.43					
Ples - 2	2.91E+07	1.80E+06	1.68E+05	1.20E+04	270	150	131	11	825	19	4.30E+05	9.30E+03	17.24	0.84	B.D.	0.042	5.52	0.57					
Ples - 3	3.14E+07	1.40E+06	1.48E+05	6.90E+03	300	1700	123	15	817	18	4.21E+05	1.30E+04	16.44	0.72	0.058	0.08	5.63	0.84					
Ples - 4	2.85E+07	1.60E+06	1.58E+05	1.00E+04	B.D.	950	78.9	8.9	489.4	8.8	4.18E+05	9.20E+03	4.33	0.45	B.D.	0.035	2.01	0.48					
Ples - 5	3.01E+07	1.30E+06	1.59E+05	6.90E+03	3.10E+06	2.00E+06	98	12	700	19	4.15E+05	7.00E+03	4.3	0.69	B.D.	0.051	2.73	0.65					
Ples - 6	3.17E+07	1.60E+06	1.52E+05	1.30E+04	990	550	80.2	8.9	659	33	4.10E+05	9.50E+03	4.62	0.51	0.049	0.07	2.44	0.53					
Ples - 7	2.85E+07	1.60E+06	1.50E+05	9.80E+03	B.D.	2.30E+03	86.6	9.1	667	11	4.09E+05	8.30E+03	4.23	0.46	0.1	0.1	2.13	0.36					
Ples - 8	2.57E+07	1.60E+06	1.64E+05	1.10E+04	B.D.	710	66	12	405.8	9.1	4.17E+05	7.30E+03	5.46	0.72	0.036	0.076	2.07	0.59					

Ples - 9	2.72E+07	1.20E+06	1.64E+05	1.30E+04	B.D.	190	90.4	9.8	623	17	4.14E+05	6.10E+03	4.98	0.57	0.095	0.091	2.64	0.56					
Ples - 10	2.75E+07	1.30E+06	1.52E+05	1.50E+04	B.D.	170	34.4	5	239.9	7.7	3.99E+05	1.10E+04	2.91	0.49	0.061	0.068	2.03	0.73					
Ples - 11	2.65E+07	1.20E+06	1.55E+05	1.20E+04	10	280	69.6	6.1	495	14	4.00E+05	1.00E+04	3.79	0.59	B.D.	0.051	1.81	0.38					
Ples - 12	2.61E+07	1.50E+06	1.51E+05	1.20E+04	600	2400	56.5	5.2	447	11	3.92E+05	8.90E+03	4.79	0.58	0.001	0.077	2.14	0.65					
Ples - 13	2.80E+07	1.40E+06	1.59E+05	9.80E+03	B.D.	3000	54.9	6.3	475.3	9.8	3.93E+05	6.60E+03	4.9	0.5	B.D.	0.039	2.4	0.48					
Ples - 14	3.10E+07	1.40E+06	1.44E+05	1.10E+04	B.D.	240	60.6	4.8	492	11	4.04E+05	9.40E+03	4.85	0.59	B.D.	0.046	2.2	0.54					
Ples - 15	2.87E+07	1.30E+06	1.53E+05	1.10E+04	180	290	69.6	7.3	472	13	3.90E+05	1.00E+04	4.53	0.5	0.02	0.053	1.89	0.35					
91500 - 1	3.04E+07	1.20E+06	1.40E+05	1.20E+04	B.D.	210	5.8	6.4	121	4.1	4.28E+05	1.40E+04	1	0.3	B.D.	0.043	2.7	1					
91500 - 2	2.61E+07	1.10E+06	1.61E+05	1.70E+04	170	140	4.9	6.6	112.2	3.7	4.25E+05	1.10E+04	1.04	0.27	B.D.	0.0034	2.12	0.78					
91500 - 3	2.75E+07	1.20E+06	1.68E+05	1.40E+04	360	130	B.D.	2.9	122.4	3	4.30E+05	1.00E+04	1.23	0.25	B.D.	0.05	2.48	0.42					
91500 - 4	2.81E+07	1.20E+06	1.56E+05	9.90E+03	B.D.	120	5.1	2.9	118.3	3.3	4.29E+05	8.70E+03	0.97	0.2	0.023	0.086	2.4	0.44					
91500 - 5	2.77E+07	1.20E+06	1.49E+05	8.80E+03	B.D.	150	6.6	3.6	118.7	2.8	4.30E+05	8.80E+03	0.66	0.19	B.D.	0.044	2.38	0.39					
91500 - 6	2.89E+07	1.60E+06	1.60E+05	1.10E+04	90	310	5.6	3.2	116.3	3.2	4.24E+05	7.10E+03	0.82	0.21	B.D.	0.045	2.3	0.39					
91500 - 7	2.91E+07	1.30E+06	1.50E+05	7.30E+03	900	1400	4.5	4.1	97.1	3.2	4.25E+05	9.20E+03	0.86	0.21	B.D.	0.03	1.64	0.5					
91500 - 8	2.97E+07	1.60E+06	1.58E+05	1.00E+04	200	2400	3	3.1	116.4	3	4.25E+05	6.80E+03	0.99	0.26	0.044	0.074	2.66	0.35					
91500 - 9	2.77E+07	1.40E+06	1.59E+05	8.70E+03	110	780	4.9	4.6	126.4	3.4	4.20E+05	9.30E+03	0.66	0.2	0.025	0.08	2.44	0.53					
91500 - 10	2.78E+07	1.40E+06	1.67E+05	9.20E+03	B.D.	2800	2.5	3.3	124.3	3.8	4.27E+05	1.00E+04	0.99	0.26	B.D.	0.045	2.2	0.62					
91500 - 11	2.81E+07	1.70E+06	1.49E+05	8.30E+03	6.00E+04	2.30E+04	4.9	3.1	120	2.9	4.21E+05	1.00E+04	0.67	0.16	0.008	0.063	2.73	0.39					
91500 - 12	2.77E+07	1.40E+06	1.51E+05	1.20E+04	100	1200	B.D.	2.7	103.3	4.2	4.13E+05	8.20E+03	1.08	0.26	B.D.	0.063	2.03	0.32					
91500 - 13	2.90E+07	1.40E+06	1.46E+05	1.10E+04	B.D.	460	3.4	3.1	118.5	2.5	4.12E+05	4.50E+03	0.68	0.16	0.029	0.059	2.31	0.46					
91500 - 14	2.84E+07	1.50E+06	1.58E+05	1.40E+04	300	880	4.9	3.7	119.3	2.9	4.13E+05	8.60E+03	0.67	0.18	0.039	0.081	2.24	0.53					
91500 - 15	2.66E+07	1.50E+06	1.56E+05	1.40E+04	300	9100	4.1	3.6	119.8	4.5	4.11E+05	7.90E+03	0.63	0.16	0.058	0.069	2.59	0.64					
91500 - 16	2.77E+07	1.40E+06	1.51E+05	1.20E+04	B.D.	770	2.2	3.1	118.1	4.7	4.17E+05	8.90E+03	0.72	0.23	B.D.	0.016	2.11	0.33					
91500 - 17	2.85E+07	1.40E+06	1.41E+05	7.50E+03	310	390	1.4	3	117.2	3.4	4.04E+05	8.10E+03	0.71	0.17	B.D.	0.042	2.47	0.44					
91500 - 18	2.82E+07	1.70E+06	1.53E+05	9.90E+03	240	290	3.5	3.8	107.7	2.9	4.12E+05	7.20E+03	0.98	0.23	0.017	0.042	1.87	0.27					
91500 - 19	2.57E+07	1.10E+06	1.58E+05	1.40E+04	20	300	7.1	3.6	117.6	3.9	4.12E+05	1.20E+04	0.74	0.25	0.02	0.061	2.25	0.52					
91500 - 20	2.83E+07	1.60E+06	1.48E+05	8.50E+03	B.D.	110	5	2.9	123	3.3	4.06E+05	8.50E+03	0.66	0.14	0.006	0.046	2.3	0.53					
91500 - 21	2.91E+07	1.50E+06	1.63E+05	1.00E+04	30	150	4.3	3	117.9	2.6	3.98E+05	6.30E+03	0.66	0.16	B.D.	0.025	2.28	0.51					
91500 - 22	2.74E+07	1.70E+06	1.51E+05	8.70E+03	1.20E+03	2.00E+03	4.9	3.6	109.1	3.3	4.00E+05	6.70E+03	0.75	0.21	B.D.	0.042	1.76	0.47					
91500 - 23	2.61E+07	9.30E+05	1.54E+05	8.60E+03	0	370	5.1	4.9	102.5	3.8	3.93E+05	7.60E+03	0.75	0.21	B.D.	0.051	1.89	0.45					
91500 - 24	2.80E+07	1.60E+06	1.43E+05	1.10E+04	180	440	4.8	3.8	120.6	2.8	4.03E+05	8.10E+03	0.66	0.15	0.006	0.037	2.37	0.46					
91500 - 25	2.83E+07	1.30E+06	1.47E+05	7.90E+03	B.D.	1.00E+03	5.9	4.1	118.3	2.4	4.00E+05	5.00E+03	0.85	0.21	0.012	0.041	2.11	0.37					

91500 - 26	2.79E+07	1.60E+06	1.48E+05	7.20E+03	0	1700	6.6	5.2	116.3	3.7	3.98E+05	7.80E+03	0.84	0.23	0.031	0.061	2.41	0.5
91500 - 27	2.84E+07	1.60E+06	1.52E+05	9.00E+03	B.D.	1.80E+03	2.6	4.1	114	3.5	4.00E+05	1.00E+04	0.91	0.29	0.088	0.077	2.85	0.75
91500 - 28	2.88E+07	1.60E+06	1.43E+05	9.70E+03	100	730	3.4	3.3	110.6	3.2	4.00E+05	1.10E+04	0.71	0.13	0.041	0.048	1.86	0.49
91500 - 29	2.79E+07	1.70E+06	1.52E+05	1.10E+04	120	280	1.1	2.2	121.3	3.6	4.00E+05	6.30E+03	0.69	0.19	B.D.	0.053	2.5	0.56
91500 - 30	2.76E+07	1.20E+06	1.45E+05	1.40E+04	140	470	2	4	108.6	3.2	3.93E+05	7.20E+03	0.73	0.28	B.D.	0.044	2.26	0.57

Sample	Pr	Pr 2SE	Nd	Nd 2SE	Sm	Sm 2SE	Eu	Eu 2SE	Gd	Gd 2SE	Tb	Tb 2SE	Dy	Dy 2SE	Ho	Ho 2SE	Er
Z16-40 - 1	8.2	1.7	48.1	8.5	31	6.2	4.9	1.5	77.2	7.2	18.8	1.9	190	16	69.1	3.6	299
Z16-40 - 2	0.024	0.079	1.1	0.96	3.1	1.8	0.46	0.4	33	6.9	13.8	1.3	222	15	90.6	4.4	443
Z16-40 - 3	0.065	0.077	1.3	1.1	3.8	1.8	0.56	0.4	19.3	3	9.1	1.2	113.2	8.1	42.3	2.5	195
Z16-40 - 4	0.36	0.11	2.9	1.3	11.8	2.9	1.59	0.62	52.5	6.1	16.5	1.3	174.6	7.7	66	3.2	273
Z16-40 - 5	0.21	0.11	3.5	1.8	9	3.2	0.95	0.37	48.7	6	14.9	1.5	168.6	9.8	65.1	2.6	270.6
Z16-40 - 6	1.83	0.42	13.8	2.9	11.3	4.2	1.73	0.77	35.4	6.5	11.3	1.5	124	8.9	43.2	2.1	200.5
Z16-40 - 7	0.255	0.096	3.7	1.3	7.1	2.1	0.73	0.34	31.4	4	10.23	0.94	129.9	9.2	50.1	2.9	213
Z16-40 - 8	0.106	0.061	2.7	1.1	6.2	2.2	0.98	0.58	42.9	7.5	13.8	1.5	158	12	57.7	3	234
Z16-40 - 9	0.74	0.28	8.8	4.4	2.1	1.5	0.96	0.59	20.7	4.5	7.5	1.2	86.8	8.1	35.3	3	184
Z16-40 - 10	68	22	394	91	194	50	71	24	279	74	54	16	480	210	86	11	400
Z16-40 - 11	1.63	0.35	11.3	3	10.2	2.9	1.73	0.9	46.7	5.8	16.09	0.98	172.5	8.3	66.2	5.2	284
Z16-40 - 12	0.78	0.43	4.5	2.2	5.8	2.9	0.88	0.52	34.3	6.7	18.7	2.1	272	19	119.7	6.5	582
Z16-40 - 13	6.7	1.1	43	6.4	21.7	5.6	8.4	2.4	36.9	9.4	8.4	1.4	100	11	38.9	3.7	195
Z16-40 - 14	0.16	0.1	1	1.3	2.9	1.3	0.08	0.42	31.9	7.8	14.5	2.5	193	22	80	9.2	376
Z16-40 - 15	3.8	2	26	13	16.2	7.4	5.2	2.8	58	19	18.4	3.7	198	33	72.5	6.3	308
Z16-40 - 16	2.1	2.2	14.9	9.9	11.8	5.9	2.1	1.7	54	22	12.7	2.4	107	28	28.9	4.6	95
Z16-40 - 17	0.097	0.068	1.4	1.1	2.8	1.2	0.33	0.25	20.6	4.3	9.8	1.3	142.3	7.4	62.4	3.4	314
Z16-40 - 18	B.D.	0.042	0.77	0.91	2.5	1.3	0.3	0.26	21.8	3	10.1	1.3	133.7	9	57	2	263.3
Z16-40 - 19	0.092	0.048	2.2	1	5.6	2.6	1.18	0.44	41.3	4.5	11.7	1.3	124.4	9.2	47.8	2.4	200.4
Z16-40 - 20	2.12	0.37	14.7	3.4	8.6	1.8	2.87	0.94	31.8	5.9	11.6	1	135.2	7.3	51.5	1.9	231.9
Z16-40 - 21	4.68	0.78	29.3	4.7	14.9	3.7	3.07	0.82	50.5	5.9	14.25	0.96	176	10	63.9	3.7	264
Z16-40 - 22	7.31	0.71	54.9	6.1	39.6	4.9	7.9	1.1	104	10	32.5	2.5	407	15	171.1	5.2	769
Z16-40 - 23	1.59	0.33	12.1	2.6	12.1	2.7	3.01	0.49	51.6	6.1	19.8	1.3	251.9	7.1	99.3	2.2	432
Z16-40 - 24	0.29	0.12	1.11	0.8	3.9	2.1	0.28	0.32	34.7	6.8	17.6	1.9	271	20	124.3	8.1	614
Z16-40 - 25	B.D.	0.045	B.D.	0.24	2.4	1.5	0.38	0.3	25	4.8	12.9	1.8	177	19	80	11	396
Z16-40 - 26	2.56	0.48	17.6	2.8	18.6	2.7	2.19	0.66	59.5	5.9	16.4	1.7	179	10	74.4	4.4	317
Z16-40 - 27	0.179	0.088	4	1.3	9.3	2.4	1.39	0.53	48.3	6.1	16	1.5	188	15	71.2	5.7	293
Z16-40 - 28	0.72	0.4	4.9	2.3	5.5	2.7	1.34	0.6	25.5	5	8.15	0.78	97	12	36.1	2.7	147
Z16-40 - 29	0.06	0.18	0.57	0.98	2.4	1.5	0.03	0.23	29.3	3	15.6	1.4	231	14	111.5	6.1	558
Z16-40 - 30	1.93	0.54	18.3	5.2	11.9	3.1	3.5	1.1	53.7	6.8	16.4	1.3	189	12	66	2.8	286
Z16-40 - 31	1	0.26	11.4	2.4	13.4	2.9	2.08	0.66	50.2	7.6	17.5	1.9	193	10	78.5	3.1	352

Z16-40 - 32	0.104	0.084	0.35	0.51	2.9	2.2	0.06	0.19	18.6	3.2	12.7	1.6	170	9.5	66	4.1	269			
Z16-40 - 33	3.6	0.38	23.7	5.9	24.2	5.2	2.43	0.81	52.1	6.5	15.9	1.5	187.7	9.2	75.9	2.8	350			
Z16-40 - 34	1.82	0.81	12.4	4.4	6.9	2.5	3.2	1.6	32.8	6.1	11.1	1.1	143	19	57.7	4.1	286			
Z16-40 - 35	0.92	0.71	8.7	6.2	9.4	3.4	0.74	0.38	30.8	5.8	10.6	1.5	122.6	5.7	45.2	1.4	195			
Z16-40 - 36	6.34	0.75	41.3	5	19.7	3.2	5.1	1.3	53.2	6.2	13.9	1.4	145.6	9	52.7	1.5	227			
Z16-40 - 37	0.65	0.19	4.9	1.7	5.2	1.7	1.53	0.47	29.5	4	12.3	1.2	152.6	6.7	66.2	2.8	306			
Z16-40 - 38	0	0.055	0.75	0.81	3.1	1.2	B.D.	0.074	24.5	3	12.9	1.2	205.2	9	95.8	3.4	486			
Z16-40 - 39	75	49	320	210	79	39	6.9	3.2	118	38	28	4.7	318	43	112.4	6.6	544			
Z16-40 - 40	0.81	0.25	4	1.5	3.2	1.8	0.54	0.3	32.1	5.6	11.6	1.6	167	12	64.7	3.5	319			
Z16-40 - 41	1	0.33	8.2	2.3	6	1.9	1.29	0.49	22.2	4.2	7.03	0.92	92.6	6.2	36.7	2.3	168.6			
Z16-40 - 42	0.78	0.18	8.9	2.7	11.7	1.6	1.44	0.55	63.8	7.1	17.36	0.92	189.6	8.6	71.2	3.6	280.8			
Z16-40 - 43	8.79	0.98	58	11	45.2	5.8	7.3	1.1	104	9.1	28.3	2.2	272	14	96.1	4.4	402			
Z16-40 - 44	3.26	0.53	15.5	3.3	7.3	2.1	3.1	1.2	30.3	4.9	11.6	1.4	160	14	66.7	4.3	325			
Z16-40 - 45	0.63	0.16	9.9	2.4	16.5	3.1	2.33	0.72	100	10	33.6	2.6	415	30	164	12	734			
Z16-40 - 46	0.059	0.054	0.28	0.58	1.6	1.1	0.34	0.25	20.9	3.7	8.7	1.2	123.3	5.6	51.3	2.7	243.1			
Z16-40 - 47	0.095	0.057	1.6	0.82	4.2	1.5	0.42	0.25	33.5	3.5	15.8	1.1	217.6	7.9	94.6	3.2	441			
Z16-40 - 48	0.6	0.25	3.9	1.7	11.8	3.3	1.49	0.65	50.7	4.1	17.4	1.7	221	12	87.3	4.4	388			
Z16-40 - 49	7.3	0.6	54.9	7.2	40.3	4.7	4.11	0.92	86.6	7.9	17.3	1.8	144	10	41.3	4.2	171			
Z16-40 - 50	0.039	0.074	3	1.3	5.4	1.8	0.83	0.33	27.6	4.3	8.9	1.3	113.7	8.6	41.3	3.6	179			
Z16-40 - 51	4.36	0.85	34.8	4.5	19.1	2.9	8.5	1.8	75.3	7	25	2.4	276	21	103.2	4.7	419			
Z16-40 - 52	0.86	0.35	6.7	3.2	4	1.8	1.39	0.78	30.4	4.9	15.4	1.9	213	22	89.2	9.9	418			
Z16-40 - 53	8.1	0.83	45.9	7.7	27.3	5.9	6.2	1.4	44.3	8.2	13.6	1.9	119.7	6.3	42	2.5	196			
Z16-40 - 54	171	35	1210	240	548	97	103	17	780	150	108	18	636	97	139	17	441			
Z16-40 - 55	0.74	0.28	3.85	0.82	5.2	2.9	0.7	0.46	32.5	4	13.1	1.3	168.7	7.9	74.7	3.2	358			
Z16-40 - 56	1.6	0.6	12.4	3.6	12.3	2.1	1.58	0.34	36.4	5.5	11.2	1.2	119.6	8.5	45.5	2.4	195			
Z16-40 - 57	0.114	0.085	3.5	1.2	9.9	2.3	1.72	0.6	50.2	6.1	15.6	1.7	166	10	59.6	2.8	246			
Z16-40 - 58	0.137	0.056	2.2	1.2	5.9	1.9	0.24	0.23	27.9	5.8	11.3	1.1	146.1	8.8	58	2.8	266			
Z16-40 - 59	0.96	0.32	7.3	3.1	6.2	2.7	1.02	0.44	31.7	6.9	14.8	2	194	15	87.2	4.7	410			
Z16-40 - 60	6.1	1.8	48	17	31.6	6.9	4.66	0.98	82.5	9.9	23	2.4	213.2	8.4	72.3	2.7	286			
Z16-40 - 61	0.64	0.15	4.1	1.7	3.2	1.2	0.62	0.41	16.1	2.2	6.04	0.64	75.3	3.9	31	2.6	153			
Z16-41 - 1	0.35	0.19	5.1	1.9	11.7	4.3	0.94	0.64	63.7	9.2	19.9	1.6	211	14	76.5	1.7	334			
Z16-41 - 2	0.62	0.15	9.1	1.9	13.8	2.1	2.27	0.65	59.9	5.3	18.2	1.2	184	12	63.1	3.3	263.5			

Z16-41 - 3	0.24	0.12	7	2.6	13	3.8	2.6	1.1	50	7.1	14.8	2.1	152	17	53.4	5	215					
Z16-41 - 4	0.21	0.18	4.7	1.3	11	5.4	1.04	0.72	42.3	8.7	14.7	2.2	157	26	57.7	9.9	238					
Z16-41 - 5	B.D.	0.064	0.36	0.66	3.3	1.4	0.05	0.19	11.4	3	4.19	0.66	57.6	5.9	23.4	2.4	114.2					
Z16-41 - 6	0.018	0.057	1.8	1.2	2.2	1.6	0.74	0.47	17.2	6.1	5.5	1.1	72.8	8.6	30.1	2.7	128					
Z16-41 - 7	0.095	0.067	2.3	1.6	5.2	1.7	0.39	0.31	22	3.3	6.89	0.71	88.1	6.4	33.6	1.7	147.7					
Z16-41 - 8	0.178	0.095	3.3	1.5	6.2	2.1	0.51	0.31	27	3.3	8.74	0.7	101.5	6.2	41.8	1.9	184.7					
Z16-41 - 9	0.071	0.063	0.9	1	2.5	2.1	0.34	0.37	13.5	3.9	5.27	0.77	51.4	4.4	23.3	1.6	109.9					
Z16-41 - 10	0.007	0.052	1.8	1.2	3.3	1.9	0.4	0.42	19.1	4.1	7.1	1.5	80	10	30.8	3.2	139					
Z16-41 - 11	0.26	0.16	5.04	0.87	8.8	2.9	0.82	0.4	51.5	5.6	16.3	1.1	188	11	71.2	5	291					
Z16-41 - 12	0.053	0.075	3.1	2.3	5	2.2	0.52	0.45	25.9	3.9	8.7	1.4	96	7.3	34.6	3	150					
Z16-41 - 13	0.41	0.13	7.5	1.9	11.3	2.7	2.63	0.6	55.9	4.6	14.3	1	159.3	8	52	2	215.5					
Z16-41 - 14	5.7	5.9	29	28	13.9	5.6	1.03	0.7	59	12	15.2	1.1	170	14	62.7	3.5	271					
Z16-41 - 15	0.081	0.061	0.38	0.46	1.6	0.83	0.34	0.22	7.5	2.1	3.07	0.51	42.1	3.7	18	1.4	83.6					
Z16-41 - 16	0.086	0.094	1	1.1	1.8	1.1	0.28	0.27	11.5	4.3	4.5	0.92	56.9	6.5	22.5	2.4	108					
Z16-41 - 17	0.15	0.1	2.1	1.1	5.9	2.2	0.63	0.35	24.4	3.7	8	1.2	88.9	8.6	33.2	2.3	145					
Z16-41 - 18	0.058	0.073	2	1	5.8	2.3	0.64	0.33	29.4	6.9	10	1.4	116	18	42.6	6.3	191					
Z16-41 - 19	0.67	0.15	7.8	2.3	18.5	5.3	0.58	0.42	88.7	7	28.1	2.2	296	18	108.5	6.1	444					
Z16-41 - 20	30	21	160	110	50	27	3.3	2	111	30	32.6	6.4	341	50	117	16	488					
Z16-41 - 21	15.1	6.5	84	37	27.7	9.4	1.64	0.62	50.5	9.9	11.7	1.5	105	4.8	37.8	2.4	156.1					
Z16-41 - 22	3.3	1.3	25.1	7.1	21.6	4.9	1.19	0.49	96	10	28.4	2.3	311	16	113.3	6.4	472					
Z16-41 - 23	0.062	0.046	1	0.73	2.2	1	0.13	0.15	10	1.7	3.74	0.46	48.8	4.5	19	1.3	92.2					
Z16-41 - 24	0.082	0.072	1.2	0.84	2.4	1.4	0.59	0.4	11.9	1.9	4.2	0.9	59.3	4.4	24.3	1.3	105.6					
Z16-41 - 25	0.014	0.054	0.88	0.66	1.4	1.2	0.21	0.21	15.8	4	5.24	0.76	61.8	5	25.3	1.8	116.5					
Z16-41 - 26	0.096	0.075	1.01	0.85	1.04	0.8	0.24	0.22	12.1	2.1	5.07	0.6	61.8	7.3	27.4	2.2	120.7					
Z16-41 - 27	0.15	0.12	2.9	1.8	4.3	1.8	0.26	0.32	23.7	4.8	8.1	1.7	92	11	36	2.5	156					
Z16-41 - 28	0.065	0.064	1.5	1.1	3.1	1.4	0.15	0.2	21.4	3.7	7.07	0.73	84.5	5.5	29.6	1.6	135.8					
Z16-41 - 29	0.45	0.2	5.5	1.7	11.6	2.6	1.17	0.49	48.6	6.6	13.2	1.8	155.7	9	54.5	2.6	234.2					
Z16-41 - 30	0.41	0.14	2.3	1.2	1.77	0.91	0.36	0.2	19.2	2.1	5.5	0.55	63.3	3.3	23.6	1.4	105.5					
Z16-41 - 31	0.17	0.11	4.7	1.7	9.3	2.6	1	0.45	43.9	5.6	13.8	2.1	150	16	53.6	4.6	227					
Z16-41 - 32	0.048	0.054	0.88	0.84	2.7	1.5	B.D.	0.086	10.4	1.7	4.14	0.62	50.8	4.5	20.9	1.6	98.7					
Z16-41 - 33	122.3	3.1	794	34	228	13	17.4	1.7	262	12	44.2	2.3	274	10	63.5	3.4	204.7					
Z16-41 - 34	0.42	0.11	5.4	2.4	8.1	2.1	1.67	0.64	39.8	6.6	12.6	1.7	129	18	47.8	4.5	198					
Z16-41 - 35	0.255	0.084	5	1.9	8.2	2.1	0.9	0.47	53.2	5.5	15.1	1.1	168.1	9.7	59.7	3	255.9					

Z16-41 - 36	0.083	0.069	0.64	0.58	1.7	0.86	0.008	0.091	11.5	1.8	3.32	0.62	45.2	3.9	19.4	1.4	88.8			
Z16-41 - 37	0.071	0.078	1.4	1.4	1.3	1.5	0.33	0.33	11.7	2.4	5.2	0.78	59.4	4.1	23.2	1.5	116			
Z16-41 - 38	0.035	0.051	1.27	0.79	2.6	1.1	0.24	0.22	14.8	2.2	4.85	0.5	56.5	5.1	21	1.5	95.6			
Z16-41 - 39	0.2	0.18	3.5	2	7.2	3.2	0.26	0.19	47	7.1	15.2	1.8	176	17	69	5.7	276			
Z16-41 - 40	0.357	0.099	5.6	1.4	9.8	2.1	1.59	0.52	41.1	4.5	11.9	1.3	131.8	9.3	46.5	2.3	190			
Z16-41 - 41	0.085	0.055	0.36	0.34	1.11	0.97	0.19	0.16	7.9	1.7	3.48	0.54	39.5	3.2	17.4	1.4	82.3			
Z16-41 - 42	0.005	0.052	1.1	1	2.7	1.8	0.31	0.41	9.2	2.7	3.5	1	48.7	3.3	22.4	1.6	102.3			
Z16-41 - 43	2.7	3.1	18	20	10.2	6.4	1.37	0.46	40	11	10.7	1	111.5	6.7	38.4	1.3	164.9			
Z16-41 - 44	0.21	0.17	4.4	2.3	6.1	2.2	0.72	0.39	39	11	12.3	2.9	130	25	50.3	7.5	221			
Z16-41 - 45	0.09	0.1	2	0.89	1.74	0.74	0.41	0.35	22.6	5.4	7.58	0.86	84.7	5	31.8	1.9	138.6			
Z16-41 - 46	0.073	0.09	0.19	0.54	2.7	1.3	0.31	0.35	14.7	5.3	5.5	2	71	14	25.5	3.1	125			
Z16-41 - 47	0.4	0.15	5.5	1	11.5	2.4	1.65	0.59	51	3.8	15.2	1.2	162	7.5	57.8	2	242			
Z16-41 - 48	0.53	0.19	5.4	1.7	6	1.9	1.17	0.37	33.5	3.3	11	1	113.4	5.2	41.8	1.5	176.4			
Z16-41 - 49	0.33	0.23	9.5	2.3	18.1	3.8	2.75	0.94	80.1	8.6	22.9	1.7	247	12	84.7	2.8	352.3			
Z16-41 - 50	54	28	250	130	63	31	3.8	1.6	80	25	15.8	3.8	122	20	36.2	4.4	151			
Z16-41 - 51	0.09	0.089	1.46	0.92	2.4	1.2	0.26	0.25	13.7	4.2	4.6	1	53	9.1	23.4	2.3	104			
Z16-41 - 52	0.41	0.19	8.4	2.7	12.5	3.1	0.86	0.53	71	6.4	21.6	1.9	232	12	85.1	4.6	357			
Z16-41 - 53	0.13	0.13	0.11	0.39	2	1.6	0.37	0.58	14.1	3.7	5.1	1.3	63.5	9.1	27.3	3.1	117			
Z16-41 - 54	B.D.	0.034	0.74	0.48	2	1.1	0.12	0.24	13.8	2.5	4.24	0.75	57.1	3.8	22.8	1.7	115.3			
Z16-41 - 55	0.181	0.072	2.8	1.5	5.5	3	0.97	0.49	37.6	6.9	11.6	1.9	131	10	49.3	3.1	223			
Z16-41 - 56	0.17	0.14	2.32	0.81	8.9	3.5	0.11	0.21	35	20	10	4.7	121	50	43	16	191			
Z16-41 - 57	0.022	0.056	0.38	0.48	0.84	0.98	0.2	0.31	13.9	2.6	4.73	0.81	57.6	7.8	23.4	2.6	112.8			
Z16-41 - 58	0.132	0.076	3	1.8	7.3	2.2	0.3	0.36	43.1	5	15	1.1	154.2	8.2	60	3.3	257.7			
Z16-41 - 59	0.48	0.38	5.3	2.4	5.4	2.1	0.3	0.35	27.3	3.3	9.8	1	107.1	7	41.2	2.9	181.3			
Z16-41 - 60	0.033	0.061	1.63	0.96	1.96	0.86	0	0.17	12.4	3	5.29	0.78	63.7	5	26.3	1.3	119.3			
Z16-42 - 1	0.3	0.11	9.4	1.9	14.5	3.3	2.23	0.57	60.2	5.7	18.8	1.6	185.9	7.5	64.4	3.1	262			
Z16-42 - 2	0.099	0.082	1.29	0.63	4.5	1.6	0.69	0.36	29.2	5	9.87	0.88	111	10	39.5	3.1	178			
Z16-42 - 3	0.041	0.059	1.9	1.4	2.3	1.5	0.55	0.26	14.6	3.2	4.75	0.88	62.1	5.4	24.2	1.6	109.1			
Z16-42 - 4	0.43	0.13	7.8	1.6	11.9	2.4	2.16	0.64	52	5.5	16.7	1.2	171	11	61.3	3.6	259			
Z16-42 - 5	0.099	0.093	2.4	1.4	5.4	2.5	0.33	0.25	28.6	4.4	8.3	1.1	84.3	6.8	31.6	1.6	149.9			
Z16-42 - 6	0.019	0.063	0.23	0.53	2.7	1.4	0.26	0.3	15	3.6	5.03	0.69	65.5	5.7	27.9	1.8	125.7			
Z16-42 - 7	16.6	2.5	79	13	24.4	4.6	2.53	0.63	66.8	4.8	17.6	1.2	177.9	8	61.5	3.4	246			

Z16-42 - 8	0.175	0.063	3.12	0.96	7.1	1.3	0.86	0.45	32.9	5.6	11.7	1.3	124	11	46.6	4	198						
Z16-42 - 9	0.14	0.11	1.26	0.68	3.2	1.2	0.55	0.39	17.3	4	4.72	0.65	62.8	6.4	23.9	2.1	107.5						
Z16-42 - 10	0.039	0.046	0.38	0.42	3.4	1.9	0.39	0.3	13.2	2.3	5.1	0.8	61.9	5.6	20.1	2.4	93						
Z16-42 - 11	0.077	0.073	0.99	0.48	3.39	0.91	0.4	0.26	18.8	3.7	5.9	0.89	67	10	26.4	3.3	115.6						
Z16-42 - 12	0.03	0.05	1.2	0.92	3	1.1	0.55	0.3	16.6	2.8	5.94	0.8	64	4.3	24.1	1.2	110.4						
Z16-42 - 13	1.11	0.35	13	2.9	17.3	2.5	1.14	0.5	81.4	4.3	23.9	1.2	243.1	9.8	86.9	5	371						
Z16-42 - 14	0.09	0.12	0.72	0.67	3.1	1.3	0.13	0.23	21.1	4.2	5.84	0.71	69	6.2	26.4	2.2	120.9						
Z16-42 - 15	0.152	0.078	1.25	0.7	3.2	1.1	0.6	0.31	20.5	1.9	7.15	0.96	74.9	6.6	29	1.1	124.5						
Z16-42 - 16	0.09	0.11	3.6	2.4	7.6	2.7	1.21	0.66	46.5	7	14.4	2.1	150	16	53	4.9	229						
Z16-42 - 17	1.08	0.46	11.6	2	14.3	3.2	1.43	0.54	66.8	5.5	19.6	1.9	211	15	75.3	3.6	300						
Z16-42 - 18	0.041	0.052	1.2	0.94	1.9	1.1	0.44	0.44	11.7	2.3	4.42	0.61	48.9	4.3	18.7	1.5	86.5						
Z16-42 - 19	0.06	0.09	0.25	0.57	1.7	1.2	0.12	0.35	12.9	4.2	4.51	0.84	61.2	7.9	23.9	3.1	120.9						
Z16-42 - 20	0.07	0.066	1.8	1.1	3.9	1.4	0.47	0.19	19.8	3	6.12	0.61	70.7	6	26.3	1.8	110.6						
Z16-42 - 21	0.02	0.048	0.82	0.91	4.1	2.2	0.29	0.38	13.3	4.3	5	1.1	62	14	23.6	4.4	109						
Z16-42 - 22	B.D.	0.034	1.24	0.84	2.09	0.97	0.37	0.29	10.6	2.7	4.48	0.84	50.3	5.1	21.7	1.3	103.2						
Z16-42 - 23	0.035	0.063	3.2	1.5	5.9	1.7	1.17	0.52	27.2	4.6	8.86	0.97	98	11	33.2	3	149						
Z16-42 - 24	0.126	0.083	1.6	0.94	2.7	1.4	0.52	0.5	22.2	4.6	7.12	0.86	88.7	9.5	33.6	1.8	149						
Z16-42 - 25	0.075	0.064	1.74	0.79	3	1.3	0.18	0.22	17.1	4	6.01	0.74	73.9	7.7	27.4	3	122.6						
Z16-42 - 26	0.008	0.041	0.53	0.36	0.44	0.54	0.43	0.26	9.7	1.9	3.67	0.56	48.2	3.1	17.8	1.2	83.5						
Z16-42 - 27	17.1	4.4	94	29	20.5	5.1	1.3	0.63	40	11	7.4	1.5	83.9	9	26.3	2.9	117						
Z16-42 - 28	0.085	0.071	2.05	0.95	4.3	1.6	0.42	0.22	23	3.8	7.6	1.1	79.3	6.8	31.5	2.4	141						
Z16-42 - 29	0.017	0.048	1.16	0.85	3	1.1	0.15	0.16	11.2	2	4.84	0.61	57.7	3.4	22.4	1.5	105						
Z16-42 - 30	0.01	0.039	1.16	0.72	1.09	0.77	0.38	0.24	12.4	2.1	4.06	0.59	56	3.2	21.3	1.5	104.8						
Z16-42 - 31	968	77	5150	390	1330	170	71	10	1400	120	212	19	1219	87	257	17	753						
Z16-42 - 32	0.125	0.097	1.4	1	4.6	1.9	0.56	0.42	28.3	3.5	8.6	1.1	97.6	6	35.5	3	153.1						
Z16-42 - 33	0.24	0.11	3.8	1.3	12.1	3	2.25	0.7	51.4	4.8	16.2	1.9	169.7	9.3	57.3	3.6	250						
Z16-42 - 34	0.066	0.078	0.45	0.57	1.3	1.1	0.22	0.27	11	4	4.25	0.86	47.3	4.8	19.7	2.1	91.9						
Z16-42 - 35	0.32	0.21	5.9	2.9	7.7	2.8	2	1.1	64.8	7.1	19.1	1.6	196	21	67.1	6.3	273						
Z16-42 - 36	0.4	0.11	5.8	1.8	8.4	2	0.42	0.23	42.5	5.8	12.92	0.99	149	8.2	50	2.2	223.3						
Z16-42 - 37	0.336	0.098	6.8	1.5	10.3	2.1	1.28	0.46	53.8	3.3	15.2	1.1	166	5.8	58.7	3	238.5						
Z16-42 - 38	0.23	0.14	4.6	1.2	7	1.3	1.15	0.44	31.5	4.4	10.05	0.86	110.5	6.9	40.5	2	170.2						
Z16-42 - 39	2.7	1.8	14.8	7.9	9.7	3.3	1.59	0.76	33.9	7	8.62	0.86	99.8	9.2	35.3	2.9	146						
Z16-42 - 40	0.4	0.14	7.7	2.7	15.6	2.6	1.72	0.59	61.6	9.5	18.5	2.1	175	14	62.2	4.8	261						

Z16-42 - 41	0.62	0.3	8.6	2.4	12.1	3.3	0.98	0.57	61.3	7.1	16.6	1.2	186	10	64.2	4.2	266						
Z16-42 - 42	0.35	0.2	3.7	2.4	6.2	1.6	1.15	0.62	40.4	6.1	13.2	1.8	134	17	48.7	6	195						
Z16-42 - 43	0.49	0.36	3.2	2.2	2.2	1.1	0.08	0.21	8.6	3.1	4.45	0.72	49.3	6.3	20.9	2.3	99						
Z16-42 - 44	0.32	0.19	6	4.6	15.9	5.6	1.02	0.69	53.5	9.1	16.9	2.2	187	13	68.1	5.1	279						
Z16-42 - 45	0.312	0.098	5.2	1.5	9.2	2.1	1.99	0.63	41	4.5	13.3	0.95	127.7	6.2	46.7	2.7	189.5						
Z16-42 - 46	0.024	0.063	0.25	0.7	2.2	1.6	0.16	0.25	9.2	2.3	3.59	0.49	43.1	5.3	17.7	1.1	84.7						
Z16-42 - 47	0.042	0.05	1.7	1.5	4.4	2.1	1.51	0.91	23.9	5.4	8.1	1.2	83.7	7.4	31.5	3	140						
Z16-42 - 48	0.107	0.079	2.8	1.9	6.1	2.3	0.36	0.34	37.1	7.6	12.2	1.9	121	14	45.4	4	189						
Z16-42 - 49	0.044	0.093	2.9	1.6	3.3	1.7	0.97	0.73	22.8	4.2	6.55	0.98	85.8	8.1	30.8	2.4	127						
Z16-42 - 50	0.13	0.1	3.7	1.9	6.6	2.8	1.54	0.39	36.6	5	11.23	0.99	131	8.4	44	2.7	184						
Z16-42 - 51	0.13	0.14	3.5	1.8	5.3	2	0.48	0.32	34.3	7.9	10.8	1.7	119	12	43.2	3.2	173						
Z16-42 - 52	0.292	0.094	7.2	2	11.3	3.1	1.04	0.36	41.6	4.4	12.33	0.91	124.3	8.1	46.4	2.6	189						
Z16-42 - 53	15.5	7.9	81	41	20	11	0.78	0.37	35	13	8.3	1.6	77	11	28.5	2	121.2						
Z16-42 - 54	0.46	0.47	4.6	2.7	1.6	1.4	0.57	0.37	16.9	3.6	5.02	0.74	59.5	8.3	22.3	2.5	99						
Z16-42 - 55	0.27	0.13	4.6	1.7	9.8	3.1	1.8	0.78	49.6	5.8	15.5	1.4	158.5	9.9	55	3	224						
Z16-42 - 56	58.6	7.1	296	37	78	10	4.4	1.1	122	10	24.4	1.8	215	14	65.8	4.9	251						
Z16-42 - 57	0.216	0.093	3	1.3	7.7	2.2	1.55	0.44	36.8	5.4	11.8	1.2	128	10	44.2	3.5	190						
Z16-42 - 58	0.34	0.15	6.2	2.8	9.3	3.8	1.43	0.73	49.3	9.2	15.3	1.8	155	12	55	4.4	221						
Z16-42 - 59	0.022	0.05	1.1	1.4	2	1.6	0.19	0.22	14.8	3.5	4.84	0.98	59	3.9	23.7	1.5	112.1						
Z16-42 - 60	69	30	280	120	40	16	2.35	0.87	41	12	9.7	1.6	83.7	8.8	29.1	2.1	111.8						
Z16-45 - 1	14.5	1.1	66	7.6	31.1	4.6	4.07	0.43	66.2	5.3	19.6	2	198	14	62.5	3.7	244						
Z16-45 - 2	8.5	6.2	44	32	17	9.7	1.58	0.88	54	16	13	2.1	138	17	48.4	3.4	183						
Z16-45 - 3	0.49	0.29	3.1	1.5	1.8	1.1	0.35	0.22	11.9	2.5	4.64	0.63	63.1	5.4	26.2	1.6	124.8						
Z16-45 - 4	0.068	0.061	3.2	1.2	6.1	3	1.29	0.78	39	5.5	11.2	1.2	110.9	6.2	40.1	2.5	171						
Z16-45 - 5	0.168	0.095	3.6	1.7	8.6	2.4	1.3	0.47	35.6	6.4	11.4	1.2	125	13	43.5	4.2	169						
Z16-45 - 6	0.046	0.06	1.43	0.48	3	1.3	0.56	0.3	19.9	4.3	6.61	0.77	74.7	5.5	26.6	1.3	110.9						
Z16-45 - 7	8	5.1	43	25	18.5	5.3	1.17	0.6	54.1	9.3	16	1.9	162	11	62.6	3.7	242.9						
Z16-45 - 8	27	12	153	94	28.6	7.8	4	1.8	53	12	12	2.5	95	10	32.6	3.1	140						
Z16-45 - 9	0.51	0.21	7.3	2.6	10.4	3.2	1.25	0.5	45	5.7	13.9	2.2	162	18	59.9	3.8	249						
Z16-45 - 10	B.D.	0.061	1.22	0.63	3.3	1.3	0.79	0.44	17.9	2.8	5.66	0.57	64.7	3.8	25.5	1.5	105.3						
Z16-45 - 11	0.032	0.061	1.15	0.78	4.1	1.6	0.25	0.24	19.2	3.2	5.92	0.7	76.8	6.1	26.9	1.3	122.4						
Z16-45 - 12	16.9	6.2	84	31	30	10	1.1	0.39	44.3	9.9	10.8	1.8	105.2	5.7	34.1	1.1	136.7						

Z16-45 - 13	12.5	1.1	64.4	7.7	18.1	3.2	1.41	0.42	24.1	3.9	5.9	0.56	54	4.2	18.7	1.1	83.2						
Z16-45 - 14	100	23	400	110	88	21	12.3	2.5	96	14	18.5	1.7	159.9	7.8	50.8	1.8	194.9						
Z16-45 - 15	1.33	0.28	10.9	2.9	8.6	3.2	1.89	0.77	29	4.7	8.8	1	99.3	7.1	36.9	2.8	164.6						
Z16-45 - 16	0.115	0.081	0.88	0.62	1.42	0.98	0.08	0.17	8.8	1.7	3.77	0.72	47.2	4.3	20.2	1.9	93.5						
Z16-45 - 17	1.83	0.43	10.5	3.1	4.2	1.5	0.47	0.44	15.5	2.4	5.9	1.1	60.9	5.7	24.9	2.4	120						
Z16-45 - 18	0.26	0.11	7.4	1.6	11.5	2.4	1.49	0.64	59	6.9	18.1	1.8	198	16	65.2	4	269						
Z16-45 - 19	1	0.38	7.7	2.2	4.3	1.8	0.6	0.4	10	1.8	4.07	0.62	49	3.7	22.4	1.6	113.9						
Z16-45 - 20	25.7	7.3	131	39	37	11	0.31	0.26	48.4	9.2	9.5	1.5	93	13	32.5	2.6	124.6						
Z16-45 - 21	88	36	470	200	126	46	3.7	1.6	158	47	31.4	6.2	281	40	87	6.2	343						
Z16-45 - 22	20.8	5.3	117	30	56	21	8.9	2.8	80	23	18.7	5.7	158	36	47.3	6.7	173						
Z16-45 - 23	0.053	0.085	0.92	0.79	2.9	1.6	0.27	0.25	15.7	3.9	6.36	0.86	70.7	6.2	25.9	2.9	113.8						
Z16-45 - 24	12.6	1.7	68.7	8	32.6	4.2	3.49	0.99	46.9	2.6	10.7	1.9	104	13	30.2	1.6	120.5						
Z16-45 - 25	0.193	0.091	3.5	1.6	8.1	3.7	1.58	0.69	49.2	5.3	16.6	1.4	177	15	64.8	6	252						
Z16-45 - 26	0.38	0.12	5.3	1.4	10	2.9	1.86	0.67	48.1	6.2	17.1	1.6	173	11	60.2	3.6	244						
Z16-45 - 27	75	28	304	87	69	11	2.01	0.54	70.4	9.4	13.5	1.8	125.2	9.2	40.2	2.6	154						
Z16-45 - 28	B.D.	0.031	0.86	0.59	2.9	1.3	0.22	0.2	17.6	2.2	6.85	0.75	79	4.6	31.9	2	137.2						
Z16-45 - 29	0.77	0.82	3.8	3.9	3.6	1.4	0.66	0.63	17.3	3.4	6.4	0.63	75.8	5.6	29.3	2.2	118.9						
Z16-45 - 30	2.2	1.1	14.1	5.5	11.2	3.5	0.74	0.36	32.1	5.6	9.1	1	92.2	6.9	34.4	1.5	156.1						
Z16-45 - 31	32.8	2.7	183	21	90	11	11.7	1.6	165	16	37.7	4.4	317	37	91.4	9.9	334						
Z16-45 - 32	19.1	4	90	22	20.3	4.4	1.7	0.46	43	5.2	12.3	1	131	9.8	47.1	2.9	192						
Z16-45 - 33	0.079	0.077	1.6	0.77	3.4	1.4	0.97	0.4	21.7	3.1	6.19	0.65	81.4	6.9	28.6	1.6	125.5						
Z16-45 - 34	0.86	0.2	8.7	2.4	8.6	1.8	1.03	0.57	27.1	3.9	9.16	0.85	99	5.3	33.7	1.9	137.8						
Z16-45 - 35	1.81	0.37	18.1	4.4	20.1	2.7	1.66	0.73	67.6	5.6	19.3	1	215.8	9.4	73.7	4.4	286						
Z16-45 - 36	3.04	0.45	17.9	3.4	16.9	3.9	2.02	0.78	60	15	18	4	195	33	65.4	9.8	274						
Z16-45 - 37	B.D.	0.052	B.D.	0.48	1.2	1.4	B.D.	0.074	11.6	2.6	4	0.74	54.1	4.9	19.6	1.7	91.3						
Z16-45 - 38	11.6	8.7	52	36	20.3	9	1.74	0.66	59	11	15.6	1.7	158.3	7.8	56.3	3.9	227						
Z16-45 - 39	0.5	0.15	3.8	1	4.2	1.3	0.12	0.13	18.4	4.3	5.93	0.81	77	11	29.5	3.1	132						
Z16-45 - 40	1141	70	5910	420	1650	140	362	27	1726	91	255	20	1438	94	281	20	703						
Z16-45 - 41	3.1	0.94	21.8	4.6	15.1	5.7	2.5	1	59.3	5.5	14.6	1.8	163	14	49.8	4.4	205.2						
Z16-45 - 42	2.01	0.39	12.6	3.4	10.8	4	1.43	0.7	26.1	4.8	7.5	2.2	81	10	28.7	3.3	113.7						
Z16-45 - 43	0.25	0.21	5.8	2.5	11.5	3.5	0.89	0.56	55.1	6.6	15.8	2.6	184	18	63.4	6	262						
Z16-45 - 44	0.33	0.12	4.9	1.5	9.9	3.9	2.7	1.1	46.7	7	15.5	1.9	152	16	56.6	7.1	221						
Z16-45 - 45	5.1	0.5	36.2	6.2	18.6	4.3	3.4	0.97	42.5	7.5	10.16	0.95	97.1	7.8	32.4	3.2	130						

Z16-45 - 46	14.4	3.4	94	14	48	12	6.6	2.1	96.5	5.9	23.4	2.3	231	24	72.9	7.8	299			
Z16-45 - 47	5.1	2.2	28	11	16.4	6.9	1.27	0.59	21.1	9.1	6.1	1.1	66	11	26	3.3	128.7			
Z16-45 - 48	0.28	0.11	5.4	2.3	9.8	2.7	2.33	0.9	43.5	7.5	12.7	1.3	136	10	51	4.9	197			
Z16-45 - 49	136.8	8.6	797	57	343	20	40.3	3.6	489	35	99.1	6.6	725	31	166.1	7.4	492			
Z16-45 - 50	36.8	7.7	177	35	51	11	2.77	0.85	67	12	13	1.5	112.4	9.2	34.5	2.2	133			
Z16-45 - 51	B.D.	0.038	B.D.	0.26	1.9	1.5	0.03	0.15	11.5	2	4.48	0.68	67.3	6.9	29.5	2.5	140			
Z16-45 - 52	7.91	0.86	53.1	7.9	27.5	5.2	4.16	0.94	45.1	7.8	12.2	1.2	117	10	39.6	5.3	154			
Z16-45 - 53	8.9	3.5	51	18	30.2	9.9	3.9	1.6	86	10	22	2.5	231	16	81.2	5.2	339			
Z16-45 - 54	0.62	0.2	8.6	1.9	15.1	3.6	2.88	0.76	55.3	6.8	18.5	1.4	182.9	9.3	63.5	3.7	243.4			
Z16-45 - 55	10.8	9.4	44	39	18.8	8.9	1.22	0.7	46	11	13.3	1.9	145	15	50.5	4.4	214			
Z16-45 - 56	0.2	0.16	1.5	1.5	1.7	1.2	0.38	0.4	22.7	6.8	6.7	1.1	83	11	33	3	139.2			
Z16-45 - 57	1.43	0.62	7	4.4	11.1	2.9	0.87	0.6	52.9	9.8	16.5	1.3	164.3	7.9	61.5	4.2	249			
Z16-45 - 58	0.051	0.075	1.9	1	4	1.2	0.65	0.42	20.5	3.4	6.92	0.67	82.4	7	30.1	1.9	134.1			
Z16-45 - 59	0.17	0.12	2.8	1.2	8.6	3.4	0.66	0.65	48.3	6.3	14.6	1.6	171.1	9.5	62.5	4.8	260			
Z16-45 - 60	183	11	884	50	239	13	6.2	1.5	261	22	39.2	3.2	267	21	70.5	7.4	236			
Z16-01 - 1	11.3	1.8	58	10	40.6	5	6.1	1.2	99	12	28.2	2.9	280	26	89.2	9.2	348			
Z16-01 - 2	233	12	1257	83	728	50	98.1	8.5	1213	87	337	20	2560	140	609	49	2070			
Z16-01 - 3	29.3	2.7	156	17	112	16	13.1	2.5	204	26	53.8	2.6	476	53	128.7	8.9	485			
Z16-01 - 4	0.18	0.14	3.1	1.5	6.5	1.8	0.22	0.25	39.2	7.2	13.29	0.97	151	8.4	54.4	3.1	235.6			
Z16-01 - 5	0.36	0.17	5.1	2.2	9	3.2	0.57	0.43	48.7	8.1	15	1.2	170	11	61	3	243			
Z16-01 - 6	15.2	1.8	93	11	36.9	6.4	5.3	1.2	79.9	9.3	20.6	2.4	176	15	53.9	3.6	196			
Z16-01 - 7	0.031	0.049	0.73	0.72	0.93	0.65	0.13	0.16	8.7	2.2	3.49	0.5	36.6	2.7	13.4	0.94	66.4			
Z16-01 - 8	1.23	0.77	7.2	3.1	9.7	3.7	0.46	0.32	31.4	4.5	13.3	1.4	166	11	67	3.1	287			
Z16-01 - 9	0.43	0.2	3.8	1.3	7.6	2.5	0.25	0.18	25.8	2.1	7.53	0.47	87.3	5	32.8	1.4	130.3			
Z16-01 - 10	1.91	0.57	11.4	3.1	11.3	3.9	1.69	0.61	35.5	5.2	10.1	1.3	124.4	7.8	44.5	2.4	185.3			
Z16-01 - 11	19.7	1.6	108	11	57.8	6.3	12.4	2	112.4	9.1	27.2	2	257	24	73.9	5.5	274			
Z16-01 - 12	4.4	1.2	24.6	6.5	18.7	4.6	2.93	0.98	43	5.1	13.9	1.4	126	12	40.8	3.5	166			
Z16-01 - 13	0.014	0.038	0.51	0.53	1.37	0.86	0.1	0.14	9.5	2.8	4.12	0.45	48.8	3.2	18.59	0.88	76.3			
Z16-01 - 14	53.5	3.1	292	22	214	23	35.3	3.4	449	36	133.3	9.7	1119	67	295	18	979			
Z16-01 - 15	0.36	0.23	4.3	2.1	7.4	2.6	0.92	0.57	35.6	7.9	10.3	2.1	104	14	39.5	4.9	155			
Z16-01 - 16	7.8	1.1	46.2	8.6	26.2	4.6	4.8	1.2	78.2	9.4	22	2	197	11	62.7	3.5	231.4			
Z16-01 - 17	2.84	0.36	20.2	3.4	13.5	2.3	2.27	0.72	43.5	5.4	13.74	0.98	132.4	8.6	46.4	3.7	184			

Z16-01 - 18	1.47	0.51	12.3	4.9	8.9	2.2	1.18	0.54	31.7	4.3	10.37	0.69	114.1	7.6	40.9	1.9	168.3							
Z16-01 - 19	144	23	526	92	114	24	8.7	2.2	76	17	12	1.4	95	11	26.1	1.7	103.2							
Z16-01 - 20	0.091	0.06	1.09	0.66	2.6	1	0.2	0.21	11	1.4	3.76	0.5	42	4.3	17.7	0.83	73.5							
Z16-01 - 21	4.4	3.8	36	33	10.7	8.9	1.89	0.62	31	11	7.6	2	75	17	25.2	4	103							
Z16-01 - 22	0.16	0.12	1.2	1.1	2.8	1.9	0.37	0.23	18.8	3.7	6.34	0.91	81.8	4.8	33	1.7	158.1							
Z16-01 - 23	0.21	0.083	3.1	1.1	4.4	1.3	0.77	0.38	22.6	3.1	7.41	0.88	75.3	5.9	28	1.4	117.9							
Z16-01 - 24	0.129	0.063	1.7	1	1.6	1.1	0.19	0.19	18.7	2.9	6.4	0.78	70	5.4	25.4	1.5	113.3							
Z16-01 - 25	1.66	0.84	10	4.4	8.2	2.7	1.07	0.59	25.9	4.3	9	1.5	94.9	8.9	32.7	2.1	143.3							
Z16-01 - 26	0.71	0.17	9.4	1.7	12.8	2.1	1.93	0.54	54.2	4.3	15.5	1.3	152.7	8.4	52.4	3.1	202.7							
Z16-01 - 27	0.157	0.092	1.3	0.67	2.01	0.77	0.26	0.22	17.1	2.7	5.9	0.73	58.6	4.1	23.5	1.2	104.9							
Z16-01 - 28	1.81	0.7	11.8	4.6	5.4	1.9	0.52	0.25	23.4	3.4	7.06	0.59	83.9	5.7	31.3	1.8	132.8							
Z16-01 - 29	1.5	0.78	9.5	3.9	8.3	2.7	0.8	0.36	30.7	4.2	9.77	0.99	114.1	7.6	40.3	2.3	165.6							
Z16-01 - 30	3.48	0.47	24.6	4.6	18.8	4.2	3.6	1.1	50	6.9	13.24	0.81	129.3	9.5	41.7	1.9	170.8							
Z16-01 - 31	0.65	0.18	6.7	2.2	6.5	2	0.6	0.39	25.9	3.8	8.56	0.9	90	6.3	34.2	1.9	140.4							
Z16-01 - 32	0.83	0.21	4.6	2	6.2	2.5	0.49	0.44	16.9	4.9	6.37	0.88	71.1	8.7	24.9	2.8	107							
Z16-01 - 33	5.1	2.3	27.9	8.8	15	3.2	2.47	0.85	62	11	16.1	1.6	157	17	53.8	2.9	211							
Z16-01 - 34	1.03	0.22	5.2	1.2	3.8	1.5	0.35	0.26	15.3	3.4	5.41	0.64	67.1	4.2	25.2	1.8	107.3							
Z16-01 - 35	3.56	0.52	23	4.4	14	2.6	2.58	0.69	45.2	4.9	11.42	0.88	134.4	6.9	48	3	205							
Z16-01 - 36	2	1.1	15.5	5.3	10.8	2.4	1.4	0.79	44	13	15.1	2.6	145	11	50.4	4.4	210							
Z16-01 - 37	2.8	1.4	14.8	7.8	5.6	2.1	0.28	0.29	18.8	3.5	6.24	0.89	67.5	5.3	25.9	1.4	122.9							
Z16-01 - 38	0.78	0.32	11.5	2.3	15.5	3.3	0.56	0.37	76.1	6.9	20.3	1.4	231	12	80.6	2.3	326							
Z16-01 - 39	1.89	0.53	9.3	3.1	5.8	1.7	0.28	0.26	16.9	2.5	6.25	0.62	75	4.2	29.6	1.1	126.4							
Z16-01 - 40	1.51	0.21	11	2	9	1.9	1.02	0.4	31.7	4.9	10	1	116	7.3	40.1	2.1	178.6							
Z16-01 - 41	8.5	2.8	40	13	16.4	4.1	0.47	0.39	31.9	6	10.1	1.9	91.1	7	33	2.4	140.1							
Z16-01 - 42	1.1	0.22	9.6	2.3	8.6	2.1	1.57	0.54	40.4	5.9	12.3	1.3	130.5	6.4	44.2	2.1	179.5							
Z16-01 - 43	38.1	3	278	24	152	18	6.4	1.5	238	19	48.8	4.3	370	22	101.1	3.8	353							
Z16-01 - 44	0.136	0.088	2.1	0.9	5	1.5	0.49	0.41	37.1	4	12.28	0.97	138.4	7.2	51.9	3.2	206.8							
Z16-01 - 45	0.049	0.07	0.4	0.84	2.3	1.5	0.17	0.37	6.9	2	2.85	0.4	29.3	2.5	12.3	1	56.9							
Z16-01 - 46	13.6	1.1	79.5	8.8	51	10	18.3	2.3	96	12	20.4	2.4	196	16	57	4.5	194.9							
Z16-01 - 47	0.23	0.1	5.8	2.2	9.5	2.5	1.61	0.32	44.2	4.7	12.39	0.85	136.5	7.7	47.3	2.5	185.1							
Z16-01 - 48	0.095	0.072	0.71	0.49	0.81	0.77	0.12	0.18	11.7	1.9	4.1	0.56	55.4	3.4	24.1	1.3	107.7							
Z16-01 - 49	0.043	0.075	0.89	0.87	3.2	1.5	0.25	0.22	17.6	3.1	6	1.1	69.7	5.2	30	1.6	135.8							
Z16-01 - 50	29	3.7	168	24	104	15	13.3	1.2	220	28	54.9	8.4	516	61	121	10	447							

Z16-01 - 51	9.6	1.1	96.3	8.5	91	8.8	1.7	300	25	73.1	3.4	697	32	225	12	810							
Z16-01 - 52	0.18	0.12	2.9	1.9	3.7	1.7	0.29	20.4	3.9	6.27	0.75	73.9	7.8	26.7	2.9	107.6							
Z16-01 - 53	0.013	0.046	1	1.1	3.5	2.1	0.41	15.3	4.5	5.14	0.75	64.1	6.3	23	1.4	109.4							
Z16-01 - 54	0.104	0.083	0.71	0.81	2.1	1	0.19	13.2	2.8	5.18	0.7	63.4	6.4	24.1	2.1	102.2							
Z16-01 - 55	3.13	0.36	23.7	4.8	15.1	3	0.88	54.2	6.1	13.9	1.1	155.1	8	47.9	2.9	203							
Z16-01 - 56	0.059	0.09	1.37	0.81	3.6	1.6	0.3	15.8	4.7	5.66	0.62	72.4	4.6	28.3	2.2	115.8							
Z16-01 - 57	0.22	0.13	3.8	2	6.9	2.2	0.53	29.8	7	8.8	1.6	94.6	5.4	32.7	2.5	142							
Z16-01 - 58	6.57	0.78	33.1	4.5	28.6	5.5	0.93	69.1	9.4	21.1	2.1	205	12	58.4	3.2	237							
Z16-01 - 59	0.62	0.26	5.6	1.9	4	2.6	0.49	21	4	6.5	1.4	65.7	8	22.7	2.1	93							
Z16-01 - 60	1.87	0.31	16.9	3.2	12.1	2.6	0.68	46.4	8.4	13.9	1.5	143	15	46.4	4.3	187							
Z16-01 - 61	10.9	1.7	64.7	8.5	41.2	6.5	1.4	131	20	34.2	1.9	368	22	116.8	3.7	445							
Z16-01 - 62	0.55	0.37	5.5	2.3	5.3	2.9	0.57	15.4	5.4	5.08	0.97	45	6.7	18.5	2.6	80.1							
Z16-01 - 63	0.06	0.071	1.09	0.73	1.9	1.2	0.21	11.3	2.2	4.16	0.52	48.8	4.1	17.1	1	77.3							
Z16-01 - 64	1.9	1.2	13.6	7.5	14.8	4.6	0.72	70.9	5.2	26.7	3.3	309	29	118	14	517							
Z16-01 - 65	3.62	0.3	22.6	4.9	16.2	6.3	1.3	52.3	8.4	12.5	1.6	117	5.9	37.6	2.6	157.2							
Z16-33 - 1	106	30	610	170	350	100	21	470	140	91	27	690	210	146	40	440							
Z16-33 - 2	30.8	9	188	75	107	34	7.1	127	38	27.2	7.2	189	48	44	11	153							
Z16-33 - 3	25	4.8	136	26	80	12	5	113	19	24.9	3.8	183	20	52.1	5.6	192							
Z16-33 - 4	54.3	5.2	267	30	156	21	5.1	182	19	36.3	4.8	272	32	60.3	4.9	192.9							
Z16-33 - 5	75	12	392	60	171	26	5.7	227	23	47	9.8	284	36	62.5	7.9	206							
Z16-33 - 6	9.6	2	71	15	31.6	8.4	1.7	45	13	9.1	1.8	67	11	18.7	3.4	76.1							
Z16-33 - 7	0.61	0.39	3.1	1.5	1.5	1.2	0.24	3.9	2	0.64	0.28	10.8	4.1	3.69	0.74	20.3							
Z16-33 - 8	7.5	4.4	42	28	27	13	1.7	27	14	7.5	4.3	58	34	15.1	6.4	68							
Z16-33 - 9	146.2	8.1	724	39	431	31	5.3	498	34	104.1	9.8	678	37	143	11	429							
Z16-33 - 10	169	20	890	140	550	190	17	615	95	126	14	860	100	191	16	690							
Z16-33 - 11	18.3	2.1	98	16	53.7	8.2	4.2	75	13	16.8	2.8	101	23	24.5	5.2	84							
Z16-33 - 12	219	19	1306	86	751	66	27	840	41	182	23	1450	270	273	22	844							
Z16-33 - 13	1.46	0.85	9.7	3.2	7.3	7.5	1.1	13.7	5.4	4	1.3	33.3	8.7	12.8	2.3	53							
Z16-33 - 14	19.3	2.4	144	14	49.2	6.8	2	63	11	11	2.2	78	14	20.1	3.3	73							
Z16-33 - 15	407	15	2166	94	1282	63	13	1739	72	340	21	2290	110	492	28	1509							
Z16-33 - 16	179	37	1030	230	440	110	23	520	110	87	17	630	120	173	26	641							
Z16-33 - 17	120	11	602	50	287	23	6.7	323	25	62.5	3.9	436	25	96.9	6.2	318							

Z16-33 - 18	45.4	9.3	272	57	117	35	30.9	7.8	179	32	31.4	7	252	67	53.7	9.1	195						
Z16-33 - 19	139	14	634	76	190	26	45.8	6.9	193	24	27.5	3.3	168	16	40.8	3.5	130						
Z16-33 - 20	21.3	1.5	141	11	52.2	5.4	15.1	1.4	82	7.4	14.6	1.1	108	12	26.5	2.4	103.3						
Z16-33 - 21	5.4	2.3	29	12	17.8	8.4	4	2.6	18.1	8.7	4.8	1.9	37	14	8.2	2	39						
Z16-33 - 22	0.22	0.12	1.7	1.2	1.8	1.2	0.43	0.29	7.5	2.2	2.65	0.34	33.8	3.7	13.62	0.87	64.5						
Z16-33 - 23	125	12	716	82	154	30	127	15	151	17	19.3	3.5	150	14	54.2	4.9	258						
Z16-33 - 24	14.9	1.2	119	12	66	15	19.7	2.3	160.6	7.8	34.6	2.3	308	20	90.7	7.5	347						
Z16-33 - 25	36.6	3.4	180	21	82	12	17.2	2.7	93	12	19.8	2.2	132	13	30.7	2.8	107.1						
Z16-33 - 26	513	18	2240	180	819	83	180	23	840	160	177	19	1130	120	210	13	760						
Z16-33 - 27	0.003	0.042	0.13	0.63	1.2	1.4	0.23	0.36	4.4	1.3	1.98	0.51	25.1	4.2	11.2	1.5	54.8						
Z16-33 - 28	3.13	0.85	22.5	5.1	23.7	4.4	7.8	1.7	104.4	9.9	22.6	1.7	219	16	70.4	3.9	285						
Z16-33 - 29	18.9	3.1	113	15	59.4	6.8	12.8	2.7	79.9	8.4	15.2	1.1	128	12	35.2	3.3	138.2						
Z16-33 - 30	119.2	5.7	713	54	396	31	93.6	7.5	511	40	111.4	4.2	759	34	162	13	547						
Z16-33 - 31	31.8	1.5	162.7	9.5	103	13	27.7	4.2	153	13	30.5	3	236	13	59.9	5.7	208						
Z16-33 - 32	30.5	4	191	21	101	11	24.6	2.8	126	17	22.5	2.9	193	29	39.6	2.4	127						
Z16-33 - 33	332	26	1720	130	914	75	214	14	1082	78	208	16	1390	120	298	17	923						
Z16-33 - 34	4.9	2.2	22	10	14.3	5.4	5.4	1.9	18	7.8	5.3	1.7	44	14	14.3	2.3	75						
Z16-33 - 35	0.65	0.31	5.5	3.1	3.2	2.1	0.16	0.22	4.5	2.4	1.27	0.46	11.4	3.3	4.1	0.93	23.1						
Z16-50 - 1	51.5	5	261	33	128	11	31.4	4.3	169.1	8.8	35.6	4.5	306	27	88.5	5.4	411						
Z16-50 - 2	0.098	0.089	0.84	0.6	0.13	0.42	0.24	0.18	2.33	0.79	0.65	0.22	5.9	1.2	2.45	0.38	11.6						
Z16-50 - 3	10.8	1.5	75	10	40.9	8.9	10.2	2.6	45	11	10.4	2.4	81	19	23.5	2.8	94						
Z16-50 - 4	157	14	892	83	392	50	98	11	500	57	118	14	840	100	206	19	768						
Z16-50 - 5	24	11	146	60	72	25	22.6	9.5	115	37	26.2	7.8	210	59	58	11	229						
Z16-50 - 6	15.4	4.8	82	27	49	17	12.4	4.3	65	17	13	3.5	113	21	33.7	5.7	133						
Z16-50 - 7	8.6	5.1	47	28	34	10	7.4	2.1	82	43	13.6	2.4	148	35	46.3	9.5	224						
Z16-50 - 8	17.7	9.3	60	16	34	5.5	10.1	1.9	63.9	9.6	17.6	1.8	147	17	46.9	3.2	195						
Z16-50 - 9	1.21	0.21	5.5	2.9	5.2	3.6	1.19	0.59	8.2	4	2.46	0.47	25.6	3.8	10.1	1.7	67.7						
Z16-50 - 10	16.3	5.5	100	34	58	20	14.2	5.3	72	22	17.7	4.8	143	42	35.8	7	149						
Z16-50 - 11	129.7	9.3	768	91	422	83	96	10	459	47	105	15	738	87	167	21	569						
Z16-50 - 12	19.3	2	117	12	62.9	8.5	16.9	2.8	99	15	21.6	2.8	175	20	51.1	6	197						
Z16-50 - 13	2.09	0.36	11.4	3.3	9.2	3.6	2.27	0.69	20.1	3.1	6.2	1.1	57.2	6	19.7	1.4	87.3						
Z16-50 - 14	3.7	1.6	19.6	8.3	7.6	3	2.91	0.76	17.9	6.3	3.95	0.98	39.1	5.5	12	1.3	60.5						

Z16-50 - 15	8	1.1	45.7	5.5	25.5	4.2	6.24	0.78	41.1	5.6	9	1	77	5	22	1.8	95.9						
Z16-50 - 16	303	38	1640	200	769	98	164	19	836	96	175	21	1120	110	255	27	867						
Z16-50 - 17	470	130	2340	570	1010	310	235	60	1220	280	237	52	1740	390	379	93	1370						
Z16-50 - 18	3.38	0.57	17.4	4.2	10.8	3.3	2.48	0.63	16.3	3.5	4	1.5	44	12	10.6	1.7	42.2						
Z16-50 - 19	5.2	1.3	28.5	8.1	17	5.1	3.7	1.8	25.4	6.5	6.5	2.1	50	12	18.3	3.2	79						
Z16-50 - 20	800	49	4070	190	1682	64	437	21	2004	88	361	15	2400	180	494	27	1590						
Z16-50 - 21	107	21	508	64	242	33	54.8	8.3	328	61	66	12	468	38	120.7	6	468						
Z16-50 - 22	104	32	540	140	285	79	65	19	340	110	61	15	420	110	104	27	400						
Z16-50 - 23	21	6.7	108	32	46	14	13.5	3.7	96	24	20	3.9	199	35	55.9	7.5	245						
Z16-50 - 24	39.1	3	210	24	98	11	29	3	155	14	42.6	2.6	385	29	111.3	7.6	488						
Z16-50 - 25	1.7	0.74	13.1	5.1	11.2	4.8	3	1.5	26.9	8.7	6.5	1.9	65	11	23.3	2.8	93						
Z16-50 - 26	6.6	2.1	42	13	20.7	6.8	5.6	2.1	34	11	8.5	1.6	72	18	21.9	3.2	100						
Z16-50 - 27	3.99	0.48	20.8	5	11.4	2.9	4	1.2	21.1	6.8	5.4	1.6	30.4	5	8.6	1.6	29.1						
Z16-50 - 28	87.7	4.9	492	33	213	19	53.2	5.6	290	27	63.9	6.4	527	57	147	14	579						
Z16-50 - 29	11.77	0.92	75	10	41.1	2.9	10.2	1.5	60	5.9	13.5	1.4	96.7	7.9	27.9	4.2	108.2						
Z16-50 - 30	5.76	0.74	35	6.5	20.4	4.9	5.3	1.1	31.1	6.3	7.9	1.2	61.8	5.9	18.2	1.3	81						
Z16-50 - 31	25.3	3.2	149	13	93	15	22.4	2.2	131	16	27.1	1.2	202	14	51.9	2.8	220						
Z16-50 - 32	2.61	0.41	15.7	3.7	7.7	2.6	2.06	0.68	13.9	3.8	4.61	0.59	43.6	4.8	15.3	1.3	84						
Z16-50 - 33	1.44	0.35	6.7	1.9	4.3	1.6	1.29	0.5	8.6	1.5	2.62	0.43	30.6	4.1	10.7	1.2	56.4						
Z16-50 - 34	0.2	0.16	1.4	1	1.3	1.1	0.38	0.19	8.8	2.9	2.83	0.76	41.1	3.4	17.8	2.1	107.2						
Z16-50 - 35	136	12	731	51	306	38	78.7	8.2	396	32	73.2	4	473	33	101.6	4.6	383						
Z16-50 - 36	10	2	57	16	31.9	7.7	7.1	2.4	45	11	11.1	1.5	95	15	27.4	2.4	124						
Z16-50 - 37	69.5	8.8	397	70	180	23	43.3	6.4	206	29	39.1	4.9	277	29	64.3	5.9	264						
Z16-50 - 38	307	79	1960	500	1100	610	218	52	1060	250	202	39	2.50E+03	2.30E+03	317	74	1080						
Z16-50 - 39	80.2	6.4	406	38	199	29	45.9	5.9	260	22	49.4	4.6	374	42	86.1	4.9	352						
Z16-50 - 40	52.4	7.9	247	29	128	28	30.7	6.4	143	19	30.3	4.9	214	33	45.2	5.5	173						
Z16-50 - 41	81.5	8.2	426	37	187	17	51.4	4.3	260	23	56.5	5.1	444	26	118.1	8.7	455						
Z16-50 - 42	12.4	0.93	90.1	6.9	33.4	5.4	6.9	1.4	43.6	7	10.3	1.1	76.5	5.9	21.3	3.1	86						
Z16-50 - 43	316	29	1670	100	687	65	195	20	810	89	154	14	1000	110	192	10	694						
Z16-50 - 44	61.2	9.2	319	67	163	32	44.8	9.7	231	45	42	6.5	305	56	75	15	259						
Z16-50 - 45	3.38	0.56	18.9	3.1	12.2	2.9	2.6	0.77	22.6	3.8	5.04	0.71	43.2	5.2	13.5	1.3	68.6						
Z16-50 - 46	5.2	3.4	28	18	15.4	6.5	4.8	2.9	36.4	6.9	10.1	1.4	108.3	8.8	39.2	3.9	181						
Z16-50 - 47	11.8	2	61.4	7.9	34	6.9	9	1.6	46.3	8.9	10.7	2.1	98	13	25.4	2.5	121						

Z16-50 - 48	20.6	6	105	29	38.5	9.4	8.3	2.4	49	13	9.7	2.4	74	12	24.6	3.6	108.8					
Z16-50 - 49	1.93	0.52	12.7	2.9	5.9	2.7	1.19	0.34	11.2	2.9	2.14	0.43	21.4	3	8.24	0.77	33.9					
Z16-50 - 50	216	35	1080	170	570	130	118	21	610	110	117	16	742	89	158	21	565					
Z16-50 - 51	61.4	7.2	338	37	151	23	41	5.4	228	17	49.3	4.2	397	35	109.3	8.9	411					
Z16-50 - 52	2.3	1.4	14.2	4.9	12.8	7.1	2.66	0.89	39.4	8.8	11.8	2.3	134	21	49.6	6.7	257					
Z16-50 - 53	99	42	530	190	226	83	62	24	290	100	63	18	410	130	101	26	396					
Z16-50 - 54	45.5	9.7	233	53	115	32	29.8	4	155	28	40	12	296	48	77.1	6.1	355					
Z16-50 - 55	36.7	4.5	183	19	95	12	20.4	2.2	127	14	27.2	2.4	224	15	62.1	3.2	250					
Z16-50 - 56	67	18	324	81	161	39	39.1	9.8	195	46	40.8	9	263	46	57.4	9.2	218					
Z16-50 - 57	309	40	1540	210	750	100	171	22	850	110	164	19	1020	130	214	28	772					
Z16-50 - 58	2.07	0.65	8.4	3.6	6.4	2	1.07	0.55	14	3.9	3.18	0.72	32.6	6	14.9	1.6	83.1					
Z16-50 - 59	0.285	0.089	1.7	0.83	1.2	0.64	0.39	0.36	4.4	1.6	1.97	0.48	25	2.9	9.95	0.75	46					
Z16-50 - 60	0.035	0.052	0.27	0.58	0.01	0.29	0.28	0.25	2	1.1	1.47	0.5	23.1	2.5	11	0.93	67					
Z16-50 - 61	172	32	970	210	393	88	89	17	466	94	91	13	620	110	154	23	513					
Z16-50 - 62	12	2.3	64	14	33.5	7.6	6.9	2.2	37.5	7.3	10.7	2	76	12	21.9	3.1	102					
Z16-52 - 1	6.02	0.8	31.7	5.7	17.6	3.9	6.5	1.4	37.4	3.4	13.7	1.2	139	10	42.2	2.3	191.1					
Z16-52 - 2	38.7	3.9	199	17	112	21	37.5	4.7	209	30	54.7	6.5	433	54	111	12	413					
Z16-52 - 3	221	29	1150	170	700	73	204	23	1140	130	283	38	2050	320	425	47	1250					
Z16-52 - 4	62.3	5.7	339	40	183	20	58.8	6.1	314	42	72.8	7.9	514	43	134	15	503					
Z16-52 - 5	100.9	4.6	553	39	306	22	69.4	9.4	512	51	118.3	9.9	835	55	169	11	543					
Z16-52 - 6	16.5	1.3	89	12	47.5	8.3	12.1	2	88.8	7.1	28.2	3.9	217	19	57	2.6	219					
Z16-52 - 7	41.1	5	178	30	131	33	31.6	8.9	221	41	50.7	7.2	480	170	105	11	392					
Z16-52 - 8	4.92	0.75	21.7	2.8	12.8	2.7	2.9	1.6	31.4	6.5	11.3	1.5	120.5	9.4	41.6	3.5	216					
Z16-52 - 9	94.1	6	453	53	221	21	85.3	8.7	412	64	86.4	4.8	585	40	123.2	6.8	398					
Z16-52 - 10	23.9	5.8	128	34	69	15	16.3	5.3	120	31	36.2	9.4	290	50	69.2	7	262					
Z16-52 - 11	48	5.1	249	23	120	16	49.9	4.6	233	25	59.3	4.5	442	33	103.4	5.7	350					
Z16-52 - 12	299	35	1490	140	970	150	261	24	1460	120	362	28	2640	230	547	27	1698					
Z16-52 - 13	136	11	742	79	446	52	117	15	690	120	162	24	1120	150	278	51	751					
Z16-52 - 14	71.8	6.1	369	30	239	30	64.1	9.4	464	33	120	16	855	85	191	17	571					
Z16-52 - 15	103.8	5.3	511	42	313	37	75.8	6.2	495	37	112.4	6.5	798	39	164	10	533					
Z16-52 - 16	13.2	1.6	64	16	55	23	10.4	3.9	78	15	21.9	2.2	230	17	83.1	4.5	401					
Z16-52 - 17	47.5	5	286	35	168	26	45.4	2.8	309	38	89	10	703	74	175	13	667					

Z16-52 - 18	74	24	390	130	252	89	100	30	540	160	139	45	1120	330	248	74	780			
Z16-52 - 19	10.1	4.2	40	11	24.7	9.9	6.6	3.3	50	17	15.6	3.8	158	34	56.6	6.2	325			
Z16-52 - 20	112	15	581	75	297	29	78.4	8.9	522	47	107.4	8.8	842	72	193.1	8.7	617			
Z16-52 - 21	172	25	860	140	476	77	119	19	790	120	182	24	1230	120	279	29	914			
Z16-52 - 22	273	40	1500	220	870	120	224	38	1350	240	309	55	2140	320	432	72	1260			
Z16-52 - 23	300	25	1600	200	920	110	250	20	1435	82	328	27	2190	130	460	47	1335			
Z16-52 - 24	144	17	755	97	465	72	185	29	850	110	244	27	1900	210	450	43	1460			
Z16-52 - 25	119	14	614	70	403	54	110	15	667	56	181	29	1330	150	286	27	990			
Z16-52 - 26	275	22	1490	140	823	72	260	31	1444	91	348	48	2280	300	496	63	1490			
Z16-52 - 27	6.6	1.5	38	10	30.3	6.9	7.1	1.8	64	16	22	3.8	194	31	58.2	6.4	246			
Z16-52 - 28	315	38	1810	250	1010	150	324	40	1740	210	415	53	3260	360	804	99	2710			
Z16-52 - 29	559	31	2940	210	1800	120	519	43	2950	210	705	54	5040	350	1032	83	3140			
Z16-03 - 1	0.153	0.074	4.8	1.2	8.8	2.3	1.15	0.5	35.9	6.2	11.4	1.1	119.1	8.3	44.7	2.7	189			
Z16-03 - 2	0.09	0.11	0.07	0.35	1.01	0.99	0.37	0.44	4.7	2	2.16	0.44	27	2.3	10.81	0.76	56.2			
Z16-03 - 3	12.1	1.7	53.9	5.5	17.8	4.5	0.73	0.53	32.4	5	8.36	0.86	91.5	7.1	33.1	1.8	146			
Z16-03 - 4	2.54	0.41	24.3	4.1	19.3	3.7	2.56	0.94	57.9	5.9	16.06	0.99	161.7	6.2	50.5	1.9	195.8			
Z16-03 - 5	2.74	0.48	13.4	2.8	10.7	2.8	1.79	0.3	32.1	5.2	8.8	1	89.5	6.9	31	2.4	140.6			
Z16-03 - 6	0.75	0.23	3.9	1.6	4.3	1.1	0.83	0.35	14	2.7	4.64	0.63	52.6	3.2	18.7	1.3	86			
Z16-03 - 7	0.82	0.26	8.1	2.5	6	1.9	1.84	0.41	28.8	4.9	7.4	1.1	83	8.3	29.5	2	127.5			
Z16-03 - 8	1.31	0.42	9.1	1.6	6.7	3.3	0.71	0.39	26.8	5.7	8.6	1.2	97	11	38.5	2.8	172			
Z16-03 - 9	1.91	0.46	11.8	2.5	8.7	3.8	1.1	0.54	26.6	4	10.8	1.1	104.1	7.4	37	2.2	168.1			
Z16-03 - 10	12.2	3.4	52	11	24.1	8.5	6.7	1.7	67.8	7.2	19.8	3.3	179	20	63.1	5.1	266			
Z16-03 - 11	B.D.	0.052	0.86	0.84	2.9	1.2	0.11	0.2	19.2	2.7	7.3	0.53	90.4	8	32.1	2.8	139			
Z16-03 - 12	0.48	0.41	2.3	2.3	3	1.4	0.49	0.74	19.2	8.8	7.4	1.2	100	12	39.1	2.7	190			
Z16-03 - 13	0.44	0.28	2.2	1.2	2.5	1.9	0.47	0.37	16.8	3.9	5.03	0.77	60.8	6	20.2	2.3	103.3			
Z16-03 - 14	0.113	0.058	1.01	0.75	3.4	1.4	0.34	0.33	20.7	4.7	7	1.2	81.1	8.6	30	3.3	133			
Z16-03 - 15	1.18	0.33	10.8	3.3	8	1.8	2	0.83	35.5	4.9	10.44	0.69	120.4	7.9	43.4	1.9	195.7			
Z16-03 - 16	5.88	0.53	36.4	6	20.1	3.7	7.3	1.3	60.9	7.5	16.4	1.7	157	11	50.7	3.4	196.9			
Z16-03 - 17	0.7	0.35	2.8	1.8	6.8	4.4	2.9	1	26.8	6.2	7.6	1.5	81.3	9.7	29.6	2.7	128.8			
Z16-03 - 18	6.32	0.78	45.3	5.8	41.9	7.3	4.7	1.5	143	14	43.3	1.9	493	25	167.3	9.8	675			
Z16-03 - 19	28	3.3	120	15	47.7	8.2	15.8	2.2	109	16	24.3	2.7	205	19	67.4	3.4	287			

Z16-17 - 1	no value	NAN	no value	NAN	no value	NAN	no value	NAN	no value	NAN	no value	NAN	no value	NAN	no value	NAN	no value
Z16-17 - 2	1.13E+05	1.10E+04	1.49E+06	1.50E+05	2.74E+06	2.60E+05	7.05E+05	7.40E+04	1.59E+07	1.60E+06	5.54E+06	5.70E+05	5.07E+07	5.60E+06	1.33E+07	1.50E+06	4.01E+07
Z16-17 - 3	28.5	3.2	128	16	68	14	22.7	5.6	139	18	34.2	3.5	298	22	92	7.3	381
Z16-17 - 4	343	20	1850	150	824	31	272	20	1570	110	333	15	2250	110	518	28	1454
Z16-17 - 5	17.2	1.4	81.1	6.4	25.7	4.9	7.9	2	56.3	6	12.7	1.7	102	5.9	25.6	3.2	110.1
Z16-26 - 1	9.08	0.71	33.5	4	11.9	3.2	4.3	1.2	28.3	3.5	6.61	0.8	71	8.1	25	1.6	115.9
Z16-26 - 2	14.7	1.6	80	17	31.3	7.4	9.9	2.3	61.3	6.8	20.2	2.4	200.4	9.8	65.9	3.2	282
Z16-26 - 3	0.39	0.19	5.1	2	5.8	2.9	0.73	0.51	30.1	7.4	8.8	1.6	113	14	40.9	6.4	187
Z16-26 - 4	12.5	2.6	78	25	28.1	6.7	15.4	3.2	116	16	25.5	2.7	140.2	9.2	29.4	3.6	111
Z16-26 - 5	2.34	0.36	12	2.3	5.2	2.1	1.5	0.72	23.3	3	9	1.2	107.8	6.1	42.1	2.6	194.7
Z16-26 - 6	6.3	1	31.7	3.7	10.7	3.3	4.8	1.3	27.5	5	7.7	1.5	97	11	34.4	2.7	144
Z16-26 - 7	14.3	5.7	73	37	24	9.2	8.4	4.3	76	15	17.3	3.8	161	33	44.1	5.9	163
Z16-26 - 8	0.251	0.092	4.3	1.1	11.3	2.5	1.15	0.35	78.7	6.9	25	1	220	11	45.9	3.3	105
Z16-26 - 9	1.44	0.2	8.7	2.8	8.1	1.9	1.16	0.58	43.3	4.3	14.8	1.7	180	11	67.2	3.2	306
Z16-26 - 10	0.19	0.097	4.8	2.2	7.8	2.3	0.81	0.54	48.2	6.5	15.8	1.6	189	13	73	2.7	318
Z16-26 - 11	8.2	1.1	35.8	4.2	12.5	2.6	5	1.5	24	3.5	8.2	1.1	83.1	6.6	28.8	1.7	125.7
Z16-26 - 12	2.15	0.26	11.8	3.9	8	2.6	2	0.78	59.7	6.4	24.5	2.9	396	31	195	14	1008
Z16-26 - 13	0.017	0.051	0.55	0.61	2	1.3	0.02	0.13	8.5	1.4	3.58	0.51	50.6	4.2	17.9	1.4	93.1
Z16-26 - 14	0.74	0.22	4.4	1.3	4.6	1.7	0.5	0.35	18.6	3	6.03	0.69	74.8	5.8	29.1	1.7	134.8
Z16-26 - 15	14	1.3	72.5	8.6	21.4	4.8	14.5	1.9	59.7	9.8	16.5	2.3	170	13	50.1	2.4	214.7
Z16-26 - 16	0.18	0.13	2.4	1.4	4.6	1.4	1.43	0.4	24.1	2.4	7.12	0.97	78.7	4.1	28.2	1.9	128.6
Z16-26 - 17	16.3	1.3	80.3	9.2	15	2.8	9.2	1.4	32.9	3.9	5.92	0.66	67	6.2	28.7	1.7	151.4
Z16-26 - 18	2.53	0.43	18.3	4.4	15.9	4.2	2.42	0.99	73	11	21.4	1.4	242	20	89.4	7.7	406
Z16-26 - 19	4.3	1.5	18	5.7	9	1.9	1.84	0.82	29.7	5.1	10.8	1.4	119.7	9.8	45	2.6	215
Z16-26 - 20	1.1	0.24	7	2	8.1	2.2	0.59	0.34	44.7	3.9	16.7	1.1	186.8	9.2	73.8	3.3	331
Z16-26 - 21	9.4	1.5	45.3	8	15.3	3.8	4	1.1	25.9	7	7.7	1.3	67	12	26.8	3.4	122.5
Z16-26 - 22	36	4.3	198	26	88	18	63	14	206	36	48.9	4.8	430	46	126	15	503
Z16-26 - 23	122	74	500	290	104	47	12.9	5.3	88	31	16.2	4.1	111	21	28.6	2.5	108
Z16-27 - 1	47.3	8.7	216	39	43.2	8.5	7.9	1.5	80	14	20.8	3.2	230	21	88.8	4.8	446
Z16-27 - 2	12.6	1.3	68	10	32.9	5.2	5.8	1.2	114	12	37.7	3.2	425	14	155.1	4.8	666
Z16-27 - 3	1.26	0.37	10.5	4.3	13.6	4.3	2.6	1.6	68	11	23.1	2.9	261	32	101.6	9.8	439

Z16-27 - 4	0.09	0.086	2.1	1.4	4.7	2.6	1.31	0.44	36.7	8	10.75	0.76	109	12	30.6	2.4	114						
Z16-27 - 5	2.5	1.3	13	8.2	3.2	1.9	1.1	0.53	12.8	2.8	4.61	0.89	63	14	23.4	3	115						
Z16-27 - 6	1	0.47	5.9	2.6	8.7	2.4	1.19	0.43	38.6	4	16	1.6	216	12	83.6	3.4	380						
Z16-27 - 7	13.3	2.7	66	14	19.9	5.2	5.5	1.1	35.7	6.2	9.6	1.1	90.8	8.4	31	2.4	132.1						
Z16-27 - 8	14.4	6.3	62	29	20	7.1	2.3	1.7	45	7.7	15	2.2	182	12	83	5.8	421						
Z16-27 - 9	4.5	0.94	20	4.4	9.7	1.8	2.54	0.53	28.8	3.3	6.54	0.66	67.5	6.4	23.1	1.9	92.2						
Z16-27 - 10	14.3	3.1	72	20	14.6	4.9	2.98	0.68	28.7	5.9	9.4	1.4	124	11	52.1	2.5	272.4						
Z16-27 - 11	11	2	42	15	16.6	4.6	3.97	0.99	51.3	4.4	19.1	2.8	261	27	86.6	5.5	414						
Z16-27 - 12	19.6	8	101	43	30	11	11	3.3	93	16	24.5	3.9	273	28	99	11	440						
Z16-27 - 13	0.113	0.096	1.7	1.3	2.7	1.5	1.04	0.38	19.7	3.4	7.1	1.1	83	11	34.5	5.6	164						
Z16-27 - 14	31.2	2.9	137	13	23.8	5.1	5.86	0.97	73.9	5.8	25.4	2.9	330	16	128.8	5.2	645						
Z16-27 - 15	187	21	690	110	84	10	11.5	2.3	93	16	24	3.8	197	28	40.9	3.8	138						
Z16-27 - 16	1.09	0.4	4.8	1.6	4	2.1	1.39	0.5	37.3	4.5	14.9	1.5	195	12	82.2	4.9	403						
Z16-27 - 17	1.41	0.44	11.1	3.1	8.3	1.8	1.26	0.38	40.6	6.3	12.39	0.91	138.9	7.5	52.8	2.9	227						
Z16-27 - 18	22.3	3.2	99	11	33.8	4.2	8.6	2	110	27	30.2	7.6	332	79	128	32	580						
Z16-27 - 19	1.44	0.43	10.6	3.4	10.1	2.2	2.92	0.76	38.4	4.3	12.7	1.2	151.9	7.4	58.4	2.9	260						
Z16-27 - 20	0.25	0.17	3.5	2.5	8.1	2.4	1.22	0.68	54.1	8.1	18.4	1.4	213	17	81.1	2.7	349						
Z16-27 - 21	9.3	2	46	15	22.6	6.5	5.4	2.1	64	13	19.6	3.2	210	25	74.4	6	302						
Z16-27 - 22	0.41	0.27	1.6	1.3	1	1	0.19	0.25	9.6	2	2.97	0.59	42.3	7.7	18.4	1.1	104.3						
Z16-27 - 23	13.2	1.6	68	13	26.4	5.6	5.6	1.4	37.6	6.4	10.8	1.4	117	14	45.8	4.5	244						
Z16-27 - 24	10.1	1	52	11	15.9	2.6	3.26	0.53	40.2	8	14.4	1.2	227	18	105.1	5.1	535						
Z16-27 - 25	1.28	0.72	8.4	4.1	7.6	2.1	1.85	0.82	32.5	6.3	12.86	0.87	168	8.8	69.4	3.3	333						
Z16-27 - 26	23.8	1.3	107.9	8.9	25.6	3.8	8.4	1.9	58.7	7.3	18.2	2.1	185	12	60.4	3.4	267						
Z16-27 - 27	0.165	0.087	2.2	1.1	6.1	1.8	1.53	0.49	32.9	3.6	10.1	0.8	126.6	7.8	49	2.4	206.8						
Z16-27 - 28	36.1	4.9	153	21	35.3	7.7	9.5	1.9	83.9	9.4	29	1.9	327	15	133.5	4.9	612						
Z16-27 - 29	0.066	0.066	0.75	0.92	1.7	1.4	1.23	0.59	10.4	2.6	2.69	0.4	34.5	3.1	13.2	1.3	65.8						
Z16-27 - 30	11.11	0.78	60	6.2	22.5	2.5	3.51	0.75	65	6.7	16.82	0.91	173.5	7.8	58.4	2.8	233						
Z16-27 - 31	20.1	2.9	82.7	7.5	33.4	7.9	7.5	2	53.3	6.6	15.3	2.3	171	13	68.5	5.2	334						
Z16-27 - 32	4.75	0.85	25.5	5.7	15.9	3.3	3.08	0.65	58.6	8.1	17.5	3	201	22	71.4	5.5	293						
Z16-27 - 33	0.024	0.054	0.6	0.89	1.16	0.83	0.06	0.22	13.2	2.1	5.45	0.79	64.9	6	25.2	1.6	115.7						
Z16-27 - 34	0.75	0.4	5	2.4	5.3	2	0.92	0.42	29.1	5	9.26	0.69	114.1	7.7	43.6	3	200						
Z16-27 - 35	34.6	4.1	170	21	32	4.8	8.3	1.4	49.2	8.4	11.8	1	118.1	6.9	40	2.7	203						
Z16-27 - 36	2.13	0.42	11.2	2.7	6.2	2.2	0.9	0.34	24.1	3.6	8.6	0.98	106.1	4.7	47.1	3.1	227						

Z16-27 - 37	0.33	0.13	7	2.7	6	1.8	1.22	0.58	39.7	4.8	11.6	1	131.4	7.8	45.2	2.4	183.8					
Z16-27 - 38	4.32	0.82	20.2	3.8	9.6	2.7	6	1.1	47.2	6.6	16	1.2	222	11	95.6	3.4	477					
Z16-27 - 39	4.6	1.8	18.3	4.8	6.4	1.9	2.4	1.1	36	3.8	17.6	2.4	259	14	109.3	5.4	606					
Z16-27 - 40	15.2	2.9	94	20	37.3	9.1	6.4	1.5	75	10	17.2	2.4	172	12	55.3	5.4	241					
Z16-27 - 41	0.58	0.18	6.9	1.3	11.9	2.2	3.8	1.1	66.3	6.9	21.7	1.6	255	14	104.4	5.3	502					
Z16-35 - 1	0.84	0.43	10.4	3.1	15	3.7	2.11	0.79	70.2	8.7	18.2	1.3	205	15	70.3	6.3	288					
Z16-35 - 2	0.009	0.061	2.5	1.9	2.4	1.8	0.13	0.29	24.2	6.8	8.6	1.4	105	9.7	38.4	3.9	166					
Z16-35 - 3	1.1	0.35	7.6	2	8.6	3.4	2.09	0.8	36.8	4.9	13.5	1.1	151.9	5.9	60.4	3	260					
Z16-35 - 4	0.112	0.092	1.26	0.9	6.3	1.8	0.09	0.23	31.1	3.7	11.9	1.2	117.3	6.4	34.9	2.2	134.4					
Z16-35 - 5	1.37	0.42	5.4	1.9	4	2.4	2.2	1.2	14.8	3.2	4.56	0.75	56	5	22.2	1.5	122					
Z16-35 - 6	0.058	0.095	1.5	1.1	5.2	2.1	0.24	0.32	40.6	4.8	17.5	2.3	243	13	89.6	4.6	421					
Z16-35 - 7	0.13	0.11	1.8	1.1	2.9	1.5	0.65	0.4	14.7	3.5	4.59	0.69	48.4	4.2	17.9	1.5	81.5					
Z16-35 - 8	0.005	0.066	1.9	1.6	3.3	2.4	0.08	0.18	29.4	8.3	12.8	1.5	176	23	66.6	5.7	304					
Z16-35 - 9	0.42	0.2	2.9	1.2	2.4	1.3	1.5	0.45	17	3.4	6	1.2	79	10	32.2	3.1	156					
Z16-35 - 10	2.39	0.41	11.2	2.4	5.7	2.1	1.72	0.6	24.5	5	8.3	1.2	87.4	6.4	34.2	1.7	150.7					
Z16-35 - 11	B.D.	0.046	0.51	0.89	1.7	1.1	0.59	0.46	15.6	2.9	6.71	0.7	92	12	39.4	2.9	179					
Z16-35 - 12	0.18	0.11	3.4	1.4	8.3	2.7	0.63	0.49	58.2	6.7	18.3	1.4	238	18	93.9	5.2	399					
Z16-35 - 13	0.61	0.43	6	2.2	8	2.8	3.2	1.1	34.1	4.8	12.2	1.2	134	19	37.2	4.9	139					
Z16-35 - 14	2.5	0.62	10.4	4.6	5.2	2.6	3.3	1.5	32.1	7.2	9.1	1.3	114.8	7.8	46.4	3.3	222					
Z16-35 - 15	3.85	0.71	22.9	4.8	13.8	2.5	16.6	2.6	30.5	4.5	8.97	0.75	87.3	6.1	31.7	2.2	145.7					
Z16-35 - 16	0.28	0.12	2.8	1.5	3.9	1.4	0.65	0.31	28.1	3.7	13.7	1.2	192.2	6.9	84.2	3.2	415					
Z16-35 - 17	0.38	0.28	3.8	2	5.6	1.7	1.15	0.46	39	3.4	13.02	0.98	166	8.5	65.2	3.5	300					
Z16-35 - 18	1.39	0.44	6.7	4.2	6.6	4.4	2.88	0.77	14.8	3.4	4.75	0.82	68.4	7	30.2	2.2	142					
Z16-35 - 19	3.12	0.38	18	2.9	13.2	2.4	7.8	1.1	54	5.7	16.6	1.3	183.8	7.8	61.6	2.1	266					
Z16-35 - 20	0.018	0.065	1.1	1.5	3.6	1.4	0.07	0.18	22.8	5.2	10.4	1.3	145.5	7	60.5	2.9	285					
Z16-35 - 21	0.002	0.037	1.3	0.85	3.9	1.4	0.42	0.18	17.9	2.9	5.51	0.5	68.9	5.7	28.6	0.88	124.6					
Z16-35 - 22	0.046	0.066	1.11	0.74	2.2	1.3	0.44	0.4	19.2	3.4	8.2	1	110.9	8.4	39.6	2	181.6					
Z16-35 - 23	0.15	0.17	2.08	0.95	6.4	1.7	1.06	0.58	31.4	5.4	8.5	1.8	101.9	7.5	41.7	2.1	182.7					
Z16-35 - 24	0.32	0.15	3.2	2	2	1	1.04	0.54	16	4.1	5.17	0.83	64.9	4	24.6	2.4	120.9					
Z16-35 - 25	0.014	0.056	1.26	0.7	3.2	1.4	B.D.	0.0018	26.8	3.6	12.1	1.1	172	11	74.8	2.9	335					
Z16-35 - 26	0.11	0.11	2	1.1	2.7	2.2	0.79	0.63	29	4.3	8.41	0.98	113	10	47.2	3.6	239.4					
Z16-35 - 27	0.7	0.24	4.6	2.1	6.2	1.4	2.5	0.69	35.7	6	12	1.2	150	11	59.5	2.8	261.8					

Z16-35 - 28	0.106	0.049	0.93	0.82	7.5	1.8	0.19	0.35	37	3.7	12.7	1.1	165.8	7.4	63.7	2.1	274						
Z16-35 - 29	0.17	0.1	2.47	0.94	9.7	2.2	1.63	0.51	58.8	5.8	19.1	1.6	203	9.1	78.8	2.8	322						
Z16-35 - 30	0.53	0.2	5.2	1.8	9.6	3	3.4	2	56.5	7.1	15.2	2.2	208	18	78.5	7.6	344						
Z16-35 - 31	0.73	0.16	4.2	2.2	6	2.5	1.82	0.69	26.4	5	8.6	1.5	110	10	41.8	2.5	179						
Z16-35 - 32	1.16	0.21	18.1	2.7	31.1	3.6	15.5	1.8	147.1	8.9	44	1.6	477	14	173.2	4.1	682						
Z16-35 - 33	0.26	0.14	6.2	2.1	10.8	3.2	1.43	0.72	60.9	6.7	21.1	1.4	245	13	101.2	4.8	440						
Z16-35 - 34	0.037	0.063	0.98	0.52	2.33	0.99	0.23	0.18	17	2.9	5.6	0.67	72.1	4.7	29.5	1.7	133						
Z16-35 - 35	0.011	0.048	0.59	0.66	0.8	0.69	0.02	0.11	5.3	1.1	2.61	0.36	37.5	3.7	16	1.1	83.1						
Z16-35 - 36	0.158	0.081	1.35	0.63	4.2	1.5	0.28	0.31	27	3	9.27	0.71	119.9	6.5	51.1	2.4	240.7						
Z16-35 - 37	4.34	0.64	27.6	5.3	16.4	2.5	13.4	2	32.9	4.9	10.9	1.2	129	13	47.5	2.7	227						
Z16-35 - 38	0.026	0.04	1.83	0.93	1.76	0.85	0.8	0.35	23.5	3	6.79	0.59	85.1	4.6	31.7	1.7	143.9						
Z16-35 - 39	24.7	3.6	157	25	85	13	111	15	146	24	31.6	4.4	283	27	79.2	7	333						
Z16-35 - 40	9.1	3	39	12	16.7	5.7	5.7	2.3	38.4	7.1	11.9	1.3	146	16	56.2	4.1	268						
Z16-35 - 41	0.22	0.15	2.57	0.92	3.6	1.8	1.64	0.79	24.4	4.9	8.7	1.2	104.5	9.7	39.4	2.9	175.8						
Z16-35 - 42	0.65	0.36	3.1	2.3	5.9	3.8	0.82	0.54	27.9	8.8	9.8	2.5	109	10	40.8	3.5	186						
Z16-35 - 43	0.14	0.12	1.36	0.9	3.55	0.81	0.72	0.34	26	3.3	8.87	0.77	104.4	6.3	39.5	1.7	185.4						
Z16-35 - 44	B.D.	0.035	B.D.	0.29	2.5	1.4	0.22	0.23	22.6	4.2	8	0.98	106.7	6.9	41.2	2.6	180.9						
Z16-35 - 45	2.79	0.74	14.7	5.9	16.5	4.2	7.8	2	36	6	12.7	1.4	145	11	54.6	3.7	230.5						
Z16-35 - 46	0.36	0.27	3.7	1.8	4.6	2.4	2.22	0.65	26.8	4.3	9.4	1.5	134	12	52.2	5.3	251						
Z16-35 - 47	8.5	1.8	42.7	7.8	32.1	3.4	3.7	1	132.8	4.2	41.8	2.2	492	14	177.2	5.3	771						
Z16-35 - 48	2.49	0.3	14.5	2.2	10.7	1.8	3.89	0.76	45.1	4.7	13.9	1	178.9	8.7	67.4	3.5	295.4						
Z16-35 - 49	1.97	0.25	10.5	2.9	6.5	4.1	9.8	1.5	28	7	5.83	0.96	71	11	27.5	3.8	119.9						
Z16-35 - 50	0.05	0.12	1.7	1.5	1.4	1.1	0.77	0.47	15.5	2.9	4.83	0.85	70	4.5	27.3	1.6	123.9						
Z16-35 - 51	0.026	0.05	0.8	0.99	2.7	1.1	0.45	0.54	11.6	4.6	4.7	1.4	61.4	3	27.4	2.3	134						
Z16-35 - 52	0.14	0.1	1.39	0.79	2.5	1.5	0.51	0.28	17.3	3	5.12	0.8	65.5	5.4	25.6	1.6	114.6						
Z16-35 - 53	0.014	0.045	1.26	0.88	3.2	2.3	0.67	0.41	15.7	3.4	5.62	0.73	67.7	4.5	26.6	1.6	124.6						
Z16-35 - 54	0.084	0.083	3	1.2	7	2.2	1.09	0.52	27.2	4.1	9.19	0.62	104.3	4.7	40.6	2	178.4						
Z16-35 - 55	0.81	0.37	8.9	3.1	11.7	2.8	7	2.6	50.7	9.9	16.5	1.8	186	19	66.7	4.4	289						
Z16-35 - 56	0.83	0.27	5.2	1.9	4.6	2.3	4.6	2.4	19.6	5	7.4	1.4	103.3	9.9	38.9	2.7	208						
Z16-35 - 57	B.D.	0.043	B.D.	0.32	3.4	1.2	0.24	0.21	20.5	3.8	7.51	0.78	101.4	6.3	36.8	1.9	166.8						
Z16-35 - 58	0.133	0.088	1.95	0.96	3.2	1	0.54	0.31	18.3	3.1	5.84	0.61	66.3	2.8	24.4	1.3	108.3						
Z16-35 - 59	3.04	0.86	13.7	3.2	7.9	3	1.03	0.55	20.3	4.1	5.21	0.98	52.6	4.9	19.7	1.8	85						
Z16-35 - 60	0.09	0.087	0.69	0.75	2.5	1.8	0.48	0.46	9.8	2.5	3.01	0.74	39	4.8	15.3	1.4	77.1						

Z16-35 - 61	0.259	0.089	3.5	2.1	6.8	2.9	0.73	0.46	40.9	6	11.9	1.1	150	11	55.6	3.5	228						
Z16-35 - 62	16.7	2.8	84	14	46.5	6.8	38	5.6	109	31	23.9	1.8	207	11	56.3	9.7	193						
Z16-35 - 63	0.2	0.12	3.4	1.4	2.1	1.4	2.13	0.95	13.4	4.1	5.78	0.83	72.1	9.3	30.1	3.1	153.8						
Z16-35 - 64	13	13	45	42	16	12	1.7	1	49	11	17.3	2.4	215	10	82.7	5.3	376						
Z16-35 - 65	0.069	0.055	1.79	0.75	1.8	1.1	0.24	0.22	22.2	3	7.99	0.74	100.5	6.5	40.6	1.9	195						
Z16-35 - 66	0.19	0.14	2.1	1.1	5.9	1.5	0.23	0.3	49.5	2.6	17.7	2.3	221.7	9.4	84	3.8	374						
Z16-35 - 67	0.171	0.099	3.2	1	6.1	1.8	1.66	0.52	38.9	4.9	12.4	1.4	154	10	59.5	3.7	262						
Z16-35 - 68	2.94	0.31	15	3.3	9.2	3.3	7.1	1.8	26.7	6.5	9.1	1.4	101.8	8.9	34.9	1.4	149.9						
Z16-35 - 69	0.136	0.093	2.8	1.5	4.8	1.6	B.D.	0.004	29.5	6	9.2	1.2	113.4	8.9	42.6	2	185.1						
Z16-35 - 70	1.3	1.5	3.6	3.6	2.3	1.8	0.31	0.36	15.4	5.1	5.87	0.6	63.7	5.1	28.5	2.6	134.4						
Z16-35 - 71	0.61	0.22	7.4	2.3	13.2	4.2	1.95	0.65	50.8	7	14.5	1.6	125.2	6.6	39.3	2.9	155						
Z16-35 - 72	3.8	1.1	22	11	16.4	3.6	9.9	5.7	43.2	8.6	13.6	1.2	161	25	57.6	2.6	241						
Z16-35 - 73	0.016	0.05	0.62	0.58	3.2	1.3	0.25	0.22	27.2	3.6	11.78	0.95	165.2	8	68.7	2.7	330						
Z16-35 - 74	37	37	140	130	36	25	1.9	1.6	43	18	10.2	2.9	118	15	42.9	2.7	188						
Z16-35 - 75	32	12	146	42	77.9	7.8	26	2.8	203	23	50.3	5	471	40	141	10	525						
Z16-35 - 76	0.3	0.15	2.1	1.2	2.5	1.4	0.38	0.41	13.2	2.9	3.68	0.52	47.5	2.8	20.4	1.4	93.8						
Z16-35 - 77	3.97	0.49	21.1	2.8	19	4.2	9.5	1.4	62.9	5.2	19.8	1.2	233.4	9.8	81.6	4.3	362						
Z16-35 - 78	0.307	0.077	4.2	1.5	7.7	1.8	1.68	0.61	30.7	4.7	8.24	0.69	94	7.5	36.1	2.3	164.9						
Z16-35 - 79	0.103	0.076	1.9	1.1	5.7	2.6	1.21	0.52	28.8	4	8.62	0.8	111.3	6.7	41.5	2.7	198.9						
Z16-35 - 80	B.D.	0.044	0.45	0.64	1.16	0.99	0.16	0.28	12.8	2.5	4.53	0.78	65.9	9.9	26.7	4.5	115						
Z16-35 - 81	0.17	0.1	2.6	1.1	6.8	2.5	1.37	0.41	33.1	3.5	11.3	1.1	137.9	9.7	50.7	3.1	218						
Z16-35 - 82	0.065	0.066	1.7	0.68	2.3	1.2	0.71	0.4	11.4	3.6	4.51	0.89	53.4	7.8	19.7	2.6	87.1						
Z16-35 - 83	0.18	0.19	1.3	1.1	4.3	2.3	0.56	0.41	15.7	2.8	6.08	0.88	79.1	9.6	30.3	4.6	146						
Z16-35 - 84	3.17	0.29	22.1	4.7	13.9	3.7	8.6	2.2	37.4	4.8	12.8	1.3	151	11	52.2	4.7	220						
Z16-35 - 85	0.213	0.086	3.7	1.1	8.4	1.8	2.42	0.61	41.3	3.9	11.22	0.81	138.2	7.6	50.6	2.4	205.8						
Z16-35 - 86	2.46	0.53	13.2	4.3	8	2.7	3.1	1.3	19.7	3.9	6.68	0.64	89	9.5	35.4	3.2	185						
Z16-35 - 87	0.11	0.12	2.1	1.1	4.4	1.8	0.49	0.27	24.3	4	7.9	1	96.1	8.4	35.9	1.4	160.4						
Z16-35 - 88	0.199	0.062	2.97	0.9	4.4	1.6	1.32	0.59	33.3	2.9	11.8	1.2	153.7	8.7	62.4	5.3	280						
Z16-35 - 89	0.076	0.07	0.31	0.63	1.9	1.7	0.1	0.18	12.6	2.2	5.29	0.76	71.5	8	28.1	2.1	128.8						
Z16-35 - 90	0.283	0.091	2.2	1.4	5.6	1.8	1.48	0.65	28.6	3.2	10.25	0.98	123.6	6.3	45.4	3	204						
Z16-35 - 91	0.164	0.068	2.1	1.1	2.5	1.3	1.13	0.66	21.4	2.8	7.2	1.4	92.8	6.5	38.3	4.3	181						
Z16-35 - 92	0.23	0.21	2.6	1.9	8.3	2.1	3.16	0.72	34.8	3.7	13.5	1.2	168	12	64.6	4	296.7						
Z16-35 - 93	0.21	0.16	3.3	1.8	6.6	2.1	1.15	0.59	34.9	6.7	11.6	1.4	133	12	49.4	4.2	223						

Z16-35 - 94	1.74	0.38	10.5	4.4	12.5	2.1	0.37	0.32	24	2.6	7.2	1.2	82.8	7.2	29.6	1.8	131.2						
Z16-35 - 95	0.95	0.33	6.9	2.7	11.1	2.9	5.1	1.3	51.4	7.7	15.1	1.9	186	15	72.9	6	324						
Z16-35 - 96	2.33	0.76	16.5	6.8	14.7	6.2	15.7	4	31.8	8.6	10.5	2.3	124	15	41.2	3.6	198						
Z16-35 - 97	12.9	2.5	75	20	53.6	9	34.4	9.1	100	12	26.5	1.8	250	20	76.2	3.9	324						
Z16-35 - 98	4.97	0.77	27.1	6.2	22.7	7.5	9	1.8	54.9	7.3	17.7	1.6	208.5	7.3	72.1	4.3	303						
Z16-35 - 99	0.251	0.098	3.4	1.2	5.9	1.5	0.84	0.4	35.5	5	12.15	0.81	135.7	4.6	50.6	2.5	215						
Z16-35 - 100	0.139	0.093	1.79	0.82	2.7	1.2	0.79	0.37	16.2	3.2	5.73	0.57	69.7	5.1	26.3	1.4	116.6						
Z16-35 - 101	1.83	0.55	14.2	3.1	11	4.6	2.72	0.91	74.5	8.9	22.2	3.5	267	30	93.7	9.8	379						
Z16-35 - 102	0.043	0.053	0.81	0.67	4.6	1.6	0.25	0.22	23.2	3.2	7.92	0.81	102.6	7.8	36.3	2.5	158.8						
Z16-35 - 103	0.145	0.074	2.36	0.76	9	2.3	0.25	0.2	39.9	5.5	13.4	1.1	147.8	8.2	55.4	2.6	239						
Z16-35 - 104	0.12	0.11	1.4	1	10.2	3.4	1.6	1.2	54.6	5.6	18.6	1	258	13	98.7	4.3	422						
Z16-35 - 105	8.8	1.8	52	17	40.4	6.7	30.7	8.3	87.8	9.4	21.9	1.8	242.2	9.9	76.7	2.5	319						
Z16-35 - 106	4.41	0.54	24.1	5.6	12.3	4.2	17.7	3.8	40	9.1	12	2.6	125	28	45.9	8.2	226						
Z16-35 - 107	B.D.	0.023	0.96	0.63	1.2	0.74	0.19	0.2	6.1	1.2	2.78	0.49	36.9	5.4	14.89	0.9	73.9						
Z16-35 - 108	1.68	0.45	7.7	2.4	4.6	1.7	6.4	1.7	12.6	2.3	4.05	0.5	56.7	5.1	23.1	1.3	108.4						
Z16-35 - 109	17	13	68	58	16	11	2.6	1.8	26	10	5.7	1.3	58.3	5.1	24.2	1.5	117.1						
Z16-35 - 110	0.074	0.092	0.8	1.1	1.4	1.2	0.18	0.27	19.8	5.6	7.92	0.72	115.4	7.8	42.3	4.6	181						
Z16-35 - 111	0.22	0.13	2.1	1.1	4.1	2.3	1.22	0.5	19.9	4.6	7	0.6	89.4	6.5	34.2	2.3	167.2						
Z16-35 - 112	0.035	0.062	1.4	1.1	2.6	1.7	0.24	0.28	21.4	4.9	7.3	1.4	88.8	9.6	37.2	3.3	162						
Z16-35 - 113	0.29	0.15	2.1	1.6	5.5	3.4	0.91	0.5	40	6.6	12	1	144	11	60.8	3.6	263						
Z16-35 - 114	0.063	0.054	1.08	0.79	4.9	1.3	0.33	0.21	27	4.3	8.8	1.1	113.6	8.5	42.1	2.8	195						
Z16-35 - 115	0.94	0.24	8.4	2.6	9.6	2.4	2.86	0.6	43.7	4.8	12.6	0.97	145.5	7.5	50	2.9	220.4						
Z16-35 - 116	0.53	0.17	2.4	1.2	1.8	1.2	2.5	1	17	3.7	4.63	0.79	53	10	22.1	2.8	106						
Z16-35 - 117	0.151	0.084	1.7	1	3	1.3	1.66	0.5	16.8	2.5	5.57	0.7	59.4	4.5	23.4	1.7	109.2						
Z16-35 - 118	0.079	0.093	0.22	0.55	1.52	0.98	0.18	0.22	16.2	3.5	4.54	0.69	56.5	6.1	20.4	2.5	95						
Z16-35 - 119	0.25	0.15	2.5	1.3	4.4	1.5	0.57	0.37	32.6	4.8	9.9	1.4	135.1	8.9	47.8	3.5	222						
Z16-35 - 120	1.56	0.27	11.8	3.8	8.9	3.8	3.3	0.79	38.9	8.1	12.5	1.1	157	14	58.7	3	269						
Z16-35 - 121	3.12	0.43	17.4	3.6	11.2	2.4	7	1.4	27.2	3.1	9.7	1.5	103.6	9.5	37.4	2.4	155						
Z16-35 - 122	0.41	0.16	5.9	2.2	6.9	2	2.13	0.53	36.9	5.6	12.07	0.71	153	13	57.9	3.4	264						
Z16-35 - 123	0.54	0.24	13.3	5.1	22.7	6.6	5.9	1.2	121	14	33.5	2.2	377	27	129.5	4	532						
Z16-35 - 124	0.55	0.13	3.5	2	3.1	1.4	0.4	0.26	19	3	7.17	0.69	87.8	6.6	35.6	1.7	168						
Z16-35 - 125	10.8	1.3	52.1	8.3	34	5.5	94	15	50.8	9.7	14.5	2	145	17	47.1	2.7	230						
Z16-35 - 126	0.11	0.12	3.3	2.1	12.1	4.3	0.64	0.48	65.9	7.5	19.7	1.3	234	18	85	7.1	352						

Z16-35 - 127	B.D.	0.046	0.63	0.43	1.85	0.85	0.51	0.26	12.9	2	4.97	0.48	61.4	4.9	24.2	1.4	119.5						
Z16-35 - 128	B.D.	0.047	2.12	0.93	5.9	1.9	0.33	0.24	28.8	3.2	10.47	0.87	127.2	5.9	51.2	2.1	222.2						
Z16-35 - 129	0.05	0.082	1.7	1.3	5.4	2.5	0.29	0.34	29.8	4.7	10.8	1.5	124.8	7	47.8	3	216.3						
Z16-35 - 130	0.078	0.069	1.51	0.77	1.88	0.84	0.38	0.28	17.5	2.8	6.11	0.66	77.5	4.1	29.9	1.7	129.2						
Z16-35 - 131	1.51	0.43	7.1	2.5	6.2	2	2.5	1.2	19.4	2.9	7.23	0.68	85.4	5.8	33.7	1.4	167.4						
Z16-35 - 132	0.064	0.056	1.32	0.65	3.5	0.93	0.48	0.32	28.7	3.8	11.78	0.97	148.6	9.7	57.2	3.3	245						
Z16-35 - 133	10.6	1.5	66	10	33.1	6.6	17.9	3.2	48	10	12.8	1.9	112	14	36.5	3.3	168.7						
Z16-35 - 134	0.006	0.055	1.2	1.1	3.1	1.5	0.19	0.24	21.8	5.5	7.58	0.87	93.2	4.9	37.5	2.6	177.8						
Z16-35 - 135	0.19	0.11	4.7	3.2	5.5	1.5	2.32	0.82	38.2	6.7	11.1	1.5	150.7	7.7	64.2	4.8	286						
Z16-35 - 136	0.055	0.061	1.63	0.82	2.2	1.2	0.7	0.43	18.6	1.9	6.08	0.78	79.3	6.6	32.5	2.1	140.9						
Z16-35 - 137	6.1	5.2	38	32	16.9	9.8	1.42	0.34	44.7	9.6	13.2	1.3	170	14	75	3.2	342						
Z16-35 - 138	0.17	0.11	1.8	1.5	2.8	2	0.34	0.33	24.9	4.1	10.3	1	150	10	63	4.8	280						
Z16-35 - 139	0.204	0.073	2.42	0.88	6.7	1.9	1.58	0.37	27.8	3.5	9.83	0.93	119.7	6.2	46.1	2.1	209.4						
Z16-35 - 140	0.21	0.11	4.4	2.1	5.1	2.5	0.75	0.41	23.8	3.6	7.6	0.78	90.7	6.1	35.4	2	160.8						
Z16-35 - 141	8.5	2.2	59	21	34	10	27.4	6.2	98	10	30.6	2.9	332	25	112	10	478						
Z16-35 - 142	0.27	0.11	3.7	1.3	5	1.2	1.02	0.43	19.7	3.7	5.75	0.44	69.2	6.5	22.7	1.6	97.3						
Z16-35 - 143	0.064	0.087	2.3	1.8	4.5	1.6	0.6	0.48	18.8	4.1	7.32	0.99	94.7	5.1	35	2.9	178.5						
Z16-35 - 144	0.133	0.098	2.6	1.1	5.6	2.8	1.31	0.42	27.3	6.7	7.2	1.2	80.1	5.5	30.1	2	132.8						
Z16-35 - 145	0.044	0.084	2.2	1.7	4.1	1.5	0.12	0.27	18.6	4.4	7.02	0.85	79.3	5.1	32	2	152.7						
Z16-35 - 146	B.D.	0.043	1.5	0.91	2.4	1.3	0.58	0.47	13.1	3.2	5.3	0.93	62.5	6.8	27.6	1.4	121.1						
Z16-35 - 147	B.D.	0.055	0.59	0.62	1.84	0.78	0.76	0.37	10.4	2.4	3.55	0.68	49.4	4.8	20.3	1.3	93.9						
Z16-35 - 148	1.56	0.24	13.1	4	10.1	2.9	4.9	1.3	40	6	11.7	1.3	133	11	52.8	3.9	222						
Z16-35 - 149	0.057	0.048	2.59	0.98	3.2	1.3	0.78	0.32	16.5	2.5	7	0.59	77	4.2	32.5	1.9	139.9						
Z16-35 - 150	1.27	0.22	8.8	2.2	5.4	1.8	4.9	1.3	17	3.1	6.12	0.57	71.6	4.6	27.9	1.2	137.6						
Z16-35 - 151	0.62	0.19	3.3	1.3	7.1	2.5	2.21	0.53	26.3	4.1	11	1.2	141	12	54	3	249						
Z16-35 - 152	0.09	0.11	0.18	0.5	1.6	1.2	0.97	0.52	14.4	3.1	3.84	0.74	52.6	5.2	21.1	1.5	112.1						
Z16-35 - 153	0.128	0.09	0.74	0.6	6.9	1.7	0.53	0.38	28.7	5.2	5.62	0.82	44.3	4.2	9.7	1.1	28.4						
Z16-35 - 154	5.45	0.63	23.8	4.2	7.7	2	2.06	0.88	30.9	4.3	9.7	1.3	108.9	7.6	43	2	194						
Z16-35 - 155	1.58	0.49	15.5	5.1	9.5	5	14.2	5.1	22.6	5	5.7	1	54.6	6.1	18	2.1	86						
Z16-35 - 156	1.18	0.27	8.7	3.1	8.3	3.3	2.87	0.9	43.5	6.5	15.9	1.7	175	18	67.3	6.5	308						
Z16-35 - 157	17.9	2.5	117	15	53	10	114.7	9.7	119	11	26.3	3.3	219	18	54	5.5	190						
Z16-35 - 158	0.099	0.084	1.06	0.73	2.22	0.96	0.51	0.28	18.3	2.6	6.62	0.9	90.8	8	36.4	1.6	157.8						
Z16-35 - 159	0.16	0.11	2	1.2	3.1	1.3	0.47	0.24	15	2.9	5.84	0.57	70.2	3.6	25.8	1.8	114.9						

Z16-35 - 160	0.68	0.17	10.9	2.1	19.8	3.7	3.24	0.56	91.2	6.4	24.2	1.4	263	11	89.5	2.8	369		
Z16-35 - 161	3.06	0.75	16.1	2.5	11	3.1	9.3	2.3	35.3	6.2	9.05	0.91	104.1	5.6	36.7	1.5	170.3		
Z16-35 - 162	0.13	0.14	1.3	1.1	1.09	0.88	0.29	0.28	11.5	2.2	3.99	0.73	62.9	5.8	30.2	2.4	201		
Z16-35 - 163	0.207	0.097	1.45	0.96	6.7	2.2	1.27	0.56	26.8	4.2	8	1.2	97.4	9.1	38.5	2.8	183		
Z16-35 - 164	0.039	0.054	B.D.	0.015	4.1	1.5	0.02	0.15	19.9	3.4	6.2	1.5	60	11	14.6	3.3	50		
Z16-35 - 165	0.47	0.18	7.7	2.1	12.3	2.9	2.18	0.76	43.1	5.3	9.81	0.87	102.3	7.8	35	2.6	137.4		
Z16-35 - 166	0.076	0.083	1.84	0.99	3.8	1.9	0.68	0.41	22.6	4.2	9.2	1.2	112.5	6.8	42.2	1.6	191.3		
Z16-35 - 167	0.27	0.13	3.9	1.3	10.8	3	4.5	1	56.3	4.1	16.8	1.2	213.9	9.3	81.7	2.5	354		
Z16-35 - 168	0.48	0.18	4	1.9	2.9	1.3	1.17	0.41	14	2.7	5.01	0.57	54.5	5.1	22.5	1.5	106.5		
Z16-35 - 169	0.02	0.12	0.01	0.4	0.8	1.1	0.45	0.39	9.6	4.2	3.03	0.86	45.6	6.1	19.3	2	102.6		
Nist610 - 1	420	21	423	22	436	25	442	21	435	23	435	22	418	21	438	14	419		
Nist610 - 2	423	24	423	29	455	33	454	24	435	28	429	24	414	30	454	24	413		
Nist610 - 3	429	23	422	24	453	30	455	17	441	27	445	24	432	25	439	19	430		
Nist610 - 4	415	18	423	17	419	29	445	20	425	29	427	18	409	24	432	22	406		
Nist610 - 5	425	24	421	30	442	33	453	23	441	30	444	25	421	29	441	20	429		
Nist610 - 6	424	19	431	35	441	27	464	24	440	22	432	19	417	26	444	24	415		
Nist610 - 7	415	26	407	35	442	40	449	34	421	30	432	27	421	30	440	26	411		
Nist610 - 8	432	18	436	27	450	26	463	21	453	32	442	19	424	22	447	18	427		
Nist610 - 9	408	18	407	26	446	42	441	27	422	28	422	20	399	30	425	22	410		
Nist610 - 10	429	19	437	25	436	34	462	25	449	31	444	22	426	22	443	20	428		
Nist610 - 11	419	17	416	18	445	14	457	19	432	16	431	15	415	17	442	19	412		
Nist610 - 12	427	17	429	24	453	25	450	26	452	36	440	20	425	20	447	22	425		
Nist610 - 13	417	19	421	23	438	25	443	28	431	27	430	19	408	24	431	21	415		
Nist610 - 14	421	21	434	38	434	38	449	21	432	30	436	23	425	25	438	26	416		
Nist610 - 15	423	21	418	28	434	26	446	24	436	19	435	24	418	25	444	23	419		
GJ1 - 1	0.011	0.06	0.28	0.79	1.8	1.1	0.77	0.53	6.8	2.9	1.77	0.44	19.5	2.8	7.38	0.87	30.7		
GJ1 - 2	0.024	0.047	0.37	0.66	1.56	0.87	0.51	0.3	5.6	1.7	1.88	0.56	21.6	2.5	7.4	1.1	31.9		
GJ1 - 3	0.026	0.057	1.28	0.9	1.06	0.72	1.43	0.55	6.4	2	1.61	0.25	19.4	2.6	7.47	0.98	32.2		
GJ1 - 4	0.019	0.08	B.D.	0.013	0.84	0.76	1.04	0.48	7.9	3.3	1.82	0.39	19.9	2.9	7.2	1	31.1		
GJ1 - 5	0.027	0.062	0.8	1.2	0.95	0.76	0.98	0.6	6.4	1.2	1.64	0.29	20.7	4.4	7.4	1	28.3		
GJ1 - 6	0.059	0.076	1.2	1	1.3	1.5	0.85	0.48	7	3.8	2.11	0.51	18.5	2.3	7.05	0.87	32.6		

GI1 - 7	0.036	0.037	0.4	0.36	1.08	0.86	0.8	0.38	9.2	1.8	2.03	0.37	19.8	2.4	6.68	0.69	31					
GI1 - 8	0.069	0.077	0.42	0.8	0.75	0.9	0.99	0.43	6.1	1.6	1.98	0.69	19.1	3	7.47	0.96	32.7					
GI1 - 9	0.001	0.053	0.7	0.79	0.73	0.71	0.82	0.34	6.2	1.7	1.48	0.26	17.5	1.7	6.12	0.81	29					
GI1 - 10	B.D.	0.049	0.49	0.66	1.3	1.1	0.63	0.47	8.4	2	1.77	0.46	18.3	2.7	7.42	0.82	30.1					
GI1 - 11	0.018	0.079	0.31	0.62	0.52	0.82	1.22	0.41	6.1	1.9	2.05	0.43	19	3	6.05	0.65	29.4					
GI1 - 12	0.048	0.067	0.82	0.89	0.41	0.63	1.25	0.74	5.4	1.9	2.01	0.6	21.1	2.8	6.85	0.47	32					
GI1 - 13	0.016	0.035	0.11	0.38	1.89	0.68	0.78	0.38	7.6	2	2.11	0.42	19.7	3.2	7.18	0.64	30.2					
GI1 - 14	0.055	0.064	1.6	1.2	0.65	0.8	0.81	0.37	5.9	1.7	1.75	0.38	19	2.9	6.76	0.86	30.1					
GI1 - 15	B.D.	0.052	0.25	0.61	0.61	0.82	0.65	0.41	7	2.3	1.77	0.44	19.5	2.9	7.2	0.93	29.6					
GI1 - 16	B.D.	0.038	0.3	0.47	0.48	0.53	0.99	0.45	6.9	1.8	1.9	0.47	19.1	2.4	6.56	0.66	31.2					
GI1 - 17	B.D.	0.055	0.6	0.53	1.49	0.8	1.08	0.45	7.7	1.6	1.69	0.4	19	2.1	6.55	0.8	29.3					
GI1 - 18	B.D.	0.041	0.43	0.63	1.61	0.98	0.88	0.56	6.7	2.3	2.06	0.44	17.5	2.4	6.98	0.6	29					
GI1 - 19	0.024	0.047	0.76	0.59	0.66	0.7	1.42	0.51	7.9	2.5	2	0.46	19.4	2.2	6.08	0.81	29.6					
GI1 - 20	0.034	0.052	B.D.	0.24	0.7	0.57	0.7	0.26	6.6	2.2	1.64	0.34	20.2	2.2	6.69	0.45	29.3					
GI1 - 21	B.D.	0.031	0.58	0.47	0.99	0.74	1.04	0.46	7.7	1.9	2.12	0.34	20.6	2	7.31	0.75	31.4					
GI1 - 22	B.D.	0.045	0.94	0.75	0.39	0.54	0.97	0.35	6.9	2.1	2.26	0.42	21.6	2.3	6.82	0.6	30.3					
GI1 - 23	0.02	0.055	0.44	0.51	2.05	0.92	1.26	0.44	7.5	1.6	2.23	0.43	20	2.5	7.58	0.88	28.4					
GI1 - 24	0.041	0.064	0.39	0.45	1.13	0.84	1.06	0.45	8	2.3	1.58	0.37	19	2.4	7.25	0.69	31					
GI1 - 25	0.003	0.059	0.64	0.69	0.65	0.67	1.25	0.46	7.1	2	1.94	0.39	20.5	2.5	6.94	0.59	30.4					
GI1 - 26	0.024	0.067	0.37	0.42	1.09	0.89	0.89	0.44	8.4	2.1	1.75	0.33	20.8	2.4	7.23	0.7	28.6					
GI1 - 27	0.018	0.061	1.05	0.75	0.89	0.64	0.73	0.28	8.6	2.2	1.93	0.45	18.7	2.7	6.54	0.85	29.8					
GI1 - 28	0.066	0.08	0.99	0.67	2.04	0.79	0.97	0.41	7.8	2	1.54	0.41	19.6	2.1	6.67	0.8	32					
GI1 - 29	B.D.	0.034	0.23	0.48	1.43	0.8	1.07	0.38	6.8	1.7	2.03	0.34	19.9	2.1	6.66	0.93	30.5					
GI1 - 30	0.095	0.071	0.53	0.53	0.93	0.7	1.06	0.33	6.5	1.6	1.91	0.37	19.5	2.9	7.08	0.72	31.4					
Ples - 1	0.08	0.1	1.8	1.2	3.8	1.5	1.02	0.39	16	2.7	5.59	0.87	58	5.9	15	1.4	44.5					
Ples - 2	0.28	0.1	5.1	1.1	8.2	2.5	1.83	0.44	30.1	4.2	9.36	0.95	94.3	4.3	25.9	2.1	88.8					
Ples - 3	0.38	0.15	2.7	1.2	5.4	2.2	2	0.67	25.6	4.9	9.6	1.4	97.2	6.3	26.7	2	84.3					
Ples - 4	0.124	0.077	1.64	0.83	3.1	1.2	0.99	0.4	12.6	3.4	4.85	0.61	51.3	3	15.8	1.2	51.8					
Ples - 5	0.27	0.14	2.2	1.3	4.5	2.4	1.48	0.63	20.3	4.5	7.92	0.86	70.2	3.6	21.8	1.7	70.7					
Ples - 6	0.183	0.086	2.6	0.95	4.5	2.6	1.43	0.33	20	4.8	6.91	0.64	73.5	6.7	20.7	1.7	69.1					
Ples - 7	0.19	0.1	2.4	1.3	6	2	0.85	0.36	15.9	2.6	7.13	0.68	69.5	2.9	20.6	1.5	71.9					
Ples - 8	0.17	0.1	0.88	0.86	2.7	1	0.76	0.3	15.8	3.4	4.78	0.77	47.5	4.6	12.1	1.2	45.1					

Ples - 9	0.21	0.14	2.9	1.4	4.5	2.5	1.21	0.59	15.4	2.6	6.79	0.88	69	4.3	19.9	1.1	65.8			
Ples - 10	0.11	0.11	1.7	1.3	2	1.1	0.18	0.23	6.9	1.6	2.27	0.54	22.3	3.3	7.32	0.81	24.2			
Ples - 11	0.081	0.059	2.1	1	3.8	1.5	0.76	0.33	16	3	4.93	0.48	50.4	5.5	15.8	1.3	53.1			
Ples - 12	0.18	0.097	2	1.3	1.6	1.1	1.05	0.76	11	3.2	5.3	1.1	55.2	4.7	15.8	1.3	45.9			
Ples - 13	0.075	0.083	1.11	0.65	3.4	1.7	0.88	0.4	13.9	2.9	5.24	0.68	58.7	4.5	15.5	1.5	45.3			
Ples - 14	0.102	0.081	1.38	0.88	3.8	2.1	1.14	0.51	16.6	3.1	5.18	0.76	57	4.4	14.8	1.5	47.4			
Ples - 15	0.11	0.11	0.88	0.75	3.1	1.7	1.21	0.5	12.5	2	4.92	0.53	53.3	3.8	15.57	0.88	48.7			
91500 - 1	B.D.	0.026	B.D.	0.23	0.62	0.86	0.14	0.18	2.3	1.4	0.64	0.22	8.2	2.2	4.79	0.92	20			
91500 - 2	B.D.	0.045	0.12	0.54	0.35	0.6	0.08	0.18	1.72	0.94	0.6	0.25	8.3	1.5	3.34	0.89	18.8			
91500 - 3	B.D.	0.046	B.D.	0.33	0.08	0.38	B.D.	0.09	2.9	1.2	0.68	0.27	9.4	1.8	4.21	0.79	23			
91500 - 4	0.004	0.05	B.D.	0.13	0.34	0.68	0.21	0.19	1.3	1.2	0.71	0.27	9.6	2	3.96	0.61	22.9			
91500 - 5	B.D.	0.036	0.26	0.34	0.64	0.72	0.39	0.3	2.4	1.2	0.81	0.25	10.1	1.5	4.29	0.54	21.5			
91500 - 6	B.D.	0.033	B.D.	0.3	0.48	0.51	0.6	0.16	2.2	1	0.67	0.16	8.9	1.7	3.92	0.53	21.7			
91500 - 7	B.D.	0.027	1.08	0.76	0.52	0.6	0.05	0.16	0.84	0.72	0.53	0.25	8.7	1.6	3.73	0.54	18.4			
91500 - 8	B.D.	0.028	0.08	0.4	0.43	0.5	0.27	0.24	1.64	0.93	0.74	0.2	7.5	1.3	4.09	0.57	20.7			
91500 - 9	B.D.	0.049	0.64	0.73	0.73	0.64	0.23	0.36	1.63	0.96	0.68	0.18	10	1.7	4.22	0.73	21.1			
91500 - 10	B.D.	0.013	0.12	0.51	0.61	0.81	0.16	0.25	2.3	1	0.85	0.3	8.3	1.7	4.21	0.58	21.2			
91500 - 11	B.D.	0.03	B.D.	0.22	B.D.	0.29	0.35	0.27	1.9	1.2	0.85	0.2	8.8	1.7	4.15	0.64	23.2			
91500 - 12	0.039	0.055	0.3	0.56	0.41	0.65	0.04	0.17	3	1.5	0.57	0.23	8.8	2.1	3.39	0.32	16.8			
91500 - 13	B.D.	0.031	0.08	0.39	0.06	0.26	0.16	0.2	1.49	0.87	0.67	0.24	8.2	1.3	3.79	0.4	18.6			
91500 - 14	0.009	0.047	0.4	0.47	0.06	0.61	0.01	0.15	1.55	0.84	0.82	0.19	8.3	1.7	3.34	0.45	22.5			
91500 - 15	0.036	0.085	0.28	0.51	0.31	0.61	0.38	0.33	2.1	1	0.6	0.27	8.4	1.4	3.84	0.75	22.6			
91500 - 16	0.018	0.067	0.28	0.45	0.08	0.42	0.54	0.27	1.07	0.72	0.65	0.21	10.1	1.5	4.2	0.64	19.6			
91500 - 17	B.D.	0.029	0.12	0.33	0.18	0.41	0.25	0.22	1.8	1.2	0.79	0.26	9.6	1.9	3.92	0.59	19.4			
91500 - 18	B.D.	0.039	0.32	0.47	0.26	0.48	0.23	0.18	2.2	1.2	0.43	0.18	7.5	1.1	3.59	0.49	17.8			
91500 - 19	B.D.	0.049	0.36	0.65	1.02	0.74	0.47	0.31	2.9	1	0.83	0.32	10.3	1.8	3.71	0.55	22.6			
91500 - 20	0.004	0.04	0.28	0.42	0.47	0.58	0.36	0.29	1.57	0.79	0.75	0.21	9.6	1.6	4.23	0.53	22.6			
91500 - 21	B.D.	0.018	0.57	0.64	0.44	0.59	0.17	0.16	1.8	1.1	0.73	0.23	9	1.6	4.01	0.45	21.6			
91500 - 22	B.D.	0.045	0.01	0.23	0.62	0.64	0.08	0.12	1.6	1.1	0.57	0.2	8.7	1.9	3.62	0.5	22.1			
91500 - 23	B.D.	0.05	0.23	0.65	0.32	0.7	0.34	0.33	2.5	1.2	0.53	0.27	9.7	2.5	3.26	0.42	17.9			
91500 - 24	0.05	0.061	B.D.	0.34	0.54	0.69	0.1	0.15	2.8	1.5	0.89	0.22	10.4	2.1	3.52	0.73	20.3			
91500 - 25	B.D.	0.043	0	0.32	0.52	0.58	0.04	0.12	2.4	1.6	0.75	0.2	10.5	1.8	4.23	0.64	22.7			

91500 - 26	0.068	0.064	0.2	0.4	0.57	0.53	B.D.	0.08	1.26	0.85	0.74	0.2	8.7	1.4	3.95	0.54	21.7			
91500 - 27	0.04	0.063	0.29	0.37	0.44	0.65	0.29	0.23	2.22	0.97	0.67	0.2	10.5	1.9	4.32	0.48	20.8			
91500 - 28	0.012	0.044	B.D.	0.014	0.21	0.49	0.24	0.22	1.88	0.89	0.49	0.17	9	1.5	3.95	0.41	18.6			
91500 - 29	B.D.	0.05	B.D.	0.15	0.73	0.82	0.28	0.21	1.31	0.95	0.74	0.26	8.5	1.3	3.89	0.57	22.8			
91500 - 30	0.046	0.049	1	0.71	1	1.2	0.15	0.17	0.83	0.57	0.6	0.27	8.3	2.1	3.54	0.54	20			

Sample	Er 2SE	Tm	Tm 2SE	Yb	Yb 2SE	Lu	Lu 2SE	Hf	Hf 2SE	Pb	Pb 2SE	Th	Th 2SE	U	U 2SE
Z16-40 - 1	8.5	66.5	3.4	662	27	152.3	4.5	13810	350	56	27	120.7	6.1	542	46
Z16-40 - 2	13	97	6.1	906	35	183	6.6	12680	380	B.D.	14	87.5	5.3	279	12
Z16-40 - 3	14	39.2	2.2	357	25	75.2	5.6	11170	280	0	14	126.9	4.5	177	6.7
Z16-40 - 4	11	50.4	2.1	436	17	86.6	4.4	10180	290	3	11	162.6	5.3	113	4.5
Z16-40 - 5	8.7	52.5	2.3	471	13	90.6	4	11150	300	4	14	189.5	4.5	139.7	4.7
Z16-40 - 6	8.7	40.1	1.6	392	24	82.1	4.3	10660	300	24	21	156.3	5.2	191	20
Z16-40 - 7	12	44.7	2.5	414	18	85.1	3.6	11140	210	6	14	82	4.6	223.6	6.6
Z16-40 - 8	11	46.4	2.5	390	15	77.2	3.5	10510	210	B.D.	12	161.8	7.7	131	4.8
Z16-40 - 9	10	38.3	2.6	388	20	74	4.6	13000	290	B.D.	30	42.8	2.3	605	32
Z16-40 - 10	160	90	13	1060	150	300	57	16070	960	356	76	17	2.5	1184	65
Z16-40 - 11	11	56.5	2.3	498	19	98.5	3.1	11670	240	23	39	184.1	7.7	193	12
Z16-40 - 12	26	134.2	5.3	1233	36	258.4	8.1	13500	580	17	26	108.4	6.1	678	84
Z16-40 - 13	13	52.4	4.1	563	38	131.8	5.8	13350	370	52	32	43	4.4	699	51
Z16-40 - 14	47	82	12	796	97	163	21	13030	430	6	23	114	10	376	35
Z16-40 - 15	19	64.3	5.2	556	37	108	6.8	12590	270	39	22	85.4	9.9	418	16
Z16-40 - 16	16	16.4	2.2	127	38	22.9	5.8	13580	400	11	26	74.7	5.2	518	90
Z16-40 - 17	11	68.6	3.1	632	21	133.8	4.3	12430	310	B.D.	15	104.2	3.3	366	14
Z16-40 - 18	9.7	57.7	2.3	542	16	113.5	4.6	12120	240	B.D.	14	57	2.2	189.5	6.6
Z16-40 - 19	9.4	38.2	1.7	336	20	69.7	2.6	10450	200	13	24	115.1	5.3	96.9	5
Z16-40 - 20	7.6	51.3	2.2	478	24	96	4.4	14010	350	15	16	76	3.2	714	13
Z16-40 - 21	14	51	2.8	472	23	90.5	5.2	10620	270	21	20	200.6	8.2	169.5	8.7
Z16-40 - 22	35	162	6.2	1450	53	287	13	13040	410	17	17	189	17	615	24
Z16-40 - 23	11	93.5	3.3	823	16	163.4	5.1	11710	230	12	16	173.6	8.9	324.4	9.2
Z16-40 - 24	41	145.1	5.9	1368	67	285	14	13180	350	B.D.	14	77.5	9.2	592	57
Z16-40 - 25	55	90	16	840	140	169	30	12970	430	B.D.	11	76	13	284	44
Z16-40 - 26	21	66.1	3.8	593	47	114.8	7.1	12610	260	4	19	118.8	9.5	220	14
Z16-40 - 27	18	55	2.8	502	32	98.1	4.5	10830	260	0	15	174	16	148.7	8.8
Z16-40 - 28	13	30.5	1.7	299	22	58	5.5	10510	250	4	13	85	9.9	78	7
Z16-40 - 29	28	124.1	7.1	1203	49	249	14	13200	500	B.D.	15	50.2	1.8	427	15
Z16-40 - 30	14	56	3.1	481	23	99.8	3.8	10570	230	27	25	214.1	9.3	208.7	8.3
Z16-40 - 31	12	70	3.2	655	29	130.9	6.9	11650	330	17	14	52.5	2.2	103.7	4.2

Z16-40 - 32	10	53.4	2.2	450.9	8.7	83.2	4.5	14650	350	9	22	27.2	2.6	661	14
Z16-40 - 33	13	68.2	4.8	654	18	133.8	5	12120	310	39	44	95.1	7	229.2	7.7
Z16-40 - 34	24	63.2	5.3	584	43	123.5	6.9	12420	290	14	15	93.6	6	271	27
Z16-40 - 35	11	41.7	2.7	367	15	74.9	2.8	11240	240	17	14	135.1	8	170	12
Z16-40 - 36	10	43.1	1.5	387	14	78.7	3.6	11780	290	47	21	94	4	367	22
Z16-40 - 37	11	65.9	2.9	618	17	128.3	4.1	11940	200	B.D.	12	68.8	4	194.6	5.2
Z16-40 - 38	12	106.9	3.6	1079	33	225.8	5.5	13310	210	3	14	47.6	2.1	545	30
Z16-40 - 39	28	129.1	4.6	1255	30	265.8	7.3	13250	320	32	26	265	94	959	92
Z16-40 - 40	17	68.3	3.9	619	31	129.9	4.7	12410	390	11	19	60.1	5.8	217	16
Z16-40 - 41	8.7	35	1.7	362	16	75.5	3.2	12530	340	4	12	72.3	2.8	191	40
Z16-40 - 42	8.5	53	2.1	467	16	89.5	2.5	10100	230	B.D.	17	191.8	6.7	131	6.8
Z16-40 - 43	19	81.4	4.7	710	25	145.1	5.6	12090	310	49	20	233	11	342	16
Z16-40 - 44	13	68.5	4.2	634	35	129.6	6.7	12300	310	11	17	77.4	4.7	251	16
Z16-40 - 45	50	147	10	1315	78	258	15	10700	200	1	13	225	24	262	20
Z16-40 - 46	7.5	53.7	2.7	514	16	104.5	3.6	12470	270	3	15	38.9	2.2	134.4	5.2
Z16-40 - 47	13	91.6	3.4	885	29	177.3	4.7	12430	210	2	13	45.9	2.3	232.1	8.5
Z16-40 - 48	10	77.6	3.1	699	26	139	6.8	11530	220	12	13	211	10	375	31
Z16-40 - 49	14	41.5	2.7	454	20	120.9	5	13410	400	40	28	83	15	233	30
Z16-40 - 50	14	35.1	2.3	306	14	59.2	4	10180	180	10	18	137	22	103.2	7.7
Z16-40 - 51	22	79.2	6.2	656	34	136.3	4.2	9440	250	44	31	389	28	230.5	7.8
Z16-40 - 52	39	90	7.4	847	68	177	12	14030	320	7	13	72.1	6.6	832	41
Z16-40 - 53	15	47.9	2.6	546	30	120.6	8	14840	640	27	14	27.9	2	958	83
Z16-40 - 54	41	83.9	7	832	78	177	11	13710	350	282	60	45.9	2.9	1014	68
Z16-40 - 55	12	77.6	4	719	31	146	4.5	12130	360	15	18	109.1	4	238	8.8
Z16-40 - 56	11	37.3	2.6	346	16	69.1	3.8	10880	330	14	13	110	10	232	21
Z16-40 - 57	9.5	47.2	1.6	398	21	78.9	2.7	10260	220	9	23	147.5	6.3	102	4
Z16-40 - 58	9.3	53.2	2.9	484	22	97.7	4.1	11840	300	B.D.	10	141.5	6	188	5.4
Z16-40 - 59	25	97.5	5.9	981	36	212	10	13870	380	10	16	89.7	4.7	428	30
Z16-40 - 60	15	57	2.9	478	15	97.2	5.3	9930	240	9	11	232	11	152	5.4
Z16-40 - 61	9.6	34.6	2.5	363	18	86.4	5.1	12860	330	0	11	57.7	3	293	13
Z16-41 - 1	14	60.2	2.5	560	22	103.5	6.5	10910	190	B.D.	8.2	83.6	4	139.4	5.9
Z16-41 - 2	8.8	49	2.6	427	21	82.7	3.3	9440	120	2.1	9.3	20.9	1.6	36.1	2.1

Z16-41 - 3	20	40.7	4.6	348	33	69.7	7.8	9020	150	20	22	16.6	2.7	25.6	2.5	
Z16-41 - 4	41	46.9	6.3	420	57	82	11	10600	650	B.D.	14	36	7.3	48.9	8.8	
Z16-41 - 5	9.6	22.8	2.8	224	13	49.1	3.1	11830	320	0	20	24.7	2	63.7	6.1	
Z16-41 - 6	12	28.7	2.5	268	19	54.4	3.5	11580	230	0	13	26.9	2.5	64.7	3.3	
Z16-41 - 7	5.8	30.5	1.9	263	12	54.2	2.6	11260	300	16	22	21.4	1.4	51.1	2	
Z16-41 - 8	8.5	39.9	2.7	356	18	73.5	3.7	11170	160	B.D.	15	43.5	3.2	110.2	4.9	
Z16-41 - 9	8.5	23.8	1.9	226	13	44.4	3.4	11390	370	B.D.	9.6	18.5	1.9	46.8	5.7	
Z16-41 - 10	13	28.1	2	255	21	52	3.8	11060	380	B.D.	16	19.6	3	46.2	8.1	
Z16-41 - 11	18	60.4	4.2	512	26	96	3.1	11760	340	7	19	67	3	111.3	7.4	
Z16-41 - 12	12	30.3	2.4	273	23	53.9	3.3	9940	160	6	10	15.3	1.5	30.7	2.2	
Z16-41 - 13	8.8	40.7	1.2	355	13	67.2	2.9	9170	170	B.D.	9.6	17.2	1.3	25.3	1.3	
Z16-41 - 14	11	53.2	2.7	447	30	85.4	4.5	11230	530	B.D.	9.4	53	7.7	87	16	
Z16-41 - 15	4.5	18.1	1.1	179.6	9.2	36.2	1.6	11670	200	15	16	18.2	1.1	58.3	2.8	
Z16-41 - 16	12	23.7	2.4	221	20	44.1	4.2	13650	440	1	24	21.6	1.5	74.7	3.7	
Z16-41 - 17	12	30.6	2.3	260	22	51.8	3.9	9840	210	B.D.	17	13.7	1.5	23.2	1.7	
Z16-41 - 18	26	37.5	4.4	335	38	67	7.8	11210	370	B.D.	12	30.6	6.8	60	12	
Z16-41 - 19	21	89.6	5.7	731	36	137.1	5.5	11570	450	B.D.	11	112.5	9.2	182	13	
Z16-41 - 20	59	93	12	785	87	150	15	11810	420	16	14	141	21	206	27	
Z16-41 - 21	9.4	29.1	1.7	267	11	53.8	2.3	10680	240	B.D.	13	18.2	1.3	36.4	1.7	
Z16-41 - 22	27	91.8	4.6	785	41	146.9	9.7	10500	400	1	18	124	10	171.6	9.7	
Z16-41 - 23	6.9	20	1.2	188.7	9.9	39.1	2.4	11980	220	5	15	21.11	0.96	62.5	2.3	
Z16-41 - 24	6.2	22	1.8	202	13	43.3	3.1	11120	290	7	14	15.5	1.3	39.5	5	
Z16-41 - 25	8.2	24.8	1.7	226	14	47.6	2.6	11850	420	B.D.	12	21.5	2.6	59.2	6.9	
Z16-41 - 26	7.8	26.1	1.5	252	13	52.1	3	11740	280	1	18	25.2	2.3	63.6	4	
Z16-41 - 27	12	29.1	2.9	273	15	54	3.1	9940	240	B.D.	9.4	16.8	1.5	31.7	3.4	
Z16-41 - 28	6.5	29.1	1.8	257	12	50.3	3.4	10390	400	0	15	21	1.8	44	4.9	
Z16-41 - 29	9.6	44.5	3.3	388	19	74	2.6	10260	240	B.D.	16	32	2.3	50.2	3.2	
Z16-41 - 30	5.7	21.2	1.2	186	8.2	39.7	1.8	9960	200	0	13	16.9	2.3	26.5	2.6	
Z16-41 - 31	20	41.6	2.9	380	26	74.3	5.4	9940	250	B.D.	13	28.2	3.3	41	4.3	
Z16-41 - 32	4	23.1	1.9	213	11	45.5	2.2	11830	300	B.D.	12	22.6	1.8	66	6.2	
Z16-41 - 33	7.6	34.8	1.5	280	13	49.3	2	11500	200	3	15	18.9	1.1	48.2	1.9	
Z16-41 - 34	20	40.5	4.6	342	30	65.5	5.2	9570	360	B.D.	8.7	24.2	3.2	36.1	3.8	
Z16-41 - 35	8.6	48.5	2.1	433	16	83.3	4.8	10400	470	2	15	44.4	6.2	66	13	

Z16-41 - 36	5.5	19.3	1.1	186.5	9.7	39.5	2.1	11710	280	2	15	17.8	1.2	54.8	3			
Z16-41 - 37	6.2	23.7	2.6	238	28	50.9	6.6	11180	350	B.D.	12	18.6	2	43.5	6.3			
Z16-41 - 38	5.6	19.8	1.2	179.9	5.6	35.3	1.8	9920	180	B.D.	13	8.42	0.63	19.6	1.5			
Z16-41 - 39	16	55.1	3.9	481	29	92.6	5.2	11750	210	8	18	59.3	5.8	112	11			
Z16-41 - 40	6.3	36.6	1.8	331	16	61.6	2.6	9340	190	B.D.	10	19.2	1.1	29.9	1.4			
Z16-41 - 41	4.2	20.11	0.95	199.8	9.5	42.8	2.8	11540	220	B.D.	10	17	1.1	63.9	3.5			
Z16-41 - 42	8.9	21.6	2.7	228	15	46.1	3.2	11920	590	B.D.	16	21	2.7	65	14			
Z16-41 - 43	5	32.6	1.1	295	10	56.8	2	9720	160	2.4	9.3	14.8	1.1	25	1.5			
Z16-41 - 44	28	42.9	5.9	372	43	69.3	7.2	10880	240	22	13	36.6	7.1	59.2	7.5			
Z16-41 - 45	7.2	26.6	1.5	250	18	50.7	2.1	9550	130	2	17	20.3	2	37.1	2.5			
Z16-41 - 46	11	27.6	5.1	238	14	52.5	1.9	11300	310	12	23	24.3	1.4	57	2.3			
Z16-41 - 47	7.3	46	1.7	399	17	79.1	3.8	10010	230	0	12	33.2	1.3	45.7	1.8			
Z16-41 - 48	7.3	35.3	1.1	309	10	59.1	2.6	9670	190	B.D.	10	21.2	1.3	35.9	1.7			
Z16-41 - 49	9	67	2.9	548	19	103.3	3.5	9650	230	B.D.	15	51.6	3.3	58	2.5			
Z16-41 - 50	20	28.7	3.2	227	29	47.2	4.7	9430	130	B.D.	13	12.5	3.8	16.1	2.4			
Z16-41 - 51	10	21.8	2.2	216	16	44.4	3.6	11040	280	B.D.	12	17.8	1.2	45.1	4.1			
Z16-41 - 52	11	69.4	4.9	602	38	111.4	3.6	10930	560	B.D.	16	74.6	3.5	114.9	6.3			
Z16-41 - 53	12	24.3	3.6	249	26	46.4	3.7	12080	370	10	14	23	4.3	53.5	7.1			
Z16-41 - 54	7.9	24.4	1.9	239	14	49.6	1.9	11350	170	B.D.	9.4	21.3	2.4	54.3	3.7			
Z16-41 - 55	19	42.9	4.3	375	34	70.8	4.9	10720	200	1	10	31.4	2.4	48.4	2.2			
Z16-41 - 56	66	38	13	360	110	69	18	12220	600	1	19	102	45	131	50			
Z16-41 - 57	9.5	23.4	2.4	232	19	44.9	3.4	11850	250	1	15	21.7	1.9	56.9	3			
Z16-41 - 58	8.8	49.7	3.1	436	21	82.2	3.1	11390	300	5	10	49.4	2.4	78.6	3.4			
Z16-41 - 59	9.1	35.8	2.7	346	18	66.4	3.4	12270	290	B.D.	12	43.1	3.2	92.6	6.7			
Z16-41 - 60	5.4	25.2	1.4	254	8.4	49.5	2.2	13580	250	11	16	28.7	1.4	82.9	2.7			
Z16-42 - 1	14	50.7	2.9	424	15	79.9	2.5	9880	290	2	14	25.4	1.6	39.2	2.2			
Z16-42 - 2	11	35	1.9	324	16	64.3	3.2	11660	260	11	16	37.6	2.9	68.1	2.8			
Z16-42 - 3	8.5	22.1	1.3	206	13	41.3	2.9	10580	220	B.D.	11	12.5	1.2	29.1	2.4			
Z16-42 - 4	14	46.7	2.2	421	26	80.5	3.9	10350	260	B.D.	14	41.4	2.9	62.2	2.5			
Z16-42 - 5	9.3	28.7	2.4	263	18	52	4	10000	240	B.D.	8.5	41.9	2.6	64.1	2			
Z16-42 - 6	7.6	27.5	1.5	253	17	51.3	3.7	11940	450	21	20	23.1	1.9	59.2	3.9			
Z16-42 - 7	11	48.3	2.4	411	19	76.9	2.9	9760	160	5	14	38.6	2.2	48.9	2.2			

Z16-42 - 8	14	39.1	3	353	20	68.6	4.3	11630	270	1	12	41.2	4.2	76.1	3.8									
Z16-42 - 9	9.9	22.1	1.9	213	15	40.8	2.8	11620	290	10	19	15.7	1.8	38.9	3.9									
Z16-42 - 10	7.7	19	1.8	186	17	35.9	3.2	9760	220	B.D.	6.2	5.79	0.6	14.8	1.4									
Z16-42 - 11	8.1	25	2.4	233	18	45.4	3	10940	370	B.D.	12	16.5	1.8	35.5	4.1									
Z16-42 - 12	6	24	1.3	216	15	42.8	3	10430	200	4	14	10.4	1.3	26.5	1.9									
Z16-42 - 13	19	71.3	4.1	619	34	112.7	5.6	10720	320	4	13	82.7	6.3	116.1	7.3									
Z16-42 - 14	7.7	25.3	1.8	240	12	48.9	2.9	12480	270	B.D.	17	33.2	2.9	69	3.5									
Z16-42 - 15	5.9	26.8	1.5	243	12	47.5	2	9950	150	15	13	9.13	0.99	16.9	1.4									
Z16-42 - 16	18	43.3	3.9	389	38	74.4	4.3	10290	270	B.D.	20	26.1	3.2	37.8	3.5									
Z16-42 - 17	16	57.9	2.8	509	28	96.1	4.2	9890	210	6	15	47.3	2.2	63.2	4.4									
Z16-42 - 18	6.1	17.7	1.9	159.9	9.7	33.8	2.2	10840	220	8	22	9.2	1.2	24.3	2.6									
Z16-42 - 19	7.4	25.4	2.6	234	14	48.2	3.6	11950	370	2	18	22.1	1.3	59.4	4.6									
Z16-42 - 20	7.4	24.7	1.8	218	15	44.1	2	11590	250	B.D.	6.4	20.3	1.2	46	2.2									
Z16-42 - 21	10	23.8	3.1	227	21	44.4	3.6	11060	250	B.D.	11	13.4	2	39.7	3									
Z16-42 - 22	7.6	20.8	1.4	214	10	43.5	3.2	11920	260	9	16	18.2	1.4	51.2	2.3									
Z16-42 - 23	13	29.6	2.3	256	18	51.1	3.2	9860	310	3	14	11.7	1.8	20.2	2.3									
Z16-42 - 24	11	29.2	2.6	278	16	55.1	2.2	10520	320	10	13	18.7	1.7	36.9	4.7									
Z16-42 - 25	9.8	25.2	1.8	242	13	47.6	2.7	11970	200	B.D.	13	31.4	4.1	63.5	5.2									
Z16-42 - 26	5.3	18.29	0.99	177.8	9.9	35.3	1.6	11910	250	B.D.	12	18.02	0.79	50.7	1.8									
Z16-42 - 27	12	22.2	2.2	206	10	42.1	2.4	11530	290	B.D.	13	15.4	1.7	40.1	2.5									
Z16-42 - 28	12	28.5	2	275	18	51.3	3	11630	280	0	10	38.1	6.1	62.2	6.1									
Z16-42 - 29	4.5	22.4	1.8	221	11	45.5	1.3	11720	260	B.D.	6.4	21.9	1.6	60	2									
Z16-42 - 30	3.3	22.4	1.2	214	11	43.3	1.3	11900	140	14	12	21.2	1.4	62.3	3.9									
Z16-42 - 31	80	112	11	773	50	123	11	11230	480	8	39	53.9	5.1	58	4.3									
Z16-42 - 32	9.7	30.4	2.2	264	11	54.8	3.2	10860	230	16	14	23.9	2.6	43.2	3.4									
Z16-42 - 33	14	46.3	4.2	422	23	77.3	3.9	10280	340	10	11	28.7	2.1	44.7	2.5									
Z16-42 - 34	6.8	20.1	1.9	182	13	36.8	1.5	12130	550	3	12	19.6	2.1	46.4	6.5									
Z16-42 - 35	25	51.9	5	448	33	87	6.5	10450	400	11	12	42.5	5.4	55.2	6.2									
Z16-42 - 36	7.9	43.3	1.8	393	12	79.9	3.5	10830	250	5	12	34.2	1.3	58.3	2.2									
Z16-42 - 37	7.2	47.6	2.2	414	11	78.1	2.4	10420	200	19	17	32.1	1.5	49.9	2.3									
Z16-42 - 38	8.1	33.2	1.6	309	14	56.7	2.9	9720	180	B.D.	11	13.7	1.1	25.9	1.4									
Z16-42 - 39	12	27.7	2.4	258	21	50.1	3.7	10010	170	B.D.	12	12	1.1	22.2	1.6									
Z16-42 - 40	21	48.7	3.9	434	28	77.1	4.4	9910	150	B.D.	14	31.6	3.3	39.1	2.4									

Z16-42 - 41	12	50.3	3.2	435	16	82.7	3.6	10060	370	B.D.	11	43	4.8	58.8	5.2										
Z16-42 - 42	18	37.4	4.2	339	30	63.9	5	10470	270	B.D.	15	22.4	3.2	34	3.7										
Z16-42 - 43	10	20.7	1.8	199	11	38.3	1.9	12040	370	B.D.	8.8	18.2	1.8	56.1	4.8										
Z16-42 - 44	22	52.7	3.3	464	15	86.8	5	11470	570	B.D.	25	48.5	6.3	71	13										
Z16-42 - 45	7.1	37.1	1.4	318.3	9.6	61.2	2.1	9460	200	0.5	9.7	17.82	0.98	26.2	0.77										
Z16-42 - 46	6.4	17.3	1.6	165.9	8.2	34.1	2.4	11650	250	B.D.	15	15.3	1.4	41.7	2.5										
Z16-42 - 47	13	27	2.4	246	22	49.8	3.9	10370	290	0	18	14.1	1.4	27.8	1.9										
Z16-42 - 48	11	38.5	3	329	34	63.5	4.4	10410	250	9	19	29.8	3.5	46.5	2.6										
Z16-42 - 49	10	26	2.2	244	15	48.4	4.4	10450	280	6	13	17.6	1.6	30.1	2.2										
Z16-42 - 50	11	37.2	1.3	324	13	63.2	2.1	10020	320	7	18	23.4	2	36.1	1.8										
Z16-42 - 51	13	37.6	2.4	332	24	61.4	3.6	10250	270	3	21	22.5	2	40.5	3.6										
Z16-42 - 52	11	37.2	2	330	19	63.7	3.7	10180	200	4	14	24.6	1.5	39.5	2										
Z16-42 - 53	6.4	25.6	1.9	227	10	49.2	2.2	13420	320	B.D.	13	30.9	1.9	83	5.4										
Z16-42 - 54	9.4	20.5	2.8	206	16	40.4	2.9	10730	280	B.D.	13	15.9	2.6	35.8	3.3										
Z16-42 - 55	12	43.5	2	381	18	71.1	3.2	9610	260	B.D.	14	24.7	2.6	34.7	2.2										
Z16-42 - 56	14	47.5	4.4	419	23	80.6	4.6	9950	220	B.D.	15	32.3	2.6	48.8	3.8										
Z16-42 - 57	12	36	2.2	330	21	63.9	3.6	10510	300	9	15	17.6	1.8	32.4	4.8										
Z16-42 - 58	21	44.5	4.1	396	19	73.3	7	10050	230	B.D.	16	26.6	3.3	40.4	3.1										
Z16-42 - 59	5.5	25.4	2.1	234	14	51.3	3	11940	550	B.D.	10	24.6	3.1	67	3.2										
Z16-42 - 60	5.3	22.3	1.3	210	11	41	1.7	9730	170	B.D.	10	15.3	1.9	20.7	0.72										
Z16-45 - 1	18	47.8	2.2	396	29	77.2	5.3	9900	350	B.D.	12	149	14	177	13										
Z16-45 - 2	12	35.8	3.2	316	17	61	2.3	10100	300	1	16	149.8	6	179	16										
Z16-45 - 3	6.4	28	1.4	280.3	9.7	57.4	2.5	12520	300	B.D.	8.2	122.4	5.4	315	35										
Z16-45 - 4	11	32.9	3.2	297	22	57.3	3.6	10180	170	B.D.	12	133.5	8.9	161	12										
Z16-45 - 5	15	35.9	3.4	304	24	55.8	4.7	9650	220	B.D.	8.7	94	12	124	10										
Z16-45 - 6	6.8	22.3	1.3	211.6	9.6	40.2	1.9	9240	210	0.5	9.8	96.1	4.1	208.6	5.5										
Z16-45 - 7	9.4	46.6	3.1	384	21	74.9	3.9	10360	260	B.D.	15	245	11	324	12										
Z16-45 - 8	10	27	1.8	253	11	48.3	2	11410	240	8	12	137.6	7.3	218.6	7.1										
Z16-45 - 9	17	48.7	2.7	410	17	81	4.9	10810	670	24	19	224	18	296	35										
Z16-45 - 10	5.7	21.9	1.4	196.5	8.3	38.7	1.5	9640	210	3	11	72	2.9	100	3.1										
Z16-45 - 11	5.3	25.7	1.6	237.7	8.9	48	1.8	10460	250	B.D.	7.9	101.8	2.9	159.7	3.8										
Z16-45 - 12	6.1	26.7	1.4	236	10	45.2	2.1	10040	190	11	14	158	15	283	29										

Z16-45 - 13	4.3	18.4	1.1	182	11	35	2.8	13390	330	16	18	113.3	4.7	335	23			
Z16-45 - 14	8.1	35.4	1.6	311	10	58.1	2.3	10220	170	14	13	175.5	7.5	259.5	9.6			
Z16-45 - 15	9.8	36.6	1.5	338	11	67.2	4.1	12160	330	14	19	189.2	9.6	530	45			
Z16-45 - 16	7.4	21.4	1.7	204	11	42.5	2.8	12620	320	B.D.	9.4	110.9	5.9	284.6	7.8			
Z16-45 - 17	11	29.4	2.6	284	19	59.2	4.5	12910	320	5	14	144	12	438	22			
Z16-45 - 18	13	51.8	2	441	18	83.4	6.3	9920	330	B.D.	14	210	15	235	20			
Z16-45 - 19	6.4	27.3	2.4	286	26	60.3	5.1	13780	260	3	14	150.7	8	599	55			
Z16-45 - 20	9.1	25.5	1.5	236	11	44.9	2.3	11810	140	B.D.	12	147.3	6.4	290	11			
Z16-45 - 21	17	66.9	5	599	32	114.1	6.9	11920	340	B.D.	15	489	19	886	42			
Z16-45 - 22	21	42.4	8.9	348	32	66.1	8.7	14030	580	3	12	156	18	829	44			
Z16-45 - 23	4	23.6	1.9	215	14	40.2	2.2	10810	240	B.D.	11	102.3	4.9	173.4	7.1			
Z16-45 - 24	6.3	26.7	2.3	233.3	6.5	42	2.3	11400	330	6	15	112.1	2.6	90	12			
Z16-45 - 25	18	50	4	435	25	82.2	6.5	10420	210	4	13	230	27	284	28			
Z16-45 - 26	17	47.8	2.6	423	24	81.3	6	9920	300	5	11	206	21	263	27			
Z16-45 - 27	10	29.4	1.7	254	11	49.2	2.1	10360	280	0	11	188	30	195	10			
Z16-45 - 28	7.4	29.2	1.7	260	10	52.4	1.8	11750	200	B.D.	8.1	166.9	4.6	301	10			
Z16-45 - 29	7.7	24.6	1.8	221	11	44.2	1.8	10650	200	B.D.	18	146.5	6	228	4.9			
Z16-45 - 30	7.1	32.9	1.7	314	12	61.9	2.1	12530	260	B.D.	8	249	13	506	45			
Z16-45 - 31	39	58.8	6.3	522	72	94	11	12490	240	B.D.	10	345	59	582	94			
Z16-45 - 32	12	39.2	2.4	354	13	66.4	2	10160	240	6	17	146	8.2	216.1	6.7			
Z16-45 - 33	4.9	25.4	1.2	249	14	48.7	2	9960	250	B.D.	13	93.3	2.7	159.6	4.1			
Z16-45 - 34	5.4	28.8	1.7	250	12	51.3	1.8	9740	230	0	15	112.2	2.3	160.8	3.7			
Z16-45 - 35	12	54.7	3.4	473	18	84.3	4.3	9870	220	7	18	243.6	8.3	400	14			
Z16-45 - 36	42	53.7	6.8	489	61	90	11	11940	360	B.D.	12	353	63	523	52			
Z16-45 - 37	6	19.1	1.8	193	12	38	2.3	12510	350	11	15	125	11	297	22			
Z16-45 - 38	12	46.1	2.3	387	23	72.5	5.3	10540	240	2	15	216	13	272	15			
Z16-45 - 39	13	27.4	1.9	267	19	54.2	3.8	11800	250	2.8	9.6	156	16	278	15			
Z16-45 - 40	38	88.8	5.5	589	45	88.5	6	11770	320	19	38	245	18	301	14			
Z16-45 - 41	9.3	39.5	3.5	339	19	67.2	6	10780	270	B.D.	16	174	18	228	19			
Z16-45 - 42	9.6	22.8	2.1	216	19	43.5	2	11190	340	8	16	82.8	5.5	167.8	9.3			
Z16-45 - 43	18	52.6	3.4	448	42	86	7.1	10920	380	16	23	255	29	315	38			
Z16-45 - 44	30	42.1	4.6	376	50	68.6	8.2	9730	250	8	19	204	39	196	36			
Z16-45 - 45	9.4	27.7	3.2	259	15	50.1	2.4	12820	340	0	20	135.5	8.8	398	43			

Z16-45 - 46	40	60.6	8.4	507	60	94	10	12530	410	5	17	337	75	740	130	
Z16-45 - 47	7	30.4	1.7	309	17	67.4	4.3	13870	340	B.D.	12	177.9	9.3	825	33	
Z16-45 - 48	15	38.6	3.6	345	16	65.6	3.7	9330	340	B.D.	12	133.4	4.9	148.4	6.3	
Z16-45 - 49	28	84.9	6	584	29	101.1	6.4	14180	260	14	21	204	12	651	16	
Z16-45 - 50	7.8	23.8	1.4	208	12	40.8	1.8	9600	150	B.D.	14	119.4	3.3	187.3	4.1	
Z16-45 - 51	13	36.4	3.1	332	21	69.7	3.8	12310	230	B.D.	10	259	24	473	49	
Z16-45 - 52	12	31.7	3	287	12	52.7	2.4	11720	350	4	16	163.7	7.8	143	14	
Z16-45 - 53	17	69.6	5.2	604	38	116	7.4	13000	440	4	21	440	45	950	160	
Z16-45 - 54	6.4	49.2	2.8	416	18	79.4	4.6	8930	270	3	11	154.4	6.4	195.7	9.1	
Z16-45 - 55	15	43.9	2.7	376	18	70.9	3.3	11130	300	1	10	214	20	293	27	
Z16-45 - 56	9.5	29.9	2.4	260	12	50.2	3.4	10470	170	B.D.	13	118.7	6.8	178.5	8.6	
Z16-45 - 57	18	50.9	3.9	426	24	83	5	10620	260	31	24	265	19	321	16	
Z16-45 - 58	5.5	28.8	2.4	244	9.3	46.2	2.3	10660	160	3	11	158.9	4	263.9	6.9	
Z16-45 - 59	15	51.4	2.2	430	22	82.3	2.4	10750	220	B.D.	11	264	13	320	20	
Z16-45 - 60	27	40.9	4.8	334	37	65.6	6.2	11290	410	15	20	181	28	273	22	
Z16-01 - 1	29	75	5.4	659	56	124	10	13710	350	B.D.	11	345	45	798	45	
Z16-01 - 2	110	368	21	2840	190	467	32	14640	370	240	48	664	47	1856	74	
Z16-01 - 3	28	90.7	6.7	785	51	146.2	8	16330	750	7	18	1000	120	1285	60	
Z16-01 - 4	9.3	46.3	2.5	395	15	74.6	3.3	11940	310	B.D.	16	409.3	9.7	396	13	
Z16-01 - 5	13	48.2	2.6	436	30	80.6	4.5	11020	300	B.D.	11	341	7.7	305	11	
Z16-01 - 6	12	37.5	2.4	317	12	59.8	3.4	11570	310	8	12	142.3	6.9	329	15	
Z16-01 - 7	3.9	13.86	0.86	128.9	6.6	26.1	1.4	12990	230	16	14	113.7	3.5	173.6	6	
Z16-01 - 8	10	62.6	2.8	568	20	108.1	4	14290	290	B.D.	8.5	174	24	722	16	
Z16-01 - 9	6.4	26.7	1.2	254	10	46.9	1.3	11420	220	B.D.	13	244.6	7	222.3	6.9	
Z16-01 - 10	8.1	40.2	2	346	18	66	2.2	12840	240	B.D.	9.7	444	11	643	16	
Z16-01 - 11	13	53.3	4.1	426	29	78.2	6.3	11230	340	B.D.	7.3	298	23	270	18	
Z16-01 - 12	11	32.6	1.7	286	10	57.7	3.9	11590	220	5.4	9.3	558	41	310	14	
Z16-01 - 13	4.4	16.1	1.1	144.7	6.7	30.4	1.3	12280	270	13.2	9.1	84.6	3.1	154	11	
Z16-01 - 14	72	170.2	9	1318	80	228	13	13280	350	47	18	820	59	943	42	
Z16-01 - 15	19	31.9	3.2	268	31	49.5	4.2	9970	150	B.D.	13	160	18	121.7	9.3	
Z16-01 - 16	9.1	46.1	2.8	432	20	91.8	3.7	13300	390	21	21	441	12	435	22	
Z16-01 - 17	10	36.9	2.1	320	18	64.7	3.8	11300	270	B.D.	13	300	12	231.1	9	

Z16-01 - 18	7.1	33.2	1.6	294	15	56.3	2.5	11390	190	0	11	136.7	5.1	189.8	8.7					
Z16-01 - 19	3.7	22.7	1.3	191	9.2	38.8	2.3	12700	350	30	18	477	78	260.7	8.6					
Z16-01 - 20	4.2	16.65	0.93	143	8.6	27.3	1.5	11270	240	B.D.	6.7	80.8	2.1	78.9	1.9					
Z16-01 - 21	13	19.7	2.9	189	21	33	2.2	10850	290	20	27	95.5	8.4	99.6	7.8					
Z16-01 - 22	8.2	32.8	1.4	336	17	69.2	2.1	10930	200	7	12	79.5	5.3	166.4	4.7					
Z16-01 - 23	5.3	23.4	1.1	198	11	37.1	1.2	10740	150	B.D.	5.2	87.2	3	62.8	2.6					
Z16-01 - 24	7.3	21.5	1.7	189	11	39.2	2.3	11210	220	6	10	194	11	140.7	8					
Z16-01 - 25	7.7	29.1	1.6	259.2	7.4	48.4	1.6	12210	250	B.D.	8.7	337	29	344	10					
Z16-01 - 26	8.9	38	2.1	319	16	57.8	2.7	9740	210	8.4	9.9	118.3	6.9	60.6	2.7					
Z16-01 - 27	5.4	21.21	0.92	185.1	7.7	36.5	1.9	11060	260	B.D.	3.9	130.5	7.4	127.1	5.5					
Z16-01 - 28	5.4	26.4	1.5	240	12	45	2.2	11210	190	6	12	209.7	3.4	174.7	6.1					
Z16-01 - 29	7.8	33.2	2	287	11	53.9	2.8	10870	190	11	12	248.7	5.2	240.2	9.6					
Z16-01 - 30	9.7	33	1.4	297	14	57.2	2.8	11880	250	10.6	9.5	237	8.7	364	20					
Z16-01 - 31	6	28.7	1.6	260.9	8.4	49.9	1.4	11560	230	2.3	9.7	231.5	8.9	235.7	7.8					
Z16-01 - 32	10	21	2.6	194	18	37	5.2	11780	240	15	20	228	30	211	22					
Z16-01 - 33	14	39.1	3.1	326	23	60.5	3.7	9540	280	3.6	8.7	146.7	8.6	77.5	4.8					
Z16-01 - 34	5.4	23.4	1.5	204.3	7.7	41.6	1.8	12780	270	B.D.	7.8	183.1	7.9	210.4	3.6					
Z16-01 - 35	9.4	40.4	1.4	351.9	9.1	64.4	2.2	12340	210	B.D.	10	269.6	4.9	405.4	6.6					
Z16-01 - 36	29	42.1	5.8	343	29	66.4	8.4	11280	240	12	18	379	24	267	16					
Z16-01 - 37	9.5	23.1	2.4	213	13	45.1	2.5	12000	290	B.D.	12	260	6.2	266.9	6.7					
Z16-01 - 38	13	64.8	3.9	525	24	98.8	4.2	10310	270	2	12	646	20	448	14					
Z16-01 - 39	5	25.8	1.1	223	12	43.7	1.6	11610	210	1	10	204	4.2	218.9	6.1					
Z16-01 - 40	8.5	36.8	1.7	310.6	9.9	58.7	2.7	11710	200	B.D.	7.1	323	12	336	11					
Z16-01 - 41	6.9	31.4	1.8	271	13	50.9	2.6	12560	380	31	19	386	20	433	14					
Z16-01 - 42	9.1	34.8	1.8	289	16	54.6	2.5	10520	330	13	13	200.1	7.5	118.8	4.2					
Z16-01 - 43	14	63.7	3.1	500	36	86.9	3.9	10470	230	B.D.	13	630	52	381	15					
Z16-01 - 44	9.5	41.1	2.4	336	12	62.8	2.7	11050	170	B.D.	10	320.6	9.2	279.3	6.7					
Z16-01 - 45	4.3	11.8	1.4	112.5	8.1	23.8	1.2	11880	330	1	14	87.3	4.5	122.2	3.6					
Z16-01 - 46	9.3	35.1	2.6	296	21	62.4	4.1	10690	280	2	26	144.4	5.4	186	19					
Z16-01 - 47	5.1	36.2	1.5	297.1	8.9	56.6	2.1	10350	190	7	13	143.1	3.5	81	3.1					
Z16-01 - 48	5.2	24.8	1.3	209.2	9.5	44.5	1.6	12960	220	B.D.	9.8	274	9.2	390	10					
Z16-01 - 49	6.9	30	2.5	249	12	48.8	3.3	12750	400	2	11	238	8.7	315	15					
Z16-01 - 50	41	90	11	688	54	128	22	11810	540	B.D.	11	760	78	485	18					

Z16-01 - 51	51	126.7	4.9	853	47	140.9	7.1	12440	290	9	17	197	9.2	336.6	9.7									
Z16-01 - 52	7.5	22.9	1.7	182	14	38.2	3.3	10510	240	13	13	94	9.3	69.6	6.1									
Z16-01 - 53	6.3	20.7	1.5	194	12	37.7	2.6	11320	250	5	15	88.3	5.2	104.3	4.2									
Z16-01 - 54	7.3	22.5	1.6	205.5	9.7	41.3	2.8	11870	330	B.D.	7.5	176.5	8.5	243.9	8.8									
Z16-01 - 55	10	38.6	2.8	325	16	65.8	2.7	11560	320	B.D.	8.2	310	11	285.8	9.4									
Z16-01 - 56	5.3	24	1.6	211.8	8.7	41	2.7	11570	240	B.D.	13	186.1	7.6	193.1	6.5									
Z16-01 - 57	15	26.5	2.3	237	14	43	1.7	10410	340	B.D.	4.3	136.2	8.5	93.8	4									
Z16-01 - 58	18	45.5	3.6	367	20	64.6	4	12620	520	12	17	296	15	602	21									
Z16-01 - 59	12	18.7	1.2	160	11	31	3.1	10930	360	1	23	83.5	8.7	78.7	5.9									
Z16-01 - 60	16	35.2	2.9	280	22	53.8	3.7	10340	220	10	13	204	31	136	14									
Z16-01 - 61	22	85.7	3.8	697	19	121.4	6.4	10890	330	10	15	1032	37	822	21									
Z16-01 - 62	7.2	17.5	2	154	15	28.7	2.6	9990	220	11	46	88	12	92	12									
Z16-01 - 63	4.4	14.86	0.96	143.6	6.9	27.5	1.5	10770	150	B.D.	6.2	66.7	1.9	64.9	2									
Z16-01 - 64	63	102	12	893	99	168	20	13660	410	B.D.	9.7	569	67	1160	140									
Z16-01 - 65	9.1	29.4	1.2	254.1	8.6	48.7	2.9	11730	360	8	11	224.6	9.9	274	31									
Z16-33 - 1	110	77	20	620	160	113	27	10710	280	30	18	1870	550	889	35									
Z16-33 - 2	37	33	7	330	70	78	10	14570	500	B.D.	12	205	30	784	52									
Z16-33 - 3	13	43.1	4.2	425	45	84.1	5.2	10900	260	B.D.	9.7	903	59	773	27									
Z16-33 - 4	9.7	41.3	5.3	385	37	75.5	5.5	13150	340	33	16	593	48	1231	51									
Z16-33 - 5	21	40.9	7.1	323	42	60.6	8.3	14800	530	22	17	256	21	691	22									
Z16-33 - 6	6.4	16.5	1.6	152	15	38.6	3.5	14260	390	3.7	7.9	169.7	8.8	765	21									
Z16-33 - 7	2.1	5.8	1	75.5	4.2	21.3	1.5	13160	390	B.D.	8.4	70	4.1	603	18									
Z16-33 - 8	16	16.8	4.4	191	33	50.8	7.2	16740	870	5	16	111	10	688	36									
Z16-33 - 9	21	85.3	5.1	688	39	129.5	9	13790	340	77	28	590	110	1428	35									
Z16-33 - 10	60	112	16	940	100	166	17	13010	600	29	24	1760	170	944	56									
Z16-33 - 11	15	14.8	2.1	153	13	32.7	3.6	14450	730	B.D.	8.3	97	11	530	26									
Z16-33 - 12	76	158	33	1190	150	224.4	8.6	1.41E+04	1.10E+03	45	55	1110	210	1637	90									
Z16-33 - 13	11	13.9	1.2	143	18	36.5	2.9	12140	540	B.D.	15	175	27	637	36									
Z16-33 - 14	12	15.2	2.3	163	18	37.1	1.9	14780	340	B.D.	6.8	112	11	675	20									
Z16-33 - 15	71	254	13	1972	90	356	15	14410	450	87	14	684	31	1551	63									
Z16-33 - 16	83	129.9	8	1211	65	246	17	9240	360	44	24	8.70E+03	1.80E+03	3080	140									
Z16-33 - 17	24	59.8	4.4	530	44	102.7	4.9	13080	280	28	21	398	20	1360	30									

Z16-33 - 18	37	39	11	323	55	62.1	8.4	13890	310	32	14	620	140	673	16
Z16-33 - 19	12	22.9	1.9	202	15	38.3	2.5	10490	180	27	32	604	28	723	22
Z16-33 - 20	5.5	20.9	2.6	194	16	46.7	3.1	13470	280	9	13	177.6	6.4	846	18
Z16-33 - 21	11	10.5	2.6	119	14	34.7	4.2	13200	520	B.D.	5.2	67.1	7	928	51
Z16-33 - 22	4	15.27	0.94	140.6	7.3	26.5	1.4	12240	220	B.D.	8.4	181.5	8	291	8.8
Z16-33 - 23	15	79.2	4.6	1039	48	312	13	2.70E+04	1.20E+03	35	22	481	20	4460	110
Z16-33 - 24	26	59.5	5.3	529	35	99.2	7.1	8270	460	6	18	1187	88	703	42
Z16-33 - 25	6	23.3	1.5	248	12	57	3.6	14640	240	4	10	250	13	1160	29
Z16-33 - 26	130	127	33	1110	450	183	28	1.16E+04	1.00E+03	430	150	1.49E+04	5.30E+03	1550	110
Z16-33 - 27	3.4	12.4	1.6	131.1	7.1	26.7	2.1	11320	330	B.D.	7.1	216.3	4.4	346.2	7.6
Z16-33 - 28	20	52.9	2.8	439	21	83.1	4.1	8700	240	B.D.	14	1059	59	376	12
Z16-33 - 29	7.5	24.3	2.5	219	12	47	3.5	11610	280	2	20	584	31	764	18
Z16-33 - 30	38	94.9	4.9	836	71	155.2	8.5	12540	540	47	20	1148	77	1066	43
Z16-33 - 31	12	39.7	3.5	351	24	60.8	2.8	11710	320	5	14	986	67	611	24
Z16-33 - 32	12	26.1	2.9	211	16	45.1	4	15140	380	16	13	237	34	820	22
Z16-33 - 33	78	159	11	1251	72	214	12	11970	490	106	33	1930	420	1800	96
Z16-33 - 34	11	18.2	2	202	14	46.5	3	12000	320	21	19	353	12	700	16
Z16-33 - 35	3.5	6.01	0.95	66.9	4.6	19.4	2	14120	350	2	13	77.2	6.6	553	12
Z16-50 - 1	25	94.1	5.4	913	42	196	10	10250	230	1	11	890	130	2073	75
Z16-50 - 2	1.4	3.18	0.55	36.2	4.2	10.42	0.72	11970	160	3	10	123.9	4.5	371	12
Z16-50 - 3	15	20.7	2.6	193.3	9.7	48.5	6.6	13150	400	B.D.	8.3	165.6	9.6	472	16
Z16-50 - 4	75	154	13	1340	140	230	18	12170	420	8	13	2230	140	1750	130
Z16-50 - 5	56	47	11	428	86	78	17	11580	520	B.D.	7.2	370	51	415	76
Z16-50 - 6	25	27.7	3.1	266	44	53.4	4.6	9960	230	7	15	988	40	755	38
Z16-50 - 7	31	40.9	5.4	373	36	73.6	6	11100	300	B.D.	8.9	702	54	533	25
Z16-50 - 8	15	40.5	2.5	378	51	70.5	6.6	10220	280	B.D.	11	671	50	538	20
Z16-50 - 9	5.2	17.9	1.6	190	11	48.9	3.6	14420	490	B.D.	18	169.2	8.9	688	41
Z16-50 - 10	23	31.5	4.9	313	40	71	6.4	14490	280	12	12	336	56	672	18
Z16-50 - 11	65	118	9.6	1104	79	219	17	13590	450	0	11	1098	83	1086	36
Z16-50 - 12	15	43.4	2.4	439	32	87.3	6.2	13830	430	3	13	2020	230	653	23
Z16-50 - 13	5.1	19.7	1.3	186.1	7.7	36.4	2.4	10060	270	1	11	450	11	475	16
Z16-50 - 14	3.4	15.2	1.1	171.6	8.1	39.4	2.2	11240	210	B.D.	8.7	533	12	985	30

Z16-50 - 15	6.5	19.7	2.1	210	14	47.9	4.4	11790	230	B.D.	9.6	251	30	729	51									
Z16-50 - 16	65	178	13	1670	140	291	15	13070	420	35	18	1.33E+04	4.30E+03	1540	120									
Z16-50 - 17	320	279	65	2560	620	460	100	1.38E+04	1.50E+03	76	62	1310	160	2050	280									
Z16-50 - 18	3.6	12.1	2.2	110.6	7.7	27.5	1.9	12990	260	B.D.	8.3	154.6	6	434	12									
Z16-50 - 19	15	17.1	3.4	169	27	36.7	5.2	11930	450	B.D.	9.9	193	15	627	33									
Z16-50 - 20	100	273.3	9.5	2420	110	433	23	11450	350	39	30	5410	200	1169	35									
Z16-50 - 21	23	101.1	5.1	898	64	180.6	9.5	12140	370	4	13	3550	220	2970	110									
Z16-50 - 22	100	81	18	750	160	142	28	11720	310	8	13	2050	820	726	81									
Z16-50 - 23	37	49.2	5.8	491	48	94.3	9.6	12920	440	1	19	1006	94	698	43									
Z16-50 - 24	38	104.3	6.8	1018	58	192	11	12020	330	1	14	2520	280	1390	120									
Z16-50 - 25	15	21.5	2.8	202	15	43.5	3.6	11010	260	10	14	405	56	368	26									
Z16-50 - 26	14	23.2	2	244	19	48.8	2.2	11300	350	12	24	289	14	498	16									
Z16-50 - 27	4.2	7.8	1.5	74	11	17.4	2.3	10610	280	11	35	106.4	4.4	268	14									
Z16-50 - 28	33	113.7	6	1119	88	204.4	7.9	11950	430	30	31	3930	970	1634	64									
Z16-50 - 29	9.7	21.5	1.3	189	17	40.3	2.6	12330	330	8	20	394	12	478	15									
Z16-50 - 30	6.8	16.6	1.1	164	10	33.3	2.3	12670	300	12	20	333	12	384	16									
Z16-50 - 31	19	42.4	6	392	34	80.4	6.2	12330	390	B.D.	19	378	22	859	78									
Z16-50 - 32	4.4	21.8	1.5	265	11	67.9	3.6	17420	300	13	13	217	27	742	16									
Z16-50 - 33	3.6	13	1	147.5	5.5	34.2	1.6	13560	330	10	11	319	27	375.2	9.6									
Z16-50 - 34	7.2	30.2	1.8	369	21	94.9	3.6	13620	390	9	13	183.2	7	461	14									
Z16-50 - 35	22	76.8	3.9	728	25	160	7.2	12920	410	1	14	1234	50	1250	38									
Z16-50 - 36	13	25.7	2.4	246	21	56.1	4.3	13010	270	B.D.	16	269	15	660	21									
Z16-50 - 37	22	53.4	3.3	492	51	105	20	14410	530	0	16	282	14	1021	33									
Z16-50 - 38	240	212	56	2120	740	309	72	1.19E+04	1.60E+03	31	19	9.50E+03	2.20E+03	1310	210									
Z16-50 - 39	28	65.9	6.2	600	75	115	11	11790	570	B.D.	9	1237	92	723	36									
Z16-50 - 40	15	37.2	4	346	21	66.7	6.4	13040	400	9	14	208.6	5.1	487	19									
Z16-50 - 41	30	96.2	7	842	51	157.5	5.5	12800	300	9	18	3820	560	1125	76									
Z16-50 - 42	10	17.8	1.8	172	13	36	3.2	12800	380	13	26	833	48	426	15									
Z16-50 - 43	75	129.9	8.5	1169	78	241	15	11180	660	33	24	4170	460	1680	110									
Z16-50 - 44	38	50.9	6	507	56	106	17	1.80E+04	1.10E+03	B.D.	11	850	180	782	39									
Z16-50 - 45	4.1	14.5	1	144.2	8.2	29.8	1.5	11930	260	B.D.	8.3	242	11	410	17									
Z16-50 - 46	11	41.2	3.5	418	27	92.8	7.3	11650	260	B.D.	16	913	97	1041	66									
Z16-50 - 47	11	27.3	2.3	302	36	64.2	5.4	12460	430	0	15	437	28	778	24									

Z16-50 - 48	9.5	23.4	2.5	264	19	60	2.8	14050	310	6	13	359	46	847	42		
Z16-50 - 49	3.3	7.3	1.2	83.4	6.4	19.2	1.5	12050	350	18	15	276.8	5.6	292.9	8		
Z16-50 - 50	73	115	17	970	130	189	25	10720	290	14	16	1190	130	1141	40		
Z16-50 - 51	26	89.8	5.4	845	53	160	12	12910	310	11	18	935	70	787	30		
Z16-50 - 52	31	60	7.2	613	71	140	18	14090	560	B.D.	17	1380	280	1840	240		
Z16-50 - 53	98	75	16	740	180	135	24	10710	500	22	23	3.20E+03	1.60E+03	1330	180		
Z16-50 - 54	30	76.5	7.7	782	69	164	22	15210	410	19	20	1330	210	949	35		
Z16-50 - 55	14	55	4.3	490	35	85.6	5.8	12120	240	12	10	1032	53	748	12		
Z16-50 - 56	28	46.7	6.7	495	63	99.6	9.7	17550	470	6	17	476	93	923	74		
Z16-50 - 57	92	149	17	1470	140	269	26	10790	360	27	20	376	59	1800	110		
Z16-50 - 58	8.3	21.8	1.6	227	18	52.4	4.1	12140	250	7.5	8.5	182	13	587	33		
Z16-50 - 59	4.6	10.75	0.78	118	7.2	23.9	1.7	12800	230	B.D.	14	181.6	4.1	285	13		
Z16-50 - 60	4.3	21.6	1.2	279	11	75.5	2.4	16910	280	B.D.	6.5	58	2.6	690	12		
Z16-50 - 61	71	98	13	873	87	172	24	11920	450	14	31	1.14E+04	2.90E+03	1080	110		
Z16-50 - 62	10	21.8	2.4	223	19	50.9	4.6	13380	220	B.D.	12	262	12	665	32		
Z16-52 - 1	8	48	2.1	540	20	110.3	5	19480	440	43	21	17.7	1.4	2148	50		
Z16-52 - 2	44	87.2	7.7	880	47	180.8	7	20170	460	146	46	36.2	2.9	2850	180		
Z16-52 - 3	140	193	23	1400	140	224	24	2.82E+04	1.10E+03	403	95	59.2	8.4	2740	140		
Z16-52 - 4	44	104.3	5.8	1051	78	214	12	16640	330	226	61	32.1	2.8	2920	160		
Z16-52 - 5	51	99.4	7.1	914	55	169	16	2.46E+04	1.10E+03	600	140	2000	420	1.45E+04	1.50E+03		
Z16-52 - 6	7.9	47.9	2.7	502	23	105.2	5.1	2.42E+04	1.10E+03	44	27	27.9	2.3	2540	110		
Z16-52 - 7	40	81	5.4	887	63	186	18	16320	700	284	48	21.1	1.7	2100	130		
Z16-52 - 8	15	59.8	3.7	702	22	158.8	6.8	19930	540	50	31	28.3	2.5	2730	86		
Z16-52 - 9	21	71.2	4.1	729	47	137.6	6.4	2.96E+04	1.20E+03	353	92	37.2	4.2	3022	89		
Z16-52 - 10	23	56.5	4	615	47	125.2	8.5	22440	790	122	60	46	20	2209	86		
Z16-52 - 11	28	71	4.6	642	40	111.9	7	25110	790	40	21	39.1	2.9	4380	180		
Z16-52 - 12	82	269	22	2260	220	332	19	2.46E+04	1.10E+03	950	150	156.7	8.9	3450	160		
Z16-52 - 13	92	133	22	1210	170	222	23	22170	910	184	41	37.2	6.9	3960	410		
Z16-52 - 14	50	95	11	789	47	131.3	7.8	25220	810	220	100	31.1	2.6	1836	74		
Z16-52 - 15	31	95.6	3.6	967	52	197.6	6.9	24490	800	165	46	44.7	9	3250	140		
Z16-52 - 16	29	94.7	6.5	1007	62	209	14	15470	470	58	27	22.7	2.1	2480	110		
Z16-52 - 17	59	144	13	1450	140	289	18	14050	270	46	29	156	30	4220	180		

Z16-52 - 18	230	135	30	1180	270	220	38	17850	850	259	82	62	22	2000	220			
Z16-52 - 19	34	92.9	7.8	1128	50	281	6.2	13510	260	34	22	20.7	2.3	4110	120			
Z16-52 - 20	34	124	6.1	1196	51	222.8	9.5	20860	710	710	120	30.6	4.7	4140	310			
Z16-52 - 21	85	187	16	1790	120	362	30	14550	440	455	94	28.2	3.5	3200	240			
Z16-52 - 22	200	231	45	1780	240	295	45	2.48E+04	1.30E+03	580	110	104	16	5410	710			
Z16-52 - 23	83	197	11	1550	100	259	16	2.78E+04	1.30E+03	286	67	61.2	5	5790	310			
Z16-52 - 24	180	248	22	2110	150	356	27	16700	630	710	140	42.5	4.8	2477	98			
Z16-52 - 25	110	188	16	1640	150	296	20	14730	550	511	92	64.3	8.8	3550	100			
Z16-52 - 26	140	237	33	2160	250	372	34	20570	670	450	100	58	8.3	7000	770			
Z16-52 - 27	18	59.7	3.8	640	31	128.2	9.7	20190	780	28	21	32.6	7.1	2380	180			
Z16-52 - 28	270	476	50	4050	370	653	55	17420	880	1090	190	153	14	1.29E+04	2.00E+03			
Z16-52 - 29	190	554	45	4560	240	720	62	1.66E+04	1.20E+03	1530	230	169	15	6620	440			
Z16-03 - 1	13	35.5	2.1	338	15	63.4	2.7	9350	180	11	13	69.4	2.8	86.1	3.3			
Z16-03 - 2	3.3	12.41	0.85	125.8	7	28	2.2	12580	280	7.3	9	93.2	3	241.9	9.5			
Z16-03 - 3	6.8	28.4	1.8	250	10	50.7	3.2	9030	180	B.D.	11	54.8	4	139.4	6.8			
Z16-03 - 4	8.3	38	1.7	297	13	54.5	2.3	10000	190	B.D.	12	152.5	5.2	137.8	4			
Z16-03 - 5	7.8	26.3	1.7	239	17	47.4	3.4	9650	220	B.D.	13	254.2	8.8	251.1	7.8			
Z16-03 - 6	4	17.1	1.2	168	7.1	34	1.4	10900	200	B.D.	6.7	171	5.3	380	13			
Z16-03 - 7	8	25.9	1.6	240.2	8.3	48.9	2.3	8410	180	7	11	201	13	275	18			
Z16-03 - 8	11	33.8	2.4	308	13	61.6	3.9	11290	210	B.D.	16	257.6	6.8	594	21			
Z16-03 - 9	8.4	35.1	1.3	314	16	63.3	3.5	10640	230	B.D.	8.7	282.8	9.8	574	28			
Z16-03 - 10	25	51.1	5.8	480	52	98	11	10090	190	14	20	534	65	790	130			
Z16-03 - 11	6.7	27.9	1.5	248.5	9.9	48.1	2.1	11500	190	11	12	133.9	5.4	295.2	6.8			
Z16-03 - 12	17	38.4	3.5	365	27	67.9	3.4	12610	420	8	19	134	17	379	24			
Z16-03 - 13	4.8	20.3	1.7	198	10	41.6	3.9	11080	370	15	22	163.9	4.7	417	17			
Z16-03 - 14	14	26.1	2.6	230	23	45.2	3.7	12380	110	B.D.	9.5	129.6	9.7	330	10			
Z16-03 - 15	9	39.1	2	338	10	69	1.9	11900	250	2.6	9.4	176	17	289.9	8.4			
Z16-03 - 16	7	40.1	2.4	341	17	66.2	2	10710	220	B.D.	7.8	161.6	6.5	454	14			
Z16-03 - 17	9.9	24.5	1.7	251	14	52.3	3.5	9720	210	B.D.	15	110.6	8.3	192	19			
Z16-03 - 18	37	123.5	8.3	1023	55	165.7	7.9	9760	270	2	14	711	46	988	46			
Z16-03 - 19	26	63	2.4	629	28	135.7	5.1	12290	260	B.D.	17	2320	690	1167	76			

Z16-17 - 1	NAN	no value	NAN	no value	NAN	no value	NAN	no value	NAN	no value	NAN	no value	NAN	no value	NAN
Z16-17 - 2	4.60E+06	6.21E+06	7.80E+05	3.64E+07	4.70E+06	5.14E+06	6.80E+05	1.94E+04	2.30E+03	3.80E+03	9.40E+03	5.00E+06	6.30E+05	1.36E+07	1.90E+06
Z16-17 - 3	22	74	5.7	669	37	129.7	7.6	14640	550	43	33	85.6	6.6	2160	140
Z16-17 - 4	71	228	13	1790	110	320	26	12870	810	150	39	1960	120	1.97E+04	1.40E+03
Z16-17 - 5	5.9	21.8	1.6	237	12	57	3	11670	170	2	14	201.4	5.2	1246	57
Z16-26 - 1	8.5	26.1	2.7	268	23	60	6.6	8180	470	B.D.	9	41.9	2.5	359	52
Z16-26 - 2	16	53.2	2.8	465	20	92.3	3.4	11190	270	3.3	9.5	131.1	6.5	521	33
Z16-26 - 3	28	37	4.9	342	47	66	11	10390	350	11	21	133	44	241	30
Z16-26 - 4	14	18.4	3	163.4	5.2	32.7	1.9	13290	380	19	22	131	11	958	78
Z16-26 - 5	7.9	42	1.5	372	12	79	4.2	11610	230	4	13	91	4.3	243.3	7.4
Z16-26 - 6	14	28.1	1.7	260	13	51.9	4.7	10850	310	4	18	80.3	3.1	273	9.1
Z16-26 - 7	13	28	2.2	240	21	43.9	4.4	10790	200	B.D.	13	103.4	4	434	58
Z16-26 - 8	12	12.3	1.8	67	11	8.3	1.7	11400	290	9	14	144.4	6.4	581	19
Z16-26 - 9	12	59.1	1.8	563	23	108.9	4.1	9790	210	11	14	86.5	5.1	253	12
Z16-26 - 10	12	63.6	3.3	584	20	117	5.9	10980	250	4	16	87	13	205	43
Z16-26 - 11	7.9	27	2.1	268	12	56.7	3.3	10920	230	4	19	157.3	7.7	376	13
Z16-26 - 12	74	209	11	1970	130	388	28	10420	320	14	19	114	12	226	16
Z16-26 - 13	4.9	18.9	1.2	184	12	39.1	1.5	11760	220	B.D.	8.6	100.1	3.7	276.7	9.9
Z16-26 - 14	7.9	29.4	1.6	281	11	55.6	2.4	12040	250	B.D.	8.6	303	8.8	765	26
Z16-26 - 15	8.5	44.7	3	422	15	85.8	3.4	13830	520	B.D.	11	74.3	4.9	1153	76
Z16-26 - 16	5.4	24.8	1.5	245	14	50	2.8	9670	190	B.D.	7.8	172	10	262	10
Z16-26 - 17	7.2	35.8	1.8	376	24	84.4	4.2	10800	230	8	13	112.1	9.4	859	30
Z16-26 - 18	32	88.1	3.9	803	29	164.8	5.4	9980	280	17	23	328	19	986	45
Z16-26 - 19	10	45.7	2.1	447	32	90.6	4.9	11790	370	10	17	176	21	819	51
Z16-26 - 20	12	66	2.5	585	19	111.7	5.6	10530	250	16	14	385	16	637	15
Z16-26 - 21	5	28.9	2.6	285	18	67.9	3.7	9980	330	13	26	211.4	6.3	666	27
Z16-26 - 22	44	100	10	967	72	197	10	9930	350	20	17	1680	240	2620	190
Z16-26 - 23	12	22.8	2.2	192	20	38.9	2.5	10220	260	B.D.	13	670	190	801	50
Z16-27 - 1	41	97.4	8.7	1000	120	209	16	12190	670	18	22	583	58	1110	120
Z16-27 - 2	26	124.2	4	1132	43	218.1	5.5	8530	150	B.D.	14	750	25	821	30
Z16-27 - 3	35	89.6	6.3	862	67	169.3	9.4	9620	180	B.D.	12	335	11	1004	37

Z16-27 - 4	11	20.1	3	189	26	41.2	5.3	12410	340	1	14	63.2	3.2	166	8			
Z16-27 - 5	15	24.1	2.6	269	22	56.6	5.5	11160	390	6	12	399	45	910	120			
Z16-27 - 6	15	81.7	2.9	778	23	161.6	4	12210	270	20	24	256	17	782	19			
Z16-27 - 7	7.1	27	1.7	249	14	50.1	3.3	9090	200	B.D.	12	53.5	3.2	129	12			
Z16-27 - 8	21	105.8	4.4	1150	59	250	15	13190	340	B.D.	9.9	207.6	9.9	2350	61			
Z16-27 - 9	7	18.4	1.4	178	12	37.9	2.7	10380	220	B.D.	9.1	198	8	296.4	9.4			
Z16-27 - 10	9.6	66.9	2.9	704	21	149	5.7	14890	310	25	17	242	15	1930	39			
Z16-27 - 11	25	90.2	8	847	37	174	11	10950	350	17	23	235	14	695	75			
Z16-27 - 12	44	89.9	8.4	826	86	175	17	9830	270	5	17	396	14	950	91			
Z16-27 - 13	19	38.5	5.4	354	40	79.3	7.4	9540	230	7	14	99	15	173.7	7.3			
Z16-27 - 14	18	137.1	5.6	1372	31	277	11	12880	310	11	15	484	18	1463	36			
Z16-27 - 15	17	31.2	3.8	307	30	52.3	5.8	3.77E+04	1.90E+03	26	21	75	11	3000	210			
Z16-27 - 16	20	90.1	3.8	918	34	188.6	6.1	11840	200	3	17	194.7	9.1	476	20			
Z16-27 - 17	12	47.9	1.8	409	17	81.1	3.4	10190	160	6	11	164	12	215.1	9.8			
Z16-27 - 18	130	115	18	1100	140	232	24	8420	370	0	24	1200	430	1410	65			
Z16-27 - 19	9	56.1	2.6	518	14	108.4	3.3	9360	190	1	12	155.7	5.9	215.8	9.2			
Z16-27 - 20	16	65.8	3.5	569	31	110.5	6.6	10180	160	B.D.	18	147.8	4.9	249.5	7.9			
Z16-27 - 21	19	62	4.1	618	35	127.6	5.5	12550	450	31	16	355	16	1790	110			
Z16-27 - 22	5.8	25.8	1.7	270	11	63.4	1.9	14520	550	B.D.	14	255	11	1024	28			
Z16-27 - 23	15	67	3.9	729	51	166	13	24160	720	24	16	126.1	5.5	879	34			
Z16-27 - 24	34	127.9	6.8	1387	72	303.2	8.1	14270	640	7	12	414	55	2460	200			
Z16-27 - 25	12	71.9	2.8	699	28	147.2	6.1	11690	270	B.D.	8.1	503	17	422	10			
Z16-27 - 26	15	61.3	2.5	572	32	114.5	5.6	12200	350	25	23	85.3	3.4	1001	50			
Z16-27 - 27	8.9	44.1	2.4	418	17	86.1	4.6	10090	220	B.D.	5.7	153.3	9.3	143.9	6.9			
Z16-27 - 28	33	138.8	7.2	1364	61	280	13	13400	430	23	22	462	34	1829	60			
Z16-27 - 29	4.5	15.9	1.3	174	12	35.8	1.4	8830	250	B.D.	8.5	76.7	3.8	126.7	3.4			
Z16-27 - 30	8.5	41.7	2.3	415	15	97	3.1	10000	210	B.D.	9.8	225	12	407	26			
Z16-27 - 31	19	77	4.4	795	28	175.5	7.5	11160	570	3	11	4.40E+03	1.00E+03	5360	700			
Z16-27 - 32	28	55.4	4.6	484	36	91	6.3	10370	340	B.D.	11	359	43	414	23			
Z16-27 - 33	5.2	24.3	1.7	227	16	46.5	2.8	11970	330	B.D.	11	72.4	2.6	213.2	8.1			
Z16-27 - 34	14	41.3	2.4	404	25	84.1	4.6	10610	200	2.2	9.9	85.2	5.6	249	16			
Z16-27 - 35	15	45.5	2.4	466	25	105.3	3.9	10890	250	25	16	485	18	710	22			
Z16-27 - 36	13	51.6	2.9	522	28	114.1	6.1	12120	260	8	13	151	17	325	27			

Z16-27 - 37	9.6	36.3	2.5	317	16	63	4.1	10190	260	10	13	295.2	8	289.4	9.7
Z16-27 - 38	14	110.9	5.4	1160	56	245	14	13270	330	4	18	180.5	8.8	958	24
Z16-27 - 39	23	139	5	1442	54	301	12	13140	440	6	13	261.7	9.7	1313	33
Z16-27 - 40	18	46.1	3	432	27	88.5	5.3	10160	250	4	11	133	19	388	32
Z16-27 - 41	22	109.1	5.2	1120	50	229	8.9	8380	200	1	14	539	30	770	34
Z16-35 - 1	14	52.3	2.9	483	29	92.5	6.9	10710	340	0	19	317	20	229.7	7
Z16-35 - 2	10	36.7	2.1	329	27	66.1	5	10980	290	B.D.	11	253	19	383	16
Z16-35 - 3	10	51.8	2.5	465	25	94.9	4.4	11440	190	21	20	87.3	3.6	328.9	7.3
Z16-35 - 4	7.2	22.8	2.1	178	14	33.7	2.1	13070	250	B.D.	10	54.8	2.3	485	12
Z16-35 - 5	3.6	27.3	2.3	294	11	70.3	3.2	11550	340	B.D.	7.8	332	11	428	14
Z16-35 - 6	12	85.2	4.2	781	25	144.1	6	11910	280	B.D.	15	90.7	6.2	375.1	9.5
Z16-35 - 7	4.3	18.2	1.8	173.8	6.3	37.6	1.9	9690	220	B.D.	16	89.2	3.4	94.1	3.9
Z16-35 - 8	16	61.9	6.1	557	49	112.2	8	11970	610	1	19	51.6	5.7	203	14
Z16-35 - 9	17	33.7	4	345	31	71.9	7.8	10900	320	12	30	182	22	194	18
Z16-35 - 10	6.8	34.7	2	331	13	67.7	3.3	9550	150	7	16	342.6	9.3	284	21
Z16-35 - 11	13	40.6	2	420	25	94.3	4.9	12990	260	5	16	128.3	6.4	613	21
Z16-35 - 12	17	77.4	3.3	706	36	146.5	8	11080	200	B.D.	15	113.5	5.1	284	13
Z16-35 - 13	26	24.9	3.6	211	35	38.8	8.1	12870	230	5	17	62.3	7.3	342	14
Z16-35 - 14	11	50.7	2.6	484	23	103.1	6.4	11490	280	14	32	245.7	6.8	788	19
Z16-35 - 15	7.3	31.3	2.4	292	10	59.4	2.3	11100	270	B.D.	10	237	10	293.7	9
Z16-35 - 16	14	87.2	2.6	837	29	170.8	4.3	13650	200	0	14	104.6	4	756	13
Z16-35 - 17	16	60.6	3	577	17	120.4	4	10390	330	B.D.	7.2	140.1	9.1	294	14
Z16-35 - 18	12	35.2	3	396	35	88.3	3.8	12940	630	B.D.	9.5	89.3	8.3	627	36
Z16-35 - 19	11	52.2	1.9	453	17	86.2	3.9	12550	380	1.1	9	238.4	7.9	623	53
Z16-35 - 20	12	59.7	2.2	586	25	122	3.6	13040	380	B.D.	9.5	52.6	2.6	441	13
Z16-35 - 21	5.7	24.78	0.98	233.2	9.6	48.9	1.8	10460	190	B.D.	8.3	121.8	4.2	193	4.4
Z16-35 - 22	9.5	37.6	2	334.1	9.3	61.6	2.6	12000	160	B.D.	12	170.6	5.5	530	12
Z16-35 - 23	9.3	37.5	3	349	21	70.6	4.3	10480	440	0	15	139.8	8.1	136.3	9.5
Z16-35 - 24	7.5	26.1	2.1	283	26	58.7	4.2	10960	290	B.D.	15	181.3	7.1	572	11
Z16-35 - 25	11	72.7	2.9	671	19	136.7	4.5	12950	180	B.D.	11	70.1	2	494	15
Z16-35 - 26	6.8	54	2.3	565	39	119.3	8.1	10800	280	B.D.	21	243	11	282	10
Z16-35 - 27	8.2	55.6	2.8	556	21	119.5	3.5	9370	170	0	11	444	23	472	21

Z16-35 - 28	12	53.9	2.9	500	14	98.4	5.8	11880	360	7	16	75.8	3.3	296.2	9.3				
Z16-35 - 29	10	62.6	2.3	547	21	105.6	2.2	11390	280	B.D.	8.7	274.4	6.2	376	11				
Z16-35 - 30	31	68.7	5.4	628	40	126	10	11100	220	12	12	255	36	372	18				
Z16-35 - 31	5.8	37.3	2.8	339	18	68	4.6	10510	280	9	18	226	12	169.5	6.4				
Z16-35 - 32	19	130.7	3.3	1156	29	226.3	6.3	7720	140	4	12	340	10	179.1	4.7				
Z16-35 - 33	20	88.6	4.3	781	31	160.5	5.9	11930	430	5	12	354	15	437	33				
Z16-35 - 34	5.5	29.5	1.5	281	14	61.9	2.7	11120	160	B.D.	12	137.5	4.5	150.1	3.5				
Z16-35 - 35	4.3	20.1	1.3	206.7	8.2	44.7	3	12440	220	B.D.	12	137.2	4.5	315.7	6.4				
Z16-35 - 36	9.5	51.2	2.6	490	17	103.9	3.7	9630	200	6	12	88.4	3.5	235.2	7.1				
Z16-35 - 37	17	59.2	4.3	637	39	133	9.8	12530	200	0	11	275	18	735	38				
Z16-35 - 38	7	31.6	1.1	281	11	58.6	2.3	10410	190	B.D.	6.3	162.1	3.7	233.2	6.1				
Z16-35 - 39	30	73.9	7.8	718	56	145.1	9.1	14760	350	13	12	502	24	1232	54				
Z16-35 - 40	22	58.2	3.1	558	31	117.3	6.2	13780	410	4	11	117	24	685	20				
Z16-35 - 41	8.6	38	2.1	367	18	78.9	4.3	10090	260	3	14	265	11	299	13				
Z16-35 - 42	12	41.4	3.5	386	36	83.4	7.4	10200	410	B.D.	15	301	17	264	12				
Z16-35 - 43	8	38.3	2.3	360	16	76.5	2.9	10210	270	13	10	148.6	7.1	278.7	8.1				
Z16-35 - 44	9.2	36.4	2.3	305	11	61.5	4	11460	270	7	12	126.4	5.3	377	11				
Z16-35 - 45	8.9	46	2.2	427	20	87.7	4.7	13450	290	2	11	184	9.4	847	31				
Z16-35 - 46	20	50.9	4.5	474	40	101.2	8.4	10510	230	11	16	104	11	196	22				
Z16-35 - 47	17	152.9	5.2	1376	40	290.9	6.8	9650	220	23	14	2540	220	1073	45				
Z16-35 - 48	7.9	58.8	2.1	563	22	112.2	3.1	11520	250	5	12	296	11	227.2	8.3				
Z16-35 - 49	6.4	28.7	4.1	281	27	65.2	3.8	11300	390	14	15	205	19	172	11				
Z16-35 - 50	5.4	27.4	2.1	275	16	56.9	2.3	10560	180	B.D.	13	98.8	2.5	143.1	4				
Z16-35 - 51	13	27.5	1.9	305	16	63.3	2.5	12040	360	3	15	139.4	5.9	245	10				
Z16-35 - 52	7.3	25.7	1.9	268	19	58.3	3.3	11380	180	B.D.	11	269	16	298	12				
Z16-35 - 53	5.6	25.6	1.3	255	11	50.8	2.4	10430	270	3	14	96.4	3.7	83.7	3				
Z16-35 - 54	7.2	40.2	1.9	353	20	73.7	2.1	10970	270	3	17	278	4.6	225.1	6.1				
Z16-35 - 55	29	56.3	5.1	513	56	101.8	4.3	10300	290	13	21	384	34	218	16				
Z16-35 - 56	18	45.9	4.3	504	44	112.1	8.2	13240	530	B.D.	12	137	17	623	24				
Z16-35 - 57	7.9	34.9	2.1	312.9	8.6	61.2	2	11940	220	14	13	44.7	2.3	147.1	3.1				
Z16-35 - 58	4.9	21.4	1.2	199	13	43.4	2.4	8870	190	8	11	56.5	2.2	131.2	2.6				
Z16-35 - 59	6.7	19.06	0.95	167	13	35.8	1.5	9670	270	B.D.	9.2	163.4	8.4	138	5.9				
Z16-35 - 60	5.2	19.9	1.8	225	10	51.5	2.7	12250	290	1	11	241	25	468	15				

Z16-35 - 61	12	44.9	3.1	401	23	80	4	11700	450	5	13	163.9	5.6	237	15	
Z16-35 - 62	12	37.4	2.7	357	25	75.7	6	13420	560	8	22	531	44	781	38	
Z16-35 - 63	8	35	2.7	356	23	73.4	3.6	11730	150	5	23	79	12	206	5.1	
Z16-35 - 64	20	73	4.4	676	25	135.6	5.7	11260	260	5	21	423	40	522	28	
Z16-35 - 65	10	38.1	2.2	377	17	75.5	2.8	11750	250	B.D.	7.1	99.8	4.6	169.1	6.5	
Z16-35 - 66	12	79.5	4.6	683	33	147.6	4.6	11110	440	4	16	98.5	5.5	305	17	
Z16-35 - 67	19	52.3	2.9	493	21	101.6	4.7	10250	240	11	15	179	16	150.2	8.1	
Z16-35 - 68	6.8	31.2	2.8	293	11	55.3	3.4	13110	430	3	17	142.3	4.6	527	19	
Z16-35 - 69	9	36.4	2.4	299	13	59.6	3.4	10810	230	B.D.	12	286	10	468	15	
Z16-35 - 70	9.6	29.5	2.3	275	16	61.5	2.7	11550	300	4	15	197	11	240	14	
Z16-35 - 71	11	29.7	1.3	265.4	8.2	51.9	3.1	11120	200	B.D.	15	596	12	666	13	
Z16-35 - 72	34	43.9	2.2	473	79	91	27	10290	310	20	25	280	32	563	36	
Z16-35 - 73	15	68.8	3.5	655	31	136	8.3	12320	300	2	12	62.6	4	302.6	4.9	
Z16-35 - 74	10	39.7	2.7	364	18	81.3	1.5	11120	360	3	20	236	45	224	10	
Z16-35 - 75	32	107.2	6	938	41	175.4	4.4	11570	370	B.D.	11	1790	240	1826	51	
Z16-35 - 76	6.4	21.7	1.9	229	17	52.4	4.5	10750	200	10	16	65.2	5.8	620	35	
Z16-35 - 77	15	80	3.1	767	33	159.9	5.5	10340	310	B.D.	7.5	349	13	471	14	
Z16-35 - 78	9.5	37.2	1.9	365	18	75.2	4.8	8290	180	0.1	7.9	729	45	161.7	7.4	
Z16-35 - 79	8.8	44.5	1.7	412	18	85.9	4.6	10460	280	B.D.	9.5	269.5	9.7	280.9	7.6	
Z16-35 - 80	27	19.9	4.9	196	48	40	11	12300	310	B.D.	19	29.5	2.6	172	16	
Z16-35 - 81	16	44.7	2.6	410	21	82.3	5.5	10360	230	B.D.	8.5	177	12	208.9	4	
Z16-35 - 82	8.1	20.1	2	198	16	42.8	3	10370	230	B.D.	8.3	85	12	102.4	3.9	
Z16-35 - 83	18	36.9	5.9	386	61	88	12	10510	430	17	19	40.4	3.6	133	43	
Z16-35 - 84	21	45.9	4.8	409	28	83	7.3	13290	230	7	15	110.7	5.5	402	16	
Z16-35 - 85	7.9	41	2	348	14	70.3	3	9590	190	B.D.	7.8	96.8	4.3	68.8	2.3	
Z16-35 - 86	16	46.2	4.3	585	61	132	13	12880	240	B.D.	9	122	10	787	86	
Z16-35 - 87	7.6	36.9	1.9	354	11	77.3	3.4	11210	430	B.D.	10	186.2	6.1	242	10	
Z16-35 - 88	25	63.1	5	617	55	131.1	7	11880	380	B.D.	17	376	26	442	24	
Z16-35 - 89	9.1	27	2	250	17	54.4	3.4	12310	250	B.D.	9	71.3	5.8	234.3	9.3	
Z16-35 - 90	15	41	3.2	384	19	80.5	4.3	9770	240	3	17	110.3	6.5	60.6	3	
Z16-35 - 91	15	40.2	2.3	417	21	85.4	5.6	11770	300	B.D.	7.4	249	26	280	18	
Z16-35 - 92	7.4	63.7	3.1	592	21	121.6	3.7	9300	350	B.D.	13	307.8	7.4	259.1	8.1	
Z16-35 - 93	16	46.1	3.8	424	25	90.9	5.6	10060	230	6	15	185	19	401	22	

Z16-35 - 94	8.3	25.8	1.9	261	12	49.7	2.2	11770	270	B.D.	13	78.7	2.9	230.2	8.3			
Z16-35 - 95	24	70.2	4.2	675	55	139.4	8.4	8900	240	B.D.	12	651	54	413	33			
Z16-35 - 96	15	40.2	3	425	34	84.7	6	10560	170	14	27	668	84	610	30			
Z16-35 - 97	15	68.4	3.4	662	29	136.6	7.3	10820	350	6	16	536	31	703	45			
Z16-35 - 98	11	61.6	3.9	544	20	105	5.9	11630	180	23	30	282	12	690	26			
Z16-35 - 99	8.2	41.8	2.1	380	14	77.8	2.8	10110	230	5	13	140.1	5.4	353	16			
Z16-35 - 100	4.7	23.3	1.2	213.9	7.6	43	2.2	9430	240	B.D.	9.6	48.3	1.8	43.4	1.8			
Z16-35 - 101	42	74.2	7.1	697	86	132	15	12320	480	B.D.	9.2	182	16	351	15			
Z16-35 - 102	9.1	31.7	2.8	290	20	61.2	4.7	10670	210	1	13	47.1	2.6	191.8	9.3			
Z16-35 - 103	11	47.4	2.3	435	13	86.9	3.4	11300	180	1	11	127.7	5.9	298	8.7			
Z16-35 - 104	12	86.3	6.2	749	32	144.2	4	11190	410	B.D.	7.2	229.1	8.2	169.8	4.8			
Z16-35 - 105	13	64.1	1.3	605	22	118.6	6	11550	250	18	29	468	50	820	71			
Z16-35 - 106	40	58.6	2.8	703	13	156.6	6.9	13410	490	0	15	166	13	918	62			
Z16-35 - 107	3.3	14.93	0.86	148.4	6.5	32	1.3	11550	200	7	10	61	1.7	96.8	2.4			
Z16-35 - 108	4.1	26.3	1.5	250	10	53.8	2.5	10450	210	2.2	9.5	70.2	3.9	179	11			
Z16-35 - 109	5.5	26.7	2	260	11	59	1.7	11690	200	0	10	540	170	431	12			
Z16-35 - 110	11	38.5	2.5	363	19	74	2.8	14220	310	1	17	53.7	3.2	734	44			
Z16-35 - 111	6.4	36.1	2.5	332	12	72.7	2.1	11640	240	B.D.	15	255.1	7.3	241.9	9.4			
Z16-35 - 112	11	33.7	2.8	295	21	60.5	4.5	10130	430	7	21	92.5	7.9	214.6	7.9			
Z16-35 - 113	16	61.5	3.6	594	35	123.2	9.8	12570	940	B.D.	13	801	53	898	52			
Z16-35 - 114	16	38	3.2	353	25	71.8	5.2	9950	250	B.D.	6.9	123	11	303	23			
Z16-35 - 115	8.8	47.9	1.8	460	20	97.2	4.2	10230	210	11	18	616	33	904	14			
Z16-35 - 116	12	25.1	4.3	238	25	53.5	4.9	11630	260	1	14	221	31	299	26			
Z16-35 - 117	6.3	22.8	1.4	260	10	54.5	2.6	8930	160	13	13	109.3	4.1	141.3	5.2			
Z16-35 - 118	7.9	21.3	2.4	207	16	44.4	4.2	10770	260	1	15	98.3	9.5	110	8.1			
Z16-35 - 119	14	48.7	3.9	442	24	94.2	5.5	11870	260	4	11	88.4	9	224	12			
Z16-35 - 120	11	55	3.6	509	19	105.7	1.8	10780	220	B.D.	14	170	12	416	15			
Z16-35 - 121	10	31.1	2	299	16	61.6	4.2	12060	220	7	15	206	15	488	23			
Z16-35 - 122	15	58.2	3	567	23	120	6	10620	380	5	15	285	15	185.6	7.2			
Z16-35 - 123	24	105.1	4.5	925	16	179.6	8.8	9130	360	B.D.	5.7	696	32	444	22			
Z16-35 - 124	4.7	37.9	1.6	358	13	74.2	3.1	12670	170	9	12	161.5	9.2	249	7.1			
Z16-35 - 125	17	65.8	4.3	734	44	156.9	8	14620	420	16	20	90.3	9.6	1243	42			
Z16-35 - 126	18	70.7	3.1	601	23	119.7	5.4	11530	550	B.D.	8.3	229	11	101.6	4.6			

Z16-35 - 127	8.2	26.1	1.2	257	12	55.4	3.2	11250	240	B.D.	9.8	88.5	5.7	113.7	4.2			
Z16-35 - 128	8.7	46.8	1.9	445	19	88	3.3	11920	240	4	13	69.2	2.6	189.1	5			
Z16-35 - 129	8.6	44.5	2.5	397	13	82.4	3.7	10120	320	5	18	65	2.3	197.1	7			
Z16-35 - 130	6.1	27.5	1.7	250.6	9.1	51.8	2.4	10370	220	B.D.	11	148	12	268	17			
Z16-35 - 131	7.1	37.5	1.6	371	22	75.8	2.5	13290	380	21	23	113.7	9.2	381	14			
Z16-35 - 132	13	50.5	1.8	437	19	88.6	3.4	11720	270	3	11	60.7	3.9	274	11			
Z16-35 - 133	7.6	39.4	2.4	409	28	85.4	3	13230	550	11	20	236	23	908	45			
Z16-35 - 134	7.7	38.5	2.1	381	13	75.9	4.2	12780	280	4	21	260.1	8.6	365	11			
Z16-35 - 135	26	59	6.9	602	51	122.1	6	8510	190	1	13	420	31	418	20			
Z16-35 - 136	7.5	30.9	1.7	279	12	58.8	2.7	10390	230	7	14	155.7	7.9	134.6	5.1			
Z16-35 - 137	14	73.6	3.2	631	28	132.8	5	9930	320	12	17	126.2	3.1	234.8	9			
Z16-35 - 138	22	60.8	4.2	565	32	113.3	8.9	12280	350	B.D.	12	49	2.8	293	19			
Z16-35 - 139	8.2	43.9	1.6	418	18	85	2.6	10040	250	8	11	120.7	3.4	70.2	1.7			
Z16-35 - 140	8.3	33.3	1.7	339	13	72.5	2.6	10860	230	27	21	420	15	407.6	8.8			
Z16-35 - 141	40	96	11	816	60	143	10	12270	440	20	30	251	36	622	46			
Z16-35 - 142	4.1	19.62	0.94	181	11	38.1	2.5	9240	230	1	13	79	2.5	96.9	2.5			
Z16-35 - 143	6.5	38.7	2.4	370	14	84.7	4.1	12470	270	12	19	144.1	6.5	222.3	9.8			
Z16-35 - 144	5.3	27.6	1.8	255	12	55.6	2.3	7720	130	1	18	88.8	3.3	62.5	2.4			
Z16-35 - 145	8.7	33.7	2.2	307	20	66.2	4.2	10940	400	B.D.	15	157.9	5.9	202.1	5.3			
Z16-35 - 146	6.4	28	2.5	287	13	60	2.5	10750	180	0	11	174.8	3.9	270	10			
Z16-35 - 147	7	21.5	1.9	215	10	47.4	2.3	10160	160	10	13	86	4.9	111.9	5.1			
Z16-35 - 148	10	46.5	2	414	12	79.8	3.7	9470	240	24	18	197.9	9.8	216	10			
Z16-35 - 149	7.1	30.1	2.1	285	12	57.3	3.4	9520	190	B.D.	11	131.4	4.2	118.4	4.4			
Z16-35 - 150	5.9	34	2	361	22	75.6	3.7	13170	370	7	15	37	2.3	534	21			
Z16-35 - 151	15	55.5	2.5	500	24	102.2	4.4	11230	250	4	16	159	10	235.6	7.9			
Z16-35 - 152	4.8	23.5	2	259	12	61.7	2.9	11350	300	B.D.	9.3	128.6	3.7	263.8	8			
Z16-35 - 153	1.9	5.06	0.7	37.4	5.1	6.49	0.99	12030	210	B.D.	9.8	44.4	2.6	255.9	8.8			
Z16-35 - 154	12	40	2.1	387	22	82.9	3.8	10820	230	10	12	56.6	3	387	11			
Z16-35 - 155	11	17.9	2.5	188	17	40.2	3.8	13120	350	B.D.	22	88.5	3.2	591	25			
Z16-35 - 156	21	65.6	5.6	651	49	127.6	7.1	11320	470	3	17	178	21	713	30			
Z16-35 - 157	18	36.3	4.4	310	35	56.8	5.5	13070	600	34	36	103.4	6.9	1105	98			
Z16-35 - 158	6.4	32.3	1.7	285	12	58.8	2.2	11280	220	12	16	68.1	4.9	116.8	4.4			
Z16-35 - 159	6.5	24.2	1.2	228.9	9.7	47	1.7	10210	170	10	11	105.5	2.6	123.6	2.9			

Z16-35 - 160	11	70.5	2.3	601	24	117.6	3.2	9230	190	2	11	376	12	231.4	5.8	
Z16-35 - 161	9.7	39.4	2.1	399	16	78.8	3.6	11480	230	9	16	555	19	569	15	
Z16-35 - 162	12	58.1	2.9	728	29	189.2	5.8	12240	310	3	15	696	19	596	24	
Z16-35 - 163	14	38.2	2	386	23	85.3	3.7	10610	200	B.D.	9.5	414	27	429	20	
Z16-35 - 164	13	8.6	2.6	76	26	14.6	5.7	13270	350	1	18	30.4	2.4	296	22	
Z16-35 - 165	6.4	25.7	1.1	241.5	9	47.4	1.7	9010	140	B.D.	11	135	1.6	124.2	4	
Z16-35 - 166	8.9	39.6	2.7	371	19	73.7	2.8	9490	250	0	13	142.4	5.7	235.1	6.7	
Z16-35 - 167	11	77.8	3.1	712	25	144	5.9	8060	310	7	14	206.1	7.4	174.8	6.1	
Z16-35 - 168	6.7	24.1	1.9	236.9	9.5	49.1	2.9	10780	240	9	14	136.4	4.8	159.3	4.6	
Z16-35 - 169	9.6	24.3	2.4	236	11	50.6	3.3	11310	470	0	21	64.6	6.3	160	17	
Nist610 - 1	24	409	18	431	27	424	23	420	26	417	44	447	16	448	24	
Nist610 - 2	26	418	22	449	28	432	25	429	30	419	72	452	24	462	29	
Nist610 - 3	30	418	20	442	34	430	18	431	26	422	88	456	28	464	27	
Nist610 - 4	22	402	18	427	19	417	20	416	18	415	60	443	16	443	19	
Nist610 - 5	25	412	23	440	24	432	25	434	30	421	75	448	23	454	32	
Nist610 - 6	24	416	23	437	28	427	18	423	22	391	80	455	22	456	23	
Nist610 - 7	34	408	30	438	34	426	27	421	29	473	87	435	30	450	29	
Nist610 - 8	21	420	17	445	22	432	17	433	21	415	64	457	18	460	17	
Nist610 - 9	16	401	21	420	29	412	24	408	22	387	72	435	21	438	20	
Nist610 - 10	22	411	22	445	29	434	25	438	26	473	85	456	23	458	26	
Nist610 - 11	22	407	16	429	20	422	16	421	18	397	62	445	18	454	17	
Nist610 - 12	27	419	14	447	23	435	16	426	22	428	85	455	19	456	19	
Nist610 - 13	24	407	22	430	25	420	17	422	25	434	61	441	23	445	22	
Nist610 - 14	28	408	23	440	28	427	26	419	29	396	59	449	22	459	27	
Nist610 - 15	28	413	21	435	30	429	22	425	21	431	70	449	24	452	17	
GJ1 - 1	3.3	5.99	0.89	63.4	7.1	13.2	1.5	7390	220	1	15	8.44	0.43	350	13	
GJ1 - 2	3.6	6.73	0.66	65.5	5.2	15.1	1.3	7290	200	17	14	8.93	0.87	344	11	
GJ1 - 3	3	6.7	0.95	70.6	5.7	13.8	1.3	7410	240	B.D.	13	9.03	0.96	345	10	
GJ1 - 4	4.3	6.66	0.98	61.9	6.1	13.8	1.6	7290	210	B.D.	15	8.19	0.99	337	11	
GJ1 - 5	3.6	6.7	1	62.3	4.2	13.92	0.97	7310	220	1	17	7.9	1.2	339.7	9.1	
GJ1 - 6	3.8	7.01	0.72	59.4	3	13.1	1.2	7300	180	B.D.	13	7.7	1	337	13	

GI1 - 7	2.4	6.87	0.71	57	4.7	13.37	0.82	7390	150	19	11	8.3	1.1	339.4	9.4	
GI1 - 8	3.1	5.62	0.89	65.8	6.9	12.11	0.93	7411	69	B.D.	18	7.3	1.2	332.5	6.1	
GI1 - 9	3.9	5.91	0.5	68.6	7	14	1	7590	170	B.D.	9.5	7.6	1.2	334.9	8.3	
GI1 - 10	3.2	6.23	0.81	58.3	6.4	14.1	1.2	7530	130	8	20	7.9	1.3	333	10	
GI1 - 11	2	6.62	0.73	59.4	6.8	13.8	1.4	7350	140	4	13	7.97	0.65	331.6	8.2	
GI1 - 12	2.9	6.62	0.88	63.2	8.9	13.29	0.99	7300	170	B.D.	16	7.56	0.89	344.3	8.3	
GI1 - 13	2.7	6.14	0.7	60.9	3.7	12.84	0.95	7090	110	7	14	7.2	0.58	324.2	6.9	
GI1 - 14	2.6	5.9	0.6	64.2	5.1	13.32	0.88	7250	150	B.D.	8.5	7.52	0.8	329.5	7.4	
GI1 - 15	4.3	6.04	0.77	63.6	6.3	13	0.85	7100	160	2	12	8.4	1.3	324	11	
GI1 - 16	2.8	6.89	0.47	62.2	3.6	12.4	1.3	7250	160	B.D.	8.5	8.32	0.64	332.6	8.4	
GI1 - 17	1.6	6.01	0.45	64.7	4.1	13	1.1	7150	120	B.D.	8.7	8.39	0.8	332.6	6.9	
GI1 - 18	3.1	6.24	0.65	62.3	6.2	13.23	0.88	7250	110	B.D.	9.4	7.87	0.66	330.7	7.9	
GI1 - 19	2.8	6.67	0.53	60.8	4.3	14	1.1	7350	150	3	17	7.98	0.91	335.4	8.2	
GI1 - 20	3.6	6.77	0.6	63.5	4	13.6	1.3	7220	150	11	11	8.52	0.9	332.9	7.7	
GI1 - 21	2.4	6.21	0.74	64	3.3	13.54	0.94	7200	110	B.D.	8.9	8.12	0.56	342.1	7.4	
GI1 - 22	2.7	6.63	0.77	60.9	5.1	13.3	1.1	7380	150	18	15	8.11	0.65	340.6	6.6	
GI1 - 23	2.1	6.44	0.63	61.9	5.2	14	1.2	7300	200	B.D.	12	7.83	0.52	326.8	9.6	
GI1 - 24	2	6.28	0.84	62.2	3.9	13.28	0.96	7430	120	B.D.	7.9	7.66	0.5	330.3	6.3	
GI1 - 25	2.9	5.65	0.51	59.7	4.3	12.92	0.92	7380	150	B.D.	8.3	7.58	0.66	334	7.7	
GI1 - 26	2.5	5.8	0.52	63	4.3	13.2	1.1	7440	130	7	13	7.83	0.62	335.7	7.7	
GI1 - 27	3.1	5.99	0.86	60.8	3.6	13.73	0.62	7370	120	B.D.	15	8.08	0.6	333.8	6.5	
GI1 - 28	2.3	6.21	0.73	62.3	4	12.8	1	7320	190	B.D.	10	8.15	0.67	329.3	8.6	
GI1 - 29	2.6	5.86	0.56	57.7	4.9	13.3	1	7320	120	B.D.	11	8.04	0.54	336.9	8.8	
GI1 - 30	2.9	6.53	0.75	62.1	3.1	13.4	1	7110	170	0	12	7.81	0.73	333	8.6	
Ples - 1	3.1	7.9	0.88	51.3	3.2	7.15	0.63	11780	290	7	15	105.2	2.9	908	25	
Ples - 2	4	13.6	1.2	87.9	6.8	12.44	0.81	10840	230	B.D.	7	269.9	7.4	2190	53	
Ples - 3	5	14.5	1.2	94.6	5.9	11.6	1.1	11000	350	B.D.	12	269.8	8.7	2182	56	
Ples - 4	4.1	8.31	0.71	61.1	5.5	8.55	0.81	12280	200	8	17	60.5	2.6	650	11	
Ples - 5	4.8	12.55	0.77	89.2	7.2	13	1.1	11100	250	B.D.	9.2	88.1	4.3	824	23	
Ples - 6	5.8	11.1	1.4	88	7.6	12.2	1.3	11050	290	B.D.	13	83.1	4.1	794	28	
Ples - 7	3.8	11.96	0.59	86.3	4.9	13.14	0.87	10940	160	1.4	8.7	77	1.7	775	17	
Ples - 8	4.7	7.66	0.54	46.8	6.7	6.64	0.74	11200	210	6	16	72.7	2.7	682	16	

Ples - 9	4.9	11.56	0.88	82	5.4	11.8	1.2	11540	250	B.D.	13	79.8	2.2	772	17	
Ples - 10	2.9	4.28	0.59	33.4	6.5	4.44	0.37	11500	310	B.D.	14	44.3	2.3	516	21	
Ples - 11	3.6	8.5	0.86	68.8	5.8	9.5	1.1	11720	290	B.D.	9.6	59.2	3	647	11	
Ples - 12	2.9	7.46	0.83	46	4.5	6.21	0.87	11670	210	B.D.	16	88.4	4.8	828	24	
Ples - 13	4.5	6.83	0.72	49.9	3.5	6.51	0.81	11830	220	9	10	97.1	4.1	853	17	
Ples - 14	3.1	8.2	1	48.6	4.8	7.04	0.83	11800	270	B.D.	8.4	103.4	3.8	876	23	
Ples - 15	3.2	7	0.64	50.7	4.6	6.24	0.57	11180	220	6	18	97.4	3.9	861	16	
91500 - 1	3	5.84	0.96	56.1	5.2	10.86	0.87	6170	120	5	21	25.61	0.97	70.9	2.8	
91500 - 2	2.1	4.94	0.87	50	5	10.1	1.8	6090	150	5	22	23.8	1.8	67.6	2.3	
91500 - 3	2.4	5.15	0.98	50.4	5	12.34	0.9	6160	110	1	17	25.7	1.3	71.2	2.3	
91500 - 4	1.8	4.87	0.57	58.2	3.7	12.34	0.71	6100	160	B.D.	13	24.7	1.3	69.2	2.2	
91500 - 5	2.1	5.59	0.52	55	4.5	12.19	0.83	6140	140	3	14	24.3	1.3	69.1	2.5	
91500 - 6	2.2	4.96	0.6	56.2	3.5	12.51	0.8	6070	100	B.D.	8.7	25	1.3	66.6	2.4	
91500 - 7	1.8	4.59	0.29	47	3.8	9.65	0.98	6050	110	11	14	19.87	0.84	61.4	2	
91500 - 8	1.7	4.59	0.64	53.3	4.3	11.66	0.97	6130	110	1	10	22.7	1.5	65.9	2	
91500 - 9	1.8	5.22	0.65	57.7	4.4	11.3	1	6200	110	B.D.	10	25	1.4	68.4	2.5	
91500 - 10	2.3	5.21	0.4	55.8	5	10.97	0.72	6360	170	B.D.	9.9	24.8	1.5	68.3	1.6	
91500 - 11	2.4	5.45	0.42	53.2	3.6	11.36	0.76	6150	130	2	16	24.5	1.4	67.7	1.4	
91500 - 12	1.7	4.79	0.61	51.6	3.8	10.5	0.85	6040	130	4	13	20.92	0.87	59.8	2.3	
91500 - 13	1.4	5.14	0.71	54.8	4	11.32	0.92	5890	120	3	14	24.1	1.3	66.1	2.6	
91500 - 14	2.2	5.26	0.82	49.5	3.7	10.7	1.4	5950	100	4	12	23.5	1.1	64.3	2.1	
91500 - 15	2.1	4.95	0.81	53.3	4.6	11.27	0.96	5860	170	4	14	24.5	1.5	64.9	2.1	
91500 - 16	2.1	4.99	0.6	56.7	3.2	11.99	0.83	5898	97	4	13	24	1.2	67.7	3.1	
91500 - 17	2	5.36	0.66	55.5	3.7	12	1.1	5860	160	10	11	23.7	1.3	66.1	2.2	
91500 - 18	2.4	5.33	0.44	51.5	4.7	10.16	0.74	5953	87	1	12	21.7	1.2	63.1	1.8	
91500 - 19	2.7	5.78	0.6	62.7	6.8	12.8	1.3	6110	140	B.D.	9.3	24.5	1.7	70.1	2.6	
91500 - 20	2.7	4.9	0.7	56.5	3.2	12	1	6100	110	B.D.	10	25.8	1.1	68.1	1.8	
91500 - 21	2.2	5.08	0.72	57.1	4.2	11.4	0.77	6025	84	B.D.	10	24.8	1	66.9	2.1	
91500 - 22	2.5	4.74	0.46	47.1	4.1	9.76	0.95	5970	140	8	15	23.5	1.8	66.2	3.1	
91500 - 23	2.4	3.97	0.81	44.7	4.4	9.9	1.2	6050	170	8	16	20	1.2	63.3	3.5	
91500 - 24	2.3	5.67	0.67	54.4	5.9	11.29	0.94	6140	150	B.D.	7.8	25.1	2.2	67.1	2.5	
91500 - 25	2.6	5.17	0.59	54.1	3.7	11.53	0.93	6150	130	B.D.	3.1	24.4	1.5	69.7	2	

91500 - 26	2.6	5.09	0.62	54.7	4.7	11.87	0.98	6160	130	0	11	22.7	1.1	64.7	2.7	
91500 - 27	1.4	4.63	0.63	52.5	3.7	12.4	1.2	6120	110	B.D.	8.2	23.8	1.6	66.4	2.6	
91500 - 28	2.1	4.74	0.61	50.4	3.5	10.5	0.87	6030	110	B.D.	8.9	21.7	1.5	65.2	2.8	
91500 - 29	3	6.65	0.75	53.2	3.7	11.05	0.75	6050	150	B.D.	10	22.89	0.95	67	2.7	
91500 - 30	2.6	4.42	0.49	51.6	3.6	11.68	0.91	5820	120	14	17	21.6	1.1	63.1	2.6	

REE values are in ppm unless otherwise stated

Table S5. Whole-rock major and trace element geochemical data for Nyimba-Sinda granite samples.

Element	Z16-33	Z16-50	Z16-51
Major element proportions (wt%)			
SiO2	77.37	74.50	73.08
TiO2	0.00	0.21	0.00
Al2O3	12.93	13.80	15.91
Fe2O3T	0.17	1.22	0.01
MnO	0.02	0.02	0.02
MgO	0.05	0.28	0.09
CaO	1.08	0.82	1.29
Na2O	3.76	3.24	4.26
K2O	4.34	5.49	4.99
P2O5	0.03	0.08	0.05
Total	**99.75**	**99.66**	**99.70**
LOI	0.29	0.58	0.52
Trace element concentrations (ppm)*			
Rb	112.6	205.1	116.0
Sr	265	481	940
Y	<0.5	9.6	<0.5
Zr	15	171`	50
V	4	15	6
Ni	<1	<1	2
Cr	13	1	17
Nb	<0.5	35.9	<0.5
Ga	27.6	26.2	22.1
Cu	10	43	13
Zn	9	23	8
Co	37	29	24
Ba	502	1388	2984
La	23	67	10
Ce	25	333	8
U	<0.5	0.9	0.8
Th	4.2	50.3	<0.5
Sc	<1	<1	<1
Pb	26	13	75

Appendix 3

Supplementary material for: On yoderite: Using calculated phase equilibria to investigate its rarity in the geological record of whiteschists. Journal of Metamorphic Geology, 36(3), 297-314.

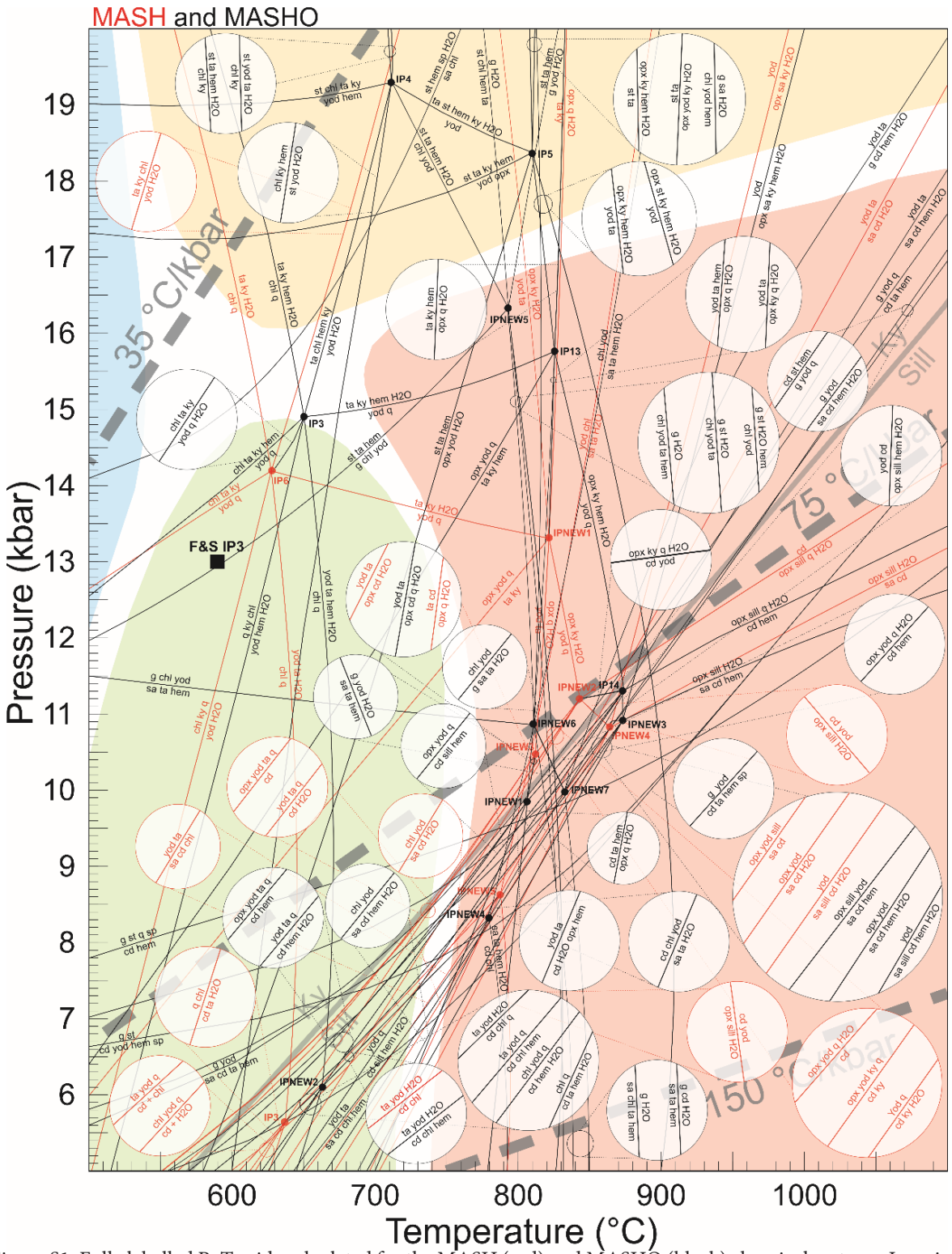

Figure S1. Fully labelled P–T grids calculated for the MASH (red) and MASHO (black) chemical systems. Invariant points are marked by circles, univariant reactions are denoted by the lines emanating from each point. Invariant points identical to those in Schreyer and Seifert (1969) and Fockenberg and Schreyer (1994) are given the same labels as those in their published grids. Points that are unique to our calculated grid are labelled as 'IPNEW'. The invariant point from which both known yoderite forming reactions emanate from, IP3, is shown for both this study (~15 kbar and 650 °C) and that by Fockenberg and Schreyer (1994; denoted by black square labelled 'F&S IP3'). The coloured fields behind the calculated grids refer to the different metamorphic facies as shown in Vernon and Clarke (2008), where red = granulite, green = amphibolite, blue = blueschist, yellow = eclogite.

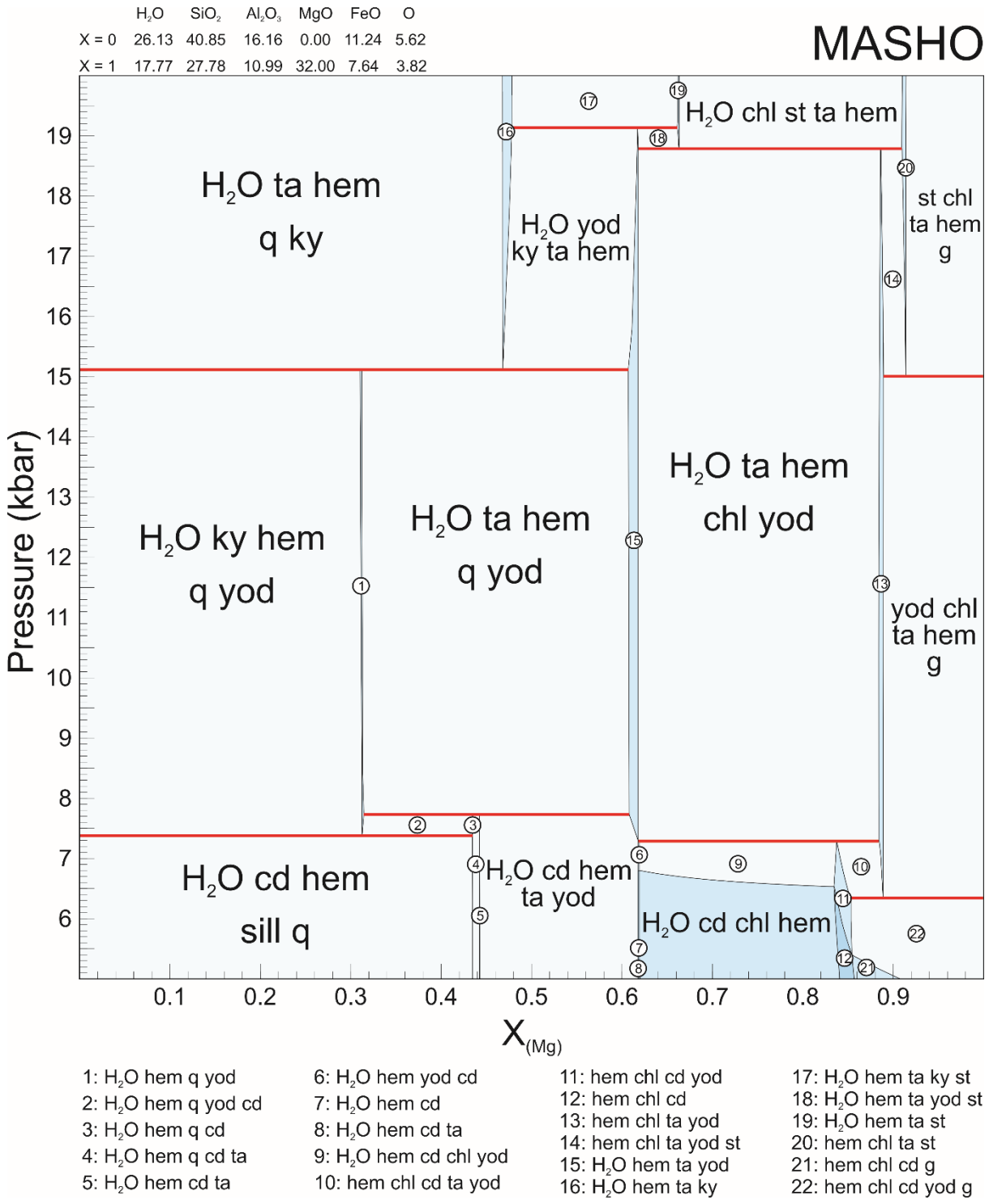

Figure S2. Calculated P–XMgO model for the MASHO system at 725 °C, based on the chemistry of the green yoderite-bearing pod from the Chewore Hills. The exact compositional range is given in the top left and is in mole%. Red horizontal lines in each model denote univariant reactions.

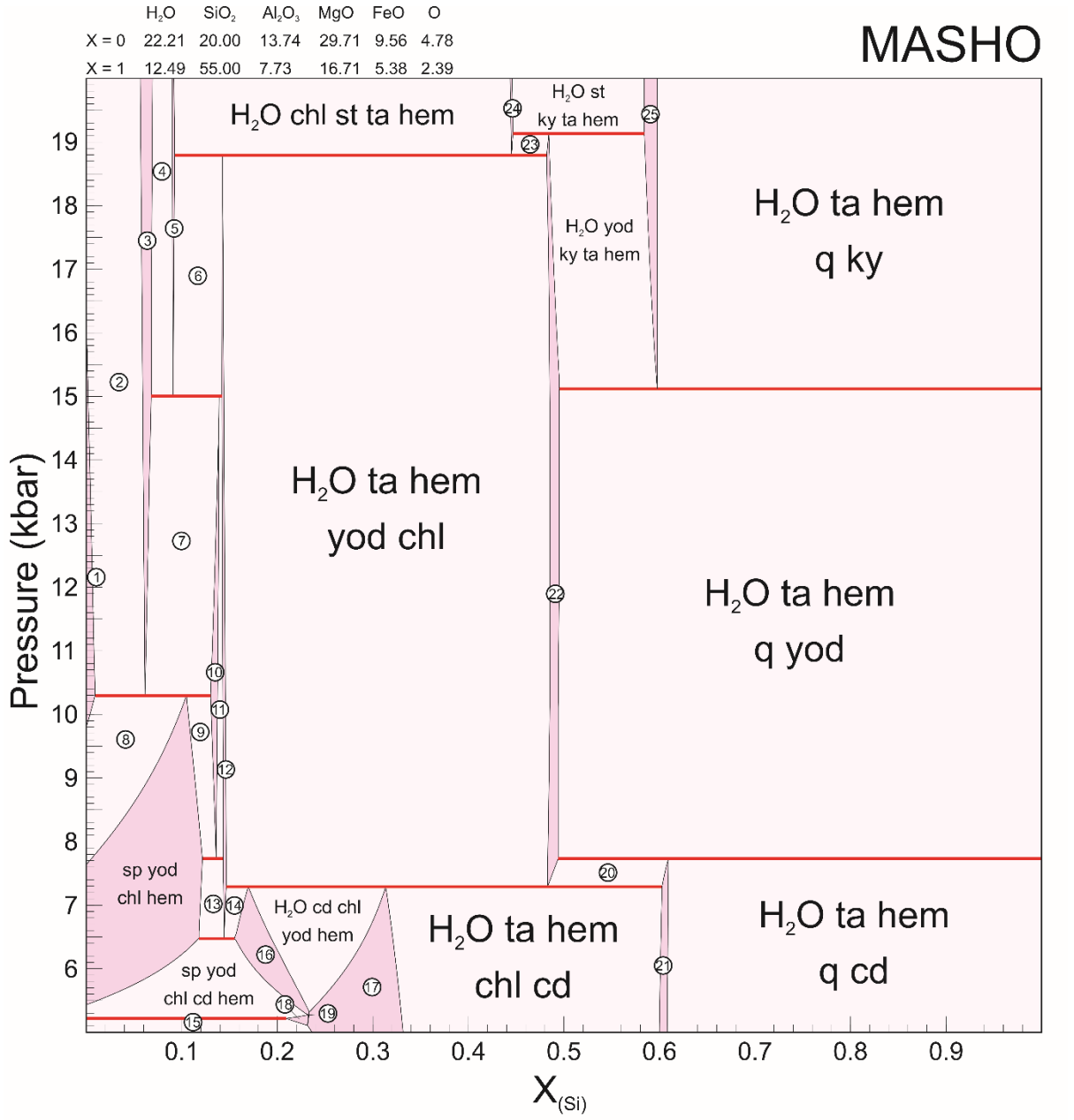

1: sp st chl hem
2: sp g st chl hem
3: g st chl hem
4: g st chl hem ta
5: st chl hem ta
6: yod st chl hem ta
7: g chl hem yod st
8: st sp yod chl hem
9: sp g yod chl hem
10: g yod chl hem
11: ta g chl hem yod
12: ta chl hem yod
13: ta chl hem yod sp
14: ta yod hem chl cd
15: H_2O sp chl cd hem
16: yod cd chl hem
17: H_2O cd chl hem
18: sp chl cd hem
19: chl cd hem
20: H_2O cd ta yod hem
21: H_2O cd ta hem
22: H_2O ta hem yod
23: H_2O st ta hem yod
24: H_2O st ta hem
25: H_2O ta hem ky

Figure S3. Calculated P–XSiO2 model for the MASHO system at 725 °C, based on the chemistry of the green yoderite-bearing pod from the Chewore Hills. The exact compositional range is given in the top left and is in mole%. Red horizontal lines in each model denote univariant reactions.

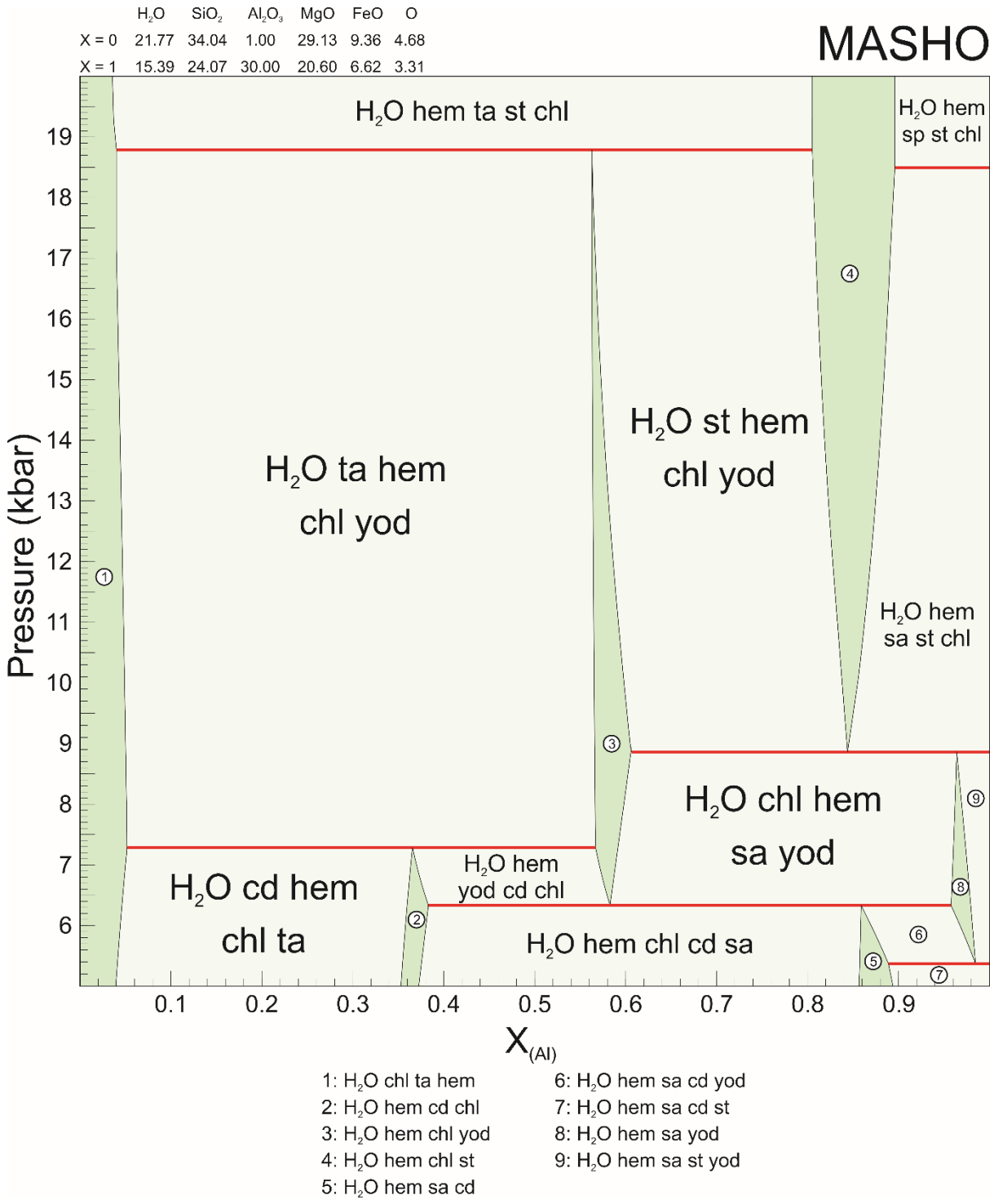

Figure S4. Calculated P–XAl2O3 model for the MASHO system at 725 °C, based on the chemistry of the green yoderite-bearing pod from the Chewore Hills. The exact compositional range is given in the top left and is in mole%. Red horizontal lines in each model denote univariant reactions.

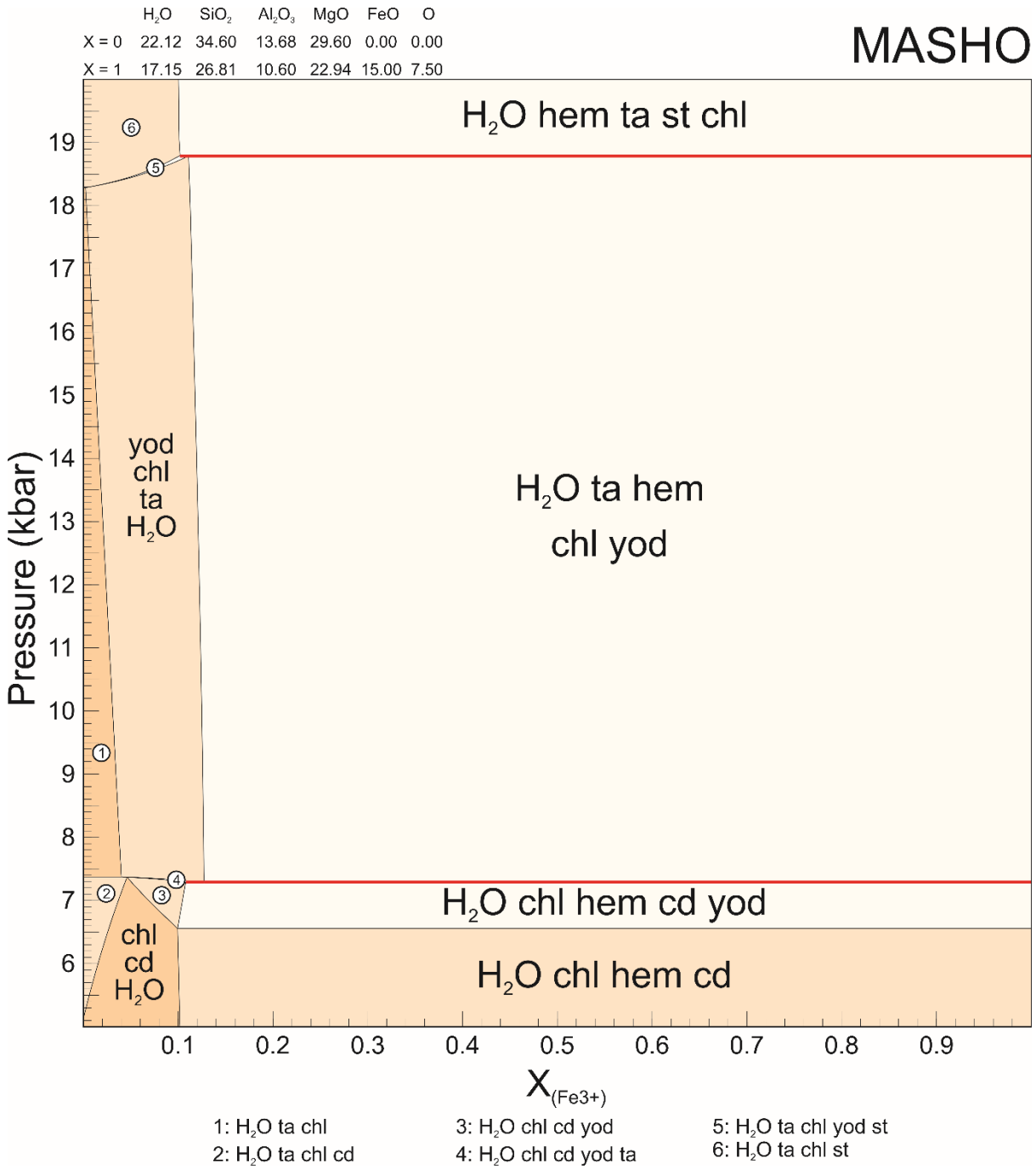

Figure S5. Calculated P–XFe2O3 model for the MASHO system at 725 °C, based on the chemistry of the green yoderite-bearing pod from the Chewore Hills. The exact compositional range is given in the top left and is in mole%. Red horizontal lines in each model denote univariant reactions.

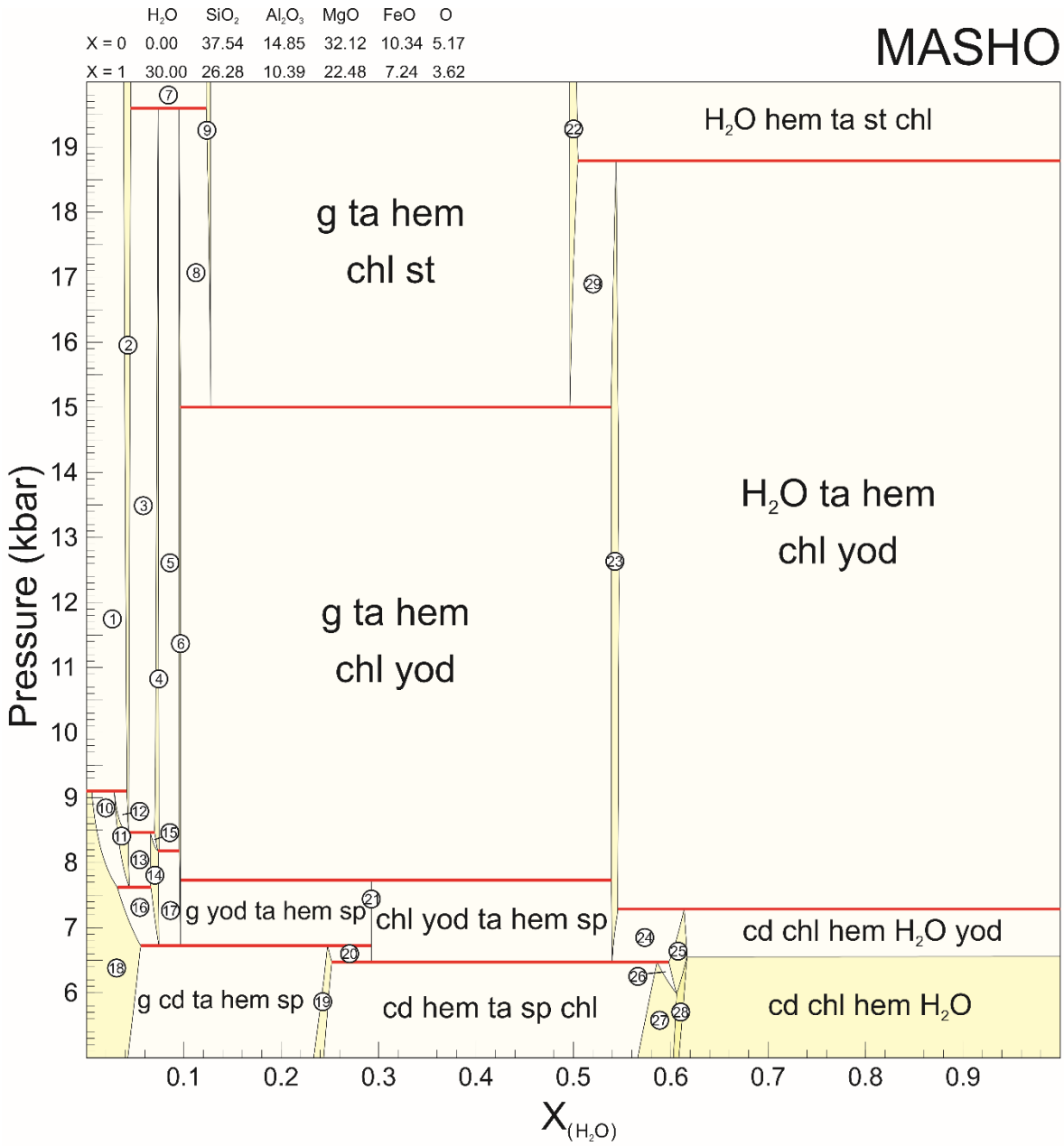

1: g st q hem sp
2: g st q hem
3: g st q hem yod
4: g q hem yod
5: g q hem yod ta
6: g hem yod ta
7: g st q hem ta
8: g hem yod ta st
9: g hem ta st
10: g cd st hem sp
11: g cd st hem
12: g cd st hem q
13: g cd st hem yod
14: g cd yod hem
15: g cd yod hem q
16: g cd yod hem sp
17: g cd yod hem ta
18: g cd hem sp
19: cd ta hem sp
20: cd ta hem sp yod
21: yod ta hem sp
22: hem ta st chl
23: ta hem chl yod
24: ta hem chl yod cd
25: hem chl yod cd
26: cd hem sp chl yod
27: cd hem sp chl
28: cd hem chl
29: hem ta st chl yod

Figure S6. Calculated P–XH2O model for the MASHO system at 725 °C, based on the chemistry of the green yoderite-bearing pod from the Chewore Hills. The exact compositional range is given in the top left and is in mole%. Red horizontal lines in each model denote univariant reactions.

Yoderite a ctivity–composition (a–x) model for use with THERMOCALC.

```
% ================================================
% ------------------------------------------------
% Yoderite "v4" (in Fe-Mg-Al-Fe3-Si-H)
%
% coded by DEK 4th October 2016
%
% myod end-member requires 'make' facility using the following reaction:
% yoderite + quartz = Tschermaks talc + kyanite.
% yodo end-member requires 'make' facility using the following reaction:
% yoderite = Tschermaks talc + kyanite + hematite.
% other two yoderite end-members require 'make' facility using the following reaction:
% yoderite + quartz = talc + kyanite + hematite + H2O

% Yoderite sites:
% vi[MgAl3] v[MgAl] v[Al,Fe3+]2 [SiO4]4 O2 (OH)2
% v=trigonal bipyramid
% vi = octahedral site
% in this model assume that some Fe3+ partitions into the Mg-Al vi & v sites

%        M1                                    B1          B2
%          Mg  Fe  Al  Fe3   Mg  Fe   Al  Fe3   Al  Fe3
% myod   1   0   3   0     1   0    1   0     2   0    [SiO4]4O2(OH)2
% fyod   0   1   3   0     0   1    1   0     2   0    [SiO4]4O2(OH)2
% yodo   1   0   5/2 1/2   1   0    1/2 1/2   1   1    [SiO4]4O2(OH)2
% fmoy   1   0   3   0     0   1    1   0     2   0    [SiO4]4O2(OH)2

% x = Fe2/(Fe2+Mg)
% f = Fe3/2
% Q = 2(x - xFeM1)  (or xFeB1 - xFeM1)
% ------------------------------------------------

yod 4  1

x(yod)  0.0
f(yod)  0.3
Q(yod)  0.0

% ------------------------------------------------

p(myod)  1 1   1  3 -1  x  -1/2 Q  -1 f

p(fyod)  1 1   0  2  1  x  -1/2 Q

p(yodo)  1 1   0  1  1  f
```

```
p(fmoy)  1 1   0  1  1  Q

% ------------------------------------------------

sf
W(myod,fyod)   10   0   -0.02
W(myod,yodo)   12   0    0
W(myod,fmoy)    4   0    0
W(fyod,yodo)   16   0    0
W(fyod,fmoy)    4   0    0
W(yodo,fmoy)   12   0    0

% ------------------------------------------------
10

xMgM1   1 2   1  1 -1 x  1  1 -1/8 f

xFeM1   1 2   0  1  1 x  1  1 -1/8 f

xFe3M1   1 1   0  1  1/8 f

xAlM1   1 1   1  1  -1/8 f

xMgB1   1 2   1  1 -1 x  1  1 -1/4 f

xFeB1   1 2   0  1  1 x  1  1 -1/4 f

xFe3B1   1 1   0  1  1/4 f

xAlB1   1 1   1  1 -1/4 f

xFe3B2   1 1   0  1  1/2 f

xAlB2   1 1   1  1 -1/2 f

% ------------------------------------------------

myod   1   5   xMgM1 1  xAlM1 3  xMgB1 1  xAlB1 1  xAlB2 2
check 0  0  0
make  3   tats 1   ky 2   q -1
DQF   -20  0  0

fyod   1   5   xFeM1 1  xAlM1 3  xFeB1 1  xAlB1 1  xAlB2 2
check 1  0  0
make  4   fta 2/3   ky 3   H2O 1/3   q -5/3
% DQF   0  0  0
```

```
yodo   1   8   xMgM1 1  xFe3M1 1/2  xAlM1 5/2  xMgB1 1  xFe3B1 1/2  xAlB1 1/2  xFe3B2 1
                                        xAlB2 1
                                      check 0  1  0
                                    make  3   tats 1   ky 1   hem 1
                                      DQF   30  0  0

                  fmoy   1   5   xMgM1 1  xAlM1 3  xFeB1 1  xAlB1 1  xAlB2 2
                                      check 0.5  0  1
                                make  5   ta 1/3   fta 1/3   ky 3   H2O 1/3   q -5/3
                                      %  DQF   0  0  0

          % ================================================
                                        *
```

Appendix 4

Supplementary material for: Identifying the tectono-metamorphic overprints of a Gondwana forming collision: a structural and thermobarometric transect of the Southern Irumide and Zambezi belts, Zambia.

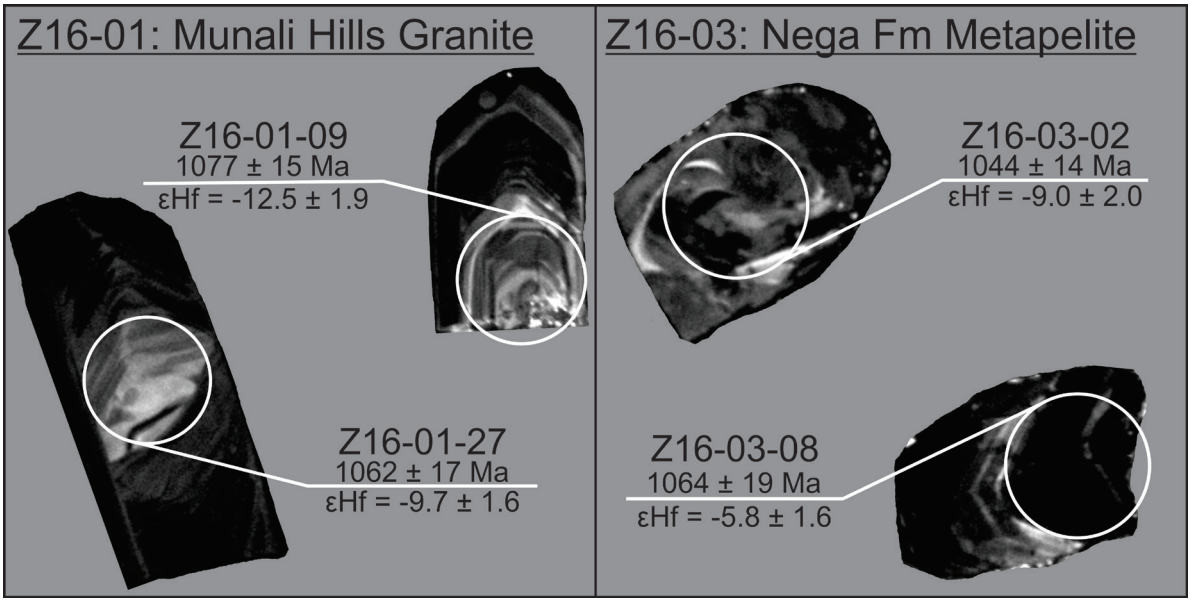

Figure S1. Representative cathodoluminescence images of zircons from Munali Hills Granite sample Z16-01 and Nega Formation sample Z16-03.

Table S1. Individual zircon U-Pb standard analyses.

	Isotope ratios and 2σ error (absolute)						Calculated age in Ma and 2σ error (absolute)						Total Isotope counts (PPM) and 2σ error (absolute)					
Analysis	$^{207}Pb/^{206Pb}$		$^{206}Pb/^{238}U$		$^{207}Pb/^{235}U$		$^{207}Pb/^{206}Pb$		$^{206}Pb/^{238}U$		$^{207}Pb/^{235}U$		U		Th		Pb	
Z_GJ1_1	0.0604	0.0007	0.0968	0.0013	0.8057	0.015	621	22	595.3	7.7	600	8.4	403	16	11.16	0.79	2.803	0.087
Z_GJ1_2	0.0602	0.0008	0.0974	0.0014	0.8063	0.016	609	28	599.1	8	600.4	9	456.8	5.9	12.72	0.93	3.18	0.13
Z_GJ1_3	0.0598	0.0007	0.0957	0.0014	0.7902	0.013	594	25	589.3	8.1	591.3	7.6	405	19	10.96	0.78	2.81	0.14
Z_GJ1_4	0.0601	0.0007	0.0961	0.0013	0.7935	0.014	606	25	591.2	7.5	593.1	8	398	18	10.6	1.2	2.807	0.064
Z_GJ1_5	0.0603	0.0007	0.097	0.0013	0.8059	0.014	613	26	596.9	7.5	600.1	8.1	426	22	11.7	1.2	2.98	0.12
Z_GJ1_6	0.0596	0.0007	0.0962	0.0013	0.7921	0.014	588	24	593.1	8.5	592.3	8.1	405	20	10.62	0.84	2.89	0.1
Z_GJ1_7	0.06	0.0007	0.0976	0.0014	0.8049	0.014	600	26	600.5	8.1	599.6	8.1	393	21	11.31	0.63	2.83	0.11
Z_GJ1_8	0.0602	0.0007	0.0972	0.0013	0.8066	0.014	609	25	597.9	7.5	600.5	7.9	406	17	12.2	1	2.782	0.086
Z_GJ1_9	0.06	0.0007	0.0976	0.0013	0.8092	0.014	601	27	600.6	7.7	602	7.9	408	23	11.3	1.4	2.79	0.14
Z_GJ1_10	0.06	0.0007	0.0958	0.0013	0.7955	0.014	602	25	589.7	7.6	594.2	8.2	424	19	11.68	0.95	2.83	0.13
Z_GJ1_11	0.0601	0.0007	0.0987	0.0014	0.8226	0.014	607	27	606.7	7.9	609.5	8	413	21	9.84	0.77	2.88	0.15
Z_GJ1_12	0.0595	0.0007	0.0977	0.0013	0.8086	0.015	584	25	601	7.9	601.7	8.2	434	20	9.3	1.1	3.12	0.12
Z_GJ1_13	0.06	0.0008	0.0961	0.0013	0.8029	0.014	602	28	591.7	7.8	598.4	8.2	383	23	9.9	1.1	2.62	0.11
Z_GJ1_14	0.06	0.0009	0.0978	0.0013	0.8191	0.016	603	31	601.4	7.8	607.5	8.8	392	20	9.5	1.1	2.81	0.14
Z_GJ1_15	0.0599	0.0007	0.0981	0.0013	0.8176	0.015	598	26	603.5	7.6	606.7	8.4	391	20	10.37	0.93	2.76	0.12
Z_GJ1_16	0.0599	0.0008	0.0953	0.0014	0.7922	0.015	599	30	586.6	8.1	592.4	8.5	375	25	10.1	1.4	2.57	0.14
Z_GJ1_17	0.0597	0.0008	0.0984	0.0014	0.8135	0.015	592	28	604.8	8	604.4	8.5	385	24	9.88	0.68	2.59	0.13
Z_GJ1_18	0.0597	0.0008	0.0978	0.0014	0.8126	0.015	590	29	601.7	8.1	603.9	8.2	391	19	9.9	1.2	2.806	0.082
Z_GJ1_19	0.06	0.0008	0.0978	0.0013	0.8143	0.016	602	28	601.7	7.9	604.8	8.8	404	17	10.3	1	2.784	0.075
Z_GJ1_20	0.0598	0.0007	0.0978	0.0013	0.809	0.015	599	28	601.3	7.8	601.8	8.4	401	19	10.82	0.88	2.693	0.092
Z_GJ1_21	0.06	0.0007	0.0975	0.0013	0.8107	0.014	602	24	599.5	7.7	602.8	7.8	391	17	10.1	1.3	2.656	0.088
Z_GJ1_22	0.0603	0.0007	0.0982	0.0014	0.8176	0.015	612	25	603.9	7.9	606.7	8.2	408	23	9.9	1	2.97	0.11
Z_GJ1_23	0.0597	0.0007	0.0972	0.0013	0.8014	0.016	590	27	597.9	7.8	597.6	8.8	431	19	10.3	0.93	3.07	0.11
Z_GJ1_24	0.0603	0.0007	0.0974	0.0014	0.8092	0.015	611	26	599	8	602	8.2	395	17	10.2	1.2	2.673	0.065
Z_GJ1_25	0.0601	0.0008	0.0967	0.0013	0.8009	0.014	604	28	595.1	7.7	597.3	8	395	19	11.05	0.98	2.65	0.1
Z_GJ1_26	0.06	0.0008	0.0971	0.0013	0.8005	0.016	602	28	597.1	7.7	597	8.8	398	24	10.5	1.3	2.81	0.11
Z_GJ1_27	0.0601	0.0008	0.0967	0.0013	0.7965	0.015	607	28	594.9	7.9	594.8	8.6	415	24	10.2	1	3.03	0.12
Z_GJ1_28	0.0604	0.0007	0.0975	0.0013	0.8049	0.014	617	25	599.5	7.6	599.6	7.8	427	20	11.9	1.2	3.031	0.091
Z_GJ1_29	0.0599	0.0007	0.0973	0.0013	0.7928	0.014	597	26	598.7	7.7	592.7	8	413	14	11.6	1.1	2.92	0.12
Z_GJ1_30	0.0602	0.0008	0.0935	0.0013	0.7647	0.015	610	29	576.2	7.7	577.9	8.2	409	21	10.8	1.1	2.894	0.087
Z_Plesovice_1	0.0534	0.0006	0.0515	0.0007	0.3794	0.007	343	27	323.45	4.1	326.6	4.8	1084	43	138.5	3.8	20.78	0.23
Z_Plesovice_2	0.0531	0.0006	0.0538	0.0007	0.3938	0.007	333	26	337.6	4.5	337.1	5.1	776	35	80.3	3.6	11.82	0.27

Z_Plesovice_3	0.0529	0.0006	0.0543	0.0007	0.3996	0.007	324	26	341.1	4.4	341.4	5	1142	26	115.9	3	21.15	0.43
Z_Plesovice_4	0.053	0.0007	0.055	0.0007	0.4057	0.007	325	28	345.1	4.4	345.8	5.2	973	40	112	3	17.06	0.49
Z_Plesovice_5	0.0535	0.0006	0.0543	0.0007	0.4038	0.007	346	26	340.6	4.5	344.4	5.1	947	53	99.9	5.4	15.96	0.54
Z_Plesovice_6	0.0533	0.0006	0.0548	0.0007	0.4034	0.007	339	25	343.6	4.4	344.1	5	810	43	91.3	5.2	14.28	0.51
Z_Plesovice_7	0.0534	0.0006	0.0549	0.0007	0.4062	0.007	343	26	344.3	4.4	346.1	5.3	891	52	93.2	4.9	14.76	0.53
Z_Plesovice_8	0.0533	0.0007	0.0538	0.0007	0.3977	0.007	338	29	337.9	4.3	340	5	650	45	61.7	4	9.39	0.42
Z_Plesovice_9	0.0535	0.0007	0.0546	0.0008	0.4032	0.008	346	31	342.9	4.6	343.9	5.9	789	42	72.5	3.9	12.65	0.33
Z_Plesovice_10	0.0532	0.0006	0.0523	0.0007	0.3832	0.007	337	27	328.7	4.3	329.4	4.9	939	62	115.8	9.4	17.2	1.1
Z_Plesovice_11	0.053	0.0007	0.0545	0.0007	0.3968	0.007	328	28	342.1	4.5	339.3	5.3	1061	42	128	6.4	19.98	0.61
Z_Plesovice_12	0.0529	0.0006	0.0546	0.0007	0.3931	0.007	324	26	342.8	4.4	336.6	4.9	1084	71	140	11	20.6	1.1
Z_Plesovice_13	0.0532	0.0007	0.0547	0.0008	0.3946	0.007	336	30	343.5	4.8	337.7	5.1	1153	47	142.1	7.2	23.04	0.75
Z_91500_1	0.0753	0.0009	0.1797	0.0026	1.865	0.038	1074	24	1065.1	14	1068.6	13	81.9	3.5	31.4	1.6	15.53	0.34
Z_91500_2	0.0748	0.0012	0.1792	0.003	1.843	0.041	1060	31	1063	16	1063	16	76	3.9	28.4	1.3	14.14	0.36
Z_91500_3	0.074	0.0011	0.1782	0.0027	1.822	0.036	1039	30	1057.1	15	1053.2	13	80.9	3.2	31.7	1.1	15.22	0.33
Z_91500_4	0.0759	0.001	0.1784	0.003	1.851	0.041	1090	27	1058	17	1066	16	80.3	2.8	30	1.3	15.01	0.25
Z_91500_5	0.0744	0.001	0.1805	0.0026	1.85	0.035	1050	26	1069.7	14	1063.4	12	79.5	2.8	29.7	1.1	14.99	0.29
Z_91500_6	0.075	0.001	0.1785	0.0025	1.837	0.035	1068	26	1058.7	14	1058.8	13	80.6	4.8	31.6	1.8	15.02	0.54
Z_91500_7	0.0754	0.001	0.1782	0.0029	1.865	0.039	1078	27	1057.3	16	1068.5	14	80.5	3.6	32.1	1.9	15.02	0.39
Z_91500_8	0.0749	0.001	0.1789	0.0029	1.851	0.038	1065	27	1061	16	1063.7	14	78.6	3.9	31.4	1.4	14.92	0.36
Z_91500_9	0.0749	0.001	0.1787	0.0029	1.845	0.039	1069	26	1059.9	16	1061.5	14	82.4	4.1	32.1	1.8	15.09	0.29
Z_91500_10	0.0746	0.0013	0.1794	0.0029	1.855	0.047	1055	35	1064	16	1065	17	78.7	3.9	26.9	1.4	14.93	0.39
Z_91500_11	0.0742	0.0011	0.1796	0.0028	1.846	0.036	1046	29	1064.9	15	1062.1	13	79.4	4.1	24.9	1.8	14.85	0.46
Z_91500_12	0.0747	0.0011	0.1795	0.0028	1.859	0.038	1060	29	1064.3	15	1066.5	13	80.7	3.1	29.8	1.6	15.12	0.33
Z_91500_13	0.0742	0.0012	0.1787	0.0028	1.845	0.039	1046	31	1059.6	15	1061.5	14	79.9	3.8	29.9	1.6	14.94	0.44
Z_91500_14	0.0753	0.0014	0.1808	0.0029	1.904	0.042	1080	34	1071.5	16	1082	15	79.5	4.6	29.2	1.9	14.97	0.49
Z_91500_15	0.0755	0.0009	0.1793	0.0028	1.878	0.04	1080	25	1063.1	15	1073	14	80.6	4.3	30	1.5	15.14	0.54
Z_91500_16	0.0747	0.0011	0.1766	0.0029	1.825	0.04	1059	30	1048.5	16	1054.4	14	79.2	5.6	27	2	14.79	0.64
Z_91500_17	0.0739	0.0009	0.181	0.0028	1.85	0.036	1037	25	1072.4	15	1063.3	13	80	4.9	28.7	1.7	15.04	0.6
Z_91500_18	0.0745	0.0009	0.1769	0.0029	1.836	0.036	1054	23	1049.9	16	1058.4	13	79.9	5.5	30.7	2	15.01	0.59
Z_91500_19	0.0751	0.001	0.18	0.0027	1.871	0.038	1075	28	1067.1	14	1070.7	13	80.4	4.3	31.3	2	15.03	0.44
Z_91500_20	0.0753	0.0011	0.1797	0.0028	1.869	0.038	1080	27	1065.1	15	1070.1	14	80.4	4.6	27.9	1.8	15.04	0.45
Z_91500_21	0.075	0.001	0.1785	0.0027	1.852	0.038	1068	27	1058.9	15	1064	14	78.6	5	26.5	2	14.7	0.67
Z_91500_22	0.0748	0.0011	0.1777	0.0032	1.83	0.046	1061	30	1055	17	1056	16	80.2	4.5	30.9	1.3	15.08	0.49
Z_91500_23	0.0751	0.0012	0.1797	0.0028	1.86	0.042	1070	31	1065.5	15	1067	15	80.5	2.7	32.1	1	15.02	0.21

Z_91500_24	0.075	0.0009	0.1798	0.0028	1.848	0.035	1068	25	1065.7	15	1062.7	13	78.8	4.1	29.3	1.6	14.84	0.47	
Z_91500_25	0.075	0.0012	0.1797	0.0029	1.841	0.045	1067	33	1065.2	16	1060	16	81.4	5.4	30.7	2.3	15.31	0.72	
Z_91500_26	0.0755	0.0015	0.1801	0.0029	1.871	0.044	1080	39	1067.4	16	1071	16	79.2	4.2	28.9	1.5	14.88	0.45	
Z_91500_27	0.0752	0.001	0.1773	0.0027	1.818	0.038	1071	28	1052.4	15	1051.7	14	80.7	4.6	33	1.6	15.15	0.58	
Z_91500_28	0.0749	0.0012	0.1806	0.0034	1.833	0.042	1063	31	1070	18	1057	15	79.9	3.9	29.3	1.3	14.98	0.45	

Table S2. Individual zircon U-Pb unknown analyses.

Analysis	Isotope ratios and 2σ error (absolute)						ρ*	Concordance (%)	Calculated age in Ma and 2σ error (absolute)						Total Isotope counts (PPM) and 2σ error (absolute)					
	$^{207}Pb/^{206}Pb$		$^{206}Pb/^{238}U$		$^{207}Pb/^{235}U$				$^{207}Pb/^{206}Pb$		$^{206}Pb/^{238}U$		$^{207}Pb/^{235}U$		U		Th		Pb	
Z16-03 - 6	0.0758	0.0008	0.1884	0.003	1.977	0.041	0.9371	102	1088	22	1112	17	1108	14	358	17	182.7	7.3	100.2	2.6
Z16-03 - 14	0.0752	0.0009	0.1836	0.003	1.91	0.033	0.507	101	1073	24	1087	14	1085	12	391	23	157	16	75.9	5.7
Z16-03 - 11	0.0755	0.0009	0.1845	0.003	1.929	0.035	0.6162	101	1080	23	1092	14	1091	12	355	12	172.4	5.4	82.9	1.6
Z16-03 - 12	0.0755	0.0009	0.1838	0.003	1.921	0.039	0.9715	101	1082	23	1088	15	1088	14	547	21	227	25	85.1	4.4
Z16-03 - 2	0.074	0.0008	0.1758	0.003	1.793	0.031	0.7909	100	1039	22	1044	14	1043	11	270.8	2.9	115.7	1.9	54.32	0.89
Z16-03 - 3	0.0759	0.0009	0.1846	0.003	1.929	0.035	0.5556	100	1092	23	1092	15	1091	12	147	11	65.7	5.1	34.8	2.3
Z16-03 - 1	0.0728	0.001	0.168	0.002	1.692	0.03	0.3212	100	1006	26	1001	13	1005	11	100.9	6.5	89.3	7.9	39.8	2.7
Z16-03 - 8	0.0791	0.001	0.1795	0.003	1.967	0.043	0.9071	91	1174	24	1064	19	1104	15	640	48	305	21	163.2	9.8
Z16-03 - 15	0.0769	0.0009	0.1661	0.004	1.758	0.048	0.9653	89	1118	23	990	24	1030	18	349	10	236	19	62.5	1.2
Z16-03 - 13	0.0773	0.0014	0.1586	0.004	1.699	0.062	0.9513	84	1128	35	949	20	1008	23	432.1	8.1	183	5.2	94.8	6.2
Z16-03 - 9	0.0791	0.0008	0.1647	0.002	1.805	0.031	0.9334	84	1174	21	982.9	12	1047	11	654	47	349	23	156.7	7.1
Z16-03 - 7	0.0778	0.001	0.156	0.008	1.683	0.077	0.9897	82	1140	27	934	46	1000	29	332	19	268.2	9.3	141.6	6.4
Z16-03 - 4	0.0703	0.0011	0.1208	0.004	1.176	0.039	0.8943	79	935	33	735	20	789	18	150.2	7.9	178	13	56.4	3.7
Z16-03 - 17	0.0816	0.0021	0.162	0.013	1.83	0.11	0.9937	79	1233	50	969	73	1052	43	226	31	128.5	7.7	72.2	2.7
Z16-03 - 5	0.0803	0.0012	0.1354	0.002	1.505	0.03	0.42	68	1203	29	818.6	11	932.3	12	344	13	358.8	9.6	120.3	4.6
Z16-03 - 18	0.072	0.001	0.1002	0.005	0.987	0.043	0.9926	62	985	29	615	28	696	22	1126	69	813	20	282.5	6.8
Z16-03 - 10	0.0785	0.001	0.098	0.011	1.06	0.12	0.998	52	1158	26	601	66	726	58	980	120	716	71	227	18
Z16-03 - 16	0.0834	0.0012	0.0888	0.003	1.017	0.022	0.9485	43	1277	28	548	15	712.1	11	546	40	204	11	82.8	1.9
Z16-03 - 19	0.1131	0.0021	0.1096	0.006	1.716	0.099	0.9529	36	1849	33	670	34	1012	37	1069	76	2040	600	269	51
Z16-01 - 13	0.0757	0.001	0.2155	0.004	2.272	0.048	0.8448	116	1086	25	1258	22	1203	15	176.3	6.5	107.6	3.6	54.8	1.1
Z16-01 - 53	0.075	0.0009	0.1899	0.003	1.991	0.036	0.6508	105	1068	23	1121	16	1112	12	138	11	117.6	8.7	61.9	2.4
Z16-01 - 63	0.0739	0.0012	0.1807	0.003	1.859	0.045	0.6036	103	1035	34	1071	17	1066	16	78.2	2.8	82.6	3	42.86	0.92
Z16-01 - 37	0.075	0.0008	0.1864	0.003	1.9479	0.033	0.5563	103	1067	22	1102	14	1098	11	312	19	324	18	169.5	7
Z16-01 - 52	0.0747	0.001	0.1844	0.003	1.925	0.043	0.7479	103	1059	28	1091	17	1090	15	82.9	5.7	112.2	8.4	60.7	2.7
Z16-01 - 47	0.0752	0.0012	0.1854	0.003	1.93	0.041	0.6101	102	1073	31	1096	16	1091	14	100.9	5.4	186	7.7	94.9	1.7
Z16-01 - 42	0.0749	0.001	0.1838	0.003	1.918	0.039	0.7671	102	1065	25	1088	15	1087	14	143	10	251	22	132.7	7.5
Z16-01 - 7	0.075	0.0008	0.1834	0.003	1.918	0.033	0.7478	102	1068	22	1086	15	1087	12	206.8	6.3	144.7	5.2	74.3	1.8
Z16-01 - 57	0.0743	0.001	0.1786	0.003	1.879	0.043	0.8914	101	1049	28	1060	17	1074	15	135.6	5.8	192.4	9.6	97.4	5.5
Z16-01 - 64	0.0758	0.0009	0.1851	0.004	1.955	0.039	0.9266	100	1090	25	1095	19	1100	13	1480	120	716	65	378	41

Z16-01 - 4	0.0747	0.0008	0.1794	0.002	1.862	0.032	0.6164	100	1060	22	1064	13	1068	11	476	22	515	23	270.5	6
Z16-01 - 23	0.0754	0.0008	0.1827	0.003	1.915	0.038	0.9309	100	1079	23	1082	17	1086	13	78.4	4.1	116.1	5.5	59.2	2
Z16-01 - 32	0.0756	0.0008	0.1833	0.003	1.928	0.035	0.8444	100	1083	22	1085	15	1091	12	572	17	926	37	428	17
Z16-01 - 34	0.0752	0.0008	0.1815	0.003	1.9	0.034	0.8395	100	1073	21	1075	15	1081	12	261	11	248	15	123	5.8
Z16-01 - 9	0.0753	0.0009	0.1818	0.003	1.896	0.032	0.773	100	1076	23	1077	15	1080	11	274	13	318	13	158.2	3.6
Z16-01 - 49	0.0749	0.0008	0.1793	0.003	1.871	0.033	0.8037	100	1064	22	1063	14	1071	12	401	27	322	20	168.3	6.6
Z16-01 - 20	0.0752	0.0012	0.1799	0.003	1.884	0.041	0.6475	100	1071	32	1067	15	1075	15	98.7	4.9	108.5	4.7	54.5	1.6
Z16-01 - 56	0.0748	0.0009	0.1779	0.004	1.853	0.045	0.9011	99	1061	25	1055	19	1064	16	238	8	233.9	7.8	123.1	3.4
Z16-01 - 45	0.0751	0.0009	0.1792	0.003	1.874	0.034	0.3478	99	1069	24	1063	14	1072	12	156.4	9.6	113.2	5.5	57.5	1.5
Z16-01 - 27	0.0752	0.001	0.1792	0.003	1.869	0.04	0.8397	99	1072	27	1062	17	1070	14	152	3.5	167.5	2.9	85.6	1.5
Z16-01 - 38	0.0753	0.0008	0.1793	0.003	1.876	0.035	0.8645	99	1076	22	1063	16	1073	12	594	13	902	19	437.1	9.1
Z16-01 - 29	0.0768	0.0011	0.1859	0.003	1.984	0.035	0.2042	99	1114	29	1099	16	1110	12	276	21	310	19	165.7	7.4
Z16-01 - 15	0.0758	0.0011	0.1799	0.003	1.896	0.038	0.3517	98	1087	30	1066	14	1080	13	171	20	275	42	130	17
Z16-01 - 24	0.0758	0.0011	0.177	0.003	1.869	0.033	0.2163	96	1089	30	1050	15	1070	12	158.7	7	237	13	118.4	5.2
Z16-01 - 8	0.0764	0.0013	0.1786	0.003	1.902	0.041	-0.676	96	1103	33	1059	14	1082	14	833	27	185.1	8.3	96	8.1
Z16-01 - 5	0.0758	0.0008	0.1747	0.003	1.841	0.033	0.9027	95	1088	21	1038	15	1060	12	396	26	419	19	207	10
Z16-01 - 44	0.076	0.0012	0.1738	0.003	1.842	0.038	0.4218	94	1094	32	1033	16	1060	14	356	13	437	15	216	4.2
Z16-01 - 54	0.0752	0.0009	0.1682	0.003	1.762	0.034	0.84	94	1072	23	1002	15	1031	12	335	20	252	14	123.6	4.1
Z16-01 - 48	0.0752	0.0009	0.1684	0.003	1.767	0.035	0.8976	93	1074	23	1004	15	1033	13	489	11	364.2	6.3	178.4	2.5
Z16-01 - 35	0.0787	0.0009	0.1797	0.002	1.966	0.034	0.7118	92	1163	22	1066	13	1104	12	477	27	350	19	187.1	6.5
Z16-01 - 26	0.0783	0.0016	0.1768	0.003	1.928	0.058	0.7295	91	1151	41	1052	18	1090	20	70.2	5.2	148	12	73	5.3
Z16-01 - 10	0.0768	0.001	0.1711	0.003	1.828	0.032	0.7628	91	1114	26	1018	15	1055	12	787	25	585	19	289.5	7.2
Z16-01 - 40	0.0779	0.0009	0.1755	0.003	1.896	0.037	0.8708	91	1144	22	1043	17	1080	13	434	11	436.3	5.9	210.5	2.6
Z16-01 - 61	0.0771	0.0009	0.1704	0.003	1.828	0.033	0.6652	90	1122	24	1014	15	1056	12	1266	19	1631	67	761	48
Z16-01 - 25	0.078	0.0017	0.1739	0.005	1.88	0.034	0.7273	90	1143	43	1033	25	1074	12	406	20	421	14	179.2	5.7
Z16-01 - 36	0.0785	0.0016	0.1757	0.004	1.927	0.038	-0.176	90	1158	40	1043	21	1090	13	376	30	600	61	247	26
Z16-01 - 28	0.0821	0.0021	0.1879	0.003	2.13	0.058	0.793	89	1244	48	1110	15	1158	19	199.9	4.9	259.5	7	147.3	2.5
Z16-01 - 59	0.0819	0.0015	0.1865	0.005	2.127	0.065	0.843	89	1241	36	1102	25	1157	21	91.1	3.6	98.9	3.2	63.7	2
Z16-01 - 22	0.0883	0.0013	0.2109	0.006	2.598	0.083	0.917	89	1393	31	1233	30	1299	23	195.5	7.6	98	8.7	64	3.7
Z16-01 - 65	0.0801	0.0018	0.1747	0.004	1.948	0.044	0.3616	87	1196	45	1038	22	1098	15	371	35	280	15	131.7	4
Z16-01 - 1	0.0814	0.0016	0.1751	0.003	1.996	0.039	-0.338	85	1230	38	1040	18	1114	13	976	25	419	52	154	14
Z16-01 - 43	0.0851	0.0019	0.1824	0.004	2.162	0.045	0.0172	82	1317	42	1080	19	1169	14	448	18	783	64	334	11
Z16-01 - 18	0.0798	0.0014	0.1627	0.003	1.815	0.057	0.8899	82	1190	34	972	17	1050	21	223	11	162.1	8.2	84.8	2.4

Z16-01 - 31	0.0964	0.0031	0.2046	0.004	2.75	0.13	0.9068	77	1550	61	1200	21	1341	34	274	12	287.3	5.9	195.2	8.8
Z16-01 - 51	0.0801	0.001	0.1544	0.002	1.72	0.035	0.8851	77	1197	24	925.7	14	1016	13	362	31	224	18	115.2	5.5
Z16-01 - 3	0.0819	0.001	0.1604	0.002	1.8282	0.03	-0.028	77	1242	25	959.2	13	1056	11	1172	27	1000	130	361.6	6.3
Z16-01 - 33	0.0873	0.0028	0.1745	0.004	2.08	0.067	0.5724	76	1362	60	1037	19	1142	22	86.4	8.3	176	17	88.6	5.4
Z16-01 - 17	0.0851	0.0014	0.156	0.003	1.849	0.036	0.3538	71	1317	33	934.6	14	1063	13	194.1	4.5	277.1	6.5	140.3	4.8
Z16-01 - 55	0.0869	0.0012	0.1609	0.002	1.961	0.041	0.5127	71	1357	26	962	13	1102	14	378	18	433	22	204	10
Z16-01 - 39	0.0949	0.0045	0.18	0.005	2.39	0.18	0.9509	71	1513	86	1067	27	1235	51	276	12	273	13	169	14
Z16-01 - 6	0.0967	0.0032	0.1697	0.004	2.266	0.05	-0.665	65	1554	61	1010	20	1202	16	399	34	164.1	4.1	116.9	4.6
Z16-01 - 46	0.1035	0.0016	0.1593	0.004	2.321	0.063	0.8406	56	1687	28	953	22	1218	20	102.5	2.7	91.3	9	59.7	4
Z16-01 - 41	0.128	0.026	0.1846	0.009	3.45	0.9	0.9832	56	1950	330	1091	48	1470	190	508	31	473	23	365	78
Z16-01 - 58	0.0861	0.0011	0.1158	0.005	1.388	0.052	0.9891	53	1339	25	706	28	883	22	704	13	361.4	7.7	183.9	1.9
Z16-01 - 50	0.0977	0.0026	0.1362	0.004	1.856	0.035	0.5795	52	1576	50	823	23	1065	12	607	32	950	29	325.7	7.7
Z16-01 - 60	0.1151	0.0026	0.1609	0.003	2.571	0.067	0.8711	51	1880	40	962	16	1292	19	178.3	5.7	295.5	9.3	156.9	5.8
Z16-01 - 12	0.1247	0.0038	0.1693	0.004	2.94	0.09	0.7492	50	2023	53	1008	21	1392	23	239	24	910	100	181	15
Z16-01 - 21	0.315	0.058	0.268	0.051	12.4	4.9	0.9989	46	3460	270	1600	280	2550	340	106.1	3.6	110.4	5.4	360	130
Z16-01 - 30	0.1415	0.0039	0.1629	0.005	3.204	0.076	0.3112	43	2242	48	973	26	1458	19	438	19	306	13	281	17
Z16-01 - 16	0.121	0.011	0.1389	0.003	2.3	0.22	0.8424	43	1940	160	839	15	1223	72	439	19	483	13	279	22
Z16-01 - 62	0.2096	0.0081	0.2061	0.005	6.07	0.32	0.8342	42	2896	62	1208	25	1982	46	32.1	1.1	29.7	1.6	42.9	2.5
Z16-01 - 19	0.229	0.012	0.2165	0.004	6.93	0.46	0.9044	42	3041	88	1263	22	2098	59	301	12	657	35	454	22
Z16-01 - 14	0.1278	0.0034	0.1276	0.004	2.286	0.072	0.6388	38	2064	47	774	22	1207	22	1106	53	991	60	478	28
Z16-01 - 11	0.1377	0.0041	0.1088	0.003	2.085	0.05	0.5671	30	2194	52	666	18	1148	19	323	19	339	37	177.3	8.2
Z16-01 - 2	0.3462	0.0036	0.118	0.002	5.684	0.1	0.9638	19	3690	16	719.3	12	1929	16	2620	200	1000	120	3050	170

* ρ denotes error correlation between $^{206}Pb/^{238}U$ and $^{207}Pb/^{235}U$ used to produce concordia diagram

** Signifies rim analyses not included in concordia or age calculations

Table S3. Individual zircon Lu-Hf analyses.

Grain number	Hf^{176}/Hf^{177}	2σ error	Lu^{176}/Hf^{177}	Yb^{176}/Hf^{177}	U-Pb AGE	Hf_i	εHf	1σ error	T(DM)	T(DM) Crustal
Z16_01_4	0.281742	0.000057	0.00112	0.03151	1096	0.281719	-13.2	2.0	2.13	2.71
Z16_01_5	0.281865	0.00008	0.00163	0.0334	1096	0.281831	-9.2	2.8	1.98	2.47
Z16_01_7	0.281853	0.000057	0.00081	0.0196	1096	0.281836	-9.0	2.0	1.96	2.46
Z16_01_8	0.281915	0.000055	0.00241	0.0531	1096	0.281865	-8.0	1.9	1.95	2.39
Z16_01_9	0.281761	0.000053	0.00111	0.02593	1096	0.281738	-12.5	1.9	2.10	2.67
Z16_01_15	0.281839	0.000054	0.00110	0.02497	1096	0.281816	-9.7	1.9	1.99	2.50
Z16_01_20	0.281833	0.000061	0.00074	0.01606	1096	0.281818	-9.7	2.1	1.98	2.50
Z16_01_22	0.281853	0.000066	0.00233	0.0459	1096	0.281805	-10.1	2.3	2.04	2.52
Z16_01_23	0.281856	0.000047	0.00112	0.01906	1096	0.281833	-9.2	1.6	1.97	2.46
Z16_01_24	0.281722	0.000045	0.00164	0.02954	1096	0.281688	-14.3	1.6	2.18	2.78
Z16_01_25	0.281795	0.000051	0.00126	0.02352	1096	0.281769	-11.4	1.8	2.06	2.60
Z16_01_26	0.28182	0.000054	0.00131	0.0232	1096	0.281793	-10.6	1.9	2.03	2.55
Z16_01_27	0.281838	0.000047	0.00099	0.01657	1096	0.281818	-9.7	1.6	1.99	2.50
Z16_01_28	0.281814	0.000055	0.00236	0.03407	1096	0.281765	-11.5	1.9	2.09	2.61
Z16_01_29	0.28178	0.000058	0.00216	0.03135	1096	0.281735	-12.6	2.0	2.13	2.67
Z16_03_1	0.282135	0.00004	0.00272	0.03284	1001	0.282084	-2.4	1.4	1.65	1.98
Z16_03_2	0.281894	0.000058	0.00124	0.01478	1044	0.281870	-9.0	2.0	1.92	2.42
Z16_03_3	0.282232	0.000054	0.00246	0.0307	1092	0.282181	3.1	1.9	1.50	1.71
Z16_03_6	0.281956	0.00005	0.00141	0.01814	1112	0.281926	-5.5	1.8	1.84	2.25
Z16_03_8	0.28199	0.000045	0.00215	0.02797	1064	0.281947	-5.8	1.6	1.83	2.24
Z16_03_11	0.282191	0.000053	0.00179	0.02116	1092	0.282154	2.1	1.9	1.53	1.77
Z16_03_12	0.281841	0.000042	0.00268	0.0393	1088	0.281786	-11.0	1.5	2.07	2.57
Z16_03_14	0.282227	0.000059	0.00133	0.01987	1086.7	0.282200	3.6	2.1	1.46	1.67
Z16_03_15	0.281943	0.000094	0.00314	0.03629	990	0.281884	-9.7	3.3	1.95	2.42

Table S4. Individual standard and unknown zircon rare eath element analyses.

Sample	Zr CPS	Zr CPS 2σ	Si	Si 2σ	P	P 2σ	Ti	Ti 2σ	Y	Y 2σ	Zr	Zr 2σ	Nb	Nb 2σ	La	La 2σ	Ce	Ce 2σ	Pr	Pr 2σ	Nd	Nd 2σ
91500 - 1	3.04E+07	1.20E+06	1.40E+05	1.20E+04	-20	210	5.8	6.4	121	4.1	4.28E+05	14000	1	0.3	-0.046	0.043	2.7	1	-0.057	0.026	-0.19	0.23
91500 - 10	2.78E+07	1.40E+06	1.67E+05	9.20E+03	-700	2800	2.5	3.3	124.3	3.8	4.27E+05	10000	0.99	0.26	-0.008	0.045	2.2	0.62	-0.045	0.013	0.12	0.51
91500 - 11	2.81E+07	1.70E+06	1.49E+05	8.30E+03	60000	23000	4.9	3.1	120	2.9	4.21E+05	10000	0.67	0.16	0.008	0.063	2.73	0.39	-0.029	0.03	-0.19	0.22
91500 - 12	2.77E+07	1.40E+06	1.51E+05	1.20E+04	100	1200	-0.5	2.7	103.3	4.2	4.13E+05	8200	1.08	0.26	-0.007	0.063	2.03	0.32	0.039	0.055	0.3	0.56
91500 - 13	2.90E+07	1.40E+06	1.46E+05	1.10E+04	-380	460	3.4	3.1	118.5	2.5	4.12E+05	4500	0.68	0.16	0.029	0.059	2.31	0.46	-0.002	0.031	0.08	0.39
91500 - 14	2.84E+07	1.50E+06	1.58E+05	1.40E+04	300	880	4.9	3.7	119.3	2.9	4.13E+05	8600	0.67	0.18	0.039	0.081	2.24	0.53	0.009	0.047	0.4	0.47
91500 - 15	2.66E+07	1.50E+06	1.56E+05	1.40E+04	300	9100	4.1	3.6	119.8	4.5	4.11E+05	7900	0.63	0.16	0.058	0.069	2.59	0.64	0.036	0.085	0.28	0.51
91500 - 16	2.77E+07	1.40E+06	1.51E+05	1.20E+04	-230	770	2.2	3.1	118.1	4.7	4.17E+05	8900	0.72	0.23	-0.069	0.016	2.11	0.33	0.018	0.067	0.28	0.45
91500 - 17	2.85E+07	1.40E+06	1.41E+05	7.50E+03	310	390	1.4	3	117.2	3.4	4.04E+05	8100	0.71	0.17	-0.041	0.042	2.47	0.44	-0.016	0.029	0.12	0.33
91500 - 18	2.82E+07	1.70E+06	1.53E+05	9.90E+03	240	290	3.5	3.8	107.7	2.9	4.12E+05	7200	0.98	0.23	0.017	0.042	1.87	0.27	-0.017	0.039	0.32	0.47
91500 - 19	2.57E+07	1.10E+06	1.58E+05	1.40E+04	20	300	7.1	3.6	117.6	3.9	4.12E+05	12000	0.74	0.25	0.02	0.061	2.25	0.52	-0.005	0.049	0.36	0.65
91500 - 2	2.61E+07	1.10E+06	1.61E+05	1.70E+04	170	140	4.9	6.6	112.2	3.7	4.25E+05	11000	1.04	0.27	-0.09	0.003	2.12	0.78	-0.045	0.045	0.12	0.54
91500 - 20	2.83E+07	1.60E+06	1.48E+05	8.50E+03	-100	110	5	2.9	123	3.3	4.06E+05	8500	0.66	0.14	0.006	0.046	2.3	0.53	0.004	0.04	0.28	0.42
91500 - 21	2.91E+07	1.50E+06	1.63E+05	1.00E+04	30	150	4.3	3	117.9	2.6	3.98E+05	6300	0.66	0.16	-0.021	0.025	2.28	0.51	-0.04	0.018	0.57	0.64
91500 - 22	2.74E+07	1.70E+06	1.51E+05	8.70E+03	1200	2000	4.9	3.6	109.1	3.3	4.00E+05	6700	0.75	0.21	-0.01	0.042	1.76	0.47	-0.022	0.045	0.01	0.23
91500 - 23	2.61E+07	9.30E+05	1.54E+05	8.60E+03	0	370	5.1	4.9	102.5	3.8	3.93E+05	7600	0.75	0.21	-0.041	0.051	1.89	0.45	-0.004	0.05	0.23	0.65
91500 - 24	2.80E+07	1.60E+06	1.43E+05	1.10E+04	180	440	4.8	3.8	120.6	2.8	4.03E+05	8100	0.66	0.15	0.006	0.037	2.37	0.46	0.05	0.061	-0.01	0.34
91500 - 25	2.83E+07	1.30E+06	1.47E+05	7.90E+03	-1100	1000	5.9	4.1	118.3	2.4	4.00E+05	5000	0.85	0.21	0.012	0.041	2.11	0.37	-0.012	0.043	0	0.32
91500 - 26	2.79E+07	1.60E+06	1.48E+05	7.20E+03	0	1700	6.6	5.2	116.3	3.7	3.98E+05	7800	0.84	0.23	0.031	0.061	2.41	0.5	0.068	0.064	0.2	0.4
91500 - 27	2.84E+07	1.60E+06	1.52E+05	9.00E+03	-1800	1800	2.6	4.1	114	3.5	4.00E+05	10000	0.91	0.29	0.088	0.077	2.85	0.75	0.04	0.063	0.29	0.37
91500 - 28	2.88E+07	1.60E+06	1.43E+05	9.70E+03	100	730	3.4	3.3	110.6	3.2	4.00E+05	11000	0.71	0.13	0.041	0.048	1.86	0.49	0.012	0.044	-0.322	0.014
91500 - 29	2.79E+07	1.70E+06	1.52E+05	1.10E+04	120	280	1.1	2.2	121.3	3.6	4.00E+05	6300	0.69	0.19	-0.022	0.053	2.5	0.56	-0.005	0.05	-0.21	0.15
91500 - 3	2.75E+07	1.20E+06	1.68E+05	1.40E+04	360	130	-2.3	2.9	122.4	3	4.30E+05	10000	1.23	0.25	-0.008	0.05	2.48	0.42	-0.008	0.046	-0.16	0.33
91500 - 30	2.76E+07	1.20E+06	1.45E+05	1.40E+04	140	470	2	4	108.6	3.2	3.93E+05	7200	0.73	0.28	-0.036	0.044	2.26	0.57	0.046	0.049	1	0.71
91500 - 4	2.81E+07	1.20E+06	1.56E+05	9.90E+03	-40	120	5.1	2.9	118.3	3.3	4.29E+05	8700	0.97	0.2	0.023	0.086	2.4	0.44	0.004	0.05	-0.32	0.13
91500 - 5	2.77E+07	1.20E+06	1.49E+05	8.80E+03	-90	150	6.6	3.6	118.7	2.8	4.30E+05	8800	0.66	0.19	-0.01	0.044	2.38	0.39	-0.031	0.036	0.26	0.34
91500 - 6	2.89E+07	1.60E+06	1.60E+05	1.10E+04	90	310	5.6	3.2	116.3	3.2	4.24E+05	7100	0.82	0.21	-0.023	0.045	2.3	0.39	-0.003	0.033	-0.2	0.3
91500 - 7	2.91E+07	1.30E+06	1.50E+05	7.30E+03	900	1400	4.5	4.1	97.1	3.2	4.25E+05	9200	0.86	0.21	-0.045	0.03	1.64	0.5	-0.023	0.027	1.08	0.76
91500 - 8	2.97E+07	1.60E+06	1.58E+05	1.00E+04	200	2400	3	3.1	116.4	3	4.25E+05	6800	0.99	0.26	0.044	0.074	2.66	0.35	-0.019	0.028	0.08	0.4
91500 - 9	2.77E+07	1.40E+06	1.59E+05	8.70E+03	110	780	4.9	4.6	126.4	3.4	4.20E+05	9300	0.66	0.2	0.025	0.08	2.44	0.53	-0.029	0.049	0.64	0.73
GJ1 - 1	3.03E+07	1.30E+06	1.55E+05	1.20E+04	70	170	2.6	4.4	258.3	7.2	4.27E+05	6900	1.55	0.47	-0.021	0.069	15	1.7	0.011	0.06	0.28	0.79
GJ1 - 10	2.93E+07	1.30E+06	1.59E+05	1.40E+04	2100	2300	1.4	3.5	262	8	4.24E+05	12000	1.73	0.28	0.022	0.084	14.4	1.5	-0.006	0.049	0.49	0.66
GJ1 - 11	2.76E+07	1.60E+06	1.51E+05	1.20E+04	-50000	34000	4.4	3.1	251.1	7	4.19E+05	6300	1.59	0.3	-0.001	0.049	14.6	1.1	0.018	0.079	0.31	0.62
GJ1 - 12	2.89E+07	1.10E+06	1.60E+05	1.10E+04	550	820	0.5	3.9	261.6	8.5	4.24E+05	9400	1.69	0.5	-0.051	0.02	14.3	1.2	0.048	0.067	0.82	0.89
GJ1 - 13	2.94E+07	1.80E+06	1.37E+05	1.10E+04	-470	460	4.6	3.9	253.1	5.4	4.11E+05	5000	1.45	0.28	0.015	0.039	13.55	0.9	0.016	0.035	0.11	0.38
GJ1 - 14	2.81E+07	1.40E+06	1.56E+05	8.80E+03	130	730	8.6	4.4	249.6	6.1	4.16E+05	9300	1.41	0.24	0.036	0.047	14.6	1.3	0.055	0.064	1.6	1.2
GJ1 - 15	2.90E+07	9.30E+05	1.56E+05	1.30E+04	-4800	8400	2.3	4	245.8	6.2	4.05E+05	11000	1.67	0.54	-0.002	0.052	14	1.5	-0.007	0.052	0.25	0.61
GJ1 - 16	2.75E+07	1.80E+06	1.54E+05	1.00E+04	690	790	1.5	3.3	249.6	6.4	4.20E+05	11000	1.17	0.3	0	0.051	13.5	1.3	-0.009	0.038	0.3	0.47

GJ1 - 17	2.81E+07	1.60E+06	1.43E+05	9.90E+03	370	380	4.4	4.6	243.6	4.7	4.15E+05	7000	1.66	0.35	-0.072	0.004	13.68	0.93	-0.003	0.055	0.6	0.53
GJ1 - 18	2.75E+07	1.40E+06	1.59E+05	9.40E+03	420	300	6.6	3.3	252.5	5.5	4.07E+05	9300	1.37	0.3	0.08	0.1	14.53	0.98	-0.032	0.041	0.43	0.63
GJ1 - 19	2.78E+07	1.50E+06	1.47E+05	8.20E+03	170	200	4.7	3.4	255.3	5.1	4.11E+05	6500	1.39	0.31	0.004	0.041	13.29	0.95	0.024	0.047	0.76	0.59
GJ1 - 2	3.10E+07	9.90E+05	1.64E+05	9.30E+03	30	200	7.7	6.2	265.6	7.3	4.31E+05	13000	1.7	0.31	-0.064	0.002	15.1	1.6	0.024	0.047	0.37	0.66
GJ1 - 20	2.92E+07	1.60E+06	1.54E+05	9.20E+03	-18	94	3.5	3.1	247.5	4.8	3.97E+05	6300	1.47	0.31	0.049	0.063	14.4	1	0.034	0.052	-0.03	0.24
GJ1 - 21	2.88E+07	1.40E+06	1.53E+05	8.10E+03	-80	180	0.4	3.1	256	4.9	4.03E+05	7500	1.52	0.26	0.054	0.051	14.5	0.89	-0.023	0.031	0.58	0.47
GJ1 - 22	2.80E+07	1.70E+06	1.54E+05	1.10E+04	-700	3000	5.4	5.3	254	6.5	4.04E+05	9400	1.66	0.32	0.032	0.056	13.9	1.1	-0.008	0.045	0.94	0.75
GJ1 - 23	2.83E+07	1.60E+06	1.53E+05	1.10E+04	210	330	5	3.3	254.3	6	3.99E+05	9500	1.48	0.25	-0.013	0.056	13.5	1.2	0.02	0.055	0.44	0.51
GJ1 - 24	2.81E+07	1.60E+06	1.46E+05	1.00E+04	170	340	4.4	3	257	5.8	4.08E+05	9000	1.41	0.28	0.047	0.069	14	1.1	0.041	0.064	0.39	0.45
GJ1 - 25	2.87E+07	1.50E+06	1.55E+05	7.00E+03	-1300	1200	2.6	3.4	246.3	4.7	3.98E+05	8100	1.43	0.34	0.003	0.043	13.2	1.1	0.003	0.059	0.64	0.69
GJ1 - 26	2.81E+07	1.50E+06	1.48E+05	8.80E+03	1200	2200	4.6	3.5	256.6	7	4.01E+05	6800	1.67	0.31	0.024	0.076	13.9	1.3	0.024	0.067	0.37	0.42
GJ1 - 27	2.90E+07	1.70E+06	1.51E+05	1.10E+04	-1100	1300	1.3	4.1	254.4	3.9	3.93E+05	9800	1.39	0.22	-0.029	0.042	14.6	1.2	0.018	0.061	1.05	0.75
GJ1 - 28	2.93E+07	1.70E+06	1.54E+05	1.00E+04	70	680	2.3	3.4	251.9	7.5	3.91E+05	9600	1.58	0.26	0.01	0.061	14.05	0.89	0.066	0.08	0.99	0.67
GJ1 - 29	2.88E+07	1.20E+06	1.54E+05	1.20E+04	-30	340	2.1	3.1	255.9	6	4.01E+05	6800	1.63	0.29	-0.007	0.051	12.65	0.97	-0.021	0.034	0.23	0.48
GJ1 - 3	3.01E+07	1.30E+06	1.53E+05	1.20E+04	-120	130	11.6	3.4	262.6	5.5	4.38E+05	7100	1.79	0.3	-0.034	0.025	14.2	1.2	0.026	0.057	1.28	0.9
GJ1 - 30	2.85E+07	1.70E+06	1.36E+05	6.60E+03	-370	280	4.2	3.3	250.3	6.4	3.95E+05	9700	1.4	0.2	-0.025	0.044	13.1	1.2	0.095	0.071	0.53	0.53
GJ1 - 4	2.90E+07	1.20E+06	1.57E+05	1.10E+04	-250	140	3.7	4.3	255	6.4	4.21E+05	15000	1.72	0.31	-0.061	0.024	14.4	1.2	0.019	0.08	-0.314	0.013
GJ1 - 5	3.19E+07	1.00E+06	1.54E+05	1.70E+04	-20	140	9.8	3.4	254.9	8	4.33E+05	11000	1.52	0.33	0.038	0.073	12.3	2	0.027	0.062	0.8	1.2
GJ1 - 6	2.98E+07	1.50E+06	1.57E+05	1.10E+04	-220	230	6.1	4.3	250.3	7.6	4.32E+05	11000	1.5	0.41	0.001	0.05	14.4	1.4	0.059	0.076	1.2	1
GJ1 - 7	3.05E+07	1.60E+06	1.61E+05	9.60E+03	200	1700	3.7	3.8	252	4.4	4.27E+05	8000	1.59	0.31	-0.004	0.04	14.07	0.53	0.036	0.037	0.4	0.36
GJ1 - 8	3.04E+07	6.90E+05	1.42E+05	1.10E+04	200	3100	0.2	4	253.1	9.5	4.36E+05	27000	1.39	0.27	0.029	0.068	14.8	1.6	0.069	0.077	0.42	0.8
GJ1 - 9	3.03E+07	1.30E+06	1.52E+05	1.30E+04	-70	770	2.9	4.8	260.3	7.3	4.25E+05	11000	1.41	0.39	-0.068	0.003	14.4	1.6	0.001	0.053	0.7	0.79
KLDF - 1	2.90E+07	1.50E+06	1.57E+05	1.10E+04	-70	140	0.1	3.3	65.9	1.8	4.26E+05	11000	0.74	0.2	-0.005	0.046	0.71	0.25	0.032	0.051	-0.03	0.51
KLDF - 10	3.03E+07	1.50E+06	1.53E+05	9.60E+03	-70	150	2.9	3.4	62.1	2.1	4.05E+05	9100	0.44	0.14	0.007	0.044	0.62	0.2	0.025	0.041	-0.25	0.24
KLDF - 11	2.88E+07	1.60E+06	1.58E+05	8.30E+03	-10	180	3.1	3.1	66	2	4.06E+05	9300	0.27	0.12	0.027	0.075	0.71	0.21	0.005	0.039	-0.14	0.23
KLDF - 12	2.97E+07	1.40E+06	1.54E+05	8.80E+03	-400	1400	5.8	4.1	64.7	1.7	4.01E+05	7300	0.25	0.1	0	0.066	0.65	0.23	0.042	0.055	0.34	0.37
KLDF - 13	2.92E+07	1.50E+06	1.51E+05	9.60E+03	300	1800	2.9	3.6	65.2	2	3.98E+05	6500	0.34	0.14	0.028	0.052	0.74	0.21	-0.003	0.044	0.17	0.37
KLDF - 14	2.81E+07	1.60E+06	1.38E+05	8.10E+03	310	210	6.3	3.5	63	1.9	3.95E+05	10000	0.4	0.15	-0.018	0.03	0.73	0.2	0.003	0.038	-0.11	0.33
KLDF - 15	2.96E+07	1.60E+06	1.48E+05	7.70E+03	10	370	2.7	3.8	63.2	2.3	3.95E+05	9200	0.36	0.1	-0.052	0.031	0.95	0.29	0.087	0.067	0.11	0.25
KLDF - 2	2.89E+07	1.80E+06	1.48E+05	1.00E+04	60	170	2.2	4.1	63.1	2	4.28E+05	10000	0.41	0.19	-0.041	0.028	0.76	0.26	0.029	0.044	-0.17	0.28
KLDF - 3	2.90E+07	1.60E+06	1.54E+05	6.60E+03	-1200	2200	-1	3.7	65	1.7	4.30E+05	8900	0.49	0.13	0.045	0.066	0.84	0.31	0.026	0.036	0.42	0.6
KLDF - 4	2.99E+07	1.70E+06	1.47E+05	1.00E+04	100	770	5	3.8	65.4	1.8	4.14E+05	5800	0.42	0.2	0.03	0.048	0.9	0.24	0.055	0.053	0.43	0.39
KLDF - 5	2.89E+07	1.70E+06	1.54E+05	9.40E+03	-29000	31000	2	3	67.2	1.8	4.17E+05	7600	0.33	0.12	-0.018	0.038	0.88	0.29	-0.015	0.034	0.05	0.35
KLDF - 6	2.86E+07	1.40E+06	1.57E+05	8.90E+03	80	470	7.2	3.8	62.7	2.3	4.18E+05	7400	0.5	0.16	0.018	0.048	0.92	0.35	0.045	0.047	0.47	0.47
KLDF - 7	2.90E+07	1.80E+06	1.62E+05	1.00E+04	-3700	4800	1.4	2.9	64.5	1.9	4.13E+05	8900	0.53	0.13	0.063	0.06	0.86	0.25	0.007	0.035	0.37	0.42
KLDF - 8	2.90E+07	2.00E+06	1.49E+05	8.80E+03	290	380	1.6	2.8	60.9	1.9	4.03E+05	6500	0.38	0.18	-0.043	0.021	0.81	0.32	-0.019	0.029	-0.12	0.21
KLDF - 9	2.89E+07	1.70E+06	1.45E+05	9.20E+03	90	130	2.5	2.6	63	2	4.11E+05	7600	0.39	0.13	-0.004	0.053	0.76	0.3	0.05	0.046	-0.17	0.14
Nist610 - 1	2.42E+04	1.80E+03	3.22E+05	1.70E+04	330	170	424	20	441	18	4.17E+02	37	409	17	446	21	436	22	420	21	423	22
Nist610 - 10	2.11E+04	1.70E+03	3.22E+05	1.90E+04	390	160	433	36	452	21	4.41E+02	54	419	20	453	21	443	18	429	19	437	25

Nist610 - 11	2.33E+04	1.70E+03	3.18E+05	1.80E+04	450	250	423	18	438	11	4.33E+02	35	408	16	445	18	438	20	419	17	416	18
Nist610 - 12	2.08E+04	1.10E+03	3.27E+05	1.60E+04	-6000	2000	429	22	449	18	4.14E+02	48	416	18	455	20	443	16	427	17	429	24
Nist610 - 13	2.23E+04	1.60E+03	3.14E+05	1.90E+04	1500	2600	431	31	436	19	4.34E+02	48	406	18	441	21	432	20	417	19	421	23
Nist610 - 14	2.17E+04	1.60E+03	3.20E+05	1.90E+04	550	460	415	35	444	24	4.29E+02	39	411	23	453	24	445	26	421	21	434	38
Nist610 - 15	2.13E+04	1.70E+03	3.25E+05	2.60E+04	420	430	427	25	441	22	4.23E+02	46	412	22	447	24	439	17	423	21	418	28
Nist610 - 2	2.15E+04	1.70E+03	3.16E+05	1.80E+04	420	280	424	25	440	24	4.04E+02	46	414	25	452	28	443	26	423	24	423	29
Nist610 - 3	2.07E+04	1.30E+03	3.38E+05	2.70E+04	-6000	2700	442	24	448	23	4.51E+02	51	418	19	460	26	445	19	429	23	422	24
Nist610 - 4	2.23E+04	1.40E+03	3.12E+05	2.30E+04	7000	1300	416	18	431	22	4.58E+02	45	402	17	437	20	429	21	415	18	423	17
Nist610 - 5	2.15E+04	2.00E+03	3.23E+05	2.20E+04	17000	58000	428	25	448	23	4.33E+02	42	415	26	457	28	446	29	425	24	421	30
Nist610 - 6	2.12E+04	1.40E+03	3.23E+05	1.60E+04	490	770	427	28	440	18	4.41E+02	45	414	19	449	20	441	22	424	19	431	35
Nist610 - 7	2.06E+04	1.30E+03	3.14E+05	1.90E+04	1600	8500	427	30	437	26	4.27E+02	56	403	26	446	31	431	26	415	26	407	35
Nist610 - 8	2.09E+04	1.30E+03	3.29E+05	1.80E+04	310	590	438	28	448	19	4.45E+02	39	418	18	453	15	446	16	432	18	436	27
Nist610 - 9	2.13E+04	1.40E+03	3.13E+05	2.10E+04	280	320	407	31	429	22	4.26E+02	43	397	22	436	20	424	23	408	18	407	26
OGC - 1	2.89E+07	1.70E+06	1.51E+05	1.00E+04	-20	160	6.6	4.2	596	61	4.26E+05	8900	0.97	0.32	-0.016	0.044	8.64	0.93	0.11	0.11	1.9	1.1
OGC - 10	2.97E+07	1.60E+06	1.58E+05	8.00E+03	-140	180	5.9	3.9	1181	27	4.08E+05	10000	0.74	0.16	0.013	0.043	12.4	1.2	0.152	0.076	3.28	0.95
OGC - 11	2.84E+07	1.70E+06	1.49E+05	8.20E+03	130	250	10.3	3.6	1600	260	4.03E+05	6600	1.04	0.27	0.07	0.11	14.6	1.9	0.38	0.23	6.2	2.2
OGC - 12	2.86E+07	1.50E+06	1.47E+05	9.30E+03	-200	1200	9.9	4.3	1898	71	4.02E+05	9100	0.94	0.17	0.028	0.077	16.9	1.2	0.55	0.15	6.4	2
OGC - 14	2.98E+07	1.80E+06	1.55E+05	9.80E+03	-280	340	6.5	3	1191	27	3.95E+05	9500	0.75	0.17	-0.006	0.026	13.5	1.1	0.29	0.1	5.2	1.5
OGC - 15	2.94E+07	1.70E+06	1.46E+05	1.00E+04	30	240	8.1	2.5	1790	88	3.93E+05	7900	0.87	0.22	0.97	0.2	20.6	1.7	1.42	0.31	16.4	3.8
OGC - 2	2.87E+07	1.60E+06	1.55E+05	9.00E+03	250	190	7.3	3.8	593	14	4.27E+05	9100	0.89	0.24	-0.038	0.025	8.72	0.73	0.012	0.038	1.6	1
OGC - 3	2.98E+07	1.60E+06	1.61E+05	9.40E+03	2100	2100	7.2	2.9	2993	56	4.22E+05	10000	1.53	0.24	0.51	0.16	25	1.5	0.78	0.15	12.9	2.6
OGC - 4	2.97E+07	1.60E+06	1.54E+05	1.00E+04	-540	640	7.5	3.7	1384	81	4.24E+05	9200	0.91	0.21	-0.011	0.044	13.8	1.4	0.35	0.11	4.4	1.4
OGC - 5	2.94E+07	1.80E+06	1.53E+05	9.80E+03	-131000	99000	8.9	4.3	2439	37	4.15E+05	7200	1.12	0.24	0.28	0.12	25.3	2	0.85	0.18	10.9	2.7
OGC - 6	2.92E+07	1.90E+06	1.60E+05	1.00E+04	420	600	13.7	3.8	2595	44	4.11E+05	9700	3.14	0.31	0.128	0.084	41.3	1.7	0.249	0.09	5.3	1.7
OGC - 7	2.90E+07	1.80E+06	1.46E+05	9.90E+03	2400	3800	4.6	2.4	1158	27	4.04E+05	8900	0.57	0.14	0.041	0.065	12.15	0.88	0.254	0.085	4	1.3
OGC - 8	2.75E+07	1.40E+06	1.64E+05	1.10E+04	-10	350	6	3.1	1174	51	4.15E+05	5500	0.59	0.13	0.16	0.11	13	1.3	0.5	0.15	5.7	2
Ples - 1	3.11E+07	1.20E+06	1.52E+05	1.20E+04	165	79	66.6	7	502	10	4.23E+05	11000	4.53	0.55	-0.06	0.019	2.49	0.43	0.08	0.1	1.8	1.2
Ples - 10	2.75E+07	1.30E+06	1.52E+05	1.50E+04	-170	170	34.4	5	239.9	7.7	3.99E+05	11000	2.91	0.49	0.061	0.068	2.03	0.73	0.11	0.11	1.7	1.3
Ples - 11	2.65E+07	1.20E+06	1.55E+05	1.20E+04	10	280	69.6	6.1	495	14	4.00E+05	10000	3.79	0.59	-0.034	0.051	1.81	0.38	0.081	0.059	2.1	1
Ples - 12	2.61E+07	1.50E+06	1.51E+05	1.20E+04	600	2400	56.5	5.2	447	11	3.92E+05	8900	4.79	0.58	0.001	0.077	2.14	0.65	0.18	0.097	2	1.3
Ples - 13	2.80E+07	1.40E+06	1.59E+05	9.80E+03	-400	3000	54.9	6.3	475.3	9.8	3.93E+05	6600	4.9	0.5	-0.012	0.039	2.4	0.48	0.075	0.083	1.11	0.65
Ples - 14	3.10E+07	1.40E+06	1.44E+05	1.10E+04	-190	240	60.6	4.8	492	11	4.04E+05	9400	4.85	0.59	-0.01	0.046	2.2	0.54	0.102	0.081	1.38	0.88
Ples - 15	2.87E+07	1.30E+06	1.53E+05	1.10E+04	180	290	69.6	7.3	472	13	3.90E+05	10000	4.53	0.5	0.02	0.053	1.89	0.35	0.11	0.11	0.88	0.75
Ples - 2	2.91E+07	1.80E+06	1.68E+05	1.20E+04	270	150	131	11	825	19	4.30E+05	9300	17.24	0.84	-0.008	0.042	5.52	0.57	0.28	0.1	5.1	1.1
Ples - 3	3.14E+07	1.40E+06	1.48E+05	6.90E+03	300	1700	123	15	817	18	4.21E+05	13000	16.44	0.72	0.058	0.08	5.63	0.84	0.38	0.15	2.7	1.2
Ples - 4	2.85E+07	1.60E+06	1.58E+05	1.00E+04	-620	950	78.9	8.9	489.4	8.8	4.18E+05	9200	4.33	0.45	-0.038	0.035	2.01	0.48	0.124	0.077	1.64	0.83
Ples - 6	3.17E+07	1.60E+06	1.52E+05	1.30E+04	990	550	80.2	8.9	659	33	4.10E+05	9500	4.62	0.51	0.049	0.07	2.44	0.53	0.183	0.086	2.6	0.95
Ples - 7	2.85E+07	1.60E+06	1.50E+05	9.80E+03	-1600	2300	86.6	9.1	667	11	4.09E+05	8300	4.23	0.46	0.1	0.1	2.13	0.36	0.19	0.1	2.4	1.3
Ples - 8	2.57E+07	1.60E+06	1.64E+05	1.10E+04	-400	710	66	12	405.8	9.1	4.17E+05	7300	5.46	0.72	0.036	0.076	2.07	0.59	0.17	0.1	0.88	0.86

Ples - 9	2.72E+07	1.20E+06	1.64E+05	1.30E+04	-260	190	90.4	9.8	623	17	4.14E+05	6100	4.98	0.57	0.095	0.091	2.64	0.56	0.21	0.14	2.9	1.4
Z16-01 - 1	2.96E+07	7.60E+05	1.64E+05	9.30E+03	1000	800	73	13	2590	200	4.22E+05	10000	16.6	2.3	18.4	2.5	98	12	11.3	1.8	58	10
Z16-01 - 10	2.83E+07	1.20E+06	1.58E+05	1.00E+04	40	450	13	3.9	1280	46	4.10E+05	10000	4.63	0.58	3.9	1.1	38.9	5.4	1.91	0.57	11.4	3.1
Z16-01 - 11	3.21E+07	1.90E+06	1.50E+05	1.10E+04	420	660	106	19	2157	97	4.14E+05	15000	10.6	1.3	53.2	6.1	168	14	19.7	1.6	108	11
Z16-01 - 12	3.09E+07	1.10E+06	1.48E+05	1.60E+04	510	490	109	78	1156	50	4.17E+05	15000	7.3	2.1	10.2	3	48.9	5.2	4.4	1.2	24.6	6.5
Z16-01 - 13	2.89E+07	1.60E+06	1.54E+05	9.10E+03	-80	490	17.3	3.7	516.9	7	4.20E+05	6700	2.02	0.3	0.053	0.089	9.5	0.81	0.014	0.038	0.51	0.53
Z16-01 - 14	2.97E+07	1.40E+06	1.54E+05	1.30E+04	1760	980	558	48	7610	400	4.10E+05	16000	64.7	5.2	166.8	8.6	544	32	53.5	3.1	292	22
Z16-01 - 15	2.63E+07	1.00E+06	1.64E+05	9.60E+03	-380	780	23.2	9.5	1130	140	4.18E+05	13000	2.16	0.36	0.4	0.31	13.5	1.9	0.36	0.23	4.3	2.1
Z16-01 - 16	2.41E+07	9.70E+05	1.74E+05	1.30E+04	-130	690	390	190	1750	78	4.20E+05	8400	12.3	1.8	16.3	2.5	82.1	8.1	7.8	1.1	46.2	8.6
Z16-01 - 17	2.03E+07	6.30E+05	2.12E+05	1.20E+04	530	920	4180	620	1328	76	4.11E+05	9200	30.8	4.3	6.36	0.72	25	2.1	2.84	0.36	20.2	3.4
Z16-01 - 18	2.74E+07	1.30E+06	1.48E+05	8.90E+03	450	540	33	20	1162	41	4.20E+05	11000	2.12	0.35	5.2	2.4	21.3	5	1.47	0.51	12.3	4.9
Z16-01 - 19	2.81E+07	1.50E+06	1.67E+05	7.60E+03	710	900	38.3	9.8	772	21	4.18E+05	14000	3.49	0.4	643	96	910	150	144	23	526	92
Z16-01 - 2	3.06E+07	2.20E+06	1.68E+05	1.60E+04	2560	930	1436	73	17010	790	4.19E+05	13000	126.6	8.5	488	28	2024	96	233	12	1257	83
Z16-01 - 20	2.97E+07	1.50E+06	1.42E+05	1.00E+04	270	550	14.9	5.5	512	11	4.16E+05	7800	1.34	0.24	0.032	0.057	10.35	0.84	0.091	0.06	1.09	0.66
Z16-01 - 21	2.51E+07	9.40E+05	1.69E+05	1.30E+04	3500	2300	122	57	730	110	4.09E+05	10000	5.2	1.4	15	13	36	18	4.4	3.8	36	33
Z16-01 - 22	3.07E+07	1.60E+06	1.41E+05	1.20E+04	480	670	14.1	6	980	29	4.07E+05	8700	1.54	0.39	0.16	0.12	7	1.1	0.16	0.12	1.2	1.1
Z16-01 - 23	2.90E+07	1.40E+06	1.56E+05	9.50E+03	200	570	22	4.2	816	17	4.21E+05	7100	1.17	0.25	0.005	0.046	9.17	0.89	0.21	0.083	3.1	1.1
Z16-01 - 24	2.81E+07	1.60E+06	1.50E+05	9.30E+03	-820	410	18.7	4.6	734	30	4.23E+05	8500	1.98	0.23	0.02	0.071	15	1.8	0.129	0.063	1.7	1
Z16-01 - 25	2.95E+07	1.70E+06	1.58E+05	1.20E+04	390	640	20.5	6.6	977	44	4.09E+05	10000	3.42	0.47	3.9	2.3	24.5	5.6	1.66	0.84	10	4.4
Z16-01 - 26	2.79E+07	1.60E+06	1.55E+05	9.10E+03	-590	720	42.6	7.7	1484	46	4.18E+05	8300	1.28	0.24	0.37	0.25	13.1	1.2	0.71	0.17	9.4	1.7
Z16-01 - 27	2.91E+07	1.50E+06	1.48E+05	9.20E+03	-180	640	13.8	3.9	687	24	4.19E+05	9500	1.65	0.27	0.008	0.047	10.48	0.96	0.157	0.092	1.3	0.67
Z16-01 - 28	2.86E+07	1.30E+06	1.59E+05	1.10E+04	-110	860	32.3	6.5	905	16	4.18E+05	7700	2.54	0.37	7.4	3	34.5	5.5	1.81	0.7	11.8	4.6
Z16-01 - 29	2.81E+07	1.50E+06	1.56E+05	1.10E+04	300	650	9.7	3.8	1126	37	4.13E+05	7500	2.44	0.44	3.1	1.7	27.9	7	1.5	0.78	9.5	3.9
Z16-01 - 3	2.96E+07	2.10E+06	1.56E+05	1.60E+04	850	640	216	21	3780	230	4.16E+05	14000	37.5	2.2	54.3	7.6	268	23	29.3	2.7	156	17
Z16-01 - 30	2.90E+07	1.40E+06	1.62E+05	1.30E+04	40	790	29.2	6.5	1230	47	4.20E+05	8200	10.5	1	5.48	0.78	48.9	4.2	3.48	0.47	24.6	4.6
Z16-01 - 31	2.89E+07	1.50E+06	1.59E+05	1.10E+04	440	570	17.3	5	970	27	4.14E+05	7400	2.76	0.23	1.35	0.44	19.4	1.6	0.65	0.18	6.7	2.2
Z16-01 - 32	2.67E+07	8.70E+05	1.66E+05	1.40E+04	510	610	13.1	6.8	757	57	4.26E+05	10000	4.03	0.7	0.7	0.31	20	2.3	0.83	0.21	4.6	2
Z16-01 - 33	3.16E+07	1.40E+06	1.48E+05	1.50E+04	730	660	34.5	5.2	1494	57	4.11E+05	10000	1.52	0.28	15	10	46	17	5.1	2.3	27.9	8.8
Z16-01 - 34	2.91E+07	1.50E+06	1.58E+05	1.00E+04	90	700	18.4	3.5	743	27	4.21E+05	7200	2.89	0.44	2.64	0.52	25.4	1.5	1.03	0.22	5.2	1.2
Z16-01 - 35	2.69E+07	1.50E+06	1.76E+05	1.10E+04	1300	1100	14.8	4.7	1393	19	4.17E+05	8500	2.91	0.49	5.58	0.85	38.2	3.2	3.56	0.52	23	4.4
Z16-01 - 36	3.14E+07	1.50E+06	1.56E+05	2.00E+04	-200	2700	14.8	5.8	1520	130	4.26E+05	19000	4.06	0.51	2.8	1.8	42	4.4	2	1.1	15.5	5.3
Z16-01 - 37	3.19E+07	8.50E+05	1.40E+05	8.40E+03	-200	1200	10.2	5.1	794	27	4.03E+05	14000	3.26	0.46	8.1	4.1	38	11	2.8	1.4	14.8	7.8
Z16-01 - 38	3.13E+07	9.80E+05	1.47E+05	1.30E+04	-480	690	12.4	5.9	2351	52	4.17E+05	7100	2.55	0.47	0.187	0.079	18.9	1.4	0.78	0.32	11.5	2.3
Z16-01 - 39	2.96E+07	1.30E+06	1.55E+05	9.00E+03	-420	860	22.9	6	833	16	4.16E+05	7700	3.29	0.44	9.2	2.2	16.7	2.2	1.89	0.53	9.3	3.1
Z16-01 - 4	2.67E+07	1.40E+06	1.61E+05	8.60E+03	-150	700	11.3	5.6	1597	33	4.26E+05	6900	2.55	0.43	0.028	0.061	18.5	1.8	0.18	0.14	3.1	1.5
Z16-01 - 40	3.00E+07	1.70E+06	1.53E+05	9.80E+03	1600	1200	16.7	3.9	1191	44	4.17E+05	8900	4.58	0.63	2.47	0.45	27.3	2.3	1.51	0.21	11	2
Z16-01 - 41	2.50E+07	6.60E+05	1.67E+05	1.40E+04	-100	1700	148	64	979	35	4.11E+05	8100	9	1.3	23	7.2	84	20	8.5	2.8	40	13
Z16-01 - 42	3.09E+07	1.30E+06	1.55E+05	8.20E+03	1400	1500	23	4.6	1249	27	4.18E+05	13000	1.99	0.35	2.94	0.69	22.1	2	1.1	0.22	9.6	2.3
Z16-01 - 43	2.79E+07	1.20E+06	1.55E+05	1.70E+04	39500	6700	127	58	2933	71	4.10E+05	11000	6.7	1.1	32.6	6.1	179	16	38.1	3	278	24

Z16-01 - 44	3.11E+07	9.80E+05	1.49E+05	1.30E+04	100	1500	12.3	6.7	1385	35	4.12E+05	8000	1.8	0.44	0.011	0.054	14.5	1.2	0.136	0.088	2.1	0.9		
Z16-01 - 45	2.67E+07	1.60E+06	1.66E+05	1.40E+04	-1000	1400	11.2	5.7	375.6	9.7	4.12E+05	12000	1.64	0.38	0.014	0.067	8.55	0.6	0.049	0.07	0.4	0.84		
Z16-01 - 46	1.34E+07	1.40E+06	3.18E+05	4.60E+04	-600	4300	57	10	1700	85	4.19E+05	13000	8.48	0.99	25.9	1.5	129.2	9.3	13.6	1.1	79.5	8.8		
Z16-01 - 47	2.83E+07	1.50E+06	1.54E+05	8.90E+03	-100	2000	26	4.5	1326	22	4.16E+05	8700	1.17	0.22	-0.02	0.039	12.3	1.4	0.23	0.1	5.8	2.2		
Z16-01 - 48	2.91E+07	1.10E+06	1.48E+05	1.10E+04	-1500	1500	9.8	3.9	705	16	4.12E+05	7000	3.24	0.39	0.26	0.13	15.5	1.4	0.095	0.072	0.71	0.49		
Z16-01 - 49	3.34E+07	1.10E+06	1.52E+05	9.60E+03	4300	2900	7.4	6.2	849	22	4.12E+05	11000	2.73	0.63	0.059	0.058	12.7	1.5	0.043	0.075	0.89	0.87		
Z16-01 - 5	2.82E+07	1.10E+06	1.51E+05	1.30E+04	380	590	9	6.2	1729	64	4.23E+05	6600	3.16	0.38	0.033	0.062	11.7	1.2	0.36	0.17	5.1	2.2		
Z16-01 - 50	2.89E+07	1.60E+06	1.55E+05	1.90E+04	12500	3600	228	38	3760	430	4.15E+05	21000	49.2	7.2	54	4.9	305	36	29	3.7	168	24		
Z16-01 - 51	2.83E+07	1.40E+06	1.50E+05	9.80E+03	80000	14000	8.7	5.8	7130	570	4.19E+05	11000	3.06	0.47	10.2	1.4	59	4.3	9.6	1.1	96.3	8.5		
Z16-01 - 52	3.16E+07	1.40E+06	1.45E+05	8.10E+03	-3200	3800	20.9	5.4	783	56	4.10E+05	12000	1.36	0.27	0.03	0.062	11.1	1.4	0.18	0.12	2.9	1.9		
Z16-01 - 53	2.61E+07	9.20E+05	1.58E+05	1.00E+04	1300	9800	5.8	4.3	680	16	4.17E+05	10000	1.74	0.38	0.044	0.08	8.6	1.2	0.013	0.046	1	1.1		
Z16-01 - 54	3.43E+07	9.20E+05	1.48E+05	8.10E+03	4100	6900	10	3.8	674	14	4.07E+05	21000	2.27	0.32	0.19	0.14	10.3	1.2	0.104	0.083	0.71	0.81		
Z16-01 - 55	3.15E+07	1.40E+06	1.57E+05	1.40E+04	9000	8300	27.9	6.2	1403	49	4.08E+05	11000	6.59	0.72	6.62	0.92	36.1	5.3	3.13	0.36	23.7	4.8		
Z16-01 - 56	2.67E+07	1.50E+06	1.67E+05	9.50E+03	17000	14000	9.4	5.8	815	17	4.12E+05	7100	2.57	0.52	0.062	0.094	15	1.6	0.059	0.09	1.37	0.81		
Z16-01 - 57	3.20E+07	1.00E+06	1.51E+05	8.80E+03	70000	29000	18.7	8.7	957	79	4.12E+05	7300	1.4	0.3	0.05	0.1	11.5	1.4	0.22	0.13	3.8	2		
Z16-01 - 58	2.71E+07	1.30E+06	1.50E+05	1.30E+04	-44000	47000	72.7	9.8	1654	73	4.19E+05	13000	17.5	2.2	12.4	2.1	86.6	8	6.57	0.78	33.1	4.5		
Z16-01 - 59	2.64E+07	1.50E+06	1.60E+05	7.80E+03	-11000	29000	16.4	5.3	656	27	4.15E+05	7700	2.05	0.44	1.68	0.64	15.2	1.9	0.62	0.26	5.6	1.9		
Z16-01 - 6	2.70E+07	1.50E+06	1.53E+05	8.20E+03	2340	650	28.6	5.7	1548	83	4.19E+05	7600	6.58	0.75	26.4	3.7	109	11	15.2	1.8	93	11		
Z16-01 - 60	2.80E+07	1.60E+06	1.54E+05	9.20E+03	-2200	1600	33.1	4.6	1320	110	4.14E+05	7800	4.54	0.49	3.67	0.65	30.7	4.8	1.87	0.31	16.9	3.2		
Z16-01 - 61	3.30E+07	1.40E+06	1.44E+05	1.50E+04	-5600	3300	27	10	3297	96	4.15E+05	12000	9.3	1.8	29	11	101	15	10.9	1.7	64.7	8.5		
Z16-01 - 62	9.10E+06	1.40E+06	4.01E+05	6.60E+04	6700	8200	30	10	527	19	4.14E+05	13000	4.69	0.88	1.8	0.75	14.3	2.2	0.55	0.37	5.5	2.3		
Z16-01 - 63	2.81E+07	1.10E+06	1.51E+05	1.10E+04	1300	1400	23.3	5.7	507	10	4.18E+05	7600	1.66	0.26	-0.025	0.044	8.74	0.92	0.06	0.071	1.09	0.73		
Z16-01 - 64	3.13E+07	1.50E+06	1.34E+05	1.50E+04	-2600	1500	17.5	7.2	3220	390	4.14E+05	8600	3.55	0.57	4.6	3.2	30	12	1.9	1.2	13.6	7.5		
Z16-01 - 65	3.01E+07	1.70E+06	1.49E+05	1.20E+04	-4200	2100	27.9	8.5	1118	45	4.15E+05	9800	3.93	0.46	6.47	0.83	48.9	4.4	3.62	0.3	22.6	4.9		
Z16-01 - 7	2.90E+07	1.40E+06	1.45E+05	1.10E+04	-270	520	4.5	3	426	8	4.16E+05	8300	2	0.39	-0.015	0.025	9.23	0.79	0.031	0.049	0.73	0.72		
Z16-01 - 8	2.88E+07	1.20E+06	1.51E+05	9.40E+03	810	510	19.7	5.5	1932	69	4.23E+05	7800	6.5	1.6	2.5	2	8.3	2.4	1.23	0.77	7.2	3.1		
Z16-01 - 9	2.89E+07	1.50E+06	1.57E+05	8.10E+03	510	700	17.6	4	927	18	4.23E+05	8600	2.76	0.36	0.73	0.41	17.6	1.9	0.43	0.2	3.8	1.3		
Z16-03 - 1	2.92E+07	1.80E+06	1.58E+05	9.50E+03	-70	120	11.5	5.1	1222	51	4.07E+05	5700	2.48	0.26	-0.04	0.026	17.8	1.2	0.153	0.074	4.8	1.2		
Z16-03 - 10	2.50E+07	1.40E+06	1.54E+05	1.20E+04	-310	230	49	16	1830	150	4.04E+05	9200	4.09	0.53	35	12	139	29	12.2	3.4	52	11		
Z16-03 - 11	2.83E+07	1.40E+06	1.60E+05	1.30E+04	-150	170	4.7	4.2	926	21	4.04E+05	10000	2.45	0.4	-0.029	0.041	8.6	1	-0.004	0.052	0.86	0.84		
Z16-03 - 12	3.36E+07	1.20E+06	1.43E+05	7.40E+03	-290	240	7.3	4	1094	39	4.01E+05	16000	2.18	0.56	0.4	0.34	11.4	3.1	0.48	0.41	2.3	2.3		
Z16-03 - 13	2.66E+07	1.50E+06	1.62E+05	1.20E+04	50	190	8.8	6.2	637	16	4.07E+05	15000	4.24	0.57	1.66	0.54	18.2	2	0.44	0.28	2.2	1.2		
Z16-03 - 14	3.22E+07	1.00E+06	1.41E+05	1.30E+04	-190	180	7.6	6	862	68	4.08E+05	11000	2.52	0.38	0.042	0.088	10.4	1.6	0.113	0.058	1.01	0.75		
Z16-03 - 15	3.04E+07	1.30E+06	1.60E+05	9.40E+03	-50	150	9.7	3.5	1244	26	4.15E+05	12000	1.18	0.26	1.4	0.33	14	2.5	1.18	0.33	10.8	3.3		
Z16-03 - 16	2.63E+07	1.70E+06	1.64E+05	6.40E+03	-200	170	17	6.2	1357	48	4.05E+05	12000	2.44	0.39	8.12	0.9	76.2	4.1	5.88	0.53	36.4	6		
Z16-03 - 17	2.72E+07	1.50E+06	1.59E+05	1.10E+04	110	210	14.9	8.6	872	39	4.03E+05	9100	1.94	0.45	0.28	0.2	29.1	4.9	0.7	0.35	2.8	1.8		
Z16-03 - 18	2.64E+07	1.50E+06	1.56E+05	1.40E+04	-250	240	16.8	4.5	4600	200	4.03E+05	13000	27	1.9	7.6	1.4	69.3	5.5	6.32	0.78	45.3	5.8		
Z16-03 - 19	2.10E+07	1.70E+06	1.91E+05	1.20E+04	-790	270	22.5	6.9	1903	91	4.09E+05	16000	4.42	0.76	59.4	6.8	179	21	28	3.3	120	15		
Z16-03 - 2	2.81E+07	1.10E+06	1.51E+05	8.30E+03	-90	140	6	3.4	338	6.2	4.08E+05	8100	1.95	0.37	0.2	0.23	8.43	0.79	0.09	0.11	0.07	0.35		

Z16-03 - 3	2.71E+07	1.50E+06	1.66E+05	8.70E+03	-210	190	5.5	5.3	952	36	4.12E+05	9500	2.61	0.62	31.7	4.7	89	11	12.1	1.7	53.9	5.5		
Z16-03 - 4	2.89E+07	1.50E+06	1.49E+05	1.10E+04	0	150	39.8	7	1379	34	4.08E+05	7800	6.82	0.63	1.91	0.41	32.1	3.9	2.54	0.41	24.3	4.1		
Z16-03 - 5	2.70E+07	1.60E+06	1.51E+05	1.10E+04	130	180	20	4.3	961	48	3.99E+05	9700	1.53	0.34	5.6	0.58	32.1	2.2	2.74	0.48	13.4	2.8		
Z16-03 - 6	2.85E+07	1.40E+06	1.59E+05	9.70E+03	-160	160	12.3	3.5	565	11	4.09E+05	7200	4.18	0.38	1.95	0.35	30.2	2.1	0.75	0.23	3.9	1.6		
Z16-03 - 7	3.01E+07	1.50E+06	1.58E+05	9.50E+03	-130	160	21.5	3.8	893	42	4.12E+05	7900	3.28	0.32	1.97	0.57	23.6	2.4	0.82	0.26	8.1	2.5		
Z16-03 - 8	2.65E+07	1.40E+06	1.64E+05	1.40E+04	50	160	4.9	5	1093	35	4.01E+05	8700	4.65	0.38	2.31	0.55	30	2.5	1.31	0.42	9.1	1.6		
Z16-03 - 9	3.36E+07	1.50E+06	1.38E+05	1.70E+04	-70	100	6.8	5.6	1115	30	4.01E+05	17000	4.73	0.46	3.31	0.47	36.5	1.9	1.91	0.46	11.8	2.5		

Sample	Sm	Sm 2σ	Eu	Eu 2σ	Gd	Gd 2σ	Tb	Tb 2σ	Dy	Dy 2σ	Ho	Ho 2σ	Er	Er 2σ	Tm	Tm 2σ	Yb	Yb 2σ	Lu	Lu 2σ	Hf	Hf 2σ	Pb	Pb 2σ	Th	Th 2σ	U	U 2σ
91500 - 1	0.62	0.86	0.14	0.18	2.3	1.4	0.64	0.22	8.2	2.2	4.79	0.92	20	3	5.84	0.96	56.1	5.2	10.86	0.87	6170	120	5	21	25.61	0.97	70.9	2.8
91500 - 10	0.61	0.81	0.16	0.25	2.3	1	0.85	0.3	8.3	1.7	4.21	0.58	21.2	2.3	5.21	0.4	55.8	5	10.97	0.72	6360	170	-14	9.9	24.8	1.5	68.3	1.6
91500 - 11	-0.17	0.29	0.35	0.27	1.9	1.2	0.85	0.2	8.8	1.7	4.15	0.64	23.2	2.4	5.45	0.42	53.2	3.6	11.36	0.76	6150	130	2	16	24.5	1.4	67.7	1.4
91500 - 12	0.41	0.65	0.04	0.17	3	1.5	0.57	0.23	8.8	2.1	3.39	0.32	16.8	1.7	4.79	0.61	51.6	3.8	10.5	0.85	6040	130	4	13	20.92	0.87	59.8	2.3
91500 - 13	0.06	0.26	0.16	0.2	1.49	0.9	0.67	0.24	8.2	1.3	3.79	0.4	18.6	1.4	5.14	0.71	54.8	4	11.32	0.92	5890	120	3	14	24.1	1.3	66.1	2.6
91500 - 14	0.06	0.61	0.01	0.15	1.55	0.8	0.82	0.19	8.3	1.7	3.34	0.45	22.5	2.2	5.26	0.82	49.5	3.7	10.7	1.4	5950	100	4	12	23.5	1.1	64.3	2.1
91500 - 15	0.31	0.61	0.38	0.33	2.1	1	0.6	0.27	8.4	1.4	3.84	0.75	22.6	2.1	4.95	0.81	53.3	4.6	11.27	0.96	5860	170	4	14	24.5	1.5	64.9	2.1
91500 - 16	0.08	0.42	0.54	0.27	1.07	0.7	0.65	0.21	10.1	1.5	4.2	0.64	19.6	2.1	4.99	0.6	56.7	3.2	11.99	0.83	5898	97	4	13	24	1.2	67.7	3.1
91500 - 17	0.18	0.41	0.25	0.22	1.8	1.2	0.79	0.26	9.6	1.9	3.92	0.59	19.4	2	5.36	0.66	55.5	3.7	12	1.1	5860	160	10	11	23.7	1.3	66.1	2.2
91500 - 18	0.26	0.48	0.23	0.18	2.2	1.2	0.43	0.18	7.5	1.1	3.59	0.49	17.8	2.4	5.33	0.44	51.5	4.7	10.16	0.74	5953	87	1	12	21.7	1.2	63.1	1.8
91500 - 19	1.02	0.74	0.47	0.31	2.9	1	0.83	0.32	10.3	1.8	3.71	0.55	22.6	2.7	5.78	0.6	62.7	6.8	12.8	1.3	6110	140	-15	9.3	24.5	1.7	70.1	2.6
91500 - 2	0.35	0.6	0.08	0.18	1.72	0.9	0.6	0.25	8.3	1.5	3.34	0.89	18.8	2.1	4.94	0.87	50	5	10.1	1.8	6090	150	5	22	23.8	1.8	67.6	2.3
91500 - 20	0.47	0.58	0.36	0.29	1.57	0.8	0.75	0.21	9.6	1.6	4.23	0.53	22.6	2.7	4.9	0.7	56.5	3.2	12	1	6100	110	-6	10	25.8	1.1	68.1	1.8
91500 - 21	0.44	0.59	0.17	0.16	1.8	1.1	0.73	0.23	9	1.6	4.01	0.45	21.6	2.2	5.08	0.72	57.1	4.2	11.4	0.77	6025	84	-2	10	24.8	1	66.9	2.1
91500 - 22	0.62	0.64	0.08	0.12	1.6	1.1	0.57	0.2	8.7	1.9	3.62	0.5	22.1	2.5	4.74	0.46	47.1	4.1	9.76	0.95	5970	140	8	15	23.5	1.8	66.2	3.1
91500 - 23	0.32	0.7	0.34	0.33	2.5	1.2	0.53	0.27	9.7	2.5	3.26	0.42	17.9	2.4	3.97	0.81	44.7	4.4	9.9	1.2	6050	170	8	16	20	1.2	63.3	3.5
91500 - 24	0.54	0.69	0.1	0.15	2.8	1.5	0.89	0.22	10.4	2.1	3.52	0.73	20.3	2.3	5.67	0.67	54.4	5.9	11.29	0.94	6140	150	-1.2	7.8	25.1	2.2	67.1	2.5
91500 - 25	0.52	0.58	0.04	0.12	2.4	1.6	0.75	0.2	10.5	1.8	4.23	0.64	22.7	2.6	5.17	0.59	54.1	3.7	11.53	0.93	6150	130	-12	3.1	24.4	1.5	69.7	2
91500 - 26	0.57	0.53	-0.056	0.08	1.26	0.9	0.74	0.2	8.7	1.4	3.95	0.54	21.7	2.6	5.09	0.62	54.7	4.7	11.87	0.98	6160	130	0	11	22.7	1.1	64.7	2.7
91500 - 27	0.44	0.65	0.29	0.23	2.22	1	0.67	0.2	10.5	1.9	4.32	0.48	20.8	1.4	4.63	0.63	52.5	3.7	12.4	1.2	6120	110	-12	8.2	23.8	1.6	66.4	2.6
91500 - 28	0.21	0.49	0.24	0.22	1.88	0.9	0.49	0.17	9	1.5	3.95	0.41	18.6	2.1	4.74	0.61	50.4	3.5	10.5	0.87	6030	110	-7.7	8.9	21.7	1.5	65.2	2.8
91500 - 29	0.73	0.82	0.28	0.21	1.31	1	0.74	0.26	8.5	1.3	3.89	0.57	22.8	3	6.65	0.75	53.2	3.7	11.05	0.75	6050	150	-14	10	22.89	0.95	67	2.7
91500 - 3	0.08	0.38	-0.035	0.09	2.9	1.2	0.68	0.27	9.4	1.8	4.21	0.79	23	2.4	5.15	0.98	50.4	5	12.34	0.9	6160	110	1	17	25.7	1.3	71.2	2.3
91500 - 30	1	1.2	0.15	0.17	0.83	0.6	0.6	0.27	8.3	2.1	3.54	0.54	20	2.6	4.42	0.49	51.6	3.6	11.68	0.91	5820	120	14	17	21.6	1.1	63.1	2.6
91500 - 4	0.34	0.68	0.21	0.19	1.3	1.2	0.71	0.27	9.6	2	3.96	0.61	22.9	1.8	4.87	0.57	58.2	3.7	12.34	0.71	6100	160	-4	13	24.7	1.3	69.2	2.2
91500 - 5	0.64	0.72	0.39	0.3	2.4	1.2	0.81	0.25	10.1	1.5	4.29	0.54	21.5	2.1	5.59	0.52	55	4.5	12.19	0.83	6140	140	3	14	24.3	1.3	69.1	2.5
91500 - 6	0.48	0.51	0.6	0.16	2.2	1	0.67	0.16	8.9	1.7	3.92	0.53	21.7	2.2	4.96	0.6	56.2	3.5	12.51	0.8	6070	100	-7.5	8.7	25	1.3	66.6	2.4
91500 - 7	0.52	0.6	0.05	0.16	0.84	0.7	0.53	0.25	8.7	1.6	3.73	0.54	18.4	1.8	4.59	0.29	47	3.8	9.65	0.98	6050	110	11	14	19.87	0.84	61.4	2
91500 - 8	0.43	0.5	0.27	0.24	1.64	0.9	0.74	0.2	7.5	1.3	4.09	0.57	20.7	1.7	4.59	0.64	53.3	4.3	11.66	0.97	6130	110	1	10	22.7	1.5	65.9	2
91500 - 9	0.73	0.64	0.23	0.36	1.63	1	0.68	0.18	10	1.7	4.22	0.73	21.1	1.8	5.22	0.65	57.7	4.4	11.3	1	6200	110	-12	10	25	1.4	68.4	2.5
GJ1 - 1	1.8	1.1	0.77	0.53	6.8	2.9	1.77	0.44	19.5	2.8	7.38	0.87	30.7	3.3	5.99	0.89	63.4	7.1	13.2	1.5	7390	220	1	15	8.44	0.43	350	13
GJ1 - 10	1.3	1.1	0.63	0.47	8.4	2	1.77	0.46	18.3	2.7	7.42	0.82	30.1	3.2	6.23	0.81	58.3	6.4	14.1	1.2	7530	130	8	20	7.9	1.3	333	10
GJ1 - 11	0.52	0.82	1.22	0.41	6.1	1.9	2.05	0.43	19	3	6.05	0.65	29.4	2	6.62	0.73	59.4	6.8	13.8	1.4	7350	140	4	13	7.97	0.65	331.6	8.2
GJ1 - 12	0.41	0.63	1.25	0.74	5.4	1.9	2.01	0.6	21.1	2.8	6.85	0.47	32	2.9	6.62	0.88	63.2	8.9	13.29	0.99	7300	170	-1	16	7.56	0.89	344.3	8.3
GJ1 - 13	1.89	0.68	0.78	0.38	7.6	2	2.11	0.42	19.7	3.2	7.18	0.64	30.2	2.7	6.14	0.7	60.9	3.7	12.84	0.95	7090	110	7	14	7.2	0.58	324.2	6.9
GJ1 - 14	0.65	0.8	0.81	0.37	5.9	1.7	1.75	0.38	19	2.9	6.76	0.86	30.1	2.6	5.9	0.6	64.2	5.1	13.32	0.88	7250	150	-9.6	8.5	7.52	0.8	329.5	7.4
GJ1 - 15	0.61	0.82	0.65	0.41	7	2.3	1.77	0.44	19.5	2.9	7.2	0.93	29.6	4.3	6.04	0.77	63.6	6.3	13	0.85	7100	160	2	12	8.4	1.3	324	11
GJ1 - 16	0.48	0.53	0.99	0.45	6.9	1.8	1.9	0.47	19.1	2.4	6.56	0.66	31.2	2.8	6.89	0.47	62.2	3.6	12.4	1.3	7250	160	-0.4	8.5	8.32	0.64	332.6	8.4

GJ1 - 17	1.49	0.8	1.08	0.45	7.7	1.6	1.69	0.4	19	2.1	6.55	0.8	29.3	1.6	6.01	0.45	64.7	4.1	13	1.1	7150	120	-2.7	8.7	8.39	0.8	332.6	6.9
GJ1 - 18	1.61	0.98	0.88	0.56	6.7	2.3	2.06	0.44	17.5	2.4	6.98	0.6	29	3.1	6.24	0.65	62.3	6.2	13.23	0.88	7250	110	-10	9.4	7.87	0.66	330.7	7.9
GJ1 - 19	0.66	0.7	1.42	0.51	7.9	2.5	2	0.46	19.4	2.2	6.08	0.81	29.6	2.8	6.67	0.53	60.8	4.3	14	1.1	7350	150	3	17	7.98	0.91	335.4	8.2
GJ1 - 2	1.56	0.87	0.51	0.3	5.6	1.7	1.88	0.56	21.6	2.5	7.4	1.1	31.9	3.6	6.73	0.66	65.5	5.2	15.1	1.3	7290	200	17	14	8.93	0.87	344	11
GJ1 - 20	0.7	0.57	0.7	0.26	6.6	2.2	1.64	0.34	20.2	2.2	6.69	0.45	29.3	3.6	6.77	0.6	63.5	4	13.6	1.3	7220	150	11	11	8.52	0.9	332.9	7.7
GJ1 - 21	0.99	0.74	1.04	0.46	7.7	1.9	2.12	0.34	20.6	2	7.31	0.75	31.4	2.4	6.21	0.74	64	3.3	13.54	0.94	7200	110	-2.1	8.9	8.12	0.56	342.1	7.4
GJ1 - 22	0.39	0.54	0.97	0.35	6.9	2.1	2.26	0.42	21.6	2.3	6.82	0.6	30.3	2.7	6.63	0.77	60.9	5.1	13.3	1.1	7380	150	18	15	8.11	0.65	340.6	6.6
GJ1 - 23	2.05	0.92	1.26	0.44	7.5	1.6	2.23	0.43	20	2.5	7.58	0.88	28.4	2.1	6.44	0.63	61.9	5.2	14	1.2	7300	200	-7	12	7.83	0.52	326.8	9.6
GJ1 - 24	1.13	0.84	1.06	0.45	8	2.3	1.58	0.37	19	2.4	7.25	0.69	31	2	6.28	0.84	62.2	3.9	13.28	0.96	7430	120	-7.4	7.9	7.66	0.5	330.3	6.3
GJ1 - 25	0.65	0.67	1.25	0.46	7.1	2	1.94	0.39	20.5	2.5	6.94	0.59	30.4	2.9	5.65	0.51	59.7	4.3	12.92	0.92	7380	150	-2	8.3	7.58	0.66	334	7.7
GJ1 - 26	1.09	0.89	0.89	0.44	8.4	2.1	1.75	0.33	20.8	2.4	7.23	0.7	28.6	2.5	5.8	0.52	63	4.3	13.2	1.1	7440	130	7	13	7.83	0.62	335.7	7.7
GJ1 - 27	0.89	0.64	0.73	0.28	8.6	2.2	1.93	0.45	18.7	2.7	6.54	0.85	29.8	3.1	5.99	0.86	60.8	3.6	13.73	0.62	7370	120	-2	15	8.08	0.6	333.8	6.5
GJ1 - 28	2.04	0.79	0.97	0.41	7.8	2	1.54	0.41	19.6	2.1	6.67	0.8	32	2.3	6.21	0.73	62.3	4	12.8	1	7320	190	-5	10	8.15	0.67	329.3	8.6
GJ1 - 29	1.43	0.8	1.07	0.38	6.8	1.7	2.03	0.34	19.9	2.1	6.66	0.93	30.5	2.6	5.86	0.56	57.7	4.9	13.3	1	7320	120	-7	11	8.04	0.54	336.9	8.8
GJ1 - 3	1.06	0.72	1.43	0.55	6.4	2	1.61	0.25	19.4	2.6	7.47	0.98	32.2	3	6.7	0.95	70.6	5.7	13.8	1.3	7410	240	-11	13	9.03	0.96	345	10
GJ1 - 30	0.93	0.7	1.06	0.33	6.5	1.6	1.91	0.37	19.5	2.9	7.08	0.72	31.4	2.9	6.53	0.75	62.1	3.1	13.4	1	7110	170	0	12	7.81	0.73	333	8.6
GJ1 - 4	0.84	0.76	1.04	0.48	7.9	3.3	1.82	0.39	19.9	2.9	7.2	1	31.1	4.3	6.66	0.98	61.9	6.1	13.8	1.6	7290	210	-14	15	8.19	0.99	337	11
GJ1 - 5	0.95	0.76	0.98	0.6	6.4	1.2	1.64	0.29	20.7	4.4	7.4	1	28.3	3.6	6.7	1	62.3	4.2	13.92	0.97	7310	220	1	17	7.9	1.2	339.7	9.1
GJ1 - 6	1.3	1.5	0.85	0.48	7	3.8	2.11	0.51	18.5	2.3	7.05	0.87	32.6	3.8	7.01	0.72	59.4	3	13.1	1.2	7300	180	-8	13	7.7	1	337	13
GJ1 - 7	1.08	0.86	0.8	0.38	9.2	1.8	2.03	0.37	19.8	2.4	6.68	0.69	31	2.4	6.87	0.71	57	4.7	13.37	0.82	7390	150	19	11	8.3	1.1	339.4	9.4
GJ1 - 8	0.75	0.9	0.99	0.43	6.1	1.6	1.98	0.69	19.1	3	7.47	0.96	32.7	3.1	5.62	0.89	65.8	6.9	12.11	0.93	7411	69	-3	18	7.3	1.2	332.5	6.1
GJ1 - 9	0.73	0.71	0.82	0.34	6.2	1.7	1.48	0.26	17.5	1.7	6.12	0.81	29	3.9	5.91	0.5	68.6	7	14	1	7590	170	-20	9.5	7.6	1.2	334.9	8.3
KLDF - 1	-0.22	0.27	0.1	0.15	2.6	1	0.42	0.17	4.9	1.1	2.72	0.41	11.2	1.8	2.26	0.41	23.2	2.7	4.19	0.58	7240	140	11	12	70.7	2.2	476	11
KLDF - 10	0.44	0.56	-0.029	0.071	1.4	1.2	0.42	0.23	6	1.2	2.12	0.39	9.6	1.4	2.35	0.47	23.3	2.3	4.23	0.62	7080	180	-7.2	8.4	65.8	2.1	454	10
KLDF - 11	-0.01	0.47	-0.04	0.11	0.68	0.7	0.46	0.18	5.4	1.2	1.94	0.2	10.2	1.2	2.62	0.31	23	3.1	4.49	0.54	7230	160	3	10	67	2	466	11
KLDF - 12	0.82	0.85	-0.05	0.062	1.01	0.9	0.46	0.14	6.3	1.3	1.97	0.37	11.1	1.3	2.34	0.35	22.7	3	4.21	0.49	7110	84	1.5	9.6	69.5	1.7	470.9	8.6
KLDF - 13	0.24	0.33	0.09	0.12	1.5	1	0.36	0.18	6.1	1.1	2.38	0.39	9.9	1.2	2.29	0.36	23.1	2.4	4.16	0.47	7290	140	7	13	68.4	2	458.7	8.3
KLDF - 14	0.11	0.41	0.21	0.14	1.57	0.9	0.31	0.19	6	1.5	2.29	0.46	9.5	1.7	2.39	0.42	22.3	3.1	4.04	0.58	7240	170	-5	11	67.1	2.5	449	10
KLDF - 15	0.62	0.72	0.32	0.27	1.06	0.7	0.49	0.25	5.26	0.96	2.25	0.37	11	1.9	2.01	0.33	22.9	2.8	4.48	0.5	7000	140	-10	8.6	64.6	3	448	11
KLDF - 2	0.02	0.35	0.21	0.19	1.57	0.9	0.39	0.17	4.9	1.1	2.26	0.39	10.3	1.6	2.53	0.37	22.9	3.3	4.67	0.53	7200	150	-7	10	67.4	2.4	448	9.2
KLDF - 3	0.43	0.56	0.04	0.15	1.2	1	0.63	0.21	4.9	1.3	2.31	0.33	12.1	1.4	2.46	0.42	22.1	1.8	4.41	0.46	7350	160	14	15	66.5	2.3	461	11
KLDF - 4	0.04	0.45	0.29	0.22	1.44	0.8	0.49	0.19	5.5	1.1	2.53	0.48	9.7	1.5	2.22	0.44	23.7	2.4	4.83	0.42	7310	140	-2	10	68.6	2.5	461.5	9.9
KLDF - 5	0.23	0.36	0.09	0.16	1.59	0.9	0.53	0.2	5	1.1	2.33	0.44	10.4	1.3	2.2	0.33	24.6	3.7	3.97	0.42	7310	110	0	15	68.4	2.7	462.6	9
KLDF - 6	0.27	0.45	-0.051	0.075	1.45	0.8	0.44	0.18	6.4	1.6	2.24	0.37	10.75	0.93	2.35	0.42	22.2	2.6	4.4	0.59	7100	130	-1	12	65	2	461	10
KLDF - 7	0.06	0.48	0.04	0.14	1.16	0.8	0.4	0.17	5.5	1.3	2.16	0.34	10.6	1.1	2.37	0.41	23.5	3.1	3.97	0.53	7030	150	-5.4	8.4	68.9	2.7	460	10
KLDF - 8	-0.07	0.39	0.08	0.18	1.23	0.7	0.46	0.23	6.6	1.3	2.52	0.36	11.5	1.3	2.01	0.33	22.4	2.5	3.89	0.52	6887	94	1.5	8.2	62.5	2.3	437	6.6
KLDF - 9	0.81	0.75	-0.132	0.075	1.41	0.8	0.36	0.16	4.9	1.4	2.08	0.36	10.7	1.2	2.02	0.33	20.4	2.7	4.02	0.48	7150	120	-1	13	66.5	2.4	440	9
Nist610 - 1	436	25	442	21	435	23	435	22	418	21	438	14	419	24	409	18	431	27	424	23	420	26	417	44	447	16	448	24
Nist610 - 10	436	34	462	25	449	31	444	22	426	22	443	20	428	22	411	22	445	29	434	25	438	26	473	85	456	23	458	26

Nist610 - 11	445	14	457	19	432	16	431	15	415	17	442	19	412	22	407	16	429	20	422	16	421	18	397	62	445	18	454	17
Nist610 - 12	453	25	450	26	452	36	440	20	425	20	447	22	425	27	419	14	447	23	435	16	426	22	428	85	455	19	456	19
Nist610 - 13	438	25	443	28	431	27	430	19	408	24	431	21	415	24	407	22	430	25	420	17	422	25	434	61	441	23	445	22
Nist610 - 14	434	38	449	21	432	30	436	23	425	25	438	26	416	28	408	23	440	28	427	26	419	29	396	59	449	22	459	27
Nist610 - 15	434	26	446	24	436	19	435	24	418	25	444	23	419	28	413	21	435	30	429	22	425	21	431	70	449	24	452	17
Nist610 - 2	455	33	454	24	435	28	429	24	414	30	454	24	413	26	418	22	449	28	432	25	429	30	419	72	452	24	462	29
Nist610 - 3	453	30	455	17	441	27	445	24	432	25	439	19	430	30	418	20	442	34	430	18	431	26	422	88	456	28	464	27
Nist610 - 4	419	29	445	20	425	29	427	18	409	24	432	22	406	22	402	18	427	19	417	20	416	18	415	60	443	16	443	19
Nist610 - 5	442	33	453	23	441	30	444	25	421	29	441	20	429	25	412	23	440	24	432	25	434	30	421	75	448	23	454	32
Nist610 - 6	441	27	464	24	440	22	432	19	417	26	444	24	415	24	416	23	437	28	427	18	423	22	391	80	455	22	456	23
Nist610 - 7	442	40	449	34	421	30	432	27	421	30	440	26	411	34	408	30	438	34	426	27	421	29	473	87	435	30	450	29
Nist610 - 8	450	26	463	21	453	32	442	19	424	22	447	18	427	21	420	17	445	22	432	17	433	21	415	64	457	18	460	17
Nist610 - 9	446	42	441	27	422	28	422	20	399	30	425	22	410	16	401	21	420	29	412	24	408	22	387	72	435	21	438	20
OGC - 1	1.1	1.1	0.54	0.38	12.1	4.6	3.67	0.79	49.8	8.4	18.2	1.6	90	11	20.4	2.4	203	11	45.9	4.4	9670	300	18	20	64	10	90.5	6.4
OGC - 10	8.7	1.6	2.3	0.62	30.9	2.7	9.94	0.96	101.8	4.8	39.1	2	179.3	8.2	35	1.9	329	14	69.1	1.5	9120	180	3	16	112.2	2.9	110.9	2.9
OGC - 11	10	2.6	2.15	0.79	41.7	5.2	11.98	0.93	139	20	55.4	9.5	254	52	52	11	461	91	96	18	8850	190	-4.3	8.3	203	64	173	43
OGC - 12	8	1.9	2.11	0.67	46.4	3.9	14.2	1	167.5	9	65.7	3.7	291	14	58.3	3.3	533	21	110.3	4.8	8860	190	-7	10	221	11	200.2	9.4
OGC - 14	6.5	2.3	1.97	0.36	24.8	4	7.58	0.92	94.8	3.6	36.7	1.4	178.7	6.1	39.7	1.4	398	11	86.8	3.2	9090	170	5	14	174.9	6.8	184.3	5
OGC - 15	10.6	3	2.8	0.84	44	4	12.9	1.3	159	12	59.3	3.3	267	14	56.9	3.5	511	23	107	5.2	8560	170	5	11	202.6	9.5	191.5	6.9
OGC - 2	2	1.2	0.62	0.38	9.7	2.5	3.7	0.55	47.6	4	20.2	1.6	93.6	4.9	21.3	1.4	202.4	7.7	43.7	1.8	9050	170	-8.1	9.3	44.6	2.2	71.5	2.3
OGC - 3	15	3.3	4.34	0.75	84.7	6.6	24.5	1.1	278	11	105.2	3	450.4	9.8	90.4	3.2	817	23	160.2	5	8550	180	4	14	371.4	7.5	286.7	6.5
OGC - 4	7.9	1.9	1.73	0.46	35.4	5	11.1	1.5	124	12	46.3	3.1	207	11	42.9	2.4	399	18	80.4	4.2	9210	210	16	14	144.3	8.6	141.1	6.5
OGC - 5	13.4	1.9	3.67	0.71	65.7	4.8	19.2	1.4	226	10	84	2.2	355	11	72.3	2.6	653	17	129.2	4.1	8720	150	0	11	297.9	5.8	231.6	3.9
OGC - 6	9.7	2.4	2.88	0.86	53.9	5.7	18.34	0.87	225.4	9.7	86.9	2.4	385	9.6	80	2.5	708	18	140.9	3.7	8120	150	-14	6.2	545	13	372.7	7.7
OGC - 7	7.9	2	1.21	0.47	29.2	2.9	9.5	0.64	103.4	5.5	40.9	1.8	165.3	3.8	37	2.5	314	12	65.4	2.7	8710	190	0	11	109.4	4.7	106.4	4.1
OGC - 8	7.9	1.9	2.01	0.47	31.9	3	9.99	0.75	111.7	7.4	40.9	2.3	177	13	36	2.3	323	18	64.7	3.9	8790	170	4	10	100.5	6.7	100.5	5.3
Ples - 1	3.8	1.5	1.02	0.39	16	2.7	5.59	0.87	58	5.9	15	1.4	44.5	3.1	7.9	0.88	51.3	3.2	7.15	0.63	11780	290	7	15	105.2	2.9	908	25
Ples - 10	2	1.1	0.18	0.23	6.9	1.6	2.27	0.54	22.3	3.3	7.32	0.81	24.2	2.9	4.28	0.59	33.4	6.5	4.44	0.37	11500	310	-4	14	44.3	2.3	516	21
Ples - 11	3.8	1.5	0.76	0.33	16	3	4.93	0.48	50.4	5.5	15.8	1.3	53.1	3.6	8.5	0.86	68.8	5.8	9.5	1.1	11720	290	-8.9	9.6	59.2	3	647	11
Ples - 12	1.6	1.1	1.05	0.76	11	3.2	5.3	1.1	55.2	4.7	15.8	1.3	45.9	2.9	7.46	0.83	46	4.5	6.21	0.87	11670	210	-6	16	88.4	4.8	828	24
Ples - 13	3.4	1.7	0.88	0.4	13.9	2.9	5.24	0.68	58.7	4.5	15.5	1.5	45.3	4.5	6.83	0.72	49.9	3.5	6.51	0.81	11830	220	9	10	97.1	4.1	853	17
Ples - 14	3.8	2.1	1.14	0.51	16.6	3.1	5.18	0.76	57	4.4	14.8	1.5	47.4	3.1	8.2	1	48.6	4.8	7.04	0.83	11800	270	-11	8.4	103.4	3.8	876	23
Ples - 15	3.1	1.7	1.21	0.5	12.5	2	4.92	0.53	53.3	3.8	15.57	0.88	48.7	3.2	7	0.64	50.7	4.6	6.24	0.57	11180	220	6	18	97.4	3.9	861	16
Ples - 2	8.2	2.5	1.83	0.44	30.1	4.2	9.36	0.95	94.3	4.3	25.9	2.1	88.8	4	13.6	1.2	87.9	6.8	12.44	0.81	10840	230	-18	7	269.9	7.4	2190	53
Ples - 3	5.4	2.2	2	0.67	25.6	4.9	9.6	1.4	97.2	6.3	26.7	2	84.3	5	14.5	1.2	94.6	5.9	11.6	1.1	11000	350	-2	12	269.8	8.7	2182	56
Ples - 4	3.1	1.2	0.99	0.4	12.6	3.4	4.85	0.61	51.3	3	15.8	1.2	51.8	4.1	8.31	0.71	61.1	5.5	8.55	0.81	12280	200	8	17	60.5	2.6	650	11
Ples - 6	4.5	2.6	1.43	0.33	20	4.8	6.91	0.64	73.5	6.7	20.7	1.7	69.1	5.8	11.1	1.4	88	7.6	12.2	1.3	11050	290	-14	13	83.1	4.1	794	28
Ples - 7	6	2	0.85	0.36	15.9	2.6	7.13	0.68	69.5	2.9	20.6	1.5	71.9	3.8	11.96	0.59	86.3	4.9	13.14	0.87	10940	160	1.4	8.7	77	1.7	775	17
Ples - 8	2.7	1	0.76	0.3	15.8	3.4	4.78	0.77	47.5	4.6	12.1	1.2	45.1	4.7	7.66	0.54	46.8	6.7	6.64	0.74	11200	210	6	16	72.7	2.7	682	16

Ples - 9	4.5	2.5	1.21	0.59	15.4	2.6	6.79	0.88	69	4.3	19.9	1.1	65.8	4.9	11.56	0.88	82	5.4	11.8	1.2	11540	250	-4	13	79.8	2.2	772	17
Z16-01 - 1	40.6	5	6.1	1.2	99	12	28.2	2.9	280	26	89.2	9.2	348	29	75	5.4	659	56	124	10	13710	350	-2	11	345	45	798	45
Z16-01 - 10	11.3	3.9	1.69	0.61	35.5	5.2	10.1	1.3	124.4	7.8	44.5	2.4	185.3	8.1	40.2	2	346	18	66	2.2	12840	240	-8.7	9.7	444	11	643	16
Z16-01 - 11	57.8	6.3	12.4	2	112.4	9.1	27.2	2	257	24	73.9	5.5	274	13	53.3	4.1	426	29	78.2	6.3	11230	340	-3.8	7.3	298	23	270	18
Z16-01 - 12	18.7	4.6	2.93	0.98	43	5.1	13.9	1.4	126	12	40.8	3.5	166	11	32.6	1.7	286	10	57.7	3.9	11590	220	5.4	9.3	558	41	310	14
Z16-01 - 13	1.37	0.86	0.1	0.14	9.5	2.8	4.12	0.45	48.8	3.2	18.59	0.88	76.3	4.4	16.1	1.1	144.7	6.7	30.4	1.3	12280	270	13.2	9.1	84.6	3.1	154	11
Z16-01 - 14	214	23	35.3	3.4	449	36	133.3	9.7	1119	67	295	18	979	72	170.2	9	1318	80	228	13	13280	350	47	18	820	59	943	42
Z16-01 - 15	7.4	2.6	0.92	0.57	35.6	7.9	10.3	2.1	104	14	39.5	4.9	155	19	31.9	3.2	268	31	49.5	4.2	9970	150	-3	13	160	18	121.7	9.3
Z16-01 - 16	26.2	4.6	4.8	1.2	78.2	9.4	22	2	197	11	62.7	3.5	231.4	9.1	46.1	2.8	432	20	91.8	3.7	13300	390	21	21	441	12	435	22
Z16-01 - 17	13.5	2.3	2.27	0.72	43.5	5.4	13.74	0.98	132.4	8.6	46.4	3.7	184	10	36.9	2.1	320	18	64.7	3.8	11300	270	-12	13	300	12	231.1	9
Z16-01 - 18	8.9	2.2	1.18	0.54	31.7	4.3	10.37	0.69	114.1	7.6	40.9	1.9	168.3	7.1	33.2	1.6	294	15	56.3	2.5	11390	190	0	11	136.7	5.1	189.8	8.7
Z16-01 - 19	114	24	8.7	2.2	76	17	12	1.4	95	11	26.1	1.7	103.2	3.7	22.7	1.3	191	9.2	38.8	2.3	12700	350	30	18	477	78	260.7	8.6
Z16-01 - 2	728	50	98.1	8.5	1213	87	337	20	2560	140	609	49	2070	110	368	21	2840	190	467	32	14640	370	240	48	664	47	1856	74
Z16-01 - 20	2.6	1	0.2	0.21	11	1.4	3.76	0.5	42	4.3	17.7	0.83	73.5	4.2	16.65	0.93	143	8.6	27.3	1.5	11270	240	-5.1	6.7	80.8	2.1	78.9	1.9
Z16-01 - 21	10.7	8.9	1.89	0.62	31	11	7.6	2	75	17	25.2	4	103	13	19.7	2.9	189	21	33	2.2	10850	290	20	27	95.5	8.4	99.6	7.8
Z16-01 - 22	2.8	1.9	0.37	0.23	18.8	3.7	6.34	0.91	81.8	4.8	33	1.7	158.1	8.2	32.8	1.4	336	17	69.2	2.1	10930	200	7	12	79.5	5.3	166.4	4.7
Z16-01 - 23	4.4	1.3	0.77	0.38	22.6	3.1	7.41	0.88	75.3	5.9	28	1.4	117.9	5.3	23.4	1.1	198	11	37.1	1.2	10740	150	-12	5.2	87.2	3	62.8	2.6
Z16-01 - 24	1.6	1.1	0.19	0.19	18.7	2.9	6.4	0.78	70	5.4	25.4	1.5	113.3	7.3	21.5	1.7	189	11	39.2	2.3	11210	220	6	10	194	11	140.7	8
Z16-01 - 25	8.2	2.7	1.07	0.59	25.9	4.3	9	1.5	94.9	8.9	32.7	2.1	143.3	7.7	29.1	1.6	259.2	7.4	48.4	1.6	12210	250	-3.4	8.7	337	29	344	10
Z16-01 - 26	12.8	2.1	1.93	0.54	54.2	4.3	15.5	1.3	152.7	8.4	52.4	3.1	202.7	8.9	38	2.1	319	16	57.8	2.7	9740	210	8.4	9.9	118.3	6.9	60.6	2.7
Z16-01 - 27	2.01	0.77	0.26	0.22	17.1	2.7	5.9	0.73	58.6	4.1	23.5	1.2	104.9	5.4	21.21	0.92	185.1	7.7	36.5	1.9	11060	260	-14	3.9	130.5	7.4	127.1	5.5
Z16-01 - 28	5.4	1.9	0.52	0.25	23.4	3.4	7.06	0.59	83.9	5.7	31.3	1.8	132.8	5.4	26.4	1.5	240	12	45	2.2	11210	190	6	12	209.7	3.4	174.7	6.1
Z16-01 - 29	8.3	2.7	0.8	0.36	30.7	4.2	9.77	0.99	114.1	7.6	40.3	2.3	165.6	7.8	33.2	2	287	11	53.9	2.8	10870	190	11	12	248.7	5.2	240.2	9.6
Z16-01 - 3	112	16	13.1	2.5	204	26	53.8	2.6	476	53	128.7	8.9	485	28	90.7	6.7	785	51	146.2	8	16330	750	7	18	1000	120	1285	60
Z16-01 - 30	18.8	4.2	3.6	1.1	50	6.9	13.24	0.81	129.3	9.5	41.7	1.9	170.8	9.7	33	1.4	297	14	57.2	2.8	11880	250	10.6	9.5	237	8.7	364	20
Z16-01 - 31	6.5	2	0.6	0.39	25.9	3.8	8.56	0.9	90	6.3	34.2	1.9	140.4	6	28.7	1.6	260.9	8.4	49.9	1.4	11560	230	2.3	9.7	231.5	8.9	235.7	7.8
Z16-01 - 32	6.2	2.5	0.49	0.44	16.9	4.9	6.37	0.88	71.1	8.7	24.9	2.8	107	10	21	2.6	194	18	37	5.2	11780	240	15	20	228	30	211	22
Z16-01 - 33	15	3.2	2.47	0.85	62	11	16.1	1.6	157	17	53.8	2.9	211	14	39.1	3.1	326	23	60.5	3.7	9540	280	3.6	8.7	146.7	8.6	77.5	4.8
Z16-01 - 34	3.8	1.5	0.35	0.26	15.3	3.4	5.41	0.64	67.1	4.2	25.2	1.8	107.3	5.4	23.4	1.5	204.3	7.7	41.6	1.8	12780	270	-5.6	7.8	183.1	7.9	210.4	3.6
Z16-01 - 35	14	2.6	2.58	0.69	45.2	4.9	11.42	0.88	134.4	6.9	48	3	205	9.4	40.4	1.4	351.9	9.1	64.4	2.2	12340	210	-1	10	269.6	4.9	405.4	6.6
Z16-01 - 36	10.8	2.4	1.4	0.79	44	13	15.1	2.6	145	11	50.4	4.4	210	29	42.1	5.8	343	29	66.4	8.4	11280	240	12	18	379	24	267	16
Z16-01 - 37	5.6	2.1	0.28	0.29	18.8	3.5	6.24	0.89	67.5	5.3	25.9	1.4	122.9	9.5	23.1	2.4	213	13	45.1	2.5	12000	290	-9	12	260	6.2	266.9	6.7
Z16-01 - 38	15.5	3.3	0.56	0.37	76.1	6.9	20.3	1.4	231	12	80.6	2.3	326	13	64.8	3.9	525	24	98.8	4.2	10310	270	2	12	646	20	448	14
Z16-01 - 39	5.8	1.7	0.28	0.26	16.9	2.5	6.25	0.62	75	4.2	29.6	1.1	126.4	5	25.8	1.1	223	12	43.7	1.6	11610	210	1	10	204	4.2	218.9	6.1
Z16-01 - 4	6.5	1.8	0.22	0.25	39.2	7.2	13.29	0.97	151	8.4	54.4	3.1	235.6	9.3	46.3	2.5	395	15	74.6	3.3	11940	310	-3	16	409.3	9.7	396	13
Z16-01 - 40	9	1.9	1.02	0.4	31.7	4.9	10	1	116	7.3	40.1	2.1	178.6	8.5	36.8	1.7	310.6	9.9	58.7	2.7	11710	200	-0.4	7.1	323	12	336	11
Z16-01 - 41	16.4	4.1	0.47	0.39	31.9	6	10.1	1.9	91.1	7	33	2.4	140.1	6.9	31.4	1.8	271	13	50.9	2.6	12560	380	31	19	386	20	433	14
Z16-01 - 42	8.6	2.1	1.57	0.54	40.4	5.9	12.3	1.3	130.5	6.4	44.2	2.1	179.5	9.1	34.8	1.8	289	16	54.6	2.5	10520	330	13	13	200.1	7.5	118.8	4.2
Z16-01 - 43	152	18	6.4	1.5	238	19	48.8	4.3	370	22	101.1	3.8	353	14	63.7	3.1	500	36	86.9	3.9	10470	230	-2	13	630	52	381	15

Z16-01 - 44	5	1.5	0.49	0.41	37.1	4	12.28	0.97	138.4	7.2	51.9	3.2	206.8	9.5	41.1	2.4	336	12	62.8	2.7	11050	170	-1	10	320.6	9.2	279.3	6.7
Z16-01 - 45	2.3	1.5	0.17	0.37	6.9	2	2.85	0.4	29.3	2.5	12.3	1	56.9	4.3	11.8	1.4	112.5	8.1	23.8	1.2	11880	330	1	14	87.3	4.5	122.2	3.6
Z16-01 - 46	51	10	18.3	2.3	96	12	20.4	2.4	196	16	57	4.5	194.9	9.3	35.1	2.6	296	21	62.4	4.1	10690	280	2	26	144.4	5.4	186	19
Z16-01 - 47	9.5	2.5	1.61	0.32	44.2	4.7	12.39	0.85	136.5	7.7	47.3	2.5	185.1	5.1	36.2	1.5	297.1	8.9	56.6	2.1	10350	190	7	13	143.1	3.5	81	3.1
Z16-01 - 48	0.81	0.77	0.12	0.18	11.7	1.9	4.1	0.56	55.4	3.4	24.1	1.3	107.7	5.2	24.8	1.3	209.2	9.5	44.5	1.6	12960	220	-0.2	9.8	274	9.2	390	10
Z16-01 - 49	3.2	1.5	0.25	0.22	17.6	3.1	6	1.1	69.7	5.2	30	1.6	135.8	6.9	30	2.5	249	12	48.8	3.3	12750	400	2	11	238	8.7	315	15
Z16-01 - 5	9	3.2	0.57	0.43	48.7	8.1	15	1.2	170	11	61	3	243	13	48.2	2.6	436	30	80.6	4.5	11020	300	-3	11	341	7.7	305	11
Z16-01 - 50	104	15	13.3	1.2	220	28	54.9	8.4	516	61	121	10	447	41	90	11	688	54	128	22	11810	540	-3	11	760	78	485	18
Z16-01 - 51	91	8.8	5.8	1.7	300	25	73.1	3.4	697	32	225	12	810	51	126.7	4.9	853	47	140.9	7.1	12440	290	9	17	197	9.2	336.6	9.7
Z16-01 - 52	3.7	1.7	0.51	0.29	20.4	3.9	6.27	0.75	73.9	7.8	26.7	2.9	107.6	7.5	22.9	1.7	182	14	38.2	3.3	10510	240	13	13	94	9.3	69.6	6.1
Z16-01 - 53	3.5	2.1	0.37	0.41	15.3	4.5	5.14	0.75	64.1	6.3	23	1.4	109.4	6.3	20.7	1.5	194	12	37.7	2.6	11320	250	5	15	88.3	5.2	104.3	4.2
Z16-01 - 54	2.1	1	0.07	0.19	13.2	2.8	5.18	0.7	63.4	6.4	24.1	2.1	102.2	7.3	22.5	1.6	205.5	9.7	41.3	2.8	11870	330	-3.2	7.5	176.5	8.5	243.9	8.8
Z16-01 - 55	15.1	3	2.73	0.88	54.2	6.1	13.9	1.1	155.1	8	47.9	2.9	203	10	38.6	2.8	325	16	65.8	2.7	11560	320	-2.8	8.2	310	11	285.8	9.4
Z16-01 - 56	3.6	1.6	0.21	0.3	15.8	4.7	5.66	0.62	72.4	4.6	28.3	2.2	115.8	5.3	24	1.6	211.8	8.7	41	2.7	11570	240	-3	13	186.1	7.6	193.1	6.5
Z16-01 - 57	6.9	2.2	0.9	0.53	29.8	7	8.8	1.6	94.6	5.4	32.7	2.5	142	15	26.5	2.3	237	14	43	1.7	10410	340	-14	4.3	136.2	8.5	93.8	4
Z16-01 - 58	28.6	5.5	3.86	0.93	69.1	9.4	21.1	2.1	205	12	58.4	3.2	237	18	45.5	3.6	367	20	64.6	4	12620	520	12	17	296	15	602	21
Z16-01 - 59	4	2.6	1.1	0.49	21	4	6.5	1.4	65.7	8	22.7	2.1	93	12	18.7	1.2	160	11	31	3.1	10930	360	1	23	83.5	8.7	78.7	5.9
Z16-01 - 6	36.9	6.4	5.3	1.2	79.9	9.3	20.6	2.4	176	15	53.9	3.6	196	12	37.5	2.4	317	12	59.8	3.4	11570	310	8	12	142.3	6.9	329	15
Z16-01 - 60	12.1	2.6	2.61	0.68	46.4	8.4	13.9	1.5	143	15	46.4	4.3	187	16	35.2	2.9	280	22	53.8	3.7	10340	220	10	13	204	31	136	14
Z16-01 - 61	41.2	6.5	4.3	1.4	131	20	34.2	1.9	368	22	116.8	3.7	445	22	85.7	3.8	697	19	121.4	6.4	10890	330	10	15	1032	37	822	21
Z16-01 - 62	5.3	2.9	0.38	0.57	15.4	5.4	5.08	0.97	45	6.7	18.5	2.6	80.1	7.2	17.5	2	154	15	28.7	2.6	9990	220	11	46	88	12	92	12
Z16-01 - 63	1.9	1.2	0.14	0.21	11.3	2.2	4.16	0.52	48.8	4.1	17.1	1	77.3	4.4	14.86	0.96	143.6	6.9	27.5	1.5	10770	150	-16	6.2	66.7	1.9	64.9	2
Z16-01 - 64	14.8	4.6	0.77	0.72	70.9	5.2	26.7	3.3	309	29	118	14	517	63	102	12	893	99	168	20	13660	410	-5.2	9.7	569	67	1160	140
Z16-01 - 65	16.2	6.3	4.6	1.3	52.3	8.4	12.5	1.6	117	5.9	37.6	2.6	157.2	9.1	29.4	1.2	254.1	8.6	48.7	2.9	11730	360	8	11	224.6	9.9	274	31
Z16-01 - 7	0.93	0.65	0.13	0.16	8.7	2.2	3.49	0.5	36.6	2.7	13.4	0.94	66.4	3.9	13.86	0.86	128.9	6.6	26.1	1.4	12990	230	16	14	113.7	3.5	173.6	6
Z16-01 - 8	9.7	3.7	0.46	0.32	31.4	4.5	13.3	1.4	166	11	67	3.1	287	10	62.6	2.8	568	20	108.1	4	14290	290	-1.8	8.5	174	24	722	16
Z16-01 - 9	7.6	2.5	0.25	0.18	25.8	2.1	7.53	0.47	87.3	5	32.8	1.4	130.3	6.4	26.7	1.2	254	10	46.9	1.3	11420	220	-1	13	244.6	7	222.3	6.9
Z16-03 - 1	8.8	2.3	1.15	0.5	35.9	6.2	11.4	1.1	119.1	8.3	44.7	2.7	189	13	35.5	2.1	338	15	63.4	2.7	9350	180	11	13	69.4	2.8	86.1	3.3
Z16-03 - 10	24.1	8.5	6.7	1.7	67.8	7.2	19.8	3.3	179	20	63.1	5.1	266	25	51.1	5.8	480	52	98	11	10090	190	14	20	534	65	790	130
Z16-03 - 11	2.9	1.2	0.11	0.2	19.2	2.7	7.3	0.53	90.4	8	32.1	2.8	139	6.7	27.9	1.5	248.5	9.9	48.1	2.1	11500	190	11	12	133.9	5.4	295.2	6.8
Z16-03 - 12	3	1.4	0.49	0.74	19.2	8.8	7.4	1.2	100	12	39.1	2.7	190	17	38.4	3.5	365	27	67.9	3.4	12610	420	8	19	134	17	379	24
Z16-03 - 13	2.5	1.9	0.47	0.37	16.8	3.9	5.03	0.77	60.8	6	20.2	2.3	103.3	4.8	20.3	1.7	198	10	41.6	3.9	11080	370	15	22	163.9	4.7	417	17
Z16-03 - 14	3.4	1.4	0.34	0.33	20.7	4.7	7	1.2	81.1	8.6	30	3.3	133	14	26.1	2.6	230	23	45.2	3.7	12380	110	-2.7	9.5	129.6	9.7	330	10
Z16-03 - 15	8	1.8	2	0.83	35.5	4.9	10.44	0.69	120.4	7.9	43.4	1.9	195.7	9	39.1	2	338	10	69	1.9	11900	250	2.6	9.4	176	17	289.9	8.4
Z16-03 - 16	20.1	3.7	7.3	1.3	60.9	7.5	16.4	1.7	157	11	50.7	3.4	196.9	7	40.1	2.4	341	17	66.2	2	10710	220	-13	7.8	161.6	6.5	454	14
Z16-03 - 17	6.8	4.4	2.9	1	26.8	6.2	7.6	1.5	81.3	9.7	29.6	2.7	128.8	9.9	24.5	1.7	251	14	52.3	3.5	9720	210	-4	15	110.6	8.3	192	19
Z16-03 - 18	41.9	7.3	4.7	1.5	143	14	43.3	1.9	493	25	167.3	9.8	675	37	123.5	8.3	1023	55	165.7	7.9	9760	270	2	14	711	46	988	46
Z16-03 - 19	47.7	8.2	15.8	2.2	109	16	24.3	2.7	205	19	67.4	3.4	287	26	63	2.4	629	28	135.7	5.1	12290	260	-5	17	2320	690	1167	76
Z16-03 - 2	1.01	0.99	0.37	0.44	4.7	2	2.16	0.44	27	2.3	10.81	0.76	56.2	3.3	12.41	0.85	125.8	7	28	2.2	12580	280	7.3	9	93.2	3	241.9	9.5

Z16-03 - 3	17.8	4.5	0.73	0.53	32.4	5	8.36	0.86	91.5	7.1	33.1	1.8	146	6.8	28.4	1.8	250	10	50.7	3.2	9030	180	-10	11	54.8	4	139.4	6.8
Z16-03 - 4	19.3	3.7	2.56	0.94	57.9	5.9	16.06	0.99	161.7	6.2	50.5	1.9	195.8	8.3	38	1.7	297	13	54.5	2.3	10000	190	-7	12	152.5	5.2	137.8	4
Z16-03 - 5	10.7	2.8	1.79	0.3	32.1	5.2	8.8	1	89.5	6.9	31	2.4	140.6	7.8	26.3	1.7	239	17	47.4	3.4	9650	220	-13	13	254.2	8.8	251.1	7.8
Z16-03 - 6	4.3	1.1	0.83	0.35	14	2.7	4.64	0.63	52.6	3.2	18.7	1.3	86	4	17.1	1.2	168	7.1	34	1.4	10900	200	-9.8	6.7	171	5.3	380	13
Z16-03 - 7	6	1.9	1.84	0.41	28.8	4.9	7.4	1.1	83	8.3	29.5	2	127.5	8	25.9	1.6	240.2	8.3	48.9	2.3	8410	180	7	11	201	13	275	18
Z16-03 - 8	6.7	3.3	0.71	0.39	26.8	5.7	8.6	1.2	97	11	38.5	2.8	172	11	33.8	2.4	308	13	61.6	3.9	11290	210	-3	16	257.6	6.8	594	21
Z16-03 - 9	8.7	3.8	1.1	0.54	26.6	4	10.8	1.1	104.1	7.4	37	2.2	168.1	8.4	35.1	1.3	314	16	63.3	3.5	10640	230	-5.4	8.7	282.8	9.8	574	28

Table S5. Individual standard and unknown U-Pb apatite analyses.

Sample	Pb^{207}/U^{235}	Pb^{207}/U^{235} 2σ	Pb^{206}/U^{238}	Pb^{206}/U^{238} 2σ	ρ*	Pb^{207}/Pb^{206}	Pb^{207}/Pb^{206} 2σ	Pb^{207} corrected Pb^{206}/U^{238} age	Pb^{207} corrected Pb^{206}/U^{238} age 2σ
A_MAD_0	0.593	0.081	0.075	0.0029	-0.30642	0.0578	0.0085	-	-
A_MAD_1	0.604	0.087	0.0759	0.0026	-0.17182	0.0567	0.0079	-	-
A_MAD_2	0.617	0.085	0.0774	0.0029	-0.23053	0.058	0.0084	-	-
A_MAD_3	0.592	0.093	0.0773	0.0029	-0.25519	0.056	0.0089	-	-
A_MAD_4	0.58	0.072	0.0747	0.0026	-0.08188	0.0562	0.0071	-	-
A_MAD_5	0.6	0.089	0.0751	0.0028	-0.15886	0.0582	0.0091	-	-
A_MAD_6	0.602	0.099	0.0767	0.0026	-0.19461	0.0561	0.0094	-	-
A_MAD_7	0.61	0.099	0.0773	0.0028	-0.10853	0.0579	0.0099	-	-
A_MAD_8	0.617	0.087	0.0775	0.0033	0.21002	0.0578	0.0079	-	-
A_MAD_9	0.61	0.078	0.0769	0.0029	-0.30098	0.0579	0.0079	-	-
A_MAD_10	0.608	0.072	0.0767	0.0029	-0.12316	0.0575	0.0072	-	-
A_MAD_11	0.62	0.1	0.079	0.0029	-0.00367	0.057	0.0094	-	-
A_MAD_12	0.57	0.1	0.0742	0.0025	-0.16625	0.056	0.01	-	-
A_MAD_13	0.601	0.092	0.0766	0.003	-0.40104	0.0577	0.0091	-	-
A_MAD_14	0.61	0.072	0.0754	0.0028	0.00767	0.059	0.0073	-	-
A_MAD_15	0.597	0.079	0.0768	0.0026	-0.2564	0.0567	0.0078	-	-
A_MAD_16	0.596	0.084	0.0773	0.0029	0.09181	0.056	0.0079	-	-
A_MAD_17	0.589	0.087	0.0748	0.0029	0.10036	0.0567	0.0087	-	-
A_McClure_0	5.22	0.27	0.1169	0.0045	0.17024	0.323	0.017	490	30
A_McClure_1	4.73	0.28	0.1179	0.005	0.06269	0.294	0.019	528	39
A_McClure_2	5.45	0.26	0.125	0.0049	0.17979	0.318	0.016	531	34
A_McClure_3	1.791	0.088	0.0937	0.003	-0.01829	0.1388	0.0072	523	21
A_McClure_4	1.733	0.074	0.0927	0.0028	0.10033	0.1351	0.006	520.1	19
A_McClure_5	1.973	0.09	0.0965	0.0034	0.1242	0.1504	0.0077	530	22
A_McClure_6	2.067	0.088	0.0955	0.0032	0.18118	0.1561	0.0067	521	20
A_McClure_7	2.88	0.16	0.1053	0.0043	0.19253	0.199	0.012	541	28
A_McClure_8	2.95	0.15	0.0994	0.0035	0.05339	0.212	0.011	501	25
Durango_0	0.189	0.037	0.00656	0.00062	0.03928	0.244	0.056	33.1	4.8
Durango_1	0.214	0.04	0.00679	0.00052	0.07045	0.242	0.048	33.9	4
Durango_2	0.266	0.043	0.00675	0.00056	0.10224	0.326	0.06	29.7	4.6
Durango_3	0.209	0.039	0.0065	0.00055	-0.17387	0.27	0.064	32	4.9
Durango_4	0.218	0.033	0.00648	0.00049	-0.0201	0.266	0.048	30.8	4
Durango_5	0.236	0.039	0.00645	0.00053	0.10636	0.288	0.052	29.4	3.8
Durango_6	0.248	0.05	0.00633	0.00068	-0.14415	0.324	0.094	28.6	5.8
Durango_7	0.234	0.051	0.00688	0.00066	0.00331	0.289	0.073	31.8	5.7
Durango_8	0.234	0.053	0.00703	0.00066	-0.0466	0.305	0.088	33.1	6.2
Z16-06_0	492	36	4.19	0.35	0.98848	0.839	0.0081	-520	360
Z16-06_1	2100	880	18	7.9	0.98972	0.831	0.0087	-500	1300
Z16-06_2	1120	300	9.44	2.7	0.99016	0.84	0.0054	-690	820
Z16-06_3	112.1	13	0.988	0.12	0.98981	0.8122	0.0075	121	79
Z16-06_4	666	270	5.69	2.4	0.99053	0.8311	0.0053	-290	460
Z16-06_5	153	15	1.38	0.14	0.98818	0.8035	0.0084	280	110
Z16-06_6	698	69	6	0.6	0.96568	0.826	0.0098	-270	1000

Z16-06_7	761	42	6.51	0.39	0.95243	0.837	0.0083	-790	740
Z16-06_8	461	98	4.01	1	0.96392	0.819	0.021	-90	580
Z16-06_9	1315	240	11.28	2.1	0.98717	0.833	0.008	-1560	1.10E+03
Z16-06_10	903	480	7.8	4.2	0.98815	0.8274	0.0062	-200	520
Z16-06_11	1305	61	11.25	0.62	0.9831	0.8306	0.0068	-1700	1.00E+03
Z16-06_12	42.8	3.5	0.395	0.031	0.96075	0.772	0.019	137	64
Z16-06_13	188.2	27	1.692	0.23	0.98663	0.8035	0.0069	300	120
Z16-06_14	732	39	6.27	0.41	0.95791	0.833	0.0079	-610	670
Z16-06_15	514	37	4.55	0.35	0.98286	0.8162	0.0087	270	340
Z16-06_16	282.8	9.6	2.473	0.11	0.95938	0.8174	0.0078	160	210
Z16-06_17	308	30	2.66	0.26	0.85087	0.85	0.048	-1350	890
Z16-06_18	279	19	2.39	0.17	0.83422	0.86	0.065	-500	1500
Z16-06_19	1550	170	13.1	1.5	0.97085	0.836	0.012	-3.10E+03	2.20E+03
Z16-06_20	740	380	6.33	3.4	0.98642	0.825	0.0072	80	710
Z16-06_21	1320	130	10.99	1.2	0.98504	0.846	0.0071	-1.90E+03	1.50E+03
Z16-06_22	574	22	5.08	0.24	0.99245	0.8107	0.003	630	140
Z16-06_23	293	58	2.61	0.51	0.99254	0.81	0.02	160	510
Z16-06_24	293	30	2.59	0.27	0.97938	0.802	0.013	220	260
Z16-06_25	3640	430	31.3	3.8	0.98629	0.838	0.007	-7.10E+03	4.10E+03
Z16-06_26	325	15	2.88	0.15	0.97948	0.8091	0.0075	410	200
Z16-06_27	571	50	5.02	0.47	0.97915	0.809	0.013	130	440
Z16-06_28	457	28	4.03	0.26	0.97272	0.818	0.008	100	400
Z16-06_29	259	35	2.27	0.32	0.98693	0.812	0.0084	290	190
Z16-06_30	223.9	8.1	2.024	0.096	0.95225	0.7956	0.0089	500	180
Z16-06_31	460	55	3.5	0.58	0.9049	0.93	0.17	-3.00E+03	3.80E+03
Z16-06_32	376	17	3.4	0.17	0.96113	0.81	0.0063	440	480
Z16-06_33	2360	280	20.3	2.4	0.98556	0.844	0.0058	-2.70E+03	2.70E+03
Z16-06_34	383	26	3.37	0.25	0.97985	0.809	0.011	320	290
Z16-06_35	149	21	1.34	0.18	0.99827	0.7928	0.0079	325	84
Z16-06_36	505	39	4.37	0.34	0.95832	0.828	0.011	-170	680
Z16-06_37	1650	160	14.4	1.4	0.98358	0.837	0.0079	-4.60E+03	4.00E+03
Z16-06_38	529	18	4.65	0.21	0.93367	0.8143	0.0095	220	430
Z16-09_0	389	38	3.01	0.35	0.92312	0.954	0.038	-2.90E+03	1.60E+03
Z16-09_1	384	44	3.19	0.41	0.93701	0.867	0.03	-900	960
Z16-09_2	314	28	2.59	0.24	0.84492	0.884	0.037	-380	830
Z16-09_3	502	69	4.12	0.61	0.95029	0.889	0.034	-2.50E+03	1.60E+03
Z16-09_4	660	100	5.33	0.79	0.97092	0.893	0.032	-2.00E+03	1.00E+03
Z16-09_5	275	37	2.27	0.26	0.91255	0.862	0.039	-160	720
Z16-09_6	1270	160	15	4.4	0.42475	0.62	0.14	no value	NAN
Z16-09_7	572	49	4.55	0.42	0.94574	0.897	0.031	-1.30E+03	1.10E+03
Z16-09_8	414	55	3.48	0.46	0.95964	0.846	0.028	200	1100
Z16-09_9	605	97	5.22	0.94	0.89932	0.9	0.051	-2.50E+03	2.60E+03
Z16-09_10	213	18	1.71	0.18	0.86181	0.904	0.043	-340	460
Z16-09_11	537	65	4.35	0.54	0.86955	0.896	0.042	-1.60E+03	1.50E+03
Z16-09_12	307	65	2.11	0.52	0.86296	0.97	0.075	-2.00E+03	2.10E+03
Z16-09_13	417	54	3.31	0.42	0.95227	0.901	0.055	-830	960
Z16-09_14	161	35	1.33	0.23	0.54904	0.89	0.092	-900	1400
Z16-09_15	158	23	1.37	0.23	0.88069	0.838	0.03	470	410
Z16-09_16	216	19	1.83	0.17	0.71961	0.833	0.045	-130	750

Z16-09_17	235	33	2.06	0.27	0.89813	0.848	0.033	-50	650
Z16-09_18	339	43	2.74	0.36	0.7786	0.875	0.048	-990	1000
Z16-09_19	134.9	17	1.104	0.16	0.82303	0.859	0.043	120	360
Z16-09_20	250	31	1.99	0.25	0.91826	0.884	0.036	-260	830
Z16-09_21	271	45	2.31	0.3	0.90006	0.885	0.071	-400	820
Z16-09_22	351	60	3.13	0.45	0.9393	0.863	0.037	400	650
Z16-09_23	413	56	3.41	0.38	0.90069	0.867	0.04	-500	1000
Z16-09_24	279	47	2.56	0.53	0.65942	0.8	0.09	-1.10E+03	2.60E+03
Z16-09_25	830	67	6.79	0.55	0.97579	0.871	0.026	-400	1400
Z16-09_26	345	47	3.03	0.47	0.89891	0.864	0.033	-700	1200
Z16-09_27	380	29	3.13	0.24	0.9002	0.866	0.034	-480	850
Z16-09_28	750	190	6.3	1.1	0.86761	0.851	0.081	-9.10E+03	9.20E+03
Z16-09_29	600	72	4.96	0.57	0.92407	0.853	0.03	100	1100
Z16-09_30	432	91	3.49	0.75	0.95183	0.893	0.035	-1220	940
Z16-09_31	670	85	5.4	0.74	0.9222	0.875	0.047	660	890
Z16-09_32	590	95	4.9	0.95	0.92991	0.872	0.026	-1.30E+03	1.80E+03
Z16-09_33	1.70E+03	880	12.5	7	0.9939	0.912	0.062	-500	1600
Z16-09_34	358	81	3.22	0.63	0.98071	0.822	0.029	80	860
Z16-09_35	384	38	3.34	0.36	0.96199	0.849	0.031	-70	840
Z16-09_36	195	99	1.71	0.91	0.88462	0.855	0.044	-130	730
Z16-09_38	232	49	1.81	0.31	0.8609	1	0.094	-1.00E+03	1.10E+03
Z16-09_39	332	42	2.84	0.34	0.8659	0.828	0.048	-300	1400

*Denotes error correlation between $^{206}Pb/^{238}U$ and $^{207}Pb/^{235}U$

Figure S2. T-$M_{(O)}$ pseudosection calculated for metapelite sample Z16-06.

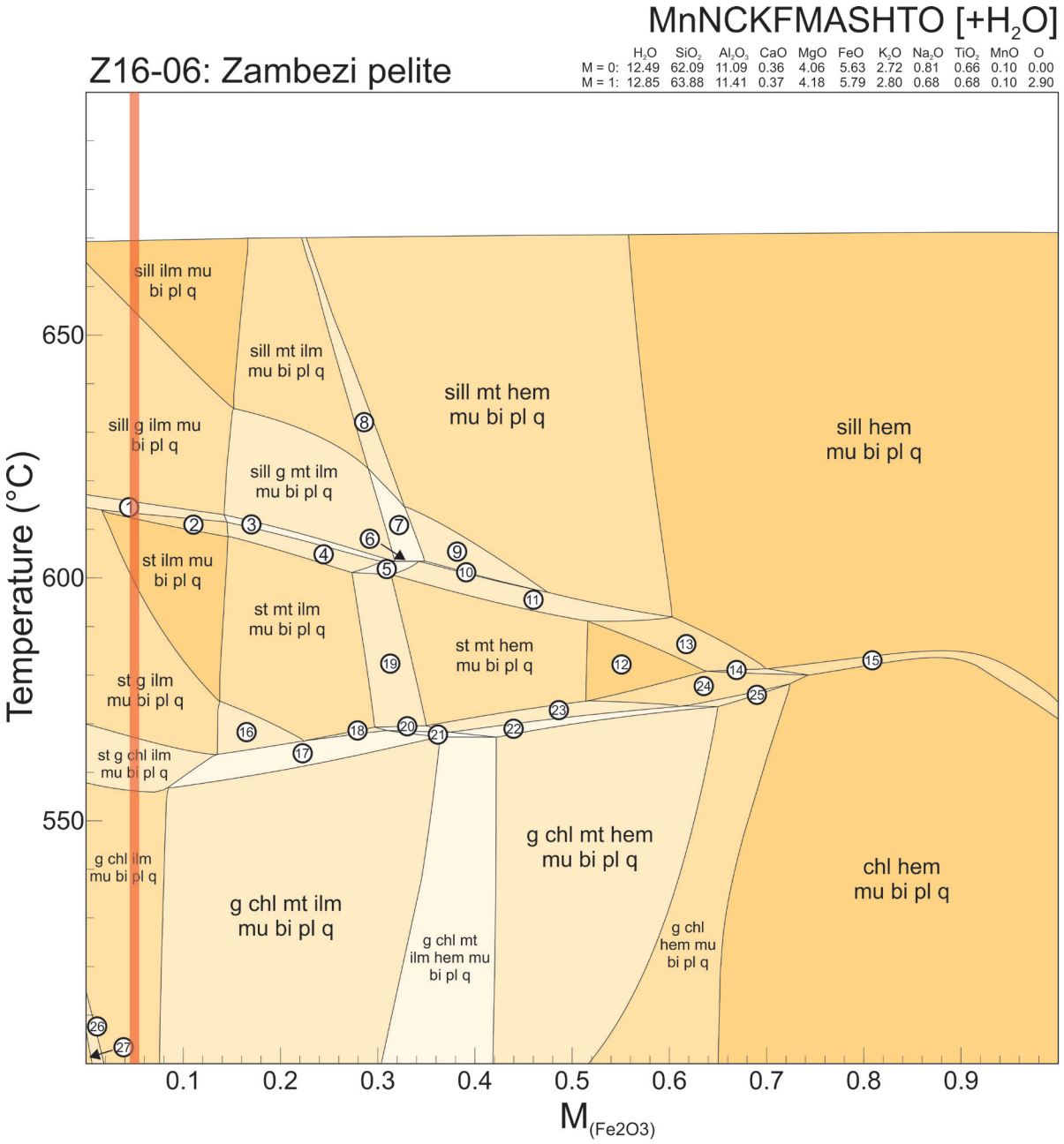

1: st sill g ilm mu bi pl q
2: st sill ilm mu bi pl q
3: st sill g mt ilm mu bi pl q
4: st sill mt ilm mu bi pl q
5: st sill mt ilm hem mu bi pl q
6: st sill g mt ilm hem mu bi pl q
7: sill g mt ilm hem mu bi pl q
8: sill mt ilm hem mu bi pl q
9: sill g mt hem mu bi pl q
10: st sill g mt hem mu bi pl q
11: st sill mt hem mu bi pl q
12: st hem mu bi pl q
13: st sill hem mu bi pl q
14: st sill chl hem mu bi pl q
15: sill chl hem mu bi pl q
16: st g mt ilm mu bi pl q
17: st g chl mt ilm mu bi pl q
18: st chl mt ilm mu bi pl q
19: st mt ilm hem mu bi pl q
20: st chl mt ilm hem mu bi pl q
21: st g chl mt ilm hem mu bi pl q
22: st g chl mt hem mu bi pl q
23: st chl mt hem mu bi pl q
24: st chl hem mu bi pl q
25: st g chl hem mu bi pl q
26: g chl ilm ru mu bi pl q
27: g chl ru mu bi pl q

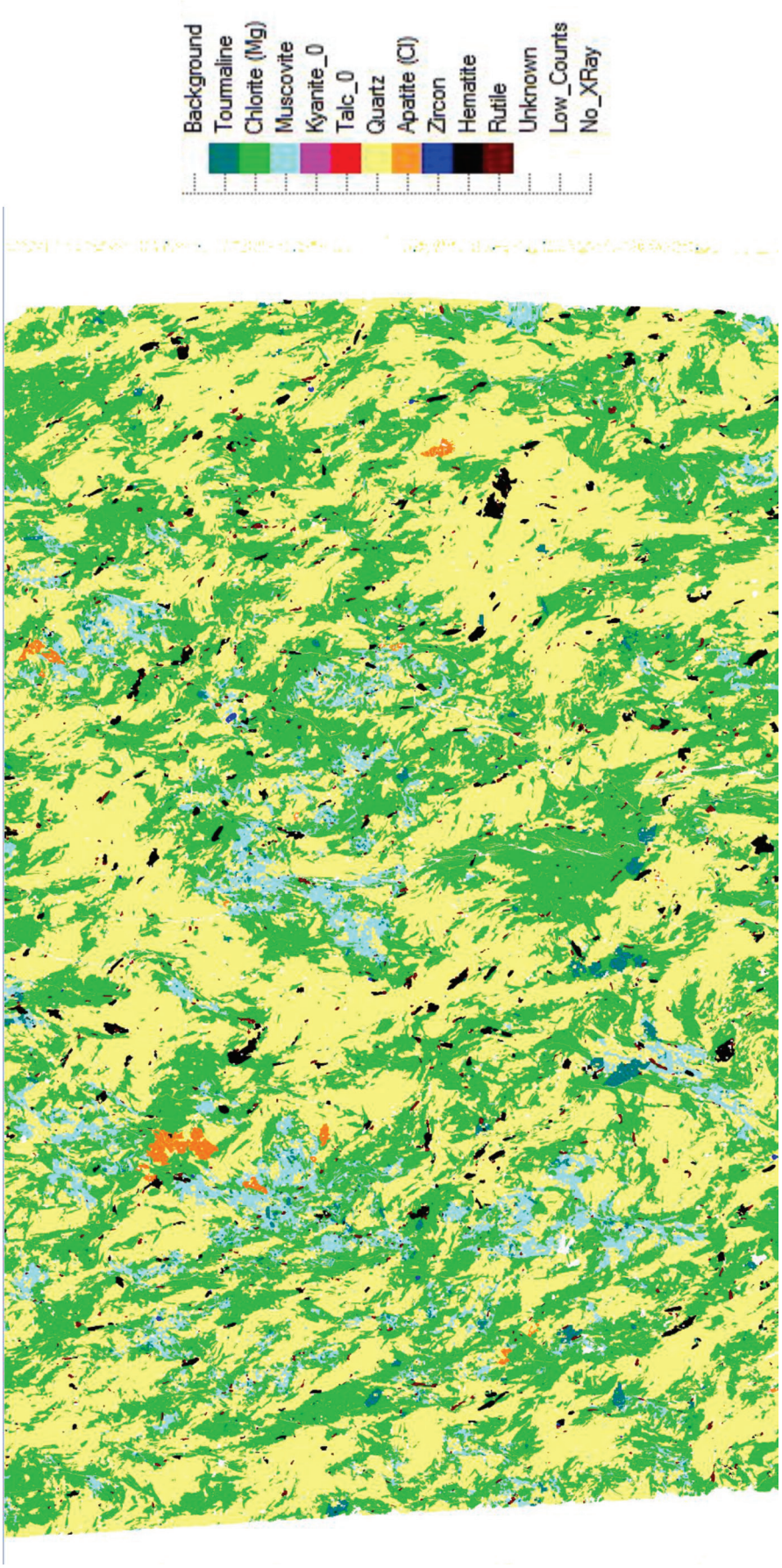

Figure S4. Map of phases within chlorite-quartz schist sample Z16-09, obtained via mineral liberation analysis.

Table S6. Bulk-rock compositions for modelled samples Z16-09 and Z16-06

	Composition (mole%)	
Oxide	Z16-09	Z16-06
H2O	14.97	12.44
SiO2	59.27	61.83
Al2O3	6	11.04
CaO	0.15	0.36
MgO	16.72	4.04
FeO	3.12	5.61
K2O	0.3	2.71
Na2O	0.15	0.81
TiO2	0.84	0.66
MnO	0.03	0.1
O	1.56	0.41

Appendix 5

Supplementary material for: The tectono-thermal evolution of the southern Congo margin as deterimined from apatite and muscovite thermochronology.

Table S1. Information for samples analysed in this study.

Sample	Lithology	Latitude (S)	Longitude (E)	Sample formation age	Reference
Chewore-Rufunsa Terrane					
Z16-17	Felsic Gneiss	15° 32' 17"	29° 41' 09"	2000 to 1000 Ma	-
Z16-18	Felsic Gneiss	15° 16' 49"	28° 46' 59"	2000 to 1000 Ma	-
Z16-27	Granodiorite	14° 59' 09"	29° 59' 11"	2000 ± 9 Ma	Alessio et al. 2019
Z16-23	Metapelite	15° 07' 38"	29° 32' 25"	*c* . 1800 to 1100 Ma (likely)	Alessio et al. 2018
Kacholola Terrane					
Z16-52	Felsic Gneiss	14° 53' 24"	30° 36' 09"	2000 to 1000 Ma	-
Nyimba Sinda Terrane					
Z14-07	Psammite	14° 32' 00"	30° 57' 23"	*c.* 1000 to 730 Ma (likely)	Alessio et al. 2018
Z16-33	Granite	14° 18' 06"	31° 32' 09"	*c* . 500 Ma	Alessio et al. 2019; Johnson et al. 2006
Chipata Terrane					
Z16-36	Quartzite	13° 59' 38"	32° 08' 04"	*c* . 1500 to 1100 Ma	Alessio et al. 2019
Z16-40	Felsic Gneiss	13° 42' 25"	32° 29' 21"	2009 ± 30 Ma	Alessio et al. 2019
Z16-41	Charnockite	13° 40' 23"	32° 32' 57"	1040 ± 5 Ma	Alessio et al. 2019
Z16-45	Charnockite	13° 52' 53"	32° 32' 22"	1039 ± 6 Ma	Alessio et al. 2019
Zambezi Belt, Kafue region					
Z16-06	Metapelite	16° 00' 52"	28° 27' 31"	*c* . 1000 to 550 Ma	Alessio et al. (Unpublished); Johnson et al. 2007
Z16-01	Granodiorite	15° 54' 03"	28° 11' 59"	1096 ± 11 Ma	Alessio et al. (Unpublished)

Table S2. Individual apatite standard U-Pb analytical data.

Sample	$^{207}Pb/^{235}U$	$^{207}Pb/^{235}U$ propagated 2σ error	$^{206}Pb/^{238}U$	$^{206}Pb/^{238}U$ propagated 2σ error	Error correlation: $^{206}Pb/^{238}U$ vs $^{207}Pb/^{235}U$	$^{207}Pb/^{206}Pb$	$^{207}Pb/^{206}Pb$ propagated 2σ error	Error correlation: $^{238}U/^{206}Pb$ vs $^{207}Pb/^{206}Pb$	^{207}Pb corrected $^{206}Pb/^{238}U$ Age	^{207}Pb corrected $^{206}Pb/^{238}U$ age propagated 2σ error
McClure Apatite*										
McC-01.d	3.25	0.31	0.1061	0.0099	0.41963	0.217	0.021	0.29912	530	57
McC-02.d	3.59	0.27	0.1066	0.0081	0.31599	0.241	0.018	0.38134	515	49
McC-03.d	3.35	0.25	0.1041	0.0074	0.22717	0.227	0.016	0.36421	516	43
McC-04.d	2.79	0.19	0.1029	0.0073	0.25114	0.193	0.014	0.32483	533	46
McC-05.d	2.15	0.19	0.0996	0.0076	0.52196	0.16	0.012	0.12656	540	44
McC-06.d	2.56	0.15	0.1011	0.0069	0.06054	0.184	0.012	0.51049	526	50
McC-07.d	3.83	0.45	0.1077	0.011	0.22885	0.258	0.036	0.51042	509	72
McC-08.d	3.15	0.28	0.1034	0.0077	0.33695	0.227	0.018	0.051425	509	45
McC-10.d	2.71	0.2	0.1	0.0072	0.21521	0.191	0.013	0.30988	517	46
McC-11.d	2.56	0.16	0.1004	0.0066	0.091917	0.188	0.013	0.47951	525	45
McC-12.d	2.25	0.13	0.0948	0.0062	0.43609	0.1728	0.0087	0.16296	506	37
McC-13.d	2.76	0.19	0.0989	0.007	0.45814	0.21	0.011	0.2558	500	41
McC-14.d	2.77	0.12	0.099	0.0068	0.42998	0.209	0.0088	0.52251	502	41
McC-15.d	3.67	0.24	0.1104	0.0075	0.23716	0.25	0.019	0.32131	525	50
McC-19.d	4.77	0.36	0.1199	0.0095	0.34721	0.301	0.022	0.5121	527	58
McC-20.d	4.17	0.35	0.1128	0.0079	0.45715	0.26	0.017	0.14147	522	48
McC-21.d	4.3	0.32	0.1125	0.0082	0.43772	0.268	0.015	0.17267	515	45
McC-22.d	5.44	0.41	0.1238	0.009	0.45365	0.316	0.02	0.20547	519	47
McC-23.d	2.18	0.18	0.0955	0.0067	0.41714	0.168	0.011	0.099417	513	39
McC-26.d	2.1	0.25	0.1001	0.0095	0.032281	0.166	0.023	0.521	539	61
McC-1.d	5.01	0.37	0.117	0.0093	0.28601	0.337	0.024	0.42287	479	56
McC-2.d	7.02	0.29	0.1373	0.011	0.42378	0.379	0.019	0.59384	524	61
McC-3.d	6.97	0.38	0.1316	0.01	0.40975	0.387	0.022	0.48177	496	61
McC-4.d	2.75	0.29	0.1002	0.0086	0.4031	0.198	0.019	0.19081	511	51
McC-5.d	2.55	0.32	0.1041	0.01	0.29024	0.179	0.026	0.28965	552	62
McC-6.d	2.12	0.26	0.1045	0.0098	0.074819	0.148	0.019	0.504	577	64

McC-7.d	3.27	0.32	0.1168	0.011	0.23808	0.205	0.024	0.5075	597	71
McC-8.d	2.75	0.34	0.109	0.012	0.18292	0.184	0.027	0.40914	576	76
McC-9.d	2.5	0.23	0.0944	0.01	0.38442	0.201	0.022	0.47094	488	60
McC-10.d	2.38	0.22	0.0953	0.0089	0.56492	0.187	0.013	0.14915	496	50
McC-11.d	3.79	0.42	0.1111	0.0097	0.10837	0.248	0.028	0.40676	525	68
McC-12.d	3.85	0.3	0.1098	0.0089	0.40423	0.251	0.019	0.25277	522	53
McC-13.d	3.84	0.26	0.1159	0.0091	0.13025	0.25	0.022	0.49865	554	61
McC-14.d	3.85	0.36	0.1172	0.01	0.49914	0.244	0.019	0.11292	562	58
McC-15.d	4.02	0.39	0.1161	0.0094	0.55754	0.244	0.02	0.1023	555	50
McC-16.d	3.95	0.35	0.1196	0.012	0.39367	0.237	0.022	0.4128	582	70
Durango Apatite*										
DurZ-01.d	0.289	0.066	0.0061	0.00076	-0.26781	0.4	0.12	0.99877	25.3	6.8
DurZ-02.d	0.215	0.056	0.0066	0.0008	-0.21006	0.249	0.066	0.51748	32.7	7.2
DurZ-03.d	0.285	0.069	0.006	0.00074	0.073606	0.372	0.097	0.21913	24.2	6.5
DurZ-04.d	0.275	0.092	0.0068	0.00084	0.21067	0.311	0.097	-0.061668	27.2	6.6
DurZ-05.d	0.267	0.094	0.0057	0.00077	-0.00034482	0.38	0.14	0.53601	23.2	8
DurZ-06.d	0.234	0.076	0.0072	0.00084	0.12355	0.211	0.07	-0.061168	35.1	7.2
DurZ-07.d	0.361	0.087	0.0072	0.00088	-0.16216	0.4	0.12	0.6979	27.6	9
DurZ-08.d	0.266	0.096	0.0074	0.0014	0.044753	0.34	0.17	0.65202	35	11
DurZ-09.d	0.294	0.072	0.0066	0.0011	0.27951	0.354	0.098	0.30835	27.2	7.7
DurZ-11.d	0.348	0.084	0.0074	0.0013	-0.15952	0.41	0.12	0.61588	28	11
DurZ-13.d	0.246	0.073	0.0081	0.0012	-0.036302	0.26	0.084	0.46107	41	9.4
DurZ-14.d	0.298	0.073	0.0069	0.0008	-0.00085724	0.312	0.087	0.62924	29.3	7.1
DurZ-15.d	0.272	0.084	0.0062	0.00089	-0.22039	0.35	0.12	0.88898	26.6	9
DurZ-16.d	0.239	0.068	0.0073	0.001	0.2735	0.253	0.091	0.49024	36	6.2
DurZ-17.d	0.19	0.11	0.0067	0.0013	-0.12329	0.26	0.16	0.38964	34	12
DurZ-18.d	0.215	0.085	0.0057	0.00087	-0.021633	0.33	0.12	0.55541	26.4	8
DurZ-19.d	0.33	0.14	0.0064	0.00096	-0.10596	0.43	0.18	0.41844	24	11
DurZ-20.d	0.257	0.084	0.0071	0.001	-0.026799	0.3	0.11	0.28977	33.3	8.8
DurZ-21.d	0.258	0.061	0.007	0.00099	0.19084	0.308	0.084	0.44893	32.3	7.2
DurZ-22.d	0.245	0.083	0.0073	0.0012	-0.16094	0.32	0.13	-0.10776	35.4	10
DurZ-23.d	0.29	0.11	0.0062	0.0014	0.39558	0.45	0.16	0.5128	24.4	9.2
DurZ-25.d	0.255	0.077	0.007	0.0013	0.098167	0.31	0.14	0.75898	32.4	9

DurZ-26.d	0.308	0.087	0.0073	0.0011	-0.13936	0.39	0.15	0.72753	31.9	9.7	
DurZ-27.d	0.43	0.13	0.0091	0.0016	-0.045165	0.37	0.14	0.43114	37	14	
DurZ-28.d	0.33	0.13	0.0073	0.0013	0.017604	0.42	0.17	0.28181	30	12	
DurZ-29.d	0.28	0.13	0.0083	0.0015	0.038857	0.28	0.17	0.73391	39	14	
DurZ-30.d	0.28	0.16	0.0071	0.0015	0.2148	0.51	0.3	0.59352	27	15	
DurZ-31.d	0.34	0.15	0.008	0.0021	-0.021895	0.56	0.28	-0.1193	34	17	
DurZ-32.d	0.42	0.17	0.0078	0.0014	0.048764	0.42	0.21	0.56776	29	14	
DurZ-33.d	0.35	0.18	0.0064	0.0019	-0.077558	0.8	0.42	0.37527	24	17	
DurZ-34.d	0.22	0.14	0.0053	0.0014	0.30312	0.56	0.36	-0.10688	24	11	
DurZ-41.d	0.31	0.14	0.0061	0.0015	-0.014292	0.43	0.39	0.39569	24	13	
DurZ-42.d	0.27	0.13	0.0063	0.0016	0.16087	0.49	0.26	0.52133	28	12	

*Note both analytical sessions are pooled, resulting in analyses with identical names

Table S3. Individual apatite U-Pb analytical data.

Sample	$^{207}Pb/^{235}U$	$^{207}Pb/^{235}U$ propagated 2σ error	$^{206}Pb/^{238}U$	$^{206}Pb/^{238}U$ propagated 2σ error	Error correlation: $^{206}Pb/^{238}U$ vs $^{207}Pb/^{235}U$	$^{207}Pb/^{206}Pb$	$^{207}Pb/^{206}Pb$ propagated 2σ error	Error correlation: $^{238}U/^{206}Pb$ vs $^{207}Pb/^{206}Pb$	^{207}Pb corrected $^{206}Pb/^{238}U$ Age	^{207}Pb corrected $^{206}Pb/^{238}U$ age propagated 2σ error
Z16-17										
Z16-17-01.d	4	0.12	0.1059	0.0067	0.58702	0.2721	0.0068	0.42294	454	38
Z16-17-02.d	5.36	0.24	0.1172	0.0079	0.67115	0.323	0.011	0.11846	448	39
Z16-17-03.d	3.46	0.13	0.1022	0.0068	0.58645	0.241	0.0078	0.36706	466	38
Z16-17-04.d	4.28	0.15	0.1083	0.0072	0.60129	0.2912	0.0081	0.49166	446	39
Z16-17-05.d	8.93	0.38	0.1588	0.011	0.23296	0.398	0.017	0.26471	501	69
Z16-17-06.d	1.704	0.093	0.0835	0.0052	0.45505	0.142	0.0062	0.020502	453	31
Z16-17-07.d	6.31	0.22	0.1282	0.0084	0.52318	0.346	0.01	0.31975	461	47
Z16-17-08.d	3.42	0.12	0.0999	0.0064	0.61952	0.2415	0.0069	0.2637	455	34
Z16-17-09.d	8.05	0.31	0.1515	0.0097	0.4772	0.393	0.016	0.083805	483	61
Z16-17-10.d	3.3	0.1	0.097	0.006	0.67463	0.2468	0.0054	0.15785	435	29
Z16-17-11.d	5.17	0.21	0.1161	0.0079	0.51285	0.315	0.012	0.34119	453	45
Z16-17-12.d	4.26	0.2	0.1108	0.0078	0.74705	0.2716	0.0081	0.3062	474	37
Z16-17-13.d	6.43	0.36	0.1291	0.01	0.58344	0.372	0.017	0.39083	440	54
Z16-17-14.d	4.77	0.66	0.1166	0.012	0.82085	0.299	0.021	-0.23898	466	47
Z16-17-15.d	2.708	0.075	0.0941	0.0058	0.39313	0.2045	0.0055	0.26949	458	36
Z16-17-16.d	3.83	0.14	0.1089	0.0069	0.51181	0.2501	0.008	0.29034	487	38
Z16-17-17.d	4.56	0.19	0.1077	0.007	0.68978	0.2993	0.0097	0.33834	439	31
Z16-17-18.d	3.63	0.1	0.1044	0.0064	0.39503	0.2479	0.0073	0.4309	466	46
Z16-17-19.d	5.77	0.28	0.1222	0.0084	0.32426	0.341	0.017	0.39775	449	54
Z16-17-20.d	5.68	0.23	0.1219	0.0084	0.74195	0.3291	0.0093	0.27756	453	35
Z16-17-21.d	4.19	0.17	0.1083	0.0072	0.45497	0.279	0.01	0.33449	458	41
Z16-17-22.d	3.1	0.12	0.099	0.0062	0.64151	0.221	0.0067	-0.058622	469	32
Z16-17-23.d	4.93	0.15	0.1161	0.0071	0.53391	0.3029	0.0084	0.34355	463	44
Z16-17-24.d	5.62	0.18	0.1232	0.0077	0.60207	0.3219	0.0085	0.26721	472	41
Z16-17-25.d	4.2	0.27	0.1106	0.009	0.56396	0.272	0.014	0.18399	474	50
Z16-17-26.d	4.14	0.16	0.1062	0.0068	0.69946	0.2838	0.0089	0.14414	444	36

Z16-17-27.d	11.6	1	0.177	0.015	0.82286	0.453	0.023	-0.34466	458	53
Z16-17-28.d	2.92	0.12	0.0961	0.0063	0.38176	0.2152	0.0093	0.40026	461	39
Z16-17-29.d	2.598	0.095	0.0937	0.0058	0.60899	0.1981	0.0057	0.10619	463	32
Z16-17-30.d	3.63	0.17	0.1047	0.0069	0.40523	0.248	0.011	0.27791	471	42
Z16-17-31.d	4.35	0.19	0.1104	0.0074	0.57743	0.279	0.011	0.26347	466	40
Z16-17-32.d	4.37	0.24	0.1152	0.0078	0.59173	0.271	0.013	0.099459	493	43
Z16-17-33.d	2.024	0.071	0.0892	0.0058	0.48692	0.1621	0.0048	0.38265	469	34
Z16-17-34.d	3.41	0.11	0.1025	0.0066	0.71258	0.2349	0.0058	0.35021	473	35
Z16-17-35.d	3.88	0.16	0.1052	0.0071	0.58942	0.2713	0.0087	0.32176	449	40
Z16-17-36.d	3.67	0.15	0.1025	0.0068	0.66967	0.2536	0.0073	0.16965	456	35
Z16-17-37.d	5.22	0.2	0.1193	0.008	0.50017	0.3076	0.0098	0.37372	470	46
Z16-17-38.d	6.04	0.2	0.1248	0.0083	0.67962	0.346	0.01	0.14083	451	42
Z16-17-39.d	4.3	0.12	0.1131	0.0071	0.57472	0.2691	0.0069	0.34832	487	40
Z16-17-40.d	2.772	0.09	0.0974	0.006	0.68801	0.2037	0.0045	0.14975	474	34
Z16-52										
Z16-52-1.d	21	1.2	0.234	0.017	0.5104	0.641	0.033	0.2939	399	100
Z16-52-10.d	32.5	2	0.337	0.027	0.77283	0.683	0.029	0.063624	459	120
Z16-52-11.d	11.28	0.41	0.1623	0.011	0.82451	0.489	0.012	0.0081518	465	43
Z16-52-12.d	15.64	0.92	0.1979	0.014	0.56234	0.576	0.022	-0.017141	434	68
Z16-52-13.d	12.63	0.89	0.178	0.015	0.69861	0.512	0.026	0.20177	480	70
Z16-52-14.d	11.36	0.37	0.1681	0.011	0.67333	0.489	0.012	0.33525	482	51
Z16-52-15.d	14.1	0.51	0.1854	0.012	0.4007	0.534	0.018	0.49304	470	68
Z16-52-16.d	15.42	0.7	0.1939	0.013	0.71911	0.572	0.018	0.081826	430	59
Z16-52-17.d	20.23	0.83	0.2365	0.017	0.54158	0.616	0.025	0.52567	448	98
Z16-52-18.d	12.83	0.52	0.1768	0.012	0.53286	0.514	0.02	0.36037	473	68
Z16-52-19.d	20.7	1.4	0.247	0.02	0.71577	0.596	0.027	0.19121	503	91
Z16-52-2.d	20.4	1.2	0.229	0.018	0.64832	0.637	0.023	0.3843	395	75
Z16-52-20.d	11.45	0.41	0.1692	0.011	0.42388	0.496	0.015	0.56548	479	63
Z16-52-21.d	17.58	0.93	0.2164	0.016	0.68572	0.576	0.022	0.21956	475	74
Z16-52-22.d	20.6	1	0.2377	0.017	0.73546	0.613	0.02	0.1913	453	74
Z16-52-23.d	16.8	1	0.213	0.017	0.64036	0.598	0.025	0.46684	436	78
Z16-52-24.d	19	0.81	0.2246	0.015	0.56767	0.6	0.023	0.39796	452	86
Z16-52-25.d	12.1	0.39	0.1715	0.011	0.63525	0.503	0.016	0.28329	474	57

Z16-52-26.d	11.37	0.33	0.1668	0.011	0.58575	0.49	0.014	0.49218	479	58
Z16-52-27.d	15.64	0.75	0.1959	0.013	0.47629	0.566	0.026	0.28704	446	84
Z16-52-28.d	19.29	0.82	0.2332	0.015	0.69646	0.587	0.018	0.099746	489	74
Z16-52-29.d	10.54	0.41	0.1576	0.011	0.73166	0.476	0.013	0.34332	469	50
Z16-52-3.d	12.67	0.49	0.1821	0.013	0.65484	0.514	0.017	0.40422	490	61
Z16-52-30.d	14.12	0.47	0.1911	0.012	0.55193	0.527	0.015	0.33445	492	67
Z16-52-31.d	54.1	3.6	0.568	0.049	0.77971	0.701	0.022	-0.012694	700	160
Z16-52-4.d	21.03	0.83	0.2393	0.016	0.7112	0.621	0.017	0.22173	441	75
Z16-52-5.d	18.44	0.9	0.227	0.015	0.54502	0.6	0.022	0.12367	455	82
Z16-52-6.d	19.26	0.83	0.233	0.017	0.34559	0.588	0.029	0.53196	494	110
Z16-52-7.d	17.91	0.78	0.2153	0.015	0.2282	0.591	0.03	0.55186	451	110
Z16-52-8.d	30.6	1.5	0.33	0.027	0.37189	0.666	0.042	0.71784	500	160
Z16-52-9.d	24.7	1	0.2717	0.018	0.65103	0.644	0.021	0.29203	453	94
Z16-41										
Z16-41-1.d	10.95	0.6	0.1634	0.012	0.57204	0.479	0.024	0.36222	530	64
Z16-41-10.d	16.9	1.1	0.239	0.02	0.35754	0.507	0.032	0.25151	725	110
Z16-41-11.d	15.85	0.87	0.2031	0.015	0.42835	0.563	0.029	0.4704	551	96
Z16-41-12.d	14.1	1.1	0.197	0.017	0.39156	0.538	0.044	0.53872	549	100
Z16-41-13.d	53.9	4	0.497	0.041	0.73217	0.789	0.039	0.28108	510	200
Z16-41-14.d	12.9	0.7	0.2006	0.015	0.3235	0.485	0.029	0.58342	644	96
~~Z16-41-15.d~~	~~no value~~	~~NAN~~	~~no value~~	~~NAN~~	~~NaN~~	~~no value~~	~~NAN~~	~~NaN~~	~~no value~~	~~NAN~~
~~Z16-41-16.d~~	~~26.6~~	~~4.2~~	~~0.346~~	~~0.051~~	~~0.19538~~	~~0.67~~	~~0.13~~	~~0.34283~~	~~780~~	~~310~~
~~Z16-41-17.d~~	~~no value~~	~~NAN~~	~~no value~~	~~NAN~~	~~NaN~~	~~no value~~	~~NAN~~	~~NaN~~	~~no value~~	~~NAN~~
Z16-41-18.d	11.54	0.55	0.1714	0.012	0.3727	0.495	0.022	0.42364	531	65
Z16-41-19.d	16.6	1.5	0.216	0.02	0.71878	0.564	0.035	0.014496	550	95
Z16-41-2.d	15.16	0.94	0.201	0.016	0.66138	0.541	0.026	0.17893	565	76
Z16-41-20.d	14.05	0.97	0.1978	0.015	0.62506	0.519	0.025	0.057945	572	65
Z16-41-21.d	30.4	1.6	0.326	0.024	0.40244	0.69	0.036	0.47119	590	150
~~Z16-41-22.d~~	~~7.86~~	~~0.92~~	~~0.166~~	~~0.016~~	~~0.87229~~	~~0.332~~	~~0.019~~	~~-0.31957~~	~~696~~	~~60~~
Z16-41-23.d	34	2	0.345	0.026	0.55428	0.724	0.035	0.30144	530	150
Z16-41-24.d	11.19	0.59	0.1684	0.012	0.55478	0.478	0.021	0.24782	545	66
Z16-41-25.d	19.29	0.8	0.238	0.016	0.51182	0.601	0.024	0.37466	569	93
Z16-41-26.d	29.3	2.8	0.319	0.028	0.46028	0.711	0.051	0.30316	510	160

Z16-41-27.d	26.7	1.9	0.302	0.027	0.3058	0.639	0.055	0.60425	650	180
Z16-41-28.d	79.7	7.9	0.695	0.071	0.69838	0.83	0.051	-0.0055449	390	330
Z16-41-29.d	14.55	0.84	0.195	0.015	0.45453	0.547	0.033	0.45561	545	88
Z16-41-3.d	28.9	4.7	0.321	0.046	0.72631	0.695	0.07	0.22045	560	190
Z16-41-30.d	19.7	1.5	0.234	0.02	0.54869	0.593	0.035	0.34284	540	99
Z16-41-31.d	14.6	3.1	0.22	0.035	0.84489	0.504	0.05	-0.28176	650	110
Z16-41-32.d	50	3.5	0.513	0.056	0.61772	0.717	0.058	0.72501	870	280
Z16-41-33.d	8.7	1	0.143	0.013	0.71528	0.458	0.035	0.11214	483	61
Z16-41-34.d	14.52	0.7	0.1997	0.015	0.48719	0.522	0.025	0.45789	589	83
Z16-41-35.d	10.96	0.63	0.1707	0.012	0.1297	0.474	0.026	0.12789	560	71
Z16-41-4.d	40.2	3.9	0.417	0.042	0.29142	0.697	0.079	0.40833	720	300
Z16-41-5.d	32	2.1	0.34	0.029	0.50745	0.673	0.039	0.52114	630	170
Z16-41-6.d	12.32	0.95	0.183	0.015	0.46808	0.494	0.026	0.34273	565	86
~~Z16-41-7.d~~	~~143~~	~~63~~	~~1.6~~	~~0.89~~	~~0.70551~~	~~0.94~~	~~0.56~~	~~0.93248~~	~~400~~	~~3100~~
Z16-41-8.d	11.4	1.4	0.168	0.017	0.51038	0.483	0.05	0.25081	542	96
Z16-41-9.d	108	11	0.969	0.11	0.84767	0.832	0.049	0.25831	510	450
Z16-01										
Z16-01-1.d	1.82	0.11	0.0937	0.0063	0.42055	0.1415	0.0079	0.16661	508	36
~~Z16-01-10.d~~	~~120~~	~~51~~	~~1.42~~	~~0.55~~	~~0.90211~~	~~0.687~~	~~0.051~~	~~-0.22382~~	~~700~~	~~510~~
~~Z16-01-11.d~~	~~2.36~~	~~0.17~~	~~0.1066~~	~~0.0074~~	~~0.26834~~	~~0.161~~	~~0.011~~	~~0.021011~~	~~563~~	~~45~~
~~Z16-01-12.d~~	~~no value~~	~~NAN~~	~~no value~~	~~NAN~~	~~NaN~~	~~no value~~	~~NAN~~	~~NaN~~	~~no value~~	~~NAN~~
Z16-01-13.d	6.44	0.56	0.1379	0.0099	0.50068	0.341	0.026	-0.11139	505	70
Z16-01-14.d	1.288	0.093	0.0826	0.0061	0.5945	0.1162	0.0073	0.061156	469	34
Z16-01-15.d	3.15	0.2	0.1025	0.0073	0.21524	0.227	0.015	0.3524	481	45
Z16-01-16.d	1.481	0.092	0.0854	0.0057	0.25263	0.1255	0.0079	0.30139	480	37
Z16-01-17.d	10.41	0.86	0.176	0.016	0.46051	0.435	0.043	0.51683	535	120
Z16-01-18.d	9.94	0.88	0.172	0.016	0.48749	0.442	0.037	0.54428	500	92
Z16-01-19.d	1.52	0.13	0.0815	0.0057	0.3519	0.137	0.011	0.16403	447	36
Z16-01-2.d	2.89	0.32	0.1055	0.0091	0.29599	0.213	0.02	0.16053	495	47
~~Z16-01-20.d~~	~~160~~	~~110~~	~~1.9~~	~~1.2~~	~~0.01615~~	~~0.62~~	~~0.27~~	~~-0.15133~~	~~0~~	~~1200~~
~~Z16-01-21.d~~	~~no value~~	~~NAN~~	~~no value~~	~~NAN~~	~~NaN~~	~~no value~~	~~NAN~~	~~NaN~~	~~no value~~	~~NAN~~
Z16-01-22.d	3.67	0.19	0.105	0.0076	0.39935	0.258	0.014	0.4652	471	46
Z16-01-23.d	9.9	1	0.164	0.015	0.23371	0.438	0.05	0.3704	482	110

Z16-01-24.d	23.7	2.1	0.289	0.029	0.42372	0.61	0.057	0.36414	420	200
Z16-01-25.d	9.26	0.98	0.146	0.013	0.43412	0.457	0.043	0.20446	402	89
~~Z16-01-26.d~~	~~740~~	~~390~~	~~7.1~~	~~2.4~~	~~0.764~~	~~0.566~~	~~0.097~~	~~-0.022467~~	~~-3.40E+03~~	~~6.10E+03~~
~~Z16-01-27.d~~	~~91.9~~	~~7~~	~~0.903~~	~~0.082~~	~~0.83966~~	~~0.754~~	~~0.033~~	~~0.12488~~	~~150~~	~~310~~
Z16-01-28.d	7.09	0.73	0.135	0.011	0.61301	0.373	0.033	0.030159	465	65
Z16-01-29.d	2.23	0.16	0.0937	0.0066	0.5879	0.174	0.011	-0.038502	481	34
Z16-01-3.d	1.305	0.063	0.0803	0.0049	0.23736	0.1162	0.0055	0.069626	456	32
Z16-01-30.d	~~10.7~~	~~1.8~~	~~0.198~~	~~0.024~~	~~0.56944~~	0.433	0.067	0.30571	580	140
Z16-01-31.d	1.029	0.059	0.0812	0.0054	0.39087	0.0938	0.0049	0.27326	478	34
Z16-01-32.d	4.97	0.37	0.1273	0.011	0.21692	0.283	0.023	0.45272	543	71
Z16-01-33.d	~~8.2~~	~~1.3~~	~~0.165~~	~~0.023~~	~~0.54145~~	0.385	0.049	0.15756	560	120
Z16-01-4.d	3.65	0.26	0.1165	0.0088	0.45129	0.224	0.015	0.25289	553	51
Z16-01-5.d	3	0.36	0.109	0.0084	0.7363	0.201	0.019	-0.38208	535	38
Z16-01-6.d	1.748	0.084	0.0882	0.0058	0.55602	0.1452	0.006	0.094363	478	33
~~Z16-01-7.d~~	~~9.6~~	~~1.6~~	~~0.136~~	~~0.035~~	~~0.22796~~	~~0.62~~	~~0.13~~	~~0.79473~~	~~190~~	~~170~~
~~Z16-01-8.d~~	~~18~~	~~11~~	~~0.297~~	~~0.069~~	~~0.22179~~	~~0.92~~	~~0.67~~	~~0.23563~~	~~810~~	~~480~~
~~Z16-01-9.d~~	~~no value~~	~~NAN~~	~~no value~~	~~NAN~~	~~NaN~~	~~no value~~	~~NAN~~	~~NaN~~	~~no value~~	~~NAN~~
Z16-45										
Z16-45-1.d	38.5	2.6	0.386	0.033	0.72826	0.755	0.038	0.22727	440	150
Z16-45-10.d	21.5	1.6	0.26	0.024	0.54112	0.632	0.043	0.30456	530	130
~~Z16-45-11.d~~	~~378~~	~~31~~	~~3.11~~	~~0.3~~	~~0.94839~~	~~0.882~~	~~0.019~~	~~-0.15678~~	~~350~~	~~510~~
Z16-45-12.d	60.6	4.2	0.572	0.046	0.84129	0.769	0.028	0.11625	590	170
Z16-45-13.d	73.4	7.4	0.659	0.071	0.86798	0.793	0.039	0.13142	560	230
Z16-45-14.d	22.6	1.6	0.258	0.021	0.77307	0.639	0.026	0.087263	512	86
Z16-45-15.d	16.5	1.9	0.205	0.019	0.7673	0.593	0.039	-0.26899	465	76
Z16-45-16.d	26.9	1.9	0.301	0.026	0.72312	0.643	0.033	0.14147	588	120
Z16-45-17.d	29.5	1.6	0.308	0.025	0.64003	0.69	0.031	0.51559	509	120
Z16-45-18.d	66.9	7.4	0.609	0.069	0.83607	0.783	0.048	0.05305	560	250
Z16-45-19.d	42.2	2.3	0.392	0.032	0.40104	0.79	0.048	0.55275	380	210
Z16-45-2.d	14.6	1.1	0.184	0.015	0.64056	0.562	0.033	0.081928	466	76
Z16-45-20.d	31.4	2.6	0.337	0.03	0.73058	0.668	0.04	0.21356	600	140
Z16-45-21.d	30	2.7	0.315	0.031	0.78829	0.682	0.041	0.2233	530	120
Z16-45-22.d	42.9	4.1	0.4	0.032	0.49437	0.765	0.067	0.071338	420	290

Z16-45-23.d	33.9	1.8	0.346	0.026	0.55202	0.699	0.035	0.35864	540	160
~~Z16-45-24.d~~	~~255~~	~~28~~	~~2.07~~	~~0.23~~	~~0.90528~~	~~0.909~~	~~0.03~~	~~0.086808~~	~~90~~	~~450~~
Z16-45-25.d	64.1	5.3	0.591	0.06	0.65269	0.823	0.056	0.3891	360	260
Z16-45-26.d	32.1	2	0.324	0.026	0.68954	0.71	0.028	0.12415	475	110
Z16-45-27.d	25.9	2.9	0.268	0.032	0.92809	0.684	0.033	-0.16115	437	81
Z16-45-28.d	56.9	3.6	0.551	0.05	0.056232	0.768	0.035	0.0080155	570	190
Z16-45-29.d	40.2	3.5	0.397	0.038	0.76669	0.727	0.04	0.27172	490	130
Z16-45-3.d	53.5	3.3	0.493	0.037	0.28376	0.791	0.032	0.34519	430	170
Z16-45-30.d	6.35	0.35	0.1238	0.0095	0.70883	0.375	0.02	-0.079292	482	47
Z16-45-31.d	38.7	2.7	0.389	0.032	0.28839	0.752	0.045	0.51957	420	230
Z16-45-32.d	24.2	1.3	0.277	0.022	0.78154	0.643	0.021	0.39472	549	87
Z16-45-33.d	44.3	3.4	0.443	0.042	0.72406	0.738	0.047	0.085927	550	220
Z16-45-34.d	8.91	0.4	0.1365	0.0091	0.49145	0.465	0.022	0.14989	444	60
Z16-45-35.d	19.6	1.2	0.241	0.018	0.71904	0.593	0.024	0.080262	555	80
Z16-45-36.d	22.5	3.5	0.258	0.04	0.93464	0.62	0.035	-0.03564	540	99
Z16-45-37.d	103.8	8.8	0.892	0.094	0.8479	0.893	0.043	0.53343	170	330
Z16-45-38.d	61.1	5.7	0.538	0.051	0.88385	0.778	0.025	0.14228	540	150
Z16-45-39.d	71.4	5.7	0.617	0.058	0.66931	0.829	0.053	0.40116	390	300
Z16-45-4.d	31.7	2.4	0.334	0.028	0.11685	0.66	0.047	0.56752	570	230
Z16-45-40.d	39.8	4.5	0.391	0.039	0.81996	0.765	0.045	0.05765	410	150
Z16-45-5.d	18.1	1.3	0.212	0.017	0.61033	0.618	0.039	0.24682	467	110
Z16-45-6.d	35.6	2.9	0.353	0.032	0.53748	0.729	0.052	0.27421	480	190
Z16-45-7.d	39.9	2.6	0.39	0.032	0.71659	0.771	0.033	0.45677	410	140
Z16-45-8.d	88.4	7.7	0.789	0.089	0.75007	0.838	0.055	0.50217	600	350
Z16-45-9.d	49.9	4	0.471	0.053	0.4872	0.772	0.073	0.73123	530	310
Z16-27										
Z16-27-1.d	9.24	0.38	0.1573	0.01	0.61676	0.428	0.013	0.15441	456	53
Z16-27-10.d	16.8	1.4	0.251	0.023	0.72126	0.469	0.023	0.14494	615	100
Z16-27-11.d	10.12	0.34	0.1684	0.011	0.38856	0.43	0.015	0.42846	485	70
Z16-27-12.d	12.03	0.5	0.1883	0.012	0.65182	0.468	0.012	0.18336	464	63
Z16-27-13.d	15.2	0.6	0.2104	0.014	0.6638	0.515	0.016	0.36997	447	70
Z16-27-14.d	13.25	0.6	0.1958	0.013	0.79894	0.492	0.014	0.0030151	452	54
Z16-27-15.d	8.06	0.23	0.1422	0.009	0.60087	0.407	0.012	0.19104	431	48

Z16-27-16.d	18.5	0.78	0.246	0.021	0.494	0.543	0.03	0.68072	474	120
Z16-27-17.d	8.37	0.29	0.1449	0.0098	0.54924	0.417	0.014	0.52095	437	55
Z16-27-18.d	13.94	0.71	0.208	0.014	0.38477	0.521	0.028	0.23833	430	120
Z16-27-19.d	8.49	0.4	0.1524	0.01	0.62712	0.411	0.013	0.38125	465	48
Z16-27-2.d	7.35	0.23	0.1417	0.0089	0.52378	0.374	0.011	0.25636	478	51
Z16-27-20.d	9.21	0.33	0.1569	0.0099	0.63608	0.429	0.01	0.19923	453	47
Z16-27-21.d	16.42	0.97	0.218	0.017	0.68034	0.539	0.024	0.23792	418	83
Z16-27-22.d	10.65	0.45	0.1672	0.011	0.61081	0.464	0.016	0.23005	431	59
Z16-27-23.d	22.7	1	0.284	0.02	0.7048	0.567	0.02	0.4044	473	110
Z16-27-24.d	14.3	1.5	0.209	0.018	0.54039	0.526	0.043	0.1987	425	120
Z16-27-25.d	12.21	0.45	0.187	0.012	0.55215	0.477	0.016	0.42696	460	69
Z16-27-26.d	12.25	0.46	0.1916	0.012	0.69964	0.466	0.013	0.18863	489	59
Z16-27-27.d	10.52	0.41	0.1721	0.011	0.58824	0.451	0.014	0.36721	462	64
Z16-27-28.d	10.78	0.55	0.1712	0.013	0.65819	0.451	0.018	0.32678	463	63
Z16-27-29.d	4.82	0.25	0.1107	0.0071	0.53644	0.315	0.012	0.0077755	432	38
Z16-27-3.d	20.7	1.2	0.257	0.02	0.68371	0.575	0.024	0.14331	409	97
Z16-27-30.d	8	1.9	0.173	0.038	0.95106	0.38	0.035	-0.40476	560	120
Z16-27-31.d	9.39	0.54	0.1583	0.012	0.74012	0.427	0.016	0.12992	450	45
Z16-27-32.d	10.97	0.34	0.1719	0.011	0.63401	0.456	0.015	0.21765	455	59
Z16-27-33.d	15.52	0.85	0.2139	0.015	0.64038	0.518	0.022	0.1548	448	82
Z16-27-34.d	10.41	0.42	0.1705	0.011	0.71518	0.446	0.01	0.14026	466	50
Z16-27-35.d	13.43	0.97	0.191	0.016	0.65202	0.502	0.027	0.12096	427	79
Z16-27-36.d	6.32	0.16	0.1296	0.0081	0.51028	0.3529	0.0088	0.43862	466	48
Z16-27-37.d	13.78	0.89	0.218	0.018	0.38854	0.457	0.033	0.49672	580	110
Z16-27-38.d	27.3	1.4	0.323	0.026	0.67065	0.61	0.028	0.52479	423	130
Z16-27-39.d	5.46	0.26	0.1224	0.0086	0.68827	0.322	0.012	0.32927	471	43
Z16-27-4.d	15.8	1.2	0.22	0.019	0.56932	0.554	0.036	0.4311	397	100
Z16-27-40.d	5.83	0.18	0.1273	0.0083	0.62921	0.3377	0.009	0.46615	472	43
Z16-27-5.d	12.41	0.45	0.1884	0.012	0.47614	0.477	0.017	0.46712	462	85
Z16-27-6.d	10.94	0.38	0.1705	0.011	0.50012	0.463	0.015	0.17907	433	60
Z16-27-7.d	11.18	0.79	0.1788	0.013	0.75823	0.449	0.016	0.046459	483	61
Z16-27-8.d	4.02	0.17	0.1073	0.0071	0.59735	0.278	0.012	0.035978	455	40
Z16-27-9.d	8.2	0.24	0.1491	0.0092	0.64509	0.4047	0.0095	0.407	463	50

Z16-40										
Z16-40-1.d	9.82	0.55	0.2066	0.014	0.53007	0.34	0.016	0.041312	830	77
Z16-40-10.d	9.32	0.42	0.1775	0.012	0.31159	0.39	0.02	0.45022	657	76
Z16-40-11.d	no value	NAN	no value	NAN	NaN	no value	NAN	NaN	no value	NAN
Z16-40-12.d	12.62	0.77	0.185	0.013	0.33684	0.492	0.03	0.31588	543	89
Z16-40-13.d	20.2	1.1	0.264	0.02	0.54581	0.556	0.027	0.42954	652	110
Z16-40-14.d	196	72	1.96	0.75	0.94511	0.758	0.067	-0.0011288	680	260
Z16-40-15.d	no value	NAN	no value	NAN	NaN	no value	NAN	NaN	no value	NAN
Z16-40-16.d	5.87	0.25	0.1589	0.011	0.49522	0.269	0.012	0.36319	726	63
Z16-40-17.d	12.03	0.56	0.1928	0.014	0.31698	0.472	0.026	0.60616	601	88
Z16-40-18.d	11.76	0.52	0.199	0.015	0.23997	0.429	0.024	0.68364	682	97
Z16-40-19.d	34	16	0.46	0.17	0.7061	0.62	0.18	0.30094	870	800
Z16-40-2.d	10.1	0.84	0.172	0.014	0.63896	0.435	0.026	0.22611	576	69
Z16-40-20.d	17.31	0.99	0.229	0.017	0.5203	0.534	0.024	0.33218	588	96
Z16-40-21.d	50	33	0.91	0.62	0.90592	0.61	0.15	-0.36139	0	1100
Z16-40-22.d	12.54	0.47	0.2057	0.013	0.16068	0.449	0.018	0.45742	669	89
Z16-40-23.d	12.4	1.8	0.199	0.017	0.70352	0.46	0.045	-0.23536	605	120
Z16-40-24.d	5.41	0.62	0.1238	0.0098	0.71192	0.297	0.02	-0.037818	546	57
Z16-40-25.d	6.77	0.38	0.1468	0.01	0.5595	0.34	0.017	0.24505	596	57
Z16-40-26.d	11.87	0.55	0.1953	0.014	0.46744	0.438	0.019	0.36026	650	77
Z16-40-27.d	9.12	0.49	0.1831	0.013	0.49414	0.355	0.016	0.25692	714	71
Z16-40-28.d	7.3	0.42	0.1438	0.012	0.56149	0.367	0.021	0.4578	559	67
Z16-40-29.d	200	120	2.7	2.8	0.31981	0.82	0.49	-0.074288	540	700
Z16-40-3.d	11.31	0.39	0.2322	0.015	0.68585	0.3528	0.0079	0.12323	904	69
Z16-40-4.d	5.81	0.25	0.1424	0.0096	0.33185	0.304	0.014	0.42287	618	59
Z16-40-5.d	4.8	0.27	0.1277	0.0092	0.42578	0.274	0.013	0.2739	580	53
Z16-40-6.d	6.67	0.51	0.1371	0.011	0.66443	0.346	0.019	0.053755	550	52
Z16-40-7.d	10.52	0.48	0.187	0.013	0.52741	0.414	0.017	0.28939	655	71
Z16-40-8.d	310	110	3.5	1.6	0.88653	0.8	0.18	-0.40907	-2.30E+03	3.00E+03
Z16-40-9.d	2.67	0.45	0.1658	0.014	0.65259	0.112	0.013	-0.31981	933	70
Z16-33										
Z16-33-1.d	1.76	0.12	0.0774	0.0059	0.53284	0.163	0.01	0.23667	426	35
Z16-33-10.d	1.78	0.1	0.0839	0.0065	0.23039	0.154	0.0078	0.18299	462	42

Z16-33-11.d	1.173	0.081	0.0772	0.0054	0.43139	0.1144	0.0076	0.17011	450	32
~~Z16-33-12.d~~	~~no value~~	~~NAN~~	~~no value~~	~~NAN~~	~~NaN~~	~~no value~~	~~NAN~~	~~NaN~~	~~no value~~	~~NAN~~
Z16-33-13.d	1.49	0.11	0.0782	0.0063	0.50626	0.139	0.011	0.24581	442	36
Z16-33-14.d	1.42	0.1	0.0788	0.0053	0.35925	0.1312	0.0095	0.099779	449	32
Z16-33-15.d	1.553	0.074	0.0769	0.0055	0.51122	0.1452	0.0059	0.2517	432	32
Z16-33-16.d	1.49	0.1	0.0761	0.0051	0.18374	0.142	0.011	0.17836	428	33
Z16-33-17.d	1.57	0.075	0.0773	0.0054	0.44042	0.1453	0.0063	0.33356	434	33
Z16-33-18.d	1.318	0.079	0.0763	0.0052	0.29535	0.1287	0.0066	0.15837	430	32
~~Z16-33-19.d~~	~~28.1~~	~~2.4~~	~~0.285~~	~~0.026~~	~~0.51989~~	~~0.711~~	~~0.062~~	~~0.35366~~	~~510~~	~~160~~
Z16-33-2.d	3.98	0.39	0.0973	0.0079	0.60386	0.287	0.024	0.078411	461	52
Z16-33-3.d	2.46	0.21	0.0836	0.0068	0.49344	0.221	0.015	0.097787	427	37
Z16-33-4.d	2.4	0.12	0.0845	0.006	0.47666	0.208	0.01	0.2595	439	35
Z16-33-5.d	3.42	0.17	0.0921	0.0065	0.41241	0.276	0.013	0.3286	436	38
Z16-33-6.d	6.8	0.55	0.1167	0.01	0.28959	0.442	0.037	0.29571	424	66
Z16-33-7.d	1.203	0.072	0.0744	0.0054	0.50365	0.1164	0.006	0.13489	433	32
Z16-33-8.d	1.93	0.11	0.0828	0.0058	0.4427	0.1724	0.0077	0.25075	450	34
Z16-33-9.d	1.85	0.1	0.0816	0.0063	0.44268	0.1651	0.0091	0.42188	448	38

Table S4. $^{40}Ar/^{39}Ar$ anlytical data.

Relative Abundances			36Ar [V]	%1σ	37Ar [V]	%1σ	38Ar [V]	%1σ	39Ar [V]	%1σ	40Ar [V]	%1σ	40(r)/39(k) ± 2σ	Age ± 2σ (Ma)	40Ar(r) (%)	39Ar(k) (%)	K/Ca ± 2σ
8M49172D	66.0 %	4	0.0000158	45.720	0.0020741	157.021	0.0000171	44.062	0.0007748	1.887	0.0146143	2.059	12.55526 ± 5.65603	422.87 ± 169.86	66.68	0.40	0.19 ± 0.61
8M49174D	68.0 %	4	0.0000324	24.630	0.0032507	101.353	0.0000626	11.588	0.0047746	0.592	0.0775787	0.448	14.16227 ± 1.02725	470.50 ± 30.05	87.20	2.47	0.76 ± 1.55
8M49175D	69.0 %	4	0.0000634	14.105	0.0005848	535.621	0.0004869	3.467	0.0413983	0.389	0.5897749	0.170	13.78989 ± 0.17507	459.58 ± 5.15	96.79	21.39	36.81 ± 394.30
8M49176D	69.5 %	4	0.0000225	44.433	0.0009640	349.650	0.0003975	2.243	0.0321822	0.307	0.4466672	0.083	13.66712 ± 0.20562	455.96 ± 6.06	98.47	16.63	17.36 ± 121.40
8M49178D	70.0 %	4	0.0000161	45.891	0.0051636	61.987	0.0004323	2.434	0.0375738	0.203	0.5154625	0.166	13.57747 ± 0.13834	453.32 ± 4.09	98.98	19.42	3.78 ± 4.69
8M49179D	70.5 %	4	0.0000134	51.406	0.0034446	98.554	0.0001445	7.051	0.0114445	0.531	0.1580037	0.215	13.42796 ± 0.39502	448.90 ± 11.69	97.28	5.91	1.73 ± 3.41
8M49180D	71.0 %	4	0.0000074	113.538	0.0074832	44.825	0.0000713	13.210	0.0060739	0.615	0.0842804	0.429	13.40291 ± 0.85344	448.15 ± 25.28	96.67	3.14	0.42 ± 0.38
8M49182D	78.0 %	4	0.0000032	193.487	0.0077185	42.519	0.0000273	25.118	0.0019915	1.414	0.0283687	1.078	13.41886 ± 1.94302	448.63 ± 57.53	94.45	1.03	0.13 ± 0.11
8M49183D	79.0 %	4	0.0000027	248.090	0.0038182	88.019	0.0000222	32.564	0.0020464	1.634	0.0280561	1.084	13.93435 ± 2.02862	463.82 ± 59.56	101.77	1.06	0.28 ± 0.49
8M49184D	80.5 %	4	0.0000114	58.211	0.0035451	94.158	0.0001034	10.183	0.0090693	0.706	0.1278857	0.284	13.68958 ± 0.48847	456.62 ± 14.40	97.11	4.69	1.33 ± 2.51
8M49186D	82.0 %	4	0.0000167	50.850	0.0026809	125.732	0.0002342	4.062	0.0196843	0.328	0.2741453	0.166	13.66147 ± 0.27757	455.79 ± 8.19	98.10	10.17	3.82 ± 9.60
8M49187D	100.0 %	4	0.0000366	20.746	0.0029701	107.389	0.0003316	4.640	0.0265012	0.337	0.3726092	0.167	13.63723 ± 0.20068	455.08 ± 5.92	97.00	13.69	4.64 ± 9.97
		Σ	0.0002362	11.400	0.0425281	26.851	0.0023309	1.555	0.1935148	0.133	2.7174467	0.066					

Information on Analysis and Constants Used in Calculations

Sample = Z16-52MUS
Material = mus
Location = Laser
Analyst = Adam Frew
Project = ALAN COLLINS_BRANDON ALESSIO18
Mass Discrimination Law = POW
Irradiation = I25t80h
J = 0.02098570 ± 0.00001574
FCs = 99.738 ± 0.100 Ma
IGSN = Undefined
Preferred Age = Undefined
Classification = Undefined
Experiment Type = Undefined
Extraction Method = Undefined
Heating = 60 sec
Isolation = 5.00 min
Instrument = MAP-215-50
Lithology = Undefined
Lat-Lon = Undefined - Undefined
Feature = Undefined

Age Equations = Min et al. (2000)
Negative Intensities = Allowed
Decay Constant 40K = 5.531 ± 0.013 E-10 1/a
Decay Constant 39Ar = 2.940 ± 0.029 E-07 1/h
Decay Constant 37Ar = 8.264 ± 0.009 E-04 1/h
Decay Constant 36Cl = 2.303 ± 0.046 E-06 1/a
Decay Constant 40K(EC,β⁺) = 0.576 ± 0.002 E-10 1/a
Decay Constant 40K(β⁻) = 4.955 ± 0.013 E-10 1/a
Atmospheric Ratio 40/36(a) = 298.56 ± 0.30
Atmospheric Ratio 38/36(a) = 0.1869 ± 0.0002
Production Ratio 39/37(ca) = 0.000695 ± 0.000009
Production Ratio 38/37(ca) = 0.000020 ± 0.000001
Production Ratio 36/37(ca) = 0.000265 ± 0.000002
Production Ratio 40/39(k) = 0.000730 ± 0.000091
Production Ratio 38/39(k) = 0.012150 ± 0.000030
Production Ratio 36/38(cl) = 263.00 ± 13.15
Scaling Ratio K/Ca = 0.520
Abundance Ratio 40K/K = 1.1700 ± 0.0100 E-04
Atomic Weight K = 39.0983 ± 0.0001 g

Results	40(a)/36(a) ± 2σ	40(r)/39(k) ± 2σ	Age ± 2σ (Ma)	MSWD	39Ar(k) (%,n)	K/Ca ± 2σ
Age Plateau		13.64921 ± 0.07910 ± 0.58%	455.43 ± 2.41 ± 0.53%	0.60	100.00	0.17 ± 0.10
				83%	12	
		Full External Error ± 3.93		1.85	2σ Confidence Limit	
		Analytical Error ± 2.33		1.0000	Error Magnification	
Total Fusion Age		13.65794 ± 0.09299 ± 0.68%	455.69 ± 2.81 ± 0.62%		12	2.37 ± 1.27
		Full External Error ± 4.19				
		Analytical Error ± 2.74				
Normal Isochron	213.85 ± 131.54 ± 61.51%	13.70871 ± 0.12826 ± 0.94%	457.19 ± 3.83 ± 0.84%	1.98	100.00	
Error Chron				3%	12	
		Full External Error ± 4.94		1.89	2σ Confidence Limit	
		Analytical Error ± 3.78		1.4064	Error Magnification	
				1	Number of Iterations	
				0.0000093909	Convergence	
Inverse Isochron	414.28 ± 156.17 ± 37.70%	13.53530 ± 0.18275 ± 1.35%	452.07 ± 5.43 ± 1.20%	0.32	100.00	
				98%	12	
		Full External Error ± 6.25		1.89	2σ Confidence Limit	
		Analytical Error ± 5.40		1.0000	Error Magnification	
				6	Number of Iterations	
				0.0000216250	Convergence	
				27%	Spreading Factor	

Relative Abundances			36Ar [V]	%1σ	37Ar [V]	%1σ	38Ar [V]	%1σ	39Ar [V]	%1σ	40Ar [V]	%1σ	40(r)/39(k) ± 2σ	Age ± 2σ (Ma)	40Ar(r) (%)	39Ar(k) (%)	K/Ca ± 2σ
8M49010D	58 °C		0.0000443	13.507	0.0017566	110.995	0.0000165	29.104	0.0010342	0.635	0.0320873	0.663	18.07695 ± 3.49653	581.53 ± 96.19	58.33	0.37	0.3 ± 0.7
8M49011D	58 °C	4	0.0000021	276.596	0.0012626	174.294	0.0000329	13.754	0.0021685	0.581	0.0332236	0.554	15.08156 ± 1.63611	497.20 ± 47.16	98.40	0.78	0.9 ± 3.1
8M49012D	58 °C	4	0.0000251	21.611	0.0008867	242.904	0.0000374	13.724	0.0031251	0.614	0.0544948	0.380	15.01091 ± 1.06778	495.16 ± 30.81	86.10	1.12	1.8 ± 8.9
8M49014D	58 °C	4	0.0002270	3.650	0.0006985	293.770	0.0002644	2.396	0.0184921	0.275	0.3358115	0.097	14.49130 ± 0.28205	480.10 ± 8.21	79.80	6.65	13.8 ± 80.9
8M49015D	59 °C	4	0.0000297	19.647	0.0027453	71.743	0.0001228	4.600	0.0102779	0.461	0.1568295	0.146	14.37112 ± 0.36813	476.60 ± 10.73	94.20	3.69	1.9 ± 2.8
8M49016D	59 °C	4	0.0001146	8.310	0.0010590	194.192	0.0004488	1.880	0.0346695	0.303	0.5350935	0.051	14.44922 ± 0.18682	478.88 ± 5.44	93.62	12.46	17.0 ± 66.1
8M49017D	60 °C	4	0.0000789	8.401	0.0015300	135.655	0.0006884	1.903	0.0588017	0.212	0.8678144	0.058	14.35445 ± 0.09250	476.12 ± 2.70	97.27	21.13	20.0 ± 54.2
8M49019D	60 °C	4	0.0000071	83.268	0.0021532	89.293	0.0007934	1.762	0.0667933	0.159	0.9588737	0.119	14.32068 ± 0.07760	475.13 ± 2.26	99.76	24.01	16.1 ± 28.8
8M49020D	61 °C	4	0.0000094	79.980	0.0007534	262.059	0.0004413	2.436	0.0361278	0.190	0.5184231	0.084	14.26951 ± 0.13786	473.64 ± 4.03	99.44	12.98	24.9 ± 130.7
8M49021D	62 °C	4	0.0000063	120.761	0.0011335	171.612	0.0001094	5.314	0.0100797	0.326	0.1442474	0.172	14.11365 ± 0.46276	469.08 ± 13.55	98.63	3.62	4.6 ± 15.9
8M49022D	64 °C	4	0.0000046	127.227	0.0010686	194.939	0.0003765	3.715	0.0317272	0.274	0.4568718	0.079	14.35933 ± 0.13692	476.26 ± 3.99	99.72	11.40	15.4 ± 60.2
8M49027D	68 °C	4	0.0000015	532.543	0.0001635	1087.209	0.0000718	9.875	0.0049391	0.498	0.0716426	0.177	14.59418 ± 0.99724	483.09 ± 28.97	100.62	1.78	15.7 ± 341.6
		Σ	0.0005476	4.419	0.0084306	82.851	0.0034035	0.918	0.2782361	0.086	4.1654133	0.037					

Information on Analysis and Constants Used in Calculations

Sample = Z16-36MUSR
Material = mus
Location = Laser
Analyst = Adam Frew
Project = ALAN COLLINS_BRANDON ALESSIO18
Mass Discrimination Law = POW
Irradiation = I25t80h
J = 0.02098570 ± 0.00001574
FCs = 28.294 ± 0.037 Ma
IGSN = Undefined
Preferred Age = Undefined
Classification = Undefined
Experiment Type = Undefined
Extraction Method = Undefined
Heating = 60 sec
Isolation = 3.00 min
Instrument = MAP-215-50
Lithology = Undefined
Lat-Lon = Undefined - Undefined
Feature = Undefined

Age Equations = Min et al. (2000)
Negative Intensities = Allowed
Decay Constant 40K = 5.531 ± 0.013 E-10 1/a
Decay Constant 39Ar = 2.940 ± 0.029 E-07 1/h
Decay Constant 37Ar = 8.264 ± 0.009 E-04 1/h
Decay Constant 36Cl = 2.303 ± 0.046 E-06 1/a
Decay Constant 40K(EC,β^+) = 0.576 ± 0.002 E-10 1/a
Decay Constant 40K(β^-) = 4.955 ± 0.013 E-10 1/a
Atmospheric Ratio 40/36(a) = 298.56 ± 0.30
Atmospheric Ratio 38/36(a) = 0.1869 ± 0.0002
Production Ratio 39/37(ca) = 0.000695 ± 0.000009
Production Ratio 38/37(ca) = 0.000020 ± 0.000001
Production Ratio 36/37(ca) = 0.000265 ± 0.000002
Production Ratio 40/39(k) = 0.000730 ± 0.000091
Production Ratio 38/39(k) = 0.012150 ± 0.000030
Production Ratio 36/38(cl) = 263.00 ± 13.15
Scaling Ratio K/Ca = 0.520
Abundance Ratio 40K/K = 1.1700 ± 0.0100 E-04
Atomic Weight K = 39.0983 ± 0.0001 g

Results	40(a)/36(a) ± 2σ	40(r)/39(k) ± 2σ	Age ± 2σ (Ma)	MSWD	39Ar(k) (%,n)	K/Ca ± 2σ
Age Plateau		14.34254 ± 0.04743 (± 0.33%)	475.77 ± 1.52 (± 0.32%)	0.76	99.63	0.9 ± 2.0
				67%	11	
		Full External Error ± 3.62		1.89	2σ Confidence Limit	
		Analytical Error ± 1.38		1.0000	Error Magnification	
Total Fusion Age		14.37981 ± 0.05867 (± 0.41%)	476.86 ± 1.82 (± 0.38%)		12	17.2 ± 28.4
		Full External Error ± 3.76				
		Analytical Error ± 1.71				
Normal Isochron	304.31 ± 34.81 (± 11.44%)	14.36304 ± 0.06045 (± 0.42%)	476.37 ± 1.87 (± 0.39%)	2.47	99.63	
Error Chron				1%	11	
		Full External Error ± 3.78		1.94	2σ Confidence Limit	
		Analytical Error ± 1.76		1.5731	Error Magnification	
				1	Number of Iterations	
				0.0000000403	Convergence	
Inverse Isochron	319.11 ± 23.49 (± 7.36%)	14.32061 ± 0.05525 (± 0.39%)	475.13 ± 1.73 (± 0.36%)	0.47	99.63	
				90%	11	
		Full External Error ± 3.71		1.94	2σ Confidence Limit	
		Analytical Error ± 1.61		1.0000	Error Magnification	
				2	Number of Iterations	
				0.0000059594	Convergence	
				21%	Spreading Factor	

Relative Abundances			36Ar [V]	%1σ	37Ar [V]	%1σ	38Ar [V]	%1σ	39Ar [V]	%1σ	40Ar [V]	%1σ	40(r)/39(k) ± 2σ	Age ± 2σ (Ma)	40Ar(r) (%)	39Ar(k) (%)	K/Ca ± 2σ
8M48054D	62 °C		0.0000306	20.548	0.0000934	771.295	0.0000056	68.902	0.0001507	5.178	0.0121793	0.526	20.16865 ± 25.08087	647.50 ± 676.80	24.94	0.07	0.8 ± 12.9
8M48055D	64 °C		0.0000657	9.923	0.0000705	973.157	0.0000150	27.880	0.0004520	1.864	0.0272411	0.645	16.86154 ± 8.67960	555.98 ± 246.38	27.97	0.21	3.3 ± 64.9
8M48056D	66 °C		0.0000515	11.806	0.0001608	431.610	0.0000262	19.042	0.0017693	1.067	0.0470532	0.343	17.88828 ± 2.09755	584.89 ± 58.60	67.27	0.83	5.7 ± 49.4
8M48057D	68 °C		0.0000621	10.881	0.0001713	397.626	0.0002016	5.569	0.0166672	0.342	0.2990462	0.087	16.83084 ± 0.26982	555.11 ± 7.66	93.81	7.83	50.6 ± 402.5
8M48059D	68 °C	4	0.0000275	19.893	0.0002514	315.342	0.0002000	4.118	0.0174450	0.434	0.2960398	0.479	16.49704 ± 0.28649	545.60 ± 8.18	97.21	8.20	36.1 ± 227.5
8M48060D	69 °C	4	0.0000200	29.879	0.0003119	217.331	0.0003091	2.639	0.0252944	0.262	0.4196999	0.166	16.35415 ± 0.17439	541.52 ± 4.99	98.56	11.89	42.2 ± 183.3
8M48061D	69 °C	4	0.0000172	37.050	0.0000017	42057.551	0.0002490	2.402	0.0205805	0.269	0.3389987	0.099	16.22226 ± 0.20673	537.74 ± 5.93	98.48	9.67	6404.5 ########
8M48062D	69 °C	4	0.0000235	23.761	0.0000881	781.176	0.0002287	3.794	0.0192366	0.250	0.3180243	0.114	16.16776 ± 0.19481	536.18 ± 5.59	97.80	9.04	113.5 ± 1773.6
8M48064D	70 °C	4	0.0000353	16.204	0.0006758	110.407	0.0002255	5.703	0.0197134	0.386	0.3302493	0.579	16.21370 ± 0.28870	537.49 ± 8.28	96.79	9.26	15.2 ± 33.5
8M48065D	70 °C	4	0.0000343	16.761	0.0005406	130.954	0.0001710	3.727	0.0147705	0.317	0.2501602	0.299	16.23881 ± 0.27382	538.21 ± 7.85	95.88	6.94	14.2 ± 37.2
8M48066D	71 °C	4	0.0000279	19.223	0.0004343	172.605	0.0000841	7.126	0.0070242	0.432	0.1200160	0.137	15.89176 ± 0.47946	528.24 ± 13.82	93.01	3.30	8.4 ± 29.0
8M48067D	71 °C	4	0.0000408	14.469	0.0001598	442.798	0.0001043	7.644	0.0087238	0.331	0.1527738	0.134	16.11781 ± 0.42054	534.74 ± 12.08	92.04	4.10	28.4 ± 251.4
8M48069D	78 °C	4	0.0000110	57.426	0.0000809	867.669	0.0000493	9.054	0.0035125	0.896	0.0612667	0.222	16.50078 ± 1.12146	545.71 ± 32.01	94.60	1.65	22.6 ± 392.0
8M48070D	79 °C	4	0.0000423	16.264	0.0001905	367.153	0.0000820	4.800	0.0073432	0.342	0.1285237	0.197	15.78346 ± 0.57430	525.11 ± 16.58	90.18	3.45	20.0 ± 147.2
8M48071D	81 °C	4	0.0001962	5.415	0.0001619	436.946	0.0005352	2.905	0.0404028	0.247	0.7090955	0.160	16.09960 ± 0.18479	534.22 ± 5.31	91.73	18.99	129.8 ± 1134.3
8M48072D	82 °C	4	0.0000360	14.621	0.0003409	211.283	0.0000721	7.931	0.0058355	0.602	0.1047043	0.256	16.10392 ± 0.58050	534.34 ± 16.68	89.75	2.74	8.9 ± 37.6
8M48074D	82 °C	4	0.0000122	48.120	0.0007941	92.270	0.0000460	9.754	0.0038842	0.888	0.0659595	0.303	16.02438 ± 0.95238	532.06 ± 27.39	94.38	1.83	2.5 ± 4.7
		Σ	0.0007343	3.588	0.0022989	127.918	0.0026048	1.253	0.2128057	0.097	3.6810315	0.080					

Information on Analysis and Constants Used in Calculations

Sample = Z16-23MUS
Material = mus
Location = Laser
Analyst = Fred Jourdan
Project = ALAN COLLINS_BRANDON ALESSIO18
Mass Discrimination Law = POW
Irradiation = I25t80h
J = 0.02135030 ± 0.00002776
WA1ms = 2613.000 ± 2.352 Ma
IGSN = Undefined
Preferred Age = Undefined
Classification = Undefined
Experiment Type = Undefined
Extraction Method = Undefined
Heating = 60 sec
Isolation = 5.00 min
Instrument = ARGUS VI
Lithology = Undefined
Lat-Lon = Undefined - Undefined
Feature = Undefined

Age Equations = Min et al. (2000)
Negative Intensities = Allowed
Decay Constant 40K = 5.531 ± 0.013 E-10 1/a
Decay Constant 39Ar = 2.940 ± 0.029 E-07 1/h
Decay Constant 37Ar = 8.264 ± 0.009 E-04 1/h
Decay Constant 36Cl = 2.303 ± 0.046 E-06 1/a
Decay Constant 40K(EC,β⁺) = 0.576 ± 0.002 E-10 1/a
Decay Constant 40K(β⁻) = 4.955 ± 0.013 E-10 1/a
Atmospheric Ratio 40/36(a) = 298.56 ± 0.30
Atmospheric Ratio 38/36(a) = 0.1869 ± 0.0002
Production Ratio 39/37(ca) = 0.000695 ± 0.000009
Production Ratio 38/37(ca) = 0.000020 ± 0.000001
Production Ratio 36/37(ca) = 0.000265 ± 0.000002
Production Ratio 40/39(k) = 0.000730 ± 0.000091
Production Ratio 38/39(k) = 0.012150 ± 0.000030
Production Ratio 36/38(cl) = 263.00 ± 13.15
Scaling Ratio K/Ca = 0.520
Abundance Ratio 40K/K = 1.1700 ± 0.0100 E-04
Atomic Weight K = 39.0983 ± 0.0001 g

Results	40(a)/36(a) ± 2σ	40(r)/39(k) ± 2σ	Age ± 2σ (Ma)	MSWD	39Ar(k) (%,n)	K/Ca ± 2σ
Age Plateau		16.21669 ± 0.08080 (± 0.50%)	537.58 ± 2.61 (± 0.49%)	1.09	91.05	2.9 ± 4.5
				36%	13	
		Full External Error ± 5.88		1.82	2σ Confidence Limit	
		Analytical Error ± 2.32		1.0452	Error Magnification	
Total Fusion Age		16.26568 ± 0.08508 (± 0.52%)	538.98 ± 2.72 (± 0.51%)		17	48.1 ± 123.1
		Full External Error ± 5.94				
		Analytical Error ± 2.44				
Normal Isochron	236.81 ± 37.80 (± 15.96%)	16.33593 ± 0.10363 (± 0.63%)	541.00 ± 3.21 (± 0.59%)	0.91	91.05	
				53%	13	
		Full External Error ± 6.19		1.85	2σ Confidence Limit	
		Analytical Error ± 2.97		1.0000	Error Magnification	
				1	Number of Iterations	
				0.0000194229	Convergence	
Inverse Isochron	253.44 ± 40.69 (± 16.05%)	16.31608 ± 0.11498 (± 0.70%)	540.43 ± 3.51 (± 0.65%)	0.85	91.05	
				59%	13	
		Full External Error ± 6.35		1.85	2σ Confidence Limit	
		Analytical Error ± 3.29		1.0000	Error Magnification	
				3	Number of Iterations	
				0.0000032287	Convergence	
				8%	Spreading Factor	

Relative Abundances			36Ar [V]	%1σ	37Ar [V]	%1σ	38Ar [V]	%1σ	39Ar [V]	%1σ	40Ar [V]	%1σ	40(r)/39(k) ± 2σ	Age ± 2σ (Ma)	40Ar(r) (%)	39Ar(k) (%)	K/Ca ± 2σ
8M48032D	62 °C		0.0000435	15.204	0.0005761	91.653	0.0000086	55.567	0.0001268	7.481	0.0138871	0.600	7.56509 ± 31.28016	266.43 ± 1024.32	6.88	0.03	0 ± 0
8M48033D	64 °C		0.0001382	5.138	0.0000732	668.765	0.0000309	13.711	0.0009798	1.312	0.0571751	0.198	16.24762 ± 4.35465	530.50 ± 123.22	27.84	0.23	7 ± 93
8M48034D	66 °C		0.0001476	4.537	0.0001507	346.917	0.0000622	11.724	0.0030748	0.688	0.0937025	0.242	16.14342 ± 1.32834	527.55 ± 37.65	52.97	0.73	11 ± 74
8M48035D	68 °C		0.0002243	5.215	0.0002792	172.137	0.0002111	3.601	0.0141683	0.260	0.3187907	0.094	17.77458 ± 0.50348	573.20 ± 13.91	79.00	3.38	26 ± 91
8M48037D	68 °C		0.0001987	2.463	0.0002630	173.305	0.0003491	2.864	0.0269030	0.236	0.5118052	0.071	16.81731 ± 0.13731	546.55 ± 3.85	88.40	6.41	53 ± 184
8M48038D	69 °C		0.0000723	7.280	0.0002266	209.702	0.0004914	3.089	0.0414855	0.109	0.7096398	0.068	16.58386 ± 0.08709	539.99 ± 2.45	96.95	9.89	95 ± 399
8M48039D	69 °C	4	0.0000457	10.669	0.0000229	2329.591	0.0004817	2.043	0.0398028	0.316	0.6722761	0.074	16.54684 ± 0.13012	538.94 ± 3.66	97.97	9.49	906 ± 42192
8M48040D	69 °C	4	0.0000741	9.713	0.0000858	648.332	0.0006487	1.731	0.0537182	0.144	0.9025264	0.095	16.38857 ± 0.09827	534.48 ± 2.77	97.54	12.81	325 ± 4220
8M48042D	70 °C	4	0.0000636	12.519	0.0000545	995.476	0.0005576	1.912	0.0455615	0.097	0.7680731	0.067	16.44043 ± 0.11145	535.95 ± 3.14	97.52	10.86	435 ± 8651
8M48043D	70 °C	4	0.0000938	6.472	0.0000968	551.448	0.0005543	2.157	0.0443798	0.197	0.7572521	0.057	16.43106 ± 0.10615	535.68 ± 3.00	96.30	10.58	238 ± 2628
8M48044D	71 °C	4	0.0000941	6.673	0.0003189	145.580	0.0004211	2.553	0.0342347	0.092	0.5937396	0.083	16.52126 ± 0.11722	538.22 ± 3.30	95.26	8.16	56 ± 163
8M48045D	71 °C	4	0.0000949	5.331	0.0002940	174.940	0.0002582	3.133	0.0204707	0.295	0.3641301	0.063	16.40494 ± 0.17783	534.94 ± 5.02	92.22	4.88	36 ± 127
8M48047D	78 °C	4	0.0000321	19.880	0.0000118	4135.930	0.0001096	5.491	0.0079584	0.381	0.1425928	0.126	16.71097 ± 0.49804	543.56 ± 13.99	93.27	1.90	350 ± 28919
8M48048D	79 °C	4	0.0001356	8.042	0.0001589	290.366	0.0001427	3.772	0.0099009	0.421	0.2013191	0.054	16.24090 ± 0.67242	530.31 ± 19.03	79.87	2.36	32 ± 188
8M48049D	81 °C	4	0.0002907	3.101	0.0003575	139.114	0.0004886	2.280	0.0357465	0.242	0.6711727	0.083	16.34842 ± 0.17304	533.35 ± 4.89	87.07	8.52	52 ± 145
8M48050D	82 °C	4	0.0001162	5.847	0.0002413	217.464	0.0002707	3.054	0.0216994	0.168	0.3901970	0.231	16.38075 ± 0.21200	534.26 ± 5.99	91.10	5.17	47 ± 203
8M48052D	82 °C	4	0.0001030	6.037	0.0001309	415.502	0.0002302	3.447	0.0192915	0.200	0.3434975	0.077	16.21097 ± 0.20508	529.46 ± 5.81	91.04	4.60	77 ± 637
		Σ	0.0019685	1.519	0.0005154	406.056	0.0053168	0.719	0.4195025	0.057	7.5117769	0.025					

Information on Analysis and Constants Used in Calculations

Sample = Z16-18MUS
Material = mus
Location = Laser
Analyst = Adam Frew
Project = ALAN COLLINS_BRANDON ALESSIO18
Mass Discrimination Law = POW
Irradiation = I25t80h
J = 0.02098570 ± 0.00001574
FCs = 28.294 ± 0.037 Ma
IGSN = Undefined
Preferred Age = Undefined
Classification = Undefined
Experiment Type = Undefined
Extraction Method = Undefined
Heating = 60 sec
Isolation = 5.00 min
Instrument = MAP-215-50
Lithology = Undefined
Lat-Lon = Undefined - Undefined
Feature = Undefined

Age Equations = Min et al. (2000)
Negative Intensities = Allowed
Decay Constant 40K = 5.531 ± 0.013 E-10 1/a
Decay Constant 39Ar = 2.940 ± 0.029 E-07 1/h
Decay Constant 37Ar = 8.264 ± 0.009 E-04 1/h
Decay Constant 36Cl = 2.303 ± 0.046 E-06 1/a
Decay Constant 40K(EC,β⁺) = 0.576 ± 0.002 E-10 1/a
Decay Constant 40K(β⁻) = 4.955 ± 0.013 E-10 1/a
Atmospheric Ratio 40/36(a) = 298.56 ± 0.30
Atmospheric Ratio 38/36(a) = 0.1869 ± 0.0002
Production Ratio 39/37(ca) = 0.000695 ± 0.000009
Production Ratio 38/37(ca) = 0.000020 ± 0.000001
Production Ratio 36/37(ca) = 0.000265 ± 0.000002
Production Ratio 40/39(k) = 0.000730 ± 0.000091
Production Ratio 38/39(k) = 0.012150 ± 0.000030
Production Ratio 36/38(cl) = 263.00 ± 13.15
Scaling Ratio K/Ca = 0.520
Abundance Ratio 40K/K = 1.1700 ± 0.0100 E-04
Atomic Weight K = 39.0983 ± 0.0001 g

Results	40(a)/36(a) ± 2σ	40(r)/39(k) ± 2σ	Age ± 2σ (Ma)	MSWD	39Ar(k) (%,n)	K/Ca ± 2σ
Age Plateau		16.43207 ± 0.05128 ± 0.31%	535.71 ± 1.61 ± 0.30%	1.37	79.32	4 ± 70
				19%	11	
			Full External Error ± 4.01	1.89	2σ Confidence Limit	
			Analytical Error ± 1.45	1.1715	Error Magnification	
Total Fusion Age		16.50481 ± 0.04740 ± 0.29%	537.76 ± 1.51 ± 0.28%		17	423 ± 3437
			Full External Error ± 3.98			
			Analytical Error ± 1.34			
Normal Isochron	274.47 ± 23.03 ± 8.39%	16.49540 ± 0.07737 ± 0.47%	537.50 ± 2.29 ± 0.43%	1.33	79.32	
				21%	11	
			Full External Error ± 4.34	1.94	2σ Confidence Limit	
			Analytical Error ± 2.18	1.1550	Error Magnification	
				1	Number of Iterations	
				0.0000365256	Convergence	
Inverse Isochron	282.57 ± 23.28 ± 8.24%	16.47561 ± 0.07929 ± 0.48%	536.94 ± 2.34 ± 0.44%	1.28	79.32	
				24%	11	
			Full External Error ± 4.36	1.94	2σ Confidence Limit	
			Analytical Error ± 2.24	1.1303	Error Magnification	
				3	Number of Iterations	
				0.0000397340	Convergence	
				17%	Spreading Factor	

Relative Abundances			36Ar [V]	%1σ	37Ar [V]	%1σ	38Ar [V]	%1σ	39Ar [V]	%1σ	40Ar [V]	%1σ	40(r)/39(k) ± 2σ	Age ± 2σ (Ma)	40Ar(r) (%)	39Ar(k) (%)	K/Ca ± 2σ
8M48013D	66.0 %		0.0000343	18.715	0.0002079	209.475	0.0000158	19.515	0.0010578	0.972	0.0267290	0.884	15.58202 ± 3.65946	511.56 ± 104.64	61.67	0.19	3 ± 11
8M48014D	68.0 %		0.0000625	10.865	0.0001762	259.146	0.0000815	8.438	0.0056976	0.521	0.1174948	0.298	17.34799 ± 0.74483	561.37 ± 20.72	84.12	1.00	17 ± 87
8M48016D	68.4 %		0.0001017	6.850	0.0001556	332.679	0.0000849	10.541	0.0056790	0.415	0.1226651	0.204	16.25761 ± 0.74990	530.78 ± 21.22	75.27	0.99	19 ± 126
8M48017D	68.6 %	4	0.0001228	7.019	0.0002511	175.414	0.0002071	4.291	0.0167282	0.201	0.2881825	0.182	15.03352 ± 0.31979	495.81 ± 9.22	87.27	2.93	35 ± 122
8M48018D	68.8 %	4	0.0000746	7.954	0.0000951	506.028	0.0006214	1.133	0.0512981	0.239	0.7921099	0.109	15.00639 ± 0.10513	495.03 ± 3.03	97.18	8.99	281 ± 2840
8M48019D	69.0 %	4	0.0000679	11.533	0.0004753	101.638	0.0007593	1.712	0.0629817	0.184	0.9666347	0.040	15.02473 ± 0.09338	495.56 ± 2.69	97.90	11.03	69 ± 140
8M48021D	70.0 %	4	0.0000317	26.847	0.0005928	78.499	0.0019926	1.034	0.1674088	0.138	2.5174990	0.064	14.98042 ± 0.05479	494.28 ± 1.58	99.62	29.32	147 ± 231
8M48022D	71.0 %	4	0.0000286	26.631	0.0003640	134.361	0.0015347	1.783	0.1258312	0.119	1.8906600	0.062	14.95655 ± 0.05394	493.59 ± 1.56	99.54	22.04	180 ± 483
8M48023D	73.0 %	4	0.0000095	63.799	0.0003572	120.854	0.0000626	7.934	0.0050552	0.453	0.0761908	0.415	15.62570 ± 0.74023	512.81 ± 21.15	103.68	0.89	7 ± 18
8M48024D	80.0 %	4	0.0000573	12.170	0.0004667	103.266	0.0011076	1.279	0.0925570	0.114	1.4076206	0.050	15.02215 ± 0.05867	495.48 ± 1.69	98.78	16.21	103 ± 213
8M48026D	81.0 %	4	0.0000318	17.438	0.0003972	122.043	0.0002383	2.715	0.0194720	0.208	0.3026799	0.139	15.05476 ± 0.18622	496.42 ± 5.37	96.85	3.41	25 ± 62
8M48027D	82.0 %	4	0.0000380	17.845	0.0000843	539.898	0.0001598	3.287	0.0124584	0.290	0.1972721	0.145	14.92350 ± 0.33916	492.63 ± 9.80	94.25	2.18	77 ± 830
8M48028D	83.0 %	4	0.0000030	199.056	0.0005372	93.392	0.0000224	19.852	0.0025249	0.904	0.0390381	0.712	15.08299 ± 1.46928	497.24 ± 42.35	97.57	0.44	2 ± 5
8M48029D	83.0 %	4	0.0000017	435.012	0.0001462	339.754	0.0000230	18.771	0.0021508	0.590	0.0329658	0.712	15.08467 ± 2.07067	497.29 ± 59.68	98.42	0.38	8 ± 52
		Σ	0.0006462	4.064	0.0036434	48.636	0.0069111	0.638	0.5709006	0.061	8.7777422	0.029					

Information on Analysis and Constants Used in Calculations

Sample = Z16-17MUS
Material = mus
Location = Laser
Analyst = Adam Frew
Project = ALAN COLLINS_BRANDON ALESSIO18
Mass Discrimination Law = POW
Irradiation = I25t80h
J = 0.02098570 ± 0.00001574
FCs = 28.294 ± 0.037 Ma
IGSN = Undefined
Preferred Age = Undefined
Classification = Undefined
Experiment Type = Undefined
Extraction Method = Undefined
Heating = 60 sec
Isolation = 5.00 min
Instrument = MAP-215-50
Lithology = Undefined
Lat-Lon = Undefined - Undefined
Feature = Undefined

Age Equations = Min et al. (2000)
Negative Intensities = Allowed
Decay Constant 40K = 5.531 ± 0.013 E-10 1/a
Decay Constant 39Ar = 2.940 ± 0.029 E-07 1/h
Decay Constant 37Ar = 8.264 ± 0.009 E-04 1/h
Decay Constant 36Cl = 2.303 ± 0.046 E-06 1/a
Decay Constant 40K(EC,β^+) = 0.576 ± 0.002 E-10 1/a
Decay Constant 40K(β^-) = 4.955 ± 0.013 E-10 1/a
Atmospheric Ratio 40/36(a) = 298.56 ± 0.30
Atmospheric Ratio 38/36(a) = 0.1869 ± 0.0002
Production Ratio 39/37(ca) = 0.000695 ± 0.000009
Production Ratio 38/37(ca) = 0.000020 ± 0.000001
Production Ratio 36/37(ca) = 0.000265 ± 0.000002
Production Ratio 40/39(k) = 0.000730 ± 0.000091
Production Ratio 38/39(k) = 0.012150 ± 0.000030
Production Ratio 36/38(cl) = 263.00 ± 13.15
Scaling Ratio K/Ca = 0.520
Abundance Ratio 40K/K = 1.1700 ± 0.0100 E-04
Atomic Weight K = 39.0983 ± 0.0001 g

Results	40(a)/36(a) ± 2σ	40(r)/39(k) ± 2σ	Age ± 2σ (Ma)	MSWD	39Ar(k) (%,n)	K/Ca ± 2σ
Age Plateau		14.99250 ± 0.02860 (± 0.19%)	494.63 ± 1.05 (± 0.21%)	0.72	97.82	3 ± 4
				71%	11	
		Full External Error ± 3.57		1.89	2σ Confidence Limit	
		Analytical Error ± 0.83		1.0000	Error Magnification	
Total Fusion Age		15.03600 ± 0.03423 (± 0.23%)	495.88 ± 1.18 (± 0.24%)		14	81 ± 79
		Full External Error ± 3.61				
		Analytical Error ± 0.99				
Normal Isochron	285.47 ± 72.05 (± 25.24%)	14.98812 ± 0.06702 (± 0.45%)	494.50 ± 2.04 (± 0.41%)	4.40	97.82	
Error Chron				0%	11	
		Full External Error ± 3.97		1.94	2σ Confidence Limit	
		Analytical Error ± 1.93		2.0968	Error Magnification	
				1	Number of Iterations	
				0.0000005268	Convergence	
Inverse Isochron	317.86 ± 39.03 (± 12.28%)	14.98096 ± 0.03711 (± 0.25%)	494.29 ± 1.25 (± 0.25%)	0.68	97.82	
				72%	11	
		Full External Error ± 3.63		1.94	2σ Confidence Limit	
		Analytical Error ± 1.07		1.0000	Error Magnification	
				5	Number of Iterations	
				0.0000124361	Convergence	
				13%	Spreading Factor	

Relative Abundances			36Ar [V]	%1σ	37Ar [V]	%1σ	38Ar [V]	%1σ	39Ar [V]	%1σ	40Ar [V]	%1σ	40(r)/39(k) ± 2σ	Age ± 2σ (Ma)	40Ar(r) (%)	39Ar(k) (%)	K/Ca ± 2σ
8M49079D	62.0 %		0.0000354	14.757	0.0031318	137.863	0.0000095	43.413	0.0003589	2.471	0.0148433	0.628	11.14638 ± 8.87762	380.06 ± 273.00	27.12	0.34	0.06 ± 0.17
8M49080D	64.0 %		0.0000487	10.931	0.0015664	257.832	0.0000284	13.100	0.0016455	0.592	0.0356615	0.271	12.75590 ± 1.97811	428.89 ± 59.21	58.90	1.53	0.55 ± 2.82
8M49081D	66.0 %		0.0000381	17.090	0.0011206	351.549	0.0000523	10.085	0.0035868	0.869	0.0715108	0.369	16.73332 ± 1.14638	544.19 ± 32.19	83.95	3.34	1.66 ± 11.70
8M49083D	68.0 %	4	0.0000953	7.584	0.0020895	189.747	0.0003334	3.820	0.0264441	0.199	0.4626657	0.051	16.41160 ± 0.17843	535.13 ± 5.04	93.81	24.59	6.58 ± 24.98
8M49084D	69.0 %	4	0.0000883	9.916	0.0005439	750.206	0.0004766	3.569	0.0386314	0.165	0.6489920	0.143	16.11501 ± 0.15412	526.74 ± 4.37	95.93	35.92	36.94 ± 554.19
8M49085D	69.5 %	4	0.0000648	11.303	0.0003924	1053.476	0.0000903	6.478	0.0066960	0.376	0.1254656	0.131	15.84005 ± 0.67346	518.93 ± 19.18	84.54	6.23	8.87 ± 186.96
8M49087D	70.0 %	4	0.0000505	9.480	0.0035854	118.457	0.0000477	9.083	0.0026686	0.474	0.0573946	0.158	15.73187 ± 1.11292	515.84 ± 31.75	73.21	2.48	0.39 ± 0.92
8M49088D	70.5 %	4	0.0000517	14.474	0.0004005	988.102	0.0000196	21.126	0.0015467	0.987	0.0396508	0.749	15.63267 ± 2.95826	513.01 ± 84.52	60.99	1.44	2.01 ± 39.70
8M49089D	71.0 %	4	0.0000521	9.414	0.0007191	543.917	0.0000276	13.421	0.0018176	0.996	0.0441067	0.412	15.66900 ± 1.68895	514.05 ± 48.23	64.59	1.69	1.31 ± 14.30
8M49091D	78.0 %	4	0.0000134	39.227	0.0009627	438.301	0.0000100	31.903	0.0010242	1.097	0.0205512	0.494	16.07297 ± 3.15873	525.55 ± 89.63	80.16	0.95	0.55 ± 4.85
8M49092D	79.0 %	4	0.0000612	12.998	0.0019754	222.576	0.0000366	15.237	0.0022422	0.679	0.0538429	0.260	15.94333 ± 2.15736	521.87 ± 61.34	66.35	2.08	0.59 ± 2.63
8M49093D	80.5 %	4	0.0000840	7.118	0.0001785	2302.354	0.0000977	3.898	0.0069099	0.790	0.1336482	0.214	15.70776 ± 0.58707	515.16 ± 16.75	81.21	6.42	20.13 ± 926.88
8M49095D	82.0 %	4	0.0000745	6.203	0.0025828	154.012	0.0001293	5.695	0.0094040	0.288	0.1724400	0.133	15.94601 ± 0.31863	521.94 ± 9.06	86.98	8.74	1.89 ± 5.83
8M49096D	100.0 %	4	0.0000712	8.873	0.0005276	766.792	0.0000692	8.366	0.0045746	1.057	0.0943031	0.544	15.97630 ± 0.92996	522.80 ± 26.43	77.49	4.25	4.51 ± 69.14
		Σ	0.0008295	2.883	0.0147705	103.817	0.0014281	1.902	0.1075503	0.117	1.9750764	0.064					

Information on Analysis and Constants Used in Calculations

Sample = Z16-06MUS
Material = mus
Location = Laser
Analyst = Adam Frew
Project = ALAN COLLINS_BRANDON ALESSIO18
Mass Discrimination Law = POW
Irradiation = I25t80h
J = 0.02098570 ± 0.00001574
FCs = 28.294 ± 0.037 Ma
IGSN = Undefined
Preferred Age = Undefined
Classification = Undefined
Experiment Type = Undefined
Extraction Method = Undefined
Heating = 60 sec
Isolation = 3.00 min
Instrument = MAP-215-50
Lithology = Undefined
Lat-Lon = Undefined - Undefined
Feature = Undefined

Age Equations = Min et al. (2000)
Negative Intensities = Allowed
Decay Constant 40K = 5.531 ± 0.013 E-10 1/a
Decay Constant 39Ar = 2.940 ± 0.029 E-07 1/h
Decay Constant 37Ar = 8.264 ± 0.009 E-04 1/h
Decay Constant 36Cl = 2.303 ± 0.046 E-06 1/a
Decay Constant 40K(EC,β⁺) = 0.576 ± 0.002 E-10 1/a
Decay Constant 40K(β⁻) = 4.955 ± 0.013 E-10 1/a
Atmospheric Ratio 40/36(a) = 298.56 ± 0.30
Atmospheric Ratio 38/36(a) = 0.1869 ± 0.0002
Production Ratio 39/37(ca) = 0.000695 ± 0.000009
Production Ratio 38/37(ca) = 0.000020 ± 0.000001
Production Ratio 36/37(ca) = 0.000265 ± 0.000002
Production Ratio 40/39(k) = 0.000730 ± 0.000091
Production Ratio 38/39(k) = 0.012150 ± 0.000030
Production Ratio 36/38(cl) = 263.00 ± 13.15
Scaling Ratio K/Ca = 0.520
Abundance Ratio 40K/K = 1.1700 ± 0.0100 E-04
Atomic Weight K = 39.0983 ± 0.0001 g

Results	40(a)/36(a) ± 2σ	40(r)/39(k) ± 2σ	Age ± 2σ (Ma)	MSWD	39Ar(k) (%,n)	K/Ca ± 2σ
Age Plateau		16.17137 ± 0.12645 ± 0.78%	528.34 ± 3.65 ± 0.69%	1.46 15%	94.80 11	0.33 ± 0.84
			Full External Error ± 5.14	1.89	2σ Confidence Limit	
			Analytical Error ± 3.58	1.2076	Error Magnification	
Total Fusion Age		16.04852 ± 0.14176 ± 0.88%	524.85 ± 4.08 ± 0.78%		14	3.79 ± 7.86
			Full External Error ± 5.44			
			Analytical Error ± 4.02			
Normal Isochron	273.17 ± 25.92 ± 9.49%	16.23804 ± 0.15225 ± 0.94%	530.23 ± 4.36 ± 0.82%	1.06 39%	94.80 11	
			Full External Error ± 5.68	1.94	2σ Confidence Limit	
			Analytical Error ± 4.31	1.0275	Error Magnification	
				1	Number of Iterations	
				0.0000443030	Convergence	
Inverse Isochron	275.27 ± 29.69 ± 10.79%	16.27504 ± 0.17135 ± 1.05%	531.27 ± 4.90 ± 0.92%	1.31 22%	94.80 11	
			Full External Error ± 6.10	1.94	2σ Confidence Limit	
			Analytical Error ± 4.85	1.1456	Error Magnification	
				3	Number of Iterations	
				0.0000270989	Convergence	
				33%	Spreading Factor	

Relative Abundances			36Ar [V]	%1σ	37Ar [V]	%1σ	38Ar [V]	%1σ	39Ar [V]	%1σ	40Ar [V]	%1σ	40(r)/39(k) ± 2σ	Age ± 2σ (Ma)	40Ar(r) (%)	39Ar(k) (%)	K/Ca ± 2σ
8M49060D	64.0 %	4	0.0000454	11.569	0.0042047	50.516	0.0000080	42.043	0.0001388	3.036	0.0141235	1.187	1.59435 ± 22.39468	59.51 ± 822.26	1.60	0.16	0.02 ± 0.02
8M49061D	66.0 %	4	0.0000342	16.060	0.0039157	69.224	0.0000101	39.709	0.0003168	2.032	0.0144642	1.086	12.31445 ± 10.41824	415.63 ± 314.14	27.21	0.35	0.04 ± 0.06
8M49062D	68.0 %	4	0.0000911	12.815	0.0008906	265.576	0.0000960	5.324	0.0075561	0.558	0.1416547	0.174	15.13565 ± 0.94155	498.75 ± 27.11	80.74	8.39	4.41 ± 23.43
8M49064D	68.8 %	4	0.0000070	82.987	0.0017010	132.323	0.0000156	29.007	0.0016328	1.008	0.0252389	0.690	14.08675 ± 2.15913	468.29 ± 63.24	91.20	1.81	0.50 ± 1.32
8M49065D	69.0 %	4	0.0000054	94.662	0.0011878	181.437	0.0000268	16.053	0.0016596	1.094	0.0259117	0.694	14.71138 ± 1.88073	486.50 ± 54.53	94.18	1.84	0.73 ± 2.64
8M49067D	69.5 %	4	0.0000346	20.331	0.0009237	256.499	0.0001094	5.869	0.0087957	0.676	0.1389706	0.396	14.61543 ± 0.53342	483.71 ± 15.49	92.51	9.77	4.95 ± 25.40
8M49068D	70.0 %	4	0.0000555	10.486	0.0009589	214.329	0.0001563	4.807	0.0118093	0.366	0.1828017	0.123	14.08368 ± 0.31519	468.20 ± 9.23	90.98	13.11	6.40 ± 27.45
8M49069D	70.5 %	4	0.0000354	17.411	0.0004615	547.389	0.0001011	5.765	0.0077740	0.403	0.1209617	0.159	14.20635 ± 0.49179	471.79 ± 14.38	91.30	8.63	8.76 ± 95.90
8M49070D	71.0 %	4	0.0000257	25.843	0.0013157	175.196	0.0000609	7.219	0.0045244	0.405	0.0706148	0.261	13.93962 ± 0.89004	463.98 ± 26.13	89.29	5.02	1.79 ± 6.26
8M49072D	78.0 %	4	0.0000016	324.877	0.0003823	669.932	0.0000207	21.308	0.0022742	0.766	0.0337614	0.541	14.61615 ± 1.42713	483.73 ± 41.44	98.47	2.53	3.09 ± 41.46
8M49073D	79.0 %	4	0.0000370	20.161	0.0012428	174.763	0.0000987	9.416	0.0074615	0.525	0.1171389	0.170	14.23250 ± 0.61957	472.56 ± 18.10	90.65	8.28	3.12 ± 10.91
8M49074D	80.5 %	4	0.0000880	7.781	0.0014202	186.924	0.0001903	6.204	0.0142047	0.279	0.2251161	0.092	13.98954 ± 0.30100	465.44 ± 8.83	88.28	15.77	5.20 ± 19.44
8M49075D	82.0 %	4	0.0000731	8.904	0.0011690	201.377	0.0001261	4.014	0.0089805	0.593	0.1475073	0.246	14.00550 ± 0.47248	465.91 ± 13.86	85.26	9.97	3.99 ± 16.09
8M49077D	100.0 %	4	0.0000519	13.016	0.0015722	148.569	0.0001615	4.270	0.0129227	0.531	0.1964897	0.086	13.99403 ± 0.34803	465.58 ± 10.21	92.04	14.35	4.27 ± 12.70
		Σ	0.0005858	4.309	0.0086748	101.820	0.0011814	2.006	0.0900511	0.157	1.4547552	0.064					

Information on Analysis and Constants Used in Calculations

Sample = Z14-07MUS
Material = mus
Location = Laser
Analyst = Adam Frew
Project = ALAN COLLINS_BRANDON ALESSIO18
Mass Discrimination Law = POW
Irradiation = I25t80h
J = 0.02098570 ± 0.00001574
FCs = 28.294 ± 0.037 Ma
IGSN = Undefined
Preferred Age = Undefined
Classification = Undefined
Experiment Type = Undefined
Extraction Method = Undefined
Heating = 60 sec
Isolation = 3.00 min
Instrument = MAP-215-50
Lithology = Undefined
Lat-Lon = Undefined - Undefined
Feature = Undefined

Age Equations = Min et al. (2000)
Negative Intensities = Allowed
Decay Constant 40K = 5.531 ± 0.013 E-10 1/a
Decay Constant 39Ar = 2.940 ± 0.029 E-07 1/h
Decay Constant 37Ar = 8.264 ± 0.009 E-04 1/h
Decay Constant 36Cl = 2.303 ± 0.046 E-06 1/a
Decay Constant 40K(EC,β^+) = 0.576 ± 0.002 E-10 1/a
Decay Constant 40K(β^-) = 4.955 ± 0.013 E-10 1/a
Atmospheric Ratio 40/36(a) = 298.56 ± 0.30
Atmospheric Ratio 38/36(a) = 0.1869 ± 0.0002
Production Ratio 39/37(ca) = 0.000695 ± 0.000009
Production Ratio 38/37(ca) = 0.000020 ± 0.000001
Production Ratio 36/37(ca) = 0.000265 ± 0.000002
Production Ratio 40/39(k) = 0.000730 ± 0.000091
Production Ratio 38/39(k) = 0.012150 ± 0.000030
Production Ratio 36/38(cl) = 263.00 ± 13.15
Scaling Ratio K/Ca = 0.520
Abundance Ratio 40K/K = 1.1700 ± 0.0100 E-04
Atomic Weight K = 39.0983 ± 0.0001 g

Results	40(a)/36(a) ± 2σ	40(r)/39(k) ± 2σ	Age ± 2σ (Ma)	MSWD	39Ar(k) (%,n)	K/Ca ± 2σ
Age Plateau		14.12659 ± 0.14512 ± 1.03%	469.46 ± 4.29 ± 0.91%	0.95	100.00	0.02 ± 0.02
				50%	14	
			Full External Error ± 5.38	1.78	2σ Confidence Limit	
			Analytical Error ± 4.25	1.0000	Error Magnification	
Total Fusion Age		14.20319 ± 0.17520 ± 1.23%	471.70 ± 5.16 ± 1.09%		14	5.40 ± 10.99
			Full External Error ± 6.10			
			Analytical Error ± 5.12			
Normal Isochron	262.63 ± 44.11 ± 16.79%	14.29432 ± 0.26976 ± 1.89%	474.36 ± 7.90 ± 1.67%	0.79	100.00	
No Convergence				66%	14	
			Full External Error ± 8.55	1.82	2σ Confidence Limit	
			Analytical Error ± 7.87	1.0000	Error Magnification	
				100	Number of Iterations	
				0.0028315083	Convergence	
Inverse Isochron	303.15 ± 50.57 ± 16.68%	14.10302 ± 0.29986 ± 2.13%	468.77 ± 8.80 ± 1.88%	1.03	100.00	
				42%	14	
			Full External Error ± 9.38	1.82	2σ Confidence Limit	
			Analytical Error ± 8.78	1.0146	Error Magnification	
				4	Number of Iterations	
				0.0000113252	Convergence	
				81%	Spreading Factor	

Table S5. Individual apatite fission track analytical data.

Sample	^{238}U ppm	2σ	Ns*	ρ s**	t (Ma)***	1σ	Cl ppm	2σ	Th ppm	2σ
Z16-01										
Z16-01-1.d	33.2	2.1	69	2.17E+06	137.13	20.3	1050	270	90	4.8
Z16-01-2.d	24.6	2.7	31	1.50E+06	128.44	28.1	10280	890	146	20
Z16-01-3.d	60	2.5	45	2.07E+06	72.31	12.0	11610	580	303	12
Z16-01-4.d	19	1.4	24	4.74E+05	52.40	11.8	3700	510	116.5	9.3
Z16-01-6.d	38.5	1.8	16	6.84E+05	37.34	9.7	330	160	208	10
Z16-01-7.d	52	33	42	1.92E+06	77.57	50.9	6.40E+04	6.30E+04	1.32E+02	55
Z16-01-8.d	17.9	3.2	5	3.87E+05	45.44	22.1	3.26E+05	5.70E+04	8.90E+01	19
Z16-01-10.d	7.2	1.3	12	4.91E+05	143.39	49.5	3.70E+03	1.50E+03	2.62E+01	4
Z16-01-11.d	27.8	1.1	27	1.41E+06	106.71	21.9	6.10E+03	1.10E+03	1.27E+02	4.6
Z16-01-13.d	5.75	0.34	30	5.87E+05	214.36	43.0	290	160	26.5	1.9
Z16-01-14.d	57.6	3.9	82	2.21E+06	80.72	11.5	-	-	307	22
Z16-01-15.d	12.7	0.63	39	1.25E+06	206.61	36.7	-	-	49.8	2.8
Z16-01-16.d	41.1	1.5	58	2.92E+06	149.00	22.1	-	-	290.5	9
Z16-01-18.d	3.8	0.21	29	2.55E+05	140.98	28.6	-	-	22.6	1.1
Z16-01-19.d	37.1	3.2	31	9.59E+05	54.31	11.3	-	-	205	17
Z16-01-20.d	32	11	25	1.64E+06	107.54	43.2	1.50E+05	1.10E+05	1.35E+02	32
Z16-01-22.d	10.74	0.49	12	4.46E+05	87.20	26.0	-	-	60.2	2.5
Z16-01-23.d	4.14	0.21	11	3.06E+05	155.49	48.4	-	-	23.77	0.9
Z16-01-24.d	3.46	0.4	4	1.42E+05	86.04	44.4	340	160	20.5	2.1
Z16-01-25.d	4.22	0.34	16	4.09E+05	203.37	54.7	420	180	22.4	2.6
Z16-01-27.d	1.88	0.14	16	1.53E+05	171.20	45.8	1770	270	10.58	0.67
Z16-01-29.d	16.8	1.3	33	1.52E+06	190.58	38.0	-	-	72.4	5
Z16-01-30.d	3.25	0.24	7	3.69E+05	238.21	92.8	2.60E+03	1.00E+03	2.11E+01	2.2
Z16-01-31.d	99.3	6.7	67	3.93E+06	83.04	12.6	370	150	536	32
Z16-01-32.d	7.49	0.37	36	6.20E+05	173.96	31.9	-	-	34.9	2.4
Z16-01-33.d	4.48	0.54	9	2.81E+05	131.87	47.4	3.30E+03	2.10E+03	1.66E+01	1.4
Z16-17										
Z16-17-01.d	97.7	4.5	143	4.62E+06	99.24	11.1	460	220	2.44	0.18
Z16-17-02.d	53.5	3.6	55	2.22E+06	87.02	14.1	-	-	1.18	0.11
Z16-17-03.d	78.3	5.8	146	4.32E+06	115.80	14.6	-	-	1.86	0.18

Z16-17-04.d	78.7	3.9	101	3.84E+06	102.56	12.9	-	-	2.3	0.17
Z16-17-05.d	26.4	0.97	55	1.69E+06	134.65	20.4	9.00E+03	1.40E+03	1.04E+00	0.11
Z16-17-07.d	51.7	2.6	62	2.61E+06	106.18	15.8	300	140	1.108	0.077
Z16-17-08.d	89.7	6.1	122	4.40E+06	103.12	13.2	620	190	1.98	0.16
Z16-17-09.d	27.5	1.3	98	3.36E+06	256.38	32.3	4500	470	1.31	0.11
Z16-17-11.d	76.9	4.3	121	3.44E+06	93.95	11.5	380	140	1.39	0.14
Z16-17-12.d	88.1	6.9	109	4.68E+06	111.51	15.3	700	220	4.88	0.39
Z16-17-13.d	27.7	1.1	55	2.14E+06	162.08	24.7	-	-	0.814	0.063
Z16-17-15.d	145	10	110	4.21E+06	60.97	8.0	510	180	2.29	0.2
Z16-17-16.d	93	6.2	163	5.29E+06	119.41	14.2	420	250	2.5	0.19
Z16-17-17.d	74.1	4.5	86	2.89E+06	81.85	11.2	460	240	1.93	0.18
Z16-17-18.d	95.2	4.9	72	3.97E+06	87.68	12.4	240	130	4.09	0.24
Z16-17-19.d	28.4	1.8	76	2.80E+06	207.20	29.8	320	140	0.95	0.11
Z16-17-20.d	43.3	1.9	40	2.36E+06	114.65	20.0	520	210	1.088	0.078
Z16-17-21.d	71.6	5	50	2.83E+06	82.92	14.0	-	-	1.1	0.11
Z16-17-22.d	87.8	5.3	95	3.37E+06	80.59	10.7	-	-	2.2	0.16
Z16-17-23.d	69.1	3.7	106	3.89E+06	118.21	14.8	-	-	1.82	0.12
Z16-17-24.d	51.6	2.5	60	2.46E+06	100.28	15.0	1980	220	1.054	0.086
Z16-17-25.d	59.9	3.7	69	3.07E+06	107.57	15.9	1560	210	1.51	0.14
Z16-17-28.d	82.2	3.9	41	3.43E+06	87.69	15.2	470	190	4.43	0.22
Z16-17-29.d	139.5	7.4	92	5.78E+06	87.03	11.4	920	180	2.12	0.14
Z16-17-30.d	61.8	3.7	117	4.67E+06	158.59	19.8	1140	270	0.802	0.07
Z16-17-31.d	53	2.2	118	3.44E+06	136.48	16.0	380	240	0.78	0.086
Z16-17-32.d	71.1	3.7	70	3.48E+06	102.68	14.7	2630	740	2.94	0.13
Z16-17-33.d	185	10	162	6.61E+06	75.05	8.4	-	-	9.17	0.73
Z16-17-34.d	106.7	5.4	149	4.77E+06	93.88	10.6	-	-	3.07	0.19
Z16-17-35.d	65	3.5	89	4.27E+06	138.11	18.3	300	160	0.862	0.064
Z16-17-36.d	100.3	6.2	76	2.99E+06	62.57	8.9	-	-	3.58	0.26
Z16-17-37.d	52	2.9	67	3.03E+06	122.50	18.0	480	170	0.858	0.061
Z16-17-38.d	48.5	2.3	55	2.09E+06	90.71	14.0	370	170	0.603	0.075
Z16-17-40.d	162.2	8.4	124	6.13E+06	79.36	9.5	420	230	5.96	0.3
Z16-27										
Z16-27-1.d	23.1	1.4	39	2.50E+06	227.73	41.2	450	210	0.83	0.095

Z16-27-2.d	30.2	1.6	65	3.58E+06	249.12	36.7	690	160	0.917		0.069
Z16-27-5.d	17.49	0.83	59	1.82E+06	218.74	32.9	430	190	0.629		0.059
Z16-27-6.d	19	1.1	60	2.22E+06	245.14	37.6	650	160	0.463		0.041
Z16-27-7.d	19.5	1.1	69	2.99E+06	322.46	46.9	450	190	0.725		0.068
Z16-27-9.d	26.3	1.2	58	2.72E+06	216.88	32.8	390	170	0.946		0.077
Z16-27-10.d	14.25	0.94	32	1.30E+06	191.22	37.8	2.98E+04	5.20E+03	5.30E-02		0.04
Z16-27-11.d	25.8	1.1	47	2.18E+06	177.19	28.9	550	190	0.894		0.076
Z16-27-12.d	19.2	1.1	44	1.65E+06	180.98	31.1	510	160	0.659		0.051
Z16-27-13.d	14.59	0.73	43	1.78E+06	256.46	43.9	410	150	0.355		0.04
Z16-27-14.d	14.25	0.81	68	1.83E+06	270.24	39.5	450	160	0.285		0.037
Z16-27-15.d	27.4	1.6	36	1.63E+06	124.67	23.2	560	160	1.022		0.081
Z16-27-16.d	11.25	0.59	29	1.25E+06	233.99	47.2	720	170	0.191		0.023
Z16-27-17.d	24.9	1.2	64	2.59E+06	218.78	32.0	440	160	0.763		0.061
Z16-27-18.d	12.49	0.85	56	1.55E+06	261.06	42.1	360	200	0.226		0.04
Z16-27-19.d	23.2	1.8	61	3.19E+06	288.60	46.4	790	200	0.393		0.045
Z16-27-20.d	26.8	1.1	54	1.81E+06	142.05	21.9	470	170	0.744		0.057
Z16-27-21.d	11.97	0.66	39	1.38E+06	241.33	43.3	580	190	0.272		0.04
Z16-27-22.d	16.24	0.99	43	1.03E+06	132.60	23.1	720	140	0.562		0.057
Z16-27-23.d	7.62	0.62	47	8.50E+05	234.41	41.5	280	140	0.227		0.032
Z16-27-24.d	6.63	0.89	27	6.41E+05	203.12	49.1	860	330	0.06		0.033
Z16-27-25.d	17.66	0.89	54	1.78E+06	212.11	33.2	470	170	0.353		0.055
Z16-27-26.d	19.48	0.95	37	1.70E+06	183.67	33.3	470	220	0.661		0.087
Z16-27-27.d	19.4	1.1	57	1.59E+06	172.51	26.9	620	230	0.623		0.06
Z16-27-28.d	21.9	1.3	19	1.01E+06	97.27	23.8	390	190	0.589		0.055
Z16-27-29.d	43.6	2.3	57	3.55E+06	170.96	26.4	640	200	0.656		0.059
Z16-27-31.d	32.3	1.6	62	1.67E+06	108.82	16.2	620	180	1.43		0.12
Z16-27-32.d	21	1.1	54	2.11E+06	211.19	33.2	830	220	0.713		0.062
Z16-27-34.d	24.6	1.1	90	3.13E+06	266.88	34.4	640	190	0.979		0.093
Z16-27-35.d	16.2	0.77	40	1.42E+06	184.02	32.3	400	200	0.355		0.054
Z16-27-36.d	39.9	1.4	51	2.66E+06	140.11	21.8	620	200	2.26		0.14
Z16-27-37.d	17.6	1.4	28	1.92E+06	229.19	48.9	480	190	0.656		0.064
Z16-27-38.d	5.5	0.24	19	6.69E+05	255.58	61.6	690	160	NA	NA	
Z16-27-39.d	46	3.3	62	3.13E+06	142.95	22.5	870	270	3.31		0.35

Z16-27-40.d	43	2.9	51	2.12E+06	103.73	17.2	570	250	1.24	0.1
Z16-33										
Z16-33-1.d	43.4	4	167	4.84E+06	234.10	31.4	-	-	314	26
Z16-33-2.d	42.2	4	142	4.92E+06	245.04	34.2	930	450	279	21
Z16-33-3.d	47.4	3.9	159	6.04E+06	267.53	34.4	-	-	316	33
Z16-33-4.d	50.2	3.5	167	6.07E+06	253.82	30.4	1340	540	270	14
Z16-33-5.d	28.8	3	120	3.60E+06	262.39	39.5	1170	700	259	23
Z16-33-7.d	82.4	4.8	133	6.76E+06	172.46	20.7	1060	500	414	25
Z16-33-8.d	60.4	3.8	153	5.90E+06	205.08	24.2	830	550	239	15
Z16-33-9.d	61.4	4.7	136	6.33E+06	216.56	28.0	660	370	214	18
Z16-33-10.d	45.3	4.1	92	4.03E+06	186.71	28.0	840	590	232	17
Z16-33-11.d	61.9	5	177	7.20E+06	244.50	30.6	1320	560	353	30
Z16-33-13.d	69.4	6.2	157	5.40E+06	163.32	21.8	1620	610	400	36
Z16-33-14.d	62.5	6.1	162	7.63E+06	256.34	35.5	1150	450	340	32
Z16-33-15.d	87.7	8.3	128	6.28E+06	150.37	21.4	1180	620	451	43
Z16-33-17.d	79.8	6.1	101	6.52E+06	171.65	23.8	930	310	254	18
Z16-33-18.d	53	4.5	83	3.77E+06	149.32	22.5	1420	390	141	15
Z16-40										
Z16-40-1.d	8.53	0.46	36	1.50E+06	369.69	68.3	660	170	0.28	0.039
Z16-40-2.d	8.71	0.56	23	1.65E+06	397.50	89.9	890	210	0.237	0.043
Z16-40-3.d	30.7	1.6	61	3.80E+06	259.98	39.1	730	250	13.71	0.71
Z16-40-4.d	17.2	1.1	57	3.04E+06	371.44	58.9	410	240	0.995	0.087
Z16-40-5.d	18.4	1.2	47	3.00E+06	342.31	58.3	470	230	2.2	0.2
Z16-40-6.d	17.2	1.5	73	2.10E+06	256.02	40.3	390	170	3.4	0.26
Z16-40-7.d	8.33	0.46	14	8.30E+05	209.28	58.4	550	180	0.24	0.033
Z16-40-7.d	8.33	0.46	14	8.30E+05	209.28	58.4	550	180	NA	NA
Z16-40-10.d	9.82	0.45	38	1.50E+06	320.91	57.3	380	220	0.037	0.015
Z16-40-12.d	9.51	0.56	41	1.38E+06	305.30	54.0	1090	200	0.0171	0.008
Z16-40-13.d	6.16	0.39	27	1.61E+06	549.1	115.9	370	140	0.138	0.026
Z16-40-14.d	3.91	0.8	11	3.77E+05	202.7	74.8	4.50E+03	2.30E+03	2.70E+00	1.6
Z16-40-16.d	16.15	0.98	56	2.84E+06	369.6	58.5	580	150	3.4	0.26
Z16-40-17.d	7.19	0.34	30	1.00E+06	293.4	58.0	330	120	0.0144	0.009

Z16-40-18.d	6.54	0.35	60	1.14E+06	366.5	55.6	500	130	0.037	0.011
Z16-40-20.d	7.93	0.36	47	1.46E+06	385.5	63.1	420	130	0.359	0.037
Z16-40-22.d	8.62	0.49	27	1.44E+06	350.2	73.3	500	150	0.05	0.013
Z16-40-23.d	11.45	0.54	49	1.86E+06	341.8	55.2	9.90E+03	2.30E+03	1.19E+00	0.1
Z16-40-24.d	27.1	2.6	66	3.20E+06	248.0	41.4	630	210	5.51	0.55
Z16-40-25.d	13.01	0.81	61	2.21E+06	357.4	55.1	480	170	0.105	0.027
Z16-40-26.d	11.53	0.68	54	2.43E+06	442.6	70.6	400	140	1.74	0.12
Z16-40-27.d	11.18	0.58	60	2.56E+06	481.6	72.8	390	140	4.42	0.22
Z16-40-28.d	12.08	0.64	14	1.22E+06	212.0	59.1	-	-	0.834	0.078
Z16-41										
Z16-41-1.d	11.02	0.63	44	1.23E+06	234.9	40.3	470	150	37.3	2
Z16-41-2.d	5.84	0.38	20	1.04E+06	374.9	90.1	4.50E+03	1.00E+03	2.00E+01	1.2
Z16-41-3.d	2.49	0.83	7	4.16E+05	350.7	178.0	4.80E+04	3.10E+04	9.00E+00	1.7
Z16-41-4.d	3.75	0.36	12	4.39E+05	245.9	76.2	3.34E+04	5.00E+03	1.93E+01	1.7
Z16-41-6.d	6.36	0.4	14	5.40E+05	178.3	50.1	2060	730	7.91	0.51
Z16-41-8.d	3.71	0.33	11	1.09E+06	616.7	197.2	460	150	20.3	1.4
Z16-41-10.d	4.68	0.27	23	1.00E+06	448.9	100.7	470	210	15.6	1.4
Z16-41-11.d	7.04	0.38	16	9.51E+05	283.8	74.5	640	150	28.4	1.4
Z16-41-14.d	8.75	0.53	13	1.02E+06	243.9	70.7	5.10E+03	1.80E+03	5.00E+01	2.7
Z16-41-18.d	8.57	0.49	25	1.30E+06	319.2	69.0	460	190	44.7	2.1
Z16-41-19.d	4.25	0.41	15	1.16E+06	575.4	162.2	300	190	16	1.1
Z16-41-20.d	6.59	0.52	14	9.71E+05	309.4	88.1	320	160	19.9	1.2
Z16-41-21.d	2.84	0.16	11	4.87E+05	360.6	112.6	530	150	9.39	0.41
Z16-41-22.d	4.66	0.77	14	1.10E+06	497.3	159.0	800	170	23.5	4.1
Z16-41-23.d	2.01	0.11	5	2.77E+05	289.9	131.7	460	140	7.03	0.43
Z16-41-24.d	5.95	0.31	21	9.48E+05	334.7	77.6	-	-	25.2	1.3
Z16-41-25.d	5.4	0.3	8	5.22E+05	203.1	73.7	420	160	27.2	1.3
Z16-41-29.d	6.43	0.29	18	9.57E+05	312.6	77.2	370	150	31	1.4
Z16-41-30.d	3.05	0.18	6	4.27E+05	293.9	122.5	310	140	6.7	0.4
Z16-41-31.d	7.98	0.9	40	1.82E+06	477.8	97.0	2240	920	42.2	3.4
Z16-41-33.d	7.75	0.52	8	9.86E+05	267.4	97.5	5.50E+03	2.30E+03	2.36E+01	1.9
Z16-41-34.d	6.9	0.41	5	6.98E+05	212.4	96.6	320	120	33.4	1.7
Z16-41-35.d	11.22	0.67	8	7.97E+05	149.3	54.2	-	-	67.8	3.9

Z16-45										
Z16-45-1.d	4.36	0.47	17	8.36E+05	402.8	109.5	530	200	33.7	4
Z16-45-2.d	4.23	0.75	11	6.88E+05	341.5	121.1	-	-	52	10
Z16-45-3.d	2.38	0.16	10	7.02E+05	620.0	203.8	300	140	31.9	1.6
Z16-45-4.d	3.85	0.22	13	7.43E+05	405.6	117.3	-	-	48.7	3
Z16-45-5.d	7.7	0.57	15	7.80E+05	212.8	58.5	-	-	62.1	3.9
Z16-45-6.d	3.9	0.31	24	6.28E+05	338.4	76.8	430	120	16.8	1.3
Z16-45-9.d	2.59	0.16	10	4.84E+05	392.2	128.5	-	-	25.8	1.3
Z16-45-10.d	7.25	0.39	26	1.75E+06	506.0	107.1	340	170	69.6	3.2
Z16-45-11.d	2.38	0.15	25	3.99E+05	351.9	76.7	610	140	18	1.2
Z16-45-13.d	2.97	0.22	31	8.20E+05	580.1	117.8	-	-	23.1	1.4
Z16-45-14.d	5.36	0.4	44	1.59E+06	622.8	111.0	-	-	73.2	4.2
Z16-45-15.d	15	1.3	73	4.29E+06	600.3	94.3	-	-	171	13
Z16-45-16.d	5.09	0.32	22	9.62E+05	397.0	91.3	-	-	54.2	2.4
Z16-45-18.d	1.53	0.11	10	2.34E+05	321.9	106.1	-	-	7.83	0.71
Z16-45-19.d	3.69	0.27	21	1.01E+06	573.3	136.2	280	160	22.6	1.6
Z16-45-20.d	4.49	0.36	26	8.45E+05	395.4	87.0	380	220	38.6	2.8
Z16-45-21.d	3	0.32	30	4.15E+05	290.6	63.8	380	250	35.9	4.3
Z16-45-22.d	3.21	0.26	31	8.05E+05	526.7	108.3	380	210	23.1	2.6
Z16-45-23.d	1.68	0.52	16	3.02E+05	377.9	152.0	-	-	17.9	6.5
Z16-45-25.d	1.84	0.13	14	5.52E+05	630.0	178.1	370	160	6.38	0.43
Z16-45-27.d	5.41	0.38	16	5.32E+05	206.5	55.0	500	170	59.4	4.9
Z16-45-28.d	2.24	0.12	8	2.21E+05	207.7	75.3	400	160	8.96	0.43
Z16-45-29.d	5.08	0.26	29	1.42E+06	588.1	118.5	-	-	39.8	1.7
Z16-45-30.d	10.6	1.7	72	3.58E+06	709.3	147.2	-	-	126	23
Z16-45-31.d	3.05	0.31	37	8.96E+05	617.2	124.7	-	-	22.4	2.3
Z16-45-32.d	5.6	0.27	22	9.99E+05	374.9	84.9	-	-	69.5	3
Z16-45-35.d	11.36	0.63	58	2.66E+06	491.2	75.8	9400	2800	167.9	7.5
Z16-45-37.d	2.53	0.15	30	6.81E+05	565.2	113.5	380	150	32.6	1.6
Z16-52										
Z16-52-1.d	11.7	0.55	27	8.18E+05	146.8	30.3	-	-	0.557	0.043
Z16-52-10.d	10.08	0.59	31	6.75E+05	140.6	27.8	450	140	0.444	0.045

Z16-52-11.d	28.8	1.5	50	1.21E+06	88.0	14.2	390	150	3.29	0.18
Z16-52-12.d	20.2	1.1	32	1.00E+06	104.3	20.3	380	180	1.8	0.12
Z16-52-14.d	24.8	1.2	40	1.54E+06	130.1	22.8	440	160	2.17	0.13
Z16-52-15.d	23.9	1	29	1.57E+06	137.9	27.5	350	120	5.71	0.26
Z16-52-16.d	15.26	0.75	29	8.72E+05	120.0	24.1	270	140	1.115	0.076
Z16-52-17.d	11.54	0.55	12	3.69E+05	67.1	20.0	-	-	0.921	0.069
Z16-52-18.d	25	1.6	87	1.55E+06	130.5	18.0	470	240	1.88	0.15
Z16-52-19.d	14.46	0.85	10	7.95E+05	115.4	37.8	330	120	1.48	0.12
Z16-52-2.d	13.1	0.65	17	8.12E+05	130.2	33.1	280	130	1.401	0.096
Z16-52-20.d	25.2	1.2	12	6.52E+05	54.3	16.2	530	210	2.82	0.21
Z16-52-21.d	16.7	1.1	17	8.44E+05	106.2	27.4	-	-	1.33	0.13
Z16-52-22.d	13.73	0.61	19	9.52E+05	145.6	35.1	270	100	1.153	0.079
Z16-52-23.d	15.65	0.71	15	9.51E+05	127.6	34.3	350	150	1.87	0.11
Z16-52-24.d	15.23	0.65	15	9.24E+05	127.5	34.2	330	130	1.53	0.11
Z16-52-25.d	21.9	1.1	32	1.25E+06	120.3	23.2	380	140	2.35	0.11
Z16-52-26.d	23.5	1.3	31	1.09E+06	97.4	19.2	570	150	2.6	0.15
Z16-52-27.d	12.31	0.75	18	7.65E+05	130.5	32.7	350	170	1.053	0.092
Z16-52-28.d	13.62	0.63	46	8.44E+05	130.1	21.5	400	160	1.035	0.07
Z16-52-29.d	26.1	1.5	22	1.33E+06	106.8	24.4	440	140	2.56	0.2
Z16-52-3.d	18.38	0.87	13	7.57E+05	86.5	24.9	370	130	1.9	0.12
Z16-52-30.d	19.07	0.94	25	1.13E+06	124.4	26.7	340	150	2.37	0.14
Z16-52-31.d	4.83	0.41	7	3.50E+05	152.3	59.7	240	190	0.136	0.027
Z16-52-4.d	15.63	0.82	15	4.59E+05	61.6	16.6	310	120	0.678	0.057
Z16-52-5.d	14.32	0.62	22	9.48E+05	139.0	31.3	290	120	0.763	0.05
Z16-52-7.d	19.18	0.89	26	8.45E+05	92.5	19.4	-	-	1.88	0.12
Z16-52-8.d	5.97	0.44	5	2.79E+05	98.2	44.9	250	140	0.307	0.035
Z16-52-9.d	12.1	0.65	18	8.13E+05	141.1	35.1	350	130	0.952	0.069

* Ns is the total number of counted spontaneous fission tracks

** ρ s is the average surface density of spontaneous dission tracks

*** t is the AFT age with its uncertainty, calculated for each grain using a zeta value of $2.03*10^{-3}$

Table S6. QTQt thermal modelling report

1. Thermochronological data	
Data treatment, uncertainties and other relevant constraints	
Initial mean track length	16.3
Track length reduction standard	0.893
Compositional parameter	Dpar
Etchant	5.0M

2. Additional geological information	
Assumption	Explanation and data source
400 to 500 °C during the late Neoproterozoic to Ordovician	Determined by the apatite U-Pb age obtained for each sample
0 to 60 °C prior to the Carboniferous (400 to 360 Ma)	Based on observed unconformities between precambrian basement and Carboniferous rocks in the region

3. System and model specific parameters	
FT annealing model	Ketcham 2007
FT c-axis projection	No
Modelling code	QTQt 5.5.0
Number of iterations	Initial exploratory run with 10,000 burn-in and 10,000 post burn-in. Subsequent runs used 50,000 iterations burn-in and 250,000 post-burn-in.
tT path characteristics	Temp. offset allowed to vary, reheating allowed
Acceptance rates	Acceptance rates 0.5-0.9. Birth/death ratio ~1
Range of General Prior	t=AFT central age ± AFT central age, T=70°C ± 70°C,

4. Thermal History Modelling Predictions vs Observed

Z16-01	FT age (Ma)	MTL (µm)	Kinetic parameter (Dpar)
Obs.	118.5	11.23	1.107
Pred.	104.8	11.42	1.39
SP	100.9 ± 3.736	11.18 ± 0.213	1.398 ± 0.445

Z16-17			
Obs.	106.9	11.68	1.27
Pred.	104.1	11.93	1.25
SP	100.8 ± 2.002	11.77 ± 0.205	1.25 ± 0.114

Z16-27			
Obs.	197.9	11.19	1.36
Pred.	201.6	11.63	1.34
SP	190.4 ± 4.968	11.28 ± 0.277	1.34 ± 0.179
Z16-33			
Obs.	208	10.97	1.478
Pred.	222.8	11.47	1.471
SP	208.3 ± 6.905	11.05 ± 0.227	1.471 ± 0.081
Z16-40 (no pre-carboniferous constraint)			
Obs.	333.4	12.05	1.418
Pred.	329.8	12.25	1.382
SP	328.2 ± 11.55	12.18 ± 0.197	1.382 ± 0.17
Z16-40			
Obs.	333.5	12.05	1.418
Pred.	341.5	12.23	1.403
SP	336.5 ± 8.753	12.12 ± 0.248	1.403 ± 0.169
Z16-41 (no pre-carboniferous constraint)			
Obs.	315.4	11.45	1.159
Pred.	300.3	11.46	1.591
SP	304.8 ± 18.05	11.53 ± 0.183	1.591 ± 0.705
Z16-41			
Obs.	315.4	11.45	1.159
Pred.	316.4	11.43	1.61
SP	319.1 ± 9.998	11.48 ± 0.183	1.618 ± 0.637
Z16-45 (no pre-carboniferous constraint)			
Obs.	446.8	11.48	1.138
Pred.	415.5	11.89	0.936

SP	412.9 ± 10.41	11.76 ± 0.16	0.936 ± 0.346
Z16-45			
Obs.	446.8	11.48	1.138
Pred.	418.9	11.96	0.951
SP	412.6 ± 10.59	11.75 ± 0.168	0.951 ± 0.344
Z16-52			
Obs.	113.1	11.91	1.15
Pred.	117.2	11.71	1.15
SP	113.2 ± 4.354	11.7 ± 0.144	1.15 ± 0.324

Table S7. Apatite fission track age data used for QTQt temperature-time modelling.

Sample	Ns	Age	Age SD	Dpar
Z16-01-1.d	69	137.13	20.3	1.15
Z16-01-2.d	31	128.44	28.1	1.19
Z16-01-3.d	45	72.31	12.0	1.34
Z16-01-4.d	24	52.40	11.8	1.03
Z16-01-6.d	16	37.34	9.7	1.28
Z16-01-7.d	42	77.57	50.9	1.14
Z16-01-8.d	5	45.44	22.1	0.89
Z16-01-10.d	12	143.39	49.5	1.28
Z16-01-11.d	27	106.71	21.9	0.95
Z16-01-13.d	30	214.36	43.0	0.65
Z16-01-14.d	82	80.72	11.5	1.26
Z16-01-15.d	39	206.61	36.7	0.95
Z16-01-16.d	58	149.00	22.1	1.32
Z16-01-18.d	29	140.98	28.6	1.04
Z16-01-19.d	31	54.31	11.3	1.17
Z16-01-20.d	25	107.54	43.2	1.1
Z16-01-22.d	12	87.20	26.0	0.95
Z16-01-23.d	11	155.49	48.4	1.27
Z16-01-24.d	4	86.04	44.4	1.09
Z16-01-25.d	16	203.37	54.7	0.57
Z16-01-27.d	16	171.20	45.8	1.03
Z16-01-29.d	33	190.58	38.0	1.19
Z16-01-30.d	7	238.21	92.8	1.28
Z16-01-31.d	67	83.04	12.6	1.39
Z16-01-32.d	36	173.96	31.9	0.96
Z16-01-33.d	9	131.87	47.4	1.04
Z16-17-01.d	143	99.24	11.1	1.27
Z16-17-02.d	55	87.02	14.1	1.39
Z16-17-03.d	146	115.80	14.6	1.28
Z16-17-04.d	101	102.56	12.9	1.31
Z16-17-05.d	55	134.65	20.4	1.13
Z16-17-07.d	62	106.18	15.8	1.39
Z16-17-08.d	122	103.12	13.2	1.34
Z16-17-09.d	98	256.38	32.3	1.11
Z16-17-11.d	121	93.95	11.5	1.19
Z16-17-12.d	109	111.51	15.3	1.25
Z16-17-13.d	55	162.08	24.7	1.14
Z16-17-15.d	110	60.97	8.0	1.4
Z16-17-16.d	163	119.41	14.2	1.39
Z16-17-17.d	86	81.85	11.2	1.21
Z16-17-18.d	72	87.68	12.4	1.64
Z16-17-19.d	76	207.20	29.8	1.25
Z16-17-20.d	40	114.65	20.0	0.98
Z16-17-21.d	50	82.92	14.0	1.03
Z16-17-22.d	95	80.59	10.7	1.13
Z16-17-23.d	106	118.21	14.8	1.33
Z16-17-24.d	60	100.28	15.0	1.27
Z16-17-25.d	69	107.57	15.9	1.18
Z16-17-28.d	41	87.69	15.2	1.69

Z16-17-29.d	92	87.03	11.4	1.19
Z16-17-30.d	117	158.59	19.8	1.36
Z16-17-31.d	118	136.48	16.0	1.42
Z16-17-32.d	70	102.68	14.7	1.19
Z16-17-33.d	162	75.05	8.4	1.21
Z16-17-34.d	149	93.88	10.6	1.3
Z16-17-35.d	89	138.11	18.3	1.38
Z16-17-36.d	76	62.57	8.9	1.17
Z16-17-37.d	67	122.50	18.0	1.21
Z16-17-38.d	55	90.71	14.0	1.24
Z16-17-40.d	124	79.36	9.5	1.39
Z16-27-1.d	39	227.73	41.2	1.35
Z16-27-2.d	65	249.12	36.7	1.69
Z16-27-5.d	59	218.74	32.9	1.3
Z16-27-6.d	60	245.14	37.6	1.31
Z16-27-7.d	69	322.46	46.9	1.27
Z16-27-9.d	58	216.88	32.8	1.31
Z16-27-10.d	32	191.22	37.8	1.26
Z16-27-11.d	47	177.19	28.9	1.22
Z16-27-12.d	44	180.98	31.1	1.27
Z16-27-13.d	43	256.46	43.9	1.08
Z16-27-14.d	68	270.24	39.5	1.34
Z16-27-15.d	36	124.67	23.2	1.19
Z16-27-16.d	29	233.99	47.2	1.21
Z16-27-17.d	64	218.78	32.0	1.38
Z16-27-18.d	56	261.06	42.1	1.94
Z16-27-19.d	61	288.60	46.4	1.23
Z16-27-20.d	54	142.05	21.9	1.25
Z16-27-21.d	39	241.33	43.3	1.38
Z16-27-22.d	43	132.60	23.1	1.21
Z16-27-23.d	47	234.41	41.5	1.26
Z16-27-24.d	27	203.12	49.1	1.79
Z16-27-25.d	54	212.11	33.2	1.36
Z16-27-26.d	37	183.67	33.3	1.35
Z16-27-27.d	57	172.51	26.9	1.25
Z16-27-28.d	19	97.27	23.8	1.28
Z16-27-29.d	57	170.96	26.4	1.37
Z16-27-31.d	62	108.82	16.2	1.14
Z16-27-32.d	54	211.19	33.2	1.26
Z16-27-34.d	90	266.88	34.4	1.46
Z16-27-35.d	40	184.02	32.3	1.34
Z16-27-36.d	51	140.11	21.8	1.3
Z16-27-37.d	28	229.19	48.9	1.22
Z16-27-38.d	19	255.58	61.6	1.75
Z16-27-39.d	62	142.95	22.5	1.4
Z16-27-40.d	51	103.73	17.2	1.31
Z16-33-1.d	167	234.10	31.4	1.43
Z16-33-2.d	142	245.04	34.2	1.41
Z16-33-3.d	159	267.53	34.4	1.54
Z16-33-4.d	167	253.82	30.4	1.57

Z16-33-5.d	120	262.39	39.5	1.52
Z16-33-7.d	133	172.46	20.7	1.46
Z16-33-8.d	153	205.08	24.2	1.42
Z16-33-9.d	136	216.56	28.0	1.36
Z16-33-10.d	92	186.71	28.0	1.52
Z16-33-11.d	177	244.50	30.6	1.61
Z16-33-13.d	157	163.32	21.8	1.57
Z16-33-14.d	162	256.34	35.5	1.5
Z16-33-15.d	128	150.37	21.4	1.59
Z16-33-17.d	101	171.65	23.8	1.21
Z16-33-18.d	83	149.32	22.5	1.5
Z16-40-1.d	36	369.69	68.3	1.33
Z16-40-2.d	23	397.50	89.9	1.67
Z16-40-3.d	61	259.98	39.1	1.58
Z16-40-4.d	57	371.44	58.9	1.73
Z16-40-5.d	47	342.31	58.3	1.29
Z16-40-6.d	73	256.02	40.3	1.32
Z16-40-7.d	14	209.28	58.4	1.4
Z16-40-10.d	38	320.91	57.3	1.33
Z16-40-12.d	41	305.30	54.0	1.43
Z16-40-13.d	27	549.1	115.9	1.38
Z16-40-14.d	11	202.7	74.8	1.44
Z16-40-16.d	56	369.6	58.5	1.48
Z16-40-17.d	30	293.4	58.0	1.37
Z16-40-18.d	60	366.5	55.6	1.43
Z16-40-20.d	47	385.5	63.1	1.42
Z16-40-22.d	27	350.2	73.3	1.4
Z16-40-23.d	49	341.8	55.2	1.22
Z16-40-24.d	66	248.0	41.4	1.41
Z16-40-25.d	61	357.4	55.1	1.37
Z16-40-26.d	54	442.6	70.6	1.62
Z16-40-27.d	60	481.6	72.8	1.52
Z16-40-28.d	14	212.0	59.1	1.42
Z16-41-1.d	44	234.9	40.3	1.03
Z16-41-2.d	20	374.9	90.1	1.05
Z16-41-3.d	7	350.7	178.0	1.09
Z16-41-4.d	12	245.9	76.2	0.92
Z16-41-6.d	14	178.3	50.1	1.14
Z16-41-8.d	11	616.7	197.2	1.24
Z16-41-10.d	23	448.9	100.7	1.23
Z16-41-11.d	16	283.8	74.5	1.15
Z16-41-14.d	13	243.9	70.7	1.02
Z16-41-18.d	25	319.2	69.0	1.22
Z16-41-19.d	15	575.4	162.2	1.37
Z16-41-20.d	14	309.4	88.1	1.13
Z16-41-21.d	11	360.6	112.6	1.31
Z16-41-22.d	14	497.3	159.0	2.82
Z16-41-23.d	5	289.9	131.7	0.83
Z16-41-24.d	21	334.7	77.6	1.33
Z16-41-25.d	8	203.1	73.7	0.9

Z16-41-29.d	18	312.6	77.2	1.23
Z16-41-30.d	6	293.9	122.5	1.51
Z16-41-31.d	40	477.8	97.0	1.42
Z16-41-33.d	8	267.4	97.5	1.02
Z16-41-34.d	5	212.4	96.6	0.94
Z16-41-35.d	8	149.3	54.2	1.01
Z16-45-1.d	17	402.8	109.5	0.91
Z16-45-2.d	11	341.5	121.1	1.55
Z16-45-3.d	10	620.0	203.8	1.33
Z16-45-4.d	13	405.6	117.3	1.29
Z16-45-5.d	15	212.8	58.5	0.9
Z16-45-6.d	24	338.4	76.8	1.38
Z16-45-9.d	10	392.2	128.5	1.11
Z16-45-10.d	26	506.0	107.1	1.37
Z16-45-11.d	25	351.9	76.7	1.48
Z16-45-13.d	31	580.1	117.8	1.15
Z16-45-14.d	44	622.8	111.0	1.35
Z16-45-15.d	73	600.3	94.3	1.47
Z16-45-16.d	22	397.0	91.3	1.11
Z16-45-18.d	10	321.9	106.1	1.04
Z16-45-19.d	21	573.3	136.2	1.15
Z16-45-20.d	26	395.4	87.0	1.2
Z16-45-21.d	30	290.6	63.8	1.16
Z16-45-22.d	31	526.7	108.3	0.77
Z16-45-23.d	16	377.9	152.0	1.35
Z16-45-25.d	14	630.0	178.1	0.9
Z16-45-27.d	16	206.5	55.0	1.56
Z16-45-28.d	8	207.7	75.3	0.85
Z16-45-29.d	29	588.1	118.5	1.41
Z16-45-30.d	72	709.3	147.2	1.22
Z16-45-31.d	37	617.2	124.7	1.07
Z16-45-32.d	22	374.9	84.9	1.68
Z16-45-35.d	58	491.2	75.8	1.14
Z16-45-37.d	30	565.2	113.5	1.17
Z16-52-1.d	27	146.8	30.3	1.33
Z16-52-10.d	31	140.6	27.8	0.99
Z16-52-11.d	50	88.0	14.2	1.33
Z16-52-12.d	32	104.3	20.3	1.44
Z16-52-14.d	40	130.1	22.8	1.12
Z16-52-15.d	29	137.9	27.5	1.25
Z16-52-16.d	29	120.0	24.1	1.31
Z16-52-17.d	12	67.1	20.0	0.93
Z16-52-18.d	87	130.5	18.0	1.08
Z16-52-19.d	10	115.4	37.8	1.09
Z16-52-2.d	17	130.2	33.1	1.38
Z16-52-20.d	12	54.3	16.2	1.16
Z16-52-21.d	17	106.2	27.4	0.8
Z16-52-22.d	19	145.6	35.1	1.31
Z16-52-23.d	15	127.6	34.3	1.23
Z16-52-24.d	15	127.5	34.2	1.09

Z16-52-25.d	32	120.3	23.2	1.12
Z16-52-26.d	31	97.4	19.2	1.23
Z16-52-27.d	18	130.5	32.7	1.17
Z16-52-28.d	46	130.1	21.5	1.24
Z16-52-29.d	22	106.8	24.4	1.11
Z16-52-3.d	13	86.5	24.9	1.06
Z16-52-30.d	25	124.4	26.7	1.13
Z16-52-31.d	7	152.3	59.7	1
Z16-52-4.d	15	61.6	16.6	1.01
Z16-52-5.d	22	139.0	31.3	0.96
Z16-52-7.d	26	92.5	19.4	0.97
Z16-52-8.d	5	98.2	44.9	1.27
Z16-52-9.d	18	141.1	35.1	1.25

Table S8. Apatite fission track length data used for QTQt temperature-time modelling.

Z16-01		
Length	Angle Caxis	Dpar
10.72	70.63	1.09
10.12	52.91	1.09
11.15	87.23	1.09
9.88	56.06	1.03
9.17	60.63	0.95
13.79	24.56	0.95
8.72	63.40	0.65
12.96	34.31	0.65
13.45	13.18	0.65
9.09	75.88	1.26
8.64	32.32	1.26
11.38	72.32	1.32
14.87	42.97	1.32
9.21	66.66	1.32
9.42	32.33	1.01
12.08	70.47	0.66
10.60	54.06	0.95
14.09	18.14	1.36
9.95	19.39	1.19
10.35	23.15	1.19
13.84	47.44	1.19
11.05	54.37	1.19
12.37	48.85	1.39
12.00	65.47	1.39
Confined tracks obtained via Cf irradiation		
Length	Angle Caxis	Dpar
9.83	23.54	1.12
12.76	62.09	1.12
9.07	41.85	1.12
13.80	34.04	1.12
10.08	41.32	1.12
11.65	43.47	1.12
12.45	81.18	1.12
9.15	82.78	1.12
9.91	78.54	1.12
13.84	38.12	1.12
12.48	51.83	1.12
11.11	58.42	1.12
14.98	8.12	1.11
10.63	32.61	1.11
10.25	31.41	1.11
14.89	27.22	1.11
10.00	31.55	1.11
9.24	41.62	1.11
12.46	55.08	1.16
11.67	46.93	1.16
10.08	89.81	1.16
9.47	27.15	1.07

10.41	43.00	1.07
11.14	41.27	0.93
9.87	42.51	1.12
12.68	26.90	1.12
10.08	34.63	1.12
10.77	37.64	1.12
10.76	22.69	1.12
9.57	53.43	1.12
11.61	37.84	1.12
10.82	77.97	1.12
15.56	37.65	1.12
10.02	61.38	1.20
10.88	83.67	1.20
12.72	33.52	1.20
9.08	69.28	1.20
9.17	86.48	1.20
13.34	60.03	1.11
10.21	77.49	1.11
13.08	69.10	1.11

Z16-17

Length	Angle Caxis	Dpar
11.43	79.98	1.27
13.15	37.94	1.27
14.64	35.96	1.27
10.43	29.87	1.27
11.96	43.28	1.27
11.72	51.57	1.27
11.31	57.11	1.27
12.26	55.88	1.27
11.64	37.50	1.27
9.27	26.41	1.39
9.64	79.92	1.39
11.77	40.09	1.39
12.97	43.55	1.39
11.71	38.07	1.28
12.15	41.12	1.28
11.08	79.44	1.28
6.42	52.37	1.28
9.75	45.50	1.31
13.60	53.00	1.31
12.70	44.19	1.31
12.95	36.54	1.31
12.89	68.28	1.31
11.32	79.26	1.31
12.81	15.22	1.31
11.68	85.74	1.31
12.87	62.66	1.66
10.37	42.48	1.39
11.70	42.81	1.34
10.04	40.17	1.34

14.68	53.07	1.34
11.79	63.03	1.34
12.61	25.97	1.34
12.42	62.59	1.11
13.72	75.07	1.11
11.58	29.36	1.15
15.52	36.62	1.15
12.02	32.87	1.19
11.95	69.81	1.19
14.33	53.83	1.19
11.28	67.19	1.19
9.99	44.02	1.19
13.86	48.35	1.19
10.00	70.13	1.19
9.54	29.06	1.19
11.26	24.33	1.25
10.30	80.33	1.14
14.06	43.41	1.14
12.16	73.31	1.14
12.64	49.01	1.14
12.94	42.52	1.14
11.73	41.53	1.14
10.48	28.27	1.28
10.83	51.68	1.40
8.44	61.83	1.40
12.84	43.08	1.40
11.13	80.54	1.40
13.13	42.88	1.39
9.94	80.24	1.39
14.22	15.96	1.39
11.62	45.64	1.39
12.82	59.94	1.21
11.64	50.98	1.64
11.97	33.87	1.25
9.15	62.98	1.13
9.66	75.18	1.13
11.76	12.05	1.13
12.40	49.01	1.13
11.61	68.07	1.33
9.91	78.21	1.33
12.05	69.17	1.33
12.05	32.50	1.27
11.99	88.49	1.27
12.48	38.92	1.27
9.65	84.83	1.18
10.59	49.10	1.18
11.43	85.69	1.27
12.48	85.31	1.19
8.32	55.72	1.36
12.71	89.43	1.19

12.20	15.66	1.19
10.56	46.09	1.21

Z16-27

Length	Angle Caxis	Dpar
10.50	88.44	1.69
10.10	24.22	1.69
11.36	58.54	1.69
10.82	83.34	1.53
10.55	30.05	1.27
11.04	36.54	1.44
11.78	67.70	1.31
10.71	84.38	1.26
12.98	58.73	1.08
12.22	43.01	1.34
10.07	52.86	1.19
14.13	14.33	1.38
10.73	58.07	1.38
10.43	40.38	1.38
11.39	21.93	1.38
10.82	19.57	1.94
9.39	86.12	1.94
13.73	51.50	1.23
14.25	21.82	1.23
11.35	72.06	1.23
9.00	26.45	1.25
12.29	38.69	1.38
10.30	71.76	1.38
9.38	15.94	1.28
9.01	16.89	1.33
10.28	39.23	1.33
14.02	48.03	1.14
12.93	35.74	1.14
11.04	17.78	1.14
10.49	56.32	1.46
13.22	64.49	1.34
9.34	32.69	1.30
11.37	80.07	1.30
8.66	16.47	1.30
11.08	56.77	1.30
11.70	32.78	1.75
12.89	14.91	1.40
9.43	83.99	1.40
11.95	75.39	1.31

Z16-33

Length	Angle Caxis	Dpar
8.71	73.27	1.43
10.10	75.43	1.41
10.86	86.94	1.41
10.96	49.36	1.54
9.74	50.05	1.54

9.74	16.57	1.54
9.74	77.61	1.54
10.34	20.59	1.54
9.29	28.52	1.54
12.63	53.83	1.54
11.28	43.82	1.54
11.29	52.26	1.54
12.73	19.94	1.57
13.90	75.95	1.57
9.93	45.78	1.57
10.04	10.53	1.57
12.04	29.03	1.57
11.99	46.61	1.57
14.10	28.71	1.57
11.05	23.60	1.52
10.50	45.72	1.46
9.71	76.95	1.46
10.22	68.32	1.46
9.50	70.63	1.46
12.56	36.36	1.46
13.36	47.61	1.46
8.85	70.68	1.46
9.68	15.17	1.42
9.40	68.05	1.42
10.26	56.38	1.42
13.01	44.74	1.42
10.27	43.41	1.42
9.62	83.98	1.42
11.25	49.17	1.42
10.92	80.33	1.36
9.70	30.95	1.36
10.09	79.04	1.36
13.06	55.85	1.36
9.12	60.17	1.52
10.00	25.88	1.50
12.03	39.92	1.50
10.65	86.55	1.59
10.74	89.17	1.59
10.64	60.00	1.49
9.97	75.26	1.49
13.57	89.79	1.49
11.98	30.14	1.49
12.36	37.99	1.49
12.02	54.17	1.49
13.27	61.22	1.49
8.57	86.92	1.21
12.88	31.70	1.21
11.57	24.10	1.50

Z16-40

Length	Angle Caxis	Dpar

12.85	53.73	1.33
13.58	57.92	1.33
12.78	69.37	1.33
11.00	8.58	1.33
12.87	84.57	1.33
10.98	81.01	1.58
10.32	65.51	1.73
10.75	76.24	1.73
10.94	28.44	1.73
13.34	56.71	1.73
12.99	19.37	1.73
12.48	51.64	1.73
11.81	38.43	1.73
10.01	29.74	1.73
10.28	67.99	1.29
11.22	61.96	1.29
12.41	49.55	1.29
11.61	57.40	1.29
8.88	30.49	1.29
10.25	23.63	1.32
14.37	69.41	1.34
11.59	72.49	1.33
15.28	33.09	1.33
11.80	45.45	1.43
11.82	34.26	1.43
13.19	31.18	1.38
11.99	43.05	1.16
12.10	25.19	1.16
11.63	68.07	1.48
14.93	6.29	1.48
12.78	36.48	1.37
10.40	37.68	1.43
12.92	67.18	0.90
8.91	87.54	0.90
11.45	68.57	1.42
11.95	60.47	1.36
10.84	52.43	1.22
12.63	71.62	1.22
13.38	11.78	1.37
13.18	74.86	1.62
14.99	89.09	1.52
13.03	38.31	1.52

Z16-41

Length	Angle Caxis	Dpar
13.57	49.61	1.09
14.22	38.19	0.92
12.75	43.11	1.14
10.01	83.14	1.04
10.50	85.26	1.23
12.47	0.26	1.23

12.42	8.09	1.23
10.67	74.20	1.23
10.24	66.71	1.23
11.92	27.67	1.23
14.39	20.73	1.09
10.44	82.01	1.12
13.38	0.00	1.23
11.04	71.51	1.37
10.31	29.01	1.13
12.77	77.86	1.33
10.60	37.12	1.34
13.36	23.78	1.51
9.94	48.26	1.42
12.97	15.90	1.42

Confined tracks obtained via Cf irradiation

Length	Angle Caxis	Dpar
9.74	73.55	1.09
10.57	77.28	1.09
11.14	61.81	1.09
10.26	36.24	1.09
10.72	37.63	1.09
11.16	61.82	1.09
11.12	26.28	1.31
12.18	55.03	1.31
12.04	60.89	1.31
10.48	70.96	1.05
11.86	34.22	1.05
11.32	43.40	1.05
12.52	41.87	1.05
9.85	42.20	0.89
13.67	24.95	0.89
9.75	75.96	0.89
11.27	85.50	1.20
10.13	28.51	1.20
11.48	50.34	1.13
10.18	63.05	1.13
10.63	53.42	1.13
9.66	55.79	1.26
15.44	12.59	1.26
11.20	60.10	1.10
10.44	38.02	1.03
10.63	17.50	1.03
10.82	40.15	1.02
10.92	37.78	1.02
10.30	70.75	1.02
11.09	24.00	0.94
11.16	46.24	0.94
14.30	60.77	1.20
10.35	86.84	1.23
12.88	49.06	1.03

10.13	51.31	1.03
12.59	57.17	1.03
11.15	52.84	1.03
	Z16-45	
Length	Angle Caxis	Dpar
12.56	73.53	0.91
11.49	89.64	0.91
8.36	53.90	1.29
9.45	37.38	0.90
10.02	86.90	1.38
9.98	56.05	1.30
9.76	19.97	1.37
12.45	87.14	1.48
8.46	33.96	1.26
10.05	32.05	1.26
12.90	69.79	1.15
11.73	29.65	1.35
10.09	33.68	1.35
13.23	88.85	1.47
9.16	54.65	1.11
8.13	48.84	1.11
10.98	63.00	1.39
10.18	24.29	1.39
13.50	27.56	1.39
15.69	10.64	1.15
8.71	58.09	1.20
10.40	45.58	1.16
9.42	22.34	0.77
12.92	21.16	1.35
10.35	84.37	0.90
12.85	11.20	1.54
10.56	70.22	1.41
10.00	28.88	1.07
12.53	14.56	1.07
10.87	59.67	1.07
11.56	68.50	1.03
11.63	34.36	1.25
Confined tracks obtained via Cf irradiation		
Length	Angle Caxis	Dpar
13.95	28.71	1.08
12.92	79.52	1.08
11.56	70.96	0.96
11.74	86.79	0.96
10.65	42.18	0.96
10.51	76.12	0.96
13.35	34.62	1.05
10.90	79.25	1.05
12.16	42.37	1.19
9.86	29.51	1.19
13.52	86.32	1.19

10.82	47.99	0.94
11.54	40.14	0.94
11.50	26.77	0.94
11.13	17.59	0.94
11.74	33.35	0.94
11.15	26.91	1.15
12.34	60.47	1.15
13.05	18.27	1.15
12.78	33.16	1.15
12.08	49.12	1.02
9.97	74.91	1.02
12.53	47.26	1.02
12.56	33.82	1.02
12.63	49.12	1.09
11.35	89.29	1.05
13.44	65.50	1.05
14.09	52.60	1.05
14.40	50.81	1.05
13.07	63.82	1.05
11.08	36.21	0.98
10.98	31.42	0.98
12.96	56.29	1.00
11.63	56.62	1.00
12.59	50.80	1.00
11.86	45.29	1.00
11.60	40.20	1.04
11.45	78.22	1.04
10.50	43.40	1.04
10.80	27.54	1.04
12.05	24.71	1.04
10.44	53.04	1.04
9.99	83.57	1.04
12.89	39.72	1.04
10.55	61.04	1.04

Z16-52

Length	Angle Caxis	Dpar
11.91	77.94	1.01
12.07	74.75	1.01
12.41	54.42	1.01
11.14	67.16	1.01
12.50	21.58	0.96
13.10	39.87	1.30
9.87	25.22	0.97
11.55	37.33	1.25
13.09	72.81	1.25
9.86	39.62	1.25
9.36	52.59	0.99
12.92	63.48	0.99
10.80	43.71	1.33
11.77	66.07	1.33

9.21	38.63	1.33
10.19	78.92	1.44
13.87	17.65	1.12
10.66	31.52	1.12
12.54	47.45	1.31
10.97	38.04	0.93
13.79	71.64	0.93
11.24	40.20	1.08
10.31	65.00	1.08
13.02	76.90	1.16
12.01	75.87	1.31
10.08	38.91	1.31
12.64	25.95	1.23
11.65	64.36	1.23
10.46	51.73	1.12
10.94	23.81	1.23
10.80	21.09	1.17
12.62	27.84	1.24

Confined tracks obtained via Cf irradiation

Length	Angle Caxis	Dpar
14.27	41.47	1.17
10.05	46.82	1.17
10.72	46.74	1.05
11.01	33.05	1.05
11.88	74.93	1.05
13.54	17.70	1.30
11.35	59.85	1.07
10.72	46.98	1.07
10.60	46.64	1.05
12.26	43.38	1.05
11.40	40.65	1.05
11.70	47.62	1.05
10.70	27.28	1.05
11.03	55.16	1.33
13.46	74.89	1.33
12.61	40.68	1.32
10.65	32.61	1.32
10.33	34.32	1.32
14.26	40.00	1.32
12.20	42.74	1.32
15.07	77.37	1.09
9.90	53.09	1.09
9.96	53.38	1.21
10.71	43.48	1.21
9.97	78.95	1.26
10.37	81.66	1.26
13.97	22.27	1.32
12.82	81.14	1.32
12.02	28.51	1.32
10.38	79.95	1.64

10.58	19.40	1.64
11.12	17.09	1.64
11.78	84.68	1.15
13.18	38.04	1.15
10.12	45.72	1.02
11.54	76.09	1.02
11.91	54.28	1.14
13.53	70.97	1.14
13.97	44.97	1.14
12.67	46.87	0.80
11.53	50.99	1.09
10.18	21.71	1.22
11.59	61.38	1.22
10.09	85.32	1.14
11.21	31.92	1.06
11.68	16.35	1.06
12.22	45.42	1.17
11.93	43.90	1.17
14.89	69.06	1.17
12.88	29.26	1.17
13.64	61.67	0.94
11.70	35.51	0.94
10.95	21.94	0.91
13.41	26.50	0.91
11.74	26.91	1.07
10.50	21.62	1.07
12.02	53.95	1.12
10.52	39.27	1.12
13.34	67.55	1.12
11.55	52.49	1.12
11.72	38.84	1.12
14.12	24.87	1.12
11.36	32.72	1.12
12.96	23.83	1.00
11.81	68.88	1.00
10.17	48.58	1.00
10.01	27.04	0.98
11.88	70.38	0.98